This Issue Contains . . .

Articles

Integrating System Engineering Software Tools — *Chow*	3
Future NASA Spaceborne SAR — *Hilland et al.*	9
MEMS Inertial Rate & Acceleration Sensor — *Hulsing*	17
Cancellation of Jammers / Multipath in GPS — *Fante & Vaccaro*	25
Integrated Digital Info Exchange for Avionics — *Zhang*	31
Inertial Micro-Electrical-Mechanical Sensors — *Allen et al.*	36
Low Cost Avionics with INS / GPS for Vehicles — *Martin & Vouse*	41

Conference Reports

Nuclear Power Developments — *Oman*	7
Fuel Cells can Show Global Warming — *Oman*	16
Cold Fusion: A Potential Heat Source — *Oman*	29

Columns

Economic Theory for Systems Engineering — *Oman*	1
PACE — *Grayson*	2

Situations Wanted 1

Conferences *(Latest Information as published in this magazine)*

Back Cover	**Complete Calendar**
Aerospace Applications	—
Autotestcon	**Held Last Month**
Battery	**April '98, 16**
Carnahan	**May '98, 13**
COMPASS	**Held June '97**
Digital Avionics (DASC)	**Held This Month**
Energy Conversion (IECEC)	**This issue, 7, 16, 23, 29**
ICIASF	—
Intelligent Transportation	—
Mine Detection	—
NAECON	**Held July '97**
Phased Array	—
PLANS	**October '98, 17**
Radar 1999	**October '98, 29**
Radar '99	**July '98, 42**
Radar 2000	**December '96, 33**

Society

Chapters	**30, 35, 47**
Directory	**Inside Back Cover**
Distinguished Lecturers	**8**
Governors	**Inside Back Cover**
BoG Meetings	**Outside Back Cover**
Officers	**Inside Back Cover**
Organization	**24**
Membership Blank	**48**

About the Cover . . .

A World War I US Army program, under the direction of Charles F. Kettering (General Motors), developed a missile called the BUG, which was powered by a 40 horsepower Ford engine. The BUG was tested in late 1918, and radio control was incorporated into a later design; but all work was dropped as the war effort wound down following the November armistice.

PLEASE **Send suggestions and/or contributions of articles & letters to the Editor-In-Chief at the address below; send routine information to the Administrative Editor at the address below. Thank you.**

IEEE AEROSPACE AND ELECTRONIC SYSTEMS SOCIETY

The Aerospace and Electronic Systems Society is a society, within the framework of the IEEE, of members with professional interests in the organization, design, development, integration and operation of complex systems for space, air, ocean or ground environments. These systems include, but are not limited to, navigation, avionics, spacecraft, aerospace power, radar, sonar, telemetry, defense, transportation, automated testing, and command and control. All members of the IEEE are eligible for membership in the Society and will receive this Magazine upon payment of the annual Society membership fee. The Society Board of Governors and its Organization will be found elsewhere in this magazine.

IEEE AEROSPACE & ELECTRONIC SYSTEMS MAGAZINE®

Editor-in-Chief	Henry Oman	19221 Normandy Park Dr., SW, Seattle, WA 98166-4129; (206) 878-4458, F (206) 878-9421, Compmail: (h.oman), Internet: (h.oman@ieee.org)
Associate Editors	Ron Schroer	118 Dan Moody Trail, Georgetown, TX 78628; (512) 864-0294, E-mail: (r.schroer@ieee.org)
	Prakash Chakravarthi	19284 Circle Gate Drive, #103, Germantown, MD 20874; (301) 428-4294, H (301) 540-3258
	Pekka Eskelinen	PL 119A, 07700 Koskenkyla, Finland; 358-5-62111, F 358-5-6212799
PACE Editor	Timothy P. Grayson	9074 Glenway Court, Burke, VA 22015; V (703) 247-8438, F (703) 247-8537, E-mail: (t.p.grayson@ieee.org)
Administrative Editor	David B. Dobson	4500 North Park Ave., Chevy Chase, MD 20815; (301) 657-0208, F (301) 657-0209, E-mail: (d.dobson@ieee.org)
Editors Emeriti	Ben J. Goldfarb; Lee D. Dickey; H. Warren Cooper	

THE INSTITUTE OF ELECTRICAL AND ELECTRONICS ENGINEERS, INC.

Joseph Bordogna, *President*
Kenneth R. Laker, *President-Elect*
Charles K. Alexander, *Past President*
Antonio C. Bastos, *Secretary*
Bruce E. Eisenstein, *Treasurer*
Arthur Winston, *Vice President - Educational Activities*
Friedolf M. Smith, *Vice President - Publication Activities*
Daniel R. Begnini, *Vice President - Regional Activities*
L. John Rankine, *Vice President - Standards Activities*
Lloyd A. Morley, *Vice President - Technical Activities*

Director, Division IX: Signals & Applications
Edward K. Reedy GTRI/RO, 400 Tenth Street, NW, Atlanta, GA 30332-0800; (404) 894-7788, F (404) 894-5233, E-mail: ed.reedy@gtri.gatech.edu

IEEE AEROSPACE AND ELECTRONIC SYSTEMS MAGAZINE® (ISSN 0885-8985; USPS 212-660) is published monthly by The Institute of Electrical and Electronics Engineers, Inc. Responsibility for the contents rests upon the authors and not upon the IEEE, the Society/Council, or its members. **IEEE Corporate Office:** 345 East 47 Street, New York, NY 10017-2394, USA. **IEEE Operations Center:** 445 Hoes Lane, P.O. Box 1331, Piscataway, NJ 08855-1331, USA. **NJ Telephone:** 908-981-0060. **Price/Publication Information:** Individual copies: IEEE members $10.00 (first copy only), nonmembers $20.00 per copy. (Note: add $4.00 postage and handling charge to any order from $1.00 to $50.00, including prepaid orders.) Member and nonmember subscription prices available on request. Available in microfiche and microfilm. **Copyright and reprint permissions:** Abstracting is permitted with credit to the source. Libraries are permitted to photocopy for private use of patrons; provided the per-copy fee indicated in the code at the bottom of the first page is paid through the Copyright Clearance Center, 222 Rosewood Drive, Danvers, MA 01923, USA. For all other copying, reprint or republication permission, write to the Copyrights and Permissions Department, IEEE Publications Administration, 445 Hoes Lane, P.O. Box 1331, Piscataway, NJ 08855-1331.

Copyright © 1998 by the Institute of Electrical and Electronics Engineers, Inc. All rights reserved.

Periodicals postage paid at New York, NY, and at additional mailing offices. Postmaster: Send address changes to *IEEE Aerospace and Electronic Systems Magazine*, IEEE, 445 Hoes Lane, P.O. Box 1331, Piscataway, NJ 08855-1331. GST Registration No. 125634188. Printed in the United States of America.

This material may be protected by Copyright law (Title 17 U.S. Code)

MEMS Inertial Rate and Acceleration Sensor

Rand Hulsing
AlliedSignal

ABSTRACT

Development of the μSCIRAS™ (pronounced micro-Cyrus) multisensor for a period of over six years has produced a practical MEMS Inertial Measurement Unit (IMU). Using only three silicon sensors, a full-up IMU suitable for tactical grade navigation and guidance applications has been achieved. Iterative improvements in silicon sensor design and bulk micromachining processes have matured to the point where an IMU with an attractive price/performance ratio is now producible. This paper summarizes the design features and test results for an IMU with < 100 deg/hr performance. Test results are shown for rate bias and acceleration bias over temperature.

Production of this initial member of the μSCIRAS product family begins this year to support applications including guided artillery shells, technology insertion to decrease missile costs, navigation of remotely-piloted vehicles, dismounted soldier location devices and other navigation aids. The small size of this silicon multisensor and its ability to measure both angular rotation rate and linear acceleration provides a useful advantage in product packaging, cost, size, and system testing. The μSCIRAS Inertial Sensor Assembly (ISA) is housed in a 2 cubic inch package weighing less than 5 ounces (140 grams) requires less than 0.8 Watts of power. Continuing development will lead to greatly improved performance on the order of 1 deg/hr at low prices in high-volume production.

Author's Current Address:
AlliedSignal, EAS, Instrument Systems 15005, NE 36th Street, Redmond, WA 98052, USA.

Based on a presentation at PLANS '98.

0885-8985/98/ $10.00 © 1998 IEEE

INTRODUCTION

In the rapidly advancing world of Micro-Electro-Mechanical Sensors, or MEMS, there are many new design approaches used to achieve rate sensors. As sizes shrink, a new set of error sources come into play which ultimately set the limits of performance. Bulk micromachining offers the benefits of mass production, but not at the price of performance. By utilizing the full thickness of the silicon wafer, sensitivity to line width, mask alignment and flatness are greatly reduced. At the same time, the long term stability of the device is enhanced due to the low stress of the lightly doped layers. While bulk machined sensors are larger than surface machined, the cost to the user is minor due to the relatively higher costs of the electronics and packaging. Thus the performance is maximized without the need for mechanical or electrical trimming.

The development of μSCIRAS is the culmination of six years of silicon work, and seven prior years of macro-size mechanisms. Leveraging off of the strength of three decades in the design of precision linear accelerometers, the rate sensor consists of two linear accelerometers etched within a unique dither mechanism. This produces a direct cost advantage in that both linear acceleration and angular rate are sensed by the same silicon and processing electronics. The dither drive mechanism was designed to not only provide a velocity

Nintendo Exhibit 1066
IPR2024-00668 - Page 241

perpendicular to the accelerometers sensitive axes to excite the Coriolis signal, but also to link the two accelerometer motions to be equal and opposite. This makes the dither drive reactionless and less sensitive to mounting, orthogonal axes dither and external vibration sources. This feature has been tested and refined to produce a vibration insensitive sensor which can meet performance in tough military vibration environments. The sensing element is sandwiched in between two cover plates which provide squeeze film damping in a 1 atmosphere, dry gas backfill. The damping adds a further measure of vibration reduction as well as providing shock stops for the accelerometers and rate sensor. This gives the sensor the capability to withstand 20,000 g shock loads along the accelerometer input axes.

The accelerometers use resonant beams as the sensing elements. The output of the accelerometer is a frequency proportional to the input acceleration. Two proof-mass sensing elements are constrained by a pair of resonant beams. They are arranged so that one beam goes into tension for a higher natural frequency while the other goes into compression. This push-pull arrangement produces a differential frequency output proportional to acceleration. The advantage is that common mode errors such as absolute clock frequency and second order non-linearities are reduced. The output of the rate sensor is a direct digital interface which takes advantage of the revolution in digital processing techniques. The use of the new fine-line digital Application Specific Integrated Circuits, ASIC, to convert frequency directly into a micro-processor digital word format eliminates the need for A/D or delta-sigma converters and their associated errors.

PRINCIPLE OF OPERATION

A simplified sensor mechanism is outlined in Figure 1. Multiple sensor elements are etched in a batch process from one piece of crystalline silicon. The sensor is comprised of three basic blocks: two resonant beam accelerometer, RBA, shuttles and an interconnecting link. Each shuttle is connected to the silicon frame by multiple high aspect ratio flexures. The link is connected to each shuttle and to the frame with three similar high aspect ratio flexures. The center flexure acts as a hinge which allows the link to rotate about an axis normal to the plane of the substrate and located at the flexure's mid-point.

In operation, the two accelerometer shuttles are driven at resonance in opposite directions. The link insures that the phase and amplitude are exactly equal, even if there are mass or spring stiffness differences between the two shuttles. This feature has several advantages which allow the silicon processing accuracy to be relaxed. Minor processing gradients will cause the two accelerometer shuttles to be mismatched. If they were not interconnected, they could resonate at the average frequency between them, but with a leader / follower phase relationship. With high Q dither frames, small differences rapidly grow to a substantial phase difference. This would lead to a sensor that is not reactionless and could lower the effective Q, induce base reactions that could couple to other sensors and leave it susceptible to input vibrations. The link prevents these adverse consequences and inhibits external vibration from inducing any differential shuttle motion. The shuttles are static g-balanced to prevent emitting reaction forces into the base mount that could otherwise couple into the other two channels.

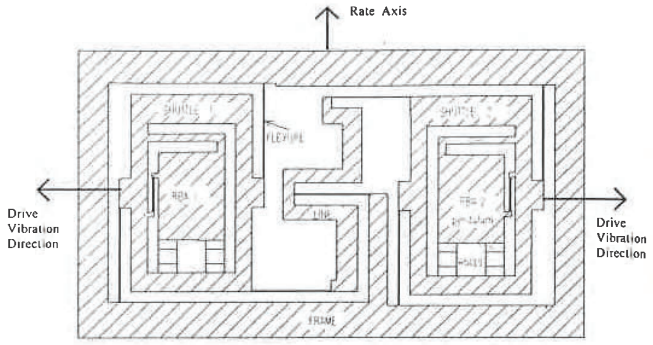


Fig. 1. Sensing Mechanism

The accelerometers are formed at the same time as the other elements. A pendulum is etched free from the substrate, except at five attachment points. The two flat flexures form a hinge at the bottom of the pendulum on the far side of the wafer. A horizontal hinge axis is formed through their mid-points, about which the pendulum can rotate out of the plane of the substrate. The pendulum is constrained against rolling about the rate axis by a strut, which remains flexible in the direction of pendulum motion out of the plane of the substrate. The pendulum is captured by the resonant beams used as the frequency sensitive output. These beams are located between the shuttle frame and the pendulum. Both pairs of beams are in a push-pull arrangement on the near side of the substrate. In Figure 1, an acceleration that is applied normal to the page causes RBA 1 beams to be pulled in tension while RBA 2 beams are pushed in compression. This configuration has the advantage of matching the accelerometer characteristics even when there are silicon process variations. The beams constrain the pendulum to a very small displacement even under high g-loads. The pendulum mass is levered to the axial spring rate of the beams. This increases sensitivity for a given proof mass by as much as ten to one. The advantage of driving a bulk etched proof mass is the greatly increased signal strength of the Coriolis acceleration relative to other error sources.

The sensor substrate is sandwiched between two silicon damping plates which are similarly bulk etched. In the central area just inside the outer frame of Figure 1, the damping plate is etched back to provide a stop for the pendulum and clearance for all the shuttle's moving parts. This gap also provides the squeeze film damping for the pendulum. The squeeze film damping prevents the pendulums from rattling against the stops during a

Nintendo Exhibit 1066
IPR2024-00668 - Page 242

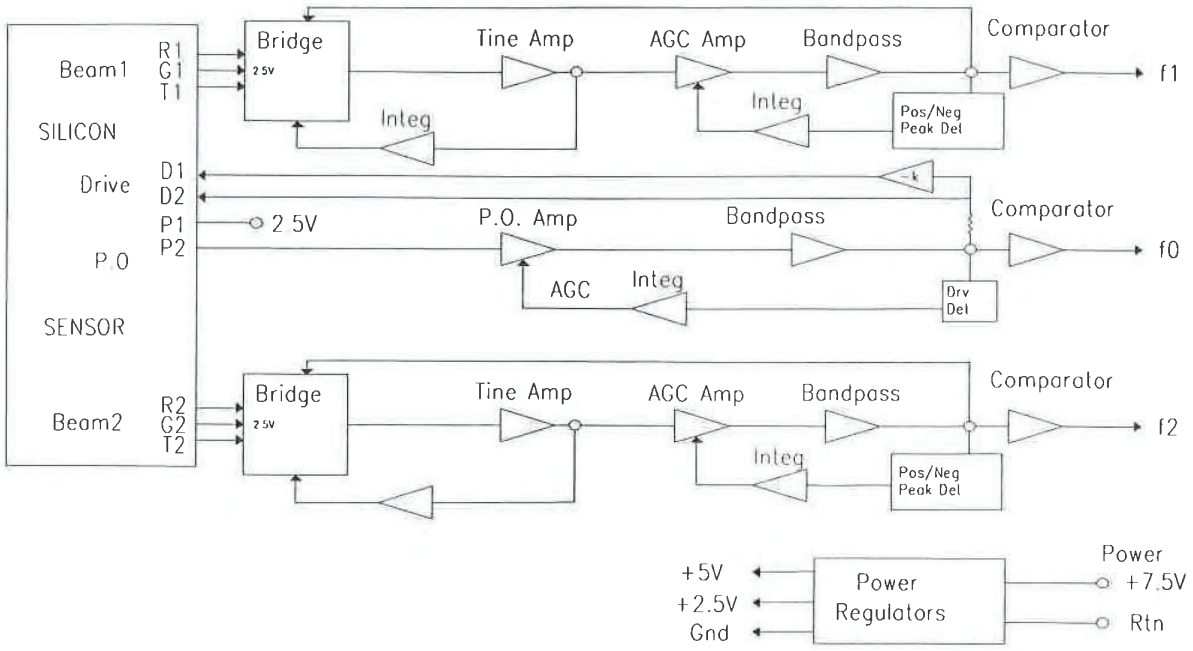


Figure 2. Hybrid Drive Electronics

vibration input. By using a 1 atmosphere backfill instead of a hard vacuum, the leak rate requirement is greatly reduced, thus further reducing processing and packaging costs. The gas damping also provides an extra measure of protection for shock overload in that the pendulum is cushioned as it approaches the stops. This prevents stress concentrations from damaging the pendulums during repeated shocks.

DRIVE ELECTRONICS

The drive electronics for the dither and two resonant beams is accomplished in a co-located ASIC hybrid circuit as shown in Figure 2. The two beam drive circuits are identical, each consists of a balanced bridge input formed by the tines and a matching reference resistor.

The difference is amplified with a variable gain, very low noise amplifier. This output is integrated and used to DC balance the bridge. The tine amp output is also bandpass filtered to reduce noise and then peak detected for input into an automatic gain control (AGC) loop. The output of the bandpass filter drives the top of the bridge to supply AC current to oscillate the beams. The output of the bandpass also drives a comparator to generate a logic level, frequency output signal. These two beam drive loops have local power supply regulation to reduce line sensitivity and to eliminate coupling to the other sensors in a triaxial unit.

The dither drive electronics is the middle block. The operation is similar to the beam drive loops except the velocity pickoff goes directly into the first amplifier without the bridge circuit. A bandpass amplifier which is tuned loosely around the drive frequency supplies a signal the peak detector, motor drive amplifier and to the output comparator. The drive amplifier must supply the peak current to sustain the dither level and is run directly off of 5VDC power to avoid coupling into the beam drives. At the low drive frequency, the op amps have adequate power supply rejection to avoid coupling between the channels.

SIGNAL PROCESSING

Acceleration sensed by the rate sensor is:

$$a = 2\omega v \quad (1)$$

where

a= Coriolis acceleration

ω = Input angular rotation rate

v = Accelerometer perpendicular velocity

For a dithered accelerometer whose position input is a sine wave at the dither frequency, the perpendicular velocity is proportional to the cosine of the dither frequency. In order to extract the rate information from the accelerometer, a synchronous demodulator is used referenced to the cosine velocity. The advantage of an inherently digital system is the precision with which the demodulation can be done. Generating two equal periods with a digital phase lock loop allows precise cancellation of any constant term like accelerometer bias. This precision can be as good as the short term stability of a quartz crystal, on the order of one part in 5 billion per day.

A single channel of signal processing is shown in Figure 3. The resonant beam frequencies, fi, are input into a digital ASIC which uses a 50 MHz clock as a fine

Nintendo Exhibit 1066
IPR2024-00668 - Page 243

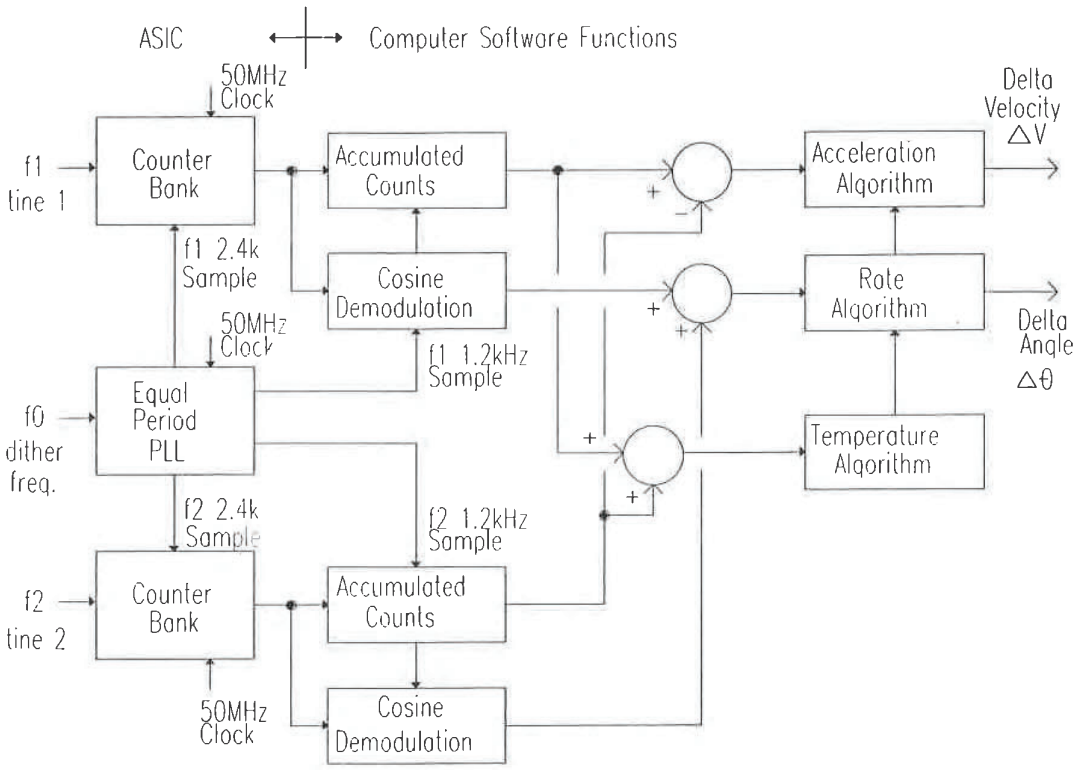


Fig. 3. Processing Block Diagam

reference. These frequencies are counted over a sample frequency of 1200 Hz. The data is taken each half cycle as determined by the input dither frequency and internal phase lock loop. If consecutive half cycles are added, the result is proportional to linear acceleration. The f2 counts are subtracted from f1 counts to form an input for delta velocity algorithm, ΔV. If two consecutive counts are subtracted, then a cosine demodulation is performed. Adding f1 and f2 demodulated counts forms an input to the delta theta algorithm, Δθ. A signal proportional to temperature can be formed by adding accumulated counts.

The ΔV algorithm is:

$$\Delta V = A[\Sigma Ni + FT + B\Delta Ni] \quad (2)$$

where

A = Scale Factor
FT = Bias Frequency Constant
B = Correction Constant
Ni = Accumulated Counts per cycle
T = Dither Period.

Similarly, the Δθ algorithm is:

$$\Delta\theta = a[\Delta Di + ft + b\Sigma Di], \quad (3)$$

where

a = Scale Factor
ft = Bias Constant
b = Correction Constant
Di = Demodulated Counts per cycle

The coefficients in each algorithm are modeled over temperature and used to convert the digital counts directly into the ΔV and Δθ outputs at 1200 Hz. Subsequent operations include low pass filtering, coordinate transformation, axis-alignment corrections and non-linearity corrections. All of these operations are done at the 1200 Hz data rate and are available for auto-pilot functions as well as navigation. Lower rate navigation data at 100 Hz can easily be done by adding 12 frames of 1200 Hz data with appropriate scaling.

TRIAXIAL ISA

The Inertial Sensor Assembly (ISA), shown in Figure 4, on next page, consists of three silicon sensors mounted within a magnetic circuit. The magnets supply a field perpendicular to the silicon substrate so that by driving current along metalized paths atop the sensor flexures, a motive force can be generated. This provides the driving force for all the oscillators to run the tines and dither drive at their natural frequencies. The sensor assembly consists of only eleven parts. Three single-axis sensors are arranged in a triad as a "cube-on-corner" with equal angles of 35.26° with respect to the horizontal plane for each of the rate axes. This forms an orthogonal relationship between the rate input axes with a minimal volume. The accelerometer axes lie along the faces of the cube-on-corner in an acute skewed relation. Each of these

Nintendo Exhibit 1066
IPR2024-00668 - Page 244

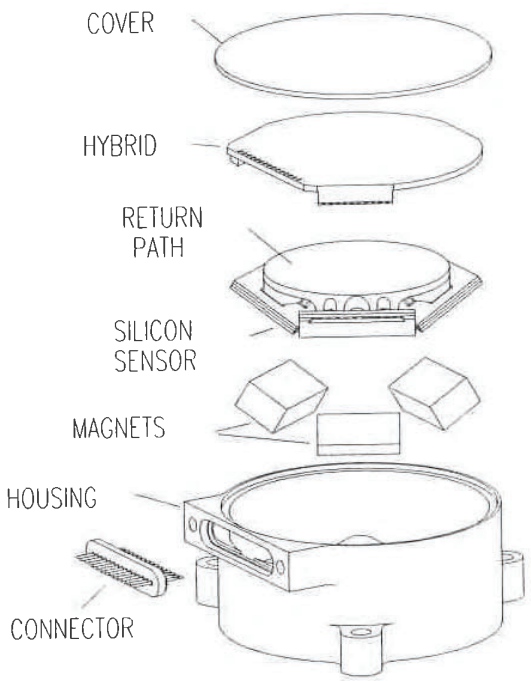


Fig. 4. ISA Exploded View

axes are 35.26° from the common vertical axis. The accelerometer axes are easily transformed to be co-located with the rate axes by a simple summing algorithm. Since the RBA's have excellent scale factor stability, this transform is accurate.

Each sensor is mounted on the magnetic field return path which is shaped to focus the magnetic flux. The return path supports the hybrid electronics and holds all three sensors in their magnet gaps. The entire assembly is bonded to a housing center support post. A top cover and connector are laser welded to the housing to seal in a dry nitrogen atmosphere which prevents moisture condensation at cold temperatures. The package is made from a magnetic grade stainless steel and serves as an EMI shield for both electric and magnetic fields. The ISA is a 1.72 inch diameter by 0.82 inch high (2 cubic inches) package weighing less than 5 ounces (140 grams) and requiring only 0.8 watts of power.

This configuration of sensor has been centrifuged to 15,000 g's and has worked before and after. The design is such that the inner sensor elements bottom out on the damping plates to protect the mechanism from excessive strain during high shock events. All of the package elements were designed to withstand 20,000 g's along the central vertical axis. This means that the device is rugged enough to be cannon launched and still provide a navigation function.

MICROPROCESSOR

A block diagram of the CPU circuit is shown in Figure 5. The major functions performed by the electronics

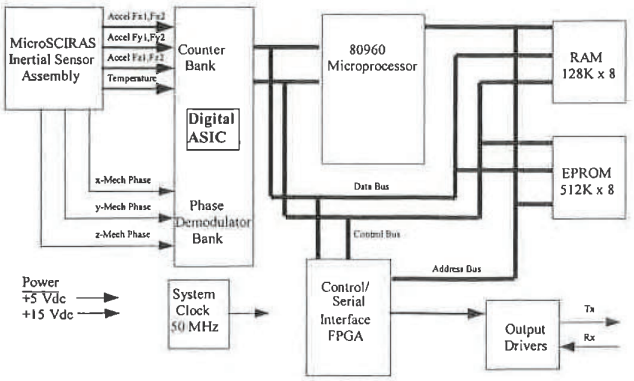


Fig. 5. Microprocessor

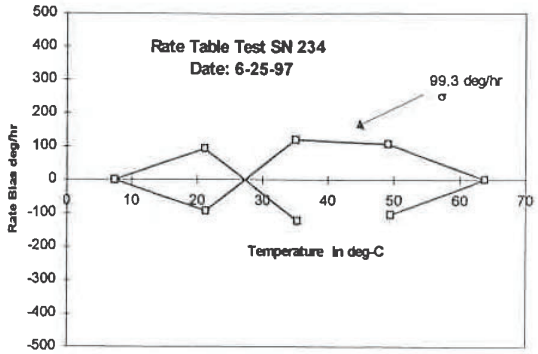


Fig. 6. Rate Sensor Residuals

are: inertial sensor interface, system processing, system timing and control, memory, and external interface. The digital ASIC provides the interface to the inertial sensors. The outputs are read by the micro-processor to derive synchronized, compensated accelerations and angular rates.

The processor loading is at 85% using an Intel 25 MHz 80960 Micro-processor. System memory consists of 512 Kbytes of EPROM and 128 Kbytes of RAM. System timing and control are achieved through the use of a field programmable gate array (FPGA) which can be mask programmed. This FPGA provides the signals necessary for the external interface. External interface signals flow to serial line drivers which interface to the host system.

A serial data output is implemented in the IMU as an RS-232 or RS-485 format. The CPU transmits six channels of inertial data over a serial data interface at 100 Hz update rate. Inertial data represents the delta linear velocity change and angular attitude change since the prior transmission.

THERMAL TEST DATA

Initial temperature test data shows good promise for tactile grade sensor performance. Rate sensor performance from 5°C to 65°C is shown in Figure 6. The rate sensor was calibrated and modeled over temperature. What is shown in Figure 6, are the residuals from the actual measurements minus a thermal model. The unit exhibits less than 100 deg/hr bias error in this test run.

Nintendo Exhibit 1066
IPR2024-00668 - Page 245

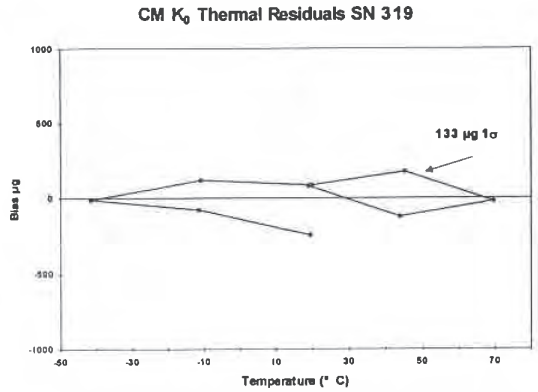


Fig. 7. Accelerometer Thermal Residuals

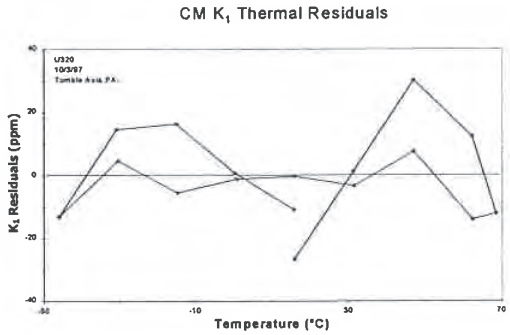


Fig. 8. Accelerometer K1 Residuals

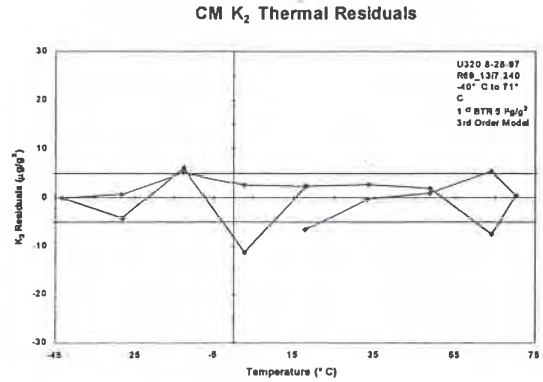


Fig. 9. Accelerometer K2 Residuals

Table 1.

Parameter	Current Target	Near Term Goal
Rate Bias	100 deg/hr	10 deg/hr
Rate Scale Factor	500 ppm	100 ppm
Random Walk	0.4 deg/√hr	0.15 deg/√hr
Accel Bias	1 mg	300 µg
Accel Scale Factor	100 ppm	25 ppm
Temperature	-40°C to 71°C	-55°C to 95°C

Accelerometer bias thermal testing was done from –40°C to 71°C. The residuals measured 133 μg, 1σ, over temperature as shown in Figure 7. The scale factor 1σ residual was 16 ppm for K1 as shown in Figure 8.

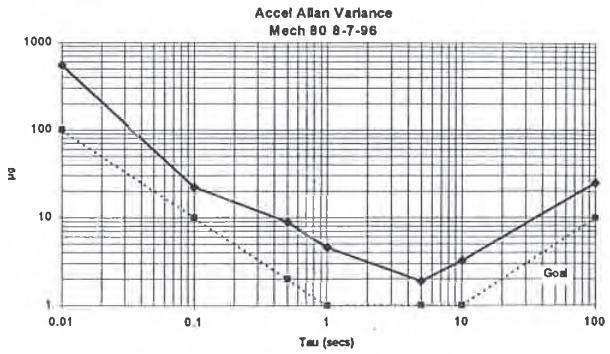


Fig. 10. Accelerometer Allan Variance

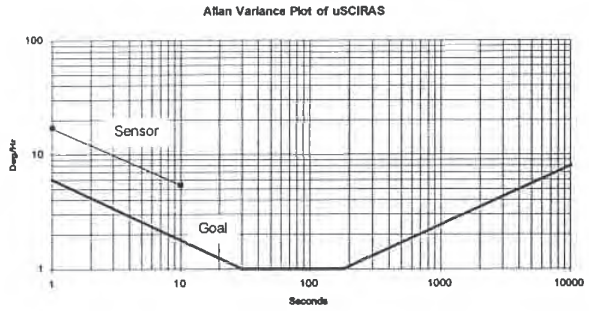


Fig. 11. Rate Allan Variance

The vibration rectification coefficient or K2 is used as the measure of vibration rejection. The K2 was measured and model residuals are shown in Figure 9. The residuals after modeling are less than 5 $\mu g/g^2$ over temperature.

The Allan Variance noise of the accelerometer and rate channels are shown in Figures 10 and 11. Both are within a factor of two of the theoretical limits.

FUTURE DEVELOPMENTS

The performance goals for the silicon sensor are summarized in Table 1. Long term goals include rate performance of 1 deg/hr and 0.1 deg/√hr random walk.

A major element of any IMU is the digital processing required to turn raw sensor signals into useful body rate information. Because the μSCIRAS sensor directly produces digital signals in frequency format, it is practical to condense the complicated front-end signal processing into an Arithmetic Logic Unit (ALU) based ASIC. Counters and simple arithmetic operations perform high speed demodulation operations that generate useful body rate information. Relegating this front-end digital processing to a low-cost ASIC yields impressive reductions in size and cost of the IMU. The basic size of an IMU with this condensed processing would be about 0.5 inches taller than the standard ISA. The interface would be a standard serial interface operating at user selectable baud rates. The signal processing ASICs embedded in the ISA would perform the

Nintendo Exhibit 1066
IPR2024-00668 - Page 246

functions of an IMU, including operations such as temperature compensation and axis-alignment to achieving fully compensated ΔV and $\Delta\theta$ values.

ACKNOWLEDGMENTS

A special word of thanks to the μSCIRAS team for their hard work and dedication to make this happen. We offer a special thank you to team leader, Randy Sprague, for his drive to get things done.

REFERENCES

[1] Hulsing, R. and MacGugan, D., January 21, 1993, Miniature IMU Based on Micro-machined Coriolis Sensors, Proceedings of the National Technical Meeting, San Francisco, pp. 353-360.

IECEC-98 Global Warming, continued from page 16

Wang's better choice is a solid-oxide fuel cell with gas-turbine and steam bottoming cycles. The oxidizer and hydrogen are heated to the fuel-cell's working temperature, without flame, by a chemical-looping combustor, rather than by the fuel-cell's exhaust gas. This eliminates the loss in a high-temperature heat exchanger that would otherwise be needed. The fuel and oxidizer go through different reactors without flame; thus nitrogen-oxide formation is avoided.

Wang predicted that with progress in fuel cells and hydrogen production, this combined cycle will achieve record efficiency without nitrogen-oxide release.

Water Electrolyzer for Making Hydrogen

Hydrogen used in launching spacecraft is shipped from oil refineries to the launch pad. Hydrogen for a fuel-cell powered car is not conveniently available at a filling station. However, hydrogen can be available anywhere there is an electrical outlet!

Takahiro Nakanori has built a polymer-electrolyte water electrolyzer that makes hydrogen from water with an efficiency of 93.2% [4]. The 200 cm^2 five-cell stack operates at atmospheric pressure and a 7.850 stack voltage. The current density is 1.0 ampere per sq cm. If you are in a hurry, you can apply 9.308 volts and go to 5 amperes per sq cm. However, energy efficiency drops to 79.7%.

A gallon of gasoline contains around 120,000 Btu of energy. A gasoline engine delivers about 25%, or about 30,000 Btu, to the transmission. This same energy in hydrogen, made with a 93.2% efficient electrolyzer from 7 cents-per-kWh electric power, would cost 66 cents.

Fuel Cell Plus Gas Turbine Plus Steam Turbine – 81% Efficiency

Giacomo Bisio observed that 30% of fuel energy is destroyed in the combustion process used in today's electric power generation [5]. An additional 15% is lost during the transfer of heat from combustion gases to the working fluid, such as water vapor. A fuel cell is not a heat engine, so is not bothered by Carnot-cycle efficiency limits based on source and sink temperatures. Its exhaust gas temperature is related only to the energy that the fuel cell didn't extract from its fuel and oxidizer. "Indeed it is impossible by configurational adjustments to approximate a situation where the irreversibilities of both coupled phenomena (chemical and electrical) vanish," he observed.

Bisio's model showed that a power plant with a solid-oxide fuel cell with gas-turbine and steam-turbine bottoming cycles could have an efficiency of 81%. The best of today's natural-gas burning combined-cycle plants is 60%, and traditional steam plants are under 40%.

Combined Heat and Power: For Manufacturers It Saves Energy, Reduces Emissions

Power plants in the US generate power by burning fuel to produce heat for turbines. The combustion products, including carbon dioxide, go into the atmosphere. The nation's overall power generating efficiency is only 30%. That means 70% of the fuel energy heats our environment. In addition, we burn fuel to heat our homes, work places and malls.

Tina Kaarsberg evaluated alternatives that reduced both carbon discharge and energy cost [6]. District heating, in which the power plant generates electricity and delivers hot water to local residences is practiced in Europe. However, people in the US don't want to live near power plants. Also, in states like Texas cooling is needed more often than heating.

Quiet fuel cells and Stirling engines can deliver electric power, heating, and cooling to homes and small businesses. Mini-gas-turbines can do the same for industries and hotels. However this practice is discouraged by utilities and government regulations in the following ways:

- Complex "gold plated" interface equipment is mandated when local power is to be paralleled with utility power.
- Fees covering interest on utility power generators must be paid by anyone selling power to a utility.
- A permit is required when nitrogen-oxide can be emitted.
- Zoning restrictions effectively prohibit such installations.
- Skilled labor for installation and maintenance is not available.
- Some state laws require a power generator rated over 30 kW have a watchman on duty 24 hours a day.

Kaarsberg's suggestions for encouraging combined heat and power generation are:

- Relieve the regulation barriers.
- Create "technology incubators" that develop units in small sizes.
- Adapt combined-heat-and-power generation to commercial air conditioning.

The goal should be to generate 7 EJ of energy annually, and reduce the annual carbon release by 30 million tons.

REFERENCES

The following references are from the *Proceedings of the 33rd Intersociety Energy Conversion Engineering Conference (IECEC '98)*, conducted by the American Nuclear Society on August 3-6, 1998. The *Proceedings,* on a hybrid CD-ROM with Search 3.01 for various platforms, can be purchased from the IEEE, 445 Hoes Lane, P.O. Box 1331, Piscataway, New Jersey 08855 USA. Copies of papers can also be purchased from the Institute. The 1998 CD-ROM Proceedings do not have numbered pages. The location of each paper is identified by its "IECEC-98-" number.

[1] Williams, Mark C., IECEC-98-099, Overview of Fuel Cell Power Plant Development in the United States.

[2] Haynes, Comas, IECEC-98-140, Thermodynamic Considerations of a Fuel Cell/Gas Turbine Cycle.

[3] Wang, Xun, and associates, IECEC-98-419, Conceptual Study and Analysis of Hydrogen Fueled Power Plants.

[4] Nakanori, Takahiro, and associates, IECEC-98-113, Development of Solid Polymer Electrolyte Water Electrolyzer With 200 cm2 5-Cell.

[5] Bisio, Giacomo, and Devia, Francesco, IECEC-98-002, Thermodynamic Analysis of a Combined System With Fuel Cells and Fuel-Fired Boiler.

[6] Kaarsberg, Tina M. and Roop, Joseph M., IECEC-98-209, Combined Heat and Power: How Much Carbon and Energy Can it Save for Manufacturers?

Nintendo Exhibit 1066
IPR2024-00668 - Page 247

MEETINGS & CONFERENCES

Russell J. Lefevre, *Vice President-Conferences*

AESS MEETINGS & CONFERENCES

DATE	MEETING	PLACE	CONTACT
January 12-15, 1999	Battery Conference	Long Beach, CA	E-mail: battery@engr.csulb.edu
April 20-22, 1999	1999 Radar	Boston, MA	IEEE Boston, (617) 890-5290; F (617) 890-5294; E-Mail: (sec.boston@ieee.org)
May 1999	National Aerospace (NAECON)	Dayton, OH	– Later
May 1999	Synthetic Aperture Radar (EUSAR '99)	Germany	D. Ausherman, V (313) 994-1200, e F (313) 994-5782
May 24-26, 1999	Integrated Navigation Systems	St. Petersburg, Russia	G. Schmidt, (US) V (617) 258-3841; F (617) 258-3355; E-mail: g.schmidt@draper.com
August 29 - September 2, 1999	Test (AUTOTESTCON)	San Antonio, TX	R. Myers, (310) 287-1463; F (310) 287-1851
October 24-29, 1999	Digital Avionics (DASC)	St. Louis, MO	– G. Logan, (703) 578-6584; E-mail: logangt@acq.osd.mil
Spring 2000	Position Location & Navigation (PLANS)	– Later	– Later
September 18-21, 2000	Test (AUTOTESTCON)	Anaheim, CA	R. Myers, (310) 287-1463; F (310) 287-1851
September 2001	Test (AUTOTESTCON)	Philadelphia, PA	R. Myers, (310) 287-1463; F (310) 287-1851

OTHER SOCIETY MEETINGS OF AESS INTEREST

DATE	MEETING	PLACE	CONTACT
December 1-4, 1998	LEOS '98	Orlando, FL	M.K. Estrin, (732) 562-3896; F (732) 562-8434; E-mail: m.estrin@ieee.org
December 2-4, 1998	System Synthesis	Hsinchu, Taiwan	Y. Min, (86) 10-6256-5533, ext. 5666; F (86) 10-6256-7724; E-mail: min@mimi.cnc.ac.cn
December 2-4, 1998	Asian Test Symposium	Singapore	Y. Min, (86) 10-6256-5533, ext 5666; F (86) 10-6256-7724; E-mail: min@mimi.cnc.ac.cn
December 3-5, 1998	Semiconductor Interface Specialists	San Diego, CA	D. Fleetwood, (505) 844-1825; F (505) 844-2991
December 6-9, 1998	International Electron Devices (IEDM)	San Francisco, CA	P. Mahoney, (301) 527-0900; F (301) 527-0994; E-mail: pwmahoney@aol.com
December 7-9, 1998	Multimedia Signal Processing	Redondo Beach, CA	J. Kuo, (213) 740-4658; F (213) 740-4651; E-mail: cckuo@sipi.usc.edu
December 9-11, 1998	Royal Institute of Navigation (NAV '98)	United Kingdom	44 (0) 171 589 5021; F 44 (0) 171 823 867 E-mail: (rindir@atlas.co.uk)
December 16-18, 1998	Decision and Control	Tampa, FL	J.D. Birdwell, (423) 974-9187; F (423) 974-9257; E-mail: birdwell@hickory_engr.utk.edu
December 17-19, 1998	Energy, Comm., Computer & Controls	New Delhi, India	T. Narang, (91)-11-643-5441; F (91)-11-646-5645; E-mail: purkay.sagrik@axcess.net.in
January 25-27, 1999	ION National Guidance Test	San Diego, CA	ION, (703) 683-7101; F (703) 683-7105

IEEE Conference Information: Telephone (908) 562-3878; Fax (908) 981-1769; E-Mail: p.sensi@ieee.org

Nintendo Exhibit 1066
IPR2024-00668 - Page 248

EXHIBIT 1047B

LIBRARY | CATALOG

1 of 1

PERIODICAL OR NEWSPAPER

IEEE aerospace and electronic systems magazine

Full Record MARC Tags

Main title

IEEE aerospace and electronic systems magazine.

Published/Created

New York, NY : Institute of Electrical and Electronics Engineers, ©1986-

Request this Item | LC Find It

More Information

LCCN Permalink	https://lccn.loc.gov/86643900
Publication history	Vol. 1, no. 1 (Jan. 1986)-
Description	volumes : illustrations ; 28 cm
Current frequency	Monthly
ISSN	0885-8985
Linking ISSN	0885-8985
LC classification	TL693 .I117

Nintendo Exhibit 1066
IPR2024-00668 - Page 250

Continues	IEEE Aerospace and Electronic Systems Society newsletter (DLC) 85643921 (OCoLC)12814086
Variant title	Institute of Electrical and Electronics Engineers aerospace and electronic systems magazine
Portion of title	Aerospace and electronic systems magazine
Running title	IEEE AES magazine
Serial key title	IEEE aerospace and electronic systems magazine
Abbreviated title	IEEE aerosp. electron. syst. mag.
Related names	IEEE Aerospace and Electronic Systems Society.
LC Subjects	Avionics--Periodicals. Astrionics--Periodicals. Electronics in military engineering--Periodicals.
Other Subjects	Astrionics. Avionics. Electronics in military engineering.
Form/Genre	Electronic journals. Periodicals. Periodicals.
Browse by shelf order	TL693
Notes	Issued by the IEEE Aerospace and Electronic Systems Society.
Reproduction no./Source	IEEE Service Center, 445 Hoes Lane, Piscataway, NJ 08854
Additional formats	Also issued by subscription via the World Wide Web. IEEE aerospace and electronic systems magazine (Online) 1557-959X (DLC) 2005214267 (OCoLC)44452100 Online version: IEEE aerospace and electronic systems magazine (OCoLC)752413226
LCCN	86643900
Invalid LCCN	sn 85004879

Nintendo Exhibit 1066
IPR2024-00668 - Page 251

CODEN	IESMEA
Dewey class no.	629.135/5/05
National bib agency no.	007529625
Other system no.	(OCoLC)ocm12760485
Additional Links	http://ieeexplore.ieee.org/servlet/opac?punumber=62
Type of material	Periodical or Newspaper
Content type	text
Media type	unmediated
Carrier type	volume
Source of description	Latest issue consulted: Vol. 1, no. 3 (Mar. 1986).

Item Availability

CALL NUMBER	TL693 .I117 Set 1
Request in	Jefferson or Adams Building Reading Rooms
Status	Not Charged
Older receipts	v.1-v.13 (1986-1998:Apr.), v.13:no.7-v.22 (1998:July-2007), v.23:no.1-v.23:no.2 (2008:Jan.-2008:Feb.), v.23:no.6-v.24:no.5 (2008:June-2009:May), v.24:no.8 (2009;Aug.), v.24:no.10-v.26:no.3 (2009:Oct.-2011:Mar.) incomplete, v.26:no.5-v.27:no.8 (2011:May-2012:Aug.), v.27:no.11-v.35:no.9 (2012:July-2020:Sept.), v.35:no.12-v.37:no.12 (2020:Dec.-2022:Dec.)

CALL NUMBER	TL693 .I117 Copy 1 Unbound issues
Request in	Newspaper & Current Periodical Reading Room (Madison LM133)

Nintendo Exhibit 1066
IPR2024-00668 - Page 252

Latest receipts	v. 40, no. 4 (2025 Apr.)
	v. 40, no. 3 (2025 Mar.)
	v. 40, no. 2 (2025 Feb.)
	v. 40, no. 1 (2025 Jan.)
	v. 39, no. 12 (2024 Dec.)
	v. 39, no. 11 (2024 Nov.)
	v. 39, no. 10 (2024 Oct.)
	v. 39, no. 9 (2024 Sept.)
	v. 39, no. 8 (2024 Aug.)
	v. 39, no. 7 (2024 July)
	v. 39, no. 6 (2024 June)
	v. 39, no. 5 (2024 May)
	v. 39, no. 4 (2024 Apr.)
	v. 39, no. 3 (2024 Mar.)
	v. 39, no. 2 (2024 Feb.)
	v. 39, no. 1 (2024 Jan.)
	v. 38, no. 12 (2023 Dec.)
	v. 38, no. 11 (2023 Nov.)
	v. 38, no. 10 (2023 Oct.)
	v. 38, no. 9 (2023 Sept.)
	v. 38, no. 8 (2023 Aug.)
	v. 38, no. 7 (2023 July)
	v. 38, no. 6 (2023 June)
	v. 38, no. 5 (2023 May)
	v. 38, no. 4 (2023 Apr.)
	v. 38, no. 3 (2023 Mar.)
	v. 38, no. 2 (2023 Feb.)
	v. 38, no. 1 (2023 Jan.)

Nintendo Exhibit 1066
IPR2024-00668 - Page 253

LIBRARY | CATALOG

1 of 1

PERIODICAL OR NEWSPAPER

IEEE aerospace and electronic systems magazine

Full Record **MARC Tags**

000		03823cas a2200721 a 4500
001		11314300
005		20250301065931.0
008		851105c19869999nyumr p 0 a0eng c
010	__	**|a** 86643900 **|z** sn 85004879
016	7_	**|a** 007529625 **|2** Uk
022	0_	**|a** 0885-8985 **|l** 0885-8985 **|2** 1
030	__	**|a** IESMEA
035	__	**|a** (OCoLC)ocm12760485
037	__	**|b** IEEE Service Center, 445 Hoes Lane, Piscataway, NJ 08854
040	__	**|a** NSD **|b** eng **|c** NSD **|d** DLC **|d** NSD **|d** NYG **|d** NST **|d** IXA **|d** DLC **|d** NST **|d** DLC **|d** NST **|d** NSD **|d** NST **|d** HUL **|d** NST **|d** MYG **|d** CUS **|d** OCL **|d** MYG **|d** SYS **|d** IEEEX **|d** OCLCQ **|d** NSD **|d** LVB **|d** CIT **|d** OCLCQ **|d** UKMGB **|d** OCLCF **|d** OCLCO **|d** AU@ **|d** I8M **|d** OCLCQ **|d** CSJ **|d** OCLCQ **|d** CPO **|d** OCLCQ **|d** DLC **|d** OCLCQ **|d** LWA **|d** OCLCO **|d** PUL **|d** OCLCQ
042	__	**|a** nsdp **|a** pcc
050	00	**|a** TL693 **|b** .I117
082	00	**|a** 629.135/5/05 **|2** 19
210	0_	**|a** IEEE aerosp. electron. syst. mag.
222	_0	**|a** IEEE aerospace and electronic systems magazine
245	00	**|a** IEEE aerospace and electronic systems magazine.
246	3_	**|a** Institute of Electrical and Electronics Engineers aerospace and electronic systems magazine
246	30	**|a** Aerospace and electronic systems magazine

Nintendo Exhibit 1066
IPR2024-00668 - Page 254

246	17	|**a** IEEE AES magazine
260	__	|**a** New York, NY : |**b** Institute of Electrical and Electronics Engineers, |**c** ©1986-
300	__	|**a** volumes : |**b** illustrations ; |**c** 28 cm
310	__	|**a** Monthly
336	__	|**a** text |**b** txt |**2** rdacontent
337	__	|**a** unmediated |**b** n |**2** rdamedia
338	__	|**a** volume |**b** nc |**2** rdacarrier
362	0_	|**a** Vol. 1, no. 1 (Jan. 1986)-
530	__	|**a** Also issued by subscription via the World Wide Web.
550	__	|**a** Issued by the IEEE Aerospace and Electronic Systems Society.
588	__	|**a** Latest issue consulted: Vol. 1, no. 3 (Mar. 1986).
590	__	|**a** SERBIB/SERLOC merged record
650	_0	|**a** Avionics |**v** Periodicals.
650	_0	|**a** Astrionics |**v** Periodicals.
650	_0	|**a** Electronics in military engineering |**v** Periodicals.
650	_6	|**a** Avionique |**v** Périodiques.
650	_6	|**a** Électronique en astronautique |**v** Périodiques.
650	_6	|**a** Électronique en génie militaire |**v** Périodiques.
650	_7	|**a** Astrionics. |**2** fast |**0** (OCoLC)fst00819376
650	_7	|**a** Avionics. |**2** fast |**0** (OCoLC)fst00824383
650	_7	|**a** Electronics in military engineering. |**2** fast |**0** (OCoLC)fst00907609
655	_0	|**a** Electronic journals.
655	_7	|**a** Periodicals. |**2** fast |**0** (OCoLC)fst01411641
655	_7	|**a** Periodicals. |**2** lcgft |**0** http://id.loc.gov/authorities/genreForms/gf2014026139 |**0** (uri) http://id.loc.gov/authorities/genreForms/gf2014026139
710	2_	|**a** IEEE Aerospace and Electronic Systems Society.
776	1_	|**t** IEEE aerospace and electronic systems magazine (Online) |**x** 1557-959X |**w** (DLC) 2005214267 |**w** (OCoLC)44452100
776	08	|**i** Online version: |**t** IEEE aerospace and electronic systems magazine | **w** (OCoLC)752413226
780	00	|**t** IEEE Aerospace and Electronic Systems Society newsletter |**w** (DLC) 85643921 | **w** (OCoLC)12814086
850	__	|**a** AAP |**a** AU |**a** ArU |**a** AzU |**a** CCC |**a** CLSU |**a** CPT |**a** CSt |**a** CU |**a** CU-A |**a** CU-I |**a** CU-RivP CU-S |**a** CU-SB |**a** CaAEU |**a** CaNBFU |**a** CaOLU |**a** CaOTU |**a** CaOWA |**a** CaOWtU | **a** CaSSU |**a** CoFS |**a** CoU |**a** CtU |**a** CtY-KS |**a** DGW |**a** DLC |**a** DeU |**a** FU |**a** GAT | **a** ICarbS |**a** IEN |**a** IaAS |**a** IaU |**a** InLP |**a** KMK |**a** KyU |**a** LNT |**a** LU |**a** MBU |**a** MCM | **a** MH-GM |**a** MMeT |**a** MdU |**a** MiEM |**a** MiU |**a** MnU |**a** MoKL |**a** MoU |**a** MsU |**a** NIC |**a** NN | **a** NNC |**a** NNE |**a** NRU |**a** NSyU |**a** NcD |**a** NcRS |**a** NdU |**a** NhU |**a** NjP |**a** NmU |**a** NjR | **a** OCU |**a** OU |**a** OkU |**a** OrCS |**a** PBL |**a** PPD |**a** PPiC |**a** PU |**a** RPB-S |**a** TU |**a** TxCM |

Nintendo Exhibit 1066
IPR2024-00668 - Page 255

		a TxDaM |**a** TxHR |**a** TxU |**a** ULA |**a** UPB |**a** UU |**a** ViBlbV |**a** ViU |**a** VtU |**a** WM |**a** WaU	**a** WvU |**a** WyU
859	41	|**u** http://ieeexplore.ieee.org/servlet/opac?punumber=62
853	00	|**8** 1 |**a** v. |**b** no. |**u** 12 |**i** (year) |**j** (month) |**w** m |**x** 01
863	40	|**8** 1 |**a** <1>- |**i** <1986>- |**x** provisional
890	__	|**a** IEEE aerospace and electronic systems magazine. New York, NY. 1986- |**i** 86-643900
906	__	|**a** 7 |**b** cbc |**c** serials |**d** 3 |**e** ncip |**f** 19 |**g** n-oclcserc
920	__	|**a** Keep 1
923	__	|**d** 20020729 |**s** Group Registration
984	__	|**a** srvf
985	__	|**e** eserial 200406
991	__	|**b** c-GenColl |**h** TL693 |**i** .I117 |**w** SERIALS
992	__	|**b** SER |**w** SERLOC

Request this Item | LC Find It

Item Availability

CALL NUMBER	TL693 .I117 Set 1
Request in	Jefferson or Adams Building Reading Rooms
Status	Not Charged
Older receipts	v.1-v.13 (1986-1998:Apr.), v.13:no.7-v.22 (1998:July-2007), v.23:no.1-v.23:no.2 (2008:Jan.-2008:Feb.), v.23:no.6-v.24:no.5 (2008:June-2009:May), v.24:no.8 (2009;Aug.), v.24:no.10-v.26:no.3 (2009:Oct.-2011:Mar.) incomplete, v.26:no.5-v.27:no.8 (2011:May-2012:Aug.), v.27:no.11-v.35:no.9 (2012:July-2020:Sept.), v.35:no.12-v.37:no.12 (2020:Dec.-2022:Dec.)

CALL NUMBER	TL693 .I117 Copy 1 Unbound issues

Nintendo Exhibit 1066
IPR2024-00668 - Page 256

Request in	Newspaper & Current Periodical Reading Room (Madison LM133)
Latest receipts	v. 40, no. 4 (2025 Apr.) v. 40, no. 3 (2025 Mar.) v. 40, no. 2 (2025 Feb.) v. 40, no. 1 (2025 Jan.) v. 39, no. 12 (2024 Dec.) v. 39, no. 11 (2024 Nov.) v. 39, no. 10 (2024 Oct.) v. 39, no. 9 (2024 Sept.) v. 39, no. 8 (2024 Aug.) v. 39, no. 7 (2024 July) v. 39, no. 6 (2024 June) v. 39, no. 5 (2024 May) v. 39, no. 4 (2024 Apr.) v. 39, no. 3 (2024 Mar.) v. 39, no. 2 (2024 Feb.) v. 39, no. 1 (2024 Jan.) v. 38, no. 12 (2023 Dec.) v. 38, no. 11 (2023 Nov.) v. 38, no. 10 (2023 Oct.) v. 38, no. 9 (2023 Sept.) v. 38, no. 8 (2023 Aug.) v. 38, no. 7 (2023 July) v. 38, no. 6 (2023 June) v. 38, no. 5 (2023 May) v. 38, no. 4 (2023 Apr.) v. 38, no. 3 (2023 Mar.) v. 38, no. 2 (2023 Feb.) v. 38, no. 1 (2023 Jan.)

Nintendo Exhibit 1066
IPR2024-00668 - Page 257

EXHIBIT 1047C

libraries.org

A directory of libraries throughout the world

Library of Congress

United States -- Library of Congress

Address: 101 Independence Avenue SE
Washington, District of Columbia
20540
United States

Phone: 202-707-5000

Connect to: Library Web Site✔ Online Catalog

Library details: **Library of Congress** is a **National** library.
This library is affiliated with Library of Congress (view map) . The collection of the library contains **175,000,000** volumes. The library circulates **250,000** items per year.

Library Hours		
Day	Open	Close
Sunday	Closed	
Monday	8:30 am	8:30 pm
Tuesday	8:30 am	8:30 pm
Wednesday	8:30 am	8:30 pm
Thursday	8:30 am	8:30 pm
Friday	8:30 am	5:00 pm
Saturday	8:30 am	5:00 pm

Other Info: Went live with Voyager on August 15, 1999. Currently planning to implement the Library Collections Access Platform (LCAP) on FOLIO and EBSCO discovery services in FY25.

Permalink: https://librarytechnology.org/library/2263
(Use this link to refer back to this listing.)

Administration: The director of the library is **Dr. Carla Hayden** .

Organizational structure: The library is part of a **publicly-funded** organization. It operates on a **Non-profit** financial model.

Affiliations: The library is a member of the Association of Research Libraries

Collection size	175,000,000	volumes
Annual Circulation	250,000	transactions

Wireless: The library offers **wireless** access to the Internet. http://www.loc.gov/rr/wirelessaccess.html

Technology Profile



Library of Congress



map location✔

Related Libraries

- All members of the Association of Research Libraries members
- Directory of ARL Member Libraries
- Libraries located in Washington (District of Columbia)
- all National libs in District of Columbia

About libraries.org

libraries.org is a free directory of libraries throughout the world.

This directory is a component of Library Technology Guides.

Please contact Marshall Breeding to report

Nintendo Exhibit 1066
IPR2024-00668 - Page 259

	Product Name	Year Contracted
Current Automation System	**FOLIO -- EBSCO Information Services**	**2023**
Previous Automation System	**Voyager**	1998
Discovery Service (w/index)	**Ex Libris CDI**	
Electronic Resource Management	**Electronic Resource Management**	
Item ID Type	Barcode	

This library is responsible for the procurement of the library automation system.

View Privacy and Security Report

corrections about information listed for this library.

Identifiers	
libraries.org ID	2263
OCLC Symbol	DLC
WorldCat Registry ID	**45266**

Record History: This listing was created on Aug 9, 1998 and was last modified on Apr 10, 2025.

Updates: Corrections or Updates? Registered members of Library Technology Guides can submit updates to library listings in libraries.org. **Registration** is free and easy. Already registered? **login**. Or, you can report corrections just by sending a message to **Marshall Breeding**.

libraries.org Update this Entry Library Technology Guides

Maintained by **Marshall Breeding**

terms of service
Copyright 1994-2024

Nintendo Exhibit 1066
IPR2024-00668 - Page 260

EXHIBIT 1047D

Copyright United States Copyright Office

Try the Copyright Public Records System (CPRS) pilot with enhanced search features and filters.

Help | Search | History | Titles | Start Over

Public Catalog

Copyright Catalog (1978 to present) at DC4
Search Request: Left Anchored Title = IEEE Aerospace and Electronic Systems Magazine
Search Results: Displaying 11 of 42 entries

previous | next

Labeled View

IEEE Aerospace and electronic systems magazine.

Type of Work: Serial
Title: IEEE Aerospace and electronic systems magazine.
Serial Publication Year: 1998
Serial Key Title: IEEE Aerospace and electronic systems magazine
Imprint: New York : IEEE, 1986-.
ISSN: 0885-8985
Description: print material.
Frequency: Monthly.
Publication History: Vol. 1, no. 1, Jan. 1986-
Continues: IEEE Aerospace and Electronic Systems Society newsletter.
Copyright Claimant: Institute of Electrical and Electronics Engineers, Inc.
Issues Registered: v. 13, no. 1, Jan98.; Pub. 1998-01-14; Reg. 1998-03-10; TX0004660526
v. 13, no. 2, Feb98.; Pub. 1998-02-13; Reg. 1998-03-10; TX0004660526
v. 13, no. 3, Mar98.; Pub. 1998-03-03; Reg. 1998-07-28; TX0004726108
v. 13, no. 4, Apr98.; Pub. 1998-04-01; Reg. 1998-07-28; TX0004726108
v. 13, no. 5, May98.; Pub. 1998-05-06; Reg. 1998-07-28; TX0004726108
v. 13, no. 6, Jun98.; Pub. 1998-06-02; Reg. 1998-09-30; TX0004765582
v. 13, no. 7, Jul98.; Pub. 1998-07-02; Reg. 1998-09-30; TX0004765582
v. 13, no. 9, Sep98.; Pub. 1998-09-02; Reg. 1999-05-28; TX0004894025
v. 13, no. 10, Oct98.; Pub. 1998-10-06; Reg. 1999-05-28; TX0004894025
v. 13, no. 11, Nov98.; Pub. 1998-10-29; Reg. 1999-05-28; TX0004893842
v. 13, no. 12, Dec98.; Pub. 1998-12-28; Reg. 1999-05-28; TX0004893842
v. 14, no. 1, Jan99. Created 1998; Pub. 1998-12-31; Reg. 1999-05-28; TX0004969516
Other Title: IEEE Aerospace and Electronic Systems Society newsletter
Names: Institute of Electrical and Electronics Engineers, Inc.

previous | next

Save, Print and Email (Help Page)		
Select Download Format	Full Record	Format for Print/Save
Enter your email address:		Email

Nintendo Exhibit 1066
IPR2024-00668 - Page 262

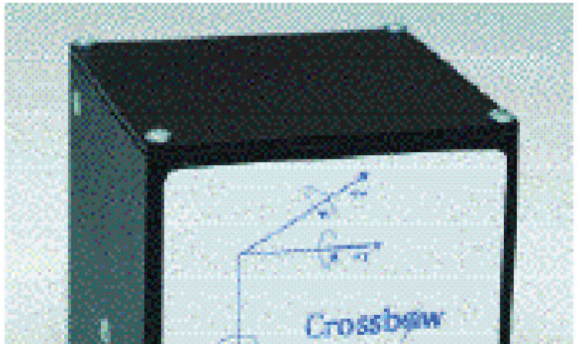
Nintendo Exhibit 1066
IPR2024-00668 - Page 263

EXHIBIT 1053A

https://web.archive.org/web/19980629124810/http://www.xbow.com/pdf/DMU-6X.pdf 133%
http://www.xbow.com/pdf/DMU-6X.pdf Go
2 captures
29 Jun 1998 - 2 May 1999
MAY JUN MAY
29
1997 1998 1999
About this capture

Crossbow

DMU-6X and DMU-VGX
Silicon IMU and Vertical Gyro

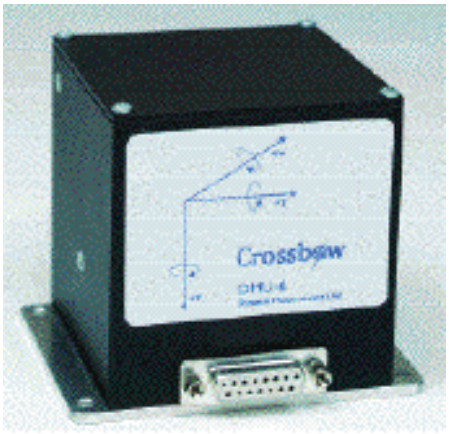


Features

X, Y, Z Acceleration
Roll, Pitch, Yaw Angular Rate
Stabilized Roll & Pitch Angle Output
Analog Signal Conditioned Output
133 Hz Digital (RS-232) Output
DSP Processing Power

Nintendo Exhibit 1066
IPR2024-00668 - Page 265

DMU-6X and DMU-VGX
Silicon IMU and Vertical Gyro



Features

X, Y, Z Acceleration
Roll, Pitch, Yaw Angular Rate
Stabilized Roll & Pitch Angle Output
Analog Signal Conditioned Output
133 Hz Digital (RS-232) Output
DSP Proccessing Power
Evaluation Software Included

Applications

Camera and Platform Stabilization
Antennae Pointing
Inertial Measurements for GPS Integration
Dynamic Positioning & Control
Automotive Testing
Flight Data Analysis

Description

The DMU is an intelligent six axis measurement system designed for accurate acceleration and angle measurement in dynamic environments. The DMU provides application-specific functionality with two product versions, the DMU-6X and DMU-VGX. The DMU-6X outputs inertial acceleration and angular rate measurements formatted for easy system integration. Example applications include GPS navigation, dynamic positioning, and automotive testing. The DMU-VGX outputs stabilized pitch and roll information in addition to the DMU-6X outputs, ideal for camera or platform stabilization. Both products allow for data to be requested via serial command or to be transferred continuously.

DMU Products	Description	Output
DMU-6X	6 degrees of freedom inertial measurement unit. Digital voltage and signal conditioned analog outputs.	XYZ Acceleration 3 Axis Angular Rate
DMU-VGX	Tilt angle (roll/pitch) is computed for measurement in dynamic environments. 133 Hz updates of RS-232 data and 400Hz updates of analog voltage output. Angular rate and acceleration outputs also included.	Roll and Pitch

Table 1. Description of DMU Products.

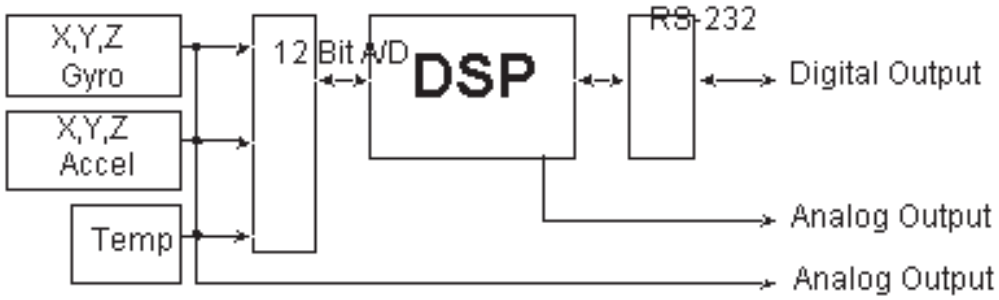


Figure 1. Block diagram of DMU

© 1998 Crossbow Technology, Inc. All rights reserved.

Crossbow Technology
41 E. Daggett Dr.
San Jose, CA 95134

http://www.xbow.com Ph: (408) 324 4830
info@xbow.com Fax: (408) 324 4840

Nintendo Exhibit 1066
IPR2024-00668 - Page 266

Specifications

Power		Operating Temperature Range	
Input Supply Voltage	+8 to 30 V DC	Operating Temperature Range	-40 to 85 °C
Input Supply Current	200 mA (max)	Storage Temperature Range	-55 to 85 °C

Packaging	
Package	Aluminum housing (3" x 3.375" x 3.250")
Weight	475 grams

DMU-VGX Performance		
Roll, Pitch Angle: Dynamic Accuracy	1° RMS	Application Dependent
Resolution	0.1°	Typical
Linearity	< 1 % of FS	FS Roll =180°, FS Pitch =90°
Full Scale Span (analog outputs)	+/- 4.096 VDC	
Analog Data Update Rate	400 Hz	See page 5 for detail.
Digital Data Update Rate	133 Hz	See page 5 for detail.

DMU-6X Performance	Gyro	Acceleration
Available Full Scale Ranges	+/- 50 to 200 °/sec	+/- 1 to 50 G
Full Scale Span (analog outputs)	+/- 4.096 V DC	0 to 5V DC
Full Scale Span (digital output)	-32,768 to +32,767	-32,768 to +32,767
Scale Factor Calibration	< 1 %	< 1 %
Bandwidth	DC - 10 Hz	DC - 100Hz
Linearity	0.5 % of FS	0. 2% of FS
Bias Stability (Room)	+/- 1 °/sec	+/- 5mG
Bias Stability (-40 to 85)	+/- 9 °/sec	+/- 70 mG
Alignment (to enclosure)	< 1 °	< 1 °
Resolution	0.05 °/sec	5 mG (FS < 8G), 50mG (FS > 8G)

Temperature Sensor Output		Mechanical Shock and Vibration	
Range	-50 to 150 °C	Shock	1000 G (1 ms half sine wave)
Accuracy	+/- 2% of FS	Vibration	10 G RMS to 2 kHz
Linearity	+/- 1% of FS		

Principle of Operation

The DMU measures acceleration in three orthogonal axes as well as rotation rate about each of these axes. This is accomplished by three accelerometers and three angular rate sensors.

The DMU employs on board digital processing to provide application-specific outputs and to compensate for deterministic error sources within the unit. The DMU accomplishes these tasks with an analog to digital converter and a high performance Digital Signal Processor. (See Figure 1)

All six of the DMU sensor elements are micromachined devices. The three angular rate sensors consist of vibrating ceramic plates that utilize the Coriolis force to output angular rate independently of acceleration. The three MEMS accelerometers are surface micro-machined silicon devices that use differential capacitance to sense acceleration. The specifications of the DMU are shown above.

© 1998 Crossbow Technology, Inc. All rights reserved.

DMU-6X

The DMU-6X has three output options, one analog and two digital, that allow for easy integration into measurement and control systems.

Analog Interface

The DMU features six fully signal conditioned analog outputs - three linear acceleration signals and three angular rate signals. The analog outputs can directly interface to an A/D or standard data acquisition hardware.

Digital Interface

The digital data output is standard UART at 38.4 kbaud. 8 bit data, 1 bit start, 1 bit stop, No parity. Other baud rates are avialable.

In **voltage mode**, the analog sensor signals are sampled and converted to digital data with 1mV resolution. This digital data is 12 bit, unsigned. Data can be requested via a serial command or set to continuously transfer to the host.

In **scaled sensor mode**, the analog sensor signals are sampled, converted to digital data, temperature compensated, and scaled to engineering units. An electronic data sheet for each sensor is stored in the DMU's on-board memory. The data sheet includes each sensor's bias (offset and scale factor). Data can be requested via a serial command or set to continuously transfer to the host. The digital data is 16 bit 2's compliment integers. A 16 bit timer value is also included in the packet. (See Timer section).

DMU-VGX

The DMU-VGX provides stabilized roll and pitch angles through sophisticated signal processing of the rate and acceleration sensors. Standard tilt sensors use earth's gravitational field to measure angle. Examples of these sensors include the older electrolytic fluid sensors as well as the newer accelerometer based tilt sensors such as the CXTILT02 from Crossbow. These sensors only measure tilt accurately when the object being measured is not accelerating. In dynamic environments such gravity-based tilt sensors can not distinguish between tilt and acceleration.

The DMU-VGX uses a combination of angular rate and acceleration signals to solve this problem. Tilt is calculated by integrating the angular rate sensor outputs to angle. Then the tilt response of the accelerometers corrects for error due to angular rate sensor drift. Drift corrections are applied continuously and the frequency of the updates can be set via the serial command 'T' <0-255>. In this way, corrections can be applied slowly, a T value between 70 - 255, in environments where accelerations are jerky and relatively short (e.g., marine, automotive applications) and more frequently, a T value closer to 0, in environments where accelerations are longer and smoother.

Roll and pitch angle, angular rate, and acceleration outputs are available in the DMU-VGX packet. The digital data is 16 bit 2's compliment integers. This data can be requested via a serial

Command (ASCII)	Response	Description
R	H	Reset: Resets the DMU Firmware. Default operating mode is Voltage Mode and Polled operation (Note 1).
G	Data Packet	Get Data: Requests a packet of data from the DMU. Data format depends on operating mode.
r	R	Change to Voltage Mode.
c	C	Change to Scaled Sensor Mode.
a	A	*DMU-VGX Only:* Change to DMU-VG output mode.
T <0 - 255>	None	*DMU-VGX Only: 2 byte command sequence that changes the integrator correction time constant.*
C	None	Change to continuous data transmit mode. Data packets streamed continuously. Packet rate is dependent on operating mode.
P	None	Change to polled mode. Data packets sent when a G is received by the DMU.
z <0-255>	Z	Calibrate and set zero bias for rate sensors by averaging over time. 1st byte initiates zeroing process. 2nd byte sets duration for averaging. Unit should be straight and level.

DMU serial command set [Firmware v1.2].

© 1998 Crossbow Technology, Inc. All rights reserved.

command or set for continuous transfer.

X-View Development Software

Crossbow development software is shipped with the DMU for use with 486 or better PCs running MS Windows95. The software demonstrates the functionality of both the DMU-6X and the DMU-VGX. It is a convenient way to get started with system development and evaluate the performance of the DMU. The software is a run-time application based on National Instrument's LabView software. The software is shipped on 3.5" floppy disks. For software installation, simply double click the SETUP file on floppy disk #1.

Value	Conversion Factors
Roll & Pitch	180° / 32,768 digits
Range of X G's	$(X * 1.5) / 2^{15}$ from binary data to G's
Range of X °/sec	$(X * 1.5) / 2^{15}$ from binary data to °/sec
Temp	=1.375V + 22.5mV*Temp(in C)
Check Sum	with 0 to 4V / 4095 digits
	Step 1: Sum all packet contents but header and checksum Step 2: Divide by 256 Step 3: The remainder of this division should equal the Check Sum

Table 2. Conversion Factors.

	DMU-VG	Scaled Sensor Mode	Voltage Mode
0	Header (255)	Header (255)	Header (255)
1	Roll (MSB)	Angular Rate X (MSB)	Gyro Voltage X (MSB)
2	Roll (LSB)	Angular Rate X (LSB)	Gyro Voltage X (LSB)
3	Pitch (MSB)	Angular Rate Y (MSB)	Gyro Voltage Y (MSB)
4	Pitch (LSB)	Angular Rate Y (LSB)	Gyro Voltage Y (LSB)
5	Roll Rate (MSB)	Angular Rate Z (MSB)	Gyro Voltage Z (MSB)
6	Roll Rate (LSB)	Angular Rate Z (LSB)	Gyro Voltage Z (LSB)
7	Pitch Rate (MSB)	Acceleration X (MSB)	Accelerometer Voltage X (MSB)
8	Pitch Rate (LSB)	Acceleration X (LSB)	Accelerometer Voltage X (LSB)
9	Yaw Rate (MSB)	Acceleration Y (MSB)	Accelerometer Voltage Y (MSB)
10	Yaw Rate (LSB)	Acceleration Y (LSB)	Accelerometer Voltage Y (LSB)
11	Acceleration X (MSB)	Acceleration Z (MSB)	Accelerometer Voltage Z (MSB)
12	Acceleration X (LSB)	Acceleration Z (LSB)	Accelerometer Voltage Z (LSB)
13	Acceleration Y (MSB)	Temp Sensor Voltage (MSB)	Temp Sensor Voltage (MSB)
14	Acceleration Y (LSB)	Temp Sensor Voltage (LSB)	Temp Sensor Voltage (LSB)
15	Acceleration Z (MSB)	Time (MSB)	Time (MSB)
16	Acceleration Z (LSB)	Time (LSB)	Time (LSB)
17	Temp Sensor Voltage (MSB)	Checksum	Checksum
18	Temp Sensor Voltage (LSB)		
19	Time (MSB)		
20	Time (LSB)		
21	Checksum		

Data packet format. [v1.2]

Timing Diagrams

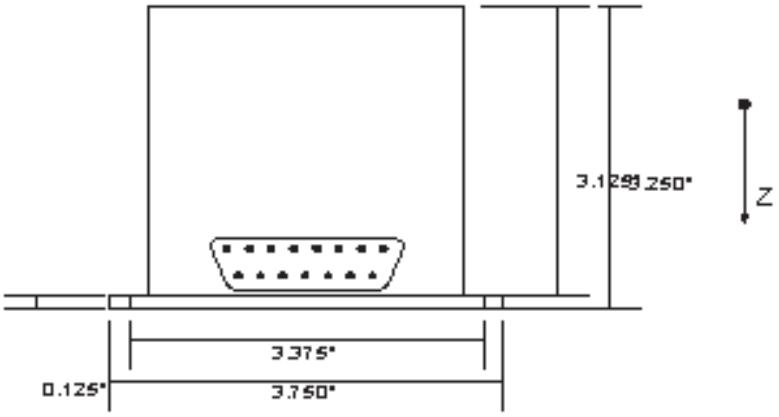
In some applications, using the DMU's digital output requires a precise understanding of the internal timing of the device. The processor internal to the DMU runs in a loop - collecting data from the sensors, processing the data, and reporting the data to the user. In continuous mode, the system processor activity is repeatable and accurate timing information can be derived based purely on the overall loop rate. The following table and graph describe these relationships.

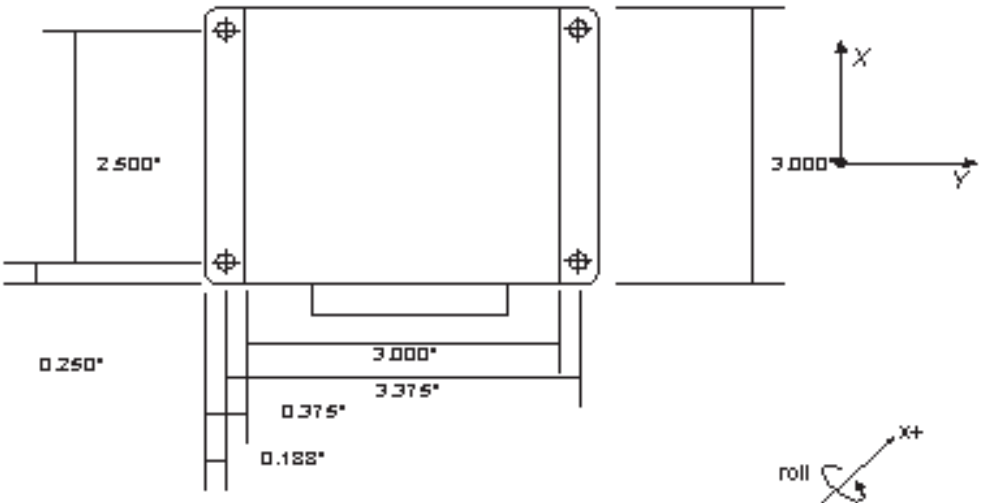
A time tag is attached to the packet in the voltage, scaled sensor, and VGX output mode. The time tag is simply the value of a free running counter at the time the A/D channels are sampled. The clock counts down from 65535 to 0, and a single tick corresponds to 0.79 micrseconds. The timer rolls over every 50 milliseconds.

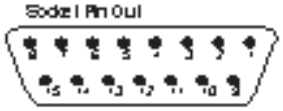
© 1998 Crossbow

Operating Mode	Conversion Time (T1)	Processing Time (T2)	Transfer Time (T3)	Total Time (Sum)	Data Rate Output
DMU-6X					
Voltage	0.8 ms	0.5 ms	4.7 ms		166 Hz
Scaled	0.8 ms	0.9 ms	4.7 ms	6.0 ms	156 Hz
DMU-VGX				6.4 ms	
Digital	0.8 ms	1.5 ms	5.2 ms		133 Hz
Analog	0.8 ms	1.5 ms	-	7.5 ms	400 Hz
				2.3 ms	

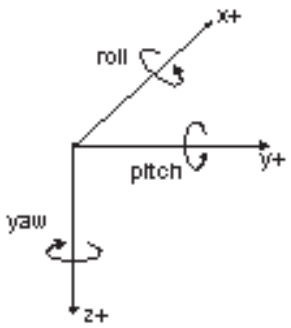
Notes:
1. Inter-channel conversion time is 0.133 milliseconds; there are a total of 6 channels which are converted on each iteration.
2. T3 assumes 38.4 Baud communications.
3. The clock signal transitions every time the 16 bit counter value rolls over. The clock signal can be used to correlate the timer stamp to an external time reference.







1 Transmit Data
2 Receive Data
3 Vcc
4 GND
5 X-axis Accelerometer Analog Voltage
6 Y-Axis Accelerometer Analog Voltage
7 Z-Axis Accelerometer Analog Voltage
8 Roll Rate Analog Voltage
9 Pitch Rate Analog Voltage
10 Yaw Rate Analog Voltage
11 Timing Pulse
12 Roll (VGX only)
13 Pitch (VGX only)
14 Unused
15 Unused



© 1998 Crossbow Technology, Inc. All rights reserved.

EXHIBIT 1057A

PCT WORLD INTELLECTUAL PROPERTY ORGANIZATION
International Bureau

INTERNATIONAL APPLICATION PUBLISHED UNDER THE PATENT COOPERATION TREATY (PCT)

(51) International Patent Classification 6 : G01C

A2

(11) International Publication Number: **WO 97/45699**

(43) International Publication Date: 4 December 1997 (04.12.97)

(21) International Application Number: PCT/US97/09150

(22) International Filing Date: 30 May 1997 (30.05.97)

(30) Priority Data:
08/658,924 31 May 1996 (31.05.96) US

(71) Applicant: THE REGENTS OF THE UNIVERSITY OF CALIFORNIA [US/US]; 21st floor, 300 Lakeside Drive, Oakland, CA 94612 (US).

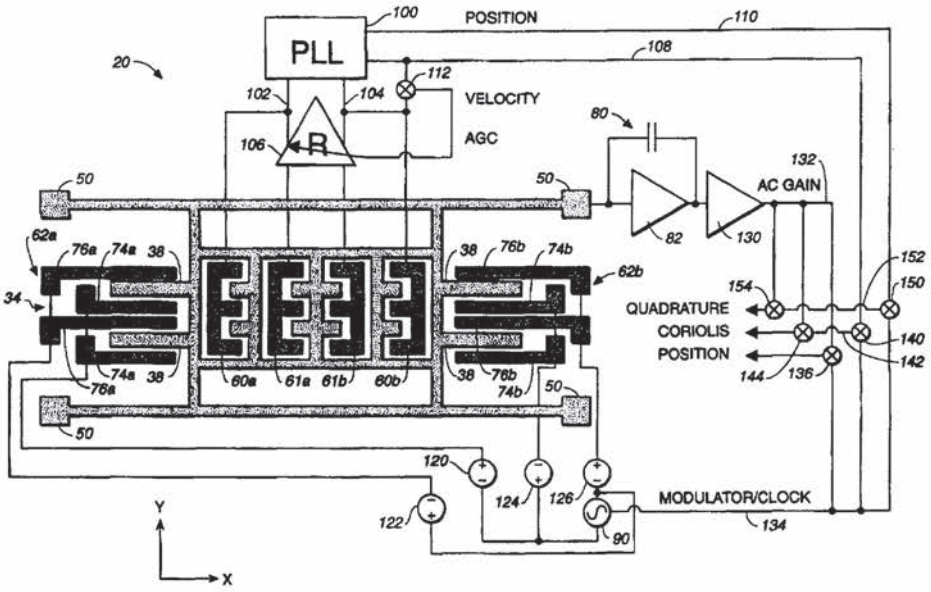
(72) Inventors: CLARK, William, A.; 35617 Pond Drive, Fremont, CA 94526 (US). JUNEAU, Thor; 1812 Delaware Street #201, Berkeley, CA 94709 (US). HOWE, Roger, T.; 3139 Sweetbriar Circle, Lafayette, CA 94549 (US).

(74) Agents: EGAN, William, J., III et al.; Fish & Richardson P.C., Suite 100, 2200 Sand Hill Road, Menlo Park, CA 94025 (US).

(81) Designated States: AL, AM, AT, AU, AZ, BA, BB, BG, BR, BY, CA, CH, CN, CU, CZ, DE, DK, EE, ES, FI, GB, GE, HU, IL, IS, JP, KE, KG, KP, KR, KZ, LC, LK, LR, LS, LT, LU, LV, MD, MG, MK, MN, MW, MX, NO, NZ, PL, PT, RO, RU, SD, SE, SG, SI, SK, TJ, TM, TR, TT, UA, UG, UZ, VN, YU, ARIPO patent (GH, KE, LS, MW, SD, SZ, UG), Eurasian patent (AM, AZ, BY, KG, KZ, MD, RU, TJ, TM), European patent (AT, BE, CH, DE, DK, ES, FI, FR, GB, GR, IE, IT, LU, MC, NL, PT, SE), OAPI patent (BF, BJ, CF, CG, CI, CM, GA, GN, ML, MR, NE, SN, TD, TG).

Published
Without international search report and to be republished upon receipt of that report.

(54) Title: MICROMACHINED VIBRATORY RATE GYROSCOPE



(57) Abstract

A microfabricated gyroscope to measure rotation about an axis parallel to the surface of the substrate. A voltage differential may be applied between pairs of electrode fingers to reduce the quadrature error. A microfabricated gyroscope includes a vibratory structure and interdigited electrodes having a high aspect ratio.

FOR THE PURPOSES OF INFORMATION ONLY

Codes used to identify States party to the PCT on the front pages of pamphlets publishing international applications under the PCT.

AL	Albania	**ES**	Spain	**LS**	Lesotho	**SI**	Slovenia
AM	Armenia	**FI**	Finland	**LT**	Lithuania	**SK**	Slovakia
AT	Austria	**FR**	France	**LU**	Luxembourg	**SN**	Senegal
AU	Australia	**GA**	Gabon	**LV**	Latvia	**SZ**	Swaziland
AZ	Azerbaijan	**GB**	United Kingdom	**MC**	Monaco	**TD**	Chad
BA	Bosnia and Herzegovina	**GE**	Georgia	**MD**	Republic of Moldova	**TG**	Togo
BB	Barbados	**GH**	Ghana	**MG**	Madagascar	**TJ**	Tajikistan
BE	Belgium	**GN**	Guinea	**MK**	The former Yugoslav Republic of Macedonia	**TM**	Turkmenistan
BF	Burkina Faso	**GR**	Greece			**TR**	Turkey
BG	Bulgaria	**HU**	Hungary	**ML**	Mali	**TT**	Trinidad and Tobago
BJ	Benin	**IE**	Ireland	**MN**	Mongolia	**UA**	Ukraine
BR	Brazil	**IL**	Israel	**MR**	Mauritania	**UG**	Uganda
BY	Belarus	**IS**	Iceland	**MW**	Malawi	**US**	United States of America
CA	Canada	**IT**	Italy	**MX**	Mexico	**UZ**	Uzbekistan
CF	Central African Republic	**JP**	Japan	**NE**	Niger	**VN**	Viet Nam
CG	Congo	**KE**	Kenya	**NL**	Netherlands	**YU**	Yugoslavia
CH	Switzerland	**KG**	Kyrgyzstan	**NO**	Norway	**ZW**	Zimbabwe
CI	Côte d'Ivoire	**KP**	Democratic People's Republic of Korea	**NZ**	New Zealand		
CM	Cameroon			**PL**	Poland		
CN	China	**KR**	Republic of Korea	**PT**	Portugal		
CU	Cuba	**KZ**	Kazakstan	**RO**	Romania		
CZ	Czech Republic	**LC**	Saint Lucia	**RU**	Russian Federation		
DE	Germany	**LI**	Liechtenstein	**SD**	Sudan		
DK	Denmark	**LK**	Sri Lanka	**SE**	Sweden		
EE	Estonia	**LR**	Liberia	**SG**	Singapore		

MICROMACHINED VIBRATORY RATE GYROSCOPE

Background of the Invention

The present invention relates generally to microfabricated sensors, and more particularly to microfabricated gyroscopic sensors.

Multi-axis sensors are highly desirable for inertial sensing of motion in three dimensions. Previously, such sensors were constructed of relatively large and expensive electromagnetic devices. More recently, micromechanical sensors have been fabricated using semiconductor processing techniques. Specifically, micromechanical accelerometers and gyroscopes have been formed from silicon wafers by using photolithographic techniques. Such microfabricated sensors hold the promise of large scale production and therefore low cost.

One objective in the construction of microfabricated sensors is to increase the sensitivity and improve the signal to noise ratio of the device. Another objective is to simplify the fabrication steps so as to reduce the cost and complexity and to increase the yield in the manufacturing process.

The integration of three gyroscopic sensors to measure the rotation rates about the three separate axes coupled with three accelerometric sensors to measure the acceleration along the three axes on a single chip would provide a monolithic, six degree-of-freedom inertial measurement system capable of measuring all possible translations and orientations of the chip.

It would be useful to provide a gyroscopic sensor to measure rotation about axes parallel to the surface of

a substrate on which the gyroscopic sensor was fabricated. It would also be useful to provide a gyroscopic sensor with reduced noise.

Summary of the Invention

In one aspect, the invention is directed to a gyroscopic sensor including a substrate, a mass connected to the substrate by a suspension system, a drive system to cause the mass to vibrate along a drive axis substantially parallel to a surface of the substrate, and a position sensor to measure a deflection of the mass along a sense axis substantially parallel to the surface of the substrate. Rotation of the mass about an axis of rotation substantially perpendicular to the surface of the substrate and vibration of the mass along the drive axis generates a Coriolis force to deflect the mass along the sense axis.

Implementations of the invention include the following. A processor may be coupled to an output of the position sensor to generate a signal varying with the rate of rotation of the mass about the axis of rotation. The gyroscopic sensor may include a first sense electrode projecting from the mass, a second sense electrode connected to the substrate and positioned on a first side of the first electrode, and a third sense electrode connected to the substrate and positioned on an opposing second side of the first electrode. The position sensor may sense a change in capacitance between the first electrode and the second and third electrodes. The first, second and third electrodes may be substantially coplanar and each electrode has a longitudinal axis substantially aligned with the drive axis. The drive system may include a first drive electrode projecting

from the mass, a second drive electrode connected to the substrate and positioned on a first side of the first electrode, and a third drive electrode connected to the substrate and positioned on an opposing second side of the first electrode. An alternating voltage may be applied between the between the first electrode and the second and third electrodes. A voltage source may apply a voltage between a plurality of correction electrodes connected to the substrate to cause the mass to vibrate, absent the Coriolis force, more precisely along the drive axis. A voltage source may apply a voltage between a first tuning electrode connected to the substrate and a second tuning electrode connected to the mass to adjust a resonant frequency of vibrations of the mass along the sense axis.

In another aspect, the invention is directed to a method of sensing rotation with a gyroscopic sensor including a mass connected to a substrate by a suspension system. The mass is rotated about an axis of rotation and the mass is caused to vibrate substantially along a drive axis. Rotation of the mass about the axis of rotation and vibration of the mass along the drive axis generates a Coriolis force to deflect the mass along a sense axis. A deflection of the mass along the sense axis is measured, and a voltage is applied between electrode fingers connected to the substrate to cause the mass to vibrate, absent a Coriolis force, more precisely along the first axis.

In another aspect, the present invention is directed to a microfabricated structure. The structure comprises a substrate, a mass connected to the substrate by a suspension system to vibrate in a plane parallel to a surface of the substrate, and three pluralities of

electrode fingers. The first plurality of electrode fingers projects from the mass along a first axis in the plane. The second and third plurality of electrode fingers, electrically isolated from each other, are coplanar with the first plurality of electrode fingers, are connected to the substrate and project substantially along the first axis. The first, second and third plurality of electrode fingers are interdigitated such that each of the first plurality of electrode fingers is adjacent to one of the second plurality of electrode fingers and one of the third plurality of electrode fingers.

Implementations include the following features. A voltage source may apply a voltage between the second and third plurality of electrode fingers. The structure may further comprise a fourth plurality of electrode fingers, coplanar with the first, second and third plurality of electrode fingers, projecting from the mass along the first axis, and a fifth plurality of electrode fingers connected to the substrate but electrically isolated from the second and third plurality of electrode fingers, the fourth and fifth plurality of electrode fingers being interdigitated. Each of the first plurality of electrode fingers may be longer than each of the fourth plurality of electrode fingers.

In another aspect, the invention is directed to a microfabricated structure. The structure comprises a substrate and a suspension system to permit a mass to vibrate in a plane parallel to a surface of the substrate. The suspension system includes first and second substantially parallel beams, each of the first and second beams anchored at both ends to the substrate, and third and fourth substantially parallel beams, one

end of each of the third and fourth beams connected to the first beam and another end connected to the second beam.

Implementations include the following features. The structure may include a plurality of fingers projecting along an axis substantially parallel to the first and second beams. The structure may comprise a fifth and a sixth beam one end of each of the fifth beam and sixth beams connected to the third beam and another end connected to the fourth beam, and a seventh beam, one end of the seventh beam connected to the fifth beam and another end connected to the sixth beam. The structure may further comprise a plurality of fingers projecting from the seventh beam along an axis substantially parallel to the first and second beams. Sections of the first and second beams located between the third and fourth beams may be substantially rigid to prevent rotation of the mass.

In another aspect, the invention is directed to a sensor. The sensor comprises a substrate, a mass connected to the substrate by a suspension system to vibrate in a plane parallel to a surface of the substrate, and three pluralities of electrode fingers. The first plurality of electrode fingers projects from the mass along a first axis in the plane. The second and third plurality of electrode fingers, are connected to the substrate and project substantially along the first axis. the first, second and third plurality of electrode fingers are interdigitated such that each of the first plurality of electrode fingers is adjacent to one of the second plurality of electrode fingers and one of the third plurality of electrode fingers. A voltage source applies a first DC voltage between the second and third

plurality of electrode fingers to cause the mass to vibrate, absent a Coriolis force, more precisely along the first axis.

Implementations may include the following features. A set of electrode fingers may be positioned opposing the three pluralities of electrode fingers, and a second voltage source for may apply a second DC voltage between a fifth and sixth plurality of electrode fingers to cause the mass to vibrate, absent a Coriolis force, more precisely along the first axis. The second DC voltage may be substantially equal in magnitude but opposite in sign to the first DC voltage. The first plurality of electrode fingers may be electrically coupled to the second plurality of electrode fingers. The sensor may include a voltage source for applying a third DC voltage between the first and third pluralities of electrode fingers and the second, third, fifth and sixth pluralities of electrode fingers to adjust the resonant frequency of vibrations of the mass along a second axis in the plane perpendicular to the first axis.

In another aspect, the invention is directed to a sensor. The sensor comprises a substrate, a mass connected to the substrate by a suspension system to vibrate in a plane parallel to a surface of the substrate, and three pluralities of electrode fingers. The first plurality of electrode fingers projects from the mass along a first axis in the plane. The second and third plurality of electrode fingers, are connected to the substrate and project substantially along the first axis. the first, second and third plurality of electrode fingers are interdigitated such that each of the first plurality of electrode fingers is adjacent to one of the second plurality of electrode fingers and one of the

third plurality of electrode fingers. A voltage source applies a DC voltage between the first plurality of electrode fingers and the second and third plurality of electrode fingers to adjust the resonant frequency of vibrations of the mass along a second axis in the plane perpendicular to the first axis.

In another aspect, the invention is directed to a gyroscope for sensing rotation about a Z-axis. The gyroscope comprises a substrate, a mass connected to the substrate by a suspension system to vibrate in a plane parallel to a surface of the substrate, a drive system to cause the mass to vibrate substantially along a first axis in the plane, and three pluralities of electrode fingers. The first plurality of electrode fingers projects from the mass along a first axis in the plane. The second and third plurality of electrode fingers, are connected to the substrate and project substantially along the first axis. The first, second and third plurality of electrode fingers are interdigitated such that each of the first plurality of electrode fingers is adjacent to one of the second plurality of electrode fingers and one of the third plurality of electrode fingers. A position sensor is coupled to the first plurality of electrode fingers for measuring the deflection of the mass along a second axis in the plane perpendicular to the first axis. Rotation of the mass about a Z-axis perpendicular to the surface and vibration of the mass along the first axis generates a coriolis force to deflect the mass along the second axis. A signal processor is coupled to an output of the position sensor to generate a signal varying with the rate of rotation of the mass about the Z-axis.

Implementations include the following features. A voltage source may apply an AC voltage having a first frequency between the second and third plurality of electrode fingers. A voltage may be applied between the second and third pluralities of electrode fingers to form a capacitive bridge with the first plurality of electrodes, and the position sensor may be coupled to the first plurality of electrodes to detect changes in capacitance when the mass is deflected along the second axis. The sensor may includes an integrator to integrate a signal from the first plurality of electrode fingers. The drive system may generate a signal to cause the mass to oscillate along the first axis at a second frequency. The drive system may include a phase-locked loop to prevent phase-shifting of the signal. The sensor may include a first mixer to mix the signal from the drive system with a signal from the voltage source. The sensor may include a second mixer to mix a signal from the first mixer with an output signal from the position sensor to produce a position quadrature signal or coriolis signal. The sensor may include a mixer to mix an output signal from the position sensor with a signal from the voltage source to produce a position signal.

In another aspect, the invention is directed to a microfabricated gyroscopic sensor for measuring rotation about an input axis. The gyroscopic sensor includes a substrate, a mass, and a suspension system connecting the mass to the substrate. A drive system causes the mass to oscillate substantially about a drive axis, and a position sensor measures a rotation of the mass about a sense axis. Rotation of the mass about the input axis and oscillation of the mass about the drive axis generates a Coriolis force to oscillate the mass about

the sense axis. A voltage source to apply a voltage between a plurality of electrodes associated with the substrate to cause the mass to oscillate, in the absence of the Coriolis force, more precisely about the drive axis.

Implementations of the invention include the following. A processor may be coupled to an output of the position sensor to generate a signal varying with the rate of rotation of the mass about the axis of rotation. A second voltage source may apply a second voltage between electrodes connected to the mass and the electrodes connected to the substrate to adjust a resonant frequency of oscillations of the mass about the sense axis. The drive axis may be substantially perpendicular to the surface of the substrate and the axis of rotation and sense axis are substantially parallel to a surface of the substrate. The mass may be substantially ring-shaped. First and second pluralities of electrode fingers may project from the mass, and third and fourth pluralities of electrode fingers projecting from the substrate and be interdigitated with the first and second pluralities of electrode fingers. The fourth plurality of electrode fingers may be positioned opposing the first plurality of electrode fingers. Fifth, sixth, seventh and eighth pluralities of electrode fingers may be similarly disposed, and the pluralities of electrode fingers are substantially co-planar. The voltage source may apply a first DC voltage between the third plurality and the fourth plurality of electrode fingers and second DC voltage, which is substantially equal in magnitude and opposite in sign, between the seventh plurality and the eighth plurality of electrode fingers.

In another aspect, the invention is directed to a method of sensing rotation with a gyroscopic sensor including a mass connected to a substrate by a suspension system. The method includes rotating the mass about an input axis and causing the mass to oscillate substantially about a drive axis. The rotation of the mass about the input axis and the oscillation of the mass about the drive axis generates a Coriolis force to oscillate the mass about a sense axis. An oscillation of the mass about the sense axis is measured, a voltage is applied between electrodes associated with the substrate to cause the mass to oscillate, in the absence of a Coriolis force, more precisely about the drive axis.

In another aspect, the invention is directed to a microfabricated gyroscopic sensor. The gyroscopic sensor includes a substrate having a first plurality of electrode teeth, a vibratory structure including a second plurality of electrode teeth and a suspension system connecting the second plurality of electrode teeth to the substrate, the second plurality of electrode teeth interdigited with the first plurality of electrode teeth, a drive system to cause the vibratory structure to oscillate relative to the substrate, and a position sensor to measure a deflection of the mass caused by a Coriolis force. The first and second pluralities of electrode teeth have thicknesses substantially greater than their widths.

Implementations of the invention include the following. The suspension system may include a plurality of flexures having an aspect ratio of at least about 10:1. The first and second pluralities of electrode teeth may have an aspect ratio of at least 5:1 and may be separated by gaps having an aspect ratio of at least

10:1.

In another aspect, the invention is directed to a method of fabricating a gyroscopic sensor. An insulative layer is formed on a first substrate, a recess is formed in a first surface of a second substrate, and the first surface of the second substrate is bonded to the first substrate so that the recess defines an enclosed cavity between the first and second substrates. Circuitry for the gyroscopic sensor is formed on a second surface of the second substrate, and a plurality of trenches are etched in the second substrate from the second surface to the cavity, the plurality of trenches defining a vibratory structure connected to the first substrate.

Implementations of the invention include the following. The vibratory structure may have a thickness of at least 25 microns and the recess may have a depth of about 1 micron. The etching step may comprise a deep reactive ion etch.

Advantages of the invention include the following. The gyroscopic sensor measures rotation about an axis parallel to the surface of the substrate. The gyroscopic sensor has reduced quadrature error. The gyroscopic sensor may include a vibratory structure and interdigited electrodes with a high aspect ratio. The gyroscopic sensor has a significantly reduced noise level.

Other advantages and features of the invention will be apparent from the description which follows, including the drawings and claims.

Brief Description of the Drawings

FIG. 1 is an schematic illustration of a spring-mass system which is equivalent to an electrostatic gyroscope.

FIG. 2 is a schematic perspective view of a microfabricated gyroscopic sensor according to the present invention.

FIG. 3 is a schematic top view of the movable elements of the gyroscopic sensor of FIG. 2.

FIG. 4 is a schematic top view of the fixed elements of the gyroscopic sensor of FIG. 2.

FIG. 5 is a schematic top view of the drive system of the gyroscopic sensor of FIG. 2.

FIG. 6 is a schematic top view of the sensing system of the gyroscopic sensor of FIG. 2.

FIGS. 7A-7C are schematic illustrations of the motion of the proof mass under the influence of the Coriolis acceleration and quadrature error.

FIG. 8A is a schematic circuit diagram of an integrator used to measure the position of the proof mass in the gyroscopic sensor of FIG. 2.

FIG. 8B is a schematic circuit diagram in which the integrator of FIG. 8A is replaced by a voltage buffer.

FIG. 8C is a schematic circuit diagram in which the integrator of FIG. 8A uses a subthreshold metal oxide semiconductor field effect transistor.

FIG. 9 is a schematic illustration of the signal processing circuitry of a gyroscopic sensor according to the present invention.

FIG. 10 is a photograph of a fabricated gyroscopic sensor.

FIG. 11 is a graph illustrating the response of the gyroscopic sensor to rotation about the Z-axis.

FIG. 12 is a graph illustrating the response of the Y-axis resonant frequency to an applied bias voltage.

FIG. 13 is a graph illustrating the response of the quadrature error to an applied voltage differential.

FIG. 14 is a schematic top view of a gyroscopic sensor in which the sensing, driving and quadrature correcting functions are performed by different electrode structures.

FIG. 15 is a schematic of the circuitry of the gyroscopic sensor of FIG. 14.

FIG. 16 is a schematic illustration of a spring-mass system which is equivalent to a dual-axis electrostatic gyroscope.

FIG. 17A is a schematic top view of a dual-axis gyroscopic sensor according to the present invention.

FIG. 17B is a photograph of a fabricated dual-axis gyroscopic sensor.

FIG. 18 is a schematic illustration of the electronic circuitry of the dual-axis gyroscopic sensor of FIG. 17A.

FIG. 19 is a cross-sectional view along line 19-19 of FIG. 17A schematically illustrating the field lines generated by the quadrature correction electrodes.

FIG. 20 is a schematic top view of a dual-axis gyroscopic sensor in which the quadrature correction system includes electrode plates.

FIG. 21 is a schematic illustration of the circuitry of a gyroscopic sensor in which the sensing, driving and quadrature functions are combined in a single electrode structure.

FIG. 22 is a schematic perspective view of a gyroscopic sensor fabricated with a high-aspect-ratio vibratory structure.

FIG. 23 is a schematic circuit diagram of the signal processing circuitry of the gyroscopic sensor of FIG. 22.

FIGS. 24A-24G are schematic cross-sectional views illustrating steps in the fabrication of the gyroscopic sensor of FIG. 22.

Description of the Preferred Embodiments

Referring to FIG. 1, a Z-axis vibratory rate gyroscope functions by generating and sensing Coriolis acceleration. The functional operation of the Z-axis vibratory rate gyroscope of the present invention is illustrated by an equivalent spring-mass system. In a vibratory rate gyroscope 10, a proof mass 12 is supported by a flexible suspension 14 from a rigid frame 16. Proof mass 12 is oscillated along the X-axis (the drive mode) by a drive force F_D as the frame rotates about the Z-axis. The combination of rotation and oscillation generates a Coriolis force F_c along the Y-axis on the oscillating proof mass. The Coriolis acceleration is detected as a deflection of the proof mass along the Y-axis (the sense mode).

Referring to FIG. 2, a micromachined gyroscopic sensor 20 designed according to the present invention includes microelectromechanical sense element or proof mass 22 connected to a rigid frame or substrate 24. The gyroscopic sensor 20 measures the Z-axis vibratory rate, i.e., the rotation of the substrate about the axis normal to the micromachined surface 26 of substrate 24. The micromachined gyroscopic sensor 20 includes three major

elements: a suspension system 30, a drive system 32 used to sustain oscillation of proof mass 22 along the X-axis, and a sensing system 34 used both to detect deflections of proof mass 22 along the Y-axis and to apply electrostatic forces to cancel any quadrature error, as will be described in detail below.

Referring to FIG. 3, suspension system 30 may be formed integrally with proof mass 22. Suspension system 30 supports the proof mass so that it may vibrate in a plane parallel to surface 26. Suspension system 30 holds proof mass 22, for example, about two microns above the surface of the substrate. The total mass of proof mass 22 may be about 0.1 to 0.3 micrograms. Suspension system 30 is generally H-shaped, with two parallel beams 40 and 42 positioned generally along the X-axis. Each beam may be about 500 to 1000 microns in length, specifically about 800 microns in length. The end of each beam is connected to an anchor 44 which connects the suspension system to the substrate (see FIG. 2). The end of each beam 40, as shown in FIG. 2, may include a folded or J-shaped flexure 45 (see FIG. 3). Alternately, beams 40 and 42 may be linear.

Two beams or crossbars 46 and 48 connect beam 40 to beam 42. Crossbars 46 and 48 may be about eight-hundred microns long, and are positioned to trisect beams 40 and 42. Two cross-beams 50 and 52 connect crossbars 46 and 48. A third beam or crossbar 54 may connect the center of cross-beam 50 to the center of cross-beam 52. The flexible elements of suspension system 30 are constructed of polysilicon and, for example, have a width and a thickness on the order of two microns. The anchors may be about eight microns square.

The suspension system 30 is designed to be flexible along the X-axis and Y-axis, and as rigid as possible to other modes of vibration. In particular, the suspension system must be substantially rigid to rotation about the Z-axis, as small rotations may degrade the performance of the gyroscopic sensor. Large deflections may also result in the movable electrode fingers crashing into the stationary electrode fingers. The suspension system provides the necessary translational compliance while maintaining rotational rigidity by thickening the portions of beams 40 and 42 located between crossbars 46 and 48 to form trusses 41 and 43. Trusses 41 and 43 may have a width three to four times the width of the remainder of the beams, i.e., about six to eight microns. The portions of crossbars 46, 48 and 54 from which fingers project may have a width of approximately four microns.

The proof mass 22 also includes a plurality of finger electrodes (or simply fingers) which are used to drive and sense oscillations of proof mass along the X-axis and Y axis. A plurality of long fingers 38 project outwardly along the X-axis from crossbars 46 and 48, and a plurality of short fingers or stubs 39 project inwardly along the X-axis from crossbars 46, 48 and 54. The crossbars 46 and 48 form the spines, and long fingers 38 form the prongs of two movable sensing electrodes 56. Similarly, crossbars 46, 48 and 54 form the spines, and short fingers 39 form the prongs of two movable driving electrodes 58 and two movable feedback electrodes 59. The short fingers 39 may be about ten to twenty-five microns in length, specifically fifteen microns in length, whereas the long fingers 38 may be about one-

hundred to two-hundred microns in length, specifically one-hundred and fifty microns in length.

Referring to FIG. 4, one or more stationary driving electrodes, one or more stationary feedback electrodes, and one or more stationary sensing electrodes may be rigidly connected to substrate 24. For example, two stationary driving electrodes 60a, 60b may be arranged relative to each other in an opposing configuration. Similarly, two stationary feedback electrodes 61a, 61b may face each other in an opposing configuration. Each stationary driving electrode 60a, 60b and each stationary feedback electrode 61a, 61b includes a plurality of short fingers 66. Stationary driving and feedback electrodes 60a, 60b and 61a, 61b may have a few to dozens of fingers. Short fingers 66 may have a length of approximately 15 microns and a width of approximately three to six microns. The width, for example, may be four microns.

Two stationary sensing electrodes 62a, 62b may face each other in an opposing configuration. Stationary sensing electrodes 62a, 62b include a plurality of long fingers 70. Each long finger 70 protrudes from a base 72. The fingers of stationary sensing electrode 62a are arranged in pairs, each pair including a right finger 74a and a left finger 76a. Similarly, the fingers of stationary electrode 62b are arranged in pairs, each pair including a right finger 74b and a left finger 76b. Each long finger 70 may be approximately one hundred and fifty microns in length, and have a width of approximately four microns.

Referring to FIG. 5, drive system 32 includes movable and stationary driving electrodes 58 and 60a, 60b, and movable and stationary feedback electrodes 59

and 61a, 61b. One set of short fingers 39 is interdigitated with short fingers 66 of stationary driving electrodes 60a, 60b. Another set of short fingers 39 is interdigitated with short fingers 66 of stationary feedback electrodes 61a, 61b. Short fingers 39 of movable electrodes 58 and 59, and short fingers 66 of stationary electrodes 60a, 60b and 61a, 61b may be formed from the same layer of polysilicon prior to the removal of the sacrificial layer so that the fingers may be co-planar.

The driving electrodes of drive system 32 act as electrical-mechanical transducers. By the application of an alternating voltage between stationary driving electrodes 60a, 60b and movable driving electrodes 58, proof mass 22 may be forced to oscillate or reciprocate along the X-axis. The motion along the X-axis induces bending in crossbars 46 and 48 so that proof mass 22 may move toward and away from stationary driving electrodes 60a, 60b. A more detailed explanation of the manner of operating drive system 32 in order to sustain oscillations in proof mass 22 may be found in U.S. Pat. No. 5,025,346, issued June 18, 1991 to Tang et al., entitled Laterally Driven Resonant Microstructures, and assigned to the assignee of the present invention, the entire disclosure of which is incorporated herein by reference; and in U.S. Pat. No. 5,491,608, issued February 13, 1996 to Nguyen, entitled Q-Controlled Microresonators and Tunable Electronic Filters Using Such Resonators, and assigned to the assignee of the present invention, the entire disclosure of which is incorporated herein by reference.

Referring to FIG. 6, sensing system 34 includes stationary sensing electrodes 62a, 62b and movable

sensing electrodes 56. The long fingers 38 of movable sensing electrodes 56 and long fingers 70 of stationary sensing electrodes 62a, 62b are interdigitated, with each long finger 38 disposed between a right finger 74a, 74b and a left finger 76a, 76b of sensing electrodes 62a, 62b. The spacing, Y_o, between fingers 70 and fingers 38 may be approximately one micron. Fingers 38 and 70 may be formed from the same layer of polysilicon so that the fingers are co-planar. Thus all of the driving and sensing elements may be formed in the same fabrication step. In addition, the driving mode and the sensing mode operate in the X-Y plane parallel to the surface of substrate 24. As will be described in more detail below, sensing system 34 is used to sense the deflection of proof mass 22 along the Y-axis, to apply electrostatic forces to balance and eliminate the effect of quadrature error, and to tune the resonant frequency of Y-axis vibrations of the proof mass.

As discussed above, drive system 32 causes proof mass 22 to oscillate along the X-axis. The position of the proof mass along the X-axis, x(t), is given by the following equation:

$$x(t) = X_0 \sin\omega_x t \qquad (1)$$

where X_o is the amplitude of the oscillation and ω_x is the frequency of the driving voltage (and thus the oscillation frequency). The frequency of the driving voltage, ω_x, may be between 7 kHz and 100 kHz, and the driving voltage may be sufficient to cause the proof mass to undergo a maximum deflection, X_o, of about one micron. The magnitude of the Coriolis acceleration, $\ddot{y}_{Coriolis}$, is given by the following equation:

$$\ddot{y}_{Coriolis} = 2 \cdot \Omega_z(t) \times \dot{x}(t) \quad (2)$$

where $\Omega_z(t)$ is the rate of rotation of the proof mass about the Z-axis and $\dot{x}$ is the velocity of the proof mass along the X-axis. Equations 1 and 2 may be combined as follows:

$$\ddot{y}_{Coriolis} = 2 \cdot \Omega_z(t) \cdot X_0 \cdot \omega_x \cdot \cos\omega_x t \quad (3)$$

For a gyroscopic sensor with an oscillation amplitude X_0=1 μm, on oscillation frequency ω_x=20 kHz, and an input rotation rate Ω_z=1 deg/sec, the Coriolis acceleration has a magnitude of 0.45 milliG's.

The Coriolis acceleration is an amplitude-modulated signal in which the carrier frequency is the oscillation frequency and the rotation rate modulates the amplitude. The resulting Coriolis acceleration is a dual sideband signal centered on the oscillation frequency. Referring to FIG. 7A, since the Y-axis accelerations are proportional to velocity, the motion of proof mass 22 is elliptical. The maximum deflection of proof mass 22 along the Y-axis will be a few nanometers. The deflection detectable by gyroscopic sensor 20 may be on the order of a picometer.

In an ideal device, the moving electrodes are perfectly aligned with the stationary electrodes so that the only motion caused by drive system 32 is along the X-axis. However, one effect of manufacturing flaws is quadrature error. Referring to FIG. 7B, quadrature error occurs if proof mass 22 oscillates along an axis that is not exactly parallel to the X-axis. If this is the case, then there is some small fraction, ε, of the drive oscillation, X(t), which lies along the Y-axis. This

quadrature displacement along the Y-axis is given by the following equation:

$$y_{Quadrature} = -\varepsilon \cdot x(t) \tag{4}$$

If this displacement is differentiated twice, the acceleration, $\ddot{y}_{quadrature}$, due to off-axis oscillation can be determined. This acceleration, given in Equation 5 below, is referred to as quadrature error.

$$\ddot{Y}_{Quadrature} = \varepsilon \cdot X_0 \cdot \omega_x^2 \cdot \sin\omega_x t \tag{5}$$

Note the similarity between the quadrature error and the Coriolis acceleration: both are sinusoidal signals centered at the frequency of oscillation. However, the signals can be distinguished by their phase relative to the driven oscillation. Specifically, the Coriolis acceleration is ninety degrees out of phase relative to the drive oscillation, ω_x, whereas the quadrature error is in phase with the driven oscillation.

The quadrature error can be quite large. In fact, the quadrature error may easily exceed the Coriolis acceleration. The ratio of quadrature error and Coriolis acceleration is given by Equation 6:

$$\frac{\ddot{Y}_{Coriolis}}{\ddot{Y}_{Quadrature}} = \frac{2\Omega_z(t) \cdot X_0 \cdot \omega_x}{\varepsilon \cdot X_0 \cdot \omega_x^2} = \frac{2\Omega_z(t)}{\varepsilon \cdot \omega_x} \tag{6}$$

Using the previous example of an input rotation rate, Ω_z, of 1 deg/sec and an oscillation frequency, ω_x, of 20 kHz, for the quadrature error to be as small as the Coriolis acceleration, the oscillation direction must be accurate to a factor of 1 part in 3.6 million. Due to manufacturing flaws and other imbalances, the quadrature error may be considerably larger than this. Accordingly,

gyroscopic sensor 20 has a mechanism to reduce, or nullify the quadrature error.

Microfabricated gyroscopic sensor 20 may apply electrostatic forces to proof mass 22 through sensing system 34. By selection of the proper electrostatic force, the quadrature error may be nullified. As shown by Equation 5, the quadrature error is directly proportional to position of the proof mass along the X-axis. To cancel this error signal without effecting the Coriolis signal, a balancing force must be applied that is also directly proportional to the position of the proof mass along the X-axis. Gyroscopic sensor 20 applies such a balancing force, using the interdigitated Y-axis position sense fingers.

Referring to FIG. 7C, proof mass 22 is shown with two fingers 38a and 38b projecting from opposite sides of the proof mass. Finger 38a is surrounded by right and left fingers 74a and 76a, whereas finger 38b is surrounded by right and left fingers 74b and 76b. A small voltage differential, $2\Delta V$, is applied between the right finger 74a and left finger 76a. The opposite voltage potential $-2\Delta V$, may be applied between right finger 74b and left finger 76b. This voltage difference creates a balancing force, F_y, which counteracts the quadrature error. The balancing force acts on proof mass 22 so that, absent the Coriolis force, fingers 39 vibrate solely along the X-axis. As mentioned above, the balancing force needs to be exactly proportional to the position of the proof mass along the X-axis. An electrostatic force between two charged surfaces is proportional to the overlapping area of the surfaces. Because the overlapping area between fingers 38 and fingers 70 is directly proportional to the position of

proof mass 22 along the X-axis, as proof mass oscillates, the position sense capacitors change proportionately. Therefore, the electrostatic balancing force F_y will also be proportional to the position of proof mass 22. Sensing system 34 applies a DC bias voltage V_{DC} to fingers 74a, 74b, 76a and 76b and a voltage differential $Z\Delta V$ between fingers 74a, 74b and 76a, 76b given by Equation 7 below:

$$F_y = \frac{C_{overlap}}{y_0} x(t) \cdot ((V_{DC}+\Delta V)^2 - (V_{DC}-\Delta V)^2) = 2\frac{C_{overlap}}{y_0} V_{DC} \Delta V \cdot x \qquad (7)$$

where $C_{overlap}$ is the maximum change in capacitance between fingers 70 and fingers 38 as the structure oscillates and y_0 is the equilibrium distance between fingers 70 and fingers 38.

By properly selecting the voltage differential ΔV, the quadrature error may be significantly reduced, e.g., by a factor ten to one-hundred. The proper voltage difference may be calculated from Equations (7) and (5) and Newton's law F = ma, as follows:

$$\Delta V = M\frac{\varepsilon y_0 \omega_x^2}{V_{DC} C_{overlap}} \qquad (8)$$

where M is the mass of proof mass 22. Because the quadrature error is a result of manufacturing defects, the proper voltage differential depends upon the specific structure and may vary from device to device. A voltage differential in the range of 1 mV to 100 mV should be appropriate. The optimum voltage differential to cancel the quadrature error may be determined experimentally (see FIG. 13 which is discussed below).

In addition to canceling the quadrature error, sensing system 34 of gyroscopic sensor 20 may be used to match the Y-axis resonant frequency ω_y of proof mass 22 to the driving oscillating frequency ω_y. Because gyroscopic sensor 20 is a high Q second order system, the response of proof mass 22 to Coriolis acceleration can be enhanced. As shown by Equation 3, the Coriolis acceleration is a signal centered around the oscillation frequency ω_x. Therefore the relative values of the oscillation frequency ω_x and the Y-axis resonant frequency ω_y have a dramatic effect on the response of the sense mode and hence the sensor sensitivity. If the Y-axis resonant frequency is matched to the oscillation frequency, the device may experience a gain of Q in the system response. However, the bandwidth of the sensor is then limited to ω_y/Q. Given that system is run in a vacuum and Q is typically greater than 10,000, the system bandwidth for $\omega_x=\omega_y$ will be only a few Hertz.

For larger bandwidth and increased sensitivity, gyroscopic sensor 20 is operated with a slight mismatch between resonant frequency ω_y and oscillation frequency ω_x. The system response of Y-axis displacement due to Coriolis acceleration is given by:

$$\frac{y}{\Omega_z} = \frac{2X_0\omega_x \sin\omega_x t}{\omega_y^2 + \frac{j\omega_x\omega_y}{Q} - \omega_x^2} = \frac{X_0\omega_x}{\omega_x\Delta\omega}\sin\omega_x t \qquad (9)$$

Provided that there is a means to tune the Y-axis resonant frequency, it is desirable to operate the gyroscopic sensor with a 5-10% frequency mismatch, $\Delta\omega/\omega_x$, yielding a gain of 5-10 in sensitivity. For example, if ω_x is about 12 kHz, then ω_y may be set to about 12.5 kHz. Alternately, the frequency mismatch may be reduced to

about 1-2%. Reducing the mismatch further might increase the sensitivity but may be difficult to maintain for any length of time because the resonant frequency changes as the temperature of the gyroscopic sensor changes.

Tuning of the Y-axis resonant to improve sensitivity is accomplished using electrostatic "negative" springs, i.e., by applying a DC bias voltage, V_{DC}, between proof mass 22 and stationary sensing electrodes 62. When the DC voltage is established between the moving proof mass and the stationary sensing electrode, the resulting attractive force reduces the total spring constant and thus adjusts the resonant frequency.

Using a first-order model for the parallel-plate capacitors, the linearized spring force due to electrostatic forces is given by:

$$F_y = \left[\frac{1}{(y_0-y)^2} - \frac{1}{(y_0+y)^2}\right]\frac{y_0 C_s V_{DC}^2}{2} \qquad (10)$$

where y is the deflection of the proof mass along the Y-axis away from its equilibrium position.

The Y-axis resonant frequency, ω_y, is given by the following equation:

$$\omega_y = \sqrt{\frac{k_y+k_e}{M}} \qquad (11)$$

where k_y is the purely mechanical spring constant, k_e is the electrostatic spring constant and M is the mass of proof mass 22. The mechanical spring constant k_y is primarily a function of the stiffness of suspension system 30.

The electromagnetic spring constant, k_e, is given by the following equation:

$$k_e = -2\frac{C_s}{y_0^2}V_{DC}^2 \qquad (12)$$

in which C_s is the sense capacitance of the gyroscopic sensor and y_o is the distance between fingers 38 and 70 (see FIG. 7A). C_s depends upon the total number of fingers and the amount of overlapping area, and should be at least 30 femtoFarads (fF). By increasing the number of fingers, C_s may be increased to about one picoFarad (pF). As mentioned above, the spacing y_o between fingers is about one micron. It may be noted that k_e has a negative value, so that as V_{DC} is increased ω_y is decreased. The system starts with ω_y larger than ω_x, and the bias voltage V_{DC} is increased, thereby reducing ω_y, until the desired mismatch $\Delta\omega/\omega_y$ is achieved. The correct valve for V_{DC} may be determined experimentally (see FIG. 12 which is discussed below), but should be in the range of one to ten volts.

In addition to canceling the quadrature error and adjusting the Y-axis resonant frequency, sensing system 34 may be used to negate the effects of centrifugal or centripetal force. As the gyroscope sensor rotates about the Z-axis, a centrifugal force will push the proof mass outwardly (assuming the axis of rotation does not pass exactly through the center of mass of the proof mass). A voltage difference, V_c, may be applied between the opposing stationary sensing electrodes 62a and 62b. Because the centripetal force varies at a low frequency, compared to the frequencies of the Coriolis force, a high pass filter may be used to remove the effect of the centripetal force from the output.

Gyroscopic sensor 20 measures the position of proof mass 22 along the Y-axis by capacitive deflection sensing. The interdigitated fingers of sensing system 34 (shown in FIG. 2) are used to sense deflection of the proof mass along the Y-axis. The fingers are arranged in a capacitor bridge so that any deflection of the proof mass results in measurable changes in the relative size of the capacitors. In a first order model, the capacitance of a parallel-plate capacitor is inversely proportional to the distance between the plates.

Referring to FIGS. 6 and 8A, the space between finger 38 of movable sensing electrode 56 and right fingers 74a, 74b of sensing electrodes 62a, 62b forms a first capacitor C_1, and the space between finger 38 and left fingers 76a, 76b forms a second capacitor C_2. As movable sensing electrode 56 is deflected along the Y-axis, C_1 and C_2 change. For example, if sensing electrode 56 is deflected leftward, the distance between finger 38 and right fingers 74a, 74b increases, thereby decreasing C_1, while the distance between finger 38 and left fingers 76a, 76b decreases, thereby increasing C_2. The change in capacitance is detected by a position sensor 80, such as an integrator or voltage buffer, which includes an amplifier 82. Finger 38 is connected to the negative input of amplifier 82. The output of amplifier 82 is connected to the negative input of the amplifier via an integrating capacitor 84 to form an integrator. The negative input of amplifier 82 is connected to ground via a parasitic capacitor 83. The positive input of amplifier 82 may be connected directly to ground.

Because capacitance cannot be measured with a DC voltage, a voltage source 90 applies an AC voltage V_S between fingers 74a, 74b and 76a, 76b. The voltage V_S is

about 0.1 to 5.0 volts, preferably about one volt, and has a frequency much higher than the driving frequency ω_x. For example, the frequency of voltage source 90 may be about one megahertz.

The integrator shown in FIG. 8A offers the flexibility of trading bandwidth for sensitivity by varying the integrating capacitor size. The integrator also provides lower distortion. Some of the parasitic capacitors involved in microelectromechanical systems are nonlinear which will vary the gain of a buffer and thereby result in distortion, and the practice of bootstrapping parasitic capacitance is a form of positive feedback which exacerbates amplifier distortion. However, because the integrator uses a fixed, linear capacitor, distortion is kept to a minimum.

Another common amplifier configurations used for capacitive position sensing is shown in FIG. 8B, in which the output of amplifier 82 is connected to its negative input and sensing electrodes 56 are connected to the positive input of the amplifier to form a voltage buffer.

Unfortunately, the integrator presents a difficult biasing problem. Ideally, biasing can be performed by placing a very large resistor in parallel with the integrating capacitor. However, any practical implementation of a large resistor results in a considerable parasitic capacitance. A diode can also be used in parallel with the integrating capacitance; however, that adds a nonlinear capacitance to the integrating capacitance resulting in distortion. Referring to FIG. 8C, this biasing problem has been solved by using a subthreshold metal oxide semiconductor field effect transistor (MOSFET) 88. The MOSFET device is connected in parallel with integrating capacitor 84 so

that the source of MOSFET 88 is connected to the output of amplifier 82, the drain is connected to the negative input of amplifier 82, and the gate is connected to ground. The negative input of amplifier 82 may be connected to ground by a diode 86, and the positive input of amplifier 82 may be connected directly to ground. In the subthreshold regime, the MOSFET device exhibits extremely low transconductance and no source-to-drain capacitance. The use of subthreshold MOSFET device has resulted in a well behaved integrator operable down to 1 kHz with a 50 F integrating capacitor without additional noise or distortion attributable to the bias circuitry.

Referring to FIG. 9, gyroscopic sensor 20 includes a phase-locked loop (PLL) 100 and several synchronous demodulators or mixers to perform signal processing. Phase-locked loop 100 produces extremely accurate digital signals having a driving frequency ω_x between about 7 kHz and 100 kHz. The drive frequency, ω_x, may be generated by dividing down the signal from voltage source 90. The phase-locked loop ensures that the position signals are exactly in phase with the position of proof mass 22. Phase-locked loop 100 may also generate a velocity signal on line 108 which is exactly ninety degrees out of phase with a position signal on line 110. Position signals on lines 102 and 104, having opposite amplitudes, are supplied by phase-locked loop 100 to the positive and negative outputs, respectively, of a transresistance amplifier 106. Opposing stationary drive electrodes 60a and 60b are also connected to the positive and negative outputs of transresistance amplifier 106. Opposing feedback electrodes 61a and 61b are connected to the positive and negative inputs of transresistance amplifier 106. One of the outputs of transresistance amplifier 106

is mixed with the velocity signal by a mixer 112. The combined output of mixer 112 is applied to trans-resistance amplifier 106 to provide an automatic gain control (AGC) circuit to control the amplitude of the oscillations of proof mass 22 along the X-axis. The phase accuracy of the phase-locked loop is critical to the operation of gyroscopic sensor 20 because any phase error will result in cross-talk between the Coriolis and quadrature signals. Assuming that a phase error $\theta_n(t)$ is generated by phase noise in the phase-locked loop, the error in the rotation rate Ω may be derived as shown in Equations 13-15 below:

$$y(t) = [\frac{X_0\omega_x}{\omega_x\Delta\omega}\Omega\cos\omega t + Y_{Quadrature}\sin\omega t] \quad (13)$$

$$\Omega_{est} = \frac{\omega_x\Delta\omega}{X_0\omega_x}y(t)\cos(\omega_x t+\theta_n(t)) \quad (14)$$

$$\Omega_{est} = \Omega + \frac{\omega_x\Delta\omega}{X_0\omega_x}Y_{Qadrature}\theta_n(t) + Higher\ terms \quad (15)$$

Because phase-locked loop 100 is extremely accurate, phase noise is minimized and variable cross-talk is extremely small. In addition, quadrature error correction reduces cross talk and phase noise.

The nulling of the quadrature error, the tuning of the Y-axis resonant frequency, and the balancing of the centrifugal forces is accomplished by the application of the proper voltages to fingers 70 of opposing stationary sensing electrodes 62a and 62b. Specifically, gyroscopic sensor 20 includes four DC bias voltage sources 120, 122,

124 and 126. Voltage source 120 applies a total voltage $V_t=V_{DC}+\Delta V+V_C$ to right fingers 74a of sensing electrode 62a. Voltage source 122 applies a total voltage of $V_{DC}-\Delta V-V_C$ to left fingers 76a. Voltage source 124 applies a total voltage of $V_{DC}-\Delta V+V_C$ to right electrode fingers 74b of sensing electrode 62b. Voltage source 126 applies a total voltage of $V_{DC}+\Delta V-V_C$ to left fingers 76b. Thus, voltage sources 120, 122, 124 and 126 provide all of the necessary bias voltages in order to nullify the quadrature error, select the desired Y-axis resonant frequency, and cancel any centrifugal or other low-frequency forces. Of course, any other combination of voltage sources providing the same effective total voltage to the fingers of the sensing electrodes could be used. Also, the voltages could be applied by different sets of fingers of the stationary sensing electrode, for example, V_{DC} could be applied by one set of fingers and ΔV could be applied by another set of fingers.

In order to extract the position, Coriolis effect, and quadrature signals from capacitive position sensor 80, the signal from amplifier 82 is boosted by an oscillation amplifier 130 to produce an output signal on line 132. This output signal may be mixed with signals from a modulator or clock and the position and velocity signals from phase locked loop 100. Voltage source 90 may produce a high frequency, e.g., one megahertz clock signal on line 134. To generate the position signal, this clock signal is mixed with the output signal on line 132 by a mixer 136. In order to produce the Coriolis signal, the clock signal on line 134 is mixed with the velocity signal on line 108 by a mixer 140 to produce a combined signal on line 142. The combined signal on line 142 is then mixed with output signal on line 132 by a

mixer 144 to produce the Coriolis signal. Finally, to produce the quadrature signal, the clock signal on line 134 is mixed with the position signal on line 110 by a mixer 150 to produce a combined signal on line 152. The combined signal on line 152 is then mixed with output signal on line 132 by a mixer 154 to produce the quadrature signal. The position, Coriolis and quadrature signals may be passed through low pass filters to filter out high frequency components.

Referring to FIG. 10, a gyroscopic sensor 20 was fabricated on a silicon substrate 24 using a combination of metal oxide semiconductor and microelectromechanical fabrication techniques. The transresistance amplifier and integrator were fabricated on the same die, and the remaining electronics was implemented off of the chip. The mechanical sensing element is about one millimeter across.

There are a number of possible noise sources in gyroscopic sensor 20. Principal among these are: Brownian noise, op-amp noise in the integrator, and phase locked loop phase noise. The Brownian noise, $\Omega_n B$, represents the fundamental limit on angular rate resolution and is given by:

$$\Omega_{nB} = \sqrt{\frac{kT\omega_y BW}{MQ\omega_x^2 X_0^2}} \qquad (16)$$

where k is Boltzman's constant, T is the temperature, M is the mass of the proof mass, BW is the bandwidth of the gyroscopic sensor, and Q is the quality factor. As an example, consider a gyroscopic sensor with mass, M=0.2μg, an oscillation amplitude X_0=1 μm, a quality factor, Q= 10,000, a bandwidth BW = 100 Hz, a drive frequency ω_x= 20

kHz and a resonant frequency ω_y= 20 kHz. For this example, we find a Brownian noise floor Ω_{nB}=0.06 deg/sec. Because the gyroscopic sensor is run in vacuum and has a high Q, Brownian noise is not the dominant noise source.

As shown by Equation 15, phase noise in the phase locked loop, represented by $\theta_n(t)$, can cause variable cross talk between quadrature and Coriolis signals. In gyroscopic sensor 20, this effect is kept to a minimum due to the low phase noise in the phase locked loop and nulled quadrature error.

The integrator op-amp noise is the dominant noise source in gyroscopic sensor 20. The input-referred noise, Ω_E, of the op-amp noise is a function of the total capacitance, C_T, attached to the summing node of the integrator, and is given by:

$$\Omega_{nE} = \frac{C_T Y_0 \nu_n}{C_S X_0 V_S} \Delta\omega \sqrt{2BW} = \frac{Y_0 \Delta\omega}{X_0 V_S} \sqrt{\frac{32kTBW}{3\pi C_S f_T}} \qquad (17)$$

where f_T is the maximum operable frequency of the transistors in gyroscopic sensor 20. The electronic noise is at best Ω_{nE}=0.08 deg/sec for a modest CMOS process with f_T=250 MHZ, a frequency mismatch $\Delta\omega$=1 kHz, a sense voltage V_s=1 volt, a sense capacitance C_s=100fF, and the oscillation amplitude and finger spacing X_0=y_o=1 μm.

An initial characterization of the gyroscopic sensor response is shown in FIG. 11. FIG. 11 is a graph of the logarithm of the output voltage of the Coriolis signal, on the Y-axis, as a function of frequency, on the X-axis. The graph was produced by measuring the output Coriolis signal in response to a 1Hz, 5 deg/sec sine wave rotation. The gyroscopic sensor was operated with an oscillation frequency, ω_x, of 12 kHz and a Y-axis resonant frequency, ω_y, of about 12.5 kHz. The noise floor for

this version of Z-axis vibratory rate gyroscopic sensor is 1 deg/sec/Hz$^{1/2}$.

Referring to FIG. 12, there is a measured mechanical resonant frequencies of proof mass 22 as a function of the DC bias voltage applied to the position sense fingers. FIG. 12 shows a graph of the resonant frequencies of proof mass 22 (on the Y-axis of the graph) as a function of the RMS voltage (on the X-axis of the graph) applied between fingers 38 and fingers 70. The RMS voltage is a combination of the DC bias voltage and the AC voltage generated by voltage source 90. The resulting electrostatic springs reduce the resonant frequency of the sense mode (ω_y), raise the resonant frequencies of the out-of-plane modes, and leaves the driven mode (ω_x) unaffected. As expected, the Y-axis resonant frequency drops as the bias voltage is increased and the oscillation frequency of proof mass 22 remains constant at 12kHz. The resonant frequencies of the vertical and tipping modes increase with DC bias due to electrostatic levitation effects.

As discussed above, gyroscopic sensor 20 includes a means to null quadrature error. FIG. 13 shows a graph of the measured voltage, V_{out} on the Y-axis, as a function of the voltage differential, ΔV, on the X-axis, which is applied between right fingers 74a, 74b and left fingers 76a, 76b. Both the quadrature and rotation rate signals were plotted for a zero rotation rate as ΔV was adjusted. Measurements of the quadrature error and rotation rate signals demonstrate that the quadrature error signal can be controlled independently of the Coriolis signal.

Another embodiment of the gyroscopic sensor, in which the sensing and quadrature correction voltages are applied by different electrode fingers, is shown by FIG.

14. Referring to FIG. 14, a micromachined gyroscopic sensor 200 includes a proof mass 202 connected to a substrate 204 by a suspension system 206. The gyroscopic sensor 200 includes three major electronic elements: a drive system 210 used to sustain oscillation of proof mass 202 along the X-axis, a sensing systems 212 used to detect deflections of proof mass 202 along the Y-axis, and a quadrature correction system 214 used to cancel any quadrature error.

The proof mass 202 includes a rectangular outer stage 220 and a rectangular inner stage 222. Each corner of outer stage 220 is connected by a folded or J-shaped first flexure 224 to an anchor 226 which secures proof mass 202 and suspension system 206 to substrate 204. Similarly, each corner of inner stage 222 is connected to outer stage 220 by a second flexure 228. The first flexure 224 is designed to permit outer stage 220 to vibrate primarily along a Y-axis with respect to substrate 204, whereas second flexure 228 is designed to permit inner stage 222 to vibrate substantially along the X-axis with respect to outer stage 220. Several beams or crossbars 230 may connect opposing sides of inner stage 222.

The physical characteristics of gyroscopic sensor 200 are similar to those of gyroscopic sensor 20. The sensor may be about 0.5 to 2.0 millimeters on a side; the proof mass may have a total mass of about 0.1 to 0.5 micrograms; the flexible elements of the suspension system may be constructed of polysilicon and may have a width and a thickness on the order of two microns. The entire assembly may be fabricated using traditional integrated circuit fabrication techniques.

Referring to FIG. 14, the drive system 210 includes two driving electrodes 232a and 232b, and two feedback electrodes 234a and 234b, all connected to substrate 204. A plurality of electrode fingers 236 project along the X-axis from each feedback electrode and each drive electrode. A plurality of electrode fingers 238 project from inner stage 222 of proof mass 202 along the X-axis, and are interdigitated with electrode fingers 236 of the sense and drive electrodes.

As shown in FIG. 15, feedback electrodes 234a and 234b are connected to the positive and negative inputs, respectively, of a transresistance amplifier 240. The driving electrodes 232a and 232b are connected to the positive and negative outputs of transresistance amplifier 240, respectively, and to a phase-locked loop 242, as previously described with respect to FIG. 9.

The sensing system 212 includes a plurality of pairs of sense electrodes fingers aligned with the X-axis. Each pair of sense electrode fingers includes a right finger 244 and a left finger 246. A plurality of electrode fingers 248 are connected to outer stage 220 and are interdigited so that each electrode finger 248 is disposed between one right finger 244 and one left finger 246. A sense voltage source 250 (see FIG. 15) applies an AC voltage between the right fingers 244 and the left fingers 246.

Quadrature correction system 214 includes several sets of correction electrodes positioned near the center-line of the sensor and connected to the substrate. Each set of correction electrodes includes an upper left electrode 260, an upper right electrode 262, a lower left electrode 264, and a lower right electrode 266. Upper right electrode 262 and lower left electrode 264 may be a

single electrode, as shown, or may be separate electrodes. A plurality of electrode fingers 268 extend from crossbars 230 and are interdigited with the connection electrodes. Specifically, each electrode finger 268 extends along the X-axis from crossbar 230 and is disposed between upper left electrode 260 and upper right electrode 262. Similarly, each electrode finger 268 extends along the X-axis from crossbar 230 and is disposed between lower left electrode 264 and lower right electrode 266. Upper left electrode 260 is electrically connected to lower right electrodes 266, and upper right electrode 262 is electrically connected to lower left electrode 264.

A voltage source 270 (FIG. 15) applies a DC bias voltage between the correction electrodes 260, 266 and 262, 264. The voltage differential between the left and right electrodes creates a balancing force to counteract the quadrature error as discussed with respect to FIG. 7C. The remainder of the circuitry, including an integrator 280 and mixers 282-286 may be assembled and function in a manner similar to the circuitry discussed above with reference to FIG. 9.

Referring to FIG. 16, quadrature correction may be used to compensate for manufacturing flaws that occur in the fabrication of other sorts of gyroscopic sensors, such as X-axis and Y-axis gyroscopic sensors. A dual-axis vibratory gyroscope functions by generating and sensing Coriolis accelerations. The functional operation of the dual-axis vibratory gyroscope is illustrated by an equivalent spring-mass system. In a dual-axis gyroscopic sensor 290, a proof mass 292 is supported by a flexible suspension 294 from a frame 296. The proof mass is generally disc-shaped, and lies in a plane generally

parallel to the surface of the substrate. The proof mass is oscillated about the Z-axis (the axis perpendicular to the surface of the substrate) by a drive torque F_d with a frequency ω_z. If the frame rotates about a first axis parallel to the surface of the substrate, e.g., the Y-axis, at a rotation rate Ω_Y, then the combination of this rotation and oscillation generates an oscillating Coriolis torque F_c about a second axis parallel to the surface of the substrate and perpendicular to the first axis, i.e., the X-axis. This Coriolis force torque will tend to oscillate the proof mass about the X-axis at a frequency ω_X. Thus, rotation of the proof mass about the Y-axis causes the proof mass to undergo a "see-saw" motion about the X-axis. Similarly, a rotation about the X-axis will induce a Coriolis oscillation about the Y-axis.

The Coriolis acceleration about the X-axis generated by rotation of the proof mass about the Y-axis is given by the following equation:

$$I_{xx}\ddot{\theta}_x + C_x\dot{\theta}_x + K_x\theta_x = -I_{zz}\Omega_y \times \theta_{z0}\omega_z \cos(\omega_z t) \qquad (18)$$

where θ_x is the sense-axis tilt angle, I_{xx} is the X-axis moment of inertia, C_x is the damping co-efficient, K_x is the spring constant, ω_z is the frequency of oscillation about the Z-axis, I_{zz} is the Z-axis movement of inertia, and Ω_y is the rotation rate of the proof mass about the Y-axis. The angular oscillation of the rotor caused by the Coriolis acceleration can be thought of as an amplitude modulated signal with a carrier frequency ω_z. The amplitude of the modulated signal is directly proportional to the Y-axis rotation rate Ω_y. The equation for Coriolis acceleration about the Y-axis is essentially

identical except that the x and y subscripts are reversed and the right-hand side of the equation is positive.

Referring to FIG. 17A, a dual-axis gyroscopic sensor 300 includes a generally ring-shaped proof mass 302 connected to a rigid frame or substrate 304 by a suspension system 306. Dual-axis gyroscopic sensor 300 measures the X-axis and Y-axis rotation rate; i.e., the rotation of the substrate about the axes parallel to the surface of substrate 304. Dual-axis gyroscopic sensor 300 includes three major electronic elements: a drive system 310 used to sustain oscillation of proof mass 302 about the Z-axis, a sensing system 312 used to detect deflections of proof mass 302 about the X-axis and Y-axis, and a quadrature correction system 314 used to cancel any quadrature error. The dual-axis gyroscopic sensor 300 may be fabricated using standard integrated circuit techniques.

The proof mass 302 includes a generally ring-shaped rotor 316. Rotor 316 may be a two micron thick polysilicon ring with an outer radius of about 250 microns and an inner radius of about 200 microns. The proof mass 302 is substantially symmetric about the X- and Y-axis.

The suspension system 306 may include four beams 320 which connect an inner edge 322 of the proof mass to an anchor 324 which secures rotor 316 to substrate 304. The beams 320 may also be constructed of polysilicon and may have a width and thickness on the order of two microns.

Alternately, the suspension system may include a serpentine suspension with folded beams. In yet another version, the proof mass may be suspended by four beams connected to an outer edge of the rotor. A serpentine

suspension system provides a lower natural frequency and can accommodate warping of the rotor.

Suspension systems 306 is designed to provide a torsional suspension for rotor 316 to allow rotation about the three perpendicular axes. However, suspension system 306 is designed to be rigid to translational accelerations along the X-axis and the Y-axis. Although rotor 316 may undergo translational acceleration along the Z-axis, the differential sensing scheme discussed below substantially cancels sensitivity to such accelerations.

For maximum mechanical sensitivity, the suspension system is designed to match the frequencies of all three rotational modes sufficiently well that electrostatic tuning may compensate for process variations during manufacture of the gyroscope sensor. In particular, the sense axis natural frequencies were designed to be about ten percent above the drive natural frequencies so that the sense frequencies may be down tuned to match the drive frequency.

A plurality of inner combs 330a-330d project inwardly from inner edge 322 of rotor 316. Each inner comb includes a spine 332 and a plurality of teeth 334 which project from both sides of the spine. The number and configuration of inner combs in FIG. 17A is merely illustrative. The dual axis gyroscope may include twelve inner combs, each having five teeth. Four outer combs 340a-340d project outwardly from an outer edge 326 of rotor 316. Each outer comb includes a spine 342 and a plurality of teeth 344 projecting from both sides of the spine. Although teeth 334 and 344 in FIG. 17A are illustrated as linear, as shown in FIG. 17B it is

advantageous for the teeth to be constructed as portions of arcs from concentric circles.

As previously mentioned, drive system 310 induces oscillations of proof mass 302 about the Z-axis. The drive system 310 includes one or more drive electrodes 350a-350b and one or more feedback electrodes 352a-352b connected to substrate 304. Preferably, the drive and feedback electrodes are arranged in opposing pairs located on either side of each inner comb 330a-330d. Each feedback and drive electrode includes a plurality of teeth 354 which are interdigited with teeth 334 of the adjacent inner comb. Teeth 354 may have an arc length of approximately twenty microns and a width of approximately two microns. The drive electrodes of drive system 310 act as electrical, mechanical transducers. By application of an alternating voltage between the drive electrodes and the proof mass, the proof mass may be forced to oscillate about the Z-axis. Specifically, beams 320 may flex or bend so that rotor 316 may rotate.

Referring to FIG. 18, dual-axis gyroscopic sensor 300 includes a transresistance amplifier 366 which produces drive signals 362 and 364 having a driving frequency ω_z of about twenty to thirty kilohertz. Drive signals 362 and 364 are equal in magnitude but opposite in sign. phase-locked loop 360. A phase-locked loop 360 generates an extremely accurate digital output signal on line 368 which is in phase with the rotational rate of the proof mass. The opposing feedback electrodes 352a and 352b are connected to the positive and negative inputs of trans-resistance amplifier 366. The opposing drive electrodes 350a and 350b are connected to the positive and negative outputs 362 and 364 of trans-resistance amplifier 366 and to phase-locked loop 360.

The positive and negative outputs of trans-resistance amplifier 366 are also mixed with the digital output signal on line 368 by a mixer 370. The output of mixer 370 is then used to modulate trans-resistance amplifier 366. This modulation provides an automatic gain control circuit to control the amplitude of the oscillations of proof mass 302. Thus, drive system 310 provides a phase-locked oscillation of constant amplitude to the proof mass and provides a clean signal for Coriolis demodulation.

Returning to FIG. 17A, sensing system 312 includes four sense electrodes 374a-374d (shown in phantom because they are located beneath the rotor 316). Each sense electrode is shaped as a quarter-pie section and may be formed of an n+ diffused region in substrate 304. Sense electrodes 374a and 374c are positioned along the X-axis whereas the sense electrodes 374b and 374d are positioned along the Y-axis. The Coriolis oscillation is measured by sensing the change in capacitance between rotor 316 and sense electrodes 374a-374d. For example, if the gyroscopic sensor rotates about the Y-axis, then the Coriolis force may cause the right portion of rotor 316 to move closer to sense electrode 374b and the left portion of rotor 316 to move farther away from sense electrode 374d. Thus, the capacitance between sense electrode 374b and rotor 316 increases whereas the capacitance between sense electrode 374d and rotor 316 decreases. Because each pair of opposing sense electrodes provides differential sensing, translation of the rotor up or down along the Z-axis does not change in sense output.

Referring to FIG. 18, a first sense voltage source 376 connects opposing sense electrodes 374a and 374c, and

a second sense voltage source 378 connects opposing sense electrodes 374b and 374d. The sense voltage sources 376 and 378 generate AC voltages with different modulation frequencies. For example, one voltage source may operate at 200 kHz and the other voltage source may operate at 300 kHz. In order to extract the position signals indicating the angular position of rotor 316 about the X-axis and Y-axis, proof mass 302 is electrically connected to an integrator 380. The integrator 380 may include a capacitor 381 having a capacitance of about 50 femtoFarrads. A benefit of integrator 380 is that it improves linearity.

The output of integrator 380 is demodulated with the signal from sense voltage source 376 by a mixer 382. The output from integrator 380 is also demodulated with the signal from sense voltage source 378 by a mixer 384. The outputs of mixers 382 and 384 are then demodulated by mixers 386 and 388 with the digital output signal on line 368 from phase-locked loop 360. The output of mixer 386 provides the angular rotation rate of the gyroscopic sensor about the X-axis, and the output of mixer 388 provides the rotation rate of the gyroscopic sensor about the Y-axis.

The combined mechanical and electrical sensitivity of dual-axis gyroscopic sensor 300 may be calculated according to the following equation:

$$\left|\frac{V_{out}}{\Omega_y}\right| = \left|\frac{\theta_x}{\Omega_y}\right|\left|\frac{V_{out}}{\theta_x}\right| = \left|\frac{2\theta_{z0}\omega_z}{\omega^{2}_{x} + \frac{j\omega_x\omega_z}{Q_x} - \omega^{2}_{z}}\right|\left|2\frac{\partial C}{\partial\theta_x}\frac{V_s}{C_I}\right| \qquad (19)$$

were V_s is the sense voltage, C_i is the capacitance of the integrating capacitor, Q_x is the quality of inverse

damping coefficient, and V_{out} is the voltage signal from the mixer. One drawback of the sensing system is that a small inherent voltage is generated at twice the drive frequency. However, this voltage is far from the sense modulation frequencies.

As described above, if dual-axis gyroscopic sensor 300 is rotating about an axis parallel to the surface of the substrate, then the oscillation of rotor 316 about the Z-axis induces an oscillation about the X-axis or Y-axis due to the Coriolis force. In an ideal device, rotor 316 is perfectly aligned so that the only motion caused by drive system 310 is within the X-Y plane. However, fabrication imperfections may cause rotor 316 to wobble as it undergoes rotation about the Z-axis. Specifically, even if the gyroscopic sensor 300 is not rotating about the X-axis or Y-axis, as rotor 316 rotates about the Z-axis, it may oscillate or wobble out of the X-Y plane. The wobble caused by the fabrication imperfections generates a false rotation rate measurement called quadrature error. The quadrature error in dual-axis gyroscopic sensor 300 is similar to the quadrature error in Z-axis gyroscopic sensor 20; the quadrature error and Coriolis acceleration are both sinusoidal signals centered at the frequency of oscillation and ninety degrees out of phase. Ideally, demodulation will eliminate the out-of-phase quadrature error. However, because the electronic components may have a small phase-lag, some percentage of the quadrature error will corrupt the measurement of the rotation rate.

Returning to FIG. 17A, quadrature correction system 314 includes eight correction electrodes 390a-390h. The correction electrodes are arranged in pairs with each outer comb 340a-340d surrounded by two opposing

correction electrodes. For example, outer comb 340a is flanked by correction electrodes 390a and 390b. Each correction electrode has a plurality of teeth 392 which are interdigitated with the teeth of the outer combs. The quadrature correction system 314 may apply voltages to the correction electrodes 390a-390h in order to levitate teeth 344 of the outer combs and cancel the quadrature error.

Returning to FIG. 18, each pair of opposing correction electrodes may be connected to a DC offset voltage source. In addition, the correction electrodes on opposite sides of the rotor may be connected. For example, correction electrode 390a may be electrically connected to correction electrode 390f. A first DC voltage source 394 may connect electrode 390a to electrode 390b, and second DC voltage source 396 may connect correction electrode 390c and 390d. The DC offset may be selected to electrostatically levitate outer combs 340a-340d and thereby cancel the quadrature error.

Referring to FIG. 19, a portion of substrate 304 beneath teeth 344 and 392 may be an n+ diffused region to provide a control pad electrode 398. The control pad electrode 398 is electrically connected to proof mass 302. By applying a generally positive voltage to teeth 392 and a generally negative voltage to teeth 344 and control pad electrode 398, the electric field (shown by field lines 399) generates an upward force F_z on teeth 344.

Returning to FIG. 17A, the correction electrodes 390a and 390f generate an upward force on the teeth on the left side of the rotor which is stronger than the upward force on the teeth on the right side of the rotor

generated by electrodes 390b and 390e. This force imbalance creates a balancing torque which tends to rotate the rotor so that, absent the Coriolis force, it vibrates solely in the X-Y plane. Because the quadrature error results in a linear displacement, the balancing forces need to be proportional to the position of the proof mass about the Z-axis. The balancing torque F_z is proportional to the overlapping area between teeth 344 and teeth 392. Because the overlapping area between teeth 344 and teeth 392 is directly proportional to the angular position of rotor 316, the balancing torque will also be proportional to the angular position of the rotor.

Referring to FIG. 20, another embodiment of dual-axis gyroscopic sensor 300' includes a modified quadrature correction system 314'. In quadrature correction system 314', four generally rectangular or wedge-shaped plates 340a'-340d' are connected to outer edge 326 of rotor 316. Two fixed electrode pads 390a' and 390b' are disposed on substrate 304 beneath each plate. The fixed electrode pads 390a' and 390b' may be formed of n+ diffused regions in the substrate. A DC offset voltage may be applied between each pair of electrode pads to correct the quadrature error. For example, a positive offset voltage may be applied so that the voltage of electrode pad 390b' is higher than the voltage of electrode pad 390a'. As rotor 316 rotates counter-clockwise and the plate 340a' moves rightwards, more of the plate will overlap electrode pad 390b', and thus the right side of the plate will be more attracted to the substrate than the left side of the plate. This will generate a torque which tends to rotate rotor 316 about the X-axis. The dual-axis gyroscopic sensor 300'

otherwise functions in a manner similar to dual-axis gyroscopic sensor 300.

Referring to FIG. 21, in a gyroscopic sensor 400 the drive system, the sensing system, and the quadrature correction system use a single set of electrodes. Gyroscopic sensor 400 includes a proof mass 402 connected to a substrate 404 by a flexible suspension 406. A plurality of opposing electrode fingers 410a and 410b (only two opposing fingers are shown) project from proof mass 402 along the X-axis. Each electrode finger 410a is flanked by respective stationary electrode fingers 412a and 414a. Similarly, each electrode finger 410b is flanked by stationary electrode fingers 412b and 414b.

To sense the position of the proof mass along the Y-axis, a voltage source 420 applies a high-frequency (e.g., one megahertz) AC voltage between upper electrode fingers 412a, 412b and lower electrode fingers 414a, 414b. Proof mass 402 is electrically connected to an integrator 422. The output of integrator 422 provides a position signal.

To drive the proof mass along the X-axis, a voltage-controlled oscillator 426 is connected to apply an AC voltage with a frequency ω between the opposing electrode fingers 412a, 414a and 412b, 414b. The output of integrator 422 is applied to a phase-sensing circuit 428, and the output of phase-sensing circuit 428 controls the voltage-controlled oscillator 426.

The output voltage V_{out} from integrator 422 is

$$V_{out} = \frac{Q_{struct}}{C_I} \qquad (20)$$

where Q_{struct} is the charge on the proof mass and C_I is the capacitance of integrator 422. Q_{struct} is given by the equation:

$$Q_{struct} = \frac{dC_s}{dy}\Delta y V_{sense} + \Delta C_x(t)\, V_F(t) \qquad (21)$$

where $V_F(t)$ is AC portion of the forcing voltage, $C_x(t)$ is the changing capacitance on the forcing electrodes as the structure displaces along the X-axis, and V_{sense} is the sense voltage applied by voltage source 420. Combining Equations 20 and 21 yields:

$$V_{out} = \frac{\Delta C_x(t)\, V_F(t)}{C_I} + other\ terms \qquad (22)$$

If the forcing voltage $V_F(t)$ is $V_F \sin(\omega t)$ then the resulting displacement $x(t)$ is given by the following equation:

$$x(t) = X_0(\omega, \omega_x)\sin(\omega t + \phi(\omega, \omega_x)) \qquad (23)$$

where ω is the drive frequency, ω_x is the driven mode resonance frequency, $X_0(\omega, \omega_x)$ is the amplitude, and $\phi(\omega, \omega_x)$ is a phase difference. Because $\Delta Cx(t)$ is proportional to $x(t)$,

$$V_{out} = \frac{\Delta C_x(\omega, \omega_x)}{C_I}\sin(\omega t + \phi(\omega, \omega_x))\sin(\omega t) \qquad (24)$$

and therefore

$$V_{out} = \frac{\Delta C_x(\omega, \omega_x)}{2C_I}[\cos(\phi(\omega, \omega_x)) - \cos(2\omega t + \phi(\omega, \omega_x))] \qquad (25)$$

When the drive frequency ω is equal to the resonant frequency ω_x, the phase ϕ will be 90°. Because

the $\cos(\phi(\omega,\omega_{x1})$ term of Equation 25 produces a DC offset, phase-sensing circuit 428 can drive the frequency ω of voltage-controlled oscillator 426 to the resonant frequency ω_x by sensing when there is no DC offset. Thus, the drive voltage will remain phase locked with the position of the proof mass.

Quadrature error correction may be accomplished in gyroscopic sensor 400 by applying a DC voltage between electrode fingers 412a and 414a and an equal but opposite DC voltage between electrode fingers 412b and 414b.

Referring to FIG. 22, a micromachined gyroscopic sensor 500 may be fabricated using high-aspect-ratio single-crystal-silicon micromachining techniques to produce an extremely thick device. Gyroscopic sensor 500 includes a vibratory structure 502 connected to a rigid frame or substrate 504 at anchor points 511. Structure 502 is configured to vibrate in a plane parallel to a surface 505 of the substrate. As such, a gap of about 0.5 to 4.0 microns, such as about 1.0 microns, separates the vibratory structure from surface 505.

Structure 502 is generally H-shaped, and includes a proof mass portion 506 and a flexible suspension portion 508. The suspension portion includes two parallel crossbeams 516 and four parallel flexures 510 positioned generally along the X-axis. One end of each flexure is connected to anchor 511 which connects structure 502 to the substrate, and the other end of each flexure is connected to one of crossbeams 516. The total length of one crossbeam 516 and two flexures 510 may be about 200 to 1500 microns in length, preferably about 1250 microns.

Proof mass portion 506 includes two crossbars 512 connected to two beams 514 to provide a generally square

arrangement. Three additional crossbars 512 are also connected between beams 514. A plurality of electrode teeth or fingers project along the X-axis from the crossbars 512. Four additional flexures 518 may connect flexures 510 to proof mass portion 506.

Structure 502 may be formed of single-crystal silicon. The structure 502 may have a thickness T of at least 25 microns, and it is advantageous for the thickness T to be at least 50 microns. The thickness may be between about 50 and 100 microns, but for some applications the thickness may be 250 microns. The flexures of the structure may have a width W_F of about two to five microns. The aspect ratio, i.e., the ratio of width to thickness, of the flexures should be greater than 10:1, and it is advantageous for the aspect ratio to be greater than 20:1. The aspect ratio may even be 50:1 or more. The beams and crossbars of the proof mass portion may have a width W_B of about five to ten microns. The total mass of structure 502 may be about 10 to 50 micrograms.

The suspension portion 508 is designed to be flexible along the X-axis and Y-axis and rigid to other modes of vibration. In particular, the high-aspect ratio of the flexures results in a structure which is very rigid to torsion and Z-axis acceleration.

Referring to FIG. 23, the micromachined gyroscopic sensor 500 includes four major electronic elements: a drive system 520 used to sustain oscillation of structure 502 along the X-axis, a sensing system 540 used both to detect deflections of structure 502 along the Y-axis, a sense tuning system 560 used to adjust the resonant frequency of structure 502 along the Y-axis, and a

quadrature correction system 580 used to apply electrostatic forces to cancel quadrature error.

As shown in FIGS. 15 and 16, the drive system 520 includes two opposing driving electrode combs 522a and 522b and two feedback electrode combs 524a and 524b, all connected to substrate 504. Each driving electrode comb and feedback electrode comb includes a plurality of electrode teeth or fingers 526 which project along the drive axis and which are interdigited with electrode teeth or fingers 528 which project from structure 502. Electrode teeth 526 and 528 may have a length L of about fifteen microns, and a width W_E of about two to six microns. Electrode teeth 526 may be separated from electrode teeth 528 by a gap of about 2.5 microns. Electrode teeth 526 and 528 may be formed from the same layer of single-crystal silicon and have a thickness of about 100 microns.

The feedback electrodes combs 524a and 524b are electrically connected to the positive and negative inputs of a trans-resistance amplifier 530. The driving electrode combs 522a and 522b are connected to the positive and negative outputs, respectively, of the transresistance amplifier and to a phase-locked loop circuit 532. At least one of the outputs from transresistance amplifier 530 may be mixed with a velocity signal from phase-locked loop 532 by a mixer 534. The output of mixer 534 is then used to modulate transresistance amplifier 530 to provide an automatic gain control circuit to control the oscillation amplitude of structure 502.

The sensing system 540 includes an opposing pair of sense electrode combs, including left sense electrode combs 542a and 542b, and right sense electrode combs 544a

and 544b. The left sense electrode combs 542a, 542b include a plurality of "left" electrode teeth 546, and the right sense electrode combs 544a, 544b include a plurality of "right" electrode teeth 548. The electrode teeth 546 and 548 are interdigited with electrode teeth 550 which project from structure 502 such that each electrode tooth 550 is disposed between one left tooth 546 and one right tooth 548.

Electrode teeth 546, 548 and 550 may have a length L of about fifteen microns, and width W_E of about two to six microns. Electrode teeth 546, 548 and 550 have a thickness of at least 25 microns, and the thickness may be between about 50 and 100 microns. The aspect ratio of the electrode teeth should be at least about 5:1. The aspect ratio may be at least 10:1, and it may be between about 10:1 and 20:1. Electrode teeth 550 may be separated from electrode teeth 546 and 548 by a gap having a width W_G between about 0.5 and 4.0 microns, such as 2.5 microns. The aspect ratio of the gap should be at least 10:1, and it may be greater than 20:1 or even greater than 50:1. Electrode teeth 546, 548 and 550 may be formed from the same layer of single-crystal silicon in the same fabrication step so that the teeth are coplanar.

A first sense voltage source 552 applies an AC voltage to left sense electrode combs 542a and 542b. A second sense voltage source 554 applies an AC voltage, 180° out of phase with the first sense voltage, to right sense electrode combs 544a and 544b. The sense voltage sources may generate AC signals having a maximum voltage of about 0.1 to 5.0 volts and a frequency of about 0.1 to 5.0 megahertz. The AC signals may have a voltage amplitude of one volt and a frequency of one megahertz.

To measure the Coriolis signal Ω_z, structure 502 is electrically connected to an integrator 556, and the output of integrator 556 is amplified by an AC amplifier 558. The signal from one of the sense voltage sources is mixed with a position signal from phase-locked loop 532 by a mixer 536. The output of mixer 536 is then mixed with the output of amplifier 558 by a mixer 538 to generate the Coriolis signal.

Tuning of the Y-axis resonant frequency may be accomplished sense tuning system 560 applying a DC bias voltage between a set of inner tuning electrodes 562 and outer tuning electrodes 564. Electrodes 566 project from structure 502 and are interdigited with the inner tuning electrodes 562 and outer tuning electrodes 564. A tuning voltage source 568 applies a bias voltage $V_{\Delta fy}$ between inner tuning electrodes 562 and outer tuning electrodes 564. Alternately, the Y-axis resonant frequency could be tuned by applying a DC bias between the vibratory structure and the tuning electrodes.

Quadrature error cancellation is accomplished by applying a voltage between diagonal pairs of electrodes. The quadrature error correction system 580 includes a lower left electrode 582a, an upper left electrode 582b, a lower right electrode 584a, and an upper right electrode 584b. Lower left electrode 582a is connected to upper right electrode 584b, and upper left electrode 582b is connected to lower right electrode 584a. A quadrature correction voltage source 586 applies a bias voltage $2V_{Quad}$ between the electrode pairs 582a, 584b and 582b, 584a. The bias voltage creates a balancing force which is proportional to the position of the proof mass along the X-axis. This bias voltage may be determined

experimentally (as shown in FIG. 13) and may be in the range of 1 mV to 100 mV.

In addition, quadrature error correction system 580 may include a feedback loop to automatically adjust the bias voltage. A velocity signal from phase-locked loop 532 may be mixed with a signal from one of the sense voltage sources by a mixer 590. The output of mixer 590 may be mixed with the output of amplifier 558 by a mixer 592. The output of mixer 592 may be used to control the voltage source 586.

Assuming that the mass M of structure 502 is 36 micrograms, the drive and sense frequencies ω_x and ω_y are each 63 kHz, the quality factor Q for single-crystal silicon is 200,000 (about three to four times higher than that of polysilicon), and the amplitude X_0 of the drive mode is five microns, then one may calculate from Equation 16 that, at room temperature, the Brownian noise Ω_{nB} for a bandwidth (BW) of 60 Hz is about 2 deg/hr.

The electronic noise floor is determined by the thermal noise level in charge integrator 556. Where the sense frequency ω_y is electrostatically tuned to the drive frequency ω_x plus an offset frequency $\Delta\omega$, the electronic noise Ω_{nE} may be calculated from the equation:

$$\Omega_{nE} = 2\frac{g_0\Delta\omega}{X_0 V_S}\sqrt{\frac{32}{3\pi}\left(\frac{k_B T}{C_S}\right)\frac{1}{f_T}\left(\left(1+\frac{C_P}{C_S}\right)BW\right.} \qquad (26)$$

where g_0 is the sense-capacitor gap width, X_0 is the oscillation amplitude, V_S is the sense voltage, k_B is Boltzmann's constant, T is the temperature, C_S is the sense capacitance, C_P is the parasitic capacitance, f_T is the CMOS transition frequency, and BW is the bandwidth.

Assuming that the sense-capacitor gap g_0 is 2.5 microns, the sense voltage V_S is 1 V, C_S is the sense capacitance C_S is 1.25 pF, the parasitic capacitance C_P is 0.25 pF, and the CMOS transition frequency f_T is 1 GHz, one may calculate from Equation 18 that a frequency offset $\Delta\omega$ of 2π(175 Hz) is required to make the electronic noise floor equal to 2.5 deg/hr. This degree of tuning is feasible in principle because the measurement bandwidth is about 60 Hz.

By increasing the thickness of electrode teeth 546, 548 and 550, the surface area between the stationary and movable electrodes is increased, resulting in a larger sense capacitance. The larger sense capacitance reduces electronic noise. Similarly, the thicker structure is more massive and thus less subject to Brownian motion. In short, a gyroscopic sensor using high-aspect-ratio single-crystal silicon structures may be about one-hundred times more sensitive than a gyroscopic sensor using structures formed of thin polysilicon layers.

Fabrication of gyroscopic sensor 500 includes six basic steps: handle wafer processing, device wafer processing, bonding, CMOS processing of the bonded structure, etching to form the vibratory structure and stationary electrodes, and capping.

Referring to FIG. 24A, processing of a bottom substrate 600 may begin with a handle wafer 602, which may be a single-crystalline silicon substrate. Handle wafer 602 is oxidized to form an oxide layer 604, and a polysilicon layer 606 is deposited on oxide layer 604. Polysilicon layer 606 is then doped, polished and patterned to form the interconnects for the electrically isolated electrodes 522a, 522b, 524a, 524b, 542a, 542b,

544a, 544b, 562, 564, 582a and 584b, and 582b and 584a, of the gyroscopic sensor.

Referring to FIG. 24B, processing of a top substrate 610 may begin with a device wafer such as a silicon-on-insulator (SOI) substrate. The device wafer includes an oxide layer 616 sandwiched between two single-crystal silicon layers 614 and 618. A shallow trench 620 is formed in a surface 622 of single-crystal silicon layer, except in regions 624. Regions 624 will form anchors 511 connecting vibratory structure 502 to substrate 504. Trench 620 may be formed by deposition of a photoresist mask, etching of the exposed portions of single-crystal silicon layer 614, and removal of the mask. Alternately, trench 620 may be formed by mechanical thinning.

The thickness of single-crystal silicon layer 614 will define the thickness of vibratory structure 502, and the depth of trench 620 will define the spacing between the vibratory structure and the substrate. Preferably, single-crystal silicon layer 614 is about 100 microns thick, and trench 620 is about one micron deep.

Referring to FIG. 24C, bottom substrate 600 and top substrate 610 are aligned with surface 622 of top substrate 610 abutting the patterned polysilicon layer 606 of bottom substrate 600. The top and bottom substrates are bonded so that trench 620 forms a sealed cavity 626 between the two substrates. Then, referring to FIG. 24D, top substrate 610 is thinned by etching or mechanical removal of single-crystal silicon layer 618 to expose oxide layer 616, and oxide layer 616 is stripped. At this point, the bonded assembly is ready for standard CMOS processing. Because sealed cavity 626 is completely internal, the bonded assembly appears as an unprocessed

silicon wafer and may processed with conventional techniques.

Referring to FIG. 24E, the integrated circuitry of gyroscopic sensor 500 is fabricated on an exposed surface 630 of single-crystal silicon layer 614 in device regions 632. Following circuit fabrication, a thermocompression bond layer 634 is deposited and patterned. The bond layer 634 may be a conductive metal, such as gold.

Referring to FIG. 24F, the structures of the gyroscopic sensor are formed in single-crystal silicon layer 614. A photoresist mask is deposited over bond layer 634 and exposed surface 630, and the photoresist mask is patterned to define the gaps between the vibratory structure 502 and the stationary electrodes (not shown in this cross-sectional view). The single-crystal silicon layer 614 is etched using inductively-coupled plasma based deep reactive ion etching until cavity 626 is exposed. The etching step forms trenches 636 which create the free-standing vibratory structure and the various electrode structures of the gyroscopic sensor. Following the reactive ion etching, an oxygen plasma may be used to remove the photoresist mask, and the assembly may undergo a UV-ozone clean.

Finally, referring to FIG. 24G, a capping wafer 640 is aligned and bonded to top substrate 610. Capping wafer 640 may be glass or oxidized silicon. An underside 642 of the capping wafer may include a patterned thermocompression bond layer 644. Bond layer 634 may be aligned with bond layer 644, and the thermocompression bond may be formed by the application of a pressure of approximately 20 psi and a temperature of about 300-350°C for several minutes. The capping wafer may also include

an etched hole 646 that permits access to bonding pads 648 in device regions 632.

The present invention has been described in terms of a preferred embodiment. The invention, however, is not limited to the embodiment depicted and described. Rather, the scope of the invention is defined by the appended claims.

What is claimed is:

1. A microfabricated structure comprising:

a substrate;

a mass connected to said substrate by a suspension system to vibrate in a plane parallel to a surface of said substrate;

a first plurality of electrode fingers projecting from said mass along a first axis in said plane;

a second plurality of electrode fingers, coplanar with said first plurality of electrode fingers, connected to said substrate and projecting substantially along said first axis;

a third plurality of electrode fingers connected to said substrate but electrically isolated from said second plurality of electrode fingers, said first third plurality of electrode fingers being coplanar with said first and second plurality of electrode fingers and projecting substantially along said first axis, said second and third plurality of electrode fingers interdigitated with said first plurality of electrode fingers such that each of said first plurality of electrode fingers is adjacent to one of said second plurality of electrode fingers and one of said third plurality of electrode fingers.

2. The structure of claim 1 further comprising a voltage source to apply a voltage between said second and third plurality of electrode fingers.

3. The structure of claim 1 further comprising

a fourth plurality of electrode fingers, coplanar with said first, second and third plurality of electrode

fingers, projecting from said mass along said first axis, and

a fifth plurality of electrode fingers connected to said substrate but electrically isolated from said second and third plurality of electrode fingers, said fourth and fifth plurality of electrode fingers interdigitated.

4. The structure of claim 3 wherein each of said first plurality of electrode fingers has a first length and each of said fourth plurality of electrode fingers has a second length.

5. The structure of claim 4 wherein said first length is greater than said second length.

6. A microfabricated structure comprising:

a substrate; and

a suspension system to permit a mass to vibrate in a plane parallel to a surface of said substrate, said suspension system including,

first and second substantially parallel beams, each of said first and second beams anchored at both ends to said substrate, and

third and fourth substantially parallel beams, one end of each of said third and fourth beams connected to said first beam and another end connected to said second beam.

7. The structure of claim 6 further comprising a plurality of fingers projecting along an axis substantially parallel to said first and second beams.

8. The structure of claim 6 further comprising

a fifth and a sixth beam, one end of each of said fifth beam and sixth beams connected to said third beam and another end connected to said fourth beam, and

a seventh beam, one end of said seventh beam connected to said fifth beam and another end connected to said sixth beam.

9. The structure of claim 8 further comprising a plurality of fingers projecting from said seventh beam along an axis substantially parallel to said first and second beams.

10. The structure of claim 6 wherein sections of said first and second beams located between said third and fourth beams are substantially rigid to prevent rotation of said mass.

11. A sensor comprising:

a substrate;

a mass connected to said substrate by a suspension system to vibrate in a plane parallel to a surface of said substrate;

a first plurality of electrode fingers projecting from said mass along a first axis in said plane;

a second plurality of electrode fingers connected to said substrate and projecting substantially along said first axis;

a third plurality of electrode fingers connected to said substrate but electrically isolated from said second plurality of electrode fingers, said third plurality of electrode fingers projecting substantially along said first axis, said second and third pluralities

of electrode fingers interdigitated with said first plurality of electrode fingers such that each of said first plurality of electrode fingers is adjacent to one of said second plurality of electrode fingers and one of said third plurality of electrode fingers;

a position sensor to mesure a deflection of said mass in said plane; and

a voltage source for applying a first DC voltage between said second and third pluralities of electrode fingers to cause said mass to vibrate, absent a Coriolis force, more precisely along said first axis.

12. The sensor of claim 11 further including,

a fourth plurality of electrode fingers projecting from said mass along a first axis in said plane and positioned opposing said first plurality of electrode fingers;

a fifth plurality of electrode fingers connected to said substrate and projecting substantially along said first axis;

a sixth plurality of electrode fingers connected to said substrate but electrically isolated from said fifth plurality of electrode fingers, said sixth plurality of electrode fingers projecting substantially along said first axis, said fifth and sixth plurality of electrode fingers interdigitated with said third plurality of electrode fingers such that each of said fourth plurality of electrode fingers is adjacent to one of said fifth plurality of electrode fingers and one of said sixth plurality of electrode fingers.

13. The sensor of claim 12 further comprising a second voltage source for applying a second DC voltage between

said fifth and sixth plurality of electrode fingers to cause said mass to vibrate, absent a Coriolis force, more precisely along said first axis.

14. The sensor of claim 13 wherein said second DC voltage is substantially equal in magnitude but opposite in sign to said first DC voltage.

15. The sensor of claim 13 wherein said first plurality of electrode fingers is electrically coupled to said second plurality of electrode fingers.

16. The sensor of claim 13 further comprising a voltage source for applying a third DC voltage between said first and third pluralities of electrode fingers and said second, third, fifth and sixth pluralities of electrode fingers to adjust the resonant frequency of vibrations of said mass along a second axis in said plane perpendicular to said first axis.

17. The sensor of claim 11 wherein the position sensor measures the deflection of said mass along a second axis substantially perpendicular to said first axis and rotation of said mass about a Z-axis perpendicular to said surface and vibration of said mass along said first axis generates a Coriolis force to deflect said mass along said second axis, and wherein the sensor further comprises a signal processor coupled to an output of said position sensor to generate a signal varying with the rate of rotation of said mass about the Z-axis.

18. The sensor of claim 17 further comprising a voltage source for applying an AC voltage between said second and third plurality of electrode fingers.

19. The sensor of claim 18 wherein a voltage is applied between said second and third pluralities of electrode fingers to form a capacitive bridge with said first plurality of electrodes, and said position sensor is coupled to said first plurality of electrodes to detect changes in capacitance when said mass is deflected along said second axis.

20. A sensor comprising:

a substrate;

a mass connected to said substrate by a suspension system to vibrate in a plane parallel to a surface of said substrate;

a first plurality of electrode fingers projecting from said mass along a first axis in said plane;

a second plurality of electrode fingers connected to said substrate and projecting substantially along said first axis;

a third plurality of electrode fingers connected to said substrate but electrically isolated from said second plurality of electrode fingers, said first third plurality of electrode fingers projecting substantially along said first axis, said second and third plurality of electrode fingers interdigitated with said first plurality of electrode fingers such that each of said first plurality of electrode fingers is adjacent to one of said second plurality of electrode fingers and one of said third plurality of electrode fingers; and

a voltage source for applying a DC voltage between said first plurality of electrode fingers and said second and third plurality of electrode fingers to adjust the resonant frequency of vibrations of said mass along a second axis in said plane perpendicular to said first axis.

21. A microfabricated gyroscopic sensor for sensing rotation about a Z-axis, comprising:

a substrate;

a mass connected to said substrate by a suspension system to vibrate in a plane parallel to a surface of said substrate;

a drive system to cause said mass to vibrate substantially along a first axis in said plane;

a first plurality of electrode fingers projecting from said mass substantially along said first axis;

a second plurality of electrode fingers connected to said substrate and projecting substantially along said first axis;

a third plurality of electrode fingers connected to said substrate and projecting substantially along said first axis, said second and third plurality of electrode fingers interdigitated with said first plurality of electrode fingers such that each of said first plurality of electrode fingers is adjacent to one of said second plurality of electrode fingers and one of said third plurality of electrode fingers;

a position sensor coupled to said first plurality of electrode fingers for measuring the deflection of said mass along a second axis in said plane perpendicular to said first axis, wherein rotation of said mass about a Z-axis perpendicular to said surface and vibration of said

mass along said first axis generates a Coriolis force to deflect said mass along said second axis; and

a signal processor coupled to an output of said position sensor to generate a signal varying with the rate of rotation of said mass about the Z-axis.

22. The sensor of claim 21 further comprising a voltage source for applying an AC voltage having a first frequency between said second and third plurality of electrode fingers.

23. The sensor of claim 22 wherein a voltage is applied between said second and third pluralities of electrode fingers to form a capacitive bridge with said first plurality of electrodes, and said position sensor is coupled to said first plurality of electrodes to detect changes in capacitance when said mass is deflected along said second axis.

24. The sensor of claim 23 wherein said position sensor further includes an integrator to integrate a signal from said first plurality of electrode fingers.

25. The sensor of claim 24 wherein said drive system generates a signal to cause said mass to oscillate along said first axis at a second frequency.

26. The sensor of claim 25 wherein said drive system said signal.

27. The sensor of claim 25 further including a first mixer to mix the signal from said drive system with a signal from said voltage source.

28. The sensor of claim 27 further including a second mixer to mix a signal from said first mixer with an output signal from said position sensor to produce a position quadrature signal.

29. The sensor of claim 27 further including a second mixer to mix a signal from said first mixer with an output signal from said position sensor to produce a Coriolis signal.

30. The sensor of claim 25 further including a mixer to mix an output signal from said position sensor with a signal from said voltage source to produce a position signal.

31. A microfabricated gyroscopic sensor, comprising:

a substrate;

a mass connected to the substrate by a suspension system;

a drive system to cause the mass to vibrate along a drive axis substantially parallel to a surface of the substrate; and

a position sensor to measure a deflection of the mass along a sense axis substantially parallel to the surface of the substrate, wherein rotation of the mass about an axis of rotation substantially perpendicular to the surface of the substrate and vibration of the mass along the drive axis generates a Coriolis force to deflect the mass along the sense axis.

32. The sensor of claim 31 further comprising a processor coupled to an output of the position sensor to

generate a signal varying with the rate of rotation of the mass about the axis of rotation.

33. The sensor of claim 31 wherein the position sensor includes a first sense electrode projecting from the mass, a second sense electrode connected to the substrate and positioned on a first side of the first electrode, and a third sense electrode connected to the substrate and positioned on an opposing second side of the first electrode.

34. The sensor of claim 33 wherein the position sensor senses a change in capacitance between the first electrode and the second and third electrodes.

35. The sensor of claim 33 wherein the first, second and third electrodes are substantially coplanar and each electrode has a longitudinal axis substantially aligned with the drive axis.

36. The sensor of claim 31 wherein the drive system includes a first drive electrode projecting from the mass, a second drive electrode connected to the substrate and positioned on a first side of the first electrode, and a third drive electrode connected to the substrate and positioned on an opposing second side of the first electrode.

37. The sensor of claim 35 wherein the drive system applies an alternating voltage between the between the first electrode and the second and third electrodes.

38. The sensor of claim 33 wherein the first, second and third electrodes are substantially coplanar and each electrode has a longitudinal axis substantially aligned with the drive axis.

39. The sensor of claim 31 further comprising a voltage source to apply a voltage between a plurality of correction electrodes connected to the substrate to cause the mass to vibrate, absent the Coriolis force, more precisely along the drive axis.

40. The sensor of claim 31 further comprising a voltage source to apply a voltage between a first tuning electrode connected to the substrate and a second tuning electrode connected to the mass to adjust a resonant frequency of vibrations of the mass along the sense axis.

41. A microfabricated gyroscopic sensor, comprising:

a substrate;

a mass connected to the substrate by a suspension system;

a drive system to cause the mass to vibrate substantially along a drive axis;

a position sensor to measure a deflection of the mass along a sense axis, wherein rotation of the mass about an axis of rotation and vibration of the mass along the drive axis generates a Coriolis force to deflect the mass along the sense axis; and

a voltage source to apply a voltage between electrodes connected to the substrate to cause the mass to vibrate, absent the Coriolis force, more precisely along the drive axis.

42. The sensor of claim 41 further comprising a processor coupled to an output of the position sensor to generate a signal varying with the rate of rotation of the mass about the axis of rotation.

43. The sensor of claim 41 further comprising a second voltage source to apply a second voltage between electrodes connected to the mass and the electrodes connected to the substrate to adjust a resonant frequency of vibrations of the mass along the sense axis.

44. The sensor of claim 41 wherein the position sensor applies an AC voltage between the electrodes connected to the substrate.

45. The sensor of claim 41 wherein the drive axis and sense axis are substantially parallel to a surface of the substrate and the axis of rotation is substantially perpendicular to the surface of the substrate.

46. The sensor of claim 41 further comprising:

a first plurality of electrode fingers projecting from the mass substantially along the drive axis;

a second plurality of electrode fingers connected to the substrate and projecting substantially along the drive axis; and

a third plurality of electrode fingers connected to the substrate and projecting substantially along the drive axis, the second and third pluralities of electrode fingers interdigitated with the first plurality of electrode fingers such that each of the first plurality of electrode fingers is adjacent to one of the second

plurality of electrode fingers and one of the third plurality of electrode fingers.

47. The sensor of claim 46 further comprising:

a fourth plurality of electrode fingers projecting from the mass substantially along the drive axis and positioned opposing the first plurality of electrode fingers;

a fifth plurality of electrode fingers connected to the substrate and projecting substantially along the drive axis and positioned opposing the second plurality of electrode fingers; and

a sixth plurality of electrode fingers connected to the substrate and projecting substantially along the drive axis and positioned opposing the third plurality of electrode fingers, the fifth and sixth pluralities of electrode fingers interdigitated with the fourth plurality of electrode fingers such that each of the fourth plurality of electrode fingers is adjacent to one of the fifth plurality of electrode fingers and one of the sixth plurality of electrode fingers.

48. The sensor of claim 47 wherein the first, second, third, fourth, fifth and sixth pluralities of electrode fingers are substantially co-planar.

49. The sensor of claim 48 wherein the voltage source applies a first DC voltage between the second plurality and the third plurality of electrode fingers and a second DC voltage between the fifth plurality and the sixth plurality of electrode fingers.

50. The sensor of claim 49 wherein the second DC voltage is substantially equal in magnitude and opposite in sign to the first DC voltage.

51. The sensor of claim 21 further comprising a voltage source for applying a DC voltage between the first plurality of electrode fingers and the second and third pluralities of electrode fingers to adjust a resonant frequency of vibrations of the mass along the second axis.

52. The sensor of claim 21 further comprising a voltage source for applying a first DC voltage between the second and third pluralities of electrode fingers to cause the mass to vibrate, absent a Coriolis force, more precisely along the first axis.

53. A method of sensing rotation with a gyroscopic sensor including a mass connected to a substrate by a suspension system, comprising:

rotating the mass about an axis of rotation substantially perpendicular to a surface of the substrate;

causing the mass to vibrate substantially along a drive axis substantially parallel to the surface of the substrate, rotation of the mass about the axis of rotation and vibration of the mass along the drive axis generating a Coriolis force to deflect the mass along a sense axis substantially parallel to the surface of the substrate; and

measuring a deflection of the mass along the sense axis.

54. A method of sensing rotation with a gyroscopic sensor including a mass connected to a substrate by a suspension system, comprising:

rotating the mass about an axis of rotation;

causing the mass to vibrate substantially along a drive axis, rotation of the mass about the axis of rotation and vibration of the mass along the drive axis generating a Coriolis force to deflect the mass along a sense axis;

measuring a deflection of the mass along the sense axis; and

applying a voltage between electrode fingers connected to the substrate to cause the mass to vibrate, absent a Coriolis force, more precisely along the first axis.

55. A microfabricated gyroscopic sensor for measuring rotation about an input axis, comprising:

a substrate;

a mass;

a suspension system connecting the mass to the substrate;

a drive system to cause the mass to oscillate substantially about a drive axis;

a position sensor to measure a rotation of the mass about a sense axis, wherein rotation of the mass about the input axis and oscillation of the mass about the drive axis generates a Coriolis force to oscillate the mass about the sense axis;

a plurality of electrodes associated with the substrate; and

a voltage source to apply a voltage between the electrodes to cause the mass to oscillate, in the absence the Coriolis force, more precisely about the drive axis.

56. The sensor of claim 55 further comprising a processor coupled to an output of the position sensor to generate a signal varying with the rate of rotation of the mass about the input axis.

57. The sensor of claim 55 further comprising a second voltage source to apply a second voltage between electrodes connected to the mass and the electrodes connected to the substrate to adjust a resonant frequency of oscillations of the mass about the sense axis.

58. The sensor of claim 55 wherein the position sensor applies an AC voltage between the electrodes connected to the substrate.

59. The sensor of claim 55 wherein the drive axis is substantially perpendicular to the surface of the substrate and the input axis and sense axis are substantially parallel to a surface of the substrate.

60. The sensor of claim 59 further comprising:

a first plurality of electrode fingers projecting from the mass;

a second plurality of electrode fingers projecting from the mass;

a third plurality of electrode fingers projecting from the substrate and interdigitated with the first plurality of electrode fingers; and

a fourth plurality of electrode fingers projecting from the substrate and positioned opposing the first plurality of electrode fingers, the fourth plurality of electrode fingers interdigitated with the second plurality of electrode fingers.

61. The sensor of claim 60 further comprising:

a fifth plurality of electrode fingers projecting from the mass;

a sixth plurality of electrode fingers projecting from the mass;

a seventh plurality of electrode fingers projecting from the substrate and interdigitated with the fifth plurality of electrode fingers; and

a eighth plurality of electrode fingers projecting from the substrate and positioned opposing the seventh plurality of electrode fingers, the eighth plurality of electrode fingers interdigitated with the sixth plurality of electrode fingers.

62. The sensor of claim 61 wherein the first, second, third, fourth, fifth, sixth, seventh and eighth pluralities of electrode fingers are substantially co-planar.

63. The sensor of claim 62 wherein the voltage source applies a first DC voltage between the third plurality and the fourth plurality of electrode fingers and a second DC voltage between the seventh plurality and the eighth plurality of electrode fingers.

64. The sensor of claim 63 wherein the second DC voltage is substantially equal in magnitude and opposite in sign to the first DC voltage.

65. The sensor of claim 55 further comprising a first electrode projecting from the mass, a second electrode connected to the substrate and positioned beneath a first portion of the first electrode, and a third electrode connected to the substrate and positioned beneath a second portion of the first electrode.

66. The sensor of claim 55 wherein the mass is substantially ring-shaped.

67. A method of sensing rotation with a gyroscopic sensor including a mass connected to a substrate by a suspension system, comprising:

rotating the mass about an input axis;

causing the mass to oscillate substantially about a drive axis, rotation of the mass about the input axis and oscillation of the mass about the drive axis generating a Coriolis force to oscillate the mass about a sense axis;

measuring an oscillation of the mass about the sense axis; and

applying a voltage between electrodes connected to the substrate to cause the mass to oscillate, in the absence of a Coriolis force, more precisely about the drive axis.

68. A microfabricated gyroscopic sensor, comprising:

a substrate having a first plurality of electrode teeth;

a vibratory structure including a second plurality of electrode teeth and a suspension system connecting the second plurality of electrode teeth to the substrate, the second plurality of electrode teeth interdigited with the first plurality of electrode teeth;

a drive system to cause the vibratory structure to oscillate relative to the substrate; and

a position sensor to measure a deflection of the mass caused by a Coriolis force;

wherein the first and second pluralities of electrode teeth have thicknesses substantially greater than their widths.

69. The sensor of claim 68 wherein the suspension system includes a plurality of flexures having an aspect ratio of at least about 10:1.

70. The sensor of claim 68 wherein the first and second pluralities of electrode teeth have an aspect ratio of at least 5:1.

71. The sensor of claim 68 wherein gaps between the first and second pluralities of electrode teeth have an aspect ratio of at least 10:1.

72. A method of fabricating a gyroscopic sensor, comprising:

forming an insulative layer on a first substrate;

forming a recess in a first surface of a second substrate;

bonding the first surface of the second substrate to the first substrate so that the recess defines an enclosed cavity between the first and second substrates;

forming circuitry for the gyroscopic sensor on a second surface of the second substrate

etching a plurality of trenches in the second substrate from the second surface to the cavity, the plurality of trenches defining a vibratory structure connected to the first substrate.

73. The method of claim 72 wherein the vibratory structure has a thickness of at least 25 microns.

74. The method of claim 72 wherein the recess has a depth of about 1 micron.

75. The method of claim 72 wherein the etching step comprises a deep reactive ion etch.

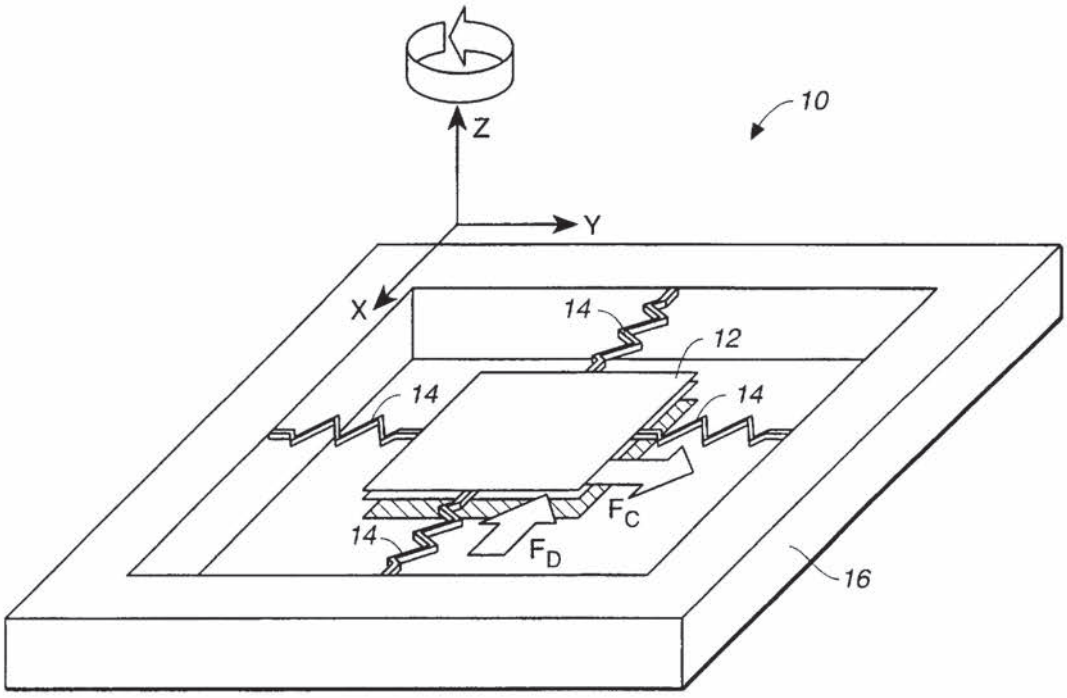


FIG._1

Nintendo Exhibit 1066
IPR2024-00668 - Page 352

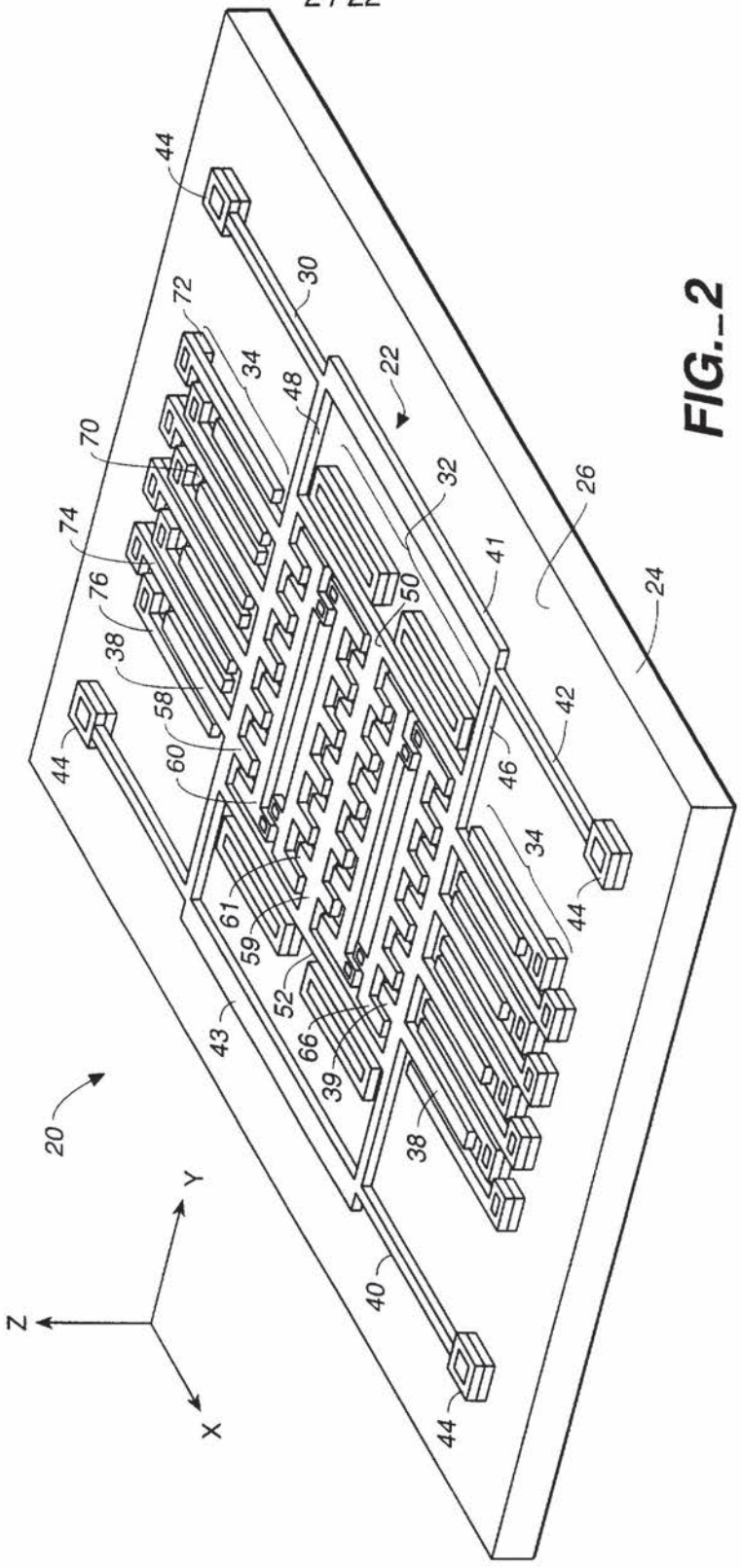


FIG._2

Nintendo Exhibit 1066
IPR2024-00668 - Page 353

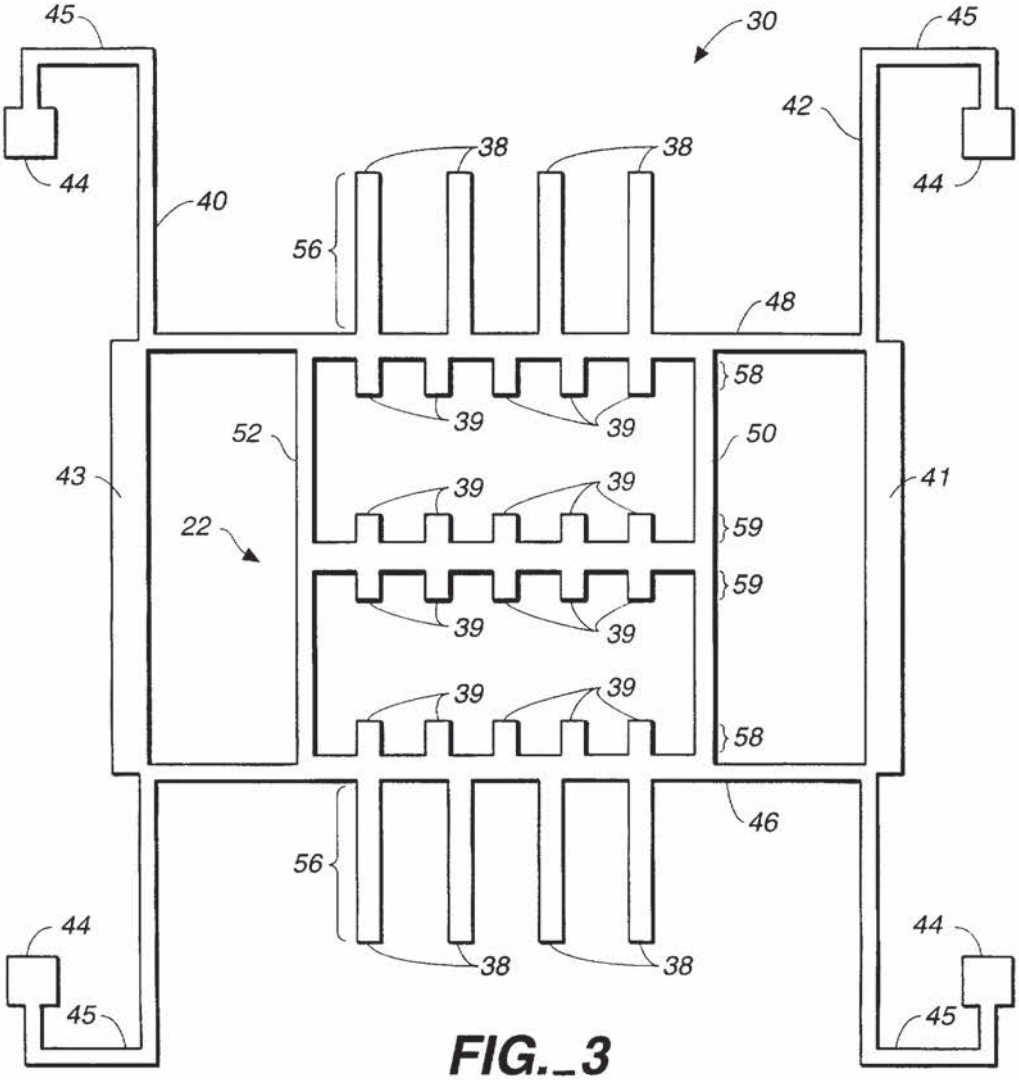


FIG._3

Nintendo Exhibit 1066
IPR2024-00668 - Page 354

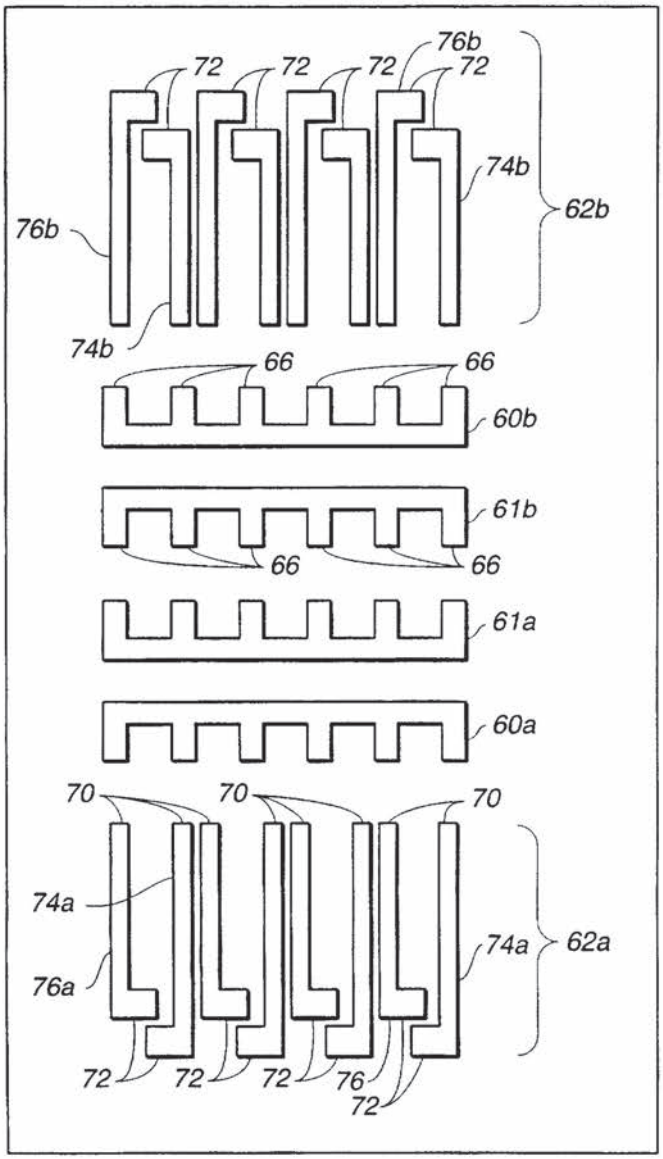


FIG._4

Nintendo Exhibit 1066
IPR2024-00668 - Page 355

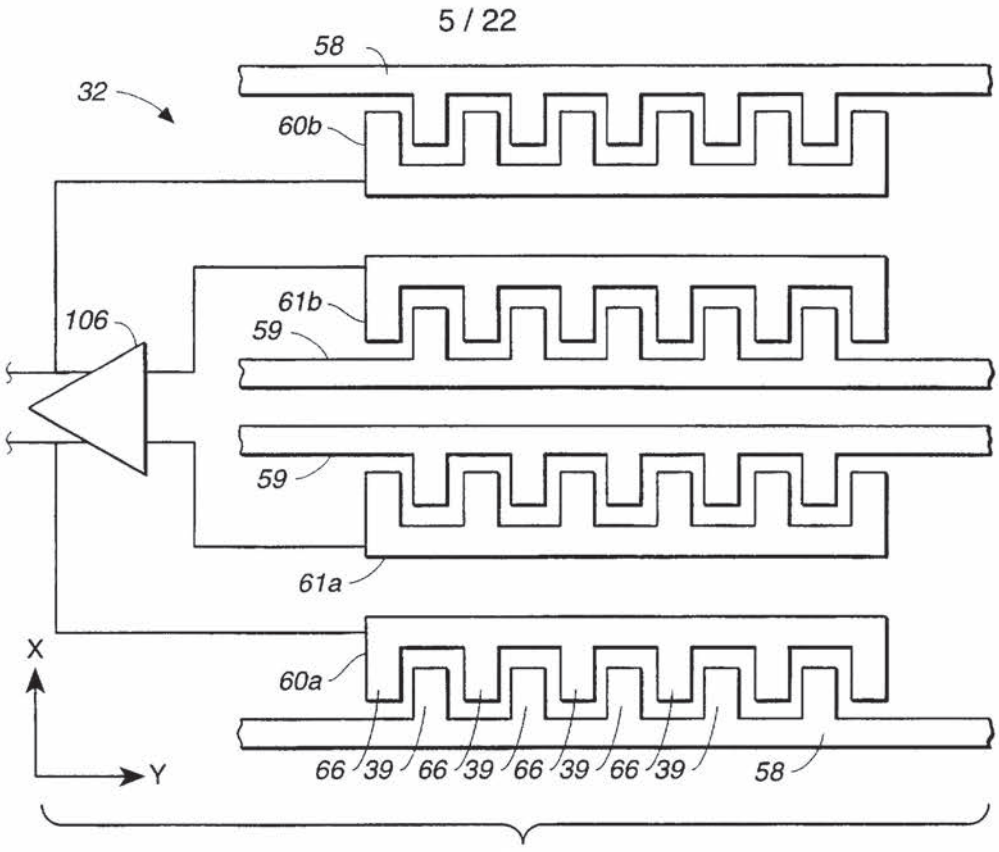


FIG._5

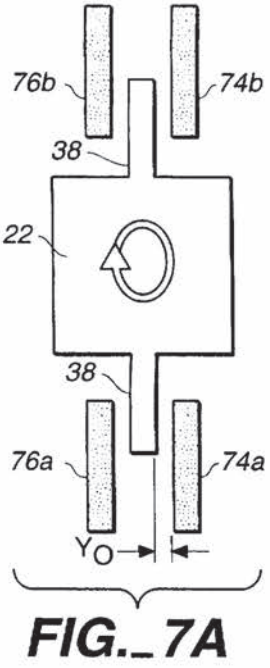


FIG._7A

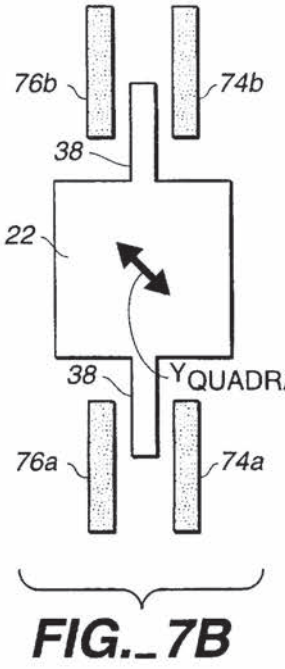


FIG._7B

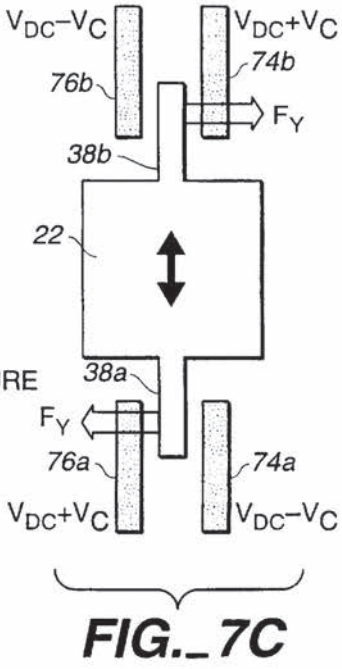


FIG._7C

Nintendo Exhibit 1066
IPR2024-00668 - Page 356

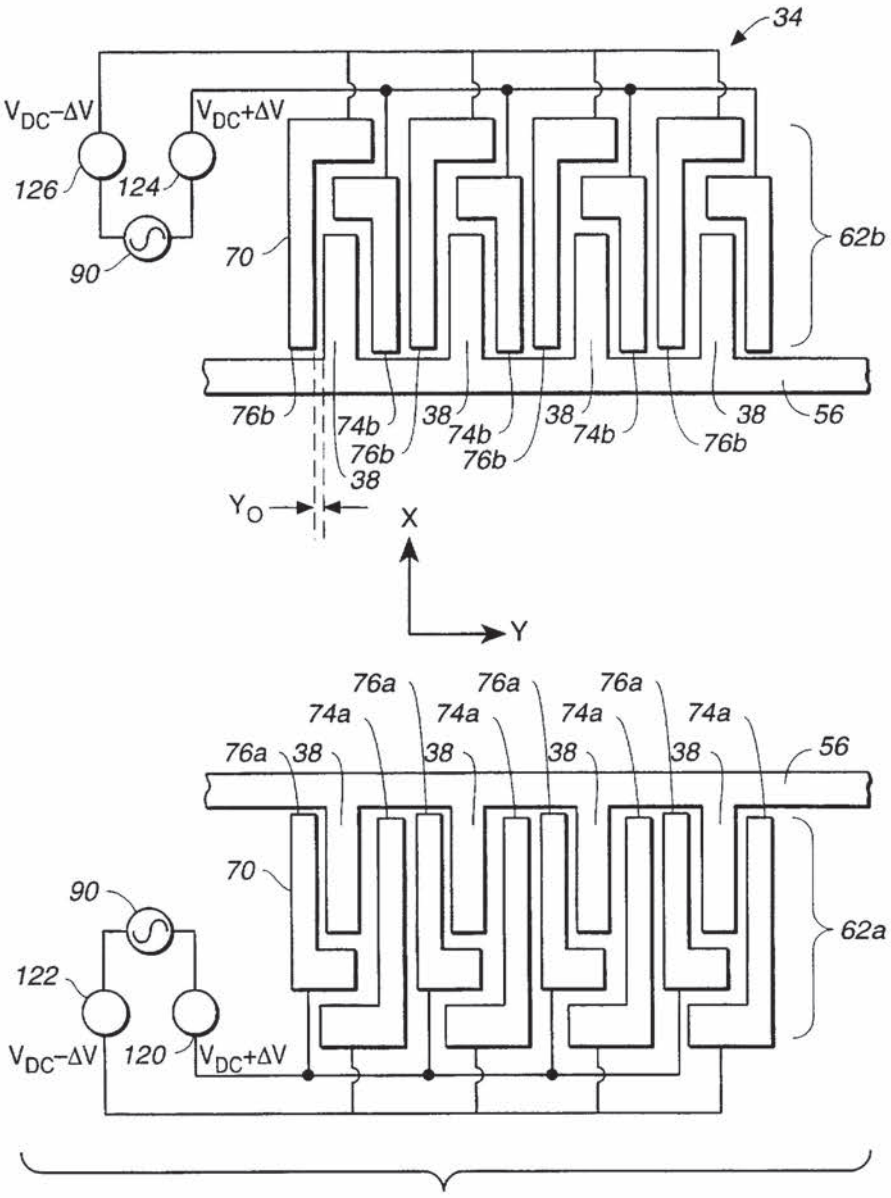


FIG._6

Nintendo Exhibit 1066
IPR2024-00668 - Page 357

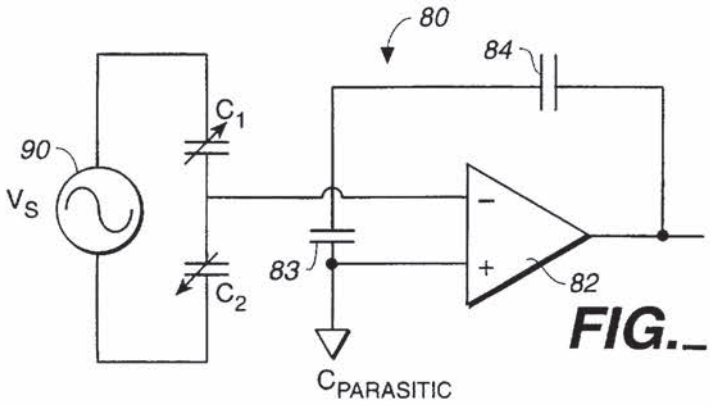


FIG._8A

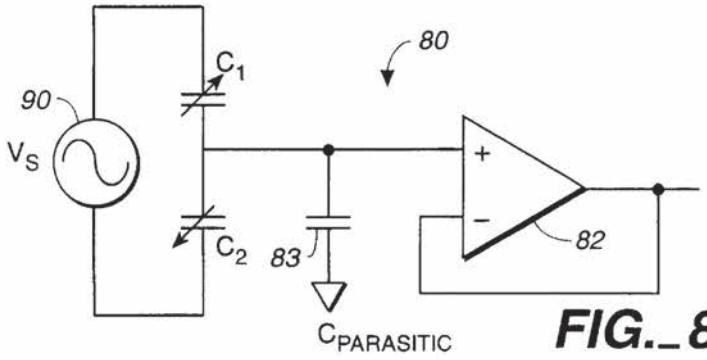


FIG._8B

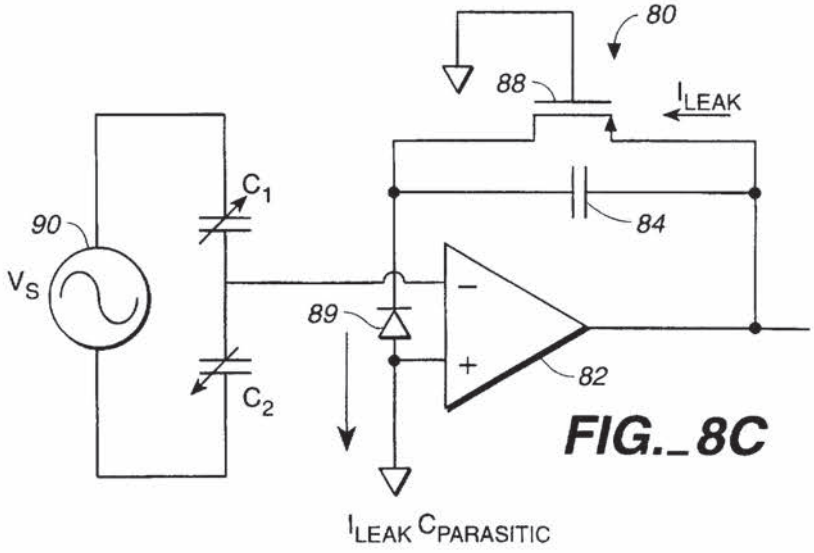


FIG._8C

Nintendo Exhibit 1066
IPR2024-00668 - Page 358

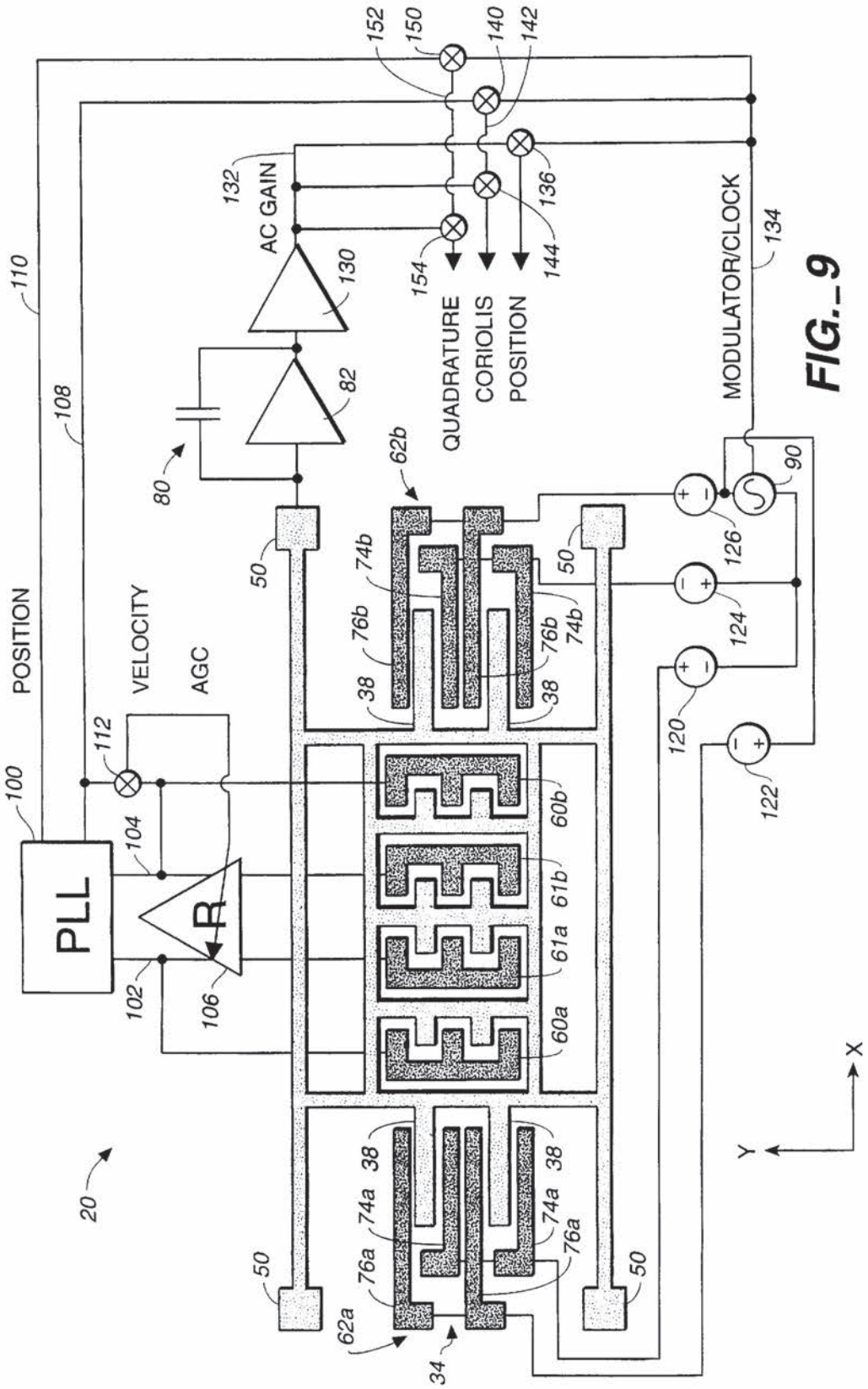


FIG._9

Nintendo Exhibit 1066
IPR2024-00668 - Page 359

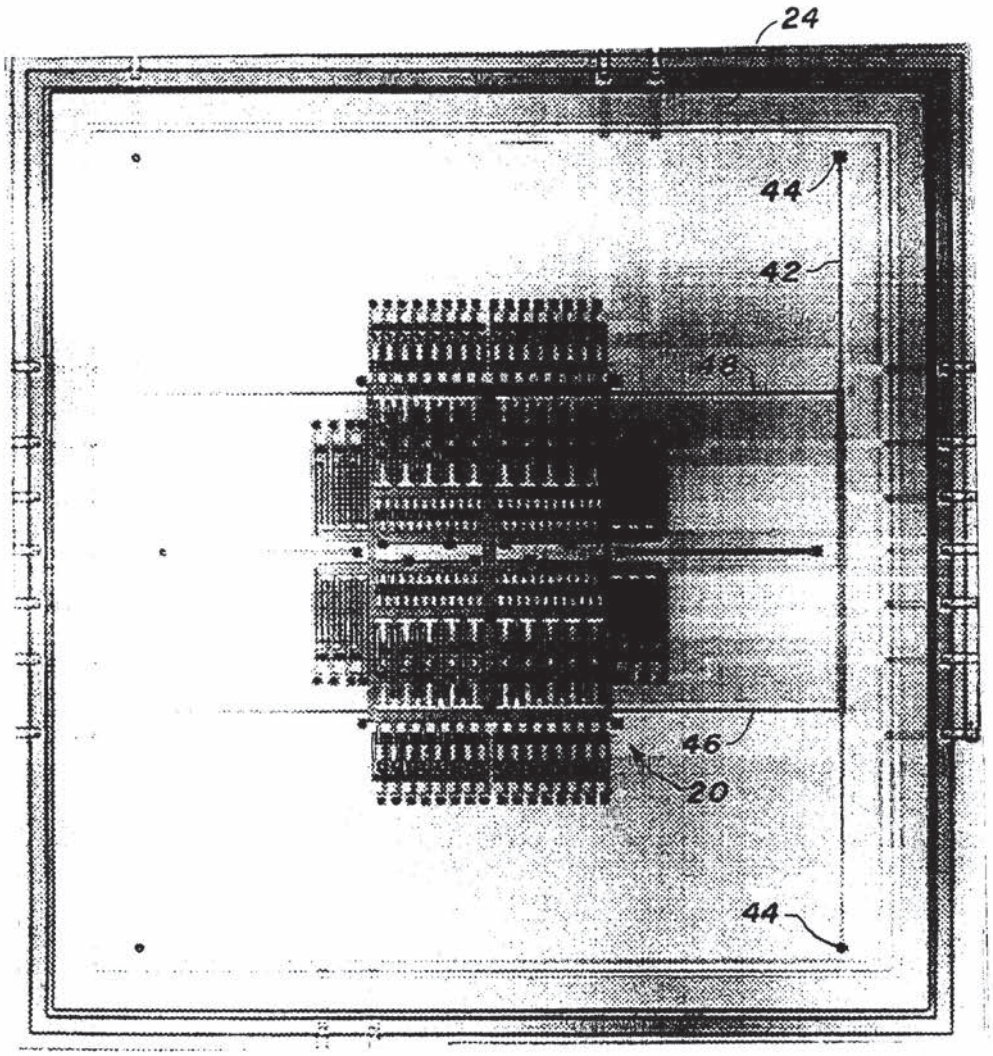


FIG._10

Nintendo Exhibit 1066
IPR2024-00668 - Page 360

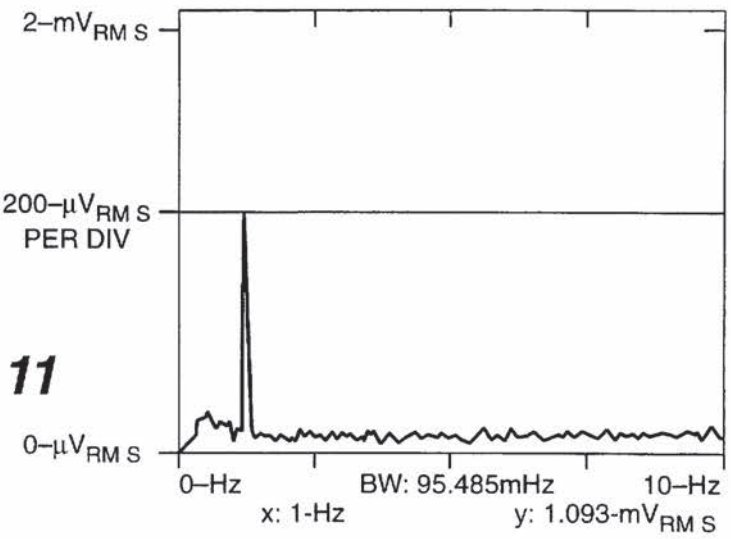


FIG._11

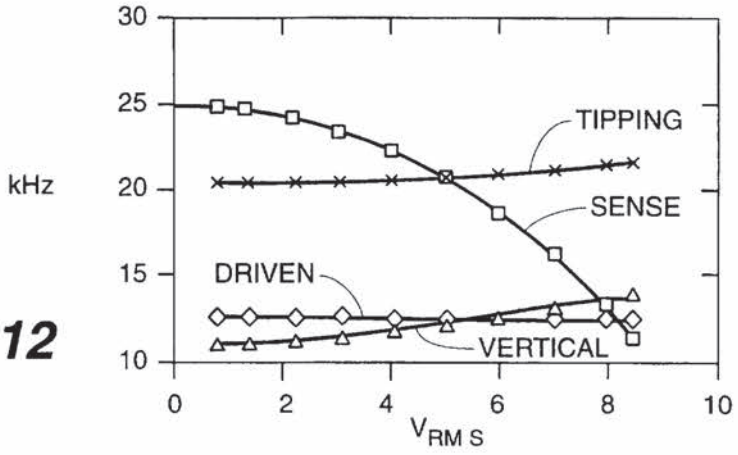


FIG._12

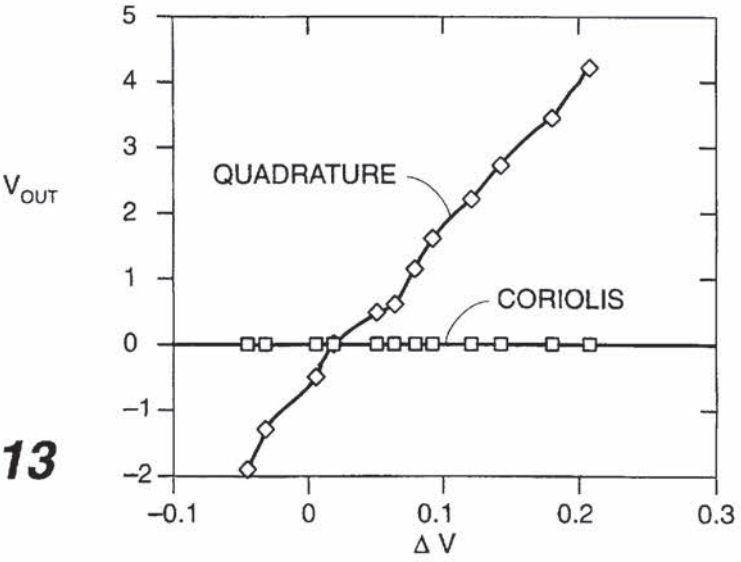


FIG._13

Nintendo Exhibit 1066
IPR2024-00668 - Page 361

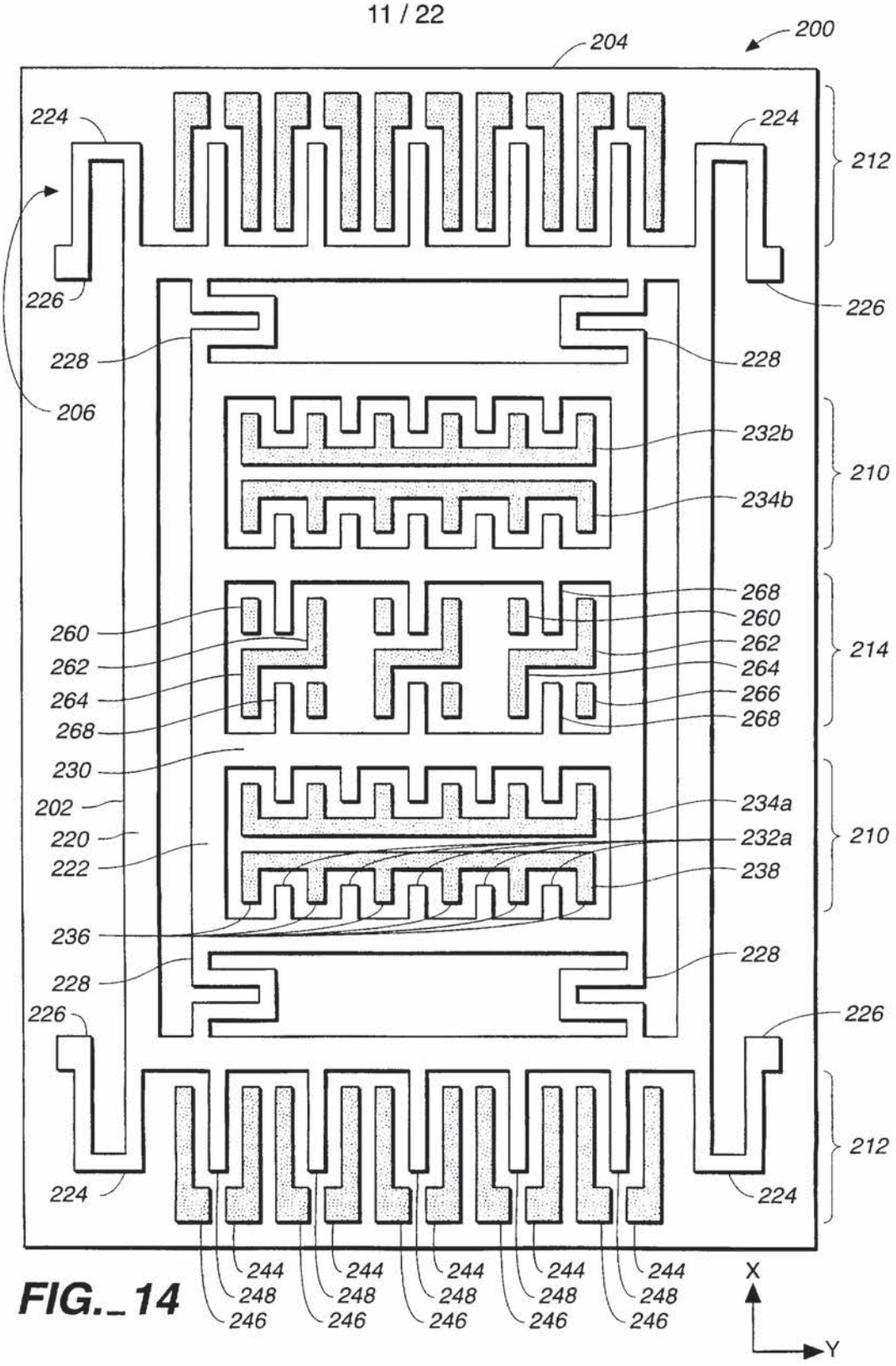
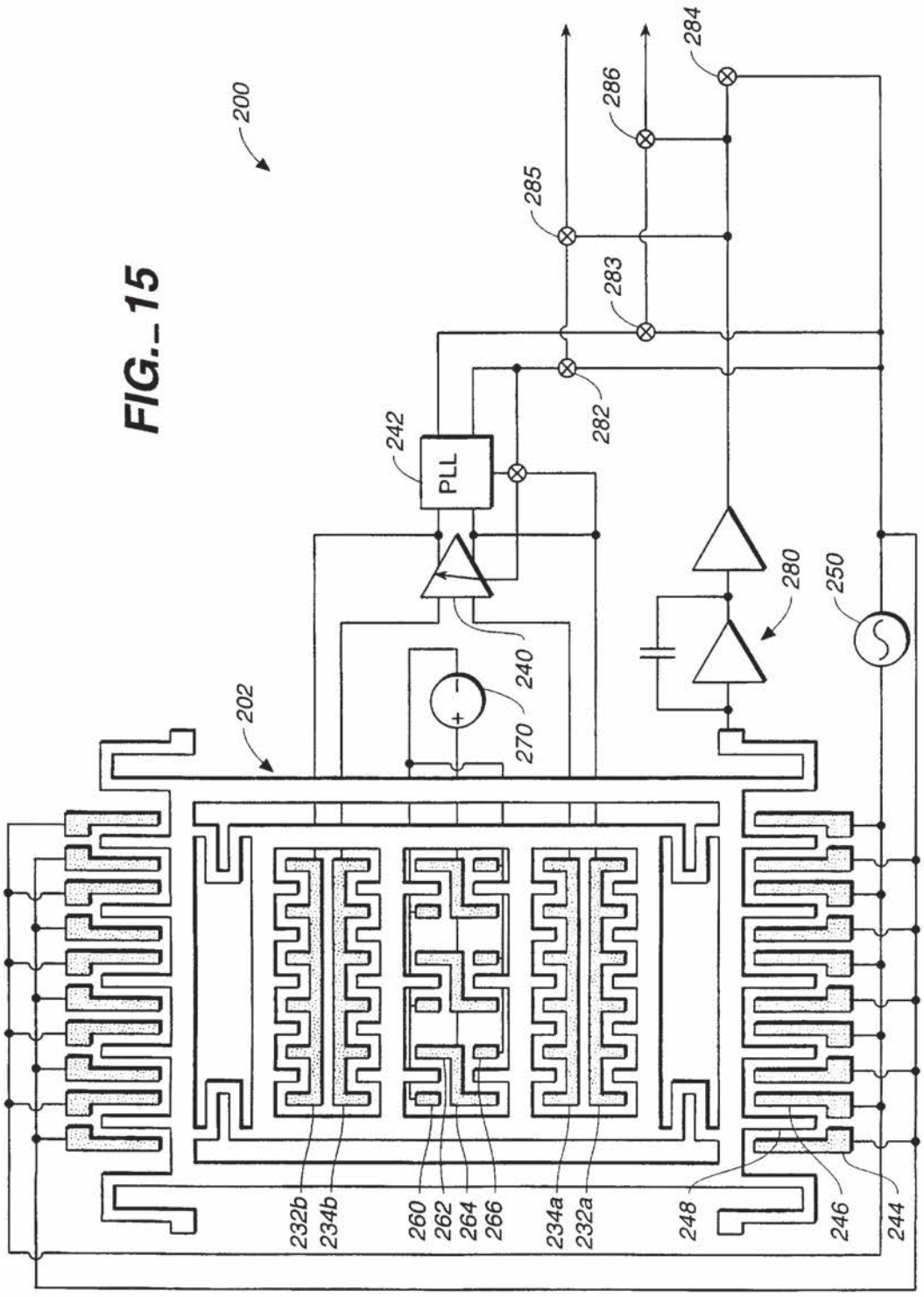


FIG._14

Nintendo Exhibit 1066
IPR2024-00668 - Page 362

FIG._15



Nintendo Exhibit 1066
IPR2024-00668 - Page 363

FIG._16

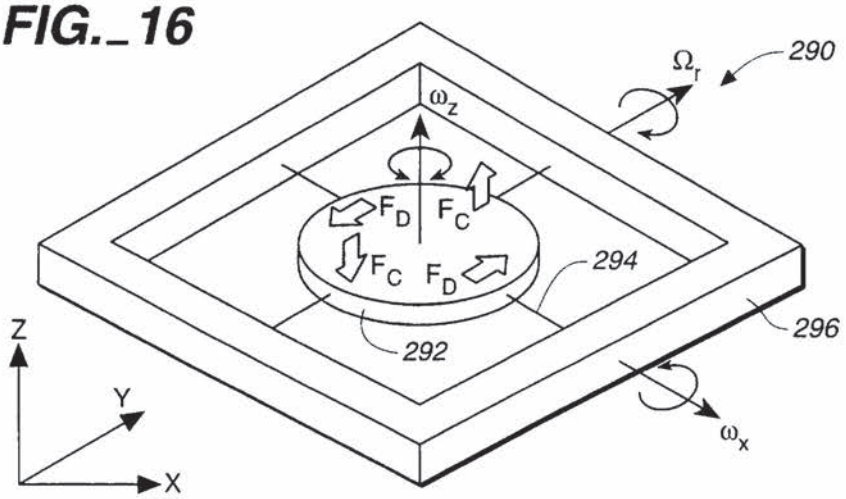
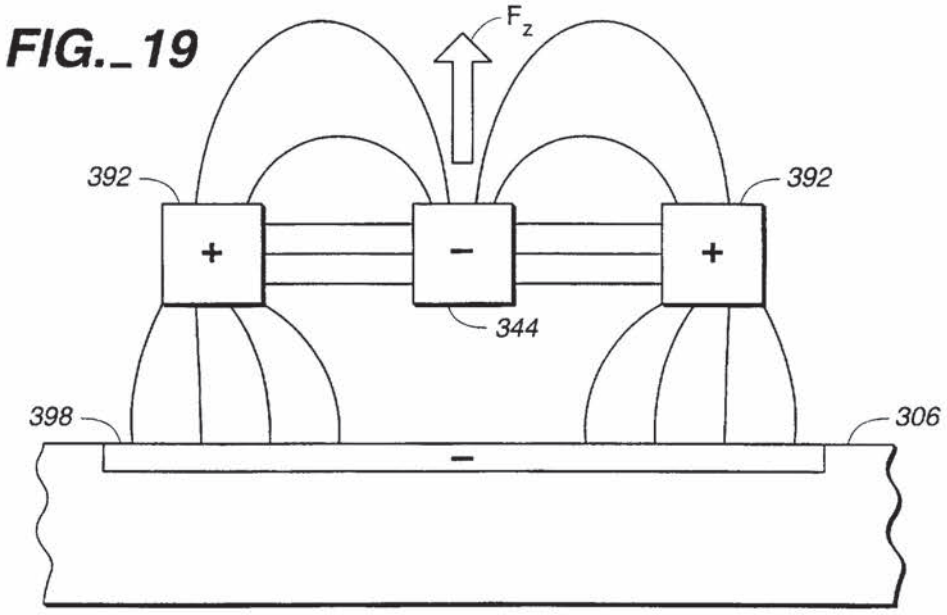
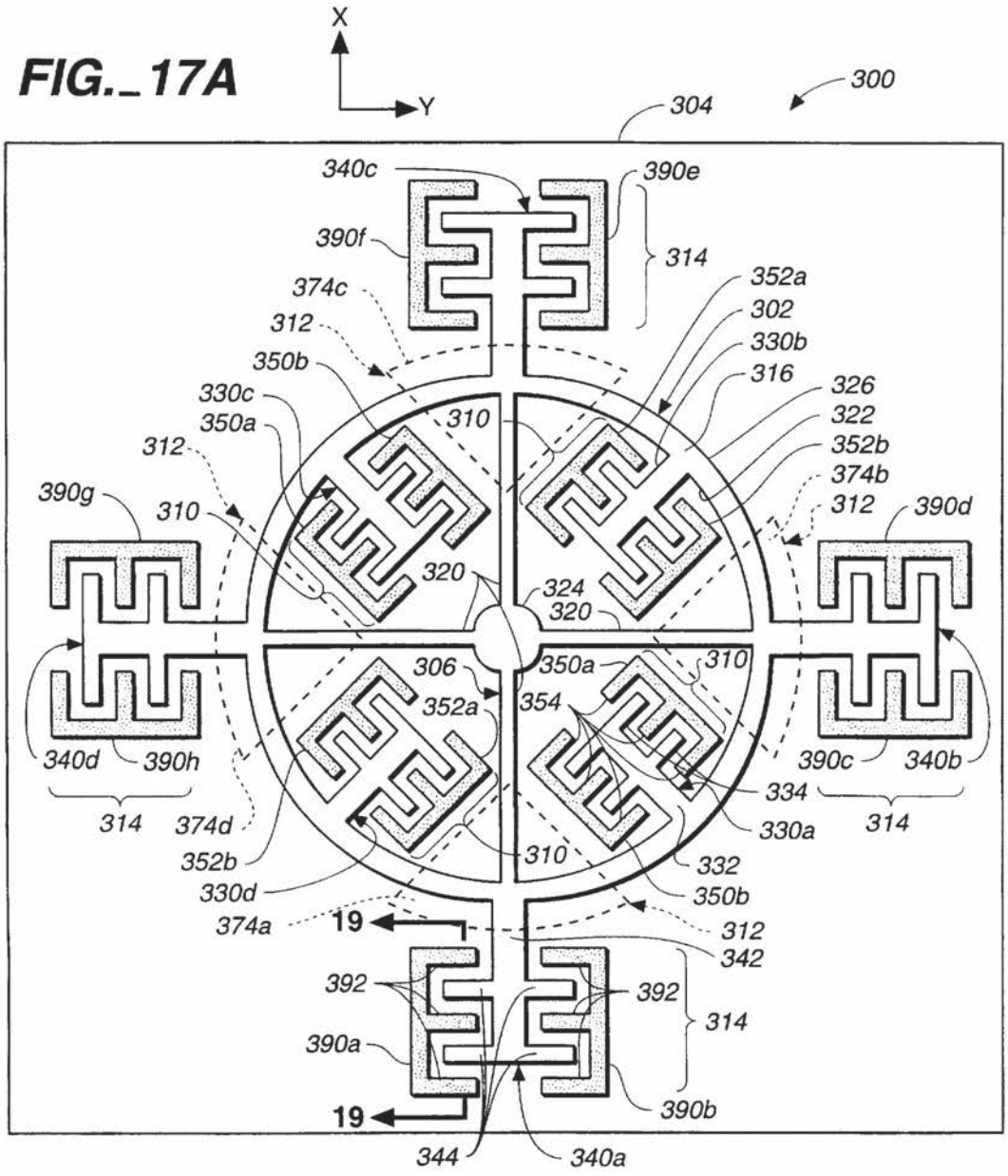


FIG._19



Nintendo Exhibit 1066
IPR2024-00668 - Page 364

FIG._17A



Nintendo Exhibit 1066
IPR2024-00668 - Page 365

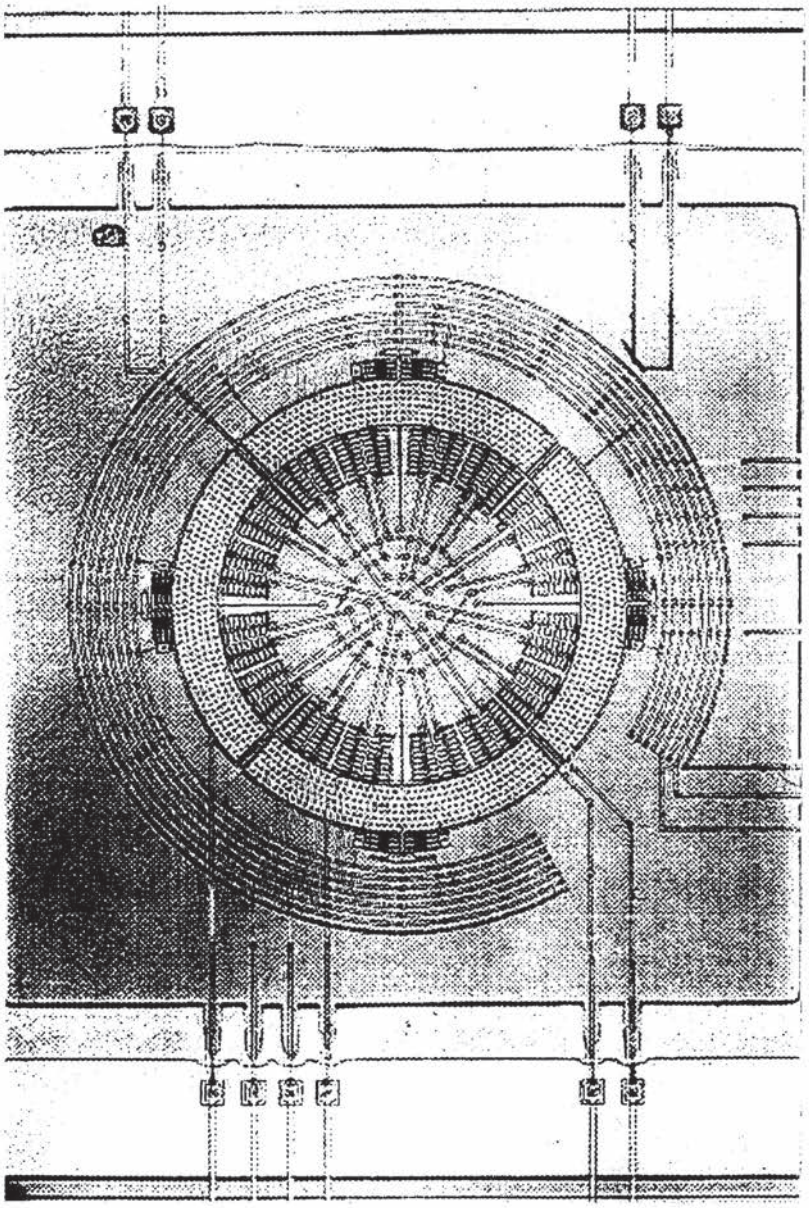
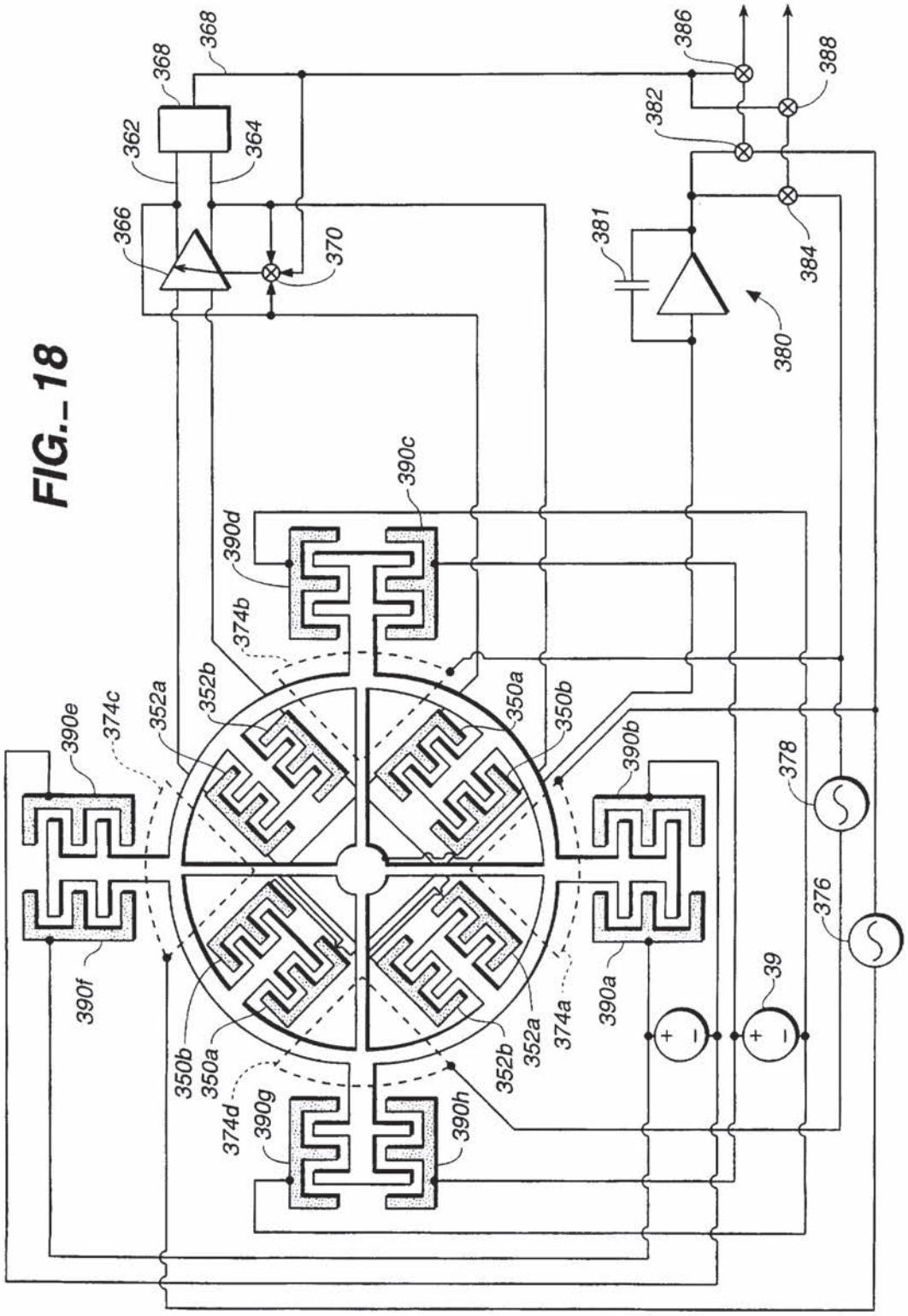


FIG._17B

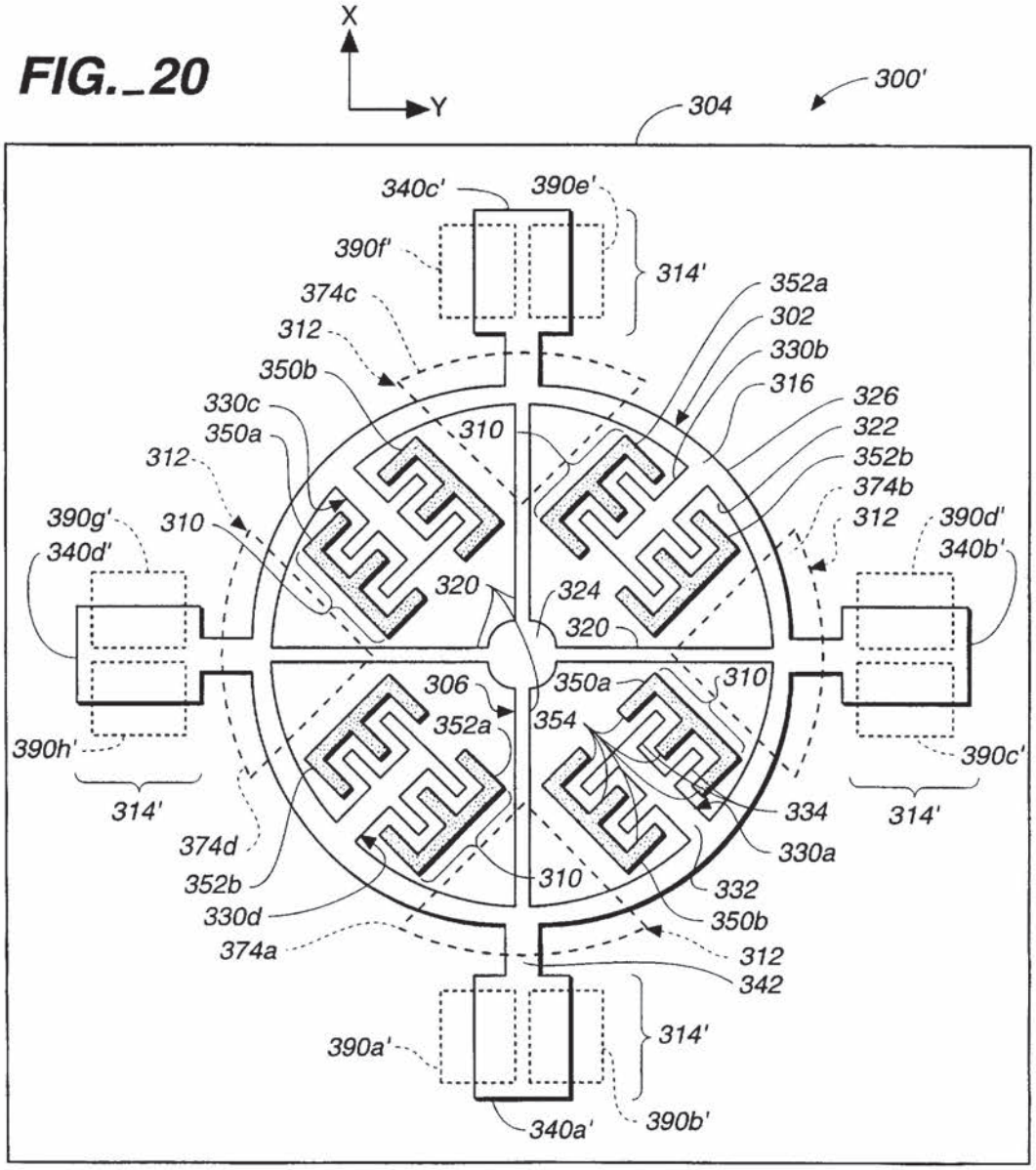
Nintendo Exhibit 1066
IPR2024-00668 - Page 366

FIG._18



Nintendo Exhibit 1066
IPR2024-00668 - Page 367

FIG._20



Nintendo Exhibit 1066
IPR2024-00668 - Page 368

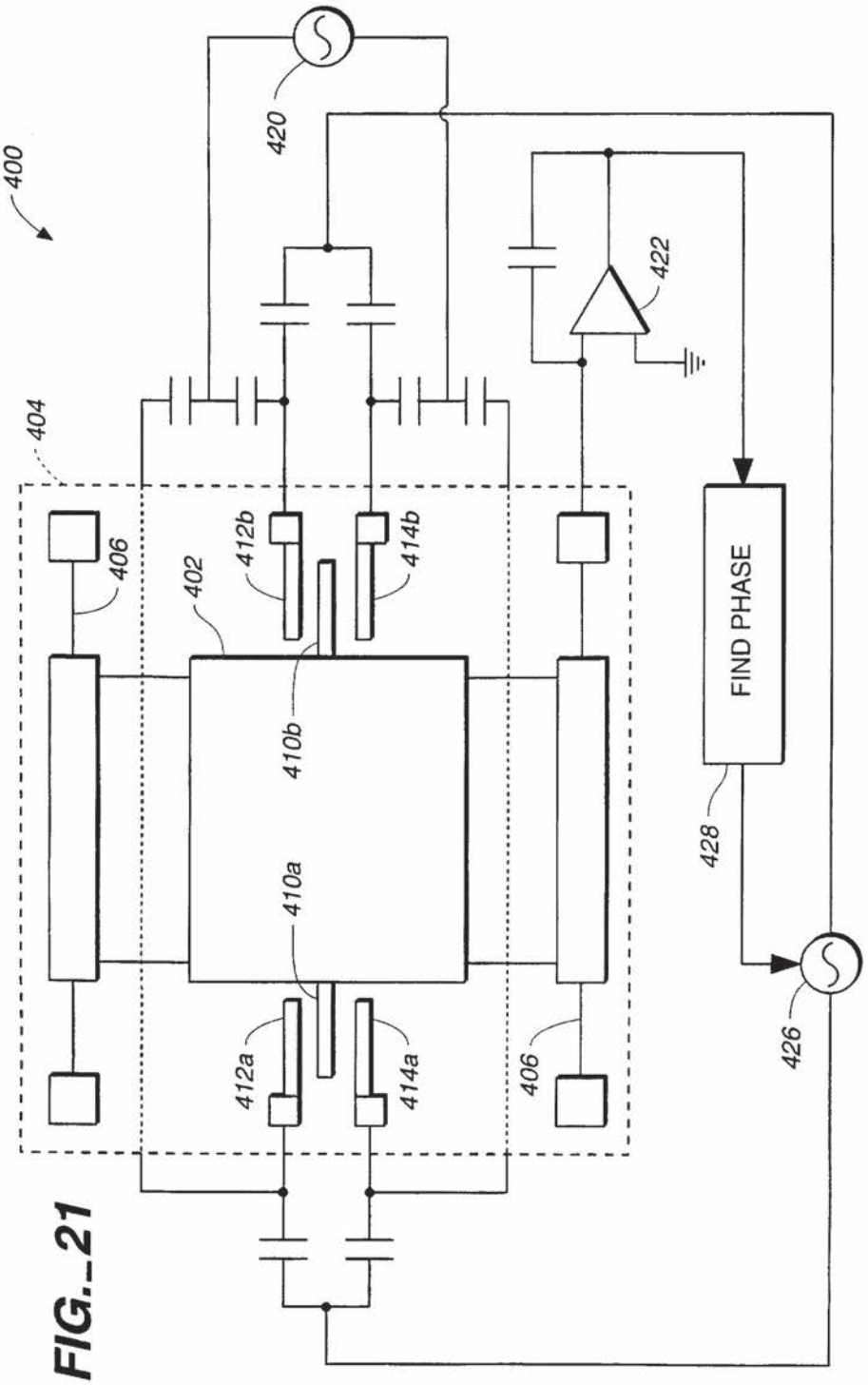


FIG._21

Nintendo Exhibit 1066
IPR2024-00668 - Page 369

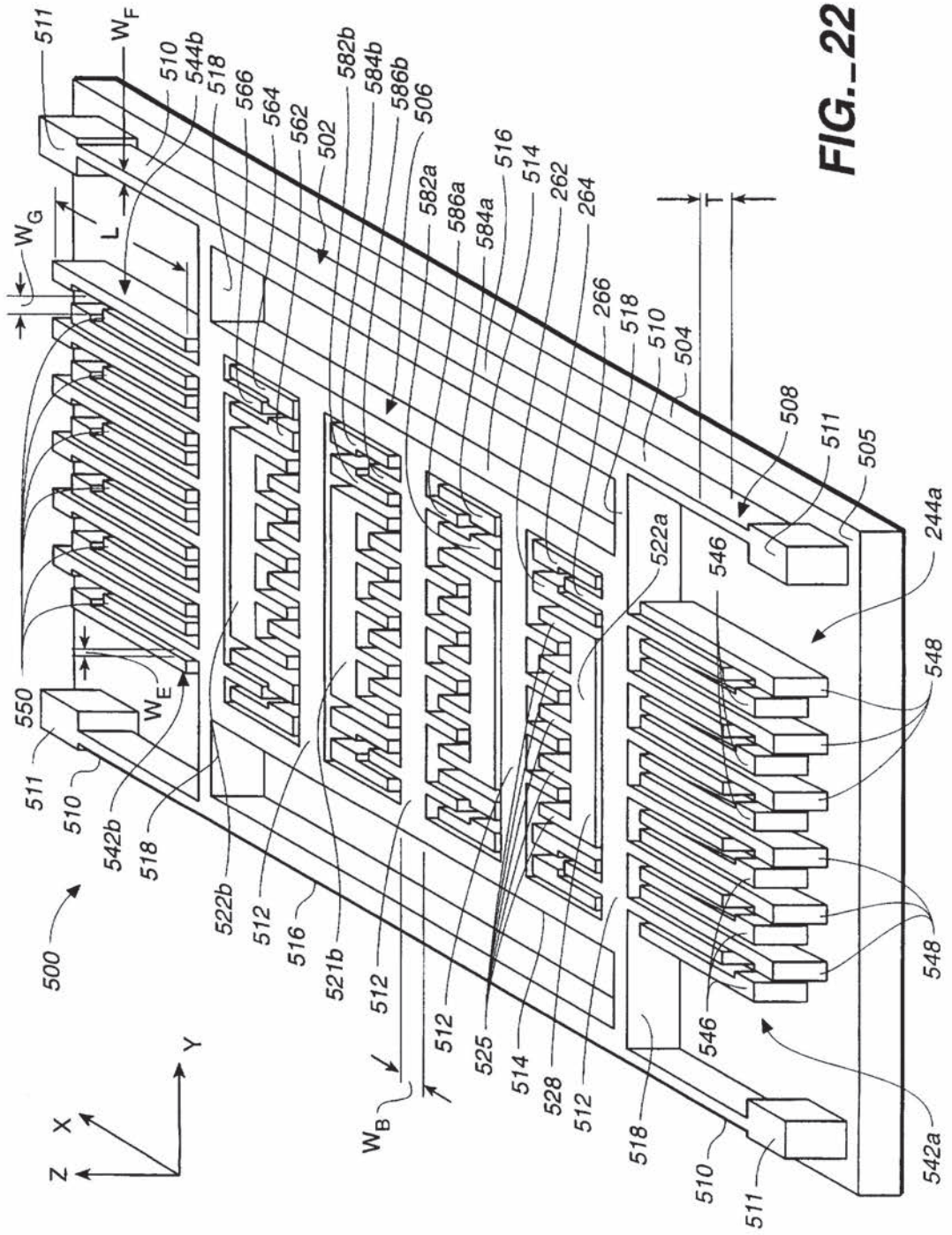


FIG._22

Nintendo Exhibit 1066
IPR2024-00668 - Page 370

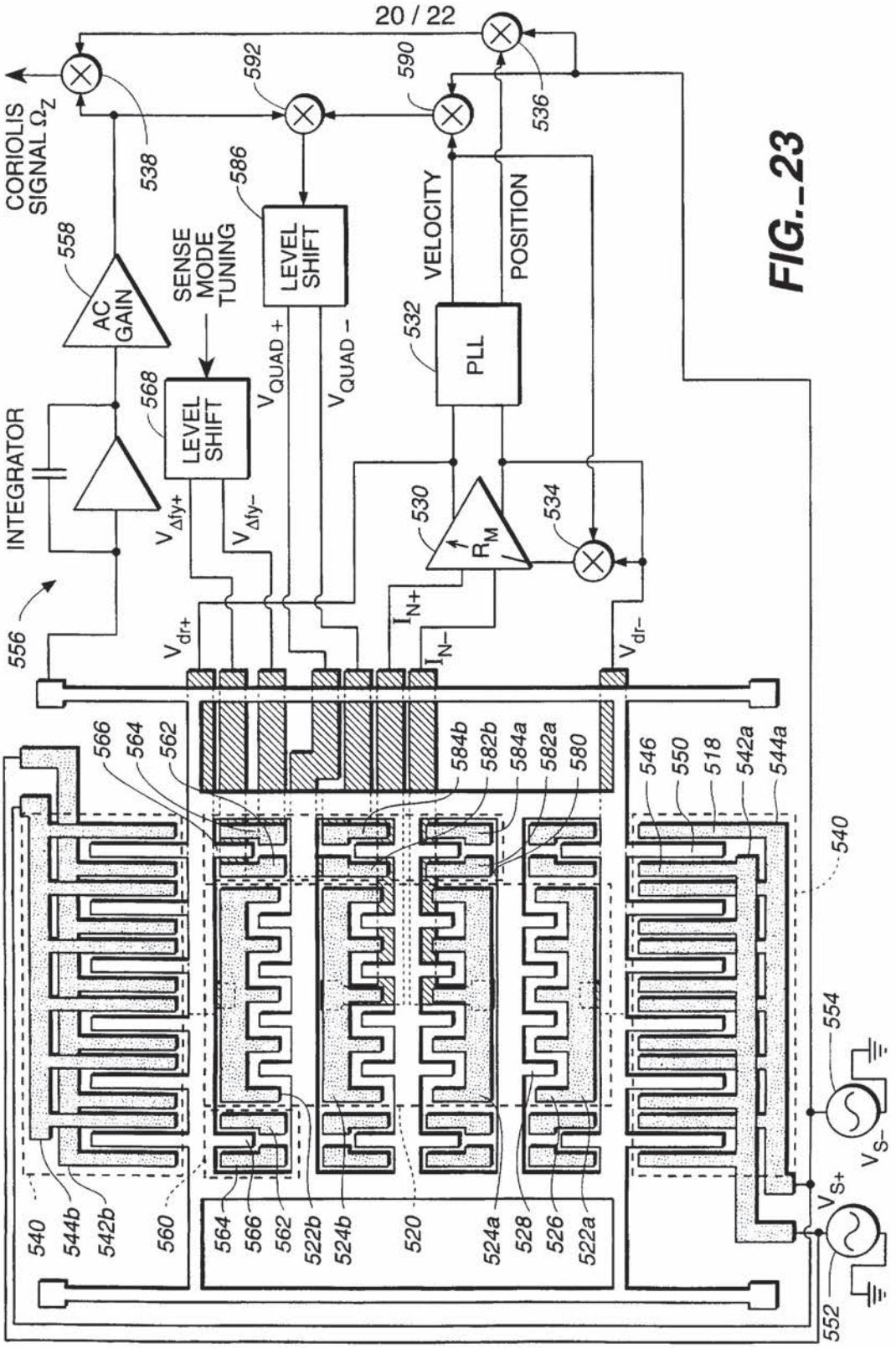


FIG._23

Nintendo Exhibit 1066
IPR2024-00668 - Page 371

FIG._24A

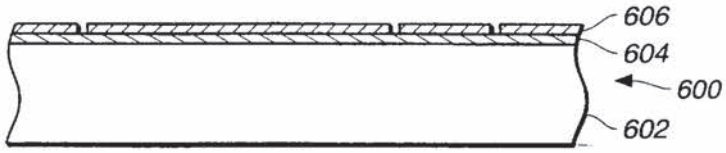


FIG._24B

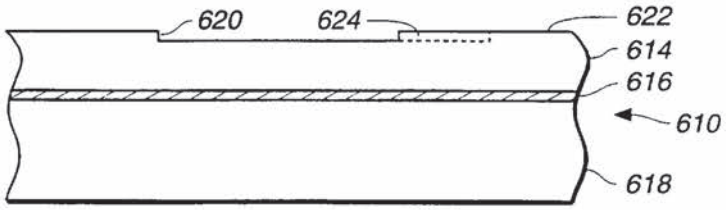


FIG._24C

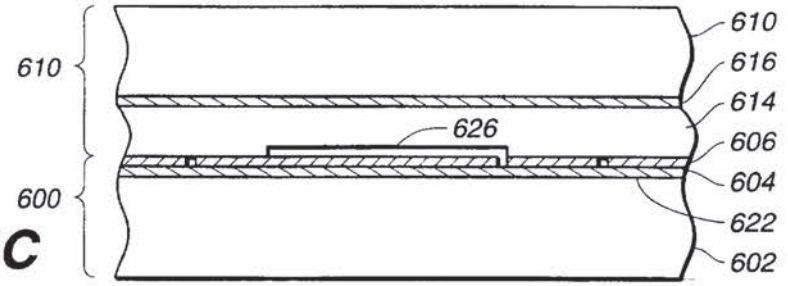


FIG._24D

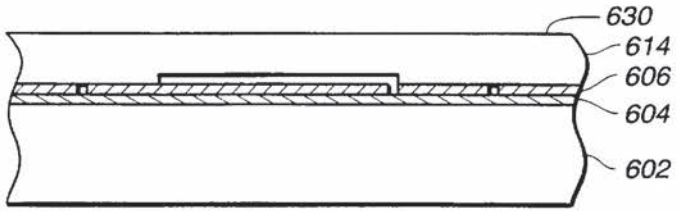
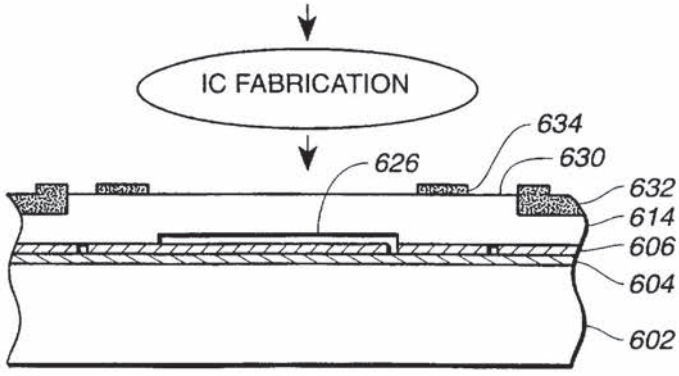


FIG._24E



Nintendo Exhibit 1066
IPR2024-00668 - Page 372

FIG._24F

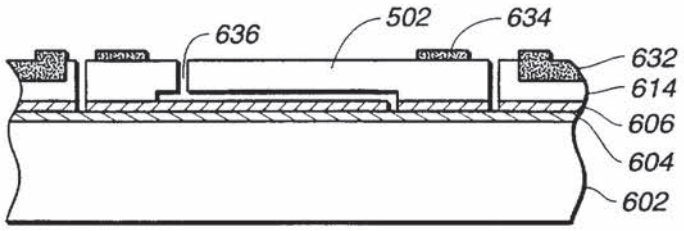
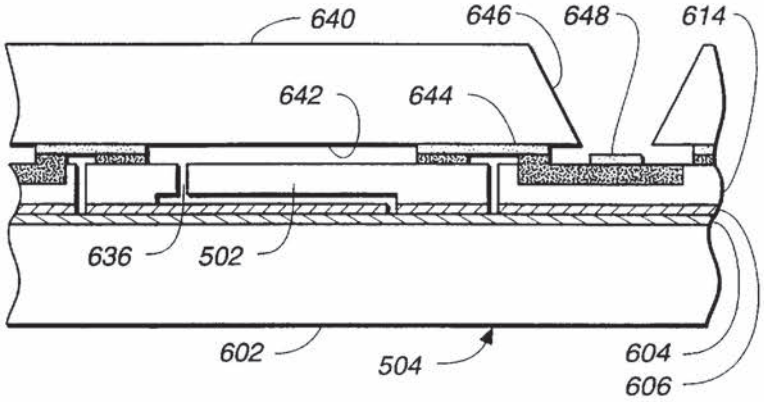


FIG._24G



Nintendo Exhibit 1066
IPR2024-00668 - Page 373

EXHIBIT 1057B

PCT WORLD INTELLECTUAL PROPERTY ORGANIZATION
International Bureau

INTERNATIONAL APPLICATION PUBLISHED UNDER THE PATENT COOPERATION TREATY (PCT)

(51) International Patent Classification 6 : G01C | A2

(11) International Publication Number: **WO 97/45699**

(43) International Publication Date: 4 December 1997 (04.12.97)

(21) International Application Number: PCT/US97/09150

(22) International Filing Date: 30 May 1997 (30.05.97)

(30) Priority Data:
08/658,924 31 May 1996 (31.05.96) US

(71) Applicant: THE REGENTS OF THE UNIVERSITY OF CALIFORNIA [US/US]; 21st floor, 300 Lakeside Drive, Oakland, CA 94612 (US).

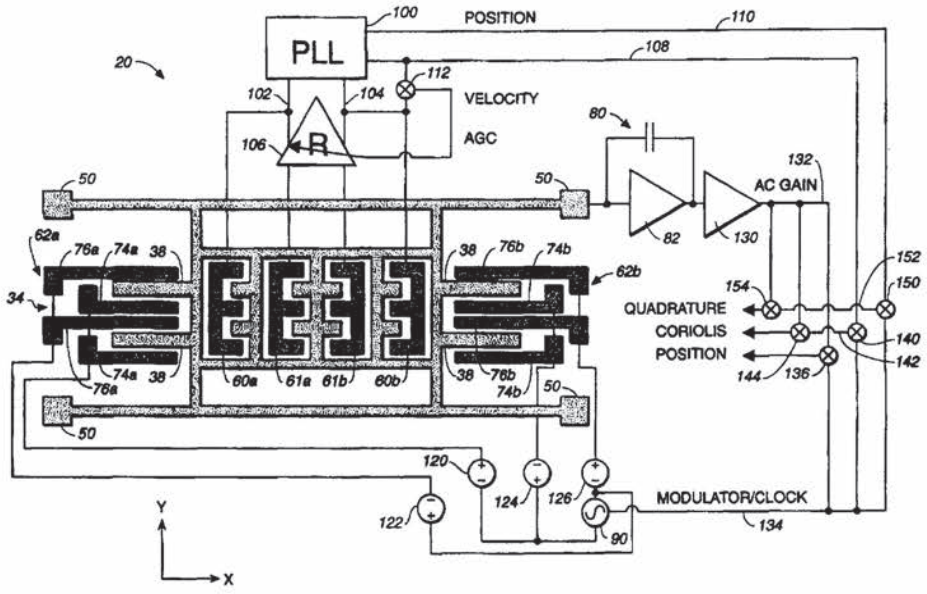
(72) Inventors: CLARK, William, A.; 35617 Pond Drive, Fremont, CA 94526 (US). JUNEAU, Thor; 1812 Delaware Street #201, Berkeley, CA 94709 (US). HOWE, Roger, T.; 3139 Sweetbriar Circle, Lafayette, CA 94549 (US).

(74) Agents: EGAN, William, J., III et al.; Fish & Richardson P.C., Suite 100, 2200 Sand Hill Road, Menlo Park, CA 94025 (US).

(81) Designated States: AL, AM, AT, AU, AZ, BA, BB, BG, BR, BY, CA, CH, CN, CU, CZ, DE, DK, EE, ES, FI, GB, GE, HU, IL, IS, JP, KE, KG, KP, KR, KZ, LC, LK, LR, LS, LT, LU, LV, MD, MG, MK, MN, MW, MX, NO, NZ, PL, PT, RO, RU, SD, SE, SG, SI, SK, TJ, TM, TR, TT, UA, UG, UZ, VN, YU, ARIPO patent (GH, KE, LS, MW, SD, SZ, UG), Eurasian patent (AM, AZ, BY, KG, KZ, MD, RU, TJ, TM), European patent (AT, BE, CH, DE, DK, ES, FI, FR, GB, GR, IE, IT, LU, MC, NL, PT, SE), OAPI patent (BF, BJ, CF, CG, CI, CM, GA, GN, ML, MR, NE, SN, TD, TG).

Published
Without international search report and to be republished upon receipt of that report.

(54) Title: MICROMACHINED VIBRATORY RATE GYROSCOPE



(57) Abstract

A microfabricated gyroscope to measure rotation about an axis parallel to the surface of the substrate. A voltage differential may be applied between pairs of electrode fingers to reduce the quadrature error. A microfabricated gyroscope includes a vibratory structure and interdigited electrodes having a high aspect ratio.

FOR THE PURPOSES OF INFORMATION ONLY

Codes used to identify States party to the PCT on the front pages of pamphlets publishing international applications under the PCT.

AL	Albania	**ES**	Spain	**LS**	Lesotho	**SI**	Slovenia
AM	Armenia	**FI**	Finland	**LT**	Lithuania	**SK**	Slovakia
AT	Austria	**FR**	France	**LU**	Luxembourg	**SN**	Senegal
AU	Australia	**GA**	Gabon	**LV**	Latvia	**SZ**	Swaziland
AZ	Azerbaijan	**GB**	United Kingdom	**MC**	Monaco	**TD**	Chad
BA	Bosnia and Herzegovina	**GE**	Georgia	**MD**	Republic of Moldova	**TG**	Togo
BB	Barbados	**GH**	Ghana	**MG**	Madagascar	**TJ**	Tajikistan
BE	Belgium	**GN**	Guinea	**MK**	The former Yugoslav Republic of Macedonia	**TM**	Turkmenistan
BF	Burkina Faso	**GR**	Greece			**TR**	Turkey
BG	Bulgaria	**HU**	Hungary	**ML**	Mali	**TT**	Trinidad and Tobago
BJ	Benin	**IE**	Ireland	**MN**	Mongolia	**UA**	Ukraine
BR	Brazil	**IL**	Israel	**MR**	Mauritania	**UG**	Uganda
BY	Belarus	**IS**	Iceland	**MW**	Malawi	**US**	United States of America
CA	Canada	**IT**	Italy	**MX**	Mexico	**UZ**	Uzbekistan
CF	Central African Republic	**JP**	Japan	**NE**	Niger	**VN**	Viet Nam
CG	Congo	**KE**	Kenya	**NL**	Netherlands	**YU**	Yugoslavia
CH	Switzerland	**KG**	Kyrgyzstan	**NO**	Norway	**ZW**	Zimbabwe
CI	Côte d'Ivoire	**KP**	Democratic People's Republic of Korea	**NZ**	New Zealand		
CM	Cameroon			**PL**	Poland		
CN	China	**KR**	Republic of Korea	**PT**	Portugal		
CU	Cuba	**KZ**	Kazakstan	**RO**	Romania		
CZ	Czech Republic	**LC**	Saint Lucia	**RU**	Russian Federation		
DE	Germany	**LI**	Liechtenstein	**SD**	Sudan		
DK	Denmark	**LK**	Sri Lanka	**SE**	Sweden		
EE	Estonia	**LR**	Liberia	**SG**	Singapore		

MICROMACHINED VIBRATORY RATE GYROSCOPE

Background of the Invention

The present invention relates generally to microfabricated sensors, and more particularly to microfabricated gyroscopic sensors.

Multi-axis sensors are highly desirable for inertial sensing of motion in three dimensions. Previously, such sensors were constructed of relatively large and expensive electromagnetic devices. More recently, micromechanical sensors have been fabricated using semiconductor processing techniques. Specifically, micromechanical accelerometers and gyroscopes have been formed from silicon wafers by using photolithographic techniques. Such microfabricated sensors hold the promise of large scale production and therefore low cost.

One objective in the construction of microfabricated sensors is to increase the sensitivity and improve the signal to noise ratio of the device. Another objective is to simplify the fabrication steps so as to reduce the cost and complexity and to increase the yield in the manufacturing process.

The integration of three gyroscopic sensors to measure the rotation rates about the three separate axes coupled with three accelerometric sensors to measure the acceleration along the three axes on a single chip would provide a monolithic, six degree-of-freedom inertial measurement system capable of measuring all possible translations and orientations of the chip.

It would be useful to provide a gyroscopic sensor to measure rotation about axes parallel to the surface of

a substrate on which the gyroscopic sensor was fabricated. It would also be useful to provide a gyroscopic sensor with reduced noise.

Summary of the Invention

In one aspect, the invention is directed to a gyroscopic sensor including a substrate, a mass connected to the substrate by a suspension system, a drive system to cause the mass to vibrate along a drive axis substantially parallel to a surface of the substrate, and a position sensor to measure a deflection of the mass along a sense axis substantially parallel to the surface of the substrate. Rotation of the mass about an axis of rotation substantially perpendicular to the surface of the substrate and vibration of the mass along the drive axis generates a Coriolis force to deflect the mass along the sense axis.

Implementations of the invention include the following. A processor may be coupled to an output of the position sensor to generate a signal varying with the rate of rotation of the mass about the axis of rotation. The gyroscopic sensor may include a first sense electrode projecting from the mass, a second sense electrode connected to the substrate and positioned on a first side of the first electrode, and a third sense electrode connected to the substrate and positioned on an opposing second side of the first electrode. The position sensor may sense a change in capacitance between the first electrode and the second and third electrodes. The first, second and third electrodes may be substantially coplanar and each electrode has a longitudinal axis substantially aligned with the drive axis. The drive system may include a first drive electrode projecting

from the mass, a second drive electrode connected to the substrate and positioned on a first side of the first electrode, and a third drive electrode connected to the substrate and positioned on an opposing second side of the first electrode. An alternating voltage may be applied between the between the first electrode and the second and third electrodes. A voltage source may apply a voltage between a plurality of correction electrodes connected to the substrate to cause the mass to vibrate, absent the Coriolis force, more precisely along the drive axis. A voltage source may apply a voltage between a first tuning electrode connected to the substrate and a second tuning electrode connected to the mass to adjust a resonant frequency of vibrations of the mass along the sense axis.

In another aspect, the invention is directed to a method of sensing rotation with a gyroscopic sensor including a mass connected to a substrate by a suspension system. The mass is rotated about an axis of rotation and the mass is caused to vibrate substantially along a drive axis. Rotation of the mass about the axis of rotation and vibration of the mass along the drive axis generates a Coriolis force to deflect the mass along a sense axis. A deflection of the mass along the sense axis is measured, and a voltage is applied between electrode fingers connected to the substrate to cause the mass to vibrate, absent a Coriolis force, more precisely along the first axis.

In another aspect, the present invention is directed to a microfabricated structure. The structure comprises a substrate, a mass connected to the substrate by a suspension system to vibrate in a plane parallel to a surface of the substrate, and three pluralities of

electrode fingers. The first plurality of electrode fingers projects from the mass along a first axis in the plane. The second and third plurality of electrode fingers, electrically isolated from each other, are coplanar with the first plurality of electrode fingers, are connected to the substrate and project substantially along the first axis. The first, second and third plurality of electrode fingers are interdigitated such that each of the first plurality of electrode fingers is adjacent to one of the second plurality of electrode fingers and one of the third plurality of electrode fingers.

Implementations include the following features. A voltage source may apply a voltage between the second and third plurality of electrode fingers. The structure may further comprise a fourth plurality of electrode fingers, coplanar with the first, second and third plurality of electrode fingers, projecting from the mass along the first axis, and a fifth plurality of electrode fingers connected to the substrate but electrically isolated from the second and third plurality of electrode fingers, the fourth and fifth plurality of electrode fingers being interdigitated. Each of the first plurality of electrode fingers may be longer than each of the fourth plurality of electrode fingers.

In another aspect, the invention is directed to a microfabricated structure. The structure comprises a substrate and a suspension system to permit a mass to vibrate in a plane parallel to a surface of the substrate. The suspension system includes first and second substantially parallel beams, each of the first and second beams anchored at both ends to the substrate, and third and fourth substantially parallel beams, one

end of each of the third and fourth beams connected to the first beam and another end connected to the second beam.

Implementations include the following features. The structure may include a plurality of fingers projecting along an axis substantially parallel to the first and second beams. The structure may comprise a fifth and a sixth beam one end of each of the fifth beam and sixth beams connected to the third beam and another end connected to the fourth beam, and a seventh beam, one end of the seventh beam connected to the fifth beam and another end connected to the sixth beam. The structure may further comprise a plurality of fingers projecting from the seventh beam along an axis substantially parallel to the first and second beams. Sections of the first and second beams located between the third and fourth beams may be substantially rigid to prevent rotation of the mass.

In another aspect, the invention is directed to a sensor. The sensor comprises a substrate, a mass connected to the substrate by a suspension system to vibrate in a plane parallel to a surface of the substrate, and three pluralities of electrode fingers. The first plurality of electrode fingers projects from the mass along a first axis in the plane. The second and third plurality of electrode fingers, are connected to the substrate and project substantially along the first axis. the first, second and third plurality of electrode fingers are interdigitated such that each of the first plurality of electrode fingers is adjacent to one of the second plurality of electrode fingers and one of the third plurality of electrode fingers. A voltage source applies a first DC voltage between the second and third

plurality of electrode fingers to cause the mass to vibrate, absent a Coriolis force, more precisely along the first axis.

Implementations may include the following features. A set of electrode fingers may be positioned opposing the three pluralities of electrode fingers, and a second voltage source for may apply a second DC voltage between a fifth and sixth plurality of electrode fingers to cause the mass to vibrate, absent a Coriolis force, more precisely along the first axis. The second DC voltage may be substantially equal in magnitude but opposite in sign to the first DC voltage. The first plurality of electrode fingers may be electrically coupled to the second plurality of electrode fingers. The sensor may include a voltage source for applying a third DC voltage between the first and third pluralities of electrode fingers and the second, third, fifth and sixth pluralities of electrode fingers to adjust the resonant frequency of vibrations of the mass along a second axis in the plane perpendicular to the first axis.

In another aspect, the invention is directed to a sensor. The sensor comprises a substrate, a mass connected to the substrate by a suspension system to vibrate in a plane parallel to a surface of the substrate, and three pluralities of electrode fingers. The first plurality of electrode fingers projects from the mass along a first axis in the plane. The second and third plurality of electrode fingers, are connected to the substrate and project substantially along the first axis. the first, second and third plurality of electrode fingers are interdigitated such that each of the first plurality of electrode fingers is adjacent to one of the second plurality of electrode fingers and one of the

third plurality of electrode fingers. A voltage source applies a DC voltage between the first plurality of electrode fingers and the second and third plurality of electrode fingers to adjust the resonant frequency of vibrations of the mass along a second axis in the plane perpendicular to the first axis.

In another aspect, the invention is directed to a gyroscope for sensing rotation about a Z-axis. The gyroscope comprises a substrate, a mass connected to the substrate by a suspension system to vibrate in a plane parallel to a surface of the substrate, a drive system to cause the mass to vibrate substantially along a first axis in the plane, and three pluralities of electrode fingers. The first plurality of electrode fingers projects from the mass along a first axis in the plane. The second and third plurality of electrode fingers, are connected to the substrate and project substantially along the first axis. The first, second and third plurality of electrode fingers are interdigitated such that each of the first plurality of electrode fingers is adjacent to one of the second plurality of electrode fingers and one of the third plurality of electrode fingers. A position sensor is coupled to the first plurality of electrode fingers for measuring the deflection of the mass along a second axis in the plane perpendicular to the first axis. Rotation of the mass about a Z-axis perpendicular to the surface and vibration of the mass along the first axis generates a coriolis force to deflect the mass along the second axis. A signal processor is coupled to an output of the position sensor to generate a signal varying with the rate of rotation of the mass about the Z-axis.

Implementations include the following features. A voltage source may apply an AC voltage having a first frequency between the second and third plurality of electrode fingers. A voltage may be applied between the second and third pluralities of electrode fingers to form a capacitive bridge with the first plurality of electrodes, and the position sensor may be coupled to the first plurality of electrodes to detect changes in capacitance when the mass is deflected along the second axis. The sensor may includes an integrator to integrate a signal from the first plurality of electrode fingers. The drive system may generate a signal to cause the mass to oscillate along the first axis at a second frequency. The drive system may include a phase-locked loop to prevent phase-shifting of the signal. The sensor may include a first mixer to mix the signal from the drive system with a signal from the voltage source. The sensor may include a second mixer to mix a signal from the first mixer with an output signal from the position sensor to produce a position quadrature signal or coriolis signal. The sensor may include a mixer to mix an output signal from the position sensor with a signal from the voltage source to produce a position signal.

In another aspect, the invention is directed to a microfabricated gyroscopic sensor for measuring rotation about an input axis. The gyroscopic sensor includes a substrate, a mass, and a suspension system connecting the mass to the substrate. A drive system causes the mass to oscillate substantially about a drive axis, and a position sensor measures a rotation of the mass about a sense axis. Rotation of the mass about the input axis and oscillation of the mass about the drive axis generates a Coriolis force to oscillate the mass about

the sense axis. A voltage source to apply a voltage between a plurality of electrodes associated with the substrate to cause the mass to oscillate, in the absence of the Coriolis force, more precisely about the drive axis.

Implementations of the invention include the following. A processor may be coupled to an output of the position sensor to generate a signal varying with the rate of rotation of the mass about the axis of rotation. A second voltage source may apply a second voltage between electrodes connected to the mass and the electrodes connected to the substrate to adjust a resonant frequency of oscillations of the mass about the sense axis. The drive axis may be substantially perpendicular to the surface of the substrate and the axis of rotation and sense axis are substantially parallel to a surface of the substrate. The mass may be substantially ring-shaped. First and second pluralities of electrode fingers may project from the mass, and third and fourth pluralities of electrode fingers projecting from the substrate and be interdigitated with the first and second pluralities of electrode fingers. The fourth plurality of electrode fingers may be positioned opposing the first plurality of electrode fingers. Fifth, sixth, seventh and eighth pluralities of electrode fingers may be similarly disposed, and the pluralities of electrode fingers are substantially co-planar. The voltage source may apply a first DC voltage between the third plurality and the fourth plurality of electrode fingers and second DC voltage, which is substantially equal in magnitude and opposite in sign, between the seventh plurality and the eighth plurality of electrode fingers.

In another aspect, the invention is directed to a method of sensing rotation with a gyroscopic sensor including a mass connected to a substrate by a suspension system. The method includes rotating the mass about an input axis and causing the mass to oscillate substantially about a drive axis. The rotation of the mass about the input axis and the oscillation of the mass about the drive axis generates a Coriolis force to oscillate the mass about a sense axis. An oscillation of the mass about the sense axis is measured, a voltage is applied between electrodes associated with the substrate to cause the mass to oscillate, in the absence of a Coriolis force, more precisely about the drive axis.

In another aspect, the invention is directed to a microfabricated gyroscopic sensor. The gyroscopic sensor includes a substrate having a first plurality of electrode teeth, a vibratory structure including a second plurality of electrode teeth and a suspension system connecting the second plurality of electrode teeth to the substrate, the second plurality of electrode teeth interdigited with the first plurality of electrode teeth, a drive system to cause the vibratory structure to oscillate relative to the substrate, and a position sensor to measure a deflection of the mass caused by a Coriolis force. The first and second pluralities of electrode teeth have thicknesses substantially greater than their widths.

Implementations of the invention include the following. The suspension system may include a plurality of flexures having an aspect ratio of at least about 10:1. The first and second pluralities of electrode teeth may have an aspect ratio of at least 5:1 and may be separated by gaps having an aspect ratio of at least

10:1.

In another aspect, the invention is directed to a method of fabricating a gyroscopic sensor. An insulative layer is formed on a first substrate, a recess is formed in a first surface of a second substrate, and the first surface of the second substrate is bonded to the first substrate so that the recess defines an enclosed cavity between the first and second substrates. Circuitry for the gyroscopic sensor is formed on a second surface of the second substrate, and a plurality of trenches are etched in the second substrate from the second surface to the cavity, the plurality of trenches defining a vibratory structure connected to the first substrate.

Implementations of the invention include the following. The vibratory structure may have a thickness of at least 25 microns and the recess may have a depth of about 1 micron. The etching step may comprise a deep reactive ion etch.

Advantages of the invention include the following. The gyroscopic sensor measures rotation about an axis parallel to the surface of the substrate. The gyroscopic sensor has reduced quadrature error. The gyroscopic sensor may include a vibratory structure and interdigited electrodes with a high aspect ratio. The gyroscopic sensor has a significantly reduced noise level.

Other advantages and features of the invention will be apparent from the description which follows, including the drawings and claims.

Brief Description of the Drawings

FIG. 1 is an schematic illustration of a spring-mass system which is equivalent to an electrostatic gyroscope.

FIG. 2 is a schematic perspective view of a microfabricated gyroscopic sensor according to the present invention.

FIG. 3 is a schematic top view of the movable elements of the gyroscopic sensor of FIG. 2.

FIG. 4 is a schematic top view of the fixed elements of the gyroscopic sensor of FIG. 2.

FIG. 5 is a schematic top view of the drive system of the gyroscopic sensor of FIG. 2.

FIG. 6 is a schematic top view of the sensing system of the gyroscopic sensor of FIG. 2.

FIGS. 7A-7C are schematic illustrations of the motion of the proof mass under the influence of the Coriolis acceleration and quadrature error.

FIG. 8A is a schematic circuit diagram of an integrator used to measure the position of the proof mass in the gyroscopic sensor of FIG. 2.

FIG. 8B is a schematic circuit diagram in which the integrator of FIG. 8A is replaced by a voltage buffer.

FIG. 8C is a schematic circuit diagram in which the integrator of FIG. 8A uses a subthreshold metal oxide semiconductor field effect transistor.

FIG. 9 is a schematic illustration of the signal processing circuitry of a gyroscopic sensor according to the present invention.

FIG. 10 is a photograph of a fabricated gyroscopic sensor.

FIG. 11 is a graph illustrating the response of the gyroscopic sensor to rotation about the Z-axis.

FIG. 12 is a graph illustrating the response of the Y-axis resonant frequency to an applied bias voltage.

FIG. 13 is a graph illustrating the response of the quadrature error to an applied voltage differential.

FIG. 14 is a schematic top view of a gyroscopic sensor in which the sensing, driving and quadrature correcting functions are performed by different electrode structures.

FIG. 15 is a schematic of the circuitry of the gyroscopic sensor of FIG. 14.

FIG. 16 is a schematic illustration of a spring-mass system which is equivalent to a dual-axis electrostatic gyroscope.

FIG. 17A is a schematic top view of a dual-axis gyroscopic sensor according to the present invention.

FIG. 17B is a photograph of a fabricated dual-axis gyroscopic sensor.

FIG. 18 is a schematic illustration of the electronic circuitry of the dual-axis gyroscopic sensor of FIG. 17A.

FIG. 19 is a cross-sectional view along line 19-19 of FIG. 17A schematically illustrating the field lines generated by the quadrature correction electrodes.

FIG. 20 is a schematic top view of a dual-axis gyroscopic sensor in which the quadrature correction system includes electrode plates.

FIG. 21 is a schematic illustration of the circuitry of a gyroscopic sensor in which the sensing, driving and quadrature functions are combined in a single electrode structure.

FIG. 22 is a schematic perspective view of a gyroscopic sensor fabricated with a high-aspect-ratio vibratory structure.

FIG. 23 is a schematic circuit diagram of the signal processing circuitry of the gyroscopic sensor of FIG. 22.

FIGS. 24A-24G are schematic cross-sectional views illustrating steps in the fabrication of the gyroscopic sensor of FIG. 22.

Description of the Preferred Embodiments

Referring to FIG. 1, a Z-axis vibratory rate gyroscope functions by generating and sensing Coriolis acceleration. The functional operation of the Z-axis vibratory rate gyroscope of the present invention is illustrated by an equivalent spring-mass system. In a vibratory rate gyroscope 10, a proof mass 12 is supported by a flexible suspension 14 from a rigid frame 16. Proof mass 12 is oscillated along the X-axis (the drive mode) by a drive force F_D as the frame rotates about the Z-axis. The combination of rotation and oscillation generates a Coriolis force F_c along the Y-axis on the oscillating proof mass. The Coriolis acceleration is detected as a deflection of the proof mass along the Y-axis (the sense mode).

Referring to FIG. 2, a micromachined gyroscopic sensor 20 designed according to the present invention includes microelectromechanical sense element or proof mass 22 connected to a rigid frame or substrate 24. The gyroscopic sensor 20 measures the Z-axis vibratory rate, i.e., the rotation of the substrate about the axis normal to the micromachined surface 26 of substrate 24. The micromachined gyroscopic sensor 20 includes three major

elements: a suspension system 30, a drive system 32 used to sustain oscillation of proof mass 22 along the X-axis, and a sensing system 34 used both to detect deflections of proof mass 22 along the Y-axis and to apply electrostatic forces to cancel any quadrature error, as will be described in detail below.

Referring to FIG. 3, suspension system 30 may be formed integrally with proof mass 22. Suspension system 30 supports the proof mass so that it may vibrate in a plane parallel to surface 26. Suspension system 30 holds proof mass 22, for example, about two microns above the surface of the substrate. The total mass of proof mass 22 may be about 0.1 to 0.3 micrograms. Suspension system 30 is generally H-shaped, with two parallel beams 40 and 42 positioned generally along the X-axis. Each beam may be about 500 to 1000 microns in length, specifically about 800 microns in length. The end of each beam is connected to an anchor 44 which connects the suspension system to the substrate (see FIG. 2). The end of each beam 40, as shown in FIG. 2, may include a folded or J-shaped flexure 45 (see FIG. 3). Alternately, beams 40 and 42 may be linear.

Two beams or crossbars 46 and 48 connect beam 40 to beam 42. Crossbars 46 and 48 may be about eight-hundred microns long, and are positioned to trisect beams 40 and 42. Two cross-beams 50 and 52 connect crossbars 46 and 48. A third beam or crossbar 54 may connect the center of cross-beam 50 to the center of cross-beam 52. The flexible elements of suspension system 30 are constructed of polysilicon and, for example, have a width and a thickness on the order of two microns. The anchors may be about eight microns square.

The suspension system 30 is designed to be flexible along the X-axis and Y-axis, and as rigid as possible to other modes of vibration. In particular, the suspension system must be substantially rigid to rotation about the Z-axis, as small rotations may degrade the performance of the gyroscopic sensor. Large deflections may also result in the movable electrode fingers crashing into the stationary electrode fingers. The suspension system provides the necessary translational compliance while maintaining rotational rigidity by thickening the portions of beams 40 and 42 located between crossbars 46 and 48 to form trusses 41 and 43. Trusses 41 and 43 may have a width three to four times the width of the remainder of the beams, i.e., about six to eight microns. The portions of crossbars 46, 48 and 54 from which fingers project may have a width of approximately four microns.

The proof mass 22 also includes a plurality of finger electrodes (or simply fingers) which are used to drive and sense oscillations of proof mass along the X-axis and Y axis. A plurality of long fingers 38 project outwardly along the X-axis from crossbars 46 and 48, and a plurality of short fingers or stubs 39 project inwardly along the X-axis from crossbars 46, 48 and 54. The crossbars 46 and 48 form the spines, and long fingers 38 form the prongs of two movable sensing electrodes 56. Similarly, crossbars 46, 48 and 54 form the spines, and short fingers 39 form the prongs of two movable driving electrodes 58 and two movable feedback electrodes 59. The short fingers 39 may be about ten to twenty-five microns in length, specifically fifteen microns in length, whereas the long fingers 38 may be about one-

hundred to two-hundred microns in length, specifically one-hundred and fifty microns in length.

Referring to FIG. 4, one or more stationary driving electrodes, one or more stationary feedback electrodes, and one or more stationary sensing electrodes may be rigidly connected to substrate 24. For example, two stationary driving electrodes 60a, 60b may be arranged relative to each other in an opposing configuration. Similarly, two stationary feedback electrodes 61a, 61b may face each other in an opposing configuration. Each stationary driving electrode 60a, 60b and each stationary feedback electrode 61a, 61b includes a plurality of short fingers 66. Stationary driving and feedback electrodes 60a, 60b and 61a, 61b may have a few to dozens of fingers. Short fingers 66 may have a length of approximately 15 microns and a width of approximately three to six microns. The width, for example, may be four microns.

Two stationary sensing electrodes 62a, 62b may face each other in an opposing configuration. Stationary sensing electrodes 62a, 62b include a plurality of long fingers 70. Each long finger 70 protrudes from a base 72. The fingers of stationary sensing electrode 62a are arranged in pairs, each pair including a right finger 74a and a left finger 76a. Similarly, the fingers of stationary electrode 62b are arranged in pairs, each pair including a right finger 74b and a left finger 76b. Each long finger 70 may be approximately one hundred and fifty microns in length, and have a width of approximately four microns.

Referring to FIG. 5, drive system 32 includes movable and stationary driving electrodes 58 and 60a, 60b, and movable and stationary feedback electrodes 59

and 61a, 61b. One set of short fingers 39 is interdigitated with short fingers 66 of stationary driving electrodes 60a, 60b. Another set of short fingers 39 is interdigitated with short fingers 66 of stationary feedback electrodes 61a, 61b. Short fingers 39 of movable electrodes 58 and 59, and short fingers 66 of stationary electrodes 60a, 60b and 61a, 61b may be formed from the same layer of polysilicon prior to the removal of the sacrificial layer so that the fingers may be co-planar.

The driving electrodes of drive system 32 act as electrical-mechanical transducers. By the application of an alternating voltage between stationary driving electrodes 60a, 60b and movable driving electrodes 58, proof mass 22 may be forced to oscillate or reciprocate along the X-axis. The motion along the X-axis induces bending in crossbars 46 and 48 so that proof mass 22 may move toward and away from stationary driving electrodes 60a, 60b. A more detailed explanation of the manner of operating drive system 32 in order to sustain oscillations in proof mass 22 may be found in U.S. Pat. No. 5,025,346, issued June 18, 1991 to Tang et al., entitled Laterally Driven Resonant Microstructures, and assigned to the assignee of the present invention, the entire disclosure of which is incorporated herein by reference; and in U.S. Pat. No. 5,491,608, issued February 13, 1996 to Nguyen, entitled Q-Controlled Microresonators and Tunable Electronic Filters Using Such Resonators, and assigned to the assignee of the present invention, the entire disclosure of which is incorporated herein by reference.

Referring to FIG. 6, sensing system 34 includes stationary sensing electrodes 62a, 62b and movable

sensing electrodes 56. The long fingers 38 of movable sensing electrodes 56 and long fingers 70 of stationary sensing electrodes 62a, 62b are interdigitated, with each long finger 38 disposed between a right finger 74a, 74b and a left finger 76a, 76b of sensing electrodes 62a, 62b. The spacing, Y_o, between fingers 70 and fingers 38 may be approximately one micron. Fingers 38 and 70 may be formed from the same layer of polysilicon so that the fingers are co-planar. Thus all of the driving and sensing elements may be formed in the same fabrication step. In addition, the driving mode and the sensing mode operate in the X-Y plane parallel to the surface of substrate 24. As will be described in more detail below, sensing system 34 is used to sense the deflection of proof mass 22 along the Y-axis, to apply electrostatic forces to balance and eliminate the effect of quadrature error, and to tune the resonant frequency of Y-axis vibrations of the proof mass.

As discussed above, drive system 32 causes proof mass 22 to oscillate along the X-axis. The position of the proof mass along the X-axis, x(t), is given by the following equation:

$$x(t) = X_0 \sin\omega_x t \qquad (1)$$

where X_o is the amplitude of the oscillation and ω_x is the frequency of the driving voltage (and thus the oscillation frequency). The frequency of the driving voltage, ω_x, may be between 7 kHz and 100 kHz, and the driving voltage may be sufficient to cause the proof mass to undergo a maximum deflection, X_o, of about one micron. The magnitude of the Coriolis acceleration, $\ddot{y}_{Coriolis}$, is given by the following equation:

$$\ddot{y}_{Coriolis} = 2 \cdot \Omega_z(t) \times \dot{x}(t) \qquad (2)$$

where $\Omega_z(t)$ is the rate of rotation of the proof mass about the Z-axis and $\dot{x}$ is the velocity of the proof mass along the X-axis. Equations 1 and 2 may be combined as follows:

$$\ddot{y}_{Coriolis} = 2 \cdot \Omega_z(t) \cdot X_0 \cdot \omega_x \cdot \cos\omega_x t \qquad (3)$$

For a gyroscopic sensor with an oscillation amplitude X_0=1 μm, on oscillation frequency ω_x=20 kHz, and an input rotation rate Ω_z=1 deg/sec, the Coriolis acceleration has a magnitude of 0.45 milliG's.

The Coriolis acceleration is an amplitude-modulated signal in which the carrier frequency is the oscillation frequency and the rotation rate modulates the amplitude. The resulting Coriolis acceleration is a dual sideband signal centered on the oscillation frequency. Referring to FIG. 7A, since the Y-axis accelerations are proportional to velocity, the motion of proof mass 22 is elliptical. The maximum deflection of proof mass 22 along the Y-axis will be a few nanometers. The deflection detectable by gyroscopic sensor 20 may be on the order of a picometer.

In an ideal device, the moving electrodes are perfectly aligned with the stationary electrodes so that the only motion caused by drive system 32 is along the X-axis. However, one effect of manufacturing flaws is quadrature error. Referring to FIG. 7B, quadrature error occurs if proof mass 22 oscillates along an axis that is not exactly parallel to the X-axis. If this is the case, then there is some small fraction, ε, of the drive oscillation, X(t), which lies along the Y-axis. This

quadrature displacement along the Y-axis is given by the following equation:

$$y_{Quadrature} = -\varepsilon \cdot x(t) \tag{4}$$

If this displacement is differentiated twice, the acceleration, $\ddot{y}_{quadrature}$, due to off-axis oscillation can be determined. This acceleration, given in Equation 5 below, is referred to as quadrature error.

$$\ddot{Y}_{Quadrature} = \varepsilon \cdot X_0 \cdot \omega_x^2 \cdot \sin\omega_x t \tag{5}$$

Note the similarity between the quadrature error and the Coriolis acceleration: both are sinusoidal signals centered at the frequency of oscillation. However, the signals can be distinguished by their phase relative to the driven oscillation. Specifically, the Coriolis acceleration is ninety degrees out of phase relative to the drive oscillation, ω_x, whereas the quadrature error is in phase with the driven oscillation.

The quadrature error can be quite large. In fact, the quadrature error may easily exceed the Coriolis acceleration. The ratio of quadrature error and Coriolis acceleration is given by Equation 6:

$$\frac{\ddot{Y}_{Coriolis}}{\ddot{Y}_{Quadrature}} = \frac{2\Omega_z(t) \cdot X_0 \cdot \omega_x}{\varepsilon \cdot X_0 \cdot \omega_x^2} = \frac{2\Omega_z(t)}{\varepsilon \cdot \omega_x} \tag{6}$$

Using the previous example of an input rotation rate, Ω_z, of 1 deg/sec and an oscillation frequency, ω_x, of 20 kHz, for the quadrature error to be as small as the Coriolis acceleration, the oscillation direction must be accurate to a factor of 1 part in 3.6 million. Due to manufacturing flaws and other imbalances, the quadrature error may be considerably larger than this. Accordingly,

gyroscopic sensor 20 has a mechanism to reduce, or nullify the quadrature error.

Microfabricated gyroscopic sensor 20 may apply electrostatic forces to proof mass 22 through sensing system 34. By selection of the proper electrostatic force, the quadrature error may be nullified. As shown by Equation 5, the quadrature error is directly proportional to position of the proof mass along the X-axis. To cancel this error signal without effecting the Coriolis signal, a balancing force must be applied that is also directly proportional to the position of the proof mass along the X-axis. Gyroscopic sensor 20 applies such a balancing force, using the interdigitated Y-axis position sense fingers.

Referring to FIG. 7C, proof mass 22 is shown with two fingers 38a and 38b projecting from opposite sides of the proof mass. Finger 38a is surrounded by right and left fingers 74a and 76a, whereas finger 38b is surrounded by right and left fingers 74b and 76b. A small voltage differential, $2\Delta V$, is applied between the right finger 74a and left finger 76a. The opposite voltage potential $-2\Delta V$, may be applied between right finger 74b and left finger 76b. This voltage difference creates a balancing force, F_y, which counteracts the quadrature error. The balancing force acts on proof mass 22 so that, absent the Coriolis force, fingers 39 vibrate solely along the X-axis. As mentioned above, the balancing force needs to be exactly proportional to the position of the proof mass along the X-axis. An electrostatic force between two charged surfaces is proportional to the overlapping area of the surfaces. Because the overlapping area between fingers 38 and fingers 70 is directly proportional to the position of

proof mass 22 along the X-axis, as proof mass oscillates, the position sense capacitors change proportionately. Therefore, the electrostatic balancing force F_y will also be proportional to the position of proof mass 22. Sensing system 34 applies a DC bias voltage V_{DC} to fingers 74a, 74b, 76a and 76b and a voltage differential $Z\Delta V$ between fingers 74a, 74b and 76a, 76b given by Equation 7 below:

$$F_y = \frac{C_{overlap}}{y_0} x(t) \cdot ((V_{DC}+\Delta V)^2 - (V_{DC}-\Delta V)^2) = 2\frac{C_{overlap}}{y_0} V_{DC} \Delta V \cdot x \qquad (7)$$

where $C_{overlap}$ is the maximum change in capacitance between fingers 70 and fingers 38 as the structure oscillates and y_0 is the equilibrium distance between fingers 70 and fingers 38.

By properly selecting the voltage differential ΔV, the quadrature error may be significantly reduced, e.g., by a factor ten to one-hundred. The proper voltage difference may be calculated from Equations (7) and (5) and Newton's law F = ma, as follows:

$$\Delta V = M\frac{\varepsilon y_0 \omega_x^2}{V_{DC} C_{overlap}} \qquad (8)$$

where M is the mass of proof mass 22. Because the quadrature error is a result of manufacturing defects, the proper voltage differential depends upon the specific structure and may vary from device to device. A voltage differential in the range of 1 mV to 100 mV should be appropriate. The optimum voltage differential to cancel the quadrature error may be determined experimentally (see FIG. 13 which is discussed below).

In addition to canceling the quadrature error, sensing system 34 of gyroscopic sensor 20 may be used to match the Y-axis resonant frequency ω_y of proof mass 22 to the driving oscillating frequency ω_y. Because gyroscopic sensor 20 is a high Q second order system, the response of proof mass 22 to Coriolis acceleration can be enhanced. As shown by Equation 3, the Coriolis acceleration is a signal centered around the oscillation frequency ω_x. Therefore the relative values of the oscillation frequency ω_x and the Y-axis resonant frequency ω_y have a dramatic effect on the response of the sense mode and hence the sensor sensitivity. If the Y-axis resonant frequency is matched to the oscillation frequency, the device may experience a gain of Q in the system response. However, the bandwidth of the sensor is then limited to ω_y/Q. Given that system is run in a vacuum and Q is typically greater than 10,000, the system bandwidth for $\omega_x=\omega_y$ will be only a few Hertz.

For larger bandwidth and increased sensitivity, gyroscopic sensor 20 is operated with a slight mismatch between resonant frequency ω_y and oscillation frequency ω_x. The system response of Y-axis displacement due to Coriolis acceleration is given by:

$$\frac{y}{\Omega_z} = \frac{2X_0\omega_x \sin\omega_x t}{\omega_y^2 + \frac{j\omega_x\omega_y}{Q} - \omega_x^2} = \frac{X_0\omega_x}{\omega_x\Delta\omega}\sin\omega_x t \qquad (9)$$

Provided that there is a means to tune the Y-axis resonant frequency, it is desirable to operate the gyroscopic sensor with a 5-10% frequency mismatch, $\Delta\omega/\omega_x$, yielding a gain of 5-10 in sensitivity. For example, if ω_x is about 12 kHz, then ω_y may be set to about 12.5 kHz. Alternately, the frequency mismatch may be reduced to

about 1-2%. Reducing the mismatch further might increase the sensitivity but may be difficult to maintain for any length of time because the resonant frequency changes as the temperature of the gyroscopic sensor changes.

Tuning of the Y-axis resonant to improve sensitivity is accomplished using electrostatic "negative" springs, i.e., by applying a DC bias voltage, V_{DC}, between proof mass 22 and stationary sensing electrodes 62. When the DC voltage is established between the moving proof mass and the stationary sensing electrode, the resulting attractive force reduces the total spring constant and thus adjusts the resonant frequency.

Using a first-order model for the parallel-plate capacitors, the linearized spring force due to electrostatic forces is given by:

$$F_y = \left[\frac{1}{(y_0-y)^2} - \frac{1}{(y_0+y)^2}\right]\frac{y_0 C_s V_{DC}^2}{2} \qquad (10)$$

where y is the deflection of the proof mass along the Y-axis away from its equilibrium position.

The Y-axis resonant frequency, ω_y, is given by the following equation:

$$\omega_y = \sqrt{\frac{k_y+k_e}{M}} \qquad (11)$$

where k_y is the purely mechanical spring constant, k_e is the electrostatic spring constant and M is the mass of proof mass 22. The mechanical spring constant k_y is primarily a function of the stiffness of suspension system 30.

The electromagnetic spring constant, k_e, is given by the following equation:

$$k_e = -2\frac{C_s}{y_0^2}V_{DC}^2 \qquad (12)$$

in which C_s is the sense capacitance of the gyroscopic sensor and y_o is the distance between fingers 38 and 70 (see FIG. 7A). C_s depends upon the total number of fingers and the amount of overlapping area, and should be at least 30 femtoFarads (fF). By increasing the number of fingers, C_s may be increased to about one picoFarad (pF). As mentioned above, the spacing y_o between fingers is about one micron. It may be noted that k_e has a negative value, so that as V_{DC} is increased ω_y is decreased. The system starts with ω_y larger than ω_x, and the bias voltage V_{DC} is increased, thereby reducing ω_y, until the desired mismatch $\Delta\omega/\omega_y$ is achieved. The correct valve for V_{DC} may be determined experimentally (see FIG. 12 which is discussed below), but should be in the range of one to ten volts.

In addition to canceling the quadrature error and adjusting the Y-axis resonant frequency, sensing system 34 may be used to negate the effects of centrifugal or centripetal force. As the gyroscope sensor rotates about the Z-axis, a centrifugal force will push the proof mass outwardly (assuming the axis of rotation does not pass exactly through the center of mass of the proof mass). A voltage difference, V_c, may be applied between the opposing stationary sensing electrodes 62a and 62b. Because the centripetal force varies at a low frequency, compared to the frequencies of the Coriolis force, a high pass filter may be used to remove the effect of the centripetal force from the output.

Gyroscopic sensor 20 measures the position of proof mass 22 along the Y-axis by capacitive deflection sensing. The interdigitated fingers of sensing system 34 (shown in FIG. 2) are used to sense deflection of the proof mass along the Y-axis. The fingers are arranged in a capacitor bridge so that any deflection of the proof mass results in measurable changes in the relative size of the capacitors. In a first order model, the capacitance of a parallel-plate capacitor is inversely proportional to the distance between the plates.

Referring to FIGS. 6 and 8A, the space between finger 38 of movable sensing electrode 56 and right fingers 74a, 74b of sensing electrodes 62a, 62b forms a first capacitor C_1, and the space between finger 38 and left fingers 76a, 76b forms a second capacitor C_2. As movable sensing electrode 56 is deflected along the Y-axis, C_1 and C_2 change. For example, if sensing electrode 56 is deflected leftward, the distance between finger 38 and right fingers 74a, 74b increases, thereby decreasing C_1, while the distance between finger 38 and left fingers 76a, 76b decreases, thereby increasing C_2. The change in capacitance is detected by a position sensor 80, such as an integrator or voltage buffer, which includes an amplifier 82. Finger 38 is connected to the negative input of amplifier 82. The output of amplifier 82 is connected to the negative input of the amplifier via an integrating capacitor 84 to form an integrator. The negative input of amplifier 82 is connected to ground via a parasitic capacitor 83. The positive input of amplifier 82 may be connected directly to ground.

Because capacitance cannot be measured with a DC voltage, a voltage source 90 applies an AC voltage V_S between fingers 74a, 74b and 76a, 76b. The voltage V_S is

about 0.1 to 5.0 volts, preferably about one volt, and has a frequency much higher than the driving frequency ω_x. For example, the frequency of voltage source 90 may be about one megahertz.

The integrator shown in FIG. 8A offers the flexibility of trading bandwidth for sensitivity by varying the integrating capacitor size. The integrator also provides lower distortion. Some of the parasitic capacitors involved in microelectromechanical systems are nonlinear which will vary the gain of a buffer and thereby result in distortion, and the practice of bootstrapping parasitic capacitance is a form of positive feedback which exacerbates amplifier distortion. However, because the integrator uses a fixed, linear capacitor, distortion is kept to a minimum.

Another common amplifier configurations used for capacitive position sensing is shown in FIG. 8B, in which the output of amplifier 82 is connected to its negative input and sensing electrodes 56 are connected to the positive input of the amplifier to form a voltage buffer.

Unfortunately, the integrator presents a difficult biasing problem. Ideally, biasing can be performed by placing a very large resistor in parallel with the integrating capacitor. However, any practical implementation of a large resistor results in a considerable parasitic capacitance. A diode can also be used in parallel with the integrating capacitance; however, that adds a nonlinear capacitance to the integrating capacitance resulting in distortion. Referring to FIG. 8C, this biasing problem has been solved by using a subthreshold metal oxide semiconductor field effect transistor (MOSFET) 88. The MOSFET device is connected in parallel with integrating capacitor 84 so

that the source of MOSFET 88 is connected to the output of amplifier 82, the drain is connected to the negative input of amplifier 82, and the gate is connected to ground. The negative input of amplifier 82 may be connected to ground by a diode 86, and the positive input of amplifier 82 may be connected directly to ground. In the subthreshold regime, the MOSFET device exhibits extremely low transconductance and no source-to-drain capacitance. The use of subthreshold MOSFET device has resulted in a well behaved integrator operable down to 1 kHz with a 50 F integrating capacitor without additional noise or distortion attributable to the bias circuitry.

Referring to FIG. 9, gyroscopic sensor 20 includes a phase-locked loop (PLL) 100 and several synchronous demodulators or mixers to perform signal processing. Phase-locked loop 100 produces extremely accurate digital signals having a driving frequency ω_x between about 7 kHz and 100 kHz. The drive frequency, ω_x, may be generated by dividing down the signal from voltage source 90. The phase-locked loop ensures that the position signals are exactly in phase with the position of proof mass 22. Phase-locked loop 100 may also generate a velocity signal on line 108 which is exactly ninety degrees out of phase with a position signal on line 110. Position signals on lines 102 and 104, having opposite amplitudes, are supplied by phase-locked loop 100 to the positive and negative outputs, respectively, of a transresistance amplifier 106. Opposing stationary drive electrodes 60a and 60b are also connected to the positive and negative outputs of transresistance amplifier 106. Opposing feedback electrodes 61a and 61b are connected to the positive and negative inputs of transresistance amplifier 106. One of the outputs of transresistance amplifier 106

is mixed with the velocity signal by a mixer 112. The combined output of mixer 112 is applied to trans-resistance amplifier 106 to provide an automatic gain control (AGC) circuit to control the amplitude of the oscillations of proof mass 22 along the X-axis. The phase accuracy of the phase-locked loop is critical to the operation of gyroscopic sensor 20 because any phase error will result in cross-talk between the Coriolis and quadrature signals. Assuming that a phase error $\theta_n(t)$ is generated by phase noise in the phase-locked loop, the error in the rotation rate Ω may be derived as shown in Equations 13-15 below:

$$y(t) = [\frac{X_0\omega_x}{\omega_x\Delta\omega}\Omega\cos\omega t + Y_{Quadrature}\sin\omega t] \quad (13)$$

$$\Omega_{est} = \frac{\omega_x\Delta\omega}{X_0\omega_x}y(t)\cos(\omega_x t+\theta_n(t)) \quad (14)$$

$$\Omega_{est} = \Omega + \frac{\omega_x\Delta\omega}{X_0\omega_x}Y_{Qadrature}\theta_n(t) + Higher\ terms \quad (15)$$

Because phase-locked loop 100 is extremely accurate, phase noise is minimized and variable cross-talk is extremely small. In addition, quadrature error correction reduces cross talk and phase noise.

The nulling of the quadrature error, the tuning of the Y-axis resonant frequency, and the balancing of the centrifugal forces is accomplished by the application of the proper voltages to fingers 70 of opposing stationary sensing electrodes 62a and 62b. Specifically, gyroscopic sensor 20 includes four DC bias voltage sources 120, 122,

124 and 126. Voltage source 120 applies a total voltage $V_t=V_{DC}+\Delta V+V_C$ to right fingers 74a of sensing electrode 62a. Voltage source 122 applies a total voltage of $V_{DC}-\Delta V-V_C$ to left fingers 76a. Voltage source 124 applies a total voltage of $V_{DC}-\Delta V+V_C$ to right electrode fingers 74b of sensing electrode 62b. Voltage source 126 applies a total voltage of $V_{DC}+\Delta V-V_C$ to left fingers 76b. Thus, voltage sources 120, 122, 124 and 126 provide all of the necessary bias voltages in order to nullify the quadrature error, select the desired Y-axis resonant frequency, and cancel any centrifugal or other low-frequency forces. Of course, any other combination of voltage sources providing the same effective total voltage to the fingers of the sensing electrodes could be used. Also, the voltages could be applied by different sets of fingers of the stationary sensing electrode, for example, V_{DC} could be applied by one set of fingers and ΔV could be applied by another set of fingers.

In order to extract the position, Coriolis effect, and quadrature signals from capacitive position sensor 80, the signal from amplifier 82 is boosted by an oscillation amplifier 130 to produce an output signal on line 132. This output signal may be mixed with signals from a modulator or clock and the position and velocity signals from phase locked loop 100. Voltage source 90 may produce a high frequency, e.g., one megahertz clock signal on line 134. To generate the position signal, this clock signal is mixed with the output signal on line 132 by a mixer 136. In order to produce the Coriolis signal, the clock signal on line 134 is mixed with the velocity signal on line 108 by a mixer 140 to produce a combined signal on line 142. The combined signal on line 142 is then mixed with output signal on line 132 by a

mixer 144 to produce the Coriolis signal. Finally, to produce the quadrature signal, the clock signal on line 134 is mixed with the position signal on line 110 by a mixer 150 to produce a combined signal on line 152. The combined signal on line 152 is then mixed with output signal on line 132 by a mixer 154 to produce the quadrature signal. The position, Coriolis and quadrature signals may be passed through low pass filters to filter out high frequency components.

Referring to FIG. 10, a gyroscopic sensor 20 was fabricated on a silicon substrate 24 using a combination of metal oxide semiconductor and microelectromechanical fabrication techniques. The transresistance amplifier and integrator were fabricated on the same die, and the remaining electronics was implemented off of the chip. The mechanical sensing element is about one millimeter across.

There are a number of possible noise sources in gyroscopic sensor 20. Principal among these are: Brownian noise, op-amp noise in the integrator, and phase locked loop phase noise. The Brownian noise, $\Omega_n B$, represents the fundamental limit on angular rate resolution and is given by:

$$\Omega_{nB} = \sqrt{\frac{kT\omega_y BW}{MQ\omega_x^2 X_0^2}} \qquad (16)$$

where k is Boltzman's constant, T is the temperature, M is the mass of the proof mass, BW is the bandwidth of the gyroscopic sensor, and Q is the quality factor. As an example, consider a gyroscopic sensor with mass, M=0.2μg, an oscillation amplitude X_0=1 μm, a quality factor, Q= 10,000, a bandwidth BW = 100 Hz, a drive frequency ω_x= 20

kHz and a resonant frequency ω_y= 20 kHz. For this example, we find a Brownian noise floor Ω_{nB}=0.06 deg/sec. Because the gyroscopic sensor is run in vacuum and has a high Q, Brownian noise is not the dominant noise source.

As shown by Equation 15, phase noise in the phase locked loop, represented by $\theta_n(t)$, can cause variable cross talk between quadrature and Coriolis signals. In gyroscopic sensor 20, this effect is kept to a minimum due to the low phase noise in the phase locked loop and nulled quadrature error.

The integrator op-amp noise is the dominant noise source in gyroscopic sensor 20. The input-referred noise, Ω_E, of the op-amp noise is a function of the total capacitance, C_T, attached to the summing node of the integrator, and is given by:

$$\Omega_{nE} = \frac{C_T Y_0 \nu_n}{C_S X_0 V_S} \Delta\omega \sqrt{2BW} = \frac{Y_0 \Delta\omega}{X_0 V_S} \sqrt{\frac{32kTBW}{3\pi C_S f_T}} \qquad (17)$$

where f_T is the maximum operable frequency of the transistors in gyroscopic sensor 20. The electronic noise is at best Ω_{nE}=0.08 deg/sec for a modest CMOS process with f_T=250 MHZ, a frequency mismatch $\Delta\omega$=1 kHz, a sense voltage V_s=1 volt, a sense capacitance C_s=100fF, and the oscillation amplitude and finger spacing X_0=y_o=1 μm.

An initial characterization of the gyroscopic sensor response is shown in FIG. 11. FIG. 11 is a graph of the logarithm of the output voltage of the Coriolis signal, on the Y-axis, as a function of frequency, on the X-axis. The graph was produced by measuring the output Coriolis signal in response to a 1Hz, 5 deg/sec sine wave rotation. The gyroscopic sensor was operated with an oscillation frequency, ω_x, of 12 kHz and a Y-axis resonant frequency, ω_y, of about 12.5 kHz. The noise floor for

this version of Z-axis vibratory rate gyroscopic sensor is 1 deg/sec/Hz$^{1/2}$.

Referring to FIG. 12, there is a measured mechanical resonant frequencies of proof mass 22 as a function of the DC bias voltage applied to the position sense fingers. FIG. 12 shows a graph of the resonant frequencies of proof mass 22 (on the Y-axis of the graph) as a function of the RMS voltage (on the X-axis of the graph) applied between fingers 38 and fingers 70. The RMS voltage is a combination of the DC bias voltage and the AC voltage generated by voltage source 90. The resulting electrostatic springs reduce the resonant frequency of the sense mode (ω_y), raise the resonant frequencies of the out-of-plane modes, and leaves the driven mode (ω_x) unaffected. As expected, the Y-axis resonant frequency drops as the bias voltage is increased and the oscillation frequency of proof mass 22 remains constant at 12kHz. The resonant frequencies of the vertical and tipping modes increase with DC bias due to electrostatic levitation effects.

As discussed above, gyroscopic sensor 20 includes a means to null quadrature error. FIG. 13 shows a graph of the measured voltage, V_{out} on the Y-axis, as a function of the voltage differential, ΔV, on the X-axis, which is applied between right fingers 74a, 74b and left fingers 76a, 76b. Both the quadrature and rotation rate signals were plotted for a zero rotation rate as ΔV was adjusted. Measurements of the quadrature error and rotation rate signals demonstrate that the quadrature error signal can be controlled independently of the Coriolis signal.

Another embodiment of the gyroscopic sensor, in which the sensing and quadrature correction voltages are applied by different electrode fingers, is shown by FIG.

14. Referring to FIG. 14, a micromachined gyroscopic sensor 200 includes a proof mass 202 connected to a substrate 204 by a suspension system 206. The gyroscopic sensor 200 includes three major electronic elements: a drive system 210 used to sustain oscillation of proof mass 202 along the X-axis, a sensing systems 212 used to detect deflections of proof mass 202 along the Y-axis, and a quadrature correction system 214 used to cancel any quadrature error.

The proof mass 202 includes a rectangular outer stage 220 and a rectangular inner stage 222. Each corner of outer stage 220 is connected by a folded or J-shaped first flexure 224 to an anchor 226 which secures proof mass 202 and suspension system 206 to substrate 204. Similarly, each corner of inner stage 222 is connected to outer stage 220 by a second flexure 228. The first flexure 224 is designed to permit outer stage 220 to vibrate primarily along a Y-axis with respect to substrate 204, whereas second flexure 228 is designed to permit inner stage 222 to vibrate substantially along the X-axis with respect to outer stage 220. Several beams or crossbars 230 may connect opposing sides of inner stage 222.

The physical characteristics of gyroscopic sensor 200 are similar to those of gyroscopic sensor 20. The sensor may be about 0.5 to 2.0 millimeters on a side; the proof mass may have a total mass of about 0.1 to 0.5 micrograms; the flexible elements of the suspension system may be constructed of polysilicon and may have a width and a thickness on the order of two microns. The entire assembly may be fabricated using traditional integrated circuit fabrication techniques.

Referring to FIG. 14, the drive system 210 includes two driving electrodes 232a and 232b, and two feedback electrodes 234a and 234b, all connected to substrate 204. A plurality of electrode fingers 236 project along the X-axis from each feedback electrode and each drive electrode. A plurality of electrode fingers 238 project from inner stage 222 of proof mass 202 along the X-axis, and are interdigitated with electrode fingers 236 of the sense and drive electrodes.

As shown in FIG. 15, feedback electrodes 234a and 234b are connected to the positive and negative inputs, respectively, of a transresistance amplifier 240. The driving electrodes 232a and 232b are connected to the positive and negative outputs of transresistance amplifier 240, respectively, and to a phase-locked loop 242, as previously described with respect to FIG. 9.

The sensing system 212 includes a plurality of pairs of sense electrodes fingers aligned with the X-axis. Each pair of sense electrode fingers includes a right finger 244 and a left finger 246. A plurality of electrode fingers 248 are connected to outer stage 220 and are interdigited so that each electrode finger 248 is disposed between one right finger 244 and one left finger 246. A sense voltage source 250 (see FIG. 15) applies an AC voltage between the right fingers 244 and the left fingers 246.

Quadrature correction system 214 includes several sets of correction electrodes positioned near the center-line of the sensor and connected to the substrate. Each set of correction electrodes includes an upper left electrode 260, an upper right electrode 262, a lower left electrode 264, and a lower right electrode 266. Upper right electrode 262 and lower left electrode 264 may be a

single electrode, as shown, or may be separate electrodes. A plurality of electrode fingers 268 extend from crossbars 230 and are interdigited with the connection electrodes. Specifically, each electrode finger 268 extends along the X-axis from crossbar 230 and is disposed between upper left electrode 260 and upper right electrode 262. Similarly, each electrode finger 268 extends along the X-axis from crossbar 230 and is disposed between lower left electrode 264 and lower right electrode 266. Upper left electrode 260 is electrically connected to lower right electrodes 266, and upper right electrode 262 is electrically connected to lower left electrode 264.

A voltage source 270 (FIG. 15) applies a DC bias voltage between the correction electrodes 260, 266 and 262, 264. The voltage differential between the left and right electrodes creates a balancing force to counteract the quadrature error as discussed with respect to FIG. 7C. The remainder of the circuitry, including an integrator 280 and mixers 282-286 may be assembled and function in a manner similar to the circuitry discussed above with reference to FIG. 9.

Referring to FIG. 16, quadrature correction may be used to compensate for manufacturing flaws that occur in the fabrication of other sorts of gyroscopic sensors, such as X-axis and Y-axis gyroscopic sensors. A dual-axis vibratory gyroscope functions by generating and sensing Coriolis accelerations. The functional operation of the dual-axis vibratory gyroscope is illustrated by an equivalent spring-mass system. In a dual-axis gyroscopic sensor 290, a proof mass 292 is supported by a flexible suspension 294 from a frame 296. The proof mass is generally disc-shaped, and lies in a plane generally

parallel to the surface of the substrate. The proof mass is oscillated about the Z-axis (the axis perpendicular to the surface of the substrate) by a drive torque F_d with a frequency ω_z. If the frame rotates about a first axis parallel to the surface of the substrate, e.g., the Y-axis, at a rotation rate Ω_Y, then the combination of this rotation and oscillation generates an oscillating Coriolis torque F_c about a second axis parallel to the surface of the substrate and perpendicular to the first axis, i.e., the X-axis. This Coriolis force torque will tend to oscillate the proof mass about the X-axis at a frequency ω_X. Thus, rotation of the proof mass about the Y-axis causes the proof mass to undergo a "see-saw" motion about the X-axis. Similarly, a rotation about the X-axis will induce a Coriolis oscillation about the Y-axis.

The Coriolis acceleration about the X-axis generated by rotation of the proof mass about the Y-axis is given by the following equation:

$$I_{xx}\ddot{\theta}_x + C_x\dot{\theta}_x + K_x\theta_x = -I_{zz}\Omega_y \times \theta_{z0}\omega_z \cos(\omega_z t) \qquad (18)$$

where θ_x is the sense-axis tilt angle, I_{xx} is the X-axis moment of inertia, C_x is the damping co-efficient, K_x is the spring constant, ω_z is the frequency of oscillation about the Z-axis, I_{zz} is the Z-axis movement of inertia, and Ω_y is the rotation rate of the proof mass about the Y-axis. The angular oscillation of the rotor caused by the Coriolis acceleration can be thought of as an amplitude modulated signal with a carrier frequency ω_z. The amplitude of the modulated signal is directly proportional to the Y-axis rotation rate Ω_y. The equation for Coriolis acceleration about the Y-axis is essentially

identical except that the x and y subscripts are reversed and the right-hand side of the equation is positive.

Referring to FIG. 17A, a dual-axis gyroscopic sensor 300 includes a generally ring-shaped proof mass 302 connected to a rigid frame or substrate 304 by a suspension system 306. Dual-axis gyroscopic sensor 300 measures the X-axis and Y-axis rotation rate; i.e., the rotation of the substrate about the axes parallel to the surface of substrate 304. Dual-axis gyroscopic sensor 300 includes three major electronic elements: a drive system 310 used to sustain oscillation of proof mass 302 about the Z-axis, a sensing system 312 used to detect deflections of proof mass 302 about the X-axis and Y-axis, and a quadrature correction system 314 used to cancel any quadrature error. The dual-axis gyroscopic sensor 300 may be fabricated using standard integrated circuit techniques.

The proof mass 302 includes a generally ring-shaped rotor 316. Rotor 316 may be a two micron thick polysilicon ring with an outer radius of about 250 microns and an inner radius of about 200 microns. The proof mass 302 is substantially symmetric about the X- and Y-axis.

The suspension system 306 may include four beams 320 which connect an inner edge 322 of the proof mass to an anchor 324 which secures rotor 316 to substrate 304. The beams 320 may also be constructed of polysilicon and may have a width and thickness on the order of two microns.

Alternately, the suspension system may include a serpentine suspension with folded beams. In yet another version, the proof mass may be suspended by four beams connected to an outer edge of the rotor. A serpentine

suspension system provides a lower natural frequency and can accommodate warping of the rotor.

Suspension systems 306 is designed to provide a torsional suspension for rotor 316 to allow rotation about the three perpendicular axes. However, suspension system 306 is designed to be rigid to translational accelerations along the X-axis and the Y-axis. Although rotor 316 may undergo translational acceleration along the Z-axis, the differential sensing scheme discussed below substantially cancels sensitivity to such accelerations.

For maximum mechanical sensitivity, the suspension system is designed to match the frequencies of all three rotational modes sufficiently well that electrostatic tuning may compensate for process variations during manufacture of the gyroscope sensor. In particular, the sense axis natural frequencies were designed to be about ten percent above the drive natural frequencies so that the sense frequencies may be down tuned to match the drive frequency.

A plurality of inner combs 330a-330d project inwardly from inner edge 322 of rotor 316. Each inner comb includes a spine 332 and a plurality of teeth 334 which project from both sides of the spine. The number and configuration of inner combs in FIG. 17A is merely illustrative. The dual axis gyroscope may include twelve inner combs, each having five teeth. Four outer combs 340a-340d project outwardly from an outer edge 326 of rotor 316. Each outer comb includes a spine 342 and a plurality of teeth 344 projecting from both sides of the spine. Although teeth 334 and 344 in FIG. 17A are illustrated as linear, as shown in FIG. 17B it is

advantageous for the teeth to be constructed as portions of arcs from concentric circles.

As previously mentioned, drive system 310 induces oscillations of proof mass 302 about the Z-axis. The drive system 310 includes one or more drive electrodes 350a-350b and one or more feedback electrodes 352a-352b connected to substrate 304. Preferably, the drive and feedback electrodes are arranged in opposing pairs located on either side of each inner comb 330a-330d. Each feedback and drive electrode includes a plurality of teeth 354 which are interdigited with teeth 334 of the adjacent inner comb. Teeth 354 may have an arc length of approximately twenty microns and a width of approximately two microns. The drive electrodes of drive system 310 act as electrical, mechanical transducers. By application of an alternating voltage between the drive electrodes and the proof mass, the proof mass may be forced to oscillate about the Z-axis. Specifically, beams 320 may flex or bend so that rotor 316 may rotate.

Referring to FIG. 18, dual-axis gyroscopic sensor 300 includes a transresistance amplifier 366 which produces drive signals 362 and 364 having a driving frequency ω_z of about twenty to thirty kilohertz. Drive signals 362 and 364 are equal in magnitude but opposite in sign. phase-locked loop 360. A phase-locked loop 360 generates an extremely accurate digital output signal on line 368 which is in phase with the rotational rate of the proof mass. The opposing feedback electrodes 352a and 352b are connected to the positive and negative inputs of trans-resistance amplifier 366. The opposing drive electrodes 350a and 350b are connected to the positive and negative outputs 362 and 364 of trans-resistance amplifier 366 and to phase-locked loop 360.

The positive and negative outputs of trans-resistance amplifier 366 are also mixed with the digital output signal on line 368 by a mixer 370. The output of mixer 370 is then used to modulate trans-resistance amplifier 366. This modulation provides an automatic gain control circuit to control the amplitude of the oscillations of proof mass 302. Thus, drive system 310 provides a phase-locked oscillation of constant amplitude to the proof mass and provides a clean signal for Coriolis demodulation.

Returning to FIG. 17A, sensing system 312 includes four sense electrodes 374a-374d (shown in phantom because they are located beneath the rotor 316). Each sense electrode is shaped as a quarter-pie section and may be formed of an n+ diffused region in substrate 304. Sense electrodes 374a and 374c are positioned along the X-axis whereas the sense electrodes 374b and 374d are positioned along the Y-axis. The Coriolis oscillation is measured by sensing the change in capacitance between rotor 316 and sense electrodes 374a-374d. For example, if the gyroscopic sensor rotates about the Y-axis, then the Coriolis force may cause the right portion of rotor 316 to move closer to sense electrode 374b and the left portion of rotor 316 to move farther away from sense electrode 374d. Thus, the capacitance between sense electrode 374b and rotor 316 increases whereas the capacitance between sense electrode 374d and rotor 316 decreases. Because each pair of opposing sense electrodes provides differential sensing, translation of the rotor up or down along the Z-axis does not change in sense output.

Referring to FIG. 18, a first sense voltage source 376 connects opposing sense electrodes 374a and 374c, and

a second sense voltage source 378 connects opposing sense electrodes 374b and 374d. The sense voltage sources 376 and 378 generate AC voltages with different modulation frequencies. For example, one voltage source may operate at 200 kHz and the other voltage source may operate at 300 kHz. In order to extract the position signals indicating the angular position of rotor 316 about the X-axis and Y-axis, proof mass 302 is electrically connected to an integrator 380. The integrator 380 may include a capacitor 381 having a capacitance of about 50 femtoFarrads. A benefit of integrator 380 is that it improves linearity.

The output of integrator 380 is demodulated with the signal from sense voltage source 376 by a mixer 382. The output from integrator 380 is also demodulated with the signal from sense voltage source 378 by a mixer 384. The outputs of mixers 382 and 384 are then demodulated by mixers 386 and 388 with the digital output signal on line 368 from phase-locked loop 360. The output of mixer 386 provides the angular rotation rate of the gyroscopic sensor about the X-axis, and the output of mixer 388 provides the rotation rate of the gyroscopic sensor about the Y-axis.

The combined mechanical and electrical sensitivity of dual-axis gyroscopic sensor 300 may be calculated according to the following equation:

$$\left|\frac{V_{out}}{\Omega_y}\right| = \left|\frac{\theta_x}{\Omega_y}\right|\left|\frac{V_{out}}{\theta_x}\right| = \left|\frac{2\theta_{z0}\omega_z}{\omega^{2}_{x} + \frac{j\omega_x\omega_z}{Q_x} - \omega^{2}_{z}}\right|\left|2\frac{\partial C}{\partial\theta_x}\frac{V_s}{C_I}\right| \qquad (19)$$

were V_s is the sense voltage, C_i is the capacitance of the integrating capacitor, Q_x is the quality of inverse

damping coefficient, and V_{out} is the voltage signal from the mixer. One drawback of the sensing system is that a small inherent voltage is generated at twice the drive frequency. However, this voltage is far from the sense modulation frequencies.

As described above, if dual-axis gyroscopic sensor 300 is rotating about an axis parallel to the surface of the substrate, then the oscillation of rotor 316 about the Z-axis induces an oscillation about the X-axis or Y-axis due to the Coriolis force. In an ideal device, rotor 316 is perfectly aligned so that the only motion caused by drive system 310 is within the X-Y plane. However, fabrication imperfections may cause rotor 316 to wobble as it undergoes rotation about the Z-axis. Specifically, even if the gyroscopic sensor 300 is not rotating about the X-axis or Y-axis, as rotor 316 rotates about the Z-axis, it may oscillate or wobble out of the X-Y plane. The wobble caused by the fabrication imperfections generates a false rotation rate measurement called quadrature error. The quadrature error in dual-axis gyroscopic sensor 300 is similar to the quadrature error in Z-axis gyroscopic sensor 20; the quadrature error and Coriolis acceleration are both sinusoidal signals centered at the frequency of oscillation and ninety degrees out of phase. Ideally, demodulation will eliminate the out-of-phase quadrature error. However, because the electronic components may have a small phase-lag, some percentage of the quadrature error will corrupt the measurement of the rotation rate.

Returning to FIG. 17A, quadrature correction system 314 includes eight correction electrodes 390a-390h. The correction electrodes are arranged in pairs with each outer comb 340a-340d surrounded by two opposing

correction electrodes. For example, outer comb 340a is flanked by correction electrodes 390a and 390b. Each correction electrode has a plurality of teeth 392 which are interdigitated with the teeth of the outer combs. The quadrature correction system 314 may apply voltages to the correction electrodes 390a-390h in order to levitate teeth 344 of the outer combs and cancel the quadrature error.

Returning to FIG. 18, each pair of opposing correction electrodes may be connected to a DC offset voltage source. In addition, the correction electrodes on opposite sides of the rotor may be connected. For example, correction electrode 390a may be electrically connected to correction electrode 390f. A first DC voltage source 394 may connect electrode 390a to electrode 390b, and second DC voltage source 396 may connect correction electrode 390c and 390d. The DC offset may be selected to electrostatically levitate outer combs 340a-340d and thereby cancel the quadrature error.

Referring to FIG. 19, a portion of substrate 304 beneath teeth 344 and 392 may be an n+ diffused region to provide a control pad electrode 398. The control pad electrode 398 is electrically connected to proof mass 302. By applying a generally positive voltage to teeth 392 and a generally negative voltage to teeth 344 and control pad electrode 398, the electric field (shown by field lines 399) generates an upward force F_z on teeth 344.

Returning to FIG. 17A, the correction electrodes 390a and 390f generate an upward force on the teeth on the left side of the rotor which is stronger than the upward force on the teeth on the right side of the rotor

generated by electrodes 390b and 390e. This force imbalance creates a balancing torque which tends to rotate the rotor so that, absent the Coriolis force, it vibrates solely in the X-Y plane. Because the quadrature error results in a linear displacement, the balancing forces need to be proportional to the position of the proof mass about the Z-axis. The balancing torque F_z is proportional to the overlapping area between teeth 344 and teeth 392. Because the overlapping area between teeth 344 and teeth 392 is directly proportional to the angular position of rotor 316, the balancing torque will also be proportional to the angular position of the rotor.

Referring to FIG. 20, another embodiment of dual-axis gyroscopic sensor 300' includes a modified quadrature correction system 314'. In quadrature correction system 314', four generally rectangular or wedge-shaped plates 340a'-340d' are connected to outer edge 326 of rotor 316. Two fixed electrode pads 390a' and 390b' are disposed on substrate 304 beneath each plate. The fixed electrode pads 390a' and 390b' may be formed of n+ diffused regions in the substrate. A DC offset voltage may be applied between each pair of electrode pads to correct the quadrature error. For example, a positive offset voltage may be applied so that the voltage of electrode pad 390b' is higher than the voltage of electrode pad 390a'. As rotor 316 rotates counter-clockwise and the plate 340a' moves rightwards, more of the plate will overlap electrode pad 390b', and thus the right side of the plate will be more attracted to the substrate than the left side of the plate. This will generate a torque which tends to rotate rotor 316 about the X-axis. The dual-axis gyroscopic sensor 300'

otherwise functions in a manner similar to dual-axis gyroscopic sensor 300.

Referring to FIG. 21, in a gyroscopic sensor 400 the drive system, the sensing system, and the quadrature correction system use a single set of electrodes. Gyroscopic sensor 400 includes a proof mass 402 connected to a substrate 404 by a flexible suspension 406. A plurality of opposing electrode fingers 410a and 410b (only two opposing fingers are shown) project from proof mass 402 along the X-axis. Each electrode finger 410a is flanked by respective stationary electrode fingers 412a and 414a. Similarly, each electrode finger 410b is flanked by stationary electrode fingers 412b and 414b.

To sense the position of the proof mass along the Y-axis, a voltage source 420 applies a high-frequency (e.g., one megahertz) AC voltage between upper electrode fingers 412a, 412b and lower electrode fingers 414a, 414b. Proof mass 402 is electrically connected to an integrator 422. The output of integrator 422 provides a position signal.

To drive the proof mass along the X-axis, a voltage-controlled oscillator 426 is connected to apply an AC voltage with a frequency ω between the opposing electrode fingers 412a, 414a and 412b, 414b. The output of integrator 422 is applied to a phase-sensing circuit 428, and the output of phase-sensing circuit 428 controls the voltage-controlled oscillator 426.

The output voltage V_{out} from integrator 422 is

$$V_{out} = \frac{Q_{struct}}{C_I} \qquad (20)$$

where Q_{struct} is the charge on the proof mass and C_I is the capacitance of integrator 422. Q_{struct} is given by the equation:

$$Q_{struct} = \frac{dC_s}{dy}\Delta y V_{sense} + \Delta C_x(t)\, V_F(t) \qquad (21)$$

where $V_F(t)$ is AC portion of the forcing voltage, $C_x(t)$ is the changing capacitance on the forcing electrodes as the structure displaces along the X-axis, and V_{sense} is the sense voltage applied by voltage source 420. Combining Equations 20 and 21 yields:

$$V_{out} = \frac{\Delta C_x(t)\, V_F(t)}{C_I} + other\ terms \qquad (22)$$

If the forcing voltage $V_F(t)$ is $V_F \sin(\omega t)$ then the resulting displacement $x(t)$ is given by the following equation:

$$x(t) = X_0(\omega, \omega_x)\sin(\omega t + \phi(\omega, \omega_x)) \qquad (23)$$

where ω is the drive frequency, ω_x is the driven mode resonance frequency, $X_0(\omega, \omega_x)$ is the amplitude, and $\phi(\omega, \omega_x)$ is a phase difference. Because $\Delta Cx(t)$ is proportional to $x(t)$,

$$V_{out} = \frac{\Delta C_x(\omega, \omega_x)}{C_I}\sin(\omega t + \phi(\omega, \omega_x))\sin(\omega t) \qquad (24)$$

and therefore

$$V_{out} = \frac{\Delta C_x(\omega, \omega_x)}{2C_I}[\cos(\phi(\omega, \omega_x)) - \cos(2\omega t + \phi(\omega, \omega_x))] \qquad (25)$$

When the drive frequency ω is equal to the resonant frequency ω_x, the phase ϕ will be 90°. Because

the $\cos(\phi(\omega,\omega_{x1})$ term of Equation 25 produces a DC offset, phase-sensing circuit 428 can drive the frequency ω of voltage-controlled oscillator 426 to the resonant frequency ω_x by sensing when there is no DC offset. Thus, the drive voltage will remain phase locked with the position of the proof mass.

Quadrature error correction may be accomplished in gyroscopic sensor 400 by applying a DC voltage between electrode fingers 412a and 414a and an equal but opposite DC voltage between electrode fingers 412b and 414b.

Referring to FIG. 22, a micromachined gyroscopic sensor 500 may be fabricated using high-aspect-ratio single-crystal-silicon micromachining techniques to produce an extremely thick device. Gyroscopic sensor 500 includes a vibratory structure 502 connected to a rigid frame or substrate 504 at anchor points 511. Structure 502 is configured to vibrate in a plane parallel to a surface 505 of the substrate. As such, a gap of about 0.5 to 4.0 microns, such as about 1.0 microns, separates the vibratory structure from surface 505.

Structure 502 is generally H-shaped, and includes a proof mass portion 506 and a flexible suspension portion 508. The suspension portion includes two parallel crossbeams 516 and four parallel flexures 510 positioned generally along the X-axis. One end of each flexure is connected to anchor 511 which connects structure 502 to the substrate, and the other end of each flexure is connected to one of crossbeams 516. The total length of one crossbeam 516 and two flexures 510 may be about 200 to 1500 microns in length, preferably about 1250 microns.

Proof mass portion 506 includes two crossbars 512 connected to two beams 514 to provide a generally square

arrangement. Three additional crossbars 512 are also connected between beams 514. A plurality of electrode teeth or fingers project along the X-axis from the crossbars 512. Four additional flexures 518 may connect flexures 510 to proof mass portion 506.

Structure 502 may be formed of single-crystal silicon. The structure 502 may have a thickness T of at least 25 microns, and it is advantageous for the thickness T to be at least 50 microns. The thickness may be between about 50 and 100 microns, but for some applications the thickness may be 250 microns. The flexures of the structure may have a width W_F of about two to five microns. The aspect ratio, i.e., the ratio of width to thickness, of the flexures should be greater than 10:1, and it is advantageous for the aspect ratio to be greater than 20:1. The aspect ratio may even be 50:1 or more. The beams and crossbars of the proof mass portion may have a width W_B of about five to ten microns. The total mass of structure 502 may be about 10 to 50 micrograms.

The suspension portion 508 is designed to be flexible along the X-axis and Y-axis and rigid to other modes of vibration. In particular, the high-aspect ratio of the flexures results in a structure which is very rigid to torsion and Z-axis acceleration.

Referring to FIG. 23, the micromachined gyroscopic sensor 500 includes four major electronic elements: a drive system 520 used to sustain oscillation of structure 502 along the X-axis, a sensing system 540 used both to detect deflections of structure 502 along the Y-axis, a sense tuning system 560 used to adjust the resonant frequency of structure 502 along the Y-axis, and a

quadrature correction system 580 used to apply electrostatic forces to cancel quadrature error.

As shown in FIGS. 15 and 16, the drive system 520 includes two opposing driving electrode combs 522a and 522b and two feedback electrode combs 524a and 524b, all connected to substrate 504. Each driving electrode comb and feedback electrode comb includes a plurality of electrode teeth or fingers 526 which project along the drive axis and which are interdigited with electrode teeth or fingers 528 which project from structure 502. Electrode teeth 526 and 528 may have a length L of about fifteen microns, and a width W_E of about two to six microns. Electrode teeth 526 may be separated from electrode teeth 528 by a gap of about 2.5 microns. Electrode teeth 526 and 528 may be formed from the same layer of single-crystal silicon and have a thickness of about 100 microns.

The feedback electrodes combs 524a and 524b are electrically connected to the positive and negative inputs of a trans-resistance amplifier 530. The driving electrode combs 522a and 522b are connected to the positive and negative outputs, respectively, of the transresistance amplifier and to a phase-locked loop circuit 532. At least one of the outputs from transresistance amplifier 530 may be mixed with a velocity signal from phase-locked loop 532 by a mixer 534. The output of mixer 534 is then used to modulate transresistance amplifier 530 to provide an automatic gain control circuit to control the oscillation amplitude of structure 502.

The sensing system 540 includes an opposing pair of sense electrode combs, including left sense electrode combs 542a and 542b, and right sense electrode combs 544a

and 544b. The left sense electrode combs 542a, 542b include a plurality of "left" electrode teeth 546, and the right sense electrode combs 544a, 544b include a plurality of "right" electrode teeth 548. The electrode teeth 546 and 548 are interdigited with electrode teeth 550 which project from structure 502 such that each electrode tooth 550 is disposed between one left tooth 546 and one right tooth 548.

Electrode teeth 546, 548 and 550 may have a length L of about fifteen microns, and width W_E of about two to six microns. Electrode teeth 546, 548 and 550 have a thickness of at least 25 microns, and the thickness may be between about 50 and 100 microns. The aspect ratio of the electrode teeth should be at least about 5:1. The aspect ratio may be at least 10:1, and it may be between about 10:1 and 20:1. Electrode teeth 550 may be separated from electrode teeth 546 and 548 by a gap having a width W_G between about 0.5 and 4.0 microns, such as 2.5 microns. The aspect ratio of the gap should be at least 10:1, and it may be greater than 20:1 or even greater than 50:1. Electrode teeth 546, 548 and 550 may be formed from the same layer of single-crystal silicon in the same fabrication step so that the teeth are coplanar.

A first sense voltage source 552 applies an AC voltage to left sense electrode combs 542a and 542b. A second sense voltage source 554 applies an AC voltage, 180° out of phase with the first sense voltage, to right sense electrode combs 544a and 544b. The sense voltage sources may generate AC signals having a maximum voltage of about 0.1 to 5.0 volts and a frequency of about 0.1 to 5.0 megahertz. The AC signals may have a voltage amplitude of one volt and a frequency of one megahertz.

To measure the Coriolis signal Ω_z, structure 502 is electrically connected to an integrator 556, and the output of integrator 556 is amplified by an AC amplifier 558. The signal from one of the sense voltage sources is mixed with a position signal from phase-locked loop 532 by a mixer 536. The output of mixer 536 is then mixed with the output of amplifier 558 by a mixer 538 to generate the Coriolis signal.

Tuning of the Y-axis resonant frequency may be accomplished sense tuning system 560 applying a DC bias voltage between a set of inner tuning electrodes 562 and outer tuning electrodes 564. Electrodes 566 project from structure 502 and are interdigited with the inner tuning electrodes 562 and outer tuning electrodes 564. A tuning voltage source 568 applies a bias voltage $V_{\Delta fy}$ between inner tuning electrodes 562 and outer tuning electrodes 564. Alternately, the Y-axis resonant frequency could be tuned by applying a DC bias between the vibratory structure and the tuning electrodes.

Quadrature error cancellation is accomplished by applying a voltage between diagonal pairs of electrodes. The quadrature error correction system 580 includes a lower left electrode 582a, an upper left electrode 582b, a lower right electrode 584a, and an upper right electrode 584b. Lower left electrode 582a is connected to upper right electrode 584b, and upper left electrode 582b is connected to lower right electrode 584a. A quadrature correction voltage source 586 applies a bias voltage $2V_{Quad}$ between the electrode pairs 582a, 584b and 582b, 584a. The bias voltage creates a balancing force which is proportional to the position of the proof mass along the X-axis. This bias voltage may be determined

experimentally (as shown in FIG. 13) and may be in the range of 1 mV to 100 mV.

In addition, quadrature error correction system 580 may include a feedback loop to automatically adjust the bias voltage. A velocity signal from phase-locked loop 532 may be mixed with a signal from one of the sense voltage sources by a mixer 590. The output of mixer 590 may be mixed with the output of amplifier 558 by a mixer 592. The output of mixer 592 may be used to control the voltage source 586.

Assuming that the mass M of structure 502 is 36 micrograms, the drive and sense frequencies ω_x and ω_y are each 63 kHz, the quality factor Q for single-crystal silicon is 200,000 (about three to four times higher than that of polysilicon), and the amplitude X_0 of the drive mode is five microns, then one may calculate from Equation 16 that, at room temperature, the Brownian noise Ω_{nB} for a bandwidth (BW) of 60 Hz is about 2 deg/hr.

The electronic noise floor is determined by the thermal noise level in charge integrator 556. Where the sense frequency ω_y is electrostatically tuned to the drive frequency ω_x plus an offset frequency $\Delta\omega$, the electronic noise Ω_{nE} may be calculated from the equation:

$$\Omega_{nE} = 2\frac{g_0\Delta\omega}{X_0 V_S}\sqrt{\frac{32}{3\pi}\left(\frac{k_B T}{C_S}\right)\frac{1}{f_T}\left(\left(1+\frac{C_P}{C_S}\right)BW\right.} \qquad (26)$$

where g_0 is the sense-capacitor gap width, X_0 is the oscillation amplitude, V_S is the sense voltage, k_B is Boltzmann's constant, T is the temperature, C_S is the sense capacitance, C_P is the parasitic capacitance, f_T is the CMOS transition frequency, and BW is the bandwidth.

Assuming that the sense-capacitor gap g_0 is 2.5 microns, the sense voltage V_S is 1 V, C_S is the sense capacitance C_S is 1.25 pF, the parasitic capacitance C_P is 0.25 pF, and the CMOS transition frequency f_T is 1 GHz, one may calculate from Equation 18 that a frequency offset $\Delta\omega$ of 2π(175 Hz) is required to make the electronic noise floor equal to 2.5 deg/hr. This degree of tuning is feasible in principle because the measurement bandwidth is about 60 Hz.

By increasing the thickness of electrode teeth 546, 548 and 550, the surface area between the stationary and movable electrodes is increased, resulting in a larger sense capacitance. The larger sense capacitance reduces electronic noise. Similarly, the thicker structure is more massive and thus less subject to Brownian motion. In short, a gyroscopic sensor using high-aspect-ratio single-crystal silicon structures may be about one-hundred times more sensitive than a gyroscopic sensor using structures formed of thin polysilicon layers.

Fabrication of gyroscopic sensor 500 includes six basic steps: handle wafer processing, device wafer processing, bonding, CMOS processing of the bonded structure, etching to form the vibratory structure and stationary electrodes, and capping.

Referring to FIG. 24A, processing of a bottom substrate 600 may begin with a handle wafer 602, which may be a single-crystalline silicon substrate. Handle wafer 602 is oxidized to form an oxide layer 604, and a polysilicon layer 606 is deposited on oxide layer 604. Polysilicon layer 606 is then doped, polished and patterned to form the interconnects for the electrically isolated electrodes 522a, 522b, 524a, 524b, 542a, 542b,

544a, 544b, 562, 564, 582a and 584b, and 582b and 584a, of the gyroscopic sensor.

Referring to FIG. 24B, processing of a top substrate 610 may begin with a device wafer such as a silicon-on-insulator (SOI) substrate. The device wafer includes an oxide layer 616 sandwiched between two single-crystal silicon layers 614 and 618. A shallow trench 620 is formed in a surface 622 of single-crystal silicon layer, except in regions 624. Regions 624 will form anchors 511 connecting vibratory structure 502 to substrate 504. Trench 620 may be formed by deposition of a photoresist mask, etching of the exposed portions of single-crystal silicon layer 614, and removal of the mask. Alternately, trench 620 may be formed by mechanical thinning.

The thickness of single-crystal silicon layer 614 will define the thickness of vibratory structure 502, and the depth of trench 620 will define the spacing between the vibratory structure and the substrate. Preferably, single-crystal silicon layer 614 is about 100 microns thick, and trench 620 is about one micron deep.

Referring to FIG. 24C, bottom substrate 600 and top substrate 610 are aligned with surface 622 of top substrate 610 abutting the patterned polysilicon layer 606 of bottom substrate 600. The top and bottom substrates are bonded so that trench 620 forms a sealed cavity 626 between the two substrates. Then, referring to FIG. 24D, top substrate 610 is thinned by etching or mechanical removal of single-crystal silicon layer 618 to expose oxide layer 616, and oxide layer 616 is stripped. At this point, the bonded assembly is ready for standard CMOS processing. Because sealed cavity 626 is completely internal, the bonded assembly appears as an unprocessed

silicon wafer and may processed with conventional techniques.

Referring to FIG. 24E, the integrated circuitry of gyroscopic sensor 500 is fabricated on an exposed surface 630 of single-crystal silicon layer 614 in device regions 632. Following circuit fabrication, a thermocompression bond layer 634 is deposited and patterned. The bond layer 634 may be a conductive metal, such as gold.

Referring to FIG. 24F, the structures of the gyroscopic sensor are formed in single-crystal silicon layer 614. A photoresist mask is deposited over bond layer 634 and exposed surface 630, and the photoresist mask is patterned to define the gaps between the vibratory structure 502 and the stationary electrodes (not shown in this cross-sectional view). The single-crystal silicon layer 614 is etched using inductively-coupled plasma based deep reactive ion etching until cavity 626 is exposed. The etching step forms trenches 636 which create the free-standing vibratory structure and the various electrode structures of the gyroscopic sensor. Following the reactive ion etching, an oxygen plasma may be used to remove the photoresist mask, and the assembly may undergo a UV-ozone clean.

Finally, referring to FIG. 24G, a capping wafer 640 is aligned and bonded to top substrate 610. Capping wafer 640 may be glass or oxidized silicon. An underside 642 of the capping wafer may include a patterned thermocompression bond layer 644. Bond layer 634 may be aligned with bond layer 644, and the thermocompression bond may be formed by the application of a pressure of approximately 20 psi and a temperature of about 300-350°C for several minutes. The capping wafer may also include

an etched hole 646 that permits access to bonding pads 648 in device regions 632.

The present invention has been described in terms of a preferred embodiment. The invention, however, is not limited to the embodiment depicted and described. Rather, the scope of the invention is defined by the appended claims.

What is claimed is:

1. A microfabricated structure comprising:

a substrate;

a mass connected to said substrate by a suspension system to vibrate in a plane parallel to a surface of said substrate;

a first plurality of electrode fingers projecting from said mass along a first axis in said plane;

a second plurality of electrode fingers, coplanar with said first plurality of electrode fingers, connected to said substrate and projecting substantially along said first axis;

a third plurality of electrode fingers connected to said substrate but electrically isolated from said second plurality of electrode fingers, said first third plurality of electrode fingers being coplanar with said first and second plurality of electrode fingers and projecting substantially along said first axis, said second and third plurality of electrode fingers interdigitated with said first plurality of electrode fingers such that each of said first plurality of electrode fingers is adjacent to one of said second plurality of electrode fingers and one of said third plurality of electrode fingers.

2. The structure of claim 1 further comprising a voltage source to apply a voltage between said second and third plurality of electrode fingers.

3. The structure of claim 1 further comprising

a fourth plurality of electrode fingers, coplanar with said first, second and third plurality of electrode

fingers, projecting from said mass along said first axis, and

a fifth plurality of electrode fingers connected to said substrate but electrically isolated from said second and third plurality of electrode fingers, said fourth and fifth plurality of electrode fingers interdigitated.

4. The structure of claim 3 wherein each of said first plurality of electrode fingers has a first length and each of said fourth plurality of electrode fingers has a second length.

5. The structure of claim 4 wherein said first length is greater than said second length.

6. A microfabricated structure comprising:

a substrate; and

a suspension system to permit a mass to vibrate in a plane parallel to a surface of said substrate, said suspension system including,

first and second substantially parallel beams, each of said first and second beams anchored at both ends to said substrate, and

third and fourth substantially parallel beams, one end of each of said third and fourth beams connected to said first beam and another end connected to said second beam.

7. The structure of claim 6 further comprising a plurality of fingers projecting along an axis substantially parallel to said first and second beams.

8. The structure of claim 6 further comprising

a fifth and a sixth beam, one end of each of said fifth beam and sixth beams connected to said third beam and another end connected to said fourth beam, and

a seventh beam, one end of said seventh beam connected to said fifth beam and another end connected to said sixth beam.

9. The structure of claim 8 further comprising a plurality of fingers projecting from said seventh beam along an axis substantially parallel to said first and second beams.

10. The structure of claim 6 wherein sections of said first and second beams located between said third and fourth beams are substantially rigid to prevent rotation of said mass.

11. A sensor comprising:

a substrate;

a mass connected to said substrate by a suspension system to vibrate in a plane parallel to a surface of said substrate;

a first plurality of electrode fingers projecting from said mass along a first axis in said plane;

a second plurality of electrode fingers connected to said substrate and projecting substantially along said first axis;

a third plurality of electrode fingers connected to said substrate but electrically isolated from said second plurality of electrode fingers, said third plurality of electrode fingers projecting substantially along said first axis, said second and third pluralities

of electrode fingers interdigitated with said first plurality of electrode fingers such that each of said first plurality of electrode fingers is adjacent to one of said second plurality of electrode fingers and one of said third plurality of electrode fingers;

a position sensor to mesure a deflection of said mass in said plane; and

a voltage source for applying a first DC voltage between said second and third pluralities of electrode fingers to cause said mass to vibrate, absent a Coriolis force, more precisely along said first axis.

12. The sensor of claim 11 further including,

a fourth plurality of electrode fingers projecting from said mass along a first axis in said plane and positioned opposing said first plurality of electrode fingers;

a fifth plurality of electrode fingers connected to said substrate and projecting substantially along said first axis;

a sixth plurality of electrode fingers connected to said substrate but electrically isolated from said fifth plurality of electrode fingers, said sixth plurality of electrode fingers projecting substantially along said first axis, said fifth and sixth plurality of electrode fingers interdigitated with said third plurality of electrode fingers such that each of said fourth plurality of electrode fingers is adjacent to one of said fifth plurality of electrode fingers and one of said sixth plurality of electrode fingers.

13. The sensor of claim 12 further comprising a second voltage source for applying a second DC voltage between

said fifth and sixth plurality of electrode fingers to cause said mass to vibrate, absent a Coriolis force, more precisely along said first axis.

14. The sensor of claim 13 wherein said second DC voltage is substantially equal in magnitude but opposite in sign to said first DC voltage.

15. The sensor of claim 13 wherein said first plurality of electrode fingers is electrically coupled to said second plurality of electrode fingers.

16. The sensor of claim 13 further comprising a voltage source for applying a third DC voltage between said first and third pluralities of electrode fingers and said second, third, fifth and sixth pluralities of electrode fingers to adjust the resonant frequency of vibrations of said mass along a second axis in said plane perpendicular to said first axis.

17. The sensor of claim 11 wherein the position sensor measures the deflection of said mass along a second axis substantially perpendicular to said first axis and rotation of said mass about a Z-axis perpendicular to said surface and vibration of said mass along said first axis generates a Coriolis force to deflect said mass along said second axis, and wherein the sensor further comprises a signal processor coupled to an output of said position sensor to generate a signal varying with the rate of rotation of said mass about the Z-axis.

18. The sensor of claim 17 further comprising a voltage source for applying an AC voltage between said second and third plurality of electrode fingers.

19. The sensor of claim 18 wherein a voltage is applied between said second and third pluralities of electrode fingers to form a capacitive bridge with said first plurality of electrodes, and said position sensor is coupled to said first plurality of electrodes to detect changes in capacitance when said mass is deflected along said second axis.

20. A sensor comprising:

a substrate;

a mass connected to said substrate by a suspension system to vibrate in a plane parallel to a surface of said substrate;

a first plurality of electrode fingers projecting from said mass along a first axis in said plane;

a second plurality of electrode fingers connected to said substrate and projecting substantially along said first axis;

a third plurality of electrode fingers connected to said substrate but electrically isolated from said second plurality of electrode fingers, said first third plurality of electrode fingers projecting substantially along said first axis, said second and third plurality of electrode fingers interdigitated with said first plurality of electrode fingers such that each of said first plurality of electrode fingers is adjacent to one of said second plurality of electrode fingers and one of said third plurality of electrode fingers; and

a voltage source for applying a DC voltage between said first plurality of electrode fingers and said second and third plurality of electrode fingers to adjust the resonant frequency of vibrations of said mass along a second axis in said plane perpendicular to said first axis.

21. A microfabricated gyroscopic sensor for sensing rotation about a Z-axis, comprising:

a substrate;

a mass connected to said substrate by a suspension system to vibrate in a plane parallel to a surface of said substrate;

a drive system to cause said mass to vibrate substantially along a first axis in said plane;

a first plurality of electrode fingers projecting from said mass substantially along said first axis;

a second plurality of electrode fingers connected to said substrate and projecting substantially along said first axis;

a third plurality of electrode fingers connected to said substrate and projecting substantially along said first axis, said second and third plurality of electrode fingers interdigitated with said first plurality of electrode fingers such that each of said first plurality of electrode fingers is adjacent to one of said second plurality of electrode fingers and one of said third plurality of electrode fingers;

a position sensor coupled to said first plurality of electrode fingers for measuring the deflection of said mass along a second axis in said plane perpendicular to said first axis, wherein rotation of said mass about a Z-axis perpendicular to said surface and vibration of said

mass along said first axis generates a Coriolis force to deflect said mass along said second axis; and

a signal processor coupled to an output of said position sensor to generate a signal varying with the rate of rotation of said mass about the Z-axis.

22. The sensor of claim 21 further comprising a voltage source for applying an AC voltage having a first frequency between said second and third plurality of electrode fingers.

23. The sensor of claim 22 wherein a voltage is applied between said second and third pluralities of electrode fingers to form a capacitive bridge with said first plurality of electrodes, and said position sensor is coupled to said first plurality of electrodes to detect changes in capacitance when said mass is deflected along said second axis.

24. The sensor of claim 23 wherein said position sensor further includes an integrator to integrate a signal from said first plurality of electrode fingers.

25. The sensor of claim 24 wherein said drive system generates a signal to cause said mass to oscillate along said first axis at a second frequency.

26. The sensor of claim 25 wherein said drive system said signal.

27. The sensor of claim 25 further including a first mixer to mix the signal from said drive system with a signal from said voltage source.

28. The sensor of claim 27 further including a second mixer to mix a signal from said first mixer with an output signal from said position sensor to produce a position quadrature signal.

29. The sensor of claim 27 further including a second mixer to mix a signal from said first mixer with an output signal from said position sensor to produce a Coriolis signal.

30. The sensor of claim 25 further including a mixer to mix an output signal from said position sensor with a signal from said voltage source to produce a position signal.

31. A microfabricated gyroscopic sensor, comprising:

a substrate;

a mass connected to the substrate by a suspension system;

a drive system to cause the mass to vibrate along a drive axis substantially parallel to a surface of the substrate; and

a position sensor to measure a deflection of the mass along a sense axis substantially parallel to the surface of the substrate, wherein rotation of the mass about an axis of rotation substantially perpendicular to the surface of the substrate and vibration of the mass along the drive axis generates a Coriolis force to deflect the mass along the sense axis.

32. The sensor of claim 31 further comprising a processor coupled to an output of the position sensor to

generate a signal varying with the rate of rotation of the mass about the axis of rotation.

33. The sensor of claim 31 wherein the position sensor includes a first sense electrode projecting from the mass, a second sense electrode connected to the substrate and positioned on a first side of the first electrode, and a third sense electrode connected to the substrate and positioned on an opposing second side of the first electrode.

34. The sensor of claim 33 wherein the position sensor senses a change in capacitance between the first electrode and the second and third electrodes.

35. The sensor of claim 33 wherein the first, second and third electrodes are substantially coplanar and each electrode has a longitudinal axis substantially aligned with the drive axis.

36. The sensor of claim 31 wherein the drive system includes a first drive electrode projecting from the mass, a second drive electrode connected to the substrate and positioned on a first side of the first electrode, and a third drive electrode connected to the substrate and positioned on an opposing second side of the first electrode.

37. The sensor of claim 35 wherein the drive system applies an alternating voltage between the between the first electrode and the second and third electrodes.

38. The sensor of claim 33 wherein the first, second and third electrodes are substantially coplanar and each electrode has a longitudinal axis substantially aligned with the drive axis.

39. The sensor of claim 31 further comprising a voltage source to apply a voltage between a plurality of correction electrodes connected to the substrate to cause the mass to vibrate, absent the Coriolis force, more precisely along the drive axis.

40. The sensor of claim 31 further comprising a voltage source to apply a voltage between a first tuning electrode connected to the substrate and a second tuning electrode connected to the mass to adjust a resonant frequency of vibrations of the mass along the sense axis.

41. A microfabricated gyroscopic sensor, comprising:

a substrate;

a mass connected to the substrate by a suspension system;

a drive system to cause the mass to vibrate substantially along a drive axis;

a position sensor to measure a deflection of the mass along a sense axis, wherein rotation of the mass about an axis of rotation and vibration of the mass along the drive axis generates a Coriolis force to deflect the mass along the sense axis; and

a voltage source to apply a voltage between electrodes connected to the substrate to cause the mass to vibrate, absent the Coriolis force, more precisely along the drive axis.

42. The sensor of claim 41 further comprising a processor coupled to an output of the position sensor to generate a signal varying with the rate of rotation of the mass about the axis of rotation.

43. The sensor of claim 41 further comprising a second voltage source to apply a second voltage between electrodes connected to the mass and the electrodes connected to the substrate to adjust a resonant frequency of vibrations of the mass along the sense axis.

44. The sensor of claim 41 wherein the position sensor applies an AC voltage between the electrodes connected to the substrate.

45. The sensor of claim 41 wherein the drive axis and sense axis are substantially parallel to a surface of the substrate and the axis of rotation is substantially perpendicular to the surface of the substrate.

46. The sensor of claim 41 further comprising:

a first plurality of electrode fingers projecting from the mass substantially along the drive axis;

a second plurality of electrode fingers connected to the substrate and projecting substantially along the drive axis; and

a third plurality of electrode fingers connected to the substrate and projecting substantially along the drive axis, the second and third pluralities of electrode fingers interdigitated with the first plurality of electrode fingers such that each of the first plurality of electrode fingers is adjacent to one of the second

plurality of electrode fingers and one of the third plurality of electrode fingers.

47. The sensor of claim 46 further comprising:

a fourth plurality of electrode fingers projecting from the mass substantially along the drive axis and positioned opposing the first plurality of electrode fingers;

a fifth plurality of electrode fingers connected to the substrate and projecting substantially along the drive axis and positioned opposing the second plurality of electrode fingers; and

a sixth plurality of electrode fingers connected to the substrate and projecting substantially along the drive axis and positioned opposing the third plurality of electrode fingers, the fifth and sixth pluralities of electrode fingers interdigitated with the fourth plurality of electrode fingers such that each of the fourth plurality of electrode fingers is adjacent to one of the fifth plurality of electrode fingers and one of the sixth plurality of electrode fingers.

48. The sensor of claim 47 wherein the first, second, third, fourth, fifth and sixth pluralities of electrode fingers are substantially co-planar.

49. The sensor of claim 48 wherein the voltage source applies a first DC voltage between the second plurality and the third plurality of electrode fingers and a second DC voltage between the fifth plurality and the sixth plurality of electrode fingers.

50. The sensor of claim 49 wherein the second DC voltage is substantially equal in magnitude and opposite in sign to the first DC voltage.

51. The sensor of claim 21 further comprising a voltage source for applying a DC voltage between the first plurality of electrode fingers and the second and third pluralities of electrode fingers to adjust a resonant frequency of vibrations of the mass along the second axis.

52. The sensor of claim 21 further comprising a voltage source for applying a first DC voltage between the second and third pluralities of electrode fingers to cause the mass to vibrate, absent a Coriolis force, more precisely along the first axis.

53. A method of sensing rotation with a gyroscopic sensor including a mass connected to a substrate by a suspension system, comprising:

rotating the mass about an axis of rotation substantially perpendicular to a surface of the substrate;

causing the mass to vibrate substantially along a drive axis substantially parallel to the surface of the substrate, rotation of the mass about the axis of rotation and vibration of the mass along the drive axis generating a Coriolis force to deflect the mass along a sense axis substantially parallel to the surface of the substrate; and

measuring a deflection of the mass along the sense axis.

54. A method of sensing rotation with a gyroscopic sensor including a mass connected to a substrate by a suspension system, comprising:

rotating the mass about an axis of rotation;

causing the mass to vibrate substantially along a drive axis, rotation of the mass about the axis of rotation and vibration of the mass along the drive axis generating a Coriolis force to deflect the mass along a sense axis;

measuring a deflection of the mass along the sense axis; and

applying a voltage between electrode fingers connected to the substrate to cause the mass to vibrate, absent a Coriolis force, more precisely along the first axis.

55. A microfabricated gyroscopic sensor for measuring rotation about an input axis, comprising:

a substrate;

a mass;

a suspension system connecting the mass to the substrate;

a drive system to cause the mass to oscillate substantially about a drive axis;

a position sensor to measure a rotation of the mass about a sense axis, wherein rotation of the mass about the input axis and oscillation of the mass about the drive axis generates a Coriolis force to oscillate the mass about the sense axis;

a plurality of electrodes associated with the substrate; and

a voltage source to apply a voltage between the electrodes to cause the mass to oscillate, in the absence the Coriolis force, more precisely about the drive axis.

56. The sensor of claim 55 further comprising a processor coupled to an output of the position sensor to generate a signal varying with the rate of rotation of the mass about the input axis.

57. The sensor of claim 55 further comprising a second voltage source to apply a second voltage between electrodes connected to the mass and the electrodes connected to the substrate to adjust a resonant frequency of oscillations of the mass about the sense axis.

58. The sensor of claim 55 wherein the position sensor applies an AC voltage between the electrodes connected to the substrate.

59. The sensor of claim 55 wherein the drive axis is substantially perpendicular to the surface of the substrate and the input axis and sense axis are substantially parallel to a surface of the substrate.

60. The sensor of claim 59 further comprising:

a first plurality of electrode fingers projecting from the mass;

a second plurality of electrode fingers projecting from the mass;

a third plurality of electrode fingers projecting from the substrate and interdigitated with the first plurality of electrode fingers; and

a fourth plurality of electrode fingers projecting from the substrate and positioned opposing the first plurality of electrode fingers, the fourth plurality of electrode fingers interdigitated with the second plurality of electrode fingers.

61. The sensor of claim 60 further comprising:

a fifth plurality of electrode fingers projecting from the mass;

a sixth plurality of electrode fingers projecting from the mass;

a seventh plurality of electrode fingers projecting from the substrate and interdigitated with the fifth plurality of electrode fingers; and

a eighth plurality of electrode fingers projecting from the substrate and positioned opposing the seventh plurality of electrode fingers, the eighth plurality of electrode fingers interdigitated with the sixth plurality of electrode fingers.

62. The sensor of claim 61 wherein the first, second, third, fourth, fifth, sixth, seventh and eighth pluralities of electrode fingers are substantially co-planar.

63. The sensor of claim 62 wherein the voltage source applies a first DC voltage between the third plurality and the fourth plurality of electrode fingers and a second DC voltage between the seventh plurality and the eighth plurality of electrode fingers.

64. The sensor of claim 63 wherein the second DC voltage is substantially equal in magnitude and opposite in sign to the first DC voltage.

65. The sensor of claim 55 further comprising a first electrode projecting from the mass, a second electrode connected to the substrate and positioned beneath a first portion of the first electrode, and a third electrode connected to the substrate and positioned beneath a second portion of the first electrode.

66. The sensor of claim 55 wherein the mass is substantially ring-shaped.

67. A method of sensing rotation with a gyroscopic sensor including a mass connected to a substrate by a suspension system, comprising:

rotating the mass about an input axis;

causing the mass to oscillate substantially about a drive axis, rotation of the mass about the input axis and oscillation of the mass about the drive axis generating a Coriolis force to oscillate the mass about a sense axis;

measuring an oscillation of the mass about the sense axis; and

applying a voltage between electrodes connected to the substrate to cause the mass to oscillate, in the absence of a Coriolis force, more precisely about the drive axis.

68. A microfabricated gyroscopic sensor, comprising:

a substrate having a first plurality of electrode teeth;

a vibratory structure including a second plurality of electrode teeth and a suspension system connecting the second plurality of electrode teeth to the substrate, the second plurality of electrode teeth interdigited with the first plurality of electrode teeth;

a drive system to cause the vibratory structure to oscillate relative to the substrate; and

a position sensor to measure a deflection of the mass caused by a Coriolis force;

wherein the first and second pluralities of electrode teeth have thicknesses substantially greater than their widths.

69. The sensor of claim 68 wherein the suspension system includes a plurality of flexures having an aspect ratio of at least about 10:1.

70. The sensor of claim 68 wherein the first and second pluralities of electrode teeth have an aspect ratio of at least 5:1.

71. The sensor of claim 68 wherein gaps between the first and second pluralities of electrode teeth have an aspect ratio of at least 10:1.

72. A method of fabricating a gyroscopic sensor, comprising:

forming an insulative layer on a first substrate;

forming a recess in a first surface of a second substrate;

bonding the first surface of the second substrate to the first substrate so that the recess defines an enclosed cavity between the first and second substrates;

forming circuitry for the gyroscopic sensor on a second surface of the second substrate

etching a plurality of trenches in the second substrate from the second surface to the cavity, the plurality of trenches defining a vibratory structure connected to the first substrate.

73. The method of claim 72 wherein the vibratory structure has a thickness of at least 25 microns.

74. The method of claim 72 wherein the recess has a depth of about 1 micron.

75. The method of claim 72 wherein the etching step comprises a deep reactive ion etch.

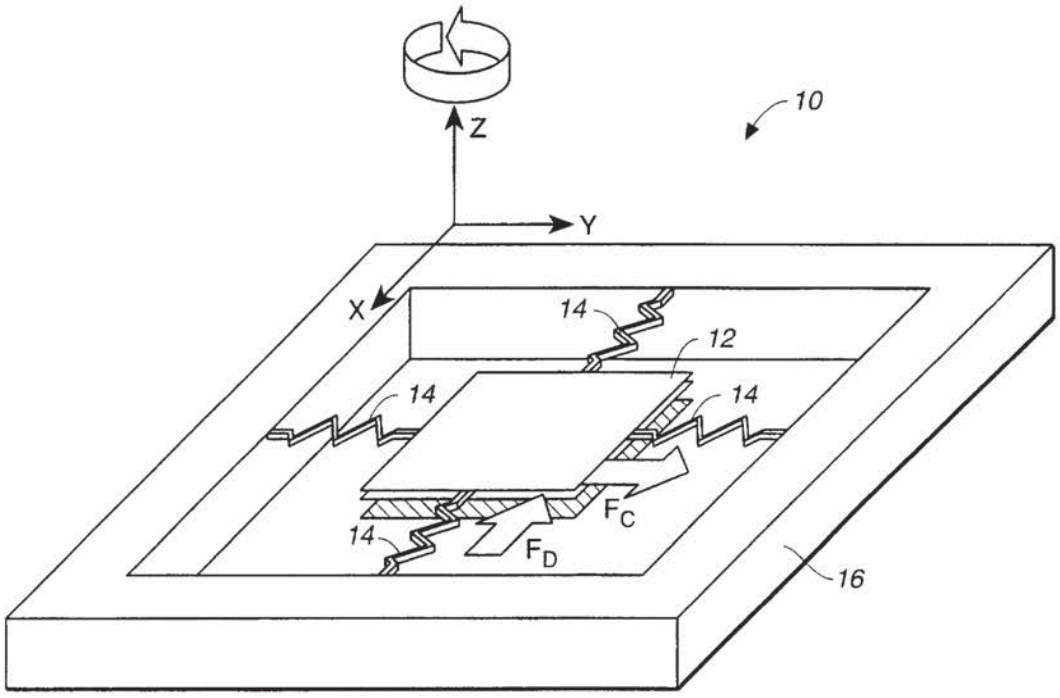


FIG._1

Nintendo Exhibit 1066
IPR2024-00668 - Page 455

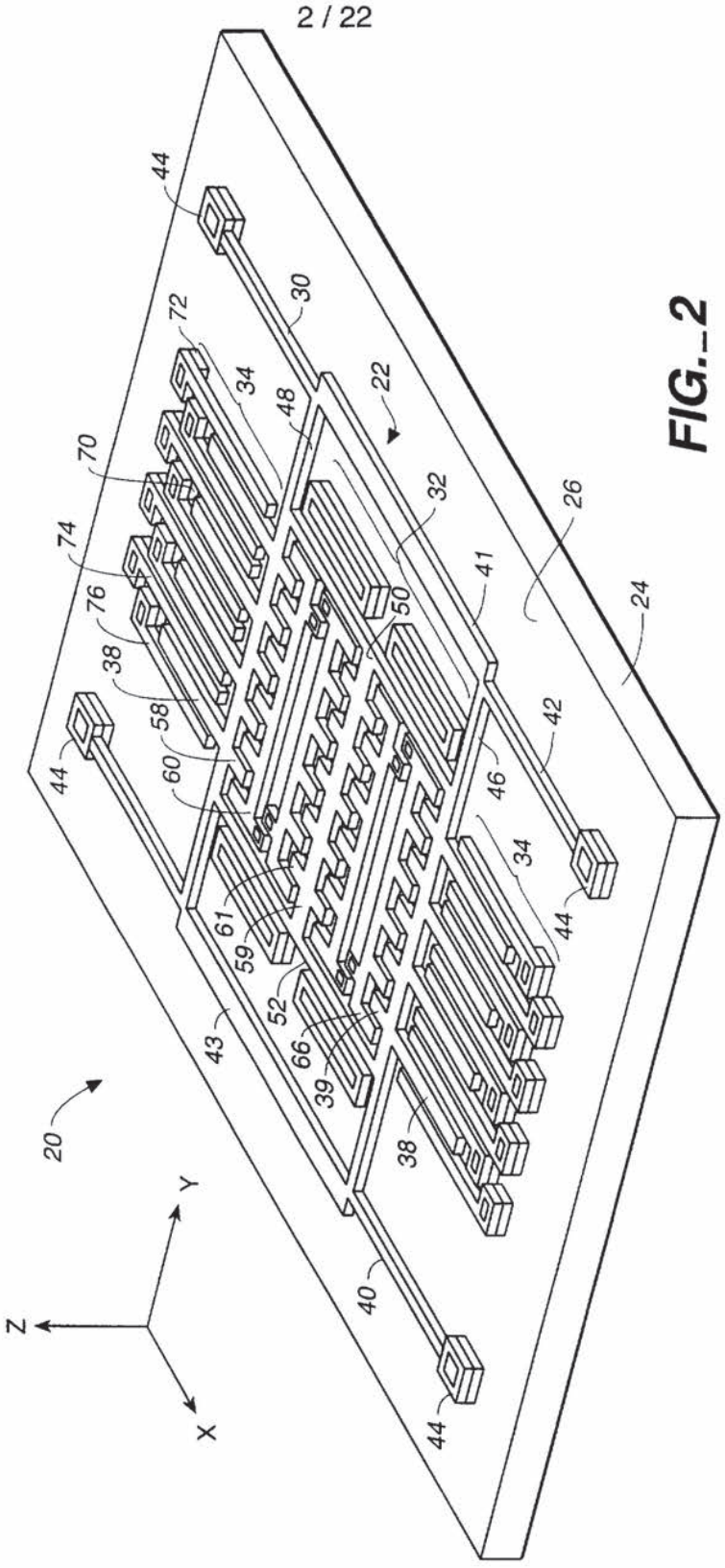


FIG._2

Nintendo Exhibit 1066
IPR2024-00668 - Page 456

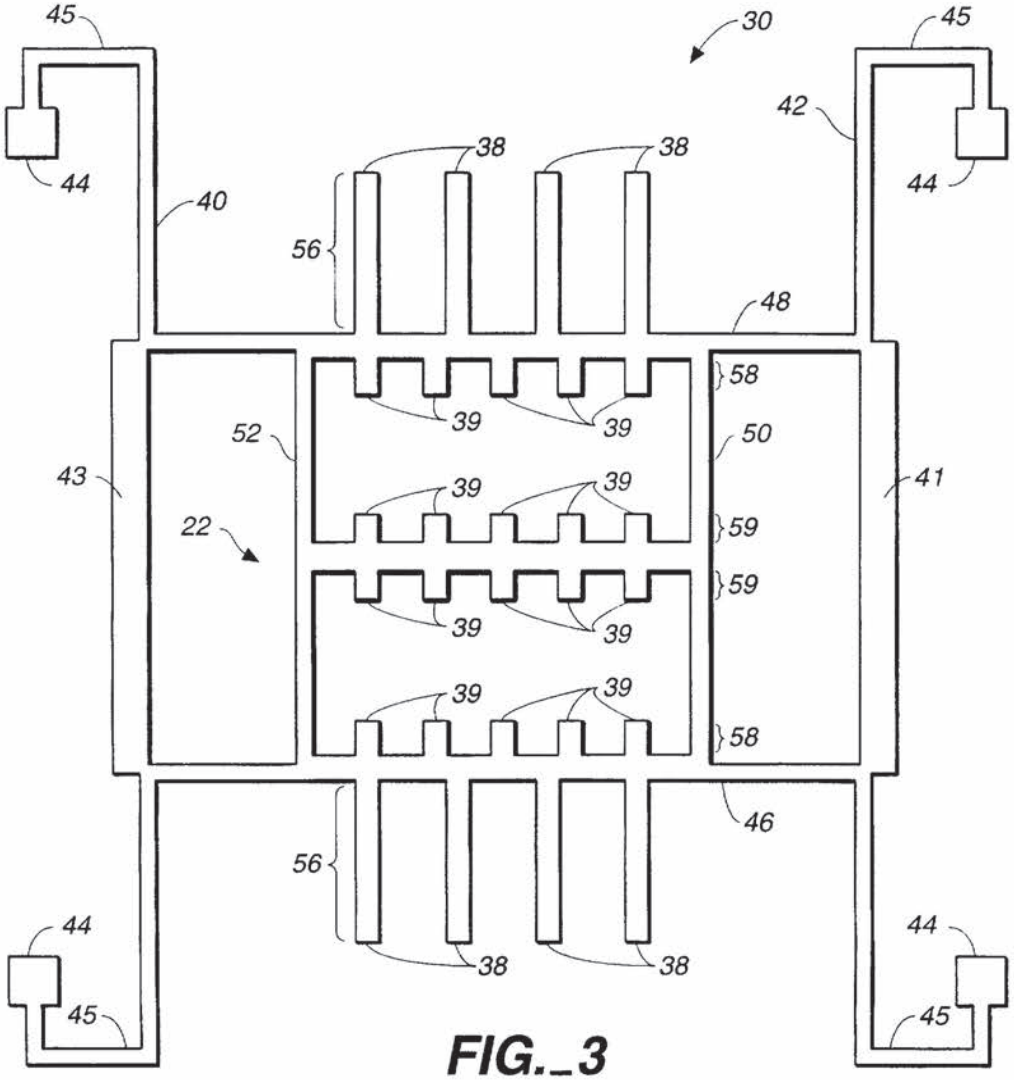


FIG._3

Nintendo Exhibit 1066
IPR2024-00668 - Page 457

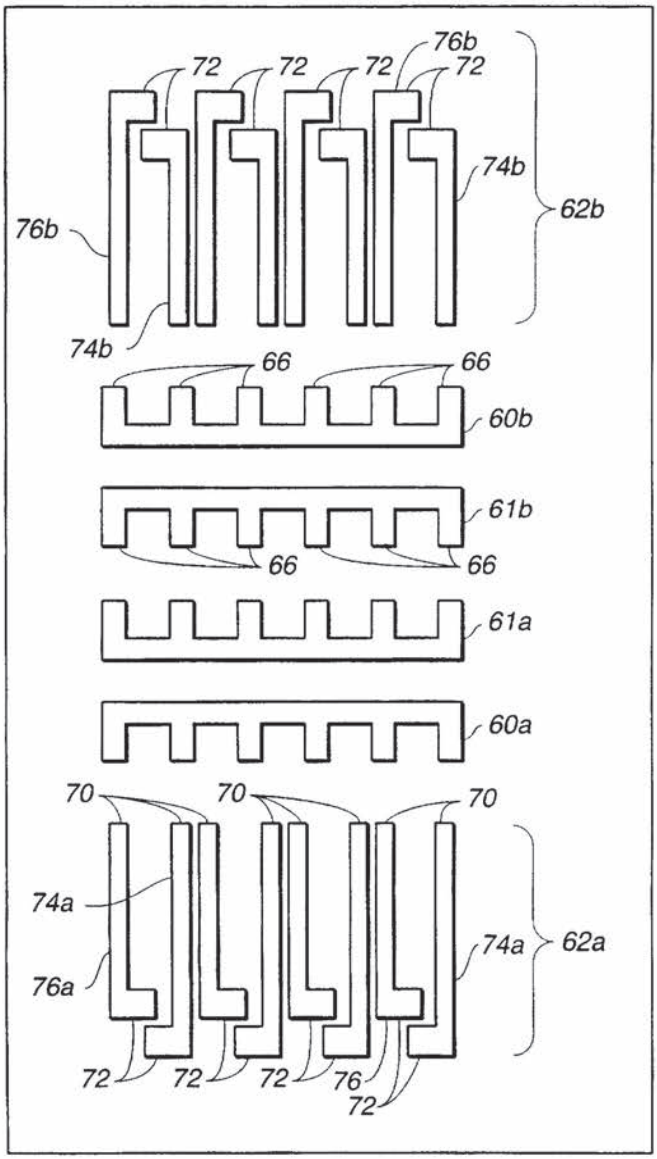


FIG._4

Nintendo Exhibit 1066
IPR2024-00668 - Page 458

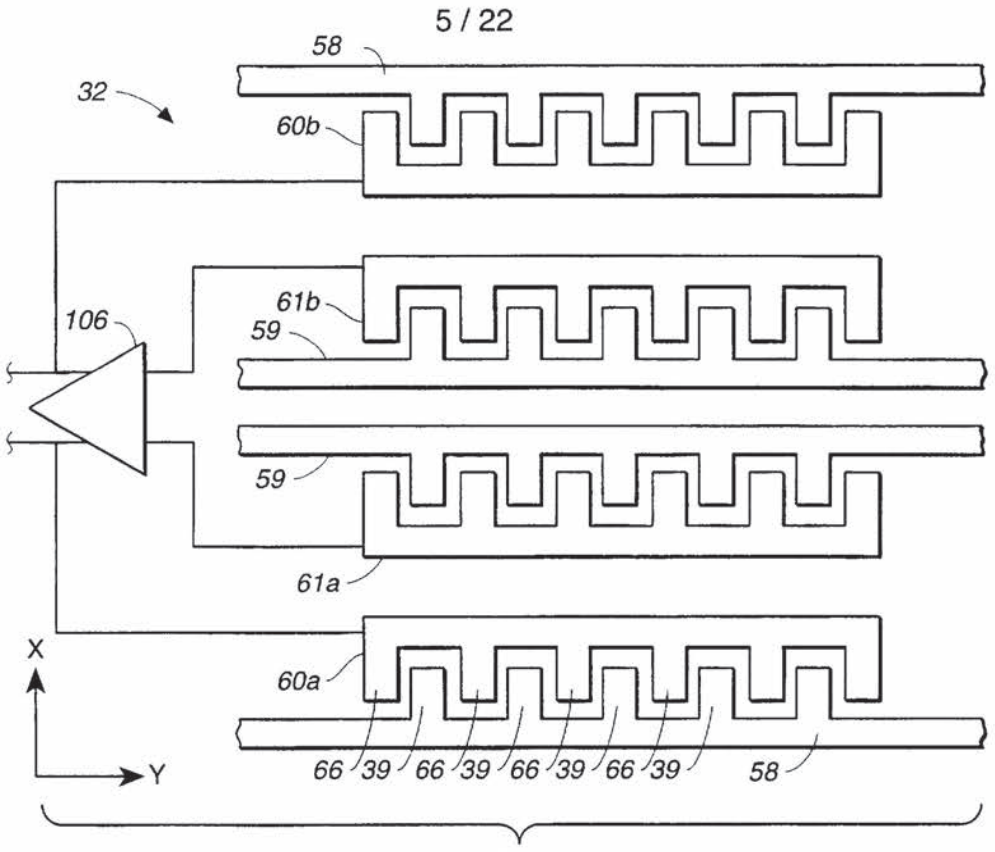


FIG._5

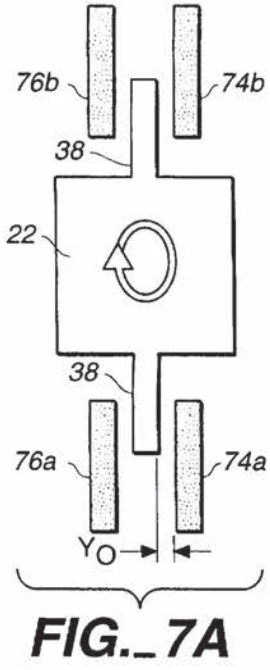


FIG._7A

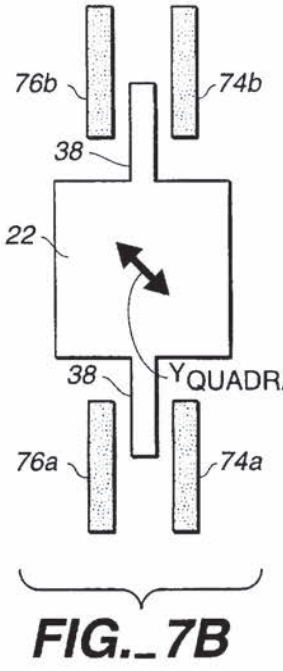


FIG._7B

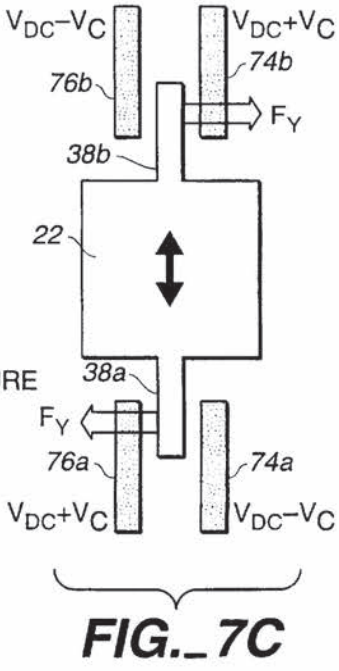


FIG._7C

Nintendo Exhibit 1066
IPR2024-00668 - Page 459

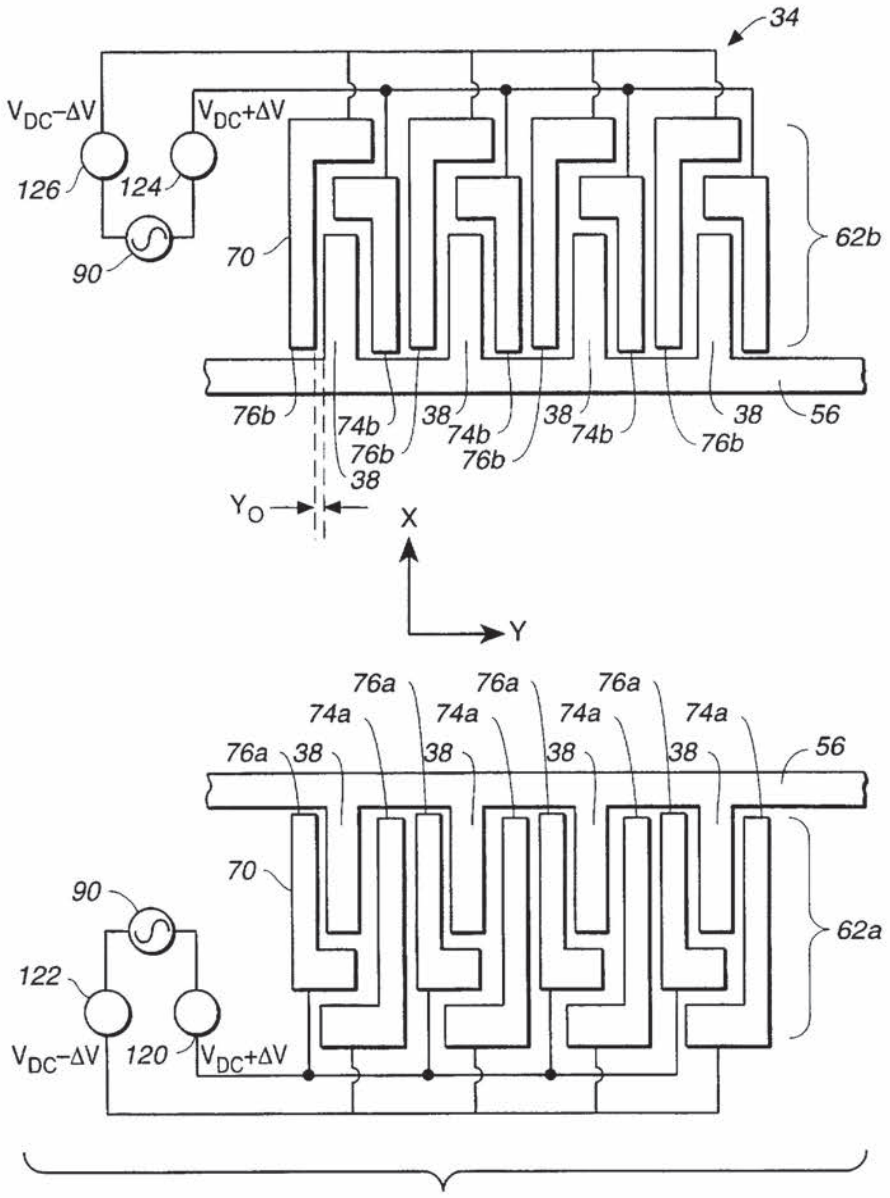


FIG._6

Nintendo Exhibit 1066
IPR2024-00668 - Page 460

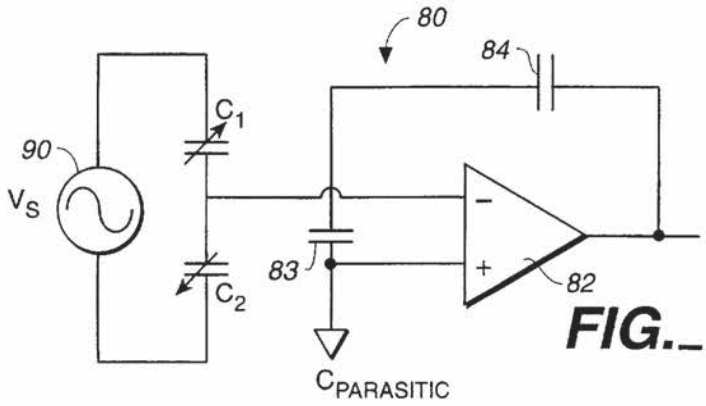


FIG._8A

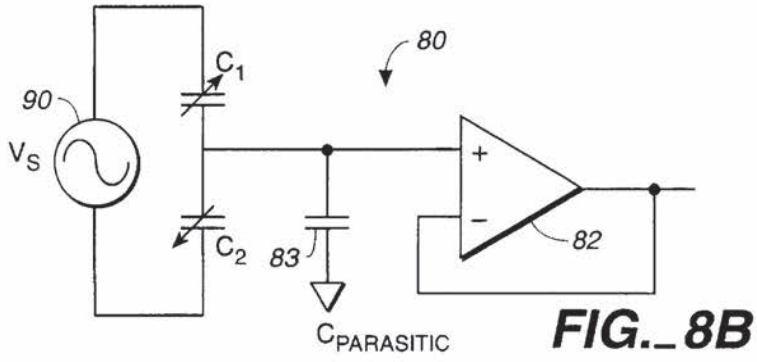


FIG._8B

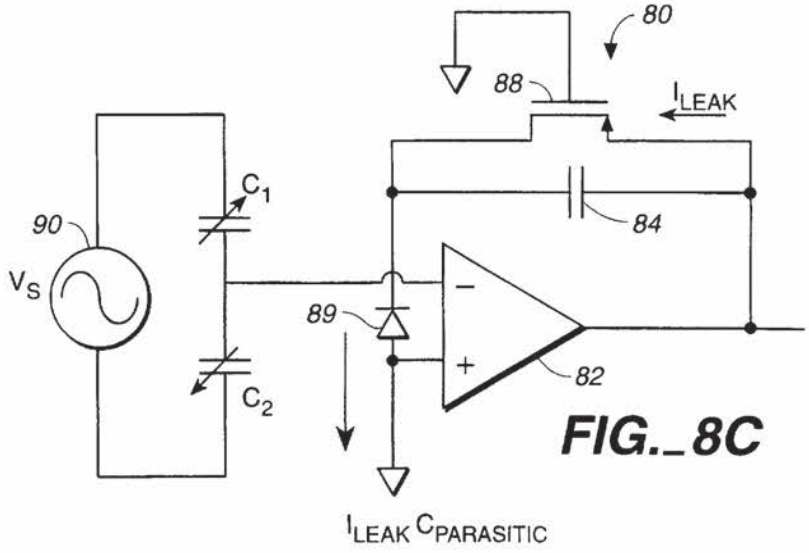


FIG._8C

Nintendo Exhibit 1066
IPR2024-00668 - Page 461

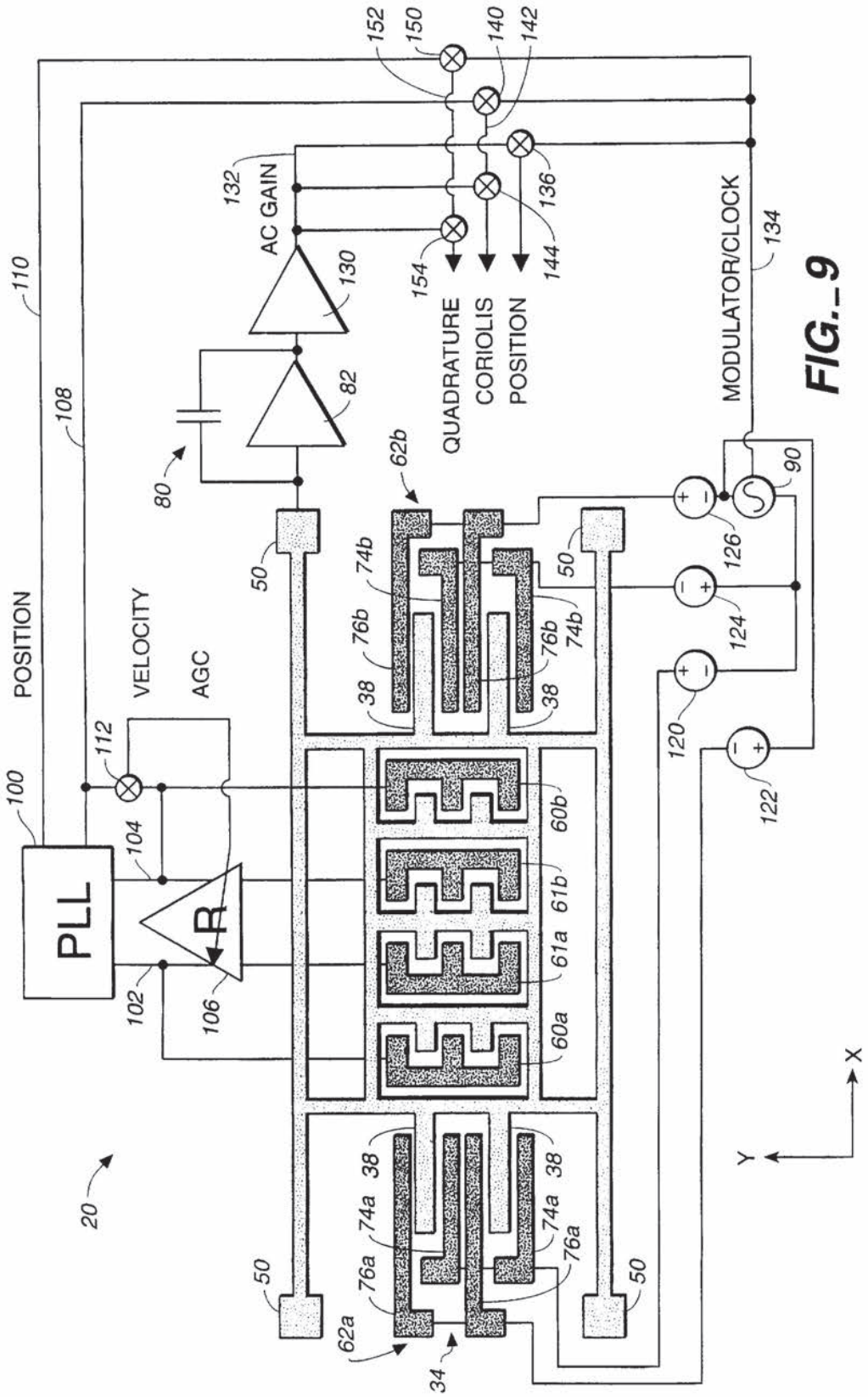


FIG._9

Nintendo Exhibit 1066
IPR2024-00668 - Page 462

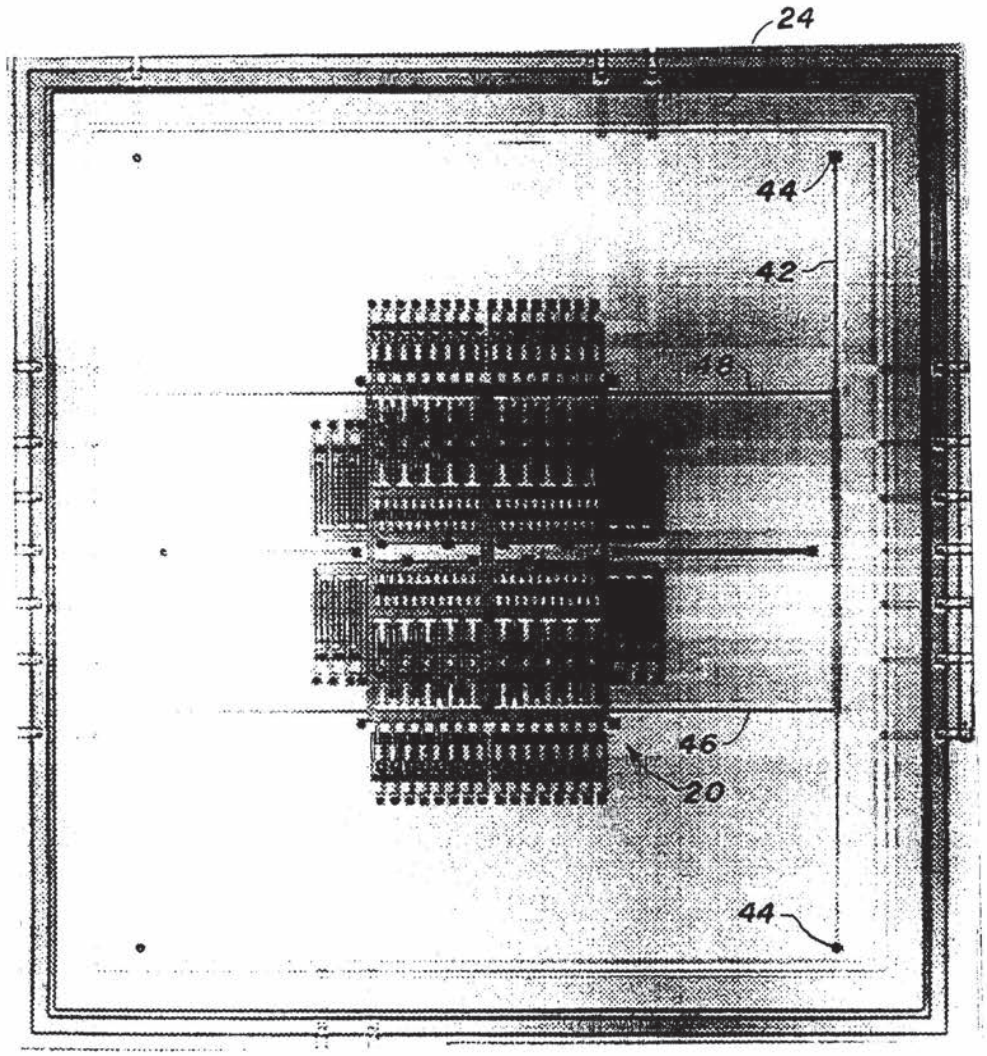


FIG._10

Nintendo Exhibit 1066
IPR2024-00668 - Page 463

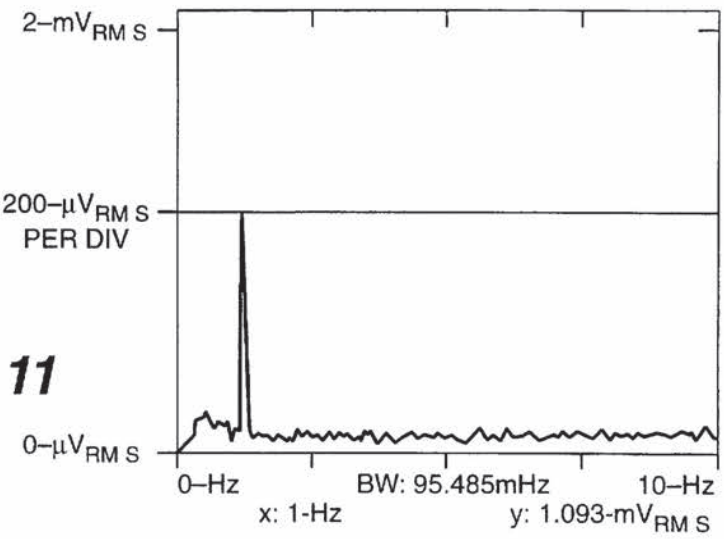


FIG._11

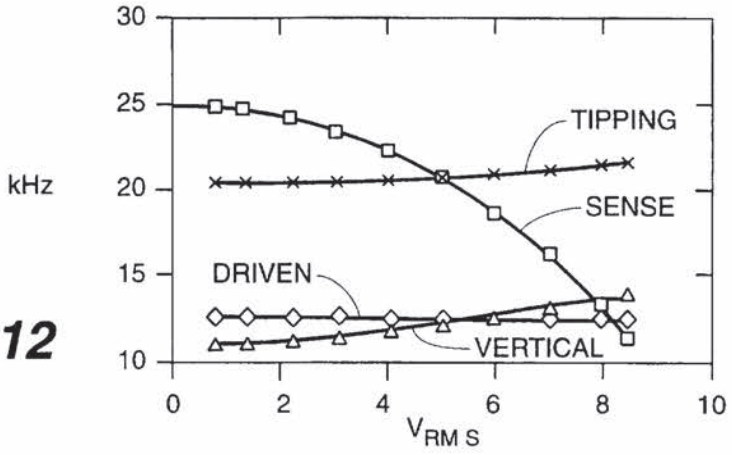


FIG._12

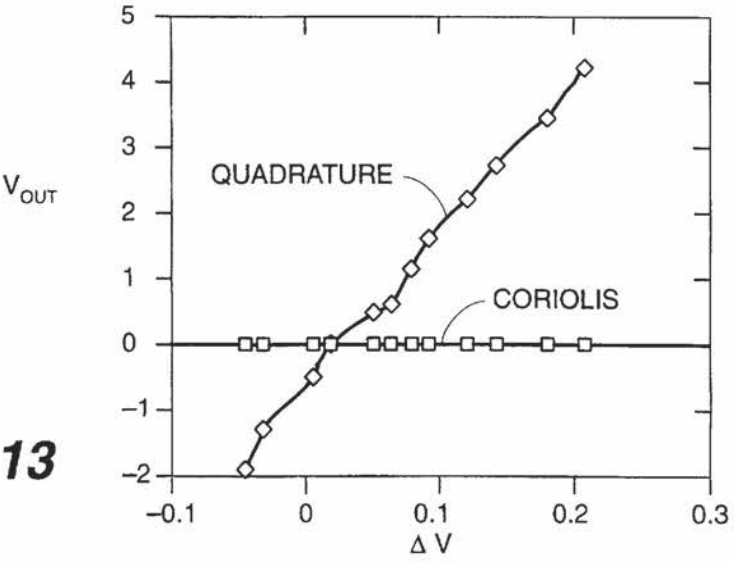


FIG._13

Nintendo Exhibit 1066
IPR2024-00668 - Page 464

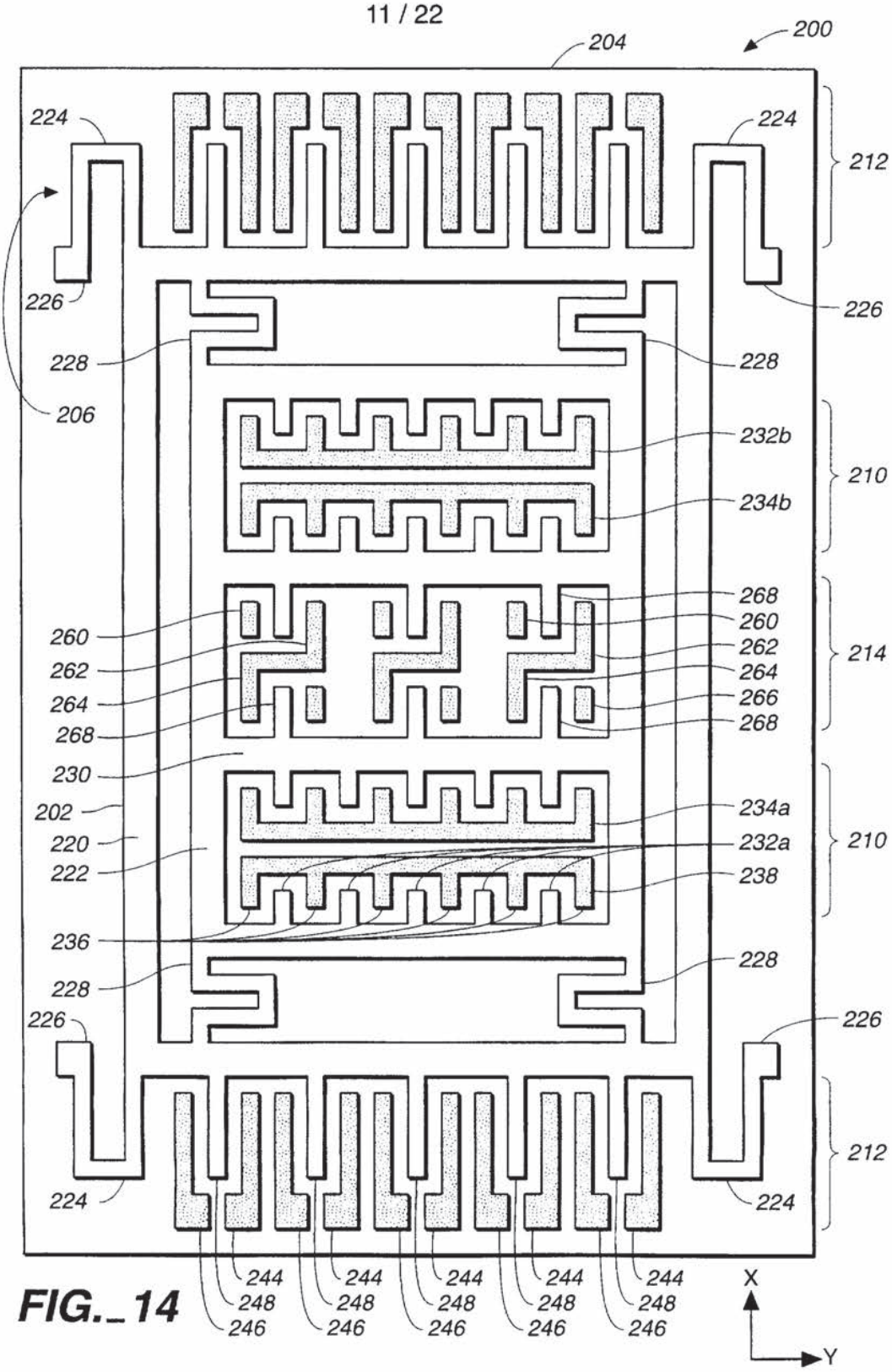
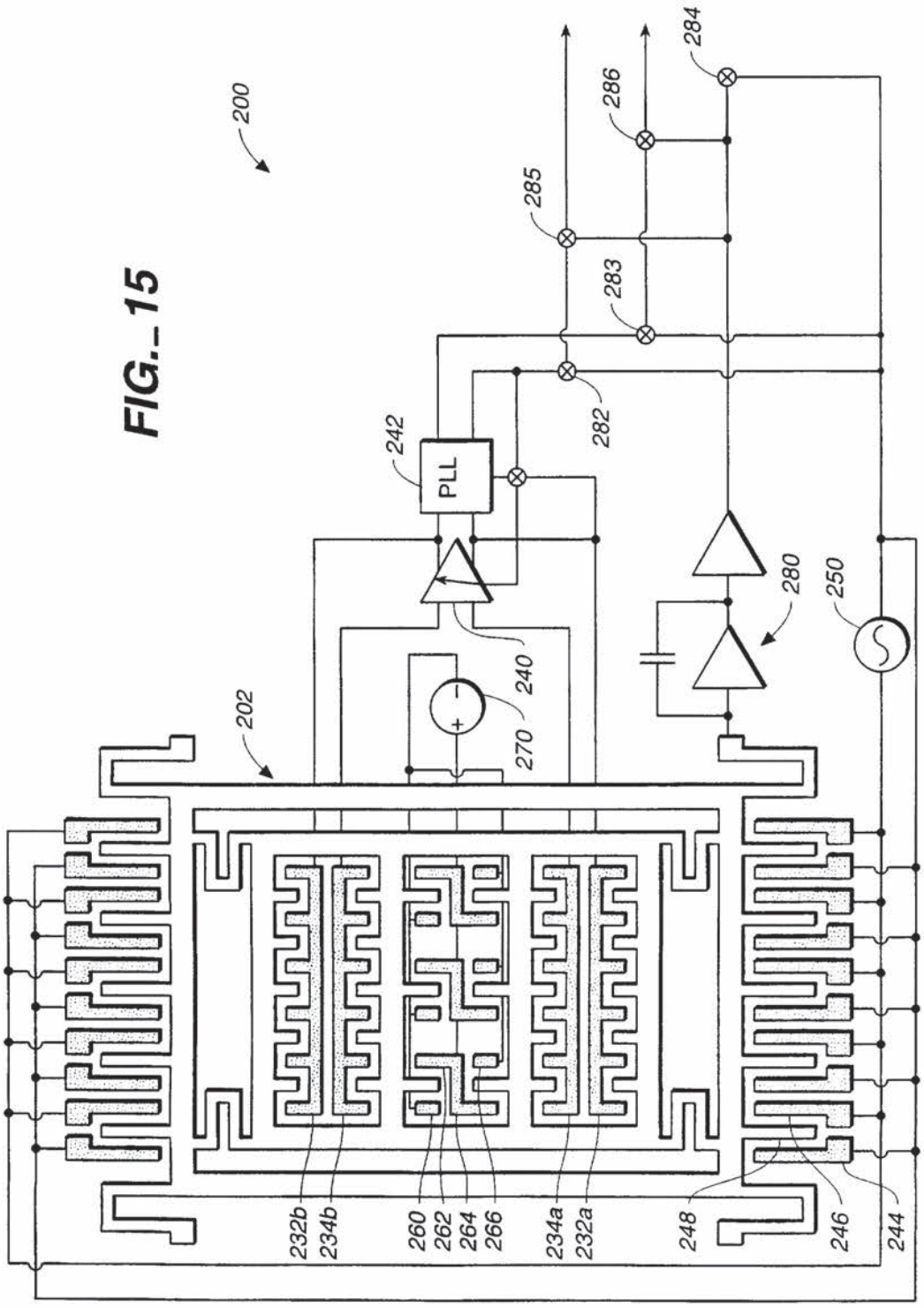


FIG._14

Nintendo Exhibit 1066
IPR2024-00668 - Page 465

FIG._15



Nintendo Exhibit 1066
IPR2024-00668 - Page 466

FIG._16

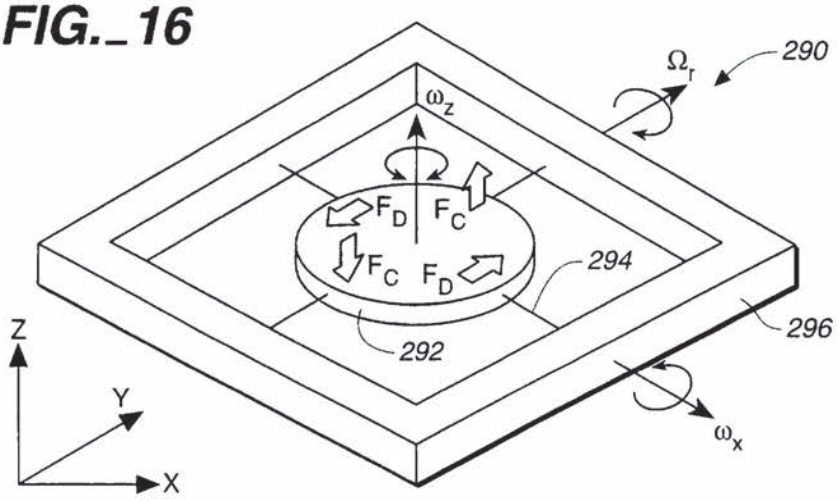
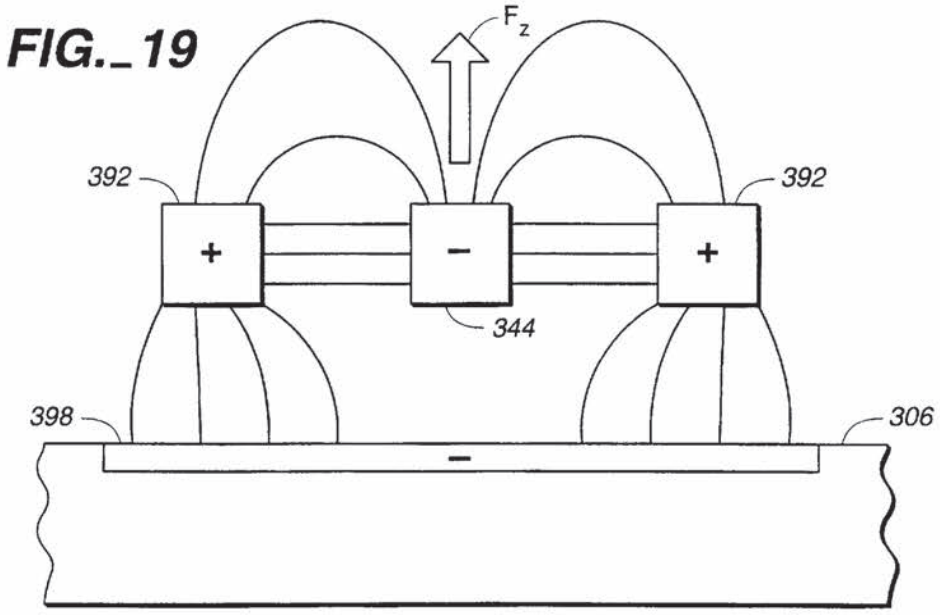
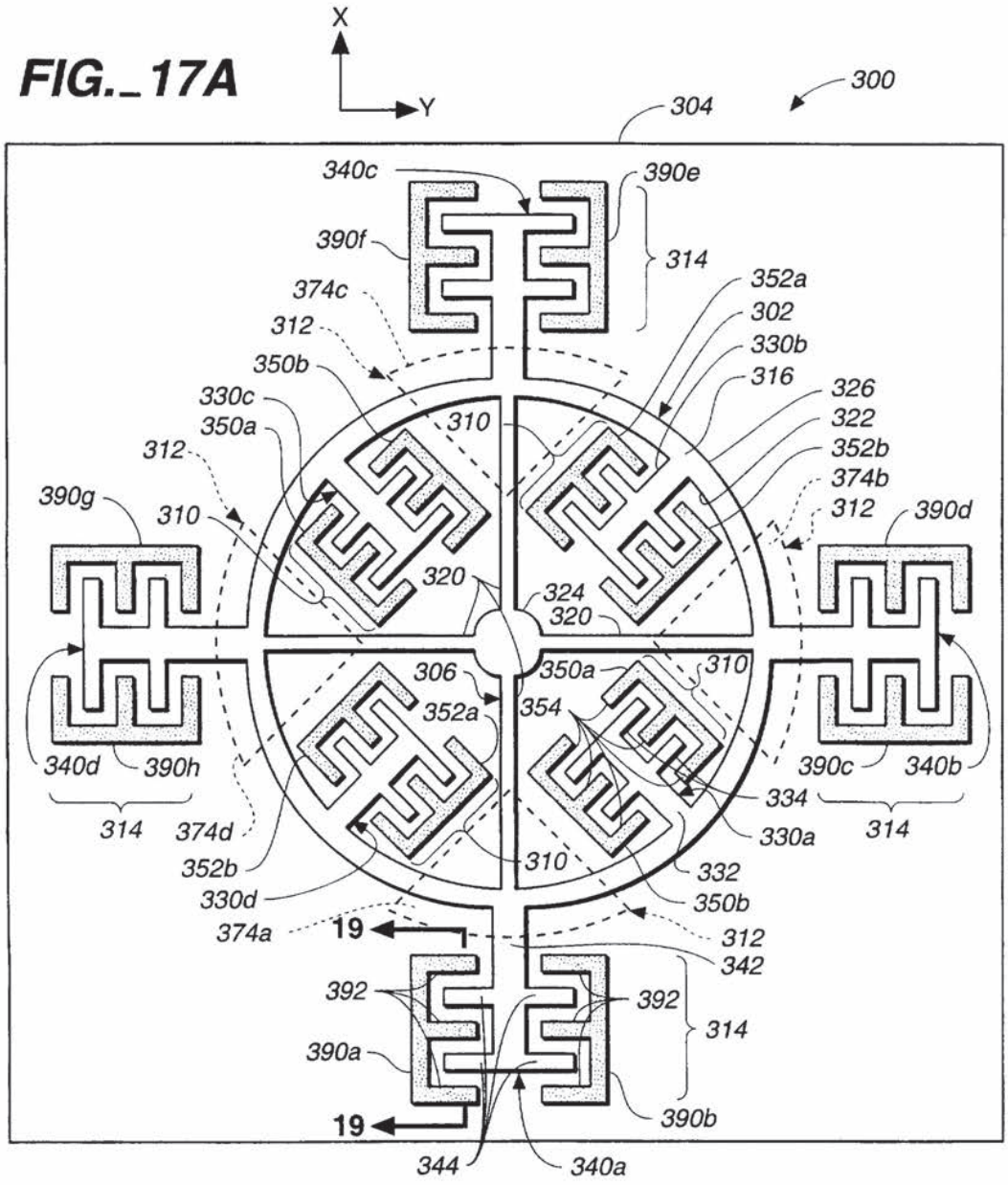


FIG._19



Nintendo Exhibit 1066
IPR2024-00668 - Page 467

FIG._17A



Nintendo Exhibit 1066
IPR2024-00668 - Page 468

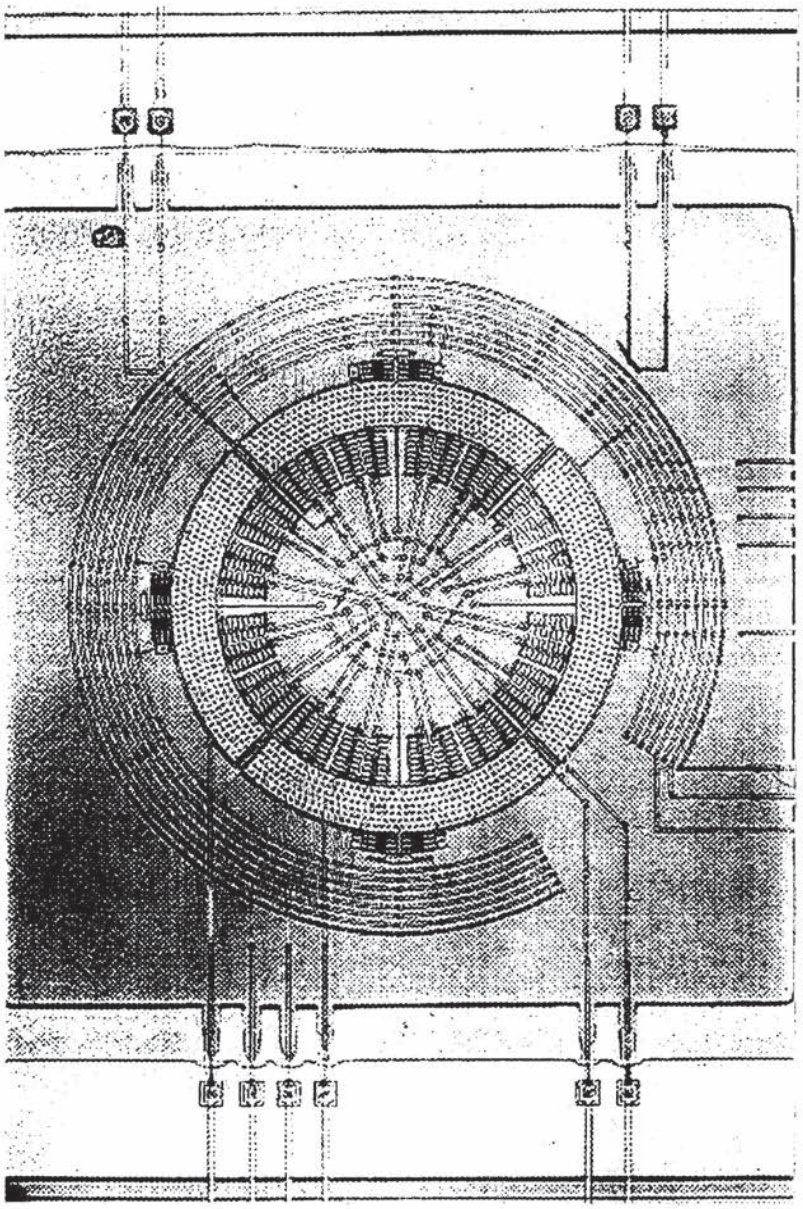
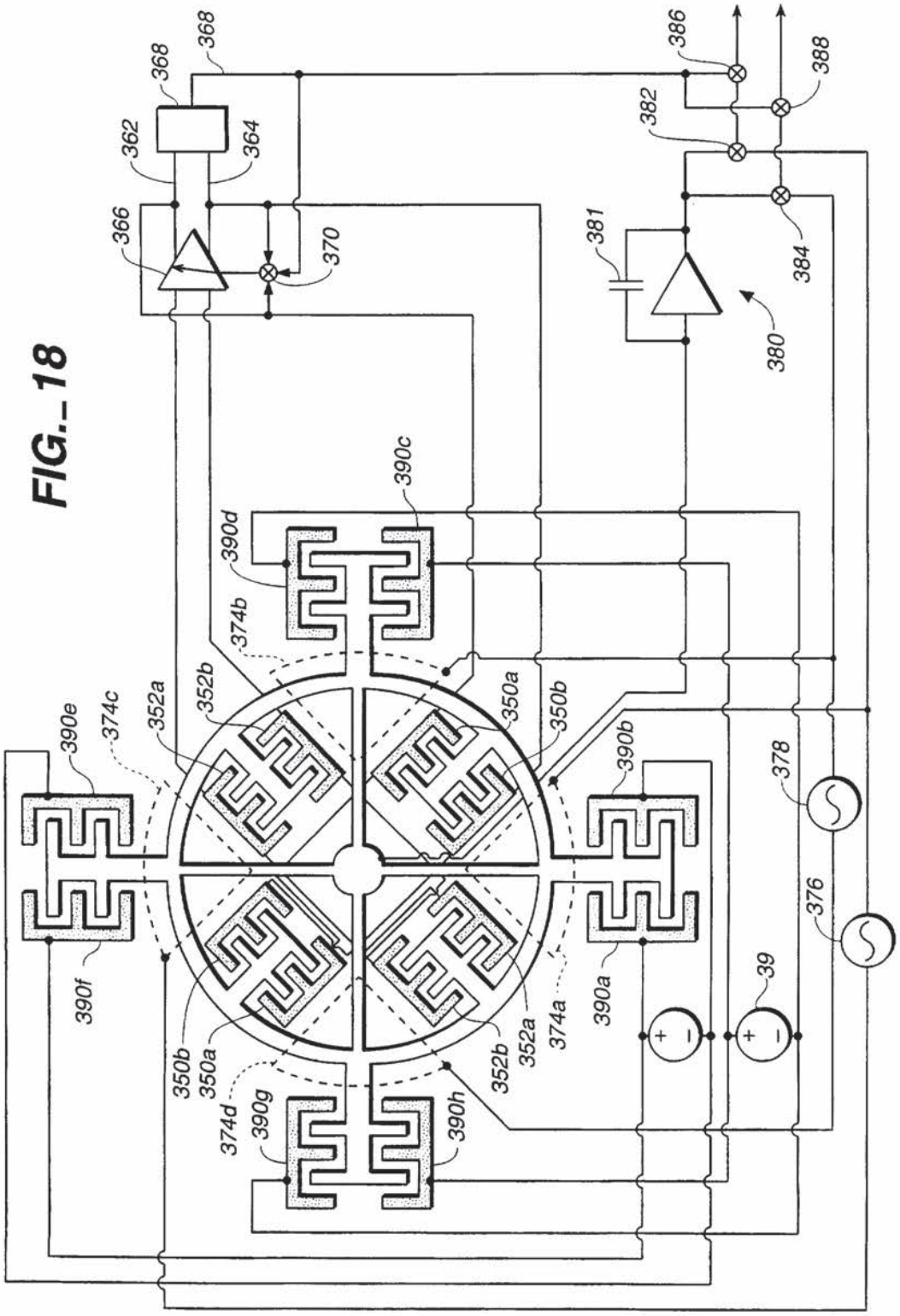


FIG._17B

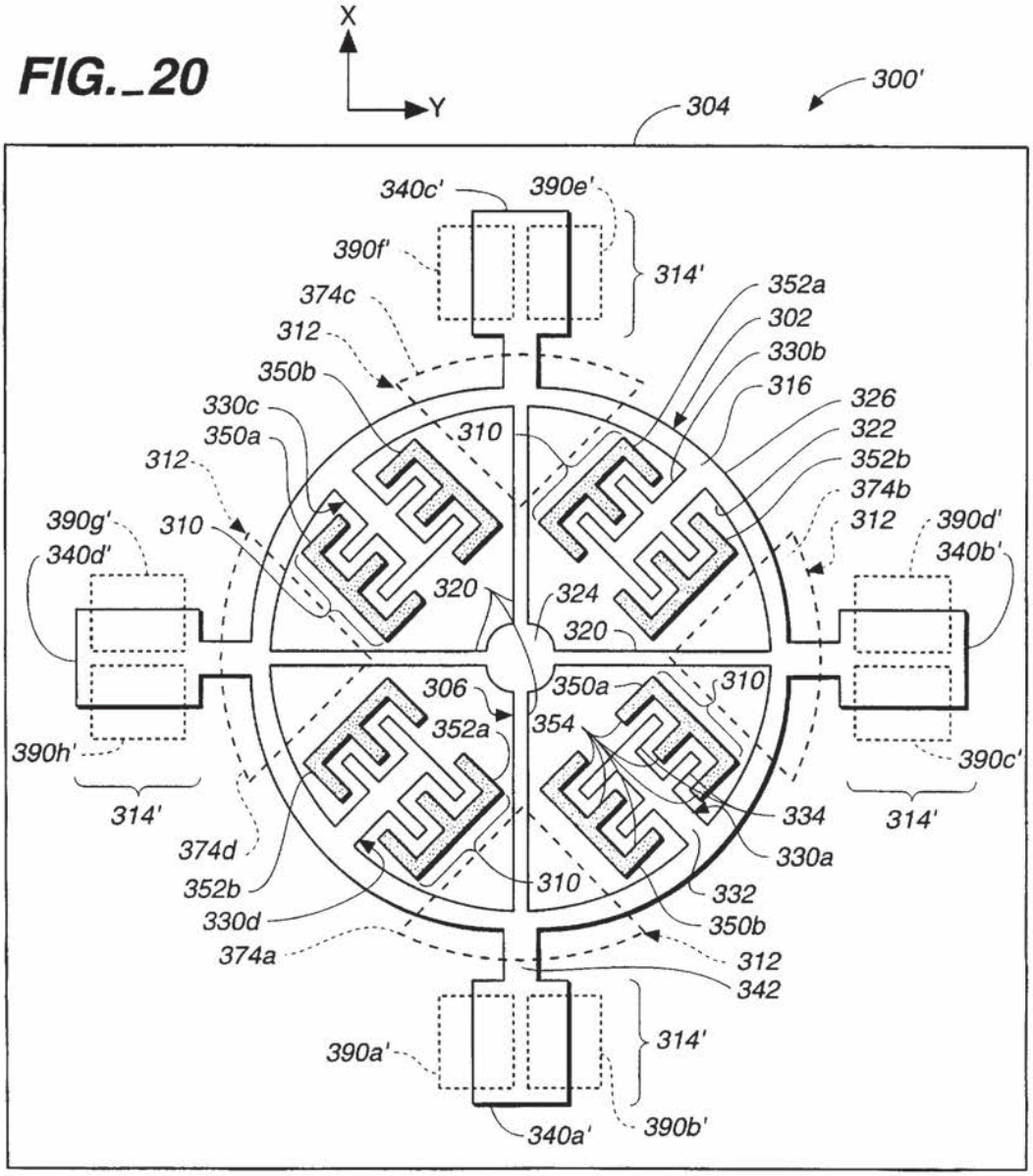
Nintendo Exhibit 1066
IPR2024-00668 - Page 469

FIG._18



Nintendo Exhibit 1066
IPR2024-00668 - Page 470

FIG._20



Nintendo Exhibit 1066
IPR2024-00668 - Page 471

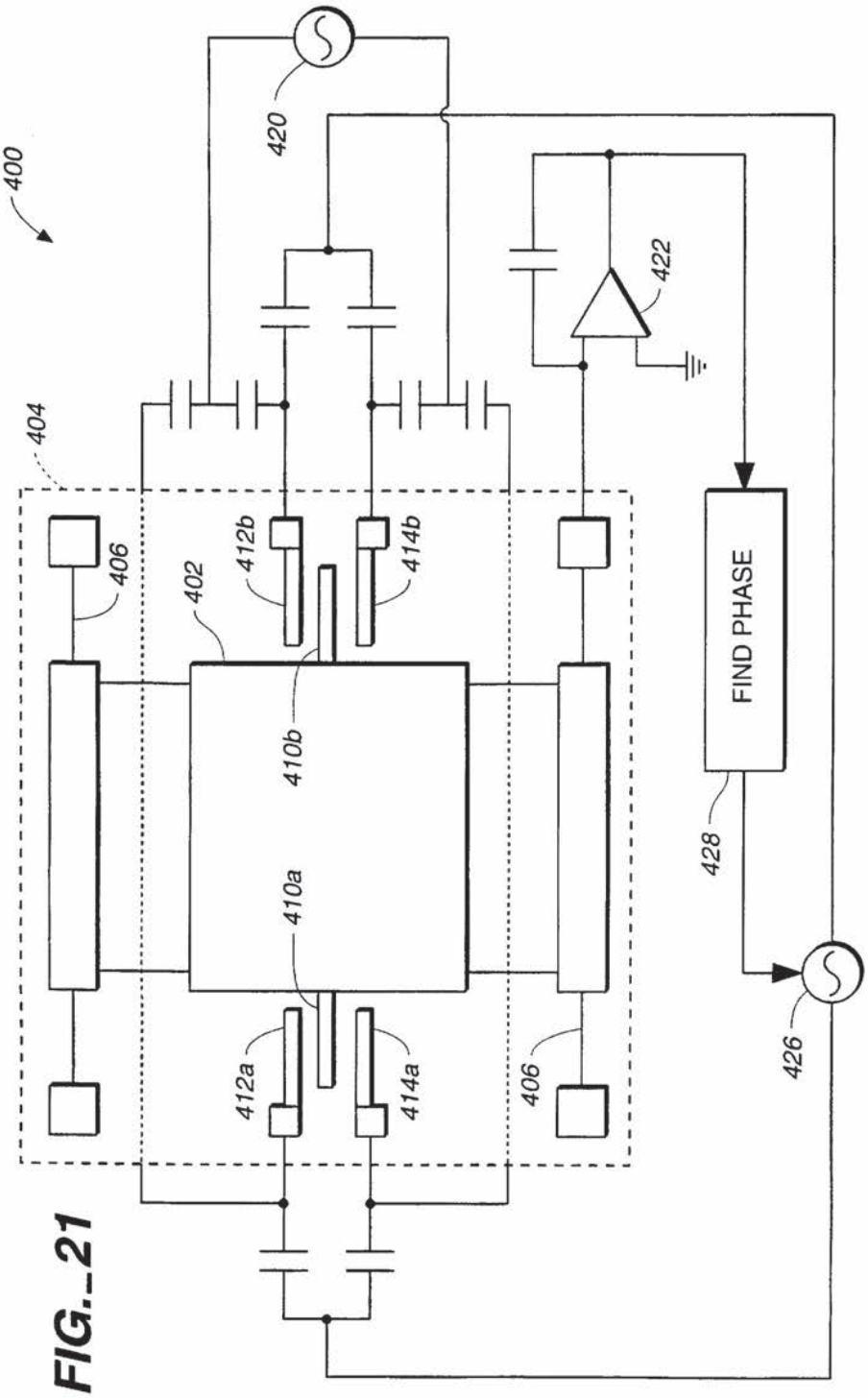


FIG._21

Nintendo Exhibit 1066
IPR2024-00668 - Page 472

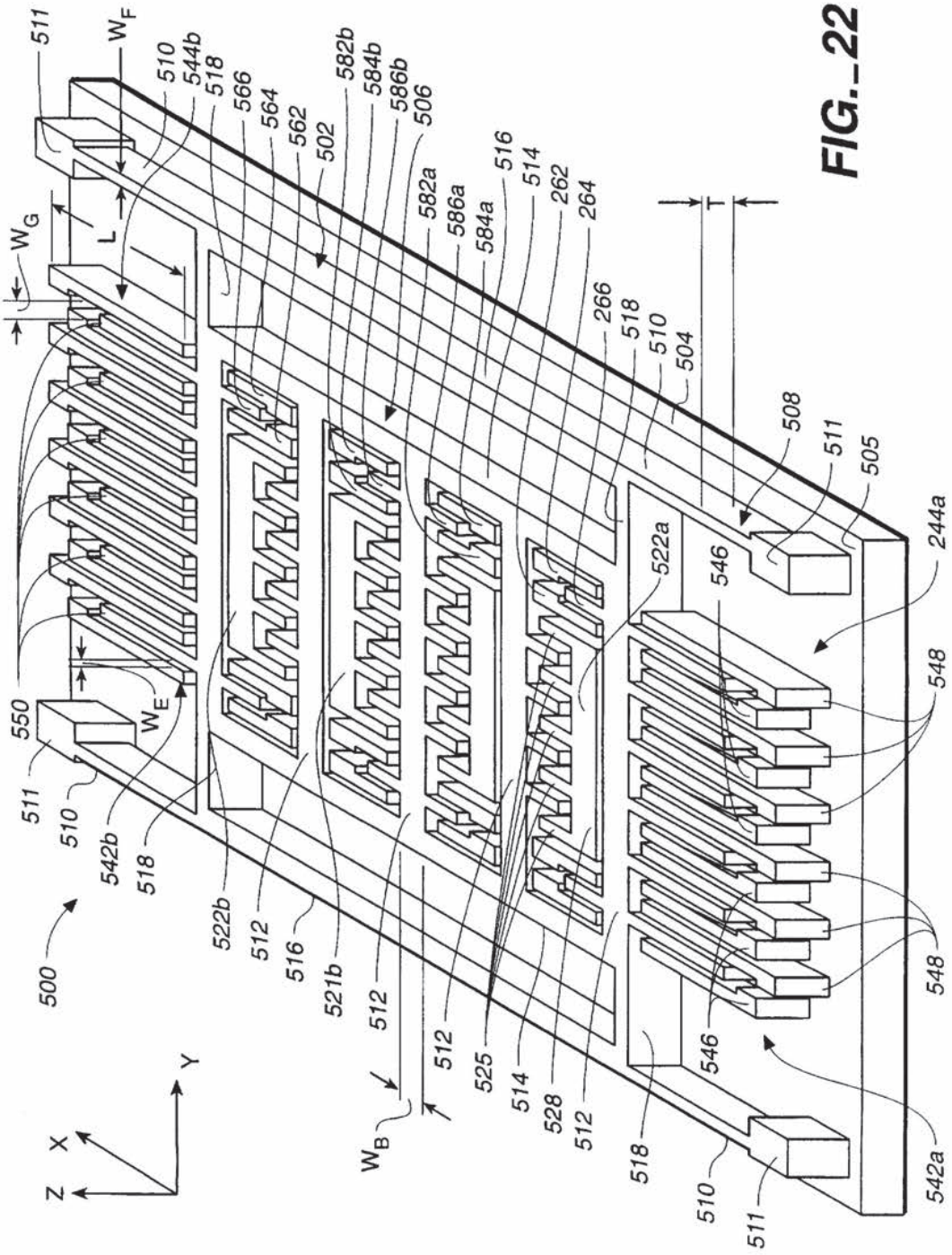


FIG._22

Nintendo Exhibit 1066
IPR2024-00668 - Page 473

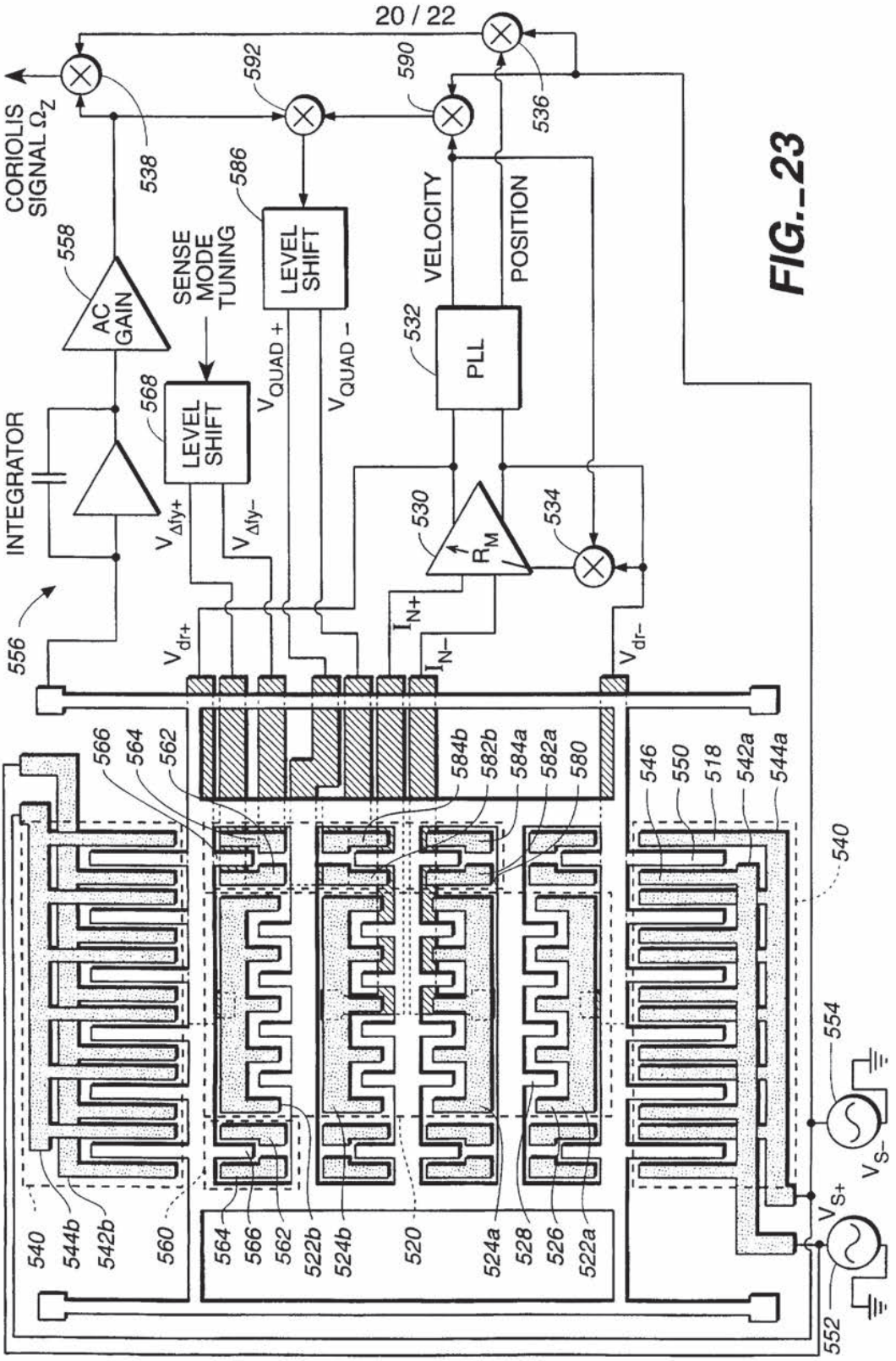


FIG._23

Nintendo Exhibit 1066
IPR2024-00668 - Page 474

FIG._24A

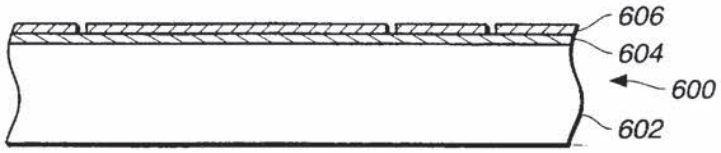


FIG._24B

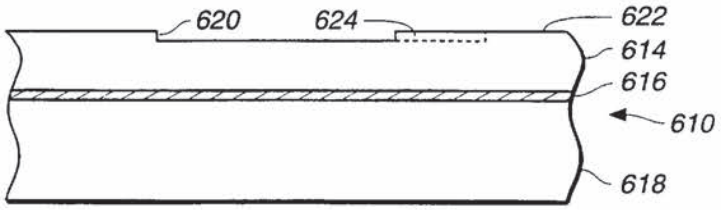


FIG._24C

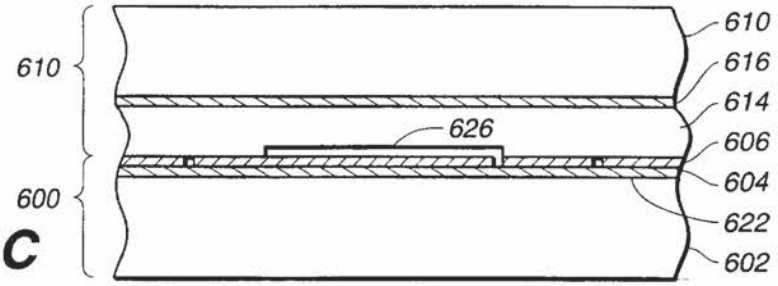


FIG._24D

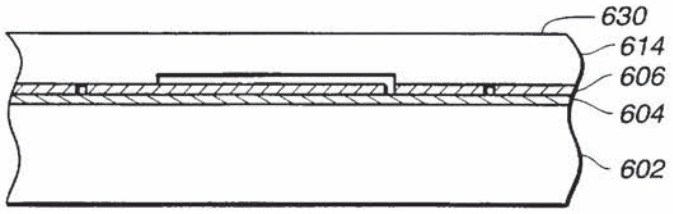
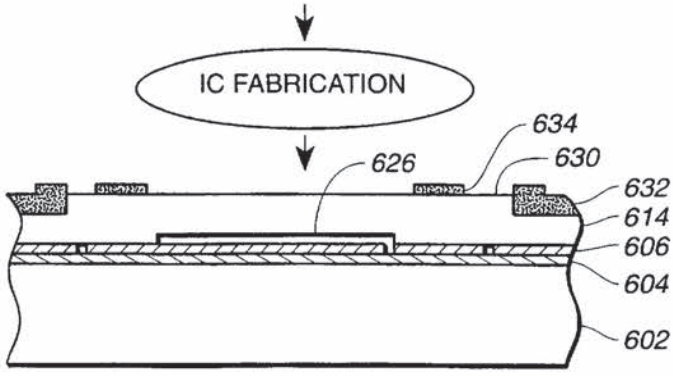


FIG._24E



Nintendo Exhibit 1066
IPR2024-00668 - Page 475

FIG._24F

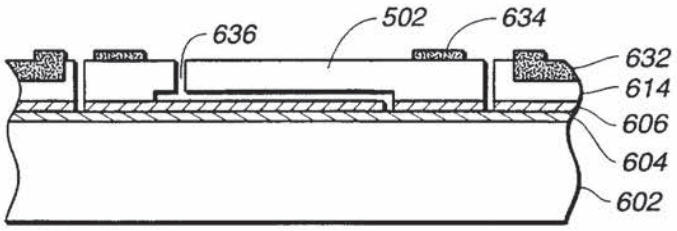
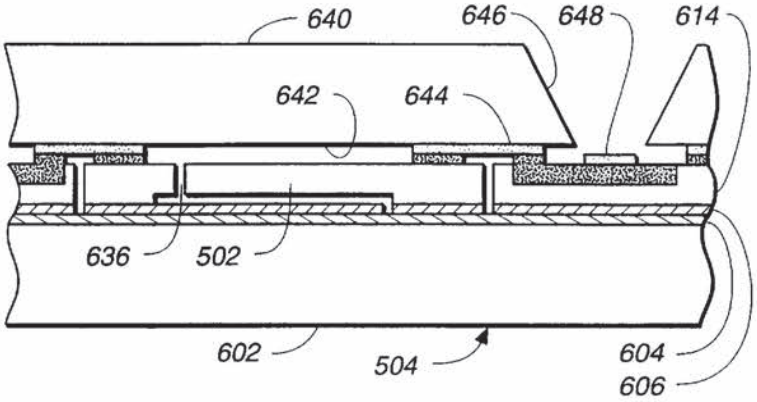


FIG._24G



Nintendo Exhibit 1066
IPR2024-00668 - Page 476

EXHIBIT 1057C

IP Portal

WIPO

Help English IP Portal login

Home › PATENTSCOPE › Search

Feedback Search Browse Tools Settings

1. WO1997045699 - MICROMACHINED VIBRATORY RATE GYROSCOPE

PCT Biblio. Data | Description | Claims | Drawings | National Phase | Patent Family | Notices | Documents

PermaLink Machine translation

Publication Number
WO/1997/045699

Publication Date
04.12.1997

International Application No.
PCT/US1997/009150

International Filing Date
30.05.1997

Chapter 2 Demand Filed
16.12.1997

IPC
G01C 19/5719 2012.1

CPC
G01C 19/5719

Applicants
THE REGENTS OF THE UNIVERSITY OF CALIFORNIA [US]/
21st floor
300 Lakeside Drive
Oakland, CA 94612
[US]United States of America

Inventors
CLARK, William, A.
JUNEAU, Thor
HOWE, Roger, T.

Agents
EGAN, William, J., III
Fish & Richardson P.C.
Suite 100
2200 Sand Hill Road
Menlo Park, CA 94025
United States of America

Priority Data
08/658,924 31.05.1996 US

Publication Language
English (en)

Filing Language
English (en)

Designated States
View all

Title
(EN) MICROMACHINED VIBRATORY RATE GYROSCOPE
(FR) GYROSCOPE MICRO-USINE A STRUCTURE VIBRATOIRE

Abstract
(EN) A microfabricated gyroscope (20) includes proof mass (22) connected to a frame or substrate (24) to measure rotation about an axis parallel to the surface of the substrate. The micromachined gyroscope includes a suspension system (30), a drive system (32) used to sustain oscillation of the proof mass (22) and a sensing system (34) used to detect deflections of the proof mass (22). The proof mass includes a plurality of electrode fingers (38). Voltage sources (120, 122, 124, 126) apply a voltage to sense fingers (74a-b, 76a-b) of sense electrodes (62a-b) to provide bias voltages to nullify quadrature error, select or adjust the resonant frequency of vibrations of the mass along the sense axis and cancel any centrifugal or other low-frequency forces.
(FR) L'invention concerne un gyroscope micro-usiné qui permet de mesurer la rotation autour d'un axe parallèle à la surface d'un substrat. On peut appliquer une différence de tension entre des paires d'électrodes digitées afin de réduire l'erreur en quadrature. Le gyroscope considéré est doté d'un structure vibratoire et d'électrodes interdigitées ayant un rapport d'allongement élevé.

Related patent documents
US5992233 US6067858 DE000069735759 EP0902876 AU1997034744 JP2002515976 US6296779 US6250156

Latest bibliographic data on file with the International Bureau

The publication of an international application under the Patent Cooperation Treaty in PATENTSCOPE (which constitutes an element of the Gazette) does not imply the expression of any opinion whatsoever on the part of the International Bureau of WIPO concerning the legal status of any country, territory, city or area or of its authorities, or concerning the delimitation of its frontiers or boundaries.

Nintendo Exhibit 1066
IPR2024-00668 - Page 478

IP Portal

WIPO

Help English IP Portal login

Home › PATENTSCOPE › Search

Feedback Search Browse Tools Settings

1. WO1997045699 - MICROMACHINED VIBRATORY RATE GYROSCOPE

PCT Biblio. Data Description Claims Drawings National Phase Patent Family Notices Documents

PermaLink

Published International Application			
Date	Title	View	Download
10.01.2002	Later publication of international search report (A3 02/2002)	PDF 3 p.	PDF 3 p. ZIP XML + TIFFs
04.12.1997	Initial Publication without ISR (A2 52/1997)	PDF 102 p.	PDF 102 p. ZIP XML + TIFFs

Nintendo Exhibit 1066
IPR2024-00668 - Page 479

EXHIBIT 1057D

SECTION II

NOTICES AND INFORMATION RELATING TO PUBLISHED INTERNATIONAL APPLICATIONS AND/OR ENTRIES IN SECTION I

NOTIFICATIONS ET INFORMATIONS RELATIVES AUX DEMANDES INTERNATIONALES PUBLIÉES ET/OU AUX RUBRIQUES DE LA SECTION I

ANNOUNCEMENT OF THE LATER PUBLICATION OF AMENDED CLAIMS AND, WHERE APPLICABLE, STATEMENT UNDER ARTICLE 19

ANNONCE DE LA PUBLICATION ULTÉRIEURE DES REVENDICATIONS MODIFIÉES ET, S'IL Y A LIEU, DE LA DÉCLARATION SELON L'ARTICLE 19

Amended claims and a statement under Article 19, relating to the already published international applications listed below, have been published on the same date as the present issue of the PCT Gazette, together with updated versions of the front pages of the pamphlets in which the said applications were published. The page numbering of the amended claims is in accordance with the page numbering of the said pamphlets.

Les revendications modifiées en vertu de l'article 19, ainsi que la déclaration, relatives aux demandes internationales mentionnées ci-dessous, ont été publiées à la date de parution du présent numéro de la Gazette du PCT avec des versions mises à jour des pages de couverture des brochures dans lesquelles lesdites demandes internationales ont été publiées. La pagination des revendications modifiées correspond à la pagination desdites brochures.

International Application Numbers **Numéros des demandes internationales**	**International Publication Numbers** **Numéros de publication internationale**	**First International Patent Classification Symbols** **Premiers symboles de la classification internationale des brevets**	**Amended Claims Received on** **Revendications modifiées reçues le**
PCT/CA97/00560	WO 98/05685	C07K 14/78	14 May/mai 1998
PCT/DE97/02474	WO 98/18705	B65H 45/16	15 May/mai 1998
PCT/DK97/00338	WO 98/10409	G10C 3/16	31 Mar/mar 1998
PCT/US97/18487	WO 98/15176	A01M 1/20	27 Mar/mar 1998
PCT/US97/19682	WO 98/18839	C08F 290/04	13 May/mai 1998
PCT/US97/20198	WO 98/21661	G06F 13/00	18 May/mai 1998

ANNOUNCEMENT OF THE WITHDRAWAL OF INTERNATIONAL APPLICATIONS AFTER INTERNATIONAL PUBLICATION

ANNONCE DU RETRAIT DE DEMANDES INTERNATIONALES APRÈS PUBLICATION INTERNATIONALE

The international applications listed below have been (considered) withdrawn after international publication.

Les demandes internationales indiquées ci-dessous ont été (considérées) retirées après publication internationale.

International Application Numbers **Numéros des demandes internationales**	**International Publication Numbers** **Numéros de publication internationale**	**First International Patent Classification Symbols** **Premiers symboles de la classification internationale des brevets**
PCT/DE97/02553	WO 98/18752	C07C 209/68
PCT/EP97/00513	WO 97/33160	G01N 23/04
PCT/IB 97/01459	WO 98/22044	A61F 2/06
PCT/IT 97/00259	WO 98/19094	F16L 17/06
PCT/RU96/00318	WO 98/20757	A24C 5/40
PCT/US97/02981	WO 97/30493	H01R 29/00
PCT/US97/20071	WO 98/20889	A61K 38/18

ANNOUNCEMENT OF THE WITHDRAWAL OF DESIGNATIONS AFTER INTERNATIONAL PUBLICATION

ANNONCE DU RETRAIT DE DÉSIGNATIONS APRÈS PUBLICATION INTERNATIONALE

The designations of the States indicated in relation to the international applications listed below have been (considered) withdrawn after international publication.

Les désignations des États indiquées dans les demandes internationales mentionnées ci-dessous ont été (considérées) retirées après publication internationale.

International Application Numbers **Numéros des demandes internationales**	**International Publication Numbers** **Numéros de publication internationale**	**First International Patent Classification Symbols** **Premiers symboles de la classification internationale des brevets**	**States** **États**
PCT/KG96/00001	WO 98/05885	F16H 21/16	AU, BG, BR, CA, CN, CZ, FI, HU, KP, MN, MX, PL, RO, ARIPO patent (KE, LS, MW, SD, SZ, UG), OAPI patent (BF, BJ, CF, CG, CI, CM, GA, GN, ML, MR, NE, SN, TD, TG) AU, BG, BR, CA, CN, CZ, FI, HU, KP, MN, MX, PL, RO, brevet ARIPO (KE, LS, MW, SD, SZ, UG), brevet OAPI (BF, BJ, CF, CG, CI, CM, GA, GN, ML, MR, NE, SN, TD, TG)
PCT/EP97/05298	WO 98/14675	E04D 3/36	DE
PCT/EP97/05570	WO 98/19071	F16B 35/04	DE

ANNOUNCEMENT OF THE LATER PUBLICATION OF REVISED VERSIONS OF INTERNATIONAL SEARCH REPORTS

ANNONCE DE LA PUBLICATION ULTÉRIEURE DE VERSIONS RÉVISÉES DE RAPPORTS DE RECHERCHE INTERNATIONALE

Revised versions of international search reports established in relation to the international applications listed below have been issued by the competent International Searching Authorities. The said revised versions have been published on the same date as the present issue of the PCT Gazette, together with updated versions of the front pages of the corresponding pamphlets bearing (in the language of publication) the indication "Published with a revised version of the international search report."

L'administration chargée de la recherche internationale compétente a établi des versions révisées des rapports de recherche internationale relatifs aux demandes internationales mentionnées ci-dessous. Lesdites versions révisées sont publiées à la date de parution du présent numéro de la Gazette du PCT, avec des versions mises à jour des pages de couverture des brochures correspondantes portant (dans la langue de publication) la mention "Publiée avec une version révisée du rapport de recherche internationale".

International Application Numbers **Numéros des demandes internationales**	**International Publication Numbers** **Numéros de publication internationale**	**International Publication Numbers** **Numéros de publication internationale**
PCT/FI 96/00618	WO 97/18681	H04Q 7/24
PCT/DE97/01624	WO 98/06136	H01L 29/78
PCT/JP 97/03065	WO 98/14785	G01N 35/10
PCT/JP 97/03474	WO 98/14507	C08J 9/06
PCT/NO97/00002	WO 97/25137	B01J 20/04

ANNOUNCEMENT OF THE LATER PUBLICATION OF INTERNATIONAL SEARCH REPORTS

ANNONCE DE LA PUBLICATION ULTÉRIEURE DE RAPPORTS DE RECHERCHE INTERNATIONALE

The international search reports, relating to the international applications listed below, which were not available when the international applications were published pursuant to Article 21(2)(a), have been published on the same date as the present issue of the PCT Gazette together with revised versions of the front pages of the pamphlets comprising the earlier publication and bearing the same international publication number.

Les rapports de recherche internationale relatifs aux demandes internationales mentionnées ci-dessous, rapports qui n'étaient pas disponibles lorsque ces demandes internationales ont été publiées en vertu de l'article 21.2)a), sont publiés à la même date que le présent numéro de la Gazette du PCT avec des versions révisées des pages de couverture des brochures publiées antérieurement. Ces versions révisées des pages de couverture portent le même numéro de publication internationale que les brochures publiées antérieurement.

International Application Numbers **Numéros des demandes internationales**	**International Publication Numbers** **Numéros de publication internationale**	**First International Patent Classification Symbols** **Premiers symboles de la classification internationale des brevets**
PCT/CA97/00728	WO 98/14445	C07D 471/04
PCT/DE97/02529	WO 98/19453	H04N 3/15
PCT/DE97/02626	WO 98/21873	H04M 15/00
PCT/EP97/06004	WO 98/21758	H01L 33/00
PCT/EP97/06095	WO 98/20123	C12N 15/12
PCT/EP97/06276	WO 98/21362	C12Q 1/68
PCT/FI 97/00544	WO 98/11675	H04B 1/707
PCT/FI 97/00650	WO 98/20663	H04M 1/274
PCT/GB97/02906	WO 98/18299	E05D 15/46
PCT/IB 97/01085	WO 98/11687	H04J 3/22
PCT/IB 97/01193	WO 98/20603	H02M 3/137
PCT/IB 97/01247	WO 98/16370	B30B 15/16
PCT/IL 97/00228	WO 98/01374	A01K 1/035
PCT/IL 97/00282	WO 98/08974	C12Q 1/68
PCT/IL 97/00352	WO 98/19130	A41H 1/02
PCT/NZ97/00114	WO 98/11765	H01F 27/08
PCT/SE97/01720	WO 98/17018	H04B 7/26
PCT/SE97/01790	WO 98/20577	H01Q 1/24
PCT/US97/06884	WO 97/40464	G06K 19/16
PCT/US97/08183	WO 97/44158	B24B 49/00
PCT/US97/09996	WO 97/48234	G06F 13/00
PCT/US97/10116	WO 98/00510	C11D 17/00
PCT/US97/11454	WO 98/11005	B65G 17/46
PCT/US97/12347	WO 98/02582	C12Q 1/68
PCT/US97/13135	WO 98/07183	H01L 41/08
PCT/US97/13372	WO 98/03956	G09F 19/12
PCT/US97/13785	WO 98/10386	G11B 7/24
PCT/US97/14215	WO 98/10178	F02M 37/04
PCT/US97/14274	WO 98/06889	F26B 3/00
PCT/US97/14430	WO 98/07459	A61M 11/00
PCT/US97/14662	WO 98/09699	F01N 3/20
PCT/US97/15045	WO 98/08370	F01D 5/14
PCT/US97/15293	WO 98/10693	A61B 17/04
PCT/US97/15390	WO 98/09529	A22C 25/16
PCT/US97/15417	WO 98/10597	G06F 3/00

(Continued on the following page)

(Suite sur la page suivante)

Nintendo Exhibit 1066
IPR2024-00668 - Page 484

ANNOUNCEMENT OF THE LATER PUBLICATION OF INTERNATIONAL SEARCH REPORTS (Continued)

ANNONCE DE LA PUBLICATION ULTÉRIEURE DE RAPPORTS DE RECHERCHE INTERNATIONALE (Suite)

International Application Numbers **Numéros des demandes internationales**	**International Publication Numbers** **Numéros de publication internationale**	**First International Patent Classification Symbols** **Premiers symboles de la classification internationale des brevets**
PCT/US97/15643	WO 98/10252	G01H 11/06
PCT/US97/16575	WO 98/12449	F16F 7/01
PCT/US97/16685	WO 98/15109	H04M 17/02
PCT/US97/16864	WO 98/13265	B29D 22/00
PCT/US97/16911	WO 98/13740	G06F 12/00
PCT/US97/17315	WO 98/16946	H01J 37/09
PCT/US97/17539	WO 98/14220	A61K 51/08
PCT/US97/17614	WO 98/14594	C12N 15/55
PCT/US97/17721	WO 98/16350	B25B 13/46
PCT/US97/17775	WO 98/15519	C07C 51/47
PCT/US97/17948	WO 98/15638	C12N 15/86
PCT/US97/17971	WO 98/14224	A61F 11/00
PCT/US97/17974	WO 98/15112	A63B 21/00
PCT/US97/18037	WO 98/15355	G01N 1/10
PCT/US97/18223	WO 98/15887	G06F 17/00
PCT/US97/18268	WO 98/18117	G06K 9/00
PCT/US97/18534	WO 98/16056	H04N 5/91
PCT/US97/18554	WO 98/17044	H04M 1/24
PCT/US97/18676	WO 98/19214	G03B 27/42
PCT/US97/18809	WO 98/16170	B68G 5/00
PCT/US97/18865	WO 98/17194	A61C 5/02
PCT/US97/18956	WO 98/17315	A61K 9/70
PCT/US97/19080	WO 98/20615	G01F 1/60
PCT/US97/19091	WO 98/17552	A47B 96/06
PCT/US97/19702	WO 98/20666	H04M 1/66
PCT/US97/20094	WO 98/19673	A61K 31/165
PCT/US97/20494	WO 98/19625	A61B 17/00
PCT/US97/20523	WO 98/20314	G01N 25/20
PCT/US97/20699	WO 98/20686	G05B 19/42
PCT/US97/20936	WO 98/21637	G06E 1/00
PCT/US97/21790	WO 98/21697	G06K 9/74

CORRECTIONS OF ENTRIES IN SECTION I

CORRECTIONS DE RUBRIQUES DE LA SECTION I

The entries appearing in Section I of the PCT Gazette, identified by the international publication numbers listed below, are corrected as follows:

Les rubriques reproduites à la Section I de la Gazette du PCT, identifiées par les numéros de publication internationale mentionnés ci-dessous, sont corrigées comme suit :

International Publication Numbers **Numéros de publication internationale**	**First International Patent Classification Symbols** **Premiers symboles de la classification internationale des brevets**		**Gazette Issue Numbers** **Numéros de Gazette**	**Corrections**
WO 97/06802(1)	A61K	31/495	10/1997	under (72, 75) replace "STOKES, Elaine, Sophie, Elisabeth" by "STOKES, Elaine, Sophie, Elizabeth" sous les numéros (72, 75) remplacer "STOKES, Elaine, Sophie, Elisabeth" par "STOKES, Elaine, Sophie, Elizabeth"
WO 97/31875(1)	C04B	28/02	38/1997	under (72) replace "GREINE, Klaus" by "GREIWE, Klaus" sous le numéro (72) remplacer "GREINE, Klaus" par "GREIWE, Klaus"
WO 97/47428(1)	B23Q	1/54	54/1997	under (22) replace "10 June 1997 (10.06.97)" by "11 June 1997 (11.06.97)" sous le numéro (22) remplacer "10 juin 1997 (10.06.97)" par "11 juin 1997 (11.06.97)"
WO 98/02580(1)	C12Q	1/68	03/1998	under (72) replace the existing text by "LANE, Michael, J.; 3044 Claybourne Lane, Baldwinsville, NY 13027 (US). BENIGHT, Albert, S.; 1630 Valley View Drive, Schaumburg, IL 60193 (US). FALDASZ, Brian, D.; 4 Bellevue Terrace, Maynard, MA 01754 (US)." sous le numéro (72) remplacer le texte existant par "LANE, Michael, J.; 3044 Claybourne Lane, Baldwinsville, NY 13027 (US). BENIGHT, Albert, S.; 1630 Valley View Drive, Schaumburg, IL 60193 (US). FALDASZ, Brian, D.; 4 Bellevue Terrace, Maynard, MA 01754 (US)."
WO 98/04560(1)	C07D	487/04	05/1998	under (72, 75) replace "STERNFIELD, Francine" by "STERNFELD, Francine" sous les numéros (72, 75) remplacer "STERNFIELD, Francine" par "STERNFELD, Francine"
WO 98/04690(1)	C12N	15/12	05/1998	under (72, 75) replace "BIDWELL, Christopher, A. [-/US]" by "BIDWELL, Christopher, A. [US/US]" and "SPURLOCK, Michael, E. [-/US]" by "SPURLOCK, Michael, E. [US/US]" sous les numéros (72, 75) remplacer "BIDWELL, Christopher, A. [-/US]" par "BIDWELL, Christopher, A. [US/US]" et "SPURLOCK, Michael, E. [-/US]" par "SPURLOCK, Michael, E. [US/US]"
WO 98/06973(1)	F17D	3/00	07/1998	under (81) add "AU, CA, CN, JP, MX"; due to late transmittal by the receiving Office sous le numéro (81) ajouter "AU, CA, CN, JP, MX"; en raison de la transmission tardive par l'office récepteur
WO 98/07946(1)	E06B	3/01	08/1998	under (72, 75) replace "LOSCH, Max [-/-]" by "LOSCH, Max [DE/DE]" sous les numéros (72, 75) remplacer "LOSCH, Max [-/-]" par "LOSCH, Max [DE/DE]"
WO 98/08569(1)	A62B	1/12	09/1998	under (81) add "GH, SL, YU, ZW" sous le numéro (81) ajouter "GH, SL, YU, ZW"
WO 98/09973(1)	C07F	5/02	10/1998	under (30) replace "Not furnished" by "08/923,054" sous le numéro (30) remplacer "Non communiqué" par "08/923,054"

(Continued on the following page)

(Suite sur la page suivante)

Nintendo Exhibit 1066
IPR2024-00668 - Page 486

CORRECTIONS OF ENTRIES IN SECTION I (Continued)

CORRECTIONS DE RUBRIQUES DE LA SECTION I (Suite)

International Publication Numbers **Numéros de publication internationale**	**First International Patent Classification Symbols** **Premiers symboles de la classification internationale des brevets**	**Gazette Issue Numbers** **Numéros de Gazette**	**Corrections**
WO 98/10334(1)	G03F 7/00	10/1998	under (81) delete "Eurasian patent (AM, AZ, BY, KG, KZ, MD, RU, TJ, TM)" sous le numéro (81) supprimer "brevet eurasien (AM, AZ, BY, KG, KZ, MD, RU, TJ, TM)"
WO 98/11859(1)	A61G 7/10	12/1998	under (72, 75) replace “WHATLEY, David, Richard" by "WHATLEY, David, Reginald" sous les numéros (72, 75) remplacer "WHATLEY, David, Richard" par "WHATLEY, David, Reginald"
WO 98/12208(1)	C07K 1/16	12/1998	under (30) replace "Not furnished" by "08/934,139" sous le numéro (30) remplacer "Non communiqué" par "08/934,139"
WO 98/13358(1)	C07D 295/22	13/1998	under (30) replace "5 May 1997 (05.05.97)" by "7 May 1997 (07.05.97)" and under (72, 75) replace "SRINIVASAN, Aloka [-/US]" by "SRINIVASAN, Aloka [IN/US]" sous le numéro (30) remplacer "5 mai 1997 (05.05.97)" par "7 mai 1997 (07.05.97)" et sous les numéros (72, 75) remplacer "SRINIVASAN, Aloka [-/US]" par "SRINIVASAN, Aloka [IN/US]"
WO 98/14447(1)	C07D 471/04	14/1998	under (81) add "IL, TR"; due to late transmittal by the receiving Office sous le numéro (81) ajouter "IL, TR"; en raison de la transmission tardive par l’office récepteur
WO 98/14606(1)	C12Q 1/42	14/1998	under (30) replace "1 October 1996 (01.10.96)" by "4 October 1996 (04.10.96)" sous le numéro (30) remplacer "1 octobre 1996 (01.10.96)" par "4 octobre 1996 (04.10.96)"
WO 98/14641(1)	C25D 5/02	14/1998	under (30) replace "1 October 1996 (01.10.96)" by "2 October 1996 (02.10.96)" sous le numéro (30) remplacer "1 octobre 1996 (01.10.96)" par "2 octobre 1996 (02.10.96)"
WO 98/15222(1)	A61B 3/10	15/1998	under (30) replace "Not furnished" by "08/947,697" sous le numéro (30) remplacer "Non communiqué" par "08/947,697"
WO 98/15456(1)	B64F 1/34	15/1998	under (30) replace "Not furnished" by "08/938,623" sous le numéro (30) remplacer "Non communiqué" par "08/938,623"
WO 98/15656(1)	C12Q 1/68	15/1998	under (71) replace "UNIVERSITY OF NEW MEXICO [-/US]" by "UNIVERSITY OF NEW MEXICO [US/US]" sous le numéro (71) remplacer "UNIVERSITY OF NEW MEXICO [-/US]" par "UNIVERSITY OF NEW MEXICO [US/US]"

(Continued on the following page)

(Suite sur la page suivante)

Nintendo Exhibit 1066
IPR2024-00668 - Page 487

CORRECTIONS OF ENTRIES IN SECTION I (Continued)

CORRECTIONS DE RUBRIQUES DE LA SECTION I (Suite)

International Publication Numbers **Numéros de publication internationale**	**First International Patent Classification Symbols** **Premiers symboles de la classification internationale des brevets**	**Gazette Issue Numbers** **Numéros de Gazette**	**Corrections**
WO 98/15688(1)	D21F 3/00	15/1998	under (81) add "CN, ID, KP, VN"; due to late transmittal by the receiving Office sous le numéro (81) ajouter "CN, ID, KP, VN"; en raison de la transmission tardive par l'office récepteur
WO 98/16225(1)	A61K 31/415	16/1998	under (81) add "IL"; due to late transmittal by the receiving Office sous le numéro (81) ajouter "IL"; en raison de la transmission tardive par l'office récepteur
WO 98/16967(1)	H04Q 1/42	16/1998	under (30) replace "15 October 1996 (15.10.96)" by "13 September 1996 (13.09.96)" sous le numéro (30) remplacer "15 octobre 1996 (15.10.96)" par "13 septembre 1996 (13.09.96)"
WO 98/17651(1)	C07D 235/06	17/1998	under (81) add "IL, TR"; due to late transmittal by the receiving Office sous le numéro (81) ajouter "IL, TR"; en raison de la transmission tardive par l'office récepteur
WO 98/17859(1)	D21F 1/00	17/1998	under (81) add "YU"; due to late transmittal by the receiving Office sous le numéro (81) ajouter "YU"; en raison de la transmission tardive par l'office récepteur
WO 98/18547(1)	B01J 8/02	18/1998	under (54) the title in English should read "PROCESS AND REACTOR FOR EPOXIDATION WITH ENERGY RECOVERY" sous le numéro (54) le titre en anglais doit se lire "PROCESS AND REACTOR FOR EPOXIDATION WITH ENERGY RECOVERY"
WO 98/18680(1)	B65D 5/40	18/1998	under (54) the title in English should read "A PROTECTED PACKAGING" sous le numéro (54) le titre en anglais doit se lire "A PROTECTED PACKAGING"
WO 98/18814(1)	C07K 1/00	18/1998	under (30) replace "Not furnished" by "60/063,140" sous le numéro (30) remplacer "Non communiqué" par "60/063,140"
WO 98/18846(1)	C08G 63/16	18/1998	under (30) replace "Not furnished" by "08/951,917" sous le numéro (30) remplacer "Non communiqué" par "08/951,917"
WO 98/18865(1)	C08L 101/00	18/1998	under (72, 75) replace "SEHANOBISH, Kalyan [US/US]" by "SEHANOBISH, Kalyan [IN/US]" sous les numéros (72, 75) remplacer "SEHANOBISH, Kalyan [US/US]" par "SEHANOBISH, Kalyan [IN/US]"

(Continued on the following page)

(Suite sur la page suivante)

CORRECTIONS OF ENTRIES IN SECTION I (Continued)

CORRECTIONS DE RUBRIQUES DE LA SECTION I (Suite)

International Publication Numbers **Numéros de publication internationale**	**First International Patent Classification Symbols** **Premiers symboles de la classification internationale des brevets**	**Gazette Issue Numbers** **Numéros de Gazette**	**Corrections**
WO 98/19718(1)	A61L 15/18	19/1998	under (51) replace "A61L 15/18" by "A61L 15/28" sous le numéro (51) remplacer "A61L 15/18" par "A61L 15/28"
WO 98/20721(1)	Not classified Non classée	20/1998	under (51) replace "Not classified" by "H01L 41/083" sous le numéro (51) remplacer "Non classée" par "H01L 41/083"
WO 98/21072(1)	B60R 21/16	20/1998	the code identifying the kind of document to which the pamphlet relates should read "A1" instead of "A2" le code identifiant le type de document que constitue la brochure doit se lire "A1" au lieu de "A2"
WO 98/21568(1)	G01N 21/89	20/1998	under (54) replace the existing text by "ARRANGEMENT AND METHOD FOR MARKING DEFECTS" sous le numéro (54) remplacer le texte existant par "AGENCEMENT ET PROCEDE POUR MARQUER DES DEFAUTS"
WO 98/21916(1)	H05B 1/02	20/1998	under (54) replace the existing text by "A DEVICE IN A MONITORING UNIT FOR HEAT-EMITTING OBJECTS" sous le numéro (54) remplacer le texte existant par "DISPOSITIF POUR UNITE DE SURVEILLANCE POUR OBJETS DIFFUSANT DE LA CHALEUR"
WO 98/22132(1)	A61K 38/46	21/1998	under "Published", replace the existing text by "Without international search report and to be republished upon receipt of that report." and replace "A1" by "A2" sous la mention "Publiée", remplacer le texte existant par "Sans rapport de recherche internationale, sera republiée dès réception de ce rapport." et remplacer "A1" par "A2"
WO 98/22901(1)	G06F 27/00	21/1998	under (51) replace "G06F 27/00" by "G09F 27/00" sous le numéro (51) remplacer "G06F 27/00" par "G09F 27/00"
WO 98/23013(1)	H02B 53/30	21/1998	under (51) replace "H02B 53/30" by "H02B 1/30" sous le numéro (51) remplacer "H02B 53/30" par "H02B 1/30"

(1) A corrected version of the front page of the corresponding pamphlet has been published on the same date as the present issue of the PCT Gazette.

(1) Une version corrigée de la page de couverture de la brochure correspondante a été publiée à la date de parution du présent numéro de la Gazette du PCT.

CORRECTED VERSIONS OF PAMPHLETS

VERSIONS CORRIGÉES DE BROCHURES

Corrected versions of the pamphlets, identified below by their international publication number, have been published on the same date as the present issue of the PCT Gazette.

Des versions corrigées des brochures, identifiées ci-dessous par leur numéro de publication internationale, ont été publiées à la date de parution du présent numéro de la Gazette du PCT.

International Publication Numbers **Numéros de publication internationale**	**International Application Numbers** **Numéros des demandes internationales**	**Corrections**
WO 97/06402	PCT/US96/12749	pages 66-71, claims, added pages 66-71, revendications, ajoutées
WO 97/34808	PCT/US97/04288	pages 1/2-2/2, drawings, replaced by new pages 1/2-2/2; due to late transmittal by the receiving Office pages 1/2-2/2, dessins, remplacées par de nouvelles pages 1/2-2/2; en raison de la transmission tardive par l'office récepteur
WO 97/39293	PCT/US97/05488	pages 1/9-9/9, drawings, replaced by new pages 1/9-9/9; due to late transmittal by the receiving Office pages 1/9-9/9, dessins, remplacées par de nouvelles pages 1/9-9/9; en raison de la transmission tardive par l'office récepteur
WO 97/41263	PCT/US97/07676	pages 4 and 16, description, replaced by new pages 4 and 16; pages 1/11-11/11, drawings, replaced by new pages 1/11-11/11; due to late transmittal by the receiving Office pages 4 et 16, description, remplacées par de nouvelles pages 4 et 16; pages 1/11-11/11, dessins, remplacées par de nouvelles pages 1/11-11/11; en raison de la transmission tardive par l'office récepteur
WO 97/41558	PCT/US97/07291	pages 1/4-4/4, drawings, replaced by new pages 1/4-4/4; due to late transmittal by the receiving Office pages 1/4-4/4, dessins, remplacées par de nouvelles pages 1/4-4/4; en raison de la transmission tardive par l'office récepteur
WO 97/42879	PCT/US97/07977	pages 1/31-31/31, drawings, replaced by new pages 1/26-26/26; due to late transmittal by the receiving Office pages 1/31-31/31, dessins, remplacées par de nouvelles pages 1/26-26/26; en raison de la transmission tardive par l'office récepteur
WO 97/45384	PCT/US97/09573	page 1/1, drawings, replaced by a new page 1/1; due to late transmittal by the receiving Office page 1/1, dessins, remplacée par une nouvelle page 1/1; en raison de la transmission tardive par l'office récepteur
WO 97/47083	PCT/US97/09382	pages 1/13-13/13, drawings, replaced by new pages 1/13-13/13; due to late transmittal by the receiving Office pages 1/13-13/13, dessins, remplacées par de nouvelles pages 1/13-13/13; en raison de la transmission tardive par l'office récepteur
WO 97/47329	PCT/US97/09292	pages 75-84, claims, replaced by new pages 75-84; due to late transmittal by the receiving Office pages 75-84, revendications, remplacées par de nouvelles pages 75-84; en raison de la transmission tardive par l'office récepteur
WO 97/47358	PCT/US97/09884	pages 21-25, claims, replaced by new pages 21-25; due to late transmittal by the receiving Office pages 21-25, revendications, remplacées par de nouvelles pages 21-25; en raison de la transmission tardive par l'office récepteur
WO 97/48631	PCT/US97/12597	pages 1/6-6/6, drawings, replaced by new pages 1/4-4/4; due to late transmittal by the receiving Office pages 1/6-6/6, dessins, remplacées par de nouvelles pages 1/4-4/4; en raison de la transmission tardive par l'office récepteur
WO 97/50130	PCT/US97/10531	pages 1/6, 2/6, 4/6 and 6/6, drawings, replaced by new pages 1/6, 2/6, 4/6 and 6/6; due to late transmittal by the receiving Office pages 1/6, 2/6, 4/6 et 6/6, dessins, remplacées par de nouvelles pages 1/6, 2/6, 4/6 et 6/6; en raison de la transmission tardive par l'office récepteur

(Continued on the following page)

(Suite sur la page suivante)

Nintendo Exhibit 1066
IPR2024-00668 - Page 490

CORRECTED VERSIONS OF PAMPHLETS (Continued)

VERSIONS CORRIGÉES DE BROCHURES (Suite)

International Publication Numbers **Numéros de publication internationale**	**International Application Numbers** **Numéros des demandes internationales**	**Corrections**
WO 97/50278	PCT/US97/11894	pages 1/10-10/10, drawings, replaced by new pages 1/10-10/10; due to late transmittal by the receiving Office pages 1/10-10/10, dessins, remplacées par de nouvelles pages 1/10-10/10; en raison de la transmission tardive par l'office récepteur
WO 98/00834	PCT/US97/11683	pages 1/11-11/11, drawings, replaced by new pages 1/11-11/11; due to late transmittal by the receiving Office pages 1/11-11/11, dessins, remplacées par de nouvelles pages 1/11-11/11; en raison de la transmission tardive par l'office récepteur
WO 98/01487	PCT/EP97/03464	pages 8, 12, 18, 23, 28, 29, 32, 44, 48, 52, 57, 65, 66, 69 and 75, description, replaced by new pages 8, 12, 18, 23, 28, 29, 32, 44, 48, 52, 57, 65, 66, 69 and 75; pages 77, 79 and 82, claims, replaced by new pages 77, 79 and 82; due to late transmittal by the receiving Office pages 8, 12, 18, 23, 28, 29, 32, 44, 48, 52, 57, 65, 66, 69 et 75, description, remplacées par de nouvelles pages 8, 12, 18, 23, 28, 29, 32, 44, 48, 52, 57, 65, 66, 69 et 75; pages 77, 79 et 82, revendications, remplacées par de nouvelles pages 77, 79 et 82; en raison de la transmission tardive par l'office récepteur
WO 98/02276	PCT/US97/12572	pages 1/7-7/7, drawings, replaced by new pages 1/7-7/7; due to late transmittal by the receiving Office pages 1/7-7/7, dessins, remplacées par de nouvelles pages 1/7-7/7; en raison de la transmission tardive par l'office récepteur
WO 98/02545	PCT/US97/12022	pages 1/33-33/33, drawings, replaced by new pages 1/34-34/34; due to late transmittal by the receiving Office pages 1/33-33/33, dessins, remplacées par de nouvelles pages 1/34-34/34; en raison de la transmission tardive par l'office récepteur
WO 98/04900	PCT/US97/13333	page 1/7, drawings, replaced by a new page 1/7; after rectification of obvious errors as authorized by the International Searching Authority page 1/7, dessins, remplacée par une nouvelle page 1/7; après rectification d'erreurs évidentes autorisée par l'administration chargée de la recherche internationale
WO 98/04923	PCT/US97/13489	pages 1/9-9/9, drawings, replaced by new pages 1/8-8/8; due to late transmittal by the receiving Office pages 1/9-9/9, dessins, remplacées par de nouvelles pages 1/8-8/8; en raison de la transmission tardive par l'office récepteur
WO 98/05087	PCT/US97/13592	pages 1/14-14/14, drawings, replaced by new pages 1/14-14/14; due to late transmittal by the receiving Office pages 1/14-14/14, dessins, remplacées par de nouvelles pages 1/14-14/14; en raison de la transmission tardive par l'office récepteur
WO 98/05226	PCT/US97/13381	page 1/1, drawings, replaced by a new page 1/1; due to late transmittal by the receiving Office page 1/1, dessins, remplacée par une nouvelle page 1/1; en raison de la transmission tardive par l'office récepteur
WO 98/06100	PCT/US97/13893	pages 1/9-9/9, drawings, replaced by new pages 1/8-8/8; due to late transmittal by the receiving Office pages 1/9-9/9, dessins, remplacées par de nouvelles pages 1/8-8/8; en raison de la transmission tardive par l'office récepteur

(Continued on the following page)

(Suite sur la page suivante)

CORRECTED VERSIONS OF PAMPHLETS (Continued)

VERSIONS CORRIGÉES DE BROCHURES (Suite)

International Publication Numbers **Numéros de publication internationale**	**International Application Numbers** **Numéros des demandes internationales**	**Corrections**
WO 98/06304	PCT/US97/14082	pages 1/30-30/30, drawings, replaced by new pages 1/29-29/29; due to late transmittal by the receiving Office pages 1/30-30/30, dessins, remplacées par de nouvelles pages 1/29-29/29; en raison de la transmission tardive par l'office récepteur
WO 98/06417	PCT/US97/14201	pages 22-26, claims, replaced by new pages 22-26; due to late transmittal by the receiving Office pages 22-26, revendications, remplacées par de nouvelles pages 22-26; en raison de la transmission tardive par l'office récepteur
WO 98/06736	PCT/US97/14266	pages 1/2-2/2, drawings, replaced by new pages 1/2-2/2; due to late transmittal by the receiving Office pages 1/2-2/2, dessins, remplacées par de nouvelles pages 1/2-2/2; en raison de la transmission tardive par l'office récepteur
WO 98/06739	PCT/US97/14487	pages 1/7-7/7, drawings, replaced by new pages 1/7-7/7; due to late transmittal by the receiving Office pages 1/7-7/7, dessins, remplacées par de nouvelles pages 1/7-7/7; en raison de la transmission tardive par l'office récepteur
WO 98/06752	PCT/US97/14597	pages 1/12-12/12, drawings, replaced by new pages 1/13-13/13; due to late transmittal by the receiving Office pages 1/12-12/12, dessins, remplacées par de nouvelles pages 1/13-13/13; en raison de la transmission tardive par l'office récepteur
WO 98/06965	PCT/US97/14091	pages 1/19-19/19, drawings, replaced by new pages 1/29-29/29; due to late transmittal by the receiving Office pages 1/19-19/19, dessins, remplacées par de nouvelles pages 1/29-29/29; en raison de la transmission tardive par l'office récepteur
WO 98/07332	PCT/US97/14473	pages 1/7-7/7, drawings, replaced by new pages 1/7-7/7; due to late transmittal by the receiving Office pages 1/7-7/7, dessins, remplacées par de nouvelles pages 1/7-7/7; en raison de la transmission tardive par l'office récepteur
WO 98/07779	PCT/US97/14510	page 1/1, drawings, replaced by a new page 1/1 page 1/1, dessins, remplacée par une nouvelle page 1/1
WO 98/07898	PCT/US97/14591	pages 1/20-20/20, drawings, replaced by new pages 1/20-20/20; due to late transmittal by the receiving Office pages 1/20-20/20, dessins, remplacées par de nouvelles pages 1/20-20/20; en raison de la transmission tardive par l'office récepteur
WO 98/07910	PCT/US97/14861	pages 1/33-33/33, drawings, replaced by new pages 1/32-32/32; due to late transmittal by the receiving Office pages 1/33-33/33, dessins, remplacées par de nouvelles pages 1/32-32/32; en raison de la transmission tardive par l'office récepteur
WO 98/07974	PCT/SE97/01378	pages 1/2-2/2, drawings, added pages 1/2-2/2, dessins, ajoutées
WO 98/08307	PCT/US97/14748	pages 1/13-13/13, drawings, replaced by new pages 1/13-13/13; due to late transmittal by the receiving Office pages 1/13-13/13, dessins, remplacées par de nouvelles pages 1/13-13/13; en raison de la transmission tardive par l'office récepteur

(Continued on the following page)

(Suite sur la page suivante)

CORRECTED VERSIONS OF PAMPHLETS (Continued)

VERSIONS CORRIGÉES DE BROCHURES (Suite)

International Publication Numbers **Numéros de publication internationale**	**International Application Numbers** **Numéros des demandes internationales**	**Corrections**
WO 98/08595	PCT/US97/16488	pages 1/19-19/19, drawings, replaced by new pages 1/14-14/14; due to late transmittal by the receiving Office pages 1/19-19/19, dessins, remplacées par de nouvelles pages 1/14-14/14; en raison de la transmission tardive par l'office récepteur
WO 98/08732	PCT/US97/14987	pages 1/20-20/20, drawings, replaced by new pages 1/19-19/19; due to late transmittal by the receiving Office pages 1/20-20/20, dessins, remplacées par de nouvelles pages 1/19-19/19; en raison de la transmission tardive par l'office récepteur
WO 98/09568	PCT/US97/15392	pages 1/4-4/4, drawings, replaced by new pages 1/4-4/4; due to late transmittal by the receiving Office pages 1/4-4/4, dessins, remplacées par de nouvelles pages 1/4-4/4; en raison de la transmission tardive par l'office récepteur
WO 98/09635	PCT/US97/17322	pages 1/9-9/9, drawings, replaced by new pages 1/12-12/12 pages 1/9-9/9, dessins, remplacées par de nouvelles pages 1/12-12/12
WO 98/09844	PCT/EP97/04671	pages 1/3-3/3, drawings, replaced by new pages 1/3-3/3; due to late transmittal by the receiving Office pages 1/3-3/3, dessins, remplacées par de nouvelles pages 1/3-3/3; en raison de la transmission tardive par l'office récepteur
WO 98/10086	PCT/US97/15691	pages 1/8-8/8, drawings, replaced by new pages 1/8-8/8; due to late transmittal by the receiving Office pages 1/8-8/8, dessins, remplacées par de nouvelles pages 1/8-8/8; en raison de la transmission tardive par l'office récepteur
WO 98/10361	PCT/US97/15492	pages 121-147, description, replaced by new pages 121-160; pages 148-176, claims, replaced by new pages 161-194; pages 50/115 and 74/115, drawings, replaced by new pages 50/115 and 74/115; due to late transmittal by the receiving Office pages 121-147, description, remplacées par de nouvelles pages 121-160; pages 148-176, revendications, remplacées par de nouvelles pages 161-194; pages 50/115 et 74/115, dessins, remplacées par de nouvelles pages 50/115 et 74/115; en raison de la transmission tardive par l'office récepteur
WO 98/10767	PCT/US97/16145	pages 1-94, description, replaced by new pages 1-82; pages 95-111, claims, replaced by new pages 83-97; pages 1/6-6/6, drawings, replaced by new pages 1/6-6/6; due to late transmittal by the receiving Office pages 1-94, description, remplacées par de nouvelles pages 1-82; pages 95-111, revendications, remplacées par de nouvelles pages 83-97; pages 1/6-6/6, dessins, remplacées par de nouvelles pages 1/6-6/6; en raison de la transmission tardive par l'office récepteur
WO 98/10796	PCT/US97/16074	pages 1/9-9/9, drawings, replaced by new pages 1/9-9/9; due to late transmittal by the receiving Office pages 1/9-9/9, dessins, remplacées par de nouvelles pages 1/9-9/9; en raison de la transmission tardive par l'office récepteur
WO 98/10967	PCT/US97/13697	page 1, description, replaced by a new page 1; due to late transmittal by the receiving Office page 1, description, remplacée par une nouvelle page 1; en raison de la transmission tardive par l'office récepteur

(Continued on the following page)

(Suite sur la page suivante)

CORRECTED VERSIONS OF PAMPHLETS (Continued)

VERSIONS CORRIGÉES DE BROCHURES (Suite)

International Publication Numbers **Numéros de publication internationale**	**International Application Numbers** **Numéros des demandes internationales**	**Corrections**
WO 98/10929	PCT/US97/13392	pages 1/5-5/5, drawings, replaced by new pages 1/5-5/5; due to late transmittal by the receiving Office pages 1/5-5/5, dessins, remplacées par de nouvelles pages 1/5-5/5; en raison de la transmission tardive par l'office récepteur
WO 98/11206	PCT/US97/16603	pages 50-59, description, replaced by new pages 50-59; due to late transmittal by the receiving Office pages 50-59, description, remplacées par de nouvelles pages 50-59; en raison de la transmission tardive par l'office récepteur
WO 98/11225	PCT/GB97/02479	page 19, description, replaced by a new page 19; after rectification of obvious errors as authorized by the International Searching Authority page 19, description, remplacée par une nouvelle page 19; après rectification d'erreurs évidentes autorisée par l'administration chargée de la recherche internationale
WO 98/11231	PCT/US97/16097	pages 1/15-5/15 and 7/15-15/15, drawings, replaced by new pages 1/26-13/26 and 15/26-26/26; page 6/15, drawings, renumbered as page 14/26; due to late transmittal by the receiving Office pages 1/15-5/15 et 7/15-15/15, dessins, remplacées par de nouvelles pages 1/26-13/26 et 15/26-26/26; page 6/15, dessins, renumérotée 14/26; en raison de la transmission tardive par l'office récepteur
WO 98/11363	PCT/US97/16006	pages 3/9-9/9, drawings, replaced by new pages 3/9-9/9; due to late transmittal by the receiving Office pages 3/9-9/9, dessins, remplacées par de nouvelles pages 3/9-9/9; en raison de la transmission tardive par l'office récepteur
WO 98/11847	PCT/US97/16737	pages 1/12-12/12, drawings, replaced by new pages 1/12-12/12; due to late transmittal by the receiving Office pages 1/12-12/12, dessins, remplacées par de nouvelles pages 1/12-12/12; en raison de la transmission tardive par l'office récepteur
WO 98/11980	PCT/US97/16898	pages 1/9-9/9, drawings, replaced by new pages 1/7-7/7; due to late transmittal by the receiving Office pages 1/9-9/9, dessins, remplacées par de nouvelles pages 1/7-7/7; en raison de la transmission tardive par l'office récepteur
WO 98/12051	PCT/US97/16572	pages 1/7-7/7, drawings, replaced by new pages 1/7-7/7; due to late transmittal by the receiving Office pages 1/7-7/7, dessins, remplacées par de nouvelles pages 1/7-7/7; en raison de la transmission tardive par l'office récepteur
WO 98/12100	PCT/US97/17070	pages 1/5-5/5, drawings, replaced by new pages 1/4-4/4; due to late transmittal by the receiving Office pages 1/5-5/5, dessins, remplacées par de nouvelles pages 1/4-4/4; en raison de la transmission tardive par l'office récepteur
WO 98/12527	PCT/US97/16870	pages 1/11-11/11, drawings, replaced by new pages 1/11-11/11; due to late transmittal by the receiving Office pages 1/11-11/11, dessins, remplacées par de nouvelles pages 1/11-11/11; en raison de la transmission tardive par l'office récepteur

(Continued on the following page)

(Suite sur la page suivante)

Nintendo Exhibit 1066
IPR2024-00668 - Page 494

CORRECTED VERSIONS OF PAMPHLETS (Continued)

VERSIONS CORRIGÉES DE BROCHURES (Suite)

International Publication Numbers **Numéros de publication internationale**	**International Application Numbers** **Numéros des demandes internationales**	**Corrections**
WO 98/13156	PCT/US97/17367	pages 1/7-7/7, drawings, replaced by new pages 1/11-11/11; due to late transmittal by the receiving Office pages 1/7-7/7, dessins, remplacées par de nouvelles pages 1/11-11/11; en raison de la transmission tardive par l'office récepteur
WO 98/13295	PCT/US97/17758	pages 1/3-3/3, drawings, replaced by new pages 1/3-3/3; due to late transmittal by the receiving Office pages 1/3-3/3, dessins, remplacées par de nouvelles pages 1/3-3/3; en raison de la transmission tardive par l'office récepteur
WO 98/13491	PCT/US97/17048	pages 1/14-14/14, drawings, replaced by new pages 1/20-20/20; due to late transmittal by the receiving Office pages 1/14-14/14, dessins, remplacées par de nouvelles pages 1/20-20/20; en raison de la transmission tardive par l'office récepteur
WO 98/13508	PCT/US97/17143	pages 1/6-6/6, drawings, replaced by new pages 1/7-7/7; due to late transmittal by the receiving Office pages 1/6-6/6, dessins, remplacées par de nouvelles pages 1/7-7/7; en raison de la transmission tardive par l'office récepteur
WO 98/13511	PCT/US97/17049	pages 1/4-4/4, drawings, replaced by new pages 1/4-4/4; due to late transmittal by the receiving Office pages 1/4-4/4, dessins, remplacées par de nouvelles pages 1/4-4/4; en raison de la transmission tardive par l'office récepteur
WO 98/13553	PCT/US97/17247	pages 1/4-4/4, drawings, replaced by new pages 1/4-4/4; due to late transmittal by the receiving Office pages 1/4-4/4, dessins, remplacées par de nouvelles pages 1/4-4/4; en raison de la transmission tardive par l'office récepteur
WO 98/13756	PCT/US97/16884	pages 1/11-11/11, drawings, replaced by new pages 1/10-10/10; due to late transmittal by the receiving Office pages 1/11-11/11, dessins, remplacées par de nouvelles pages 1/10-10/10; en raison de la transmission tardive par l'office récepteur
WO 98/13973	PCT/US97/17255	pages 1/9-9/9, drawings, replaced by new pages 1/9-9/9; due to late transmittal by the receiving Office pages 1/9-9/9, dessins, remplacées par de nouvelles pages 1/9-9/9; en raison de la transmission tardive par l'office récepteur
WO 98/14055	PCT/US97/13715	pages 1/6-6/6, drawings, replaced by new pages 1/6-6/6; due to late transmittal by the receiving Office pages 1/6-6/6, dessins, remplacées par de nouvelles pages 1/6-6/6; en raison de la transmission tardive par l'office récepteur
WO 98/14417	PCT/US97/17844	page 1/1, drawings, replaced by a new page 1/1; due to late transmittal by the receiving Office page 1/1, dessins, remplacée par une nouvelle page 1/1; en raison de la transmission tardive par l'office récepteur
WO 98/14458	PCT/EP97/05383	page 7, description, replaced by a new page 7 page 7, description, remplacée par une nouvelle page 7

(Continued on the following page)

(Suite sur la page suivante)

Nintendo Exhibit 1066
IPR2024-00668 - Page 495

CORRECTED VERSIONS OF PAMPHLETS (Continued)

VERSIONS CORRIGÉES DE BROCHURES (Suite)

International Publication Numbers **Numéros de publication internationale**	**International Application Numbers** **Numéros des demandes internationales**	**Corrections**
WO 98/14481	PCT/US97/17849	pages 1/15-15/15, drawings, replaced by new pages 1/15-15/15; due to late transmittal by the receiving Office pages 1/15-15/15, dessins, remplacées par de nouvelles pages 1/15-15/15; en raison de la transmission tardive par l'office récepteur
WO 98/14613	PCT/US97/17756	pages 1/26-26/26, drawings, replaced by new pages 1/24-24/24; due to late transmittal by the receiving Office pages 1/26-26/26, dessins, remplacées par de nouvelles pages 1/24-24/24; en raison de la transmission tardive par l'office récepteur
WO 98/14794	PCT/US97/17325	pages 1/7 and 3/7, drawings, replaced by new pages 1/7 and 3/7; due to late transmittal by the receiving Office pages 1/7 et 3/7, dessins, remplacées par de nouvelles pages 1/7 et 3/7; en raison de la transmission tardive par l'office récepteur
WO 98/14810	PCT/US97/17451	pages 1/21-21/21, drawings, replaced by new pages 1/21-21/21; due to late transmittal by the receiving Office pages 1/21-21/21, dessins, remplacées par de nouvelles pages 1/21-21/21; en raison de la transmission tardive par l'office récepteur
WO 98/14838	PCT/US97/17468	pages 1-38, description, replaced by new pages 1-38; pages 39-58, claims, replaced by new pages 39-58; pages 1/13-13/13, drawings, replaced by new pages 1/13-13/13; due to late transmittal by the receiving Office pages 1-38, description, remplacées par de nouvelles pages 1-38; pages 39-58, revendications, remplacées par de nouvelles pages 39-58; pages 1/13-13/13, dessins, remplacées par de nouvelles pages 1/13-13/13; en raison de la transmission tardive par l'office récepteur
WO 98/14903	PCT/US97/17667	pages 116-139, claims, replaced by new pages 116-139; due to late transmittal by the receiving Office pages 116-139, revendications, remplacées par de nouvelles pages 116-139; en raison de la transmission tardive par l'office récepteur
WO 98/15410	PCT/US97/18173	pages 1/2-2/2, drawings, replaced by new pages 1/2-2/2; due to late transmittal by the receiving Office pages 1/2-2/2, dessins, remplacées par de nouvelles pages 1/2-2/2; en raison de la transmission tardive par l'office récepteur
WO 98/15624	PCT/US97/18261	pages 4, 5 and 7, description, replaced by new pages 4, 5 and 7; page 98, claims, replaced by a new page 98; pages 1/15-15/15, drawings, replaced by new pages 1/18-18/18; after rectification of obvious errors as authorized by the International Searching Authority pages 4, 5 et 7, description, remplacées par de nouvelles pages 4, 5 et 7; page 98, revendications, remplacée par une nouvelle page 98; pages 1/15-15/15, dessins, remplacées par de nouvelles pages 1/18-18/18; après rectification d'erreurs évidentes autorisée par l'administration chargée de la recherche internationale

(Continued on the following page)

(Suite sur la page suivante)

Nintendo Exhibit 1066
IPR2024-00668 - Page 496

CORRECTED VERSIONS OF PAMPHLETS (Continued)

VERSIONS CORRIGÉES DE BROCHURES (Suite)

International Publication Numbers **Numéros de publication internationale**	**International Application Numbers** **Numéros des demandes internationales**	**Corrections**
WO 98/15855	PCT/US97/18038	pages 1-12, description, replaced by new pages 1-12; pages 13-15, claims, replaced by new pages 13-15; pages 1/2-2/2, drawings, replaced by new pages 1/2-2/2; due to late transmittal by the receiving Office pages 1-12, description, remplacées par de nouvelles pages 1-12; pages 13-15, revendications, remplacées par de nouvelles pages 13-15; pages 1/2-2/2, dessins, remplacées par de nouvelles pages 1/2-2/2; en raison de la transmission tardive par l'office récepteur
WO 98/15947	PCT/US97/18108	pages 1/10-10/10, drawings, replaced by new pages 1/10-10/10; due to late transmittal by the receiving Office pages 1/10-10/10, dessins, remplacées par de nouvelles pages 1/10-10/10; en raison de la transmission tardive par l'office récepteur
WO 98/16241	PCT/US97/18331	pages 1/14-14/14, drawings, replaced by new pages 1/9-9/9; due to late transmittal by the receiving Office pages 1/14-14/14, dessins, remplacées par de nouvelles pages 1/9-9/9; en raison de la transmission tardive par l'office récepteur
WO 98/16628	PCT/US97/18483	pages 1/10-10/10, drawings, replaced by new pages 1/12-12/12; due to late transmittal by the receiving Office pages 1/10-10/10, dessins, remplacées par de nouvelles pages 1/12-12/12; en raison de la transmission tardive par l'office récepteur
WO 98/17389	PCT/US97/19106	pages 1/20-20/20, drawings, replaced by new pages 1/20-20/20; due to late transmittal by the receiving Office pages 1/20-20/20, dessins, remplacées par de nouvelles pages 1/20-20/20; en raison de la transmission tardive par l'office récepteur
WO 98/18139	PCT/US97/18666	pages 1/4-4/4, drawings, replaced by new pages 1/4-4/4; due to late transmittal by the receiving Office pages 1/4-4/4, dessins, remplacées par de nouvelles pages 1/4-4/4; en raison de la transmission tardive par l'office récepteur
WO 98/19846	PCT/CA97/00827	pages 1/10-10/10, drawings, replaced by new pages 1/9-9/9; due to late transmittal by the receiving Office pages 1/10-10/10, dessins, remplacées par de nouvelles pages 1/9-9/9; en raison de la transmission tardive par l'office récepteur
WO 98/20013	PCT/EP97/06184	pages 1/3-3/3, drawings, replaced by new pages 1/3-3/3; due to late transmittal by the receiving Office pages 1/3-3/3, dessins, remplacées par de nouvelles pages 1/3-3/3; en raison de la transmission tardive par l'office récepteur

CORRECTED VERSION OF A PAMPHLET FRONT PAGE

VERSION CORRIGÉE DE LA PAGE DE COUVERTURE D'UNE BROCHURE

A corrected front page of the pamphlet, identified below by its international publication number, has been published on the same date as the present issue of the PCT Gazette.

Une version corrigée de la page de couverture de la brochure, identifiée ci-dessous par son numéro de publication internationale, a été publiée à la date de parution du présent numéro de la Gazette du PCT.

International Publication Number **Numéro de publication internationale**	**International Application Number** **Numéro de la demande internationale**	**Correction**
WO 97/35439	PCT/US97/05174	revised abstract received by the International Bureau after completion of the technical preparations for international publication abrégé révisé reçu par le Bureau international après achèvement de la préparation technique en vue de la publication internationale

ANNOUNCEMENT OF THE WITHDRAWAL OF A PRIORITY CLAIM AFTER COMPLETION OF THE TECHNICAL PREPARATIONS FOR INTERNATIONAL PUBLICATION

ANNONCE DU RETRAIT D'UNE REVENDICATION DE PRIORITÉ APRÈS ACHÈVEMENT DE LA PRÉPARATION TECHNIQUE DE LA PUBLICATION INTERNATIONALE

The priority claim made in relation to the international application indicated below has been withdrawn, under Rule 90bis.3, after completion of the technical preparations for international publication.

La revendication de priorité effectuée dans la demande internationale indiquée ci-dessous a été retirée en vertu de la règle 90bis.3, après l'achèvement de la préparation technique de la publication internationale.

International Application Number **Numéro de la demande internationale**	**International Publication Number** **Numéro de publication internationale**	**First International Patent Classification Symbol** **Premier symbole de la classification internationale des brevets**	**Priority Application Number** **Numéro de la demande prioritaire**	**Priority Date** **Date de priorité**	**Priority Country** **Pays de priorité**
PCT/AU96/00728	WO 97/18026	B01D 29/66	PN 6596	16 November 1995 (16.11.95) 16 novembre 1995 (16.11.95)	AU

INTERNATIONAL APPLICATIONS FOR WHICH A DEMAND HAS BEEN FILED PRIOR TO THE EXPIRATION OF THE 19TH MONTH FROM THE PRIORITY DATE

DEMANDES INTERNATIONALES POUR LESQUELLES UNE DEMANDE D'EXAMEN PRÉLIMINAIRE INTERNATIONAL A ÉTÉ PRÉSENTÉE AVANT L'EXPIRATION D'UNE PÉRIODE DE 19 MOIS À COMPTER DE LA DATE DE PRIORITÉ

International Application Numbers Numéros des demandes internationales	International Publication Numbers Numéros de publication internationale	Designated States not Elected in the Demand États désignés non élus dans la demande d'examen préliminaire international	International Application Numbers Numéros des demandes internationales	International Publication Numbers Numéros de publication internationale	Designated States not Elected in the Demand États désignés non élus dans la demande d'examen préliminaire international
PCT/AT97/00215	WO 98/16572	–	PCT/BR97/00062	WO 98/18982	–
PCT/AT97/00220	WO 98/17551	–	PCT/CA97/00420	WO 98/23903	–
PCT/AT97/00222	WO 98/17587	–	PCT/CA97/00728	WO 98/14445	–
PCT/AT97/00223	WO 98/17833	–	PCT/CA97/00755	WO 98/16320	–
PCT/AT97/00224	WO 98/17832	–	PCT/CA97/00768	WO 98/17823	–
PCT/AT97/00228	WO 98/18696	–	PCT/CA97/00769	WO 98/16316	–
PCT/AT97/00229	WO 98/18357	–	PCT/CA97/00774	WO 98/17784	–
PCT/AU97/00302	WO 98/24229	–	PCT/CA97/00777	WO 98/17965	–
PCT/AU97/00483	WO 98/19955	–	PCT/CA97/00778	WO 98/17999	–
PCT/AU97/00701	WO 98/17749	–	PCT/CA97/00781	WO 98/17822	–
PCT/AU97/00708	WO 98/17960	–	PCT/CA97/00786	WO 98/17132	–
PCT/AU97/00715	WO 98/17290	–	PCT/CA97/00789	WO 98/17144	–
PCT/AU97/00720	WO 98/19281	–	PCT/CA97/00790	WO 98/17656	–
PCT/AU97/00721	WO 98/18918	–	PCT/CA97/00794	WO 98/17284	–
PCT/AU97/00724	WO 98/19273	–	PCT/CA97/00795	WO 98/18971	–
PCT/AU97/00725	WO 98/19274	–	PCT/CA97/00800	WO 98/18332	–
PCT/AU97/00726	WO 98/18370	–	PCT/CA97/00808	WO 98/20449	–
PCT/AU97/00727	WO 98/20283	–	PCT/CA97/00819	WO 98/20325	–
PCT/AU97/00734	WO 98/19536	–	PCT/CA97/00848	WO 98/21361	–
PCT/AU97/00750	WO 98/20215	–	PCT/CA97/00892	WO 98/23299	–
PCT/AU97/00755	WO 98/19872	–	PCT/CA97/00914	WO 98/23175	–
PCT/AU97/00759	WO 98/20949	–	PCT/CH97/00337	WO 98/17461	–
PCT/AU97/00761	WO 98/21013	–	PCT/CH97/00368	WO 98/16231	–
PCT/AU97/00762	WO 98/21067	–	PCT/CH97/00369	WO 98/15220	–
PCT/AU97/00765	WO 98/20947	–	PCT/CH97/00377	WO 98/15465	–
PCT/AU97/00769	WO 98/21432	–	PCT/CH97/00381	WO 98/16673	–
PCT/AU97/00800	WO 98/23979	–	PCT/CH97/00382	WO 98/15310	–
PCT/AU97/00803	WO 98/23849	–	PCT/CH97/00383	WO 98/15971	–
PCT/AU97/00807	WO 98/23357	–	PCT/CH97/00403	WO 98/17987	–
PCT/BE97/00125	WO 98/18874	–	PCT/CH97/00406	WO 98/20802	–
PCT/BE97/00130	WO 98/23705	–	PCT/CN96/00094	WO 98/17348	–
PCT/BR96/00046	WO 98/16822	–	PCT/CN97/00001	WO 97/25054	–
PCT/BR97/00050	WO 98/23352	–	PCT/CN97/00099	WO 98/18373	–
PCT/BR97/00059	WO 98/18007	–	PCT/CZ97/00039	WO 98/20313	–

(Continued on the following page)

(Suite sur la page suivante)

Nintendo Exhibit 1066
IPR2024-00668 - Page 499

INTERNATIONAL APPLICATIONS FOR WHICH A DEMAND HAS BEEN FILED PRIOR TO THE EXPIRATION OF THE 19TH MONTH FROM THE PRIORITY DATE (Continued)

DEMANDES INTERNATIONALES POUR LESQUELLES UNE DEMANDE D'EXAMEN PRÉLIMINAIRE INTERNATIONAL A ÉTÉ PRÉSENTÉE AVANT L'EXPIRATION D'UNE PÉRIODE DE 19 MOIS À COMPTER DE LA DATE DE PRIORITÉ (Suite)

International Application Numbers Numéros des demandes internationales	International Publication Numbers Numéros de publication internationale	Designated States not Elected in the Demand États désignés non élus dans la demande d'examen préliminaire international	International Application Numbers Numéros des demandes internationales	International Publication Numbers Numéros de publication internationale	Designated States not Elected in the Demand États désignés non élus dans la demande d'examen préliminaire international
PCT/DE96/02271	WO 98/23476	–	PCT/DE97/02428	WO 98/17572	–
PCT/DE97/01935	WO 98/17023	–	PCT/DE97/02437	WO 98/21860	–
PCT/DE97/01967	WO 98/15428	–	PCT/DE97/02439	WO 98/18003	–
PCT/DE97/02143	WO 98/21019	–	PCT/DE97/02452	WO 98/17454	–
PCT/DE97/02198	WO 98/23859	–	PCT/DE97/02453	WO 98/18171	–
PCT/DE97/02218	WO 98/18036	–	PCT/DE97/02467	WO 98/18055	–
PCT/DE97/02227	WO 98/15138	–	PCT/DE97/02480	WO 98/19360	–
PCT/DE97/02243	WO 98/24280	–	PCT/DE97/02481	WO 98/19451	–
PCT/DE97/02251	WO 98/15498	–	PCT/DE97/02495	WO 98/20699	–
PCT/DE97/02277	WO 98/16624	–	PCT/DE97/02504	WO 98/19484	–
PCT/DE97/02309	WO 98/15665	–	PCT/DE97/02523	WO 98/18628	–
PCT/DE97/02318	WO 98/24010	–	PCT/DE97/02534	WO 98/18428	–
PCT/DE97/02320	WO 98/16953	–	PCT/DE97/02543	WO 98/23022	–
PCT/DE97/02323	WO 98/18275	–	PCT/DE97/02550	WO 98/24060	–
PCT/DE97/02327	WO 98/15998	–	PCT/DE97/02555	WO 98/19093	–
PCT/DE97/02343	WO 98/17073	–	PCT/DE97/02573	WO 98/19202	–
PCT/DE97/02346	WO 98/16824	–	PCT/DE97/02589	WO 98/20624	–
PCT/DE97/02349	WO 98/24170	–	PCT/DE97/02590	WO 98/19591	–
PCT/DE97/02350	WO 98/24239	–	PCT/DE97/02600	WO 98/24039	–
PCT/DE97/02351	WO 98/18276	–	PCT/DE97/02629	WO 98/23937	–
PCT/DE97/02357	WO 98/20579	–	PCT/DE97/02671	WO 98/23917	–
PCT/DE97/02363	WO 98/15933	–	PCT/DE97/02677	WO 98/21079	–
PCT/DE97/02366	WO 98/17415	–	PCT/DE97/02680	WO 98/24171	–
PCT/DE97/02372	WO 98/16536	–	PCT/DE97/02695	WO 98/24137	–
PCT/DE97/02375	WO 98/17398	–	PCT/DE97/02703	WO 98/24009	–
PCT/DE97/02384	WO 98/17885	–	PCT/DE97/02716	WO 98/23541	–
PCT/DE97/02386	WO 98/16877	–	PCT/DE97/02736	WO 98/23734	–
PCT/DE97/02388	WO 98/17831	–	PCT/DE97/02737	WO 98/23986	–
PCT/DE97/02389	WO 98/18056	–	PCT/DE97/02740	WO 98/23934	–
PCT/DE97/02393	WO 98/17571	–	PCT/DE97/02751	WO 98/23935	–
PCT/DE97/02400	WO 98/17122	–	PCT/DE97/02767	WO 98/24051	–
PCT/DE97/02411	WO 98/18536	–	PCT/DK96/00429	WO 98/15788	–
PCT/DE97/02414	WO 98/18058	–	PCT/DK97/00334	WO 98/09860	–
PCT/DE97/02421	WO 98/21484	–	PCT/DK97/00362	WO 98/10149	–

(Continued on the following page)

(Suite sur la page suivante)

Nintendo Exhibit 1066
IPR2024-00668 - Page 500

INTERNATIONAL APPLICATIONS FOR WHICH A DEMAND HAS BEEN FILED PRIOR TO THE EXPIRATION OF THE 19TH MONTH FROM THE PRIORITY DATE (Continued)

DEMANDES INTERNATIONALES POUR LESQUELLES UNE DEMANDE D'EXAMEN PRÉLIMINAIRE INTERNATIONAL A ÉTÉ PRÉSENTÉE AVANT L'EXPIRATION D'UNE PÉRIODE DE 19 MOIS À COMPTER DE LA DATE DE PRIORITÉ (Suite)

International Application Numbers **Numéros des demandes internationales**	**International Publication Numbers** **Numéros de publication internationale**	**Designated States not Elected in the Demand** **États désignés non élus dans la demande d'examen préliminaire international**	**International Application Numbers** **Numéros des demandes internationales**	**International Publication Numbers** **Numéros de publication internationale**	**Designated States not Elected in the Demand** **États désignés non élus dans la demande d'examen préliminaire international**
PCT/DK97/00404	WO 98/15312	–	PCT/EP97/05201	WO 98/16564	–
PCT/DK97/00405	WO 98/13957	–	PCT/EP97/05209	WO 98/12912	–
PCT/DK97/00407	WO 98/13268	–	PCT/EP97/05275	WO 98/13255	–
PCT/DK97/00432	WO 98/15806	–	PCT/EP97/05278	WO 98/16949	–
PCT/DK97/00453	WO 98/17915	–	PCT/EP97/05312	WO 98/16363	–
PCT/DK97/00471	WO 98/23501	–	PCT/EP97/05313	WO 98/16578	–
PCT/DK97/00475	WO 98/19165	–	PCT/EP97/05365	WO 98/14682	–
PCT/DK97/00478	WO 98/18771	–	PCT/EP97/05383	WO 98/14458	–
PCT/DK97/00479	WO 98/18772	–	PCT/EP97/05407	WO 98/18155	–
PCT/DK97/00480	WO 98/18773	–	PCT/EP97/05409	WO 98/24114	–
PCT/DK97/00481	WO 98/18774	–	PCT/EP97/05413	WO 98/18156	–
PCT/DK97/00482	WO 98/18775	–	PCT/EP97/05427	WO 98/14309	–
PCT/DK97/00483	WO 98/18776	–	PCT/EP97/05445	WO 98/15799	–
PCT/DK97/00484	WO 98/18777	–	PCT/EP97/05448	WO 98/14219	–
PCT/DK97/00485	WO 98/18778	–	PCT/EP97/05454	WO 98/17825	–
PCT/DK97/00486	WO 98/18779	–	PCT/EP97/05458	WO 98/16776	–
PCT/EP96/04359	WO 98/15407	–	PCT/EP97/05468	WO 98/15660	–
PCT/EP96/04427	WO 98/16356	–	PCT/EP97/05482	WO 98/15557	–
PCT/EP96/05218	WO 98/24093	–	PCT/EP97/05502	WO 98/15784	–
PCT/EP96/05291	WO 98/23878	–	PCT/EP97/05504	WO 98/21258	–
PCT/EP97/00005	WO 98/15907	–	PCT/EP97/05505	WO 98/21259	–
PCT/EP97/00466	WO 98/23526	–	PCT/EP97/05506	WO 98/21260	–
PCT/EP97/03633	WO 98/23201	–	PCT/EP97/05513	WO 98/16718	–
PCT/EP97/04021	WO 98/16331	–	PCT/EP97/05514	WO 98/16595	–
PCT/EP97/04141	WO 98/18100	–	PCT/EP97/05530	WO 98/17668	–
PCT/EP97/04416	WO 98/18278	–	PCT/EP97/05548	WO 98/15236	–
PCT/EP97/04523	WO 98/20310	–	PCT/EP97/05567	WO 98/15433	–
PCT/EP97/04650	WO 98/16838	–	PCT/EP97/05583	WO 98/15650	–
PCT/EP97/04861	WO 98/15432	–	PCT/EP97/05587	WO 98/15491	–
PCT/EP97/04940	WO 98/19897	–	PCT/EP97/05588	WO 98/23265	–
PCT/EP97/04969	WO 98/20688	–	PCT/EP97/05589	WO 98/17305	–
PCT/EP97/05122	WO 98/14815	–	PCT/EP97/05608	WO 98/23266	–
PCT/EP97/05134	WO 98/19805	–	PCT/EP97/05609	WO 98/23238	–
PCT/EP97/05146	WO 98/14345	–	PCT/EP97/05612	WO 98/23922	–

(Continued on the following page)

(Suite sur la page suivante)

Nintendo Exhibit 1066
IPR2024-00668 - Page 501

INTERNATIONAL APPLICATIONS FOR WHICH A DEMAND HAS BEEN FILED PRIOR TO THE EXPIRATION OF THE 19TH MONTH FROM THE PRIORITY DATE (Continued)

DEMANDES INTERNATIONALES POUR LESQUELLES UNE DEMANDE D'EXAMEN PRÉLIMINAIRE INTERNATIONAL A ÉTÉ PRÉSENTÉE AVANT L'EXPIRATION D'UNE PÉRIODE DE 19 MOIS À COMPTER DE LA DATE DE PRIORITÉ (Suite)

International Application Numbers Numéros des demandes internationales	International Publication Numbers Numéros de publication internationale	Designated States not Elected in the Demand États désignés non élus dans la demande d'examen préliminaire international	International Application Numbers Numéros des demandes internationales	International Publication Numbers Numéros de publication internationale	Designated States not Elected in the Demand États désignés non élus dans la demande d'examen préliminaire international
PCT/EP97/05616	WO 98/15172	–	PCT/EP97/05859	WO 98/18126	–
PCT/EP97/05619	WO 98/16814	–	PCT/EP97/05863	WO 98/17250	–
PCT/EP97/05624	WO 98/16901	–	PCT/EP97/05870	WO 98/23860	–
PCT/EP97/05629	WO 98/16146	–	PCT/EP97/05877	WO 98/18877	–
PCT/EP97/05648	WO 98/16340	–	PCT/EP97/05879	WO 98/17876	–
PCT/EP97/05651	WO 98/17488	–	PCT/EP97/05884	WO 98/19993	–
PCT/EP97/05658	WO 98/16346	–	PCT/EP97/05885	WO 98/18378	–
PCT/EP97/05663	WO 98/16589	–	PCT/EP97/05888	WO 98/18996	–
PCT/EP97/05680	WO 98/20452	–	PCT/EP97/05897	WO 98/18943	–
PCT/EP97/05684	WO 98/18014	–	PCT/EP97/05899	WO 98/19454	–
PCT/EP97/05685	WO 98/18556	–	PCT/EP97/05907	WO 98/23261	–
PCT/EP97/05688	WO 98/18555	–	PCT/EP97/05909	WO 98/18805	–
PCT/EP97/05702	WO 98/22200	–	PCT/EP97/05910	WO 98/18587	–
PCT/EP97/05722	WO 98/19584	–	PCT/EP97/05920	WO 98/17277	–
PCT/EP97/05732	WO 98/17971	–	PCT/EP97/05921	WO 98/19553	–
PCT/EP97/05736	WO 98/18093	–	PCT/EP97/05922	WO 98/17778	–
PCT/EP97/05740	WO 98/17612	–	PCT/EP97/05926	WO 98/20227	–
PCT/EP97/05743	WO 98/18795	–	PCT/EP97/05931	WO 98/17765	–
PCT/EP97/05751	WO 98/18899	–	PCT/EP97/05936	WO 98/18718	–
PCT/EP97/05752	WO 98/18868	–	PCT/EP97/05941	WO 98/19399	–
PCT/EP97/05771	WO 98/18678	–	PCT/EP97/05958	WO 98/19538	–
PCT/EP97/05772	WO 98/17866	–	PCT/EP97/05970	WO 98/18528	–
PCT/EP97/05778	WO 98/19204	–	PCT/EP97/05996	WO 98/20450	–
PCT/EP97/05793	WO 98/18885	–	PCT/EP97/06006	WO 98/18736	–
PCT/EP97/05814	WO 98/18295	–	PCT/EP97/06009	WO 98/19952	–
PCT/EP97/05820	WO 98/20862	–	PCT/EP97/06015	WO 98/18432	–
PCT/EP97/05826	WO 98/19537	–	PCT/EP97/06017	WO 98/20052	–
PCT/EP97/05830	WO 98/18977	–	PCT/EP97/06023	WO 98/21794	–
PCT/EP97/05845	WO 98/18648	–	PCT/EP97/06031	WO 98/20297	–
PCT/EP97/05848	WO 98/18474	–	PCT/EP97/06033	WO 98/20195	–
PCT/EP97/05851	WO 98/23497	–	PCT/EP97/06042	WO 98/21849	–
PCT/EP97/05853	WO 98/17596	–	PCT/EP97/06047	WO 98/21464	–
PCT/EP97/05854	WO 98/18791	–	PCT/EP97/06049	WO 98/21058	–
PCT/EP97/05855	WO 98/20012	–	PCT/EP97/06060	WO 98/20228	–

(Continued on the following page)

(Suite sur la page suivante)

Nintendo Exhibit 1066
IPR2024-00668 - Page 502

INTERNATIONAL APPLICATIONS FOR WHICH A DEMAND HAS BEEN FILED PRIOR TO THE EXPIRATION OF THE 19TH MONTH FROM THE PRIORITY DATE (Continued)

DEMANDES INTERNATIONALES POUR LESQUELLES UNE DEMANDE D'EXAMEN PRÉLIMINAIRE INTERNATIONAL A ÉTÉ PRÉSENTÉE AVANT L'EXPIRATION D'UNE PÉRIODE DE 19 MOIS À COMPTER DE LA DATE DE PRIORITÉ (Suite)

International Application Numbers Numéros des demandes internationales	International Publication Numbers Numéros de publication internationale	Designated States not Elected in the Demand États désignés non élus dans la demande d'examen préliminaire international	International Application Numbers Numéros des demandes internationales	International Publication Numbers Numéros de publication internationale	Designated States not Elected in the Demand États désignés non élus dans la demande d'examen préliminaire international
PCT/EP97/06072	WO 98/23164	–	PCT/EP97/06367	WO 98/23598	–
PCT/EP97/06079	WO 98/24008	–	PCT/EP97/06368	WO 98/23605	–
PCT/EP97/06082	WO 98/20859	–	PCT/EP97/06378	WO 98/16879	–
PCT/EP97/06085	WO 98/20845	–	PCT/EP97/06384	WO 98/23253	–
PCT/EP97/06108	WO 98/20493	–	PCT/EP97/06385	WO 98/22242	–
PCT/EP97/06111	WO 98/23515	–	PCT/EP97/06386	WO 98/23884	–
PCT/EP97/06119	WO 98/23676	–	PCT/EP97/06392	WO 98/23600	–
PCT/EP97/06136	WO 98/21161	–	PCT/EP97/06393	WO 98/23678	–
PCT/EP97/06144	WO 98/23005	–	PCT/EP97/06395	WO 98/23262	–
PCT/EP97/06148	WO 98/23001	–	PCT/EP97/06397	WO 98/21098	–
PCT/EP97/06152	WO 98/23002	–	PCT/EP97/06415	WO 98/23652	–
PCT/EP97/06154	WO 98/23010	–	PCT/EP97/06417	WO 98/23390	–
PCT/EP97/06180	WO 98/19702	–	PCT/EP97/06425	WO 98/23570	–
PCT/EP97/06181	WO 98/22591	–	PCT/EP97/06431	WO 98/23722	–
PCT/EP97/06182	WO 98/23258	–	PCT/EP97/06434	WO 98/23495	–
PCT/EP97/06195	WO 98/20233	–	PCT/EP97/06447	WO 98/23275	–
PCT/EP97/06197	WO 98/20995	–	PCT/EP97/06450	WO 98/23277	–
PCT/EP97/06204	WO 98/21790	–	PCT/EP97/06486	WO 98/23692	–
PCT/EP97/06206	WO 98/21787	–	PCT/EP97/06495	WO 98/23434	–
PCT/EP97/06208	WO 98/21495	–	PCT/EP97/06523	WO 98/23816	–
PCT/EP97/06221	WO 98/20909	–	PCT/EP97/06578	WO 98/23622	–
PCT/EP97/06257	WO 98/20856	–	PCT/EP97/06582	WO 98/23961	–
PCT/EP97/06271	WO 98/22302	–	PCT/EP97/06583	WO 98/23955	–
PCT/EP97/06275	WO 98/23651	–	PCT/EP97/06648	WO 98/23525	–
PCT/EP97/06290	WO 98/23649	–	PCT/EP97/06668	WO 98/23740	–
PCT/EP97/06291	WO 98/23688	–	PCT/EP97/06938	WO 98/21373	–
PCT/EP97/06292	WO 98/23581	–	PCT/FI96/00520	WO 98/14658	–
PCT/EP97/06295	WO 98/21616	–	PCT/FI96/00521	WO 98/14683	–
PCT/EP97/06311	WO 98/21193	–	PCT/FI97/00524	WO 98/10540	–
PCT/EP97/06347	WO 98/22726	–	PCT/FI97/00529	WO 98/09707	–
PCT/EP97/06354	WO 98/22713	–	PCT/FI97/00549	WO 98/12678	–
PCT/EP97/06357	WO 98/22763	–	PCT/FI97/00570	WO 98/14020	–
PCT/EP97/06362	WO 98/23985	–	PCT/FI97/00607	WO 98/16078	–
PCT/EP97/06363	WO 98/24178	–	PCT/FI97/00609	WO 98/16052	–

(Continued on the following page)

(Suite sur la page suivante)

Nintendo Exhibit 1066
IPR2024-00668 - Page 503

INTERNATIONAL APPLICATIONS FOR WHICH A DEMAND HAS BEEN FILED PRIOR TO THE EXPIRATION OF THE 19TH MONTH FROM THE PRIORITY DATE (Continued)

DEMANDES INTERNATIONALES POUR LESQUELLES UNE DEMANDE D'EXAMEN PRÉLIMINAIRE INTERNATIONAL A ÉTÉ PRÉSENTÉE AVANT L'EXPIRATION D'UNE PÉRIODE DE 19 MOIS À COMPTER DE LA DATE DE PRIORITÉ (Suite)

International Application Numbers Numéros des demandes internationales	International Publication Numbers Numéros de publication internationale	Designated States not Elected in the Demand États désignés non élus dans la demande d'examen préliminaire international	International Application Numbers Numéros des demandes internationales	International Publication Numbers Numéros de publication internationale	Designated States not Elected in the Demand États désignés non élus dans la demande d'examen préliminaire international
PCT/FI97/00610	WO 98/16079	–	PCT/FR97/01987	WO 98/24026	–
PCT/FI97/00611	WO 98/16037	–	PCT/FR97/02041	WO 98/21374	–
PCT/FI97/00612	WO 98/18227	–	PCT/FR97/02065	WO 98/22077	–
PCT/FI97/00613	WO 98/18267	–	PCT/FR97/02075	WO 98/22693	–
PCT/FI97/00630	WO 98/18199	–	PCT/FR97/02092	WO 98/23573	–
PCT/FI97/00631	WO 98/18197	–	PCT/FR97/02100	WO 98/24057	–
PCT/FI97/00632	WO 98/18198	–	PCT/FR97/02120	WO 98/23332	–
PCT/FI97/00717	WO 98/23394	–	PCT/FR97/02162	WO 98/23530	–
PCT/FI97/00723	WO 98/23514	–	PCT/GB97/00215	WO 97/27380	–
PCT/FR97/01695	WO 98/13715	–	PCT/GB97/02441	WO 98/16215	–
PCT/FR97/01702	WO 98/21998	–	PCT/GB97/02481	WO 98/13838	–
PCT/FR97/01745	WO 98/15848	–	PCT/GB97/02633	WO 98/13275	–
PCT/FR97/01805	WO 98/16478	–	PCT/GB97/02640	WO 98/15921	–
PCT/FR97/01820	WO 98/16740	–	PCT/GB97/02661	WO 98/13684	–
PCT/FR97/01831	WO 98/16484	–	PCT/GB97/02687	WO 98/19246	–
PCT/FR97/01835	WO 98/16780	–	PCT/GB97/02734	WO 98/15652	–
PCT/FR97/01858	WO 98/17599	–	PCT/GB97/02735	WO 98/17374	–
PCT/FR97/01861	WO 98/17378	–	PCT/GB97/02745	WO 98/17692	–
PCT/FR97/01865	WO 98/17367	–	PCT/GB97/02747	WO 98/17922	–
PCT/FR97/01869	WO 98/17158	–	PCT/GB97/02757	WO 98/15362	–
PCT/FR97/01886	WO 98/17950	–	PCT/GB97/02758	WO 98/18040	–
PCT/FR97/01894	WO 98/18308	–	PCT/GB97/02759	WO 98/19045	–
PCT/FR97/01895	WO 98/18380	–	PCT/GB97/02761	WO 98/19046	–
PCT/FR97/01902	WO 98/23246	–	PCT/GB97/02765	WO 98/17456	–
PCT/FR97/01905	WO 98/17437	–	PCT/GB97/02777	WO 98/19153	–
PCT/FR97/01908	WO 98/18317	–	PCT/GB97/02781	WO 98/16725	–
PCT/FR97/01918	WO 98/18958	–	PCT/GB97/02785	WO 98/18427	–
PCT/FR97/01937	WO 98/18369	–	PCT/GB97/02809	WO 98/17906	–
PCT/FR97/01941	WO 98/19104	–	PCT/GB97/02811	WO 98/18103	–
PCT/FR97/01947	WO 98/18360	–	PCT/GB97/02812	WO 98/17416	–
PCT/FR97/01955	WO 98/20272	–	PCT/GB97/02814	WO 98/19173	–
PCT/FR97/01966	WO 98/19967	–	PCT/GB97/02834	WO 98/16103	–
PCT/FR97/01973	WO 98/20080	–	PCT/GB97/02838	WO 98/16648	–
PCT/FR97/01981	WO 98/20384	–	PCT/GB97/02857	WO 98/17815	–

(Continued on the following page)

(Suite sur la page suivante)

Nintendo Exhibit 1066
IPR2024-00668 - Page 504

INTERNATIONAL APPLICATIONS FOR WHICH A DEMAND HAS BEEN FILED PRIOR TO THE EXPIRATION OF THE 19TH MONTH FROM THE PRIORITY DATE (Continued)

DEMANDES INTERNATIONALES POUR LESQUELLES UNE DEMANDE D'EXAMEN PRÉLIMINAIRE INTERNATIONAL A ÉTÉ PRÉSENTÉE AVANT L'EXPIRATION D'UNE PÉRIODE DE 19 MOIS À COMPTER DE LA DATE DE PRIORITÉ (Suite)

International Application Numbers Numéros des demandes internationales	International Publication Numbers Numéros de publication internationale	Designated States not Elected in the Demand États désignés non élus dans la demande d'examen préliminaire international	International Application Numbers Numéros des demandes internationales	International Publication Numbers Numéros de publication internationale	Designated States not Elected in the Demand États désignés non élus dans la demande d'examen préliminaire international
PCT/GB97/02858	WO 98/17816	–	PCT/GB97/03035	WO 98/20992	–
PCT/GB97/02860	WO 98/16535	–	PCT/GB97/03044	WO 98/20971	–
PCT/GB97/02862	WO 98/17280	–	PCT/GB97/03056	WO 98/23158	–
PCT/GB97/02865	WO 98/17930	–	PCT/GB97/03062	WO 98/20382	–
PCT/GB97/02868	WO 98/17892	–	PCT/GB97/03074	WO 98/20794	–
PCT/GB97/02869	WO 98/17893	–	PCT/GB97/03097	WO 98/21580	–
PCT/GB97/02870	WO 98/23354	–	PCT/GB97/03110	WO 98/22744	–
PCT/GB97/02883	WO 98/17383	–	PCT/GB97/03136	WO 98/22971	–
PCT/GB97/02884	WO 98/17649	–	PCT/GB97/03159	WO 98/23742	–
PCT/GB97/02885	WO 98/17648	–	PCT/GB97/03180	WO 98/24078	–
PCT/GB97/02886	WO 98/17650	–	PCT/GB97/03181	WO 98/24086	–
PCT/GB97/02896	WO 98/17216	–	PCT/GB97/03216	WO 98/23936	–
PCT/GB97/02898	WO 98/17324	–	PCT/GB97/03240	WO 98/23486	–
PCT/GB97/02901	WO 98/17262	–	PCT/GB97/03250	WO 98/24065	–
PCT/GB97/02905	WO 98/17288	–	PCT/GB97/03269	WO 98/23815	–
PCT/GB97/02907	WO 98/17661	–	PCT/GB97/03300	WO 98/24262	–
PCT/GB97/02909	WO 98/17401	–	PCT/GB97/03301	WO 98/24263	–
PCT/GB97/02918	WO 98/17812	–	PCT/GR97/00038	WO 98/19589	–
PCT/GB97/02924	WO 98/18022	–	PCT/HU97/00062	WO 98/16309	–
PCT/GB97/02925	WO 98/18039	–	PCT/HU97/00065	WO 98/17926	–
PCT/GB97/02927	WO 98/23350	–	PCT/HU97/00069	WO 98/18797	–
PCT/GB97/02928	WO 98/18318	–	PCT/HU97/00071	WO 98/18329	–
PCT/GB97/02933	WO 98/18298	–	PCT/IB97/00597	WO 98/24195	–
PCT/GB97/02935	WO 98/18387	–	PCT/IB97/00962	WO 97/49889	–
PCT/GB97/02949	WO 98/18782	–	PCT/IB97/01202	WO 98/16140	–
PCT/GB97/02950	WO 98/19226	–	PCT/IB97/01263	WO 98/18017	–
PCT/GB97/02962	WO 98/19219	–	PCT/IB97/01284	WO 98/18181	US
PCT/GB97/02969	WO 98/18934	–	PCT/IB97/01286	WO 98/18041	–
PCT/GB97/02977	WO 98/18677	–	PCT/IB97/01323	WO 98/16130	–
PCT/GB97/02980	WO 98/19073	–	PCT/IB97/01329	WO 98/17386	–
PCT/GB97/02983	WO 98/18909	–	PCT/IB97/01349	WO 98/20584	–
PCT/GB97/03013	WO 98/20355	–	PCT/IB97/01362	WO 98/20240	–
PCT/GB97/03031	WO 98/21383	–	PCT/IB97/01367	WO 98/21184	–
PCT/GB97/03033	WO 98/21188	–	PCT/IB97/01368	WO 98/23593	–

(Continued on the following page)

(Suite sur la page suivante)

INTERNATIONAL APPLICATIONS FOR WHICH A DEMAND HAS BEEN FILED PRIOR TO THE EXPIRATION OF THE 19TH MONTH FROM THE PRIORITY DATE (Continued)

DEMANDES INTERNATIONALES POUR LESQUELLES UNE DEMANDE D'EXAMEN PRÉLIMINAIRE INTERNATIONAL A ÉTÉ PRÉSENTÉE AVANT L'EXPIRATION D'UNE PÉRIODE DE 19 MOIS À COMPTER DE LA DATE DE PRIORITÉ (Suite)

International Application Numbers Numéros des demandes internationales	International Publication Numbers Numéros de publication internationale	Designated States not Elected in the Demand États désignés non élus dans la demande d'examen préliminaire international	International Application Numbers Numéros des demandes internationales	International Publication Numbers Numéros de publication internationale	Designated States not Elected in the Demand États désignés non élus dans la demande d'examen préliminaire international
PCT/IB97/01377	WO 98/15826	–	PCT/JP97/03125	WO 98/09945	–
PCT/IB97/01393	WO 98/23613	–	PCT/JP97/03236	WO 98/12175	–
PCT/IB97/01423	WO 98/20360	–	PCT/JP97/03323	WO 98/13515	–
PCT/IB97/01465	WO 98/23603	–	PCT/JP97/03338	WO 98/24021	–
PCT/IB97/01468	WO 98/24045	–	PCT/JP97/03342	WO 98/12195	–
PCT/IB97/01474	WO 98/24149	–	PCT/JP97/03357	WO 98/12715	–
PCT/IB97/01627	WO 98/20124	–	PCT/JP97/03392	WO 98/13389	–
PCT/IE97/00071	WO 98/18490	–	PCT/JP97/03418	WO 98/15076	–
PCT/IE97/00073	WO 98/19558	–	PCT/JP97/03419	WO 98/16889	–
PCT/IL96/00162	WO 98/23973	–	PCT/JP97/03421	WO 98/14484	–
PCT/IL97/00217	WO 98/19179	–	PCT/JP97/03425	WO 98/13827	–
PCT/IL97/00292	WO 98/16739	–	PCT/JP97/03522	WO 98/14831	–
PCT/IL97/00330	WO 98/16874	–	PCT/JP97/03543	WO 98/15021	–
PCT/IL97/00336	WO 98/19815	–	PCT/JP97/03603	WO 98/16497	–
PCT/IL97/00375	WO 98/23329	–	PCT/JP97/03608	WO 98/15263	–
PCT/IL97/00392	WO 98/23211	–	PCT/JP97/03627	WO 98/15943	–
PCT/IT97/00011	WO 98/21476	–	PCT/JP97/03667	WO 98/17808	–
PCT/IT97/00241	WO 98/17527	–	PCT/JP97/03687	WO 98/23628	–
PCT/IT97/00246	WO 98/17954	–	PCT/JP97/03702	WO 98/18229	–
PCT/JP96/02740	WO 98/13206	–	PCT/JP97/03717	WO 98/17438	–
PCT/JP96/02917	WO 98/15366	–	PCT/JP97/03724	WO 98/16307	–
PCT/JP96/02918	WO 98/15367	–	PCT/JP97/03742	WO 98/16145	–
PCT/JP96/02999	WO 98/16348	–	PCT/JP97/03744	WO 98/16470	–
PCT/JP96/03448	WO 98/24027	–	PCT/JP97/03745	WO 98/17739	–
PCT/JP96/03467	WO 98/23995	–	PCT/JP97/03754	WO 98/16625	–
PCT/JP96/03468	WO 98/24081	–	PCT/JP97/03778	WO 98/17869	JP
PCT/JP96/03503	WO 98/23851	–	PCT/JP97/03779	WO 98/16787	–
PCT/JP97/01995	WO 98/12098	–	PCT/JP97/03780	WO 98/16788	–
PCT/JP97/02851	WO 98/23664	–	PCT/JP97/03781	WO 98/16789	–
PCT/JP97/03022	WO 98/08527	–	PCT/JP97/03820	WO 98/18692	–
PCT/JP97/03094	WO 98/10435	–	PCT/JP97/03845	WO 98/18170	–
PCT/JP97/03096	WO 98/24082	–	PCT/JP97/03848	WO 98/16790	–
PCT/JP97/03097	WO 98/10000	–	PCT/JP97/03959	WO 98/23399	–
PCT/JP97/03098	WO 98/09784	–	PCT/JP97/03960	WO 98/23450	–

(Continued on the following page)

(Suite sur la page suivante)

Nintendo Exhibit 1066
IPR2024-00668 - Page 506

INTERNATIONAL APPLICATIONS FOR WHICH A DEMAND HAS BEEN FILED PRIOR TO THE EXPIRATION OF THE 19TH MONTH FROM THE PRIORITY DATE (Continued)

DEMANDES INTERNATIONALES POUR LESQUELLES UNE DEMANDE D'EXAMEN PRÉLIMINAIRE INTERNATIONAL A ÉTÉ PRÉSENTÉE AVANT L'EXPIRATION D'UNE PÉRIODE DE 19 MOIS À COMPTER DE LA DATE DE PRIORITÉ (Suite)

International Application Numbers Numéros des demandes internationales	International Publication Numbers Numéros de publication internationale	Designated States not Elected in the Demand États désignés non élus dans la demande d'examen préliminaire international	International Application Numbers Numéros des demandes internationales	International Publication Numbers Numéros de publication internationale	Designated States not Elected in the Demand États désignés non élus dans la demande d'examen préliminaire international
PCT/JP97/03975	WO 98/19056	–	PCT/JP97/04374	WO 98/23594	–
PCT/JP97/04003	WO 98/20542	–	PCT/JP97/04379	WO 98/24292	–
PCT/JP97/04047	WO 98/20518	–	PCT/KR97/00166	WO 98/20578	–
PCT/JP97/04055	WO 98/19960	–	PCT/KR97/00197	WO 98/19688	–
PCT/JP97/04060	WO 98/21828	–	PCT/KR97/00199	WO 98/17614	–
PCT/JP97/04100	WO 98/21005	–	PCT/NL97/00538	WO 98/13490	–
PCT/JP97/04165	WO 98/23384	–	PCT/NL97/00555	WO 98/16443	–
PCT/JP97/04177	WO 98/24108	–	PCT/NL97/00565	WO 98/16319	–
PCT/JP97/04191	WO 98/23374	–	PCT/NL97/00623	WO 98/24113	–
PCT/JP97/04194	WO 98/22498	–	PCT/NO97/00229	WO 98/10238	–
PCT/JP97/04252	WO 98/23614	–	PCT/NO97/00270	WO 98/15349	–
PCT/JP97/04265	WO 98/23562	–	PCT/NO97/00276	WO 98/16708	–
PCT/JP97/04271	WO 98/23767	–	PCT/NO97/00277	WO 98/17941	–
PCT/JP97/04276	WO 98/23615	–	PCT/NO97/00279	WO 98/19560	–
PCT/JP97/04277	WO 98/23629	–	PCT/NO97/00288	WO 98/20797	–
PCT/JP97/04285	WO 98/23557	–	PCT/NO97/00289	WO 98/20911	–
PCT/JP97/04287	WO 98/23607	–	PCT/NZ97/00134	WO 98/15579	–
PCT/JP97/04288	WO 98/23556	–	PCT/NZ97/00135	WO 98/16430	–
PCT/JP97/04295	WO 98/23918	–	PCT/NZ97/00141	WO 98/18463	–
PCT/JP97/04299	WO 98/23768	–	PCT/NZ97/00158	WO 98/23770	–
PCT/JP97/04300	WO 98/23769	–	PCT/RU96/00364	WO 98/19601	–
PCT/JP97/04301	WO 98/23916	–	PCT/RU97/00114	WO 98/13082	–
PCT/JP97/04303	WO 98/23176	–	PCT/RU97/00150	WO 98/10442	–
PCT/JP97/04313	WO 98/24112	–	PCT/RU97/00159	WO 98/21769	–
PCT/JP97/04318	WO 98/23430	–	PCT/RU97/00215	WO 98/14158	–
PCT/JP97/04323	WO 98/23271	–	PCT/RU97/00225	WO 98/13052	–
PCT/JP97/04328	WO 98/23583	–	PCT/RU97/00238	WO 98/05054	–
PCT/JP97/04330	WO 98/23563	–	PCT/RU97/00282	WO 98/11848	–
PCT/JP97/04331	WO 98/23564	–	PCT/RU97/00292	WO 98/13817	–
PCT/JP97/04334	WO 98/23624	–	PCT/RU97/00294	WO 98/13661	–
PCT/JP97/04335	WO 98/23553	–	PCT/RU97/00298	WO 98/13446	–
PCT/JP97/04337	WO 98/23406	–	PCT/RU97/00299	WO 98/14737	–
PCT/JP97/04368	WO 98/23449	–	PCT/RU97/00302	WO 98/14899	–
PCT/JP97/04373	WO 98/23568	–	PCT/RU97/00304	WO 98/14161	–

(Continued on the following page)

(Suite sur la page suivante)

Nintendo Exhibit 1066
IPR2024-00668 - Page 507

INTERNATIONAL APPLICATIONS FOR WHICH A DEMAND HAS BEEN FILED PRIOR TO THE EXPIRATION OF THE 19TH MONTH FROM THE PRIORITY DATE (Continued)

DEMANDES INTERNATIONALES POUR LESQUELLES UNE DEMANDE D'EXAMEN PRÉLIMINAIRE INTERNATIONAL A ÉTÉ PRÉSENTÉE AVANT L'EXPIRATION D'UNE PÉRIODE DE 19 MOIS À COMPTER DE LA DATE DE PRIORITÉ (Suite)

International Application Numbers Numéros des demandes internationales	International Publication Numbers Numéros de publication internationale	Designated States not Elected in the Demand États désignés non élus dans la demande d'examen préliminaire international	International Application Numbers Numéros des demandes internationales	International Publication Numbers Numéros de publication internationale	Designated States not Elected in the Demand États désignés non élus dans la demande d'examen préliminaire international
PCT/RU97/00305	WO 98/14162	–	PCT/SE97/01865	WO 98/20308	–
PCT/RU97/00307	WO 98/14791	–	PCT/SG97/00047	WO 98/20683	–
PCT/RU97/00312	WO 98/15158	–	PCT/SG97/00054	WO 98/18593	–
PCT/RU97/00314	WO 98/14166	–	PCT/SG97/00057	WO 98/20517	–
PCT/RU97/00315	WO 98/15332	–	PCT/SG97/00058	WO 98/20604	–
PCT/RU97/00318	WO 98/15495	–	PCT/SG97/00060	WO 98/24226	–
PCT/SE97/01329	WO 98/19363	–	PCT/UA96/00016	WO 98/11722	–
PCT/SE97/01330	WO 98/19364	–	PCT/US96/14899	WO 98/12026	–
PCT/SE97/01534	WO 98/15139	–	PCT/US96/16520	WO 98/15247	–
PCT/SE97/01576	WO 98/16287	–	PCT/US96/17227	WO 98/18340	–
PCT/SE97/01635	WO 98/14772	–	PCT/US96/19081	WO 98/23707	–
PCT/SE97/01656	WO 98/14238	–	PCT/US96/19112	WO 98/23708	–
PCT/SE97/01657	WO 98/16071	–	PCT/US96/19115	WO 98/23709	–
PCT/SE97/01660	WO 98/15748	–	PCT/US96/19807	WO 97/21769	–
PCT/SE97/01674	WO 98/15227	–	PCT/US96/20059	WO 98/13041	–
PCT/SE97/01680	WO 98/15334	–	PCT/US97/01324	WO 98/18596	–
PCT/SE97/01682	WO 98/15336	–	PCT/US97/02783	WO 98/21795	–
PCT/SE97/01688	WO 98/15754	–	PCT/US97/03827	WO 98/20491	–
PCT/SE97/01697	WO 98/16416	–	PCT/US97/04446	WO 98/20055	–
PCT/SE97/01699	WO 98/17080	–	PCT/US97/04575	WO 98/21023	–
PCT/SE97/01711	WO 98/19090	–	PCT/US97/04619	WO 98/00482	–
PCT/SE97/01712	WO 98/16792	–	PCT/US97/05010	WO 98/23818	–
PCT/SE97/01723	WO 98/16690	–	PCT/US97/05450	WO 98/23694	–
PCT/SE97/01730	WO 98/20504	–	PCT/US97/05527	WO 98/23518	–
PCT/SE97/01739	WO 98/18504	–	PCT/US97/05946	WO 97/40211	–
PCT/SE97/01740	WO 98/18505	–	PCT/US97/06673	WO 98/23893	–
PCT/SE97/01756	WO 98/19003	–	PCT/US97/06674	WO 98/23407	–
PCT/SE97/01762	WO 98/17861	–	PCT/US97/06702	WO 98/16855	–
PCT/SE97/01766	WO 98/19460	–	PCT/US97/08564	WO 98/20778	–
PCT/SE97/01772	WO 98/19438	–	PCT/US97/09150	WO 97/45699	–
PCT/SE97/01806	WO 98/19155	–	PCT/US97/09239	WO 97/49607	–
PCT/SE97/01834	WO 98/19953	–	PCT/US97/09857	WO 98/07892	–
PCT/SE97/01852	WO 98/23810	–	PCT/US97/10449	WO 98/12833	–
PCT/SE97/01864	WO 98/20307	–	PCT/US97/10757	WO 98/24120	–

(Continued on the following page)

(Suite sur la page suivante)

Nintendo Exhibit 1066
IPR2024-00668 - Page 508

INTERNATIONAL APPLICATIONS FOR WHICH A DEMAND HAS BEEN FILED PRIOR TO THE EXPIRATION OF THE 19TH MONTH FROM THE PRIORITY DATE (Continued)

DEMANDES INTERNATIONALES POUR LESQUELLES UNE DEMANDE D'EXAMEN PRÉLIMINAIRE INTERNATIONAL A ÉTÉ PRÉSENTÉE AVANT L'EXPIRATION D'UNE PÉRIODE DE 19 MOIS À COMPTER DE LA DATE DE PRIORITÉ (Suite)

International Application Numbers Numéros des demandes internationales	International Publication Numbers Numéros de publication internationale	Designated States not Elected in the Demand États désignés non élus dans la demande d'examen préliminaire international	International Application Numbers Numéros des demandes internationales	International Publication Numbers Numéros de publication internationale	Designated States not Elected in the Demand États désignés non élus dans la demande d'examen préliminaire international
PCT/US97/10864	WO 98/20654	–	PCT/US97/15254	WO 98/23244	–
PCT/US97/11249	WO 97/49972	–	PCT/US97/15312	WO 98/09987	–
PCT/US97/11432	WO 98/18618	–	PCT/US97/15335	WO 98/15769	–
PCT/US97/11476	WO 98/18289	–	PCT/US97/15456	WO 98/09973	–
PCT/US97/12565	WO 98/06486	–	PCT/US97/15539	WO 98/16379	–
PCT/US97/12751	WO 98/02084	–	PCT/US97/15552	WO 98/10387	–
PCT/US97/12853	WO 98/06143	–	PCT/US97/15600	WO 98/16998	–
PCT/US97/13035	WO 98/03207	–	PCT/US97/15604	WO 98/11334	–
PCT/US97/13063	WO 98/19903	–	PCT/US97/15623	WO 98/16574	–
PCT/US97/13066	WO 98/16137	–	PCT/US97/15732	WO 98/15190	–
PCT/US97/13132	WO 98/21699	–	PCT/US97/15733	WO 98/16545	–
PCT/US97/13199	WO 98/19258	–	PCT/US97/15738	WO 98/15861	–
PCT/US97/13464	WO 98/08285	–	PCT/US97/15739	WO 98/15860	–
PCT/US97/13641	WO 98/11933	–	PCT/US97/15744	WO 98/16540	–
PCT/US97/13656	WO 98/08105	–	PCT/US97/15745	WO 98/15327	–
PCT/US97/13893	WO 98/06100	–	PCT/US97/15746	WO 98/15492	–
PCT/US97/14002	WO 98/07142	–	PCT/US97/15754	WO 98/15825	–
PCT/US97/14024	WO 98/21659	–	PCT/US97/15791	WO 98/22749	–
PCT/US97/14025	WO 98/16324	–	PCT/US97/15839	WO 98/16818	–
PCT/US97/14026	WO 98/21709	–	PCT/US97/15852	WO 98/15323	–
PCT/US97/14071	WO 98/06451	–	PCT/US97/15853	WO 98/16066	–
PCT/US97/14105	WO 98/13166	–	PCT/US97/15937	WO 98/11947	–
PCT/US97/14348	WO 98/08558	–	PCT/US97/15950	WO 98/20467	–
PCT/US97/14371	WO 98/22908	–	PCT/US97/15951	WO 98/15019	–
PCT/US97/14464	WO 98/07136	–	PCT/US97/15985	WO 98/20732	–
PCT/US97/14626	WO 98/11469	–	PCT/US97/16006	WO 98/11363	–
PCT/US97/14805	WO 98/10407	–	PCT/US97/16056	WO 98/16579	–
PCT/US97/14842	WO 98/09208	–	PCT/US97/16102	WO 98/10734	–
PCT/US97/15090	WO 98/17951	–	PCT/US97/16135	WO 98/12493	–
PCT/US97/15125	WO 98/17466	–	PCT/US97/16158	WO 98/11677	–
PCT/US97/15199	WO 98/15803	–	PCT/US97/16166	WO 98/23589	–
PCT/US97/15207	WO 98/09416	–	PCT/US97/16181	WO 98/10649	–
PCT/US97/15245	WO 98/08506	–	PCT/US97/16247	WO 98/10925	–
PCT/US97/15252	WO 98/10053	–	PCT/US97/16264	WO 98/11449	–

(Continued on the following page)

(Suite sur la page suivante)

Nintendo Exhibit 1066
IPR2024-00668 - Page 509

INTERNATIONAL APPLICATIONS FOR WHICH A DEMAND HAS BEEN FILED PRIOR TO THE EXPIRATION OF THE 19TH MONTH FROM THE PRIORITY DATE (Continued)

DEMANDES INTERNATIONALES POUR LESQUELLES UNE DEMANDE D'EXAMEN PRÉLIMINAIRE INTERNATIONAL A ÉTÉ PRÉSENTÉE AVANT L'EXPIRATION D'UNE PÉRIODE DE 19 MOIS À COMPTER DE LA DATE DE PRIORITÉ (Suite)

International Application Numbers Numéros des demandes internationales	International Publication Numbers Numéros de publication internationale	Designated States not Elected in the Demand États désignés non élus dans la demande d'examen préliminaire international	International Application Numbers Numéros des demandes internationales	International Publication Numbers Numéros de publication internationale	Designated States not Elected in the Demand États désignés non élus dans la demande d'examen préliminaire international
PCT/US97/16265	WO 98/11446	–	PCT/US97/17058	WO 98/16795	–
PCT/US97/16303	WO 98/11787	–	PCT/US97/17090	WO 98/14249	–
PCT/US97/16385	WO 98/13248	–	PCT/US97/17091	WO 98/14963	–
PCT/US97/16394	WO 98/12022	–	PCT/US97/17133	WO 98/14602	–
PCT/US97/16436	WO 98/11815	–	PCT/US97/17151	WO 98/15688	–
PCT/US97/16451	WO 98/10732	–	PCT/US97/17158	WO 98/13195	–
PCT/US97/16511	WO 98/12635	–	PCT/US97/17160	WO 98/14777	–
PCT/US97/16531	WO 98/14111	–	PCT/US97/17188	WO 98/13116	–
PCT/US97/16537	WO 98/17981	–	PCT/US97/17194	WO 98/13088	–
PCT/US97/16559	WO 98/14927	–	PCT/US97/17209	WO 98/16282	–
PCT/US97/16589	WO 98/12205	–	PCT/US97/17235	WO 98/13222	–
PCT/US97/16664	WO 98/11841	–	PCT/US97/17250	WO 98/13557	–
PCT/US97/16700	WO 98/14048	–	PCT/US97/17279	WO 98/13825	–
PCT/US97/16727	WO 98/15042	–	PCT/US97/17282	WO 98/13007	–
PCT/US97/16737	WO 98/11847	–	PCT/US97/17313	WO 98/14275	–
PCT/US97/16800	WO 98/12268	–	PCT/US97/17323	WO 98/15070	–
PCT/US97/16834	WO 98/13151	–	PCT/US97/17362	WO 98/13380	–
PCT/US97/16845	WO 98/14935	–	PCT/US97/17377	WO 98/13796	–
PCT/US97/16871	WO 98/13908	–	PCT/US97/17442	WO 98/14754	–
PCT/US97/16877	WO 98/24179	–	PCT/US97/17444	WO 98/14924	–
PCT/US97/16878	WO 98/18261	–	PCT/US97/17468	WO 98/14838	–
PCT/US97/16894	WO 98/16966	–	PCT/US97/17481	WO 98/15108	–
PCT/US97/16898	WO 98/11980	–	PCT/US97/17491	WO 98/22968	–
PCT/US97/16934	WO 98/16408	–	PCT/US97/17510	WO 98/14467	–
PCT/US97/16960	WO 98/13664	–	PCT/US97/17517	WO 98/15059	–
PCT/US97/16972	WO 98/17345	–	PCT/US97/17544	WO 98/17708	–
PCT/US97/16973	WO 98/17546	–	PCT/US97/17549	WO 98/19501	–
PCT/US97/16989	WO 98/18725	–	PCT/US97/17564	WO 98/14237	–
PCT/US97/16990	WO 98/11814	–	PCT/US97/17566	WO 98/20644	–
PCT/US97/17003	WO 98/12530	–	PCT/US97/17612	WO 98/14970	–
PCT/US97/17004	WO 98/12616	–	PCT/US97/17613	WO 98/14139	–
PCT/US97/17011	WO 98/13571	–	PCT/US97/17645	WO 98/14290	–
PCT/US97/17042	WO 98/13941	–	PCT/US97/17651	WO 98/14128	–
PCT/US97/17046	WO 98/14003	–	PCT/US97/17653	WO 98/14936	–

(Continued on the following page)

(Suite sur la page suivante)

Nintendo Exhibit 1066
IPR2024-00668 - Page 510

INTERNATIONAL APPLICATIONS FOR WHICH A DEMAND HAS BEEN FILED PRIOR TO THE EXPIRATION OF THE 19TH MONTH FROM THE PRIORITY DATE (Continued)

DEMANDES INTERNATIONALES POUR LESQUELLES UNE DEMANDE D'EXAMEN PRÉLIMINAIRE INTERNATIONAL A ÉTÉ PRÉSENTÉE AVANT L'EXPIRATION D'UNE PÉRIODE DE 19 MOIS À COMPTER DE LA DATE DE PRIORITÉ (Suite)

International Application Numbers **Numéros des demandes internationales**	**International Publication Numbers** **Numéros de publication internationale**	**Designated States not Elected in the Demand** **États désignés non élus dans la demande d'examen préliminaire international**	**International Application Numbers** **Numéros des demandes internationales**	**International Publication Numbers** **Numéros de publication internationale**	**Designated States not Elected in the Demand** **États désignés non élus dans la demande d'examen préliminaire international**
PCT/US97/17661	WO 98/14886	–	PCT/US97/18055	WO 98/22418	–
PCT/US97/17682	WO 98/14641	–	PCT/US97/18056	WO 98/15795	–
PCT/US97/17696	WO 98/19013	–	PCT/US97/18062	WO 98/15811	–
PCT/US97/17699	WO 98/17702	–	PCT/US97/18104	WO 98/15293	–
PCT/US97/17702	WO 98/14485	–	PCT/US97/18112	WO 98/16199	–
PCT/US97/17706	WO 98/14901	–	PCT/US97/18118	WO 98/15857	–
PCT/US97/17725	WO 98/21678	–	PCT/US97/18129	WO 98/15198	–
PCT/US97/17731	WO 98/18016	–	PCT/US97/18132	WO 98/15473	–
PCT/US97/17733	WO 98/20185	–	PCT/US97/18139	WO 98/15621	–
PCT/US97/17742	WO 98/14570	–	PCT/US97/18141	WO 98/15920	–
PCT/US97/17744	WO 98/14571	–	PCT/US97/18143	WO 98/15645	–
PCT/US97/17745	WO 98/14612	–	PCT/US97/18145	WO 98/15179	–
PCT/US97/17749	WO 98/17777	–	PCT/US97/18162	WO 98/15812	–
PCT/US97/17751	WO 98/15862	–	PCT/US97/18167	WO 98/16069	–
PCT/US97/17752	WO 98/14179	–	PCT/US97/18182	WO 98/17494	–
PCT/US97/17765	WO 98/15396	–	PCT/US97/18194	WO 98/18006	–
PCT/US97/17780	WO 98/19000	–	PCT/US97/18200	WO 98/17474	–
PCT/US97/17798	WO 98/15413	–	PCT/US97/18202	WO 98/16627	–
PCT/US97/17808	WO 98/19356	–	PCT/US97/18217	WO 98/16150	–
PCT/US97/17819	WO 98/18910	–	PCT/US97/18222	WO 98/15570	–
PCT/US97/17828	WO 98/15275	–	PCT/US97/18228	WO 98/15194	–
PCT/US97/17855	WO 98/17758	–	PCT/US97/18230	WO 98/16571	–
PCT/US97/17878	WO 98/15810	–	PCT/US97/18238	WO 98/17603	–
PCT/US97/17891	WO 98/14572	–	PCT/US97/18243	WO 98/18527	–
PCT/US97/17909	WO 98/16492	–	PCT/US97/18247	WO 98/15994	–
PCT/US97/17915	WO 98/15894	–	PCT/US97/18248	WO 98/17045	–
PCT/US97/17919	WO 98/15218	–	PCT/US97/18259	WO 98/14579	–
PCT/US97/17927	WO 98/16174	–	PCT/US97/18265	WO 98/15380	–
PCT/US97/17979	WO 98/21641	–	PCT/US97/18280	WO 98/16503	–
PCT/US97/17996	WO 98/15228	–	PCT/US97/18288	WO 98/16164	–
PCT/US97/18000	WO 98/14514	–	PCT/US97/18293	WO 98/16646	–
PCT/US97/18013	WO 98/17301	–	PCT/US97/18296	WO 98/16821	–
PCT/US97/18023	WO 98/14402	–	PCT/US97/18304	WO 98/16720	–
PCT/US97/18048	WO 98/14534	–	PCT/US97/18323	WO 98/15563	–

(Continued on the following page)

(Suite sur la page suivante)

INTERNATIONAL APPLICATIONS FOR WHICH A DEMAND HAS BEEN FILED PRIOR TO THE EXPIRATION OF THE 19TH MONTH FROM THE PRIORITY DATE (Continued)

DEMANDES INTERNATIONALES POUR LESQUELLES UNE DEMANDE D'EXAMEN PRÉLIMINAIRE INTERNATIONAL A ÉTÉ PRÉSENTÉE AVANT L'EXPIRATION D'UNE PÉRIODE DE 19 MOIS À COMPTER DE LA DATE DE PRIORITÉ (Suite)

International Application Numbers Numéros des demandes internationales	International Publication Numbers Numéros de publication internationale	Designated States not Elected in the Demand États désignés non élus dans la demande d'examen préliminaire international	International Application Numbers Numéros des demandes internationales	International Publication Numbers Numéros de publication internationale	Designated States not Elected in the Demand États désignés non élus dans la demande d'examen préliminaire international
PCT/US97/18332	WO 98/15816	–	PCT/US97/18584	WO 98/16903	–
PCT/US97/18336	WO 98/16046	–	PCT/US97/18586	WO 98/17513	–
PCT/US97/18351	WO 98/16068	–	PCT/US97/18592	WO 98/16373	–
PCT/US97/18366	WO 98/16450	–	PCT/US97/18600	WO 98/16151	–
PCT/US97/18386	WO 98/20170	–	PCT/US97/18602	WO 98/16729	–
PCT/US97/18387	WO 98/16184	–	PCT/US97/18606	WO 98/17252	–
PCT/US97/18388	WO 98/16444	–	PCT/US97/18613	WO 98/16907	–
PCT/US97/18412	WO 98/16256	–	PCT/US97/18615	WO 98/16142	–
PCT/US97/18415	WO 98/16160	–	PCT/US97/18616	WO 98/17369	–
PCT/US97/18430	WO 98/16236	–	PCT/US97/18618	WO 98/17871	–
PCT/US97/18433	WO 98/16671	–	PCT/US97/18623	WO 98/16968	–
PCT/US97/18435	WO 98/19164	–	PCT/US97/18626	WO 98/23980	–
PCT/US97/18437	WO 98/16771	–	PCT/US97/18628	WO 98/16801	–
PCT/US97/18447	WO 98/16779	–	PCT/US97/18630	WO 98/16192	–
PCT/US97/18456	WO 98/17467	–	PCT/US97/18633	WO 98/18249	–
PCT/US97/18465	WO 98/16211	–	PCT/US97/18636	WO 98/17157	–
PCT/US97/18489	WO 98/18922	–	PCT/US97/18637	WO 98/16226	–
PCT/US97/18497	WO 98/17224	–	PCT/US97/18646	WO 98/16115	–
PCT/US97/18500	WO 98/18507	–	PCT/US97/18651	WO 98/16532	–
PCT/US97/18504	WO 98/16757	–	PCT/US97/18652	WO 98/16154	–
PCT/US97/18515	WO 98/19738	–	PCT/US97/18662	WO 98/17396	–
PCT/US97/18518	WO 98/16165	–	PCT/US97/18665	WO 98/17821	–
PCT/US97/18532	WO 98/16278	–	PCT/US97/18675	WO 98/16893	–
PCT/US97/18535	WO 98/17071	–	PCT/US97/18678	WO 98/15740	–
PCT/US97/18536	WO 98/17770	–	PCT/US97/18699	WO 98/17307	–
PCT/US97/18537	WO 98/15399	–	PCT/US97/18711	WO 98/17619	–
PCT/US97/18542	WO 98/16939	–	PCT/US97/18712	WO 98/16890	–
PCT/US97/18546	WO 98/16200	–	PCT/US97/18716	WO 98/17299	–
PCT/US97/18554	WO 98/17044	–	PCT/US97/18718	WO 98/16238	–
PCT/US97/18557	WO 98/16134	–	PCT/US97/18720	WO 98/18572	–
PCT/US97/18562	WO 98/15454	–	PCT/US97/18724	WO 98/17725	–
PCT/US97/18567	WO 98/17505	–	PCT/US97/18732	WO 98/20290	–
PCT/US97/18580	WO 98/16289	–	PCT/US97/18733	WO 98/17487	–
PCT/US97/18582	WO 98/16265	–	PCT/US97/18743	WO 98/15273	–

(Continued on the following page)

(Suite sur la page suivante)

INTERNATIONAL APPLICATIONS FOR WHICH A DEMAND HAS BEEN FILED PRIOR TO THE EXPIRATION OF THE 19TH MONTH FROM THE PRIORITY DATE (Continued)

DEMANDES INTERNATIONALES POUR LESQUELLES UNE DEMANDE D'EXAMEN PRÉLIMINAIRE INTERNATIONAL A ÉTÉ PRÉSENTÉE AVANT L'EXPIRATION D'UNE PÉRIODE DE 19 MOIS À COMPTER DE LA DATE DE PRIORITÉ (Suite)

International Application Numbers Numéros des demandes internationales	International Publication Numbers Numéros de publication internationale	Designated States not Elected in the Demand États désignés non élus dans la demande d'examen préliminaire international	International Application Numbers Numéros des demandes internationales	International Publication Numbers Numéros de publication internationale	Designated States not Elected in the Demand États désignés non élus dans la demande d'examen préliminaire international
PCT/US97/18753	WO 98/16168	–	PCT/US97/19047	WO 98/18145	–
PCT/US97/18754	WO 98/17227	–	PCT/US97/19054	WO 98/18159	–
PCT/US97/18764	WO 98/16401	–	PCT/US97/19055	WO 98/17316	–
PCT/US97/18765	WO 98/16709	–	PCT/US97/19058	WO 98/17171	–
PCT/US97/18767	WO 98/16186	–	PCT/US97/19063	WO 98/18815	–
PCT/US97/18769	WO 98/16626	–	PCT/US97/19067	WO 98/17842	–
PCT/US97/18802	WO 98/15171	–	PCT/US97/19071	WO 98/16515	–
PCT/US97/18816	WO 98/16783	–	PCT/US97/19092	WO 98/20513	–
PCT/US97/18818	WO 98/18412	–	PCT/US97/19108	WO 98/17209	–
PCT/US97/18821	WO 98/17243	–	PCT/US97/19127	WO 98/17366	–
PCT/US97/18825	WO 98/15453	–	PCT/US97/19130	WO 98/16897	–
PCT/US97/18831	WO 98/17524	–	PCT/US97/19136	WO 98/16617	–
PCT/US97/18850	WO 98/19320	–	PCT/US97/19139	WO 98/16734	–
PCT/US97/18853	WO 98/17242	–	PCT/US97/19143	WO 98/16257	–
PCT/US97/18856	WO 98/17169	–	PCT/US97/19144	WO 98/17843	–
PCT/US97/18890	WO 98/16717	–	PCT/US97/19150	WO 98/19131	–
PCT/US97/18900	WO 98/23183	–	PCT/US97/19152	WO 98/23411	–
PCT/US97/18901	WO 98/16205	–	PCT/US97/19182	WO 98/17737	–
PCT/US97/18922	WO 98/18110	–	PCT/US97/19208	WO 98/18734	–
PCT/US97/18925	WO 98/18015	–	PCT/US97/19210	WO 98/17275	–
PCT/US97/18931	WO 98/17136	–	PCT/US97/19219	WO 98/18939	–
PCT/US97/18941	WO 98/18130	–	PCT/US97/19228	WO 98/22471	–
PCT/US97/18944	WO 98/18480	–	PCT/US97/19230	WO 98/18473	–
PCT/US97/18968	WO 98/17679	–	PCT/US97/19233	WO 98/23451	–
PCT/US97/18976	WO 98/16742	–	PCT/US97/19236	WO 98/18523	–
PCT/US97/18980	WO 98/21211	–	PCT/US97/19240	WO 98/18531	–
PCT/US97/18999	WO 98/19237	–	PCT/US97/19246	WO 98/19229	–
PCT/US97/19005	WO 98/22768	–	PCT/US97/19247	WO 98/19183	–
PCT/US97/19009	WO 98/17637	–	PCT/US97/19265	WO 98/18546	–
PCT/US97/19010	WO 98/16919	–	PCT/US97/19277	WO 98/19059	–
PCT/US97/19023	WO 98/17826	–	PCT/US97/19278	WO 98/18978	–
PCT/US97/19039	WO 98/17483	–	PCT/US97/19284	WO 98/19088	–
PCT/US97/19041	WO 98/23761	–	PCT/US97/19287	WO 98/19877	–
PCT/US97/19044	WO 98/16554	–	PCT/US97/19291	WO 98/19294	–

(Continued on the following page)

(Suite sur la page suivante)

Nintendo Exhibit 1066
IPR2024-00668 - Page 513

INTERNATIONAL APPLICATIONS FOR WHICH A DEMAND HAS BEEN FILED PRIOR TO THE EXPIRATION OF THE 19TH MONTH FROM THE PRIORITY DATE (Continued)

DEMANDES INTERNATIONALES POUR LESQUELLES UNE DEMANDE D'EXAMEN PRÉLIMINAIRE INTERNATIONAL A ÉTÉ PRÉSENTÉE AVANT L'EXPIRATION D'UNE PÉRIODE DE 19 MOIS À COMPTER DE LA DATE DE PRIORITÉ (Suite)

International Application Numbers Numéros des demandes internationales	International Publication Numbers Numéros de publication internationale	Designated States not Elected in the Demand États désignés non élus dans la demande d'examen préliminaire international	International Application Numbers Numéros des demandes internationales	International Publication Numbers Numéros de publication internationale	Designated States not Elected in the Demand États désignés non élus dans la demande d'examen préliminaire international
PCT/US97/19292	WO 98/19408	–	PCT/US97/19597	WO 98/18914	–
PCT/US97/19317	WO 98/17205	–	PCT/US97/19607	WO 98/18925	–
PCT/US97/19322	WO 98/17707	–	PCT/US97/19611	WO 98/19721	–
PCT/US97/19330	WO 98/17110	–	PCT/US97/19615	WO 98/19599	–
PCT/US97/19340	WO 98/17609	–	PCT/US97/19619	WO 98/18312	–
PCT/US97/19343	WO 98/17253	–	PCT/US97/19625	WO 98/19879	–
PCT/US97/19348	WO 98/18460	–	PCT/US97/19626	WO 98/20422	–
PCT/US97/19349	WO 98/18461	–	PCT/US97/19674	WO 98/17254	–
PCT/US97/19352	WO 98/17430	–	PCT/US97/19714	WO 98/20810	–
PCT/US97/19361	WO 98/17111	–	PCT/US97/19734	WO 98/20668	–
PCT/US97/19390	WO 98/17541	–	PCT/US97/19750	WO 98/19268	–
PCT/US97/19398	WO 98/19210	–	PCT/US97/19773	WO 98/18376	–
PCT/US97/19417	WO 98/17337	–	PCT/US97/19774	WO 98/19262	–
PCT/US97/19425	WO 98/17112	–	PCT/US97/19788	WO 98/20129	–
PCT/US97/19432	WO 98/17580	–	PCT/US97/19796	WO 98/21087	–
PCT/US97/19433	WO 98/17618	–	PCT/US97/19799	WO 98/18311	–
PCT/US97/19439	WO 98/19196	–	PCT/US97/19800	WO 98/20720	–
PCT/US97/19446	WO 98/18290	–	PCT/US97/19804	WO 98/18932	–
PCT/US97/19457	WO 98/17828	–	PCT/US97/19825	WO 98/20709	–
PCT/US97/19459	WO 98/18081	–	PCT/US97/19846	WO 98/19739	–
PCT/US97/19470	WO 98/16849	–	PCT/US97/19868	WO 98/21902	–
PCT/US97/19473	WO 98/18955	–	PCT/US97/19877	WO 98/24190	–
PCT/US97/19476	WO 98/17626	–	PCT/US97/19898	WO 98/20312	–
PCT/US97/19507	WO 98/19850	–	PCT/US97/19905	WO 98/18709	–
PCT/US97/19531	WO 98/18314	–	PCT/US97/19948	WO 98/19618	–
PCT/US97/19538	WO 98/19272	–	PCT/US97/19950	WO 98/21492	–
PCT/US97/19540	WO 98/17108	–	PCT/US97/19994	WO 98/23645	–
PCT/US97/19543	WO 98/18077	–	PCT/US97/20019	WO 98/19977	–
PCT/US97/19554	WO 98/17740	–	PCT/US97/20050	WO 98/20590	–
PCT/US97/19575	WO 98/18323	–	PCT/US97/20052	WO 98/20060	–
PCT/US97/19585	WO 98/19700	–	PCT/US97/20053	WO 98/20348	–
PCT/US97/19589	WO 98/17113	–	PCT/US97/20062	WO 98/19751	–
PCT/US97/19590	WO 98/17687	–	PCT/US97/20067	WO 98/19595	–
PCT/US97/19595	WO 98/19682	–	PCT/US97/20069	WO 98/20036	–

(Continued on the following page)

(Suite sur la page suivante)

INTERNATIONAL APPLICATIONS FOR WHICH A DEMAND HAS BEEN FILED PRIOR TO THE EXPIRATION OF THE 19TH MONTH FROM THE PRIORITY DATE (Continued)

DEMANDES INTERNATIONALES POUR LESQUELLES UNE DEMANDE D'EXAMEN PRÉLIMINAIRE INTERNATIONAL A ÉTÉ PRÉSENTÉE AVANT L'EXPIRATION D'UNE PÉRIODE DE 19 MOIS À COMPTER DE LA DATE DE PRIORITÉ (Suite)

International Application Numbers / **Numéros des demandes internationales**	**International Publication Numbers** / **Numéros de publication internationale**	**Designated States not Elected in the Demand** / **États désignés non élus dans la demande d'examen préliminaire international**	**International Application Numbers** / **Numéros des demandes internationales**	**International Publication Numbers** / **Numéros de publication internationale**	**Designated States not Elected in the Demand** / **États désignés non élus dans la demande d'examen préliminaire international**
PCT/US97/20216	WO 98/19565	–	PCT/US97/20603	WO 98/21348	–
PCT/US97/20235	WO 98/21269	–	PCT/US97/20690	WO 98/20857	–
PCT/US97/20243	WO 98/20704	–	PCT/US97/20702	WO 98/20131	–
PCT/US97/20255	WO 98/20197	–	PCT/US97/20748	WO 98/21376	–
PCT/US97/20277	WO 98/23079	–	PCT/US97/20773	WO 98/23220	–
PCT/US97/20307	WO 98/20445	–	PCT/US97/20838	WO 98/23492	–
PCT/US97/20331	WO 98/21170	–	PCT/US97/20839	WO 98/21609	–
PCT/US97/20360	WO 98/23255	–	PCT/US97/20846	WO 98/19635	–
PCT/US97/20363	WO 98/23789	–	PCT/US97/20847	WO 98/19636	–
PCT/US97/20368	WO 98/21572	–	PCT/US97/20869	WO 98/20770	–
PCT/US97/20369	WO 98/21108	–	PCT/US97/20922	WO 98/20321	–
PCT/US97/20388	WO 98/19701	–	PCT/US97/20923	WO 98/19681	–
PCT/US97/20438	WO 98/20347	–	PCT/US97/20931	WO 98/22396	–
PCT/US97/20463	WO 98/22932	–	PCT/US97/21063	WO 98/21235	–
PCT/US97/20508	WO 98/20828	–	PCT/US97/21082	WO 98/22837	–
PCT/US97/20538	WO 98/20439	–	PCT/US97/21196	WO 98/23355	–
PCT/US97/20543	WO 98/23681	–	PCT/US97/21203	WO 98/21610	–
PCT/US97/20559	WO 98/20925	–	PCT/US97/21248	WO 98/21343	–
PCT/US97/20573	WO 98/21276	–	PCT/US97/21257	WO 98/24162	–
PCT/US97/20575	WO 98/20865	–	PCT/US97/21379	WO 98/23226	–
PCT/US97/20588	WO 98/21732	–	PCT/US97/21422	WO 98/24041	–
PCT/US97/20592	WO 98/20649	–	PCT/US97/21607	WO 98/24242	–
			PCT/US97/21615	WO 98/23838	–
			PCT/US97/21704	WO 98/23217	–
			PCT/US97/21865	WO 98/23782	–
			PCT/US97/22503	WO 98/23643	–
			PCT/US97/22511	WO 98/23448	–

EXHIBIT 1063A

web.archive.org/web/19990221083428/http://www.msiusa.com/piezo_film_manual.htm

http://www.msiusa.com/piezo_film_manual.htm Go JAN FEB APR

18 captures
21 Feb 1999 - 10 Apr 2021

1998 21 1999 2000 About this capture



Home
MSI Profile
Investors
Consumer
Sensors
Piezo Film
Accelerometers
Piezo Cable
Shockwriter
Sonar Hydrophones
Traffic Sensors
Vibration and Dynamic Strain Sensors
Transducers
Search
Contact Us





Technical Manual

Contents

PART1-INT.pdf
PART2-INT.pdf
PART3-INT.pdf
PART4-INT.pdf
PART5-INT.pdf
PART6-INT.pdf
PART7-INT.pdf
PART8-INT.pdf
PART9-INT.pdf
PART10-INT.pdf
PART11-INT.pdf
PART12-INT.pdf
PART13-INT.pdf
PART14-INT.pdf
PART15-INT.pdf
PART16-INT.pdf
PART17-INT.pdf
PART18-INT.pdf

Product Information

Accelerometer
ACH Specifications
805SPEC3.pdf

Accelerometer
ACH Analog Test PCB
805SPCB1.pdf

Piezo Coax Cable
Piezo_Cable.pdf

BL Sensor Package
BL Traffic Info.pdf

Piezo-Polymer Speakers
AN1242138.pdf

Solid State Switches
1141084.pdf

Download Our Piezo Film Products Guide!

Sensors_Product_Guide.pdf

The Wayback Machine - https://web.archive.org/web/19990221083428/http://www.msiusa.com:80/piezo_film…

back_button.gif

info_downloads.gif (2044 bytes)

Home
MSI Profile
Investors
Consumer
Sensors
Piezo Film
Accelerometers
Piezo Cable
Shockwriter
Sonar Hydrophones
Traffic Sensors
Vibration and Dynamic Strain Sensors
Transducers
Search
Contact Us

Technical Manual

Contents

PART1-INT.pdf
PART2-INT.pdf
PART3-INT.pdf
PART4-INT.pdf
PART5-INT.pdf
PART6-INT.pdf
PART7-INT.pdf
PART8-INT.pdf
PART9-INT.pdf
PART10-INT.pdf
PART11-INT.pdf
PART12-INT.pdf
PART13-INT.pdf
PART14-INT.pdf
PART15-INT.pdf
PART16-INT.pdf
PART17-INT.pdf
PART18-INT.pdf

Product Information

Accelerometer ACH Specifications
805SPEC3.pdf

Accelerometer ACH Analog Test PCB
805SPCB1.pdf

Piezo Coax Cable
Piezo_Cable.pdf

BL Sensor Package
BL Traffic Info.pdf

Piezo-Polymer Speakers
AN1242138.pdf

Solid State Switches
1141084.pdf

Download Our Piezo Film Products Guide!

Sensors_Product_Guide.pdf

Can't read PDF files?

Get Acrobat Reader

Transducers | Piezo Film
Home | Profile | Investors | Consumer | Sensors | Contact | Search

MEASUREMENT SPECIALTIES

Nintendo Exhibit 1066
IPR2024-00668 - Page 518

https://web.archive.org/web/20000925200945/http://www.msiusa.com/805spec3.pdf 133%
http://www.msiusa.com/805spec3.pdf Go AUG SEP JUN
6 captures 25 25
25 Sep 2000 - 1 Feb 2022 1999 2000 2004 About this capture
1 of 10 Automatic Zoom

MEASUREMENT SPECIALTIES

Accelerometer ACH-04-08-05

Application Specification
114-27002
27 AUG 98 Rev A

1.0 INTRODUCTION

This specification covers the application requirements of Measurement Specialties Accelerometer ACH-04-08-05. The accelerometer contains three piezoelectric sensing elements oriented to simultaneously measure acceleration in three orthogonal, linear axes. Internal JFET's provide for a low impedance, buffered output with a wide variety of possible, application specific, signal conditioning circuitry. The sensor responds over a broad frequency range, from below 0.5Hz to above 5kHz, as a result of the integrated electronics and the damped sensing elements.

The ACH-04-08-05 accelerometer can be used in a wide range of applications including motional measurement and control systems, speaker feedback systems, vibration switches, shipment monitor and material handling systems, security systems, computer input/output devices, and data loggers. The device is not IR reflow solderable.

Features of the accelerometer include:

Accelerometer ACH-04-08-05

1.0 INTRODUCTION

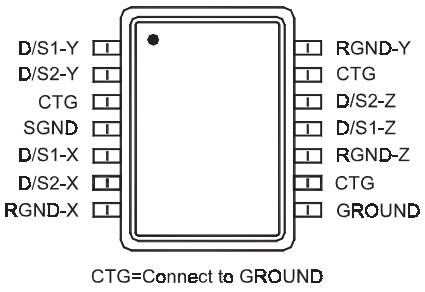
This specification covers the application requirements of Measurement Specialties Accelerometer ACH-04-08-05. The accelerometer contains three piezoelectric sensing elements oriented to simultaneously measure acceleration in three orthogonal, linear axes. Internal JFET's provide for a low impedance, buffered output with a wide variety of possible, application specific, signal conditioning circuitry. The sensor responds over a broad frequency range, from below 0.5Hz to above 5kHz, as a result of the integrated electronics and the damped sensing elements.

The ACH-04-08-05 accelerometer can be used in a wide range of applications including motional measurement and control systems, speaker feedback systems, vibration switches, shipment monitor and material handling systems, security systems, computer input/output devices, and data loggers. The device is not IR reflow solderable.

Features of the accelerometer include:

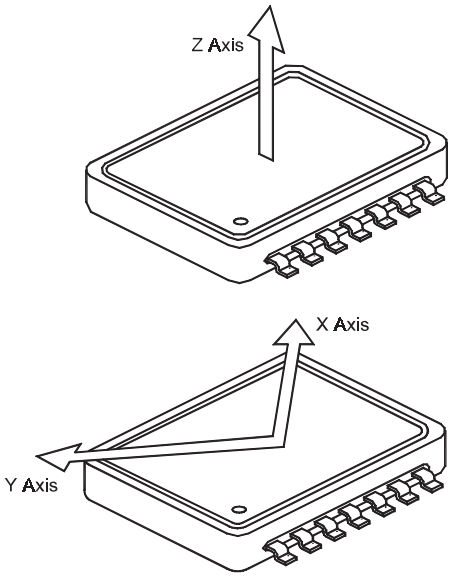
- Fully Contained 3-Axis Accelerometer
- Low Frequency Response
- High Resonant Frequency & Low Q
- Excellent Linearity
- Three Simultaneous Analog Outputs
- Low-Impedance Output
- Ultra-Low Power
- Low Cost

Pinout



CTG=Connect to GROUND

Sensitive Axes



2.0 REFERENCE MATERIALS

2.1 Revision Summary

This paragraph is reserved for a revision summary of changes and additions made to this specification. Revision A changes include: document format, improved transverse sensitivity, interface circuit corrections, Analog Test PCB Kit description, and additional performance curves.

©Copyright 1996 by MSI. All International Rights Reserved.

INFORMATIONAL NOTES AND DISCLAIMER
For drawings, technical data or samples, call 610-650-1500
Specifications subject to change. Consult MSI for latest specifications.

PN: 1003800-5 LOC ER

Nintendo Exhibit 1066
IPR2024-00668 - Page 520

2.2 Customer Assistance

Reference MSI Part Number 1003800-5 and call (610) 650-1500 in the USA or +49 6074 862 822 in Europe to obtain additional product information.

2.3 Drawings

MSI Customer Drawings are available for specific products. The information contained in Customer Drawings takes priority if there is a conflict with this specification or with any other technical document supplied by MSI.

2.4 Absolute Maximum Ratings

CHARACTERISTICS	VALUE	UNITS
Applied Voltage (V_{DD} with respect to GND)	+28	V
Package Power Dissipation	100	mW
ESD (Mil-Std-883, Method 3015.6)	2000	V

2.5 Pin Descriptions

PIN NUMBER	NAME	DESCRIPTION
1	D/S1-Y	Y-Axis JFET Drain or Source
2	D/S2-Y	Y-Axis JFET Source or Drain
3	CTG	Connect to GND
4	SGND	Sensor Common
5	D/S1-X	X-Axis JFET Drain or Source
6	D/S2-X	X-Axis JFET Source or Drain
7	RGND-X	Resistor GND for the X-Axis
8	GND	Device power - negative voltage with respect to V_{DD}
9	CTG	Connect to GND
10	RGND-Z	Resistor GND for the Z-Axis
11	D/S1-Z	Z-Axis JFET Drain or Source
12	D/S2-Z	Z-Axis JFET Source or Drain
13	CTG	Connect to GND
14	RGND-Y	Resistor GND for the Y-Axis

Note: JFET is symmetrical. The DRAIN and SOURCE are interchangeable.

2.6 Environmental Characteristics

CHARACTERISTICS (T=25°C)	SYMBOL	MIN	TYP	MAX	UNITS
Operating Temperature †	T_{OP}	-40	-	+85	°C
Storage Temperature	T_S	-40	-	+105	°C
Relative Humidity ‡	RH	0	-	95	%R.H.
Maximum Shock (Any Axis)	S_{MAX}	1,000	-	-	g

† Nominal sensitivity will typically change less than ±15% over temperature range. ‡ Humidity must be non-condensing.

Printed in U.S.A. For drawings, technical data or samples, contact call 610-650-1500.
Specifications subject to change. Consult MSI for latest specifications.

Nintendo Exhibit 1066
IPR2024-00668 - Page 521

2.7 Specification

CHARACTERISTIC (T=25°C) ●	SYMBOL	MIN	TYP	MAX	UNITS
X Axis Sensitivity ■ ▲	M_X	1.07	1.80	-	mV/g
Y Axis Sensitivity ■ ▲	M_Y	1.07	1.80	-	mV\g
Z Axis Sensitivity ■ ▲	M_Z	1.07	1.35	-	mV/g
Lower Frequency Limit (3dB Point)	f_{L3dB}	-	0.35	0.7	Hz
Upper Frequency Limit (3dB Point)	f_{U3dB}	4,000	5,000	-	Hz
Resonant Frequency	f_o	-	9,200	-	Hz
Resonant Q	Q_R	-	10	-	Hz/Hz
Transverse Sensitivity	M_T	-	10	-	%
Base Strain Sensitivity	-	-	0.05	-	g/$\mu\epsilon$
Temperature Transient Sensitivity	-	-	0.2	-	g/°C/min
Dynamic Range	-	-	±250	-	g's
Linearity	-	-	0.1	1.0	%
Equivalent Noise (100Hz)	e_{100}	-	0.2	-	mg/√Hz
Weight	-	-	0.35	-	grams

● Reference Frequency is 10 Hz.
■ Assumes constant current bias, guarded Drain & Source
▲ Tighter sensitivity tolerances available. Consult factory for options.

2.8 Electrical Specifications

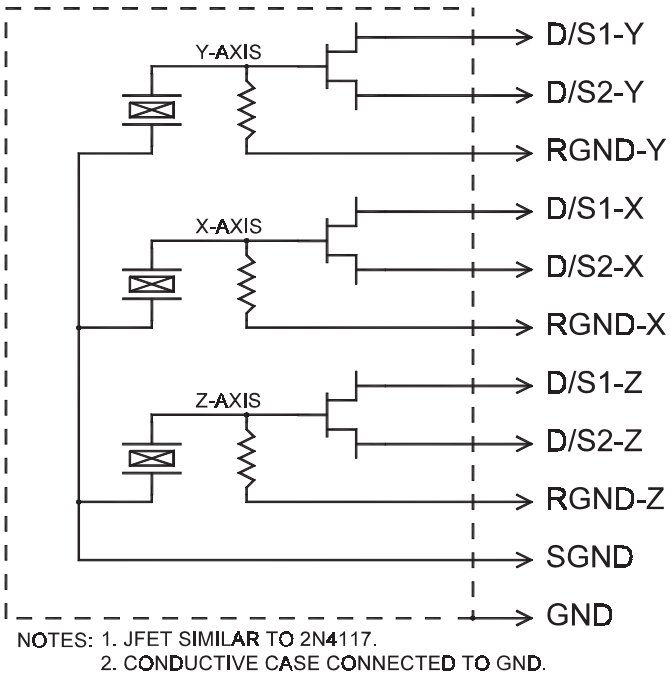
CHARACTERISTICS (T=25°C) ✦	SYMBOL	MIN	TYP	MAX	UNITS
Gate-Drain Voltage	-	-30	-	-	V
Gate-Source Voltage	-	-30	-	-	V
Gate Current	-	-	-	10	mA
Power Dissipation	-	-	-	360	mW
Power Derating	-	-	3.27	-	mW/ºC
Gate-Source Cut-Off Voltage	$V_{GS(OFF)}$	-0.5	-	-1.8	V
Saturation Drain Current ✣	I_{DSS}	10	-	150	μA
CS Forward Transconductance ✣	g_{FS}	50	-	210	μS

✦ JFET's similar to 2N4117. Three per unit.
✣ Specifications modified from standard 2N4117 JFET's.

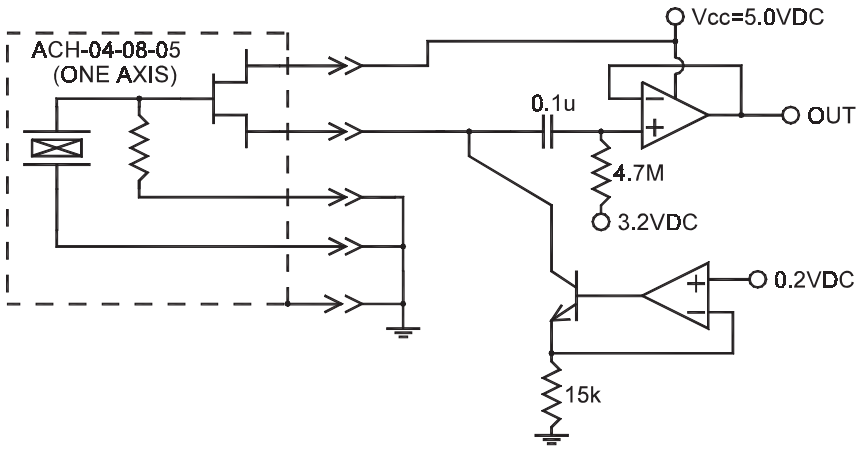
Printed in U.S.A. For drawings, technical data or samples, contact call 610-650-1500.
Specifications subject to change. Consult MSI for latest specifications.

Nintendo Exhibit 1066
IPR2024-00668 - Page 522

2.9.1 Equivalent Electrical Schematic



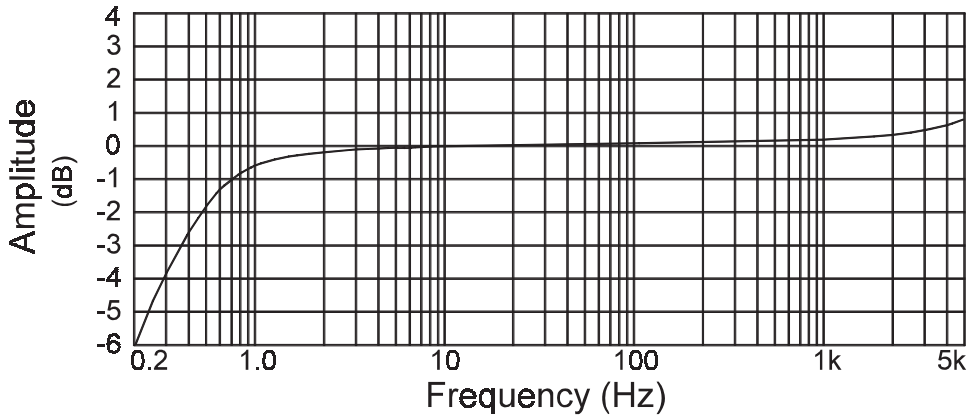
2.9.2 Interface Test Circuit (One Channel Shown)



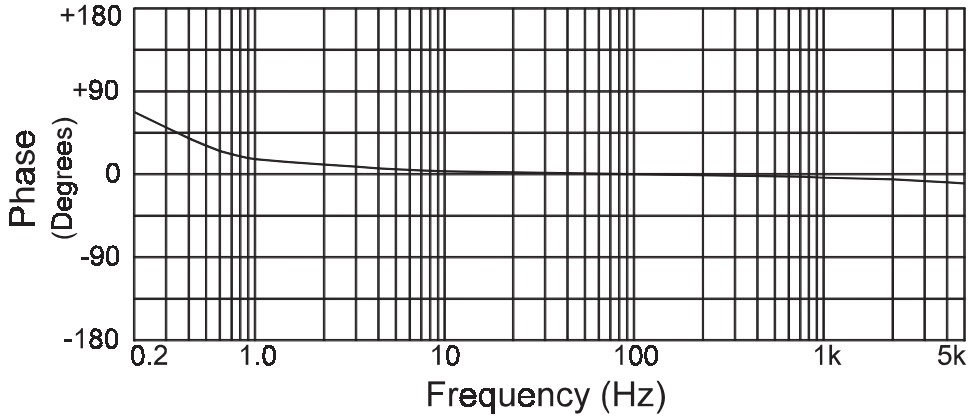
Printed in U.S.A. For drawings, technical data or samples, contact call 610-650-1500.
Specifications subject to change. Consult MSI for latest specifications.

Nintendo Exhibit 1066
IPR2024-00668 - Page 523

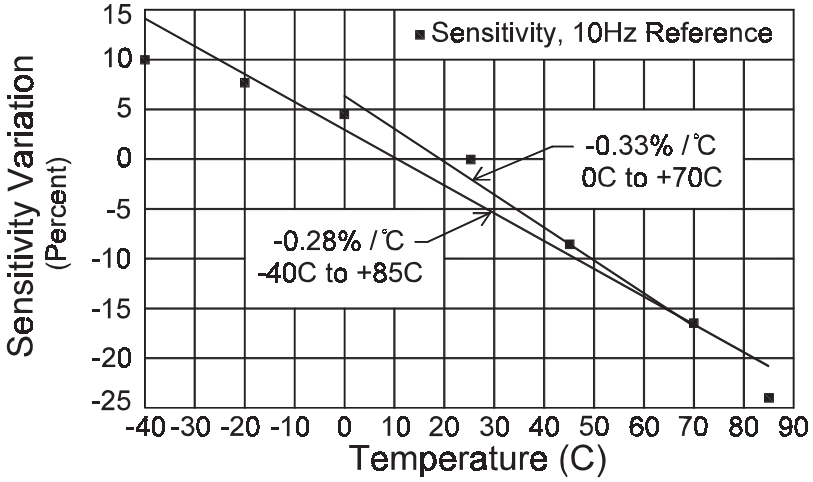
2.9.3 Typical Amplitude Response versus Frequency



2.9.4 Typical Phase Response versus Frequency



2.9.5 Typical Sensitivity Variation versus Temperature



Printed in U.S.A. For drawings, technical data or samples, contact call 610-650-1500.
Specifications subject to change. Consult MSI for latest specifications.

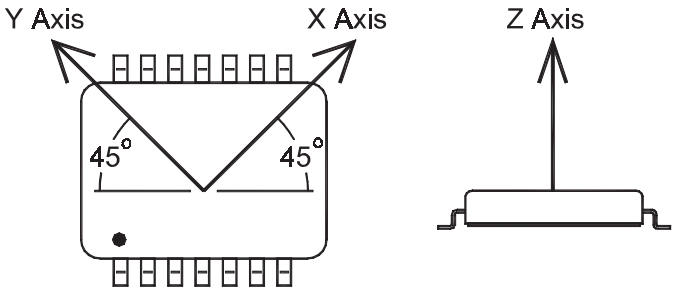
Nintendo Exhibit 1066
IPR2024-00668 - Page 524

3.0 REQUIREMENTS

3.1 Detailed Description

Each of the three sensing elements is a small cantilever beam consisting of a metal substrate with a piezoelectric polymer element affixed to one side. Each beam is supported at one end while the opposite end is allowed to flex in response to acceleration. The beam flex strains the piezoelectric material which in turn generates a charge proportional to the applied acceleration.

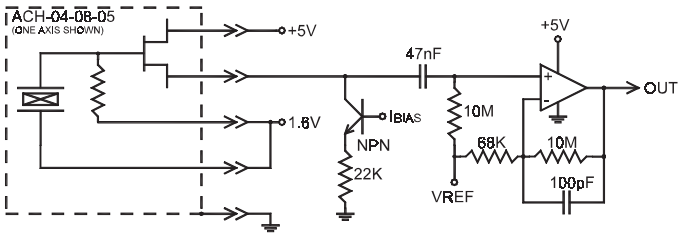
The beams are oriented to sense acceleration in the defined X, Y, and Z axes. Note that the X and Y axes are at a 45° angle relative to the accelerometer's package.

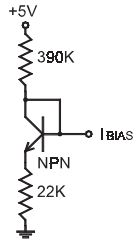


3.2 Electrical Interface

The ACH-04-08-05 contains three JFET's, one for each channel, which function as impedance converters easing electrical interface requirements. The JFET's are similar to the industry standard part number 2N4117. The JFET's MUST be biased for the accelerometer to function properly. There are many possible interface circuits. The JFET biasing circuit, used in MSI's final production test, is shown on page 4. Two other example circuits are shown below.

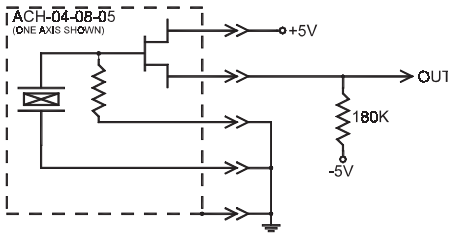
Constant Current Bias and Gain/Filter Stage





Notes:
1. VREF is typically 2.0V but should be scaled according to the operational amplifier's input common-mode range.
2. Circuit Gain: x148
3. High Pass Corner Frequency: 0.34 Hz
4. Low Pass Corner Frequency: 159 Hz
5. Circuit gain and corner frequencies can be adjusted. Circuit can also be scaled to operate at various supply voltages.

Resistor Bias with Split Supply



Notes:
1. Resistor value can be adjusted for individual applications.
2. +/- supply voltage can be scaled.

Printed in U.S.A. For drawings, technical data or samples, contact call 610-650-1500.
Specifications subject to change. Consult MSI for latest specifications.

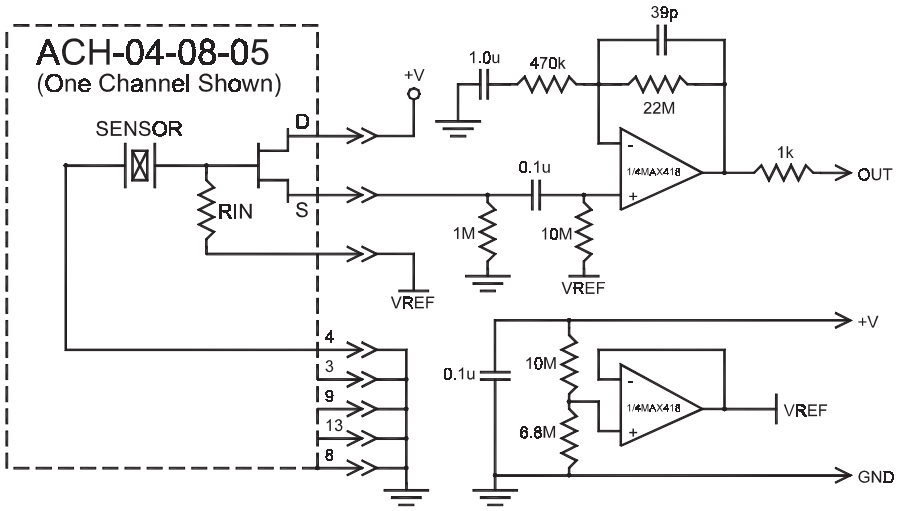
Nintendo Exhibit 1066
IPR2024-00668 - Page 525

The constant-current bias circuit minimizes device-to-device and temperature related JFET transconductance variations keeping the JFET gain near one (1). With the additional operational amplifier, the circuit has a gain of x148, a one-pole low-pass filter at 159Hz, and a one-pole high-pass filter at 0.34Hz. The circuit's component values and DC reference/supply voltages can be scaled to fit many applications.

The resistor bias circuit positions the operating point in the middle of the transconductance curve again minimizing transconductance variations. This circuit can also be powered from a single-supply voltage by creating an artificial ground, VREF.

The following figure shows the circuit used in MSI's Analog Test PCB (only one channel shown) which is available to quickly evaluate the basic characteristics of the ACH-04-08-05 accelerometer. Contact the factory to receive more information about the Analog Test PCB. Here, a resistor biasing scheme is used. The circuit runs from a single supply voltage by generating a reference voltage, VREF. The circuit has a gain of x47.8, a high-pass corner frequency of 0.34Hz, and a low-pass corner frequency of 185Hz. These values, as well as the operational amplifier, are easily changed to suit specific applications. As shown, the circuit typically draws only 13µA for all three axes.

Analog Test PCB: Low Power, Single Supply Circuit



3.3 Sensitivity Variation versus Temperature

The ACH-04-08-05's typical sensitivity variation versus temperature is shown on Page 5. As shown, the sensor output varies +10% / -24% from -40°C to +85°C, respectively, relative to 25°C. From 0°C to +70°C, the sensitivity variation is typically +5% / -16%, respectively. For many applications, this variation is acceptable (less than ±2dB from -40°C to +85°C). If a tighter tolerance is required, the ACH-04-08-05 is easily temperature compensated. A

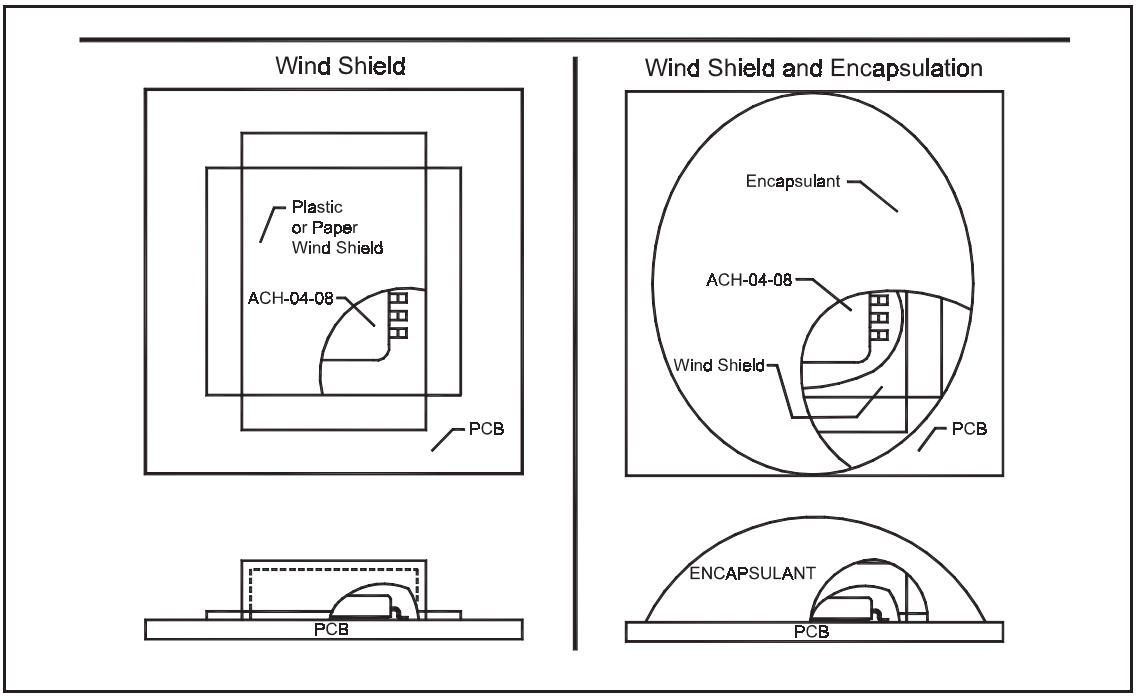
Printed in U.S.A. For drawings, technical data or samples, contact call 610-650-1500.
Specifications subject to change. Consult MSI for latest specifications.

Nintendo Exhibit 1066
IPR2024-00668 - Page 526

simple method is to use linear temperature coefficient resistors in the feedback network of the operational amplifier used to condition the accelerometer's signal. KOA Speer Electronics, Inc.® (Bradford, PA) manufactures a variety of these resistors (LT73 and MLT product family). Using a -2800ppm/°C temperature compensating resistor yields a sensitivity variation of ±4% from -40°C to +85°C. From 0°C to +70°C, a variation of only ±2% is obtained using a -3300ppm/°C resistor. Note that since the resistors have negative temperature coefficients, they need to be placed in the circuit such that the gain increases with increasing temperature.

3.4 Temperature Transient Sensitivity

Because of the its very low operating frequency, the ACH-04-08-05 exhibits high Temperature Transient Sensitivity (TTS). TTS is defined as the accelerometer's output response to RAPID temperature changes and is expressed in equivalent g's per degree C. This effect should not be confused with the ACH-04-08-05's sensitivity shift versus



temperature which is defined at static (unchanging) temperatures and is unrelated to TTS (see above). The ACH-04-08-05's TTS will manifest itself as a low frequency ("DC") drift when the device is subjected to temperature gradients. Even small temperature changes can produce significant DC drift.

TTS results primarily from differences in the thermal coefficients of expansion (TCE) of the various materials in the accelerometer. During product development, every effort is made to match TCE's, however, many mismatches are unavoidable. Even small TCE mismatches can lead to high TTS when combined with low frequency measurement capability since TTS is primarily a low frequency phenomena.

Fortunately, it is easy to minimize TTS effects. The key is to prevent air currents, which are at various temperatures, from circulating around the ACH-04-08-05. These "wind currents" can be minimized by encasing the accelerometer in a shell. The shell can be made of almost anything. Successful TTS minimization shells have been made from

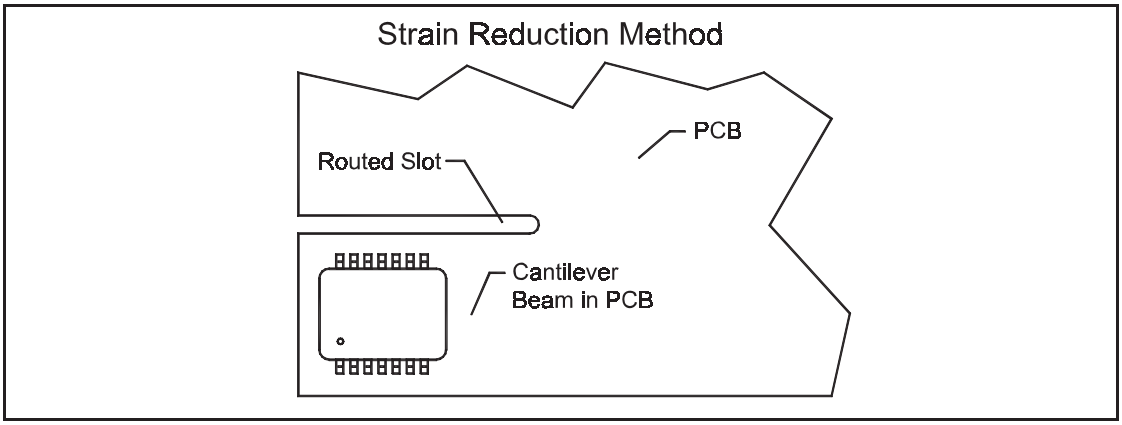
Printed in U.S.A. For drawings, technical data or samples, contact call 610-650-1500.
Specifications subject to change. Consult MSI for latest specifications.

Nintendo Exhibit 1066
IPR2024-00668 - Page 527

plastic, paper, metal, etc. In fact, wind shields have been successfully integrated into the housing of the final circuit board assembly negating the need for additional parts. While the shell does not have to be air-tight, tighter seals provide better performance. Encapsulating the ACH-04-08-05 can also provide an effective wind shield. To ensure that the ACH-04-08-05's housing is not compressed under the weight of the encapsulant, MSI recommends that a spacer be placed above the unit. Note that the best performance is obtained by combining a wind shell with encapsulation.

3.5 Base Strain Sensitivity

The ACH-04-08-05 displays Base Strain Sensitivity (BSS) for many of the same reasons that it displays TTS; namely, low frequency operation and low modulus/high TCE materials. BSS is defined as the amount of output signal generated as a result of bending in the accelerometer's mounting surface and is expressed in terms of equivalent g's per input micro-strain, g/με.



The best way to minimize BSS effects is to stiffen the mounting structure. Stiffer mounting structures are typically less susceptible to bending. However, since the ACH-04-08-05 is designed to be attached to a circuit board, it may be impractical to stiffen the mounting surface. In this situation, the accelerometer can be mounted at the end of a "cantilever beam" routed into the circuit board, where minimal strain is coupled into the accelerometer. Mounting arrangements such as this are very effective for low frequency applications. However, they are unacceptable for high frequency measurements where the signal to be measured is near or above the resonant frequency of the circuit board, cantilever beam. Implementation of a cantilever beam, strain minimization design requires careful analysis to accurately position the cantilever resonance well above the frequency range of interest.

3.6 IC Package

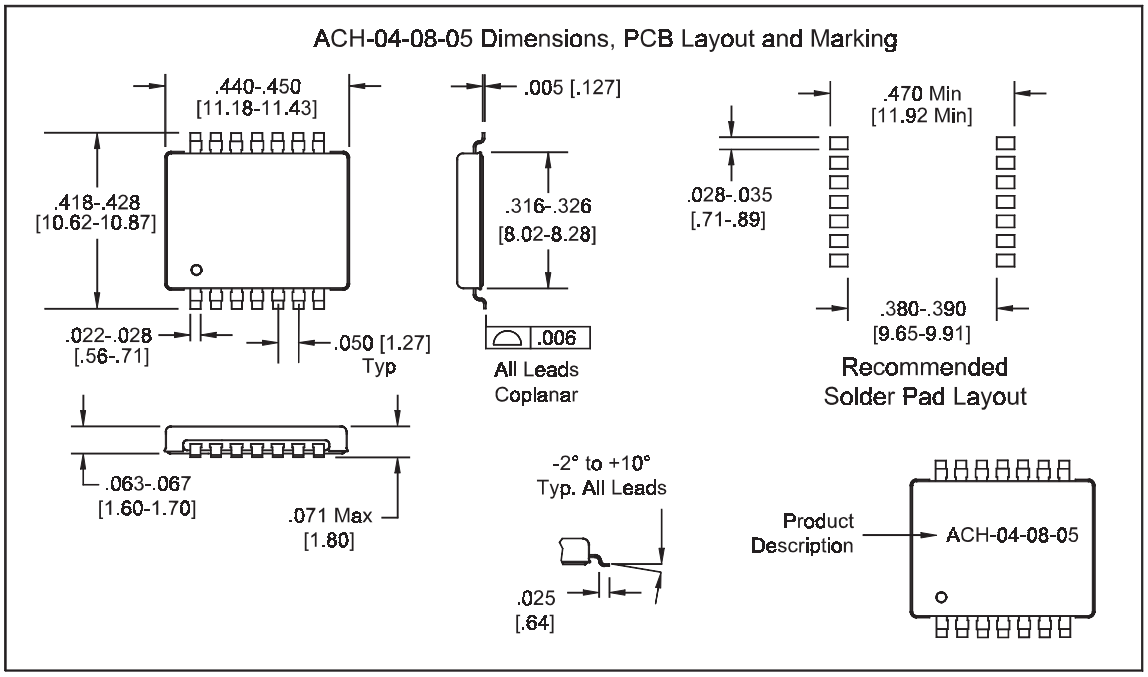
To insure proper protection against RF and EM interference, the outer surface of the package is conductive and electrically connected to the GND pin. Exercise caution when laying out PC boards to ensure that no uninsulated traces are located under the package. They could contact the package surface and be shorted to GND. It is recommended that all 14 pins of the package be soldered to the PC board to insure good mechanical coupling of acceleration, motion, and shock. Complete soldering will also eliminate undesirable mechanical resonances of the IC package.

Printed in U.S.A. For drawings, technical data or samples, contact call 610-650-1500.
Specifications subject to change. Consult MSI for latest specifications.

Nintendo Exhibit 1066
IPR2024-00668 - Page 528

The package is sealed to eliminate the effects of normal exposure to the environment and typical cleaning processes found in an electronic manufacturing facility. However, the package seal is not hermetic and exposure to acidic, basic, corrosive, or aqueous environments is not recommended. Because of process variations, the ACH-04-08-05 should be qualified through the intended production assembly processes (soldering, wash, etc.) before releasing to production. **The device is NOT IR reflow solderable**. Recommended alternative soldering processes include laser, hand and hot bar soldering. The ACH-04-08-05 can be manufactured to suit wave (not IR) soldering processes. Contact MSI for more detailed information.

3.7 ACH-04-08-05 Mechanical Dimensions



Printed in U.S.A. For drawings, technical data or samples, contact call 610-650-1500.
Specifications subject to change. Consult MSI for latest specifications.

Nintendo Exhibit 1066
IPR2024-00668 - Page 529

EXHIBIT 1063B

Texas Instruments

3-V Accelerometer Featuring TLV2772

Application Report

1998 *Advanced Analog Products*

SLVA040

Nintendo Exhibit 1066
IPR2024-00668 - Page 531

IMPORTANT NOTICE

Texas Instruments and its subsidiaries (TI) reserve the right to make changes to their products or to discontinue any product or service without notice, and advise customers to obtain the latest version of relevant information to verify, before placing orders, that information being relied on is current and complete. All products are sold subject to the terms and conditions of sale supplied at the time of order acknowledgement, including those pertaining to warranty, patent infringement, and limitation of liability.

TI warrants performance of its semiconductor products to the specifications applicable at the time of sale in accordance with TI's standard warranty. Testing and other quality control techniques are utilized to the extent TI deems necessary to support this warranty. Specific testing of all parameters of each device is not necessarily performed, except those mandated by government requirements.

CERTAIN APPLICATIONS USING SEMICONDUCTOR PRODUCTS MAY INVOLVE POTENTIAL RISKS OF DEATH, PERSONAL INJURY, OR SEVERE PROPERTY OR ENVIRONMENTAL DAMAGE ("CRITICAL APPLICATIONS"). TI SEMICONDUCTOR PRODUCTS ARE NOT DESIGNED, AUTHORIZED, OR WARRANTED TO BE SUITABLE FOR USE IN LIFE-SUPPORT DEVICES OR SYSTEMS OR OTHER CRITICAL APPLICATIONS. INCLUSION OF TI PRODUCTS IN SUCH APPLICATIONS IS UNDERSTOOD TO BE FULLY AT THE CUSTOMER'S RISK.

In order to minimize risks associated with the customer's applications, adequate design and operating safeguards must be provided by the customer to minimize inherent or procedural hazards.

TI assumes no liability for applications assistance or customer product design. TI does not warrant or represent that any license, either express or implied, is granted under any patent right, copyright, mask work right, or other intellectual property right of TI covering or relating to any combination, machine, or process in which such semiconductor products or services might be or are used. TI's publication of information regarding any third party's products or services does not constitute TI's approval, warranty or endorsement thereof.

Copyright © 1998, Texas Instruments Incorporated

3-V Accelerometer Featuring TLV2772

Application Report

Jim Karki
Advanced Analog Products
Advanced Analog Applications Group

Abstract

This paper describes a complete solution for digital measurement of acceleration. An AMP accelerometer sensor is used for the conversion between mechanical acceleration and electrical analog. This electrical signal is then conditioned using Texas Instruments' TLV2772 op amp (on the Universal Op Amp EVM), digitized using the TLV1544 ADC EVM, and processed with the TMS320C5X EVM. This provides the user with a quick and easy way to evaluate a complete 3-axis accelerometer solution.

Contents

1 Introduction 5
2 System Description 6
2.1 Sensor 7
2.2 Signal Conditioning 7
2.3 ADC 7
2.4 Processor, Memory, and Display 7
3 System Specification Requirements 7
3.1 G-Force Measurement Requirements 7
3.2 Power Requirements 7
4 Sensor and Signal Conditioning Design 8
4.1 Hand Analysis 8
4.2 Spice Simulation 11
5 Circuit Realization 14
5.1 Test of Signal Conditioning Circuit 17
5.2 Test of Shock Sensor and Signal Conditioning Circuit 17
5.3 TLV1544 EVM 18
5.4 Interfacing the TLV1544 EVM to the TMS320C5C EVM 19
5.5 The TMS320C5X EVM 19
6 Error and Noise Analysis 20
6.1 System Gain Error Analysis 20
6.2 System Noise Analysis 21
7 System Test and Evaluation 23
8 Calibration Data/Analysis 24
8.1 Calibration 24
9 References 27
Appendix A. Source Code Listings 28

TEXAS INSTRUMENTS

Figures

1–1 Typical Analog Data Collection System 5
2–1 Accelerometer System Diagram 6
4–1 1-Axis Accelerometer Sensor and Signal Conditioning Circuit 8
4–2 DC Circuit Model 8
4–3 AC Circuit Model 9
4–4 Bode Plot H1(s) = Vp/Vi 10
4–5 Bode Plot of H2(s) = Vo/Vp 10
4–6 Bode Plot of H3(s) = Vadc/Vo 11
4–7 Bode Plot of H(s) = Vadc/Vi 11
4–8 TLV2772 Sub-Circuit Model 12
4–9 SPICE Simulation Schematic 13
4–10 SPICE Simulation Results 13
5–1 Signal Conditioning Schematic using Two Universal Operational Amplifier EVM Boards . . . 16
5–2 Network Analyzer Display 17
5–3 Spring Test Fixture 17
5–4 Output Displayed on Oscilloscope 18
5–5 Schematic – Signal Conditioning to TLV1544 ADC 19
5–6 Interface Between TLV1544 EVM and TMS320C5X EVM 19
6–1 Sampling Input Model 21
7–1 X-Axis Acceleration Graphed in Excel 23
8–1 X-Axis Output Vs. Input 24
8–2 X-Axis % Error 25
8–3 Y-Axis Output vs. Input 25
8–4 Y-Axis % Error 26
8–5 Z-Axis Output vs. Input 26
8–6 Z-Axis % Error 27
8–7 Average Output vs. Input Over Frequency for Each Axis 27

Tables

5–1 Board 1 – Universal Operational Amplifier EVM Area 100 14
5–2 Board 2 – Universal Operational Amplifier EVM Area 100 14
5–3 Board 1 – Universal Operational Amplifier EVM Area 100 ACH-04-08-05 Connections 16
5–4 Interface Between Signal Conditiioning Circuit and TLV1544 EVM 18
8–1 X-Axis Output Vs. Input Using X-Axis Mean Sensitivity = 1.16 mV/g 24
8–2 X-Axis % Error 25
8–3 Y-Axis Output Vs. Input Using Y-Axis Mean Sensitivity = 1.35 mV/g 25
8–4 Y-Axis % Error 26
8–5 Z-Axis Output Vs. Input Using Z-Axis Mean Sensitivity = 1.01 mV/g 26
8–6 Z-Axis % Error 27

1 Introduction

Accelerometers are used in aerospace, defense, automotive, household appliances, instrumentation, audio, transport, material handling, etc. This application report develops a data collection system for acceleration in 3 axis.

Figure 1 shows a block diagram of a typical analog data collection system. This application presents information about the sensor, signal conditioning, ADC, processor, display, and memory.

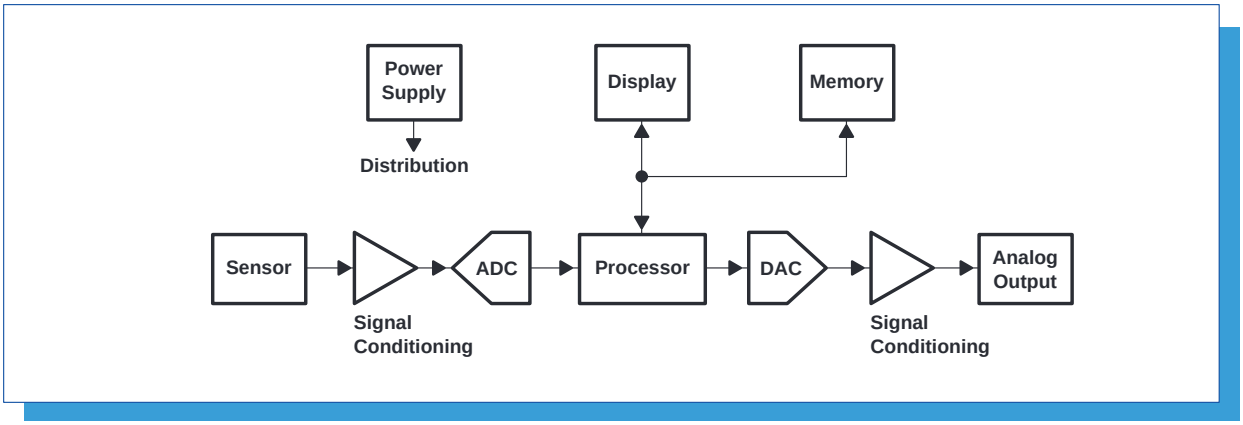


Figure 1–1. Typical Analog Data Collection System

Nintendo Exhibit 1066
IPR2024-00668 - Page 535

2 System Description

Figure 2.1 shows the accelerometer system diagram

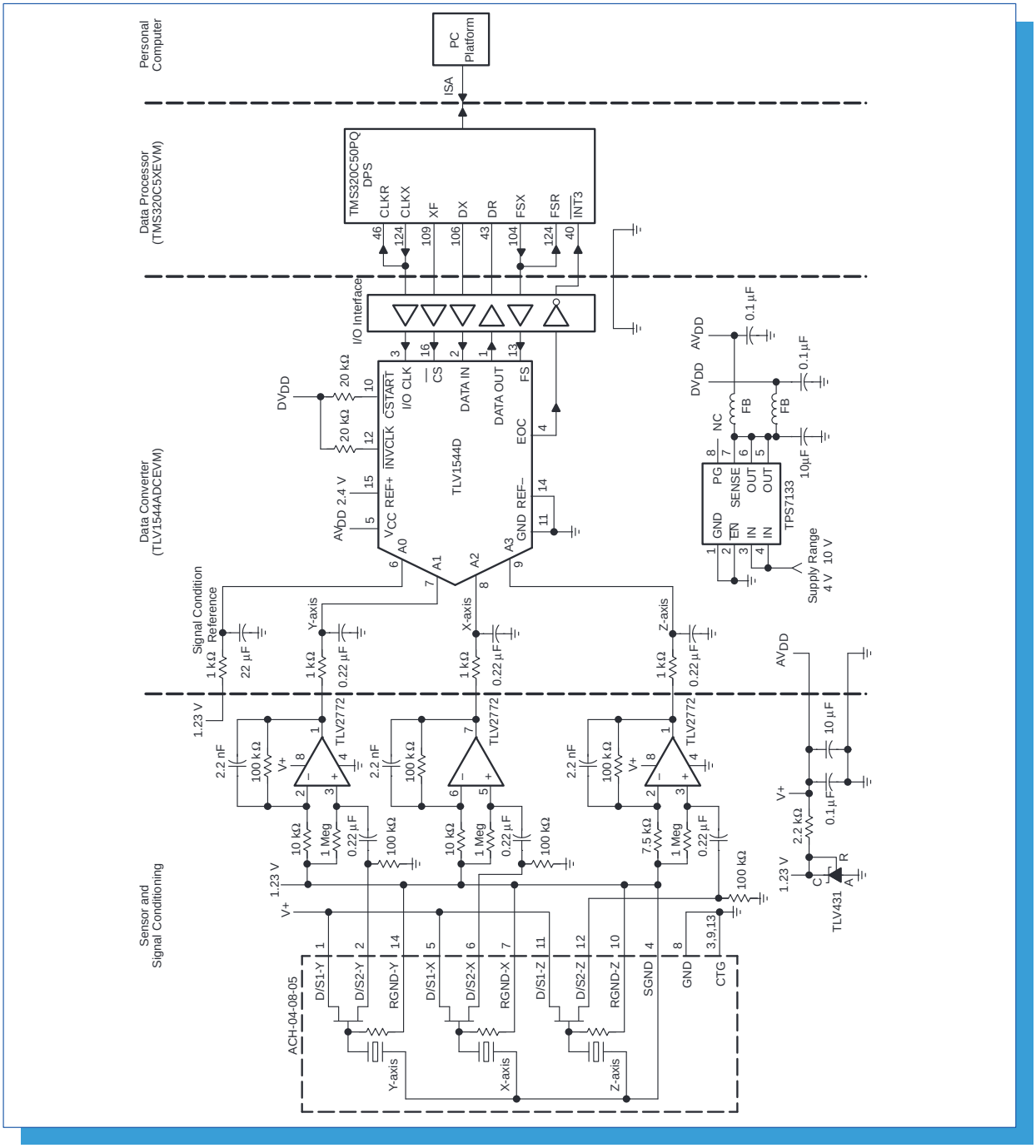


Figure 2–1. Accelerometer System Diagram

Nintendo Exhibit 1066
IPR2024-00668 - Page 536

2.1 Sensor

An AMP ACH04-08-05 shock sensor converts mechanical acceleration into electrical signals. The shock sensor contains three piezoelectric sensing elements oriented to simultaneously measure acceleration in three orthogonal linear axes. The sensor responds from 0.5 Hz to above 5 kHz. An internal JFET buffers the output. Typical output voltage for x and y axis is 1.80 mV/g. Typical output voltage for the z axis is 1.35 mV/g. Refer to AMP's web site at http://www.amp.com/sensors for in-depth information about this sensor, piezo materials in general, and other related products.

2.2 Signal Conditioning

Circuitry using the Texas Instruments TLV2772 operational amplifier provides amplification and frequency shaping of the shock sensor output. Due to its high slew rate and bandwidth, rail-to-rail output swing, high input impedance, high output drive and excellent dc precision the TLV2772 is ideal for this application. The device provides 10.5 V/μs slew rate and 5.1 MHz gain bandwidth product while consuming only 1 mA of supply current per amplifier. The rail-to-rail output swing and high output drive make this device ideal for driving the analog input to the TLV1544 analog-to-digital converter. The amplifier typically has 360 μV input offset voltage, 17 nV/vHz input noise voltage, and 2 pA input bias current. Refer to Texas Instruments' web site at http://www.ti.com and search on TLV2772 to download a TLV2772 data sheet, literature #SLOS209.

The Universal Operational Amplifier EVM is used to construct the ACH04-08-05 shock sensor and TLV2772 operational amplifier circuitry. The Universal Operational Amplifier EVM facilitates construction of surface mount operational amplifier circuits for engineering evaluation. Refer to Texas Instruments' web site at http://www.ti.com to download the Universal Operational Amplifier EVM User's Manual, literature #SLVU006.

2.3 ADC

The TLV1544 EVM provides analog-to-digital conversion. The TLV1544 is a low-voltage (2.7 V to 5.5 V dc single supply), 10-bit analog-to-digital converter (ADC) with serial control, 4 analog inputs, conversion time = 10 μs, and programmable 1 μA power down mode. Refer to Texas Instruments' web site at http://www.ti.com to download a TLV1544 data sheet, literature #SLAS139B, TLV1544 EVM User's Manual, literature #SLAU014, and related information.

2.4 Processor, Memory, and Display

The TMS320C5x EVM controls and collects data samples from the TLV1544. Refer to Texas Instruments' web site at http://www.ti.com to download the TMS320C5x EVM Technical Reference, literature #SPRU087, and related information .

The TMS320C5x EVM installs into a PC platform. The PC provides programming and control of the TMS320C5x EVM , and provides resources for file storage or other processing of the collected data.

3 System Specification Requirements

The following system specification requirements were derived to guide the design.

3.1 G-Force Measurement Requirements

Range: ±50g

Noise: 0.05g pk-pk (equivalent input noise measured in g)

Resolution: 0.1g

Frequency Response: 1 Hz to 500 Hz (min 3 dB BW)

3.2 Power Requirements

Input Voltage: 3 V ±10%, Noise = 30 mV pk-pk (20 MHz BW)

Input Current: 5 mA (max) (power requirements for sensor and signal conditioning circuitry)

Nintendo Exhibit 1066
IPR2024-00668 - Page 537

4 Sensor and Signal Conditioning Design

Circuit design is a 3-step process:

1. Hand analysis
2. SPICE simulation
3. Circuit breadboard and lab testing

The signal from the sensor must be amplified and frequency shaped to provide a signal that the ADC can properly convert into a digital number.

The schematic in Figure 4–1 shows the topology used in this application for 1 axis of the sensor and signal conditioning circuit.

Input power is 3 V and ground. The TLV431 precision voltage regulator, when configured as shown, produces a nominal 1.23-V reference voltage. This voltage provides the signal reference for the signal conditioning circuitry and the bias voltage for the internal JFETs in the shock sensor.

The transfer function of the signal conditioning circuit is derived by several means, the easiest of which may be by using super position. Perform a dc analysis, perform an ac analysis, and superimpose the results.

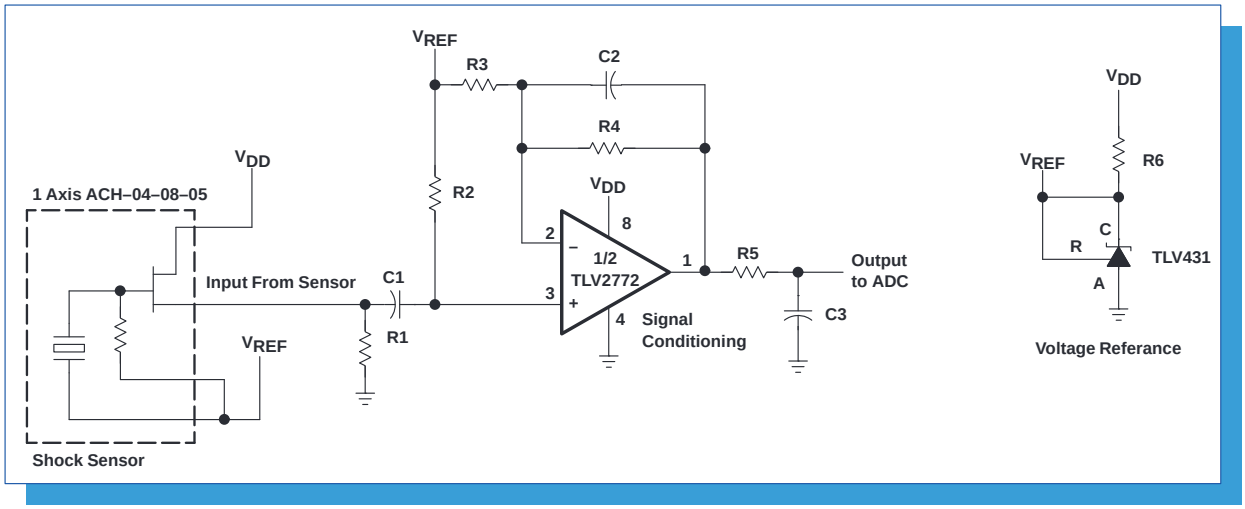


Figure 4–1. 1-Axis Accelerometer Sensor and Signal Conditioning Circuit

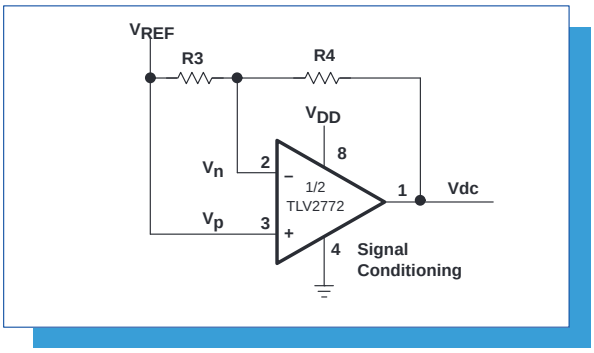


Figure 4–2. DC Circuit Model

4.1 Hand Analysis

In hand analysis, simplifying assumptions make solutions easier to derive. If the circuit does not function as anticipated, these assumption must be reevaluated.

4.1.1 DC Analysis

To perform a dc analysis, assume all inductors are short circuits and all capacitors are open circuits.

Assume that the resistance of R2 is insignificant compared to the input impedance of the op amp. Therefore, Vref will appear at the positive input to the op amp.

Assuming the ADC input does not impose a significant load on the circuit, the voltage divider formed between the ADC input and R5 can be disregarded.

Nintendo Exhibit 1066
IPR2024-00668 - Page 538

The dc model shown in Figure 4–2 is based on the assumptions made above.

The gain of the amplifier with reference to the negative input, Vn, is:

$$\frac{Vdc}{Vref} = -\frac{R4}{R3} \quad or \quad Vdc = -Vref\,\frac{R4}{R3}$$

The gain of the amplifier with reference to the positive input, Vp is:

$$\frac{Vdc}{Vref} = \left(1 + \frac{R4}{R3}\right) \quad or \quad Vdc = Vref\,\left(1 + \frac{R4}{R3}\right)$$

Superimposing the positive and negative dc gains of the amplifier results in:

$$Vdc = Vref$$

The output of the amplifier is referenced to Vref. The ac response is superimposed upon this dc level.

4.1.2 AC Analysis

For ac analysis break the circuit into 3 parts and determine the transfer functions;

- H1(s) = Vp / Vi
- H2(s) = Vo / Vp
- H3(s) = Vadc / Vo

Combine the results to obtain the overall transfer function:

- H(s) = Vadc / Vi

Where Vi is the input signal from the shock sensor and Vadc is the output signal to the analog-to-digital converter. Figure 4–3 shows the ac model with the dc sources shorted.

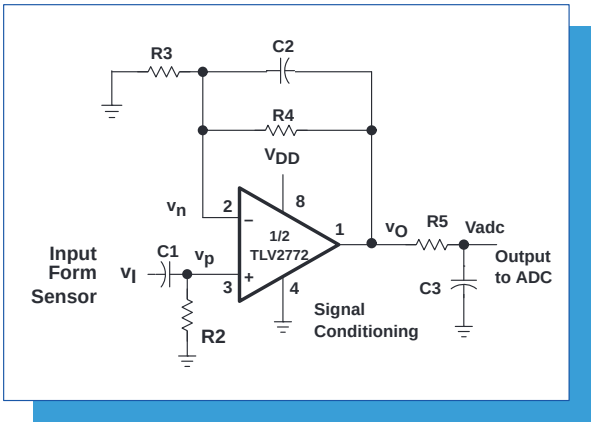


Figure 4–3. AC Circuit Model

4.1.2.1 H1(s)=Vp /Vi

Capacitor C1 and resistor R2 form a passive high-pass filter from the sensor input to the high impedance positive input to the TLV2772 where:

$$Vp = Vi\,\frac{R2}{R2 + 1/sC1} \quad or$$

$$H1(s) = \frac{Vp}{Vi} = \frac{R2}{R2 + 1/sC1}$$

4.1.2.2 H2(s) = Vo / Vp

The amplifier gain is found by solving for H2(s) = Vo/Vp. The solution is a non-inverting amplifier with:

$$H2(s) = \frac{Vo}{Vp} = \left(1 + \frac{Z}{R3}\right)$$

Where:

$$Z = \frac{R4}{1 + sC2R4}$$

substituting

$$H2(s) = \frac{Vo}{Vp} = 1 + \frac{R4}{R3}\left(\frac{1}{1 + sC2R4}\right)$$

4.1.2.3 H3(s) = Vadc / Vo

Assuming that the input impedance to the TLV1544 ADC is very high in comparison to the impedance of C3 and R5, C3 and R5 form a passive low-pass filter where:

$$Vadc = Vo\,\frac{1}{1 + sC3R5} \quad or$$

$$H3(s) = \frac{Vadc}{Vo} = \frac{1}{1 + sC3R5}$$

4.1.2.4 H(s) = Vadc / Vi

Superimposing the results from above gives the overall transfer function:

$$H(s) = \frac{Vadc}{Vi} = \left(\frac{R2}{R2 + 1/sC1}\right) \times \left(1 + \frac{R4}{R3}\left(\frac{1}{1 + sC2R4}\right)\right) \times \left(\frac{1}{1 + sC3R5}\right)$$

To find the complete response, add the ac and dc components so that:

$$Vadc = Vi\,H(s) + Vref$$

4.1.3 Gain Calculation

Since the TLV2772 is capable of rail-to-rail output, with a 3 V supply, Vout min = 0 V and Vout max = 3 V. With no signal from the sensor, Vout nom = reference voltage = 1.23 V. Therefore, the maximum negative swing from nominal is 0 V – 1.23 V = –1.23 V, and the maximum positive swing is 3 V – 1.23 V = 1.77 V.

Model the shock sensor as a low impedance voltage source with output of 2.25 mV/g max in the x and y axis and 1.70 mV/g max in the z axis, and calculate the required amplification of the signal conditioning circuit as follows:

Gain = Output Swing ÷ (Sensor Sensitivity · Acceleration)

Nintendo Exhibit 1066
IPR2024-00668 - Page 539

To avoid saturating the op amp, base the gain calculations on the maximum negative swing of –1.23 V and the maximum sensor output of 2.25 mV/g for the x and y axis, and 1.70 mV/g for the z axis. Therefore:

Gain(x,y) = –1.23 V ÷ (2.25 mV/g × (–50g)) = 10.9 and
Gain(z) = –1.23 V ÷ (1.70 mV/g × (–50g)) = 14.5

Choosing R3 = 10 kΩ and R4 = 100 kΩ, gives a gain of 11 in the x and y channels. Choosing R3 = 7.5 kΩ and R4 = 100 kΩ, gives a gain of 14.3 in the z channel.

4.1.4 Bandwidth Calculations

To calculate the component values for the frequency shaping characteristics of the signal conditioning circuit, use 1 Hz and 500 Hz as the minimum required 3-dB bandwidth from the specifications requirements.

4.1.4.1 Component Values for H1(s) = Vp / Vi

To minimize the value of the input capacitor required to set the lower cutoff frequency, a large value resistor is required for R2. A 1 MΩ resistor is used here. To set the lower cutoff frequency, the value for capacitor C1 must be:

C1 = 1 ÷ (2π × lower cutoff frequency (Hz) × R2 (Ω))

C1 = 1 ÷ (6.28 × 1 Hz × 1 MΩ) = 0.159 µF

A more common 0.22-µF capacitor is used for C1. This moves the lower cutoff frequency to 0.724 Hz.

Figure 4–4 shows the bode plot approximation to the input transfer function, H1(s) = Vp/Vi.

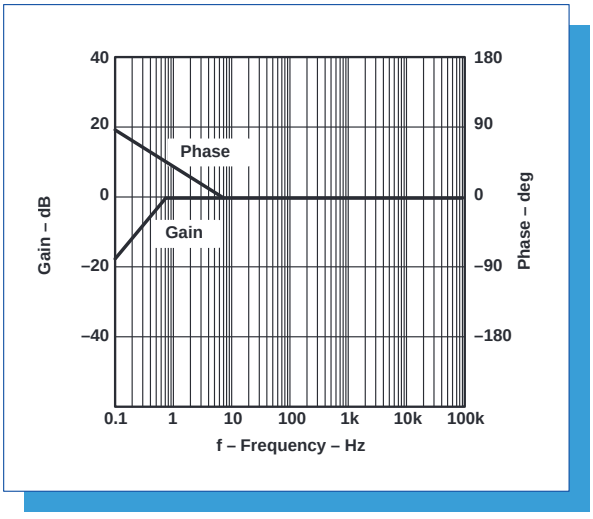


Figure 4–4. Bode Plot H1(s) = Vp/Vi

4.1.4.2 Component Values for H2(s) = Vo/Vp

To minimize phase shift in the feedback loop caused by the input capacitance of the TLV2772, it is best to minimize the value of feedback resistor R4. Also, to reduce the required capacitance in the feedback loop, a large-value resistor is required for R4. A compromise value of 100 kΩ is used for R4. To set the upper cutoff frequency, the required capacitor value for C2 is:

C2 = 1 ÷ (2π × upper cutoff frequency (Hz) × R4 (Ω))

C2 = 1 ÷ (6.28 × 500 Hz × 100 kΩ) = 3.18 nF

A more common 2.2 nF capacitor is used for C2. This changes the upper cutoff frequency to 724 Hz.

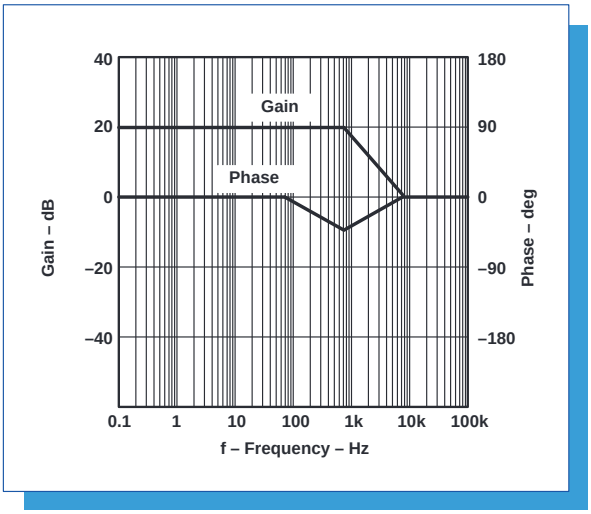


Figure 4–5. Bode Plot of H2(s) = Vo/Vp

Using the amplifier gain calculated above, Figure 4–5 shows the bode plot approximation to the transfer function H2(s) = Vo/Vp for the x and y channels. The z channel is the same except the gain is slightly higher in the pass band.

4.1.4.3 Component Values for H3(s) = Vadc/Vo

Resistor R5 and capacitor C3 cause the signal response to roll-off further. To set the frequency for this roll off to begin at the upper cutoff frequency, select 1÷(2π·C3(F) × R4(Ω)) = upper cutoff frequency(Hz).

With R5 = 1 kΩ and C3 = 0.22 µF, the roll-off frequency = 1 ÷ (6.28 × 0.22 µF × 1 kΩ) = 724 Hz.

Figure 4–6 shows the bode plot approximation to the transfer function H3(s) – Vadc/Vo.

Nintendo Exhibit 1066
IPR2024-00668 - Page 540

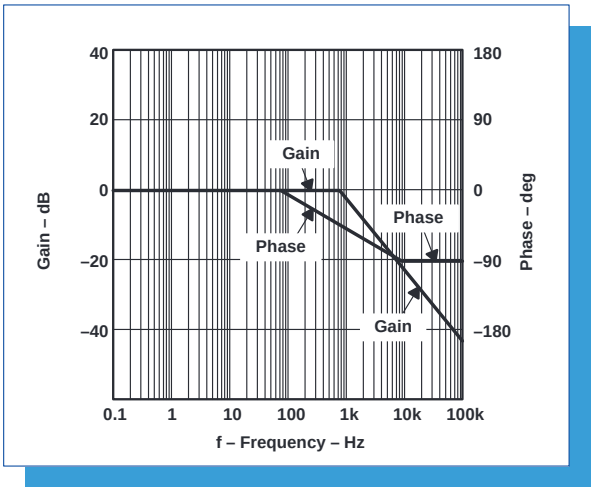


Figure 4–6. Bode Plot of H3(s) = Vadc/Vo

4.1.4.4 Transfer Function H(s) = Vadc / Vi

Superimposing the previous bode plot approximations results in the bode plot approximation for the overall transfer function to be expected from the signal conditioning circuit as shown in Figure 4–7.

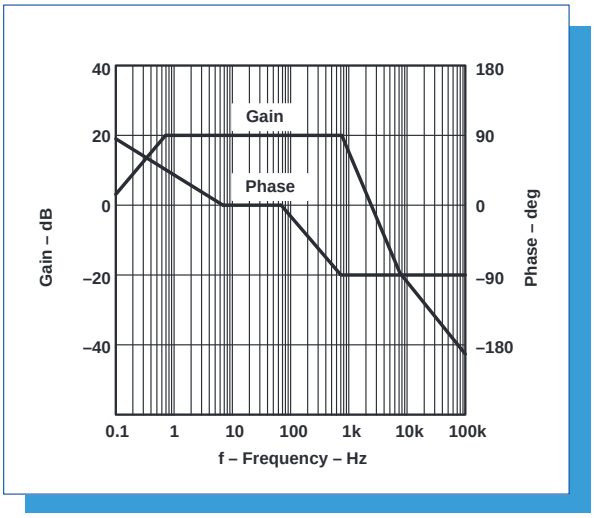


Figure 4–7. Bode Plot of H(s) = Vadc/Vi

4.2 Spice Simulation

Spice simulation verifies the results of hand analysis and provides a more accurate result than what is practical by hand.

The proper models must be used to perform SPICE simulation of the shock sensor and signal conditioning circuit.

The data sheet for the ACH-04-05-08 shock sensor states that the internal JFET used to drive the output is similar to the industry standard 2N4117. To model the sensor, a signal source is used to drive the gate of a 2N4117 JFET and proper bias is applied.

Modeling the signal conditioning circuit is straight forward except that most available SPICE versions do not have a library model for the TLV2772. This is easily remedied. Place a similar part on the schematic and modify its model with the model editor to match that of the TLV2772. Figure 4–8 below shows the TLV2772 sub-circuit model (as printed in the TLV2772 data sheet).

Nintendo Exhibit 1066
IPR2024-00668 - Page 541

```
.SUBCKT TLV2772-X 1  2  3  4  5
    C1      11    12   2.3094E-12
    C2      6     7    8.0000E-12
    CSS     10    99   2.1042E-12
    DC      5     53   DY
    DE      54    5    DY
    DLP     90    91   DX
    DLN     92    90   DX
    DP      4     3    DX
    EGND    99    0    POLY(2)  (3,0)  (4,0)  0  .5  .5
    FB      7     99   POLY(5)  VB  VC  VE  VLP  VLN  0  19.391E6 – 1E3  1E3  19E6 – 19E6
    GA  6   0     11   12    150.80E-6
    GCM 0 6     10   99    7.5576E-9
    ISS     3     10   DC    116.40E-6
    HLIM    90    0    VLIM  IK
    J1      11    2    10    JX1
    J2      12    1    10    JX2
    R2      6     9    100.0E3
    RD1     4     11   6.6315E3
    RD2     4     12   6.6315E3
    RO1     8     5    17.140
    RO2     7     99   17.140
    RP      3     4    4.5455E3
    RSS     10    99   1.7182E6
    VB      9     0    DC 0
    VC      3     53   DC .1
    VE      54    4    DC .1
    VLIM    7     8    DC 0
    VLP     91    0    DC 47
    VLN     0     92   DC 47
    .MODEL DX D(IS=800.0E-18)
    .MODEL DY D(IS=800.0E-18  Rs=1m  Cjo=10p)
    .MODEL JX1 PJF(IS=2.250E-12  BETA=195.36E-6  VTO=–1)
    .MODEL JX2 PJF(IS=1.750E-12  BETA=195.36E-6  VTO=–1)
    .ENDS
```

Figure 4–8. TLV2772 Sub-Circuit Model

Figure 4–9 shows the schematic used for SPICE simulation. Figures 4–10 show the simulation results.

Nintendo Exhibit 1066
IPR2024-00668 - Page 542

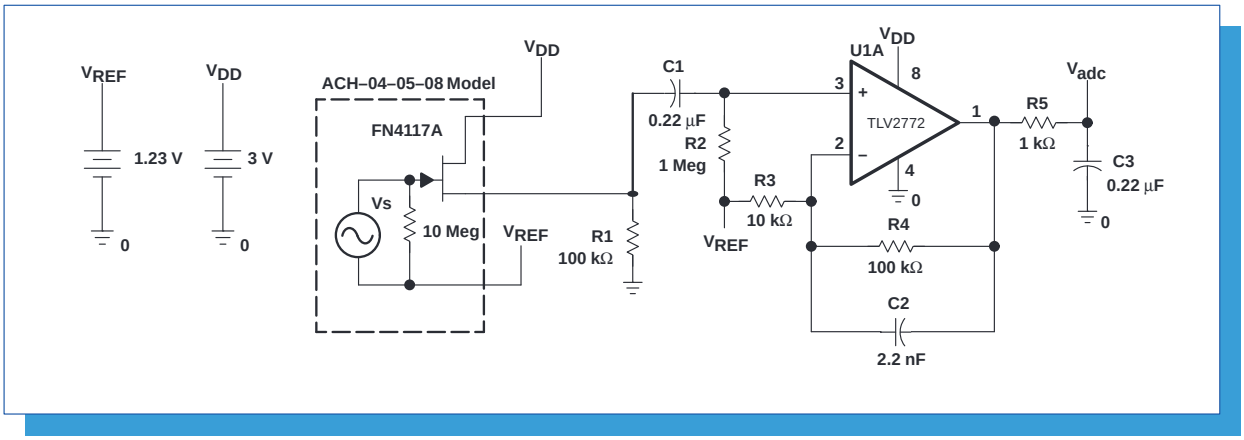


Figure 4–9. SPICE Simulation Schematic

The SPICE simulations show agreement with the hand calculations and the bode plot approximations.

The analyses above do not consider the frequency response of the shock sensor, which falls off below 0.5 Hz and above 5 kHz. The data sheet for the ACH-04-08-05 does not specify the role-off characteristics of the shock sensor's frequency response, but in general it is expected that there will be more attenuation in the signal below 0.5 Hz and above 5 kHz.

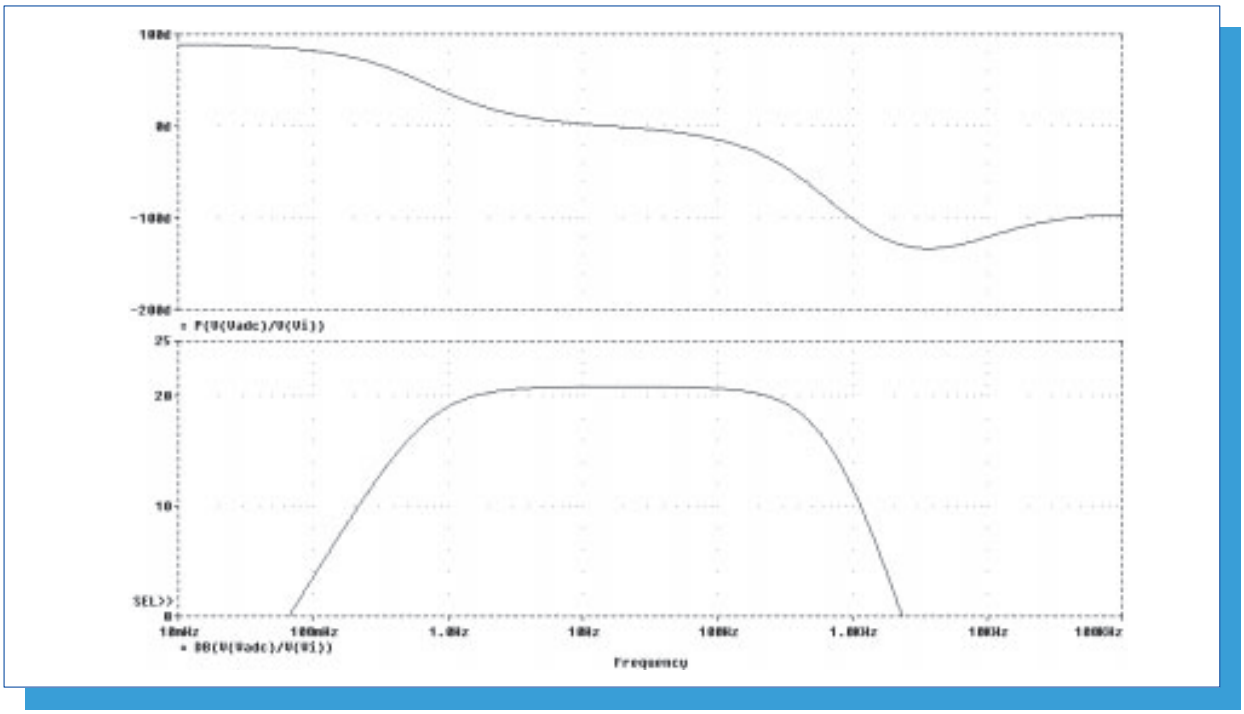


Figure 4–10. SPICE Simulation Results

Nintendo Exhibit 1066
IPR2024-00668 - Page 543

5 Circuit Realization

The shock sensor and signal conditioning circuits are built on area 100 of two Universal Operational Amplifier EVM boards (SLOP 120–1). One EVM board holds a TLV2772, an ACH-04-05-08, a TLV431, and required ancillary devices. The other board has only a TLV2772 and required ancillary devices. The signal conditioning circuit is constructed by installing required components and wiring. The two boards share signals and sources through board-to-board connectors. Standoffs and screws secure the two boards together. Figure 5–1 shows the schematic diagram with reference designators for using area 100 on two Universal Operational Amplifier EVM boards.

Tables 5–1 and 5–2 summarize reference designator part descriptions to construct the shock sensor and signal conditioning circuits.

Table 5–1. Board 1 – Universal Operational Amplifier EVM Area 100

REFERENCE DESIGNATOR	DESCRIPTION	REFERENCE DESIGNATOR	DESCRIPTION
R101	1 MΩ 1% SMT	C101	Not used
R102	10 kΩ 1% SMT	C102	2200 pF 5% NPO SMT
R103	Not used	C103	2.2 µF 20% Y5V SMT
R104	100 kΩ 1% SMT	C104	0.1 µF 10% X7R SMT
R105	100 kΩ 1% SMT	C105	2200 pF 5% NPO SMT
R106	Not used	C106	Not used
R107	10 kΩ 1% SMT	C107	Not used
R108	1 MΩ 1% SMT	C108	Not used
R109	Use 0.22 µF 10% X7R SMT Capacitor	C109	0 Ω or Jumper
R110	Use 0.22 µF 10% X7R SMT Capacitor	C110	Not used
R111	0 Ω or Jumper	C111	Not used
R112	Not used	C112	Not used
R113	Not used	U101	TLV2772CD
R114	2.2 kΩ 5% SMT	U102	TLV431ACDBV5
R115	0 Ω or Jumper	V1+	3 V power input
R116	Not used	VREF1	Signal conditioning reference
R117	Not used	GND1	Signal and power ground
R118	Not used	R119	0 Ω or Jumper
A1OUT	X Axis output	B104+	Y Axis input form ACH-04-05-08 pin 2
A101–	Not used	B103+	Jump to VREF1
A102–	Jump to VREF1	B102–	Jump VREF1
A103+	Jump to VREF1	B101–	Not used
A104+	X Axis input from ACH-04-05-08 pin 6	B1OUT	Y Axis output

Table 5–2. Board 2 – Universal Operational Amplifier EVM Area 100

REFERENCE DESIGNATOR	DESCRIPTION	REFERENCE DESIGNATOR	DESCRIPTION
R101	Not used	C101	Not used
R102	Not used	C102	Not used
R103	Not used	C103	Not used
R104	0 Ω or Jumper	C104	0.1 µF 10% X7R SMT
R105	100 kΩ 1% SMT	C105	2200 pF 5% NPO SMT

Nintendo Exhibit 1066
IPR2024-00668 - Page 544

Table 5–2. Board 2 – Universal Operational Amplifier EVM Area 100

REFERENCE DESIGNATOR	DESCRIPTION	REFERENCE DESIGNATOR	DESCRIPTION
R106	Not used	C106	Not used
R107	7.5 kΩ 1% SMT	C107	Not used
R108	1 MΩ 1% SMT	C108	Not used
R109	Use 0.22 µF 10% X7R SMT Capacitor	C109	0 Ω or Jumper
R110	Not used	C110	Not used
R111	Not used	C111	Not used
R112	Not used	C112	Not used
R113	0 Ω or Jumper	U101	TLV2772CD
R114	Not used	U102	Not used
R115	Not used	V1+	3 V from Board 1
R116	Not used	VREF1	Signal conditioning reference from Board 1
R117	Not used	GND1	Circuit common connect to board 1 GND1
R118	Not used	R119	0 Ω or Jumper
A1OUT	Z Axis output	B104+	Not used
A101–	Not used	B103+	Not used
A102–	Jump to VREF1	B102–	Not used
A103+	Jump to VREF1	B101–	Not used
A104+	Z Axis input from ACH-04-05-08 pin 12	B1OUT	Not used

The ACH-04-08-05 shock sensor mounts in the breadboard area on board 1. Table 5–3 summarizes the connections.

Table 5–3. Board 1 – Universal Operational Amplifier EVM Area 100 ACH-04-08-05 Connections

ACH-04-08-05		
PIN	NAME	BOARD 1 CONNECTIONS
1	D/S1–Y	V1+
2	D/S2–Y	B104+
3	CTG	GND1
4	SGND	VREF1
5	D/S1–X	V1+
6	D/S2–X	A104+
7	RGND–X	VREF1
8	GND	GND1
9	CTG	GND1
10	RGND–Z	VREF1
11	D/S1/Z	V1+
12	D/S2–Z	To board 2
13	CTG	GND1
14	RGND–Y	VREF1

Board-to-board connectors provide required connections between board 1 and board 2. The required board-to-board connections are GND1, V1+, and VREF. Also, pin 12 of the ACH-04-08–05 must be connected to A104+ on board 2. This is accomplished by using board-to-board connectors in the breadboard area and connecting the appropriate nodes thereto.

Figure 5–1 is the schematic of the 3-axis realization of the 1-axis circuit shown in Figure 4–1, except for output filter components R5 and C3. To ease component placement, the output filters for each channel are placed on the TLV1544 EVM. For standalone testing of the signal conditioning circuit without the TLV1544 EVM, temporarily place the filter components on board 1 and board 2. Remove them for final integration.

Nintendo Exhibit 1066
IPR2024-00668 - Page 545

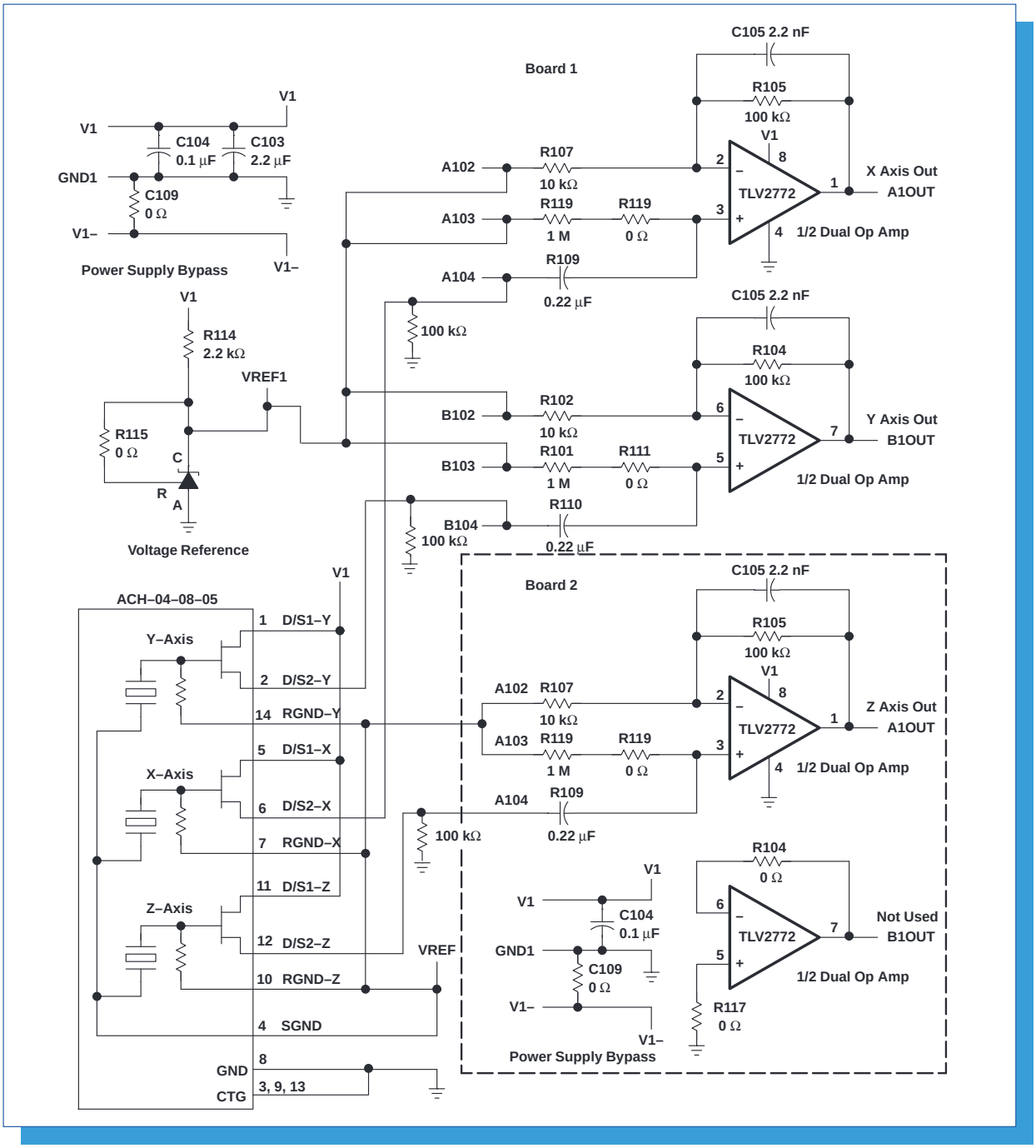


Figure 5–1. Signal Conditioning Schematic using Two Universal Operational Amplifier EVM Boards

Nintendo Exhibit 1066
IPR2024-00668 - Page 546

5.1 Test of Signal Conditioning Circuit

After constructing the signal conditioning circuit, and before connecting the shock sensor, tests were run to verify the signal conditioning circuit performed as expected. An AP Instruments network analyzer was used to measure the gain and phase response. Figure 5–2 shows the results are very much the same as the SPICE simulation predicted.

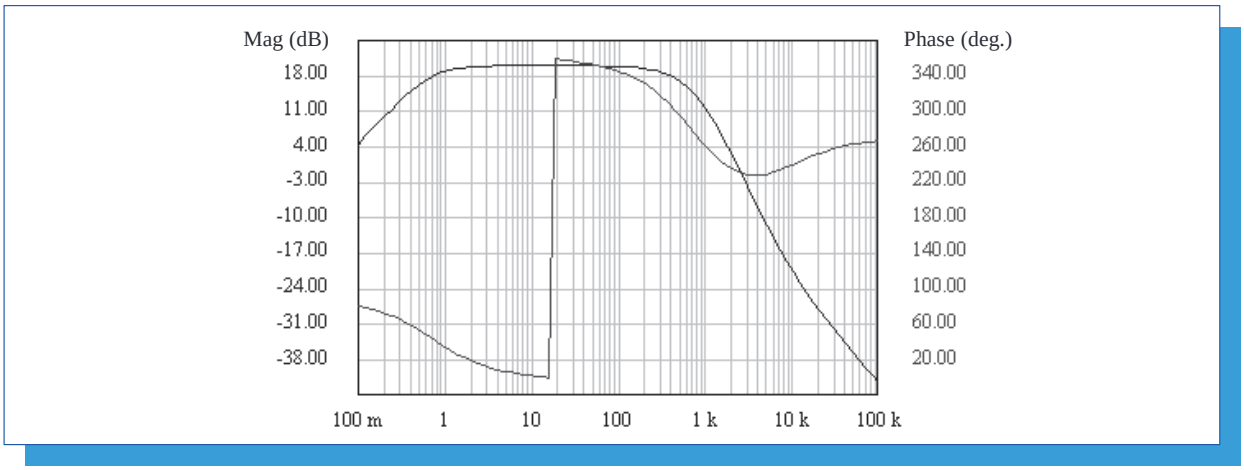


Figure 5–2. Network Analyzer Display

5.2 Test of Shock Sensor and Signal Conditioning Circuit

After connecting the shock sensor, the measurement of acceleration was verified. A spring loaded test fixture was constructed to induce simple harmonic motion into the sensor. Figure 5–3 shows a diagram of the test fixture. By measuring the deflection from center and the frequency of the oscillation, the acceleration is calculated as:

$$a = -\omega^2 \times \cos(\omega t + \phi)$$

Where

a is acceleration

ω is frequency of oscillation in radians

x is the maximum deflection from center

ϕ is the phase

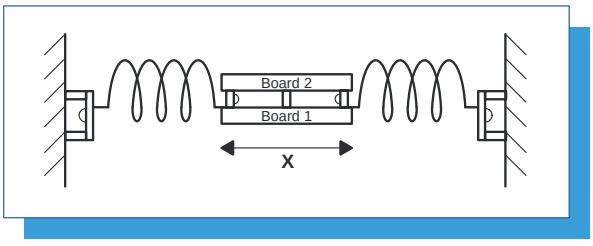


Figure 5–3. Spring Test Fixture

While monitoring the output of all 3 axes with an oscilloscope, the system was set into motion along the x-axis. Figure 5–4 shows the result displayed on an oscilloscope. Channel 1 is the x-axis, channel 2 is the y-axis, and channel 3 is the z-axis.

About 0.25” mechanical deflection was measured visually. An oscilloscope was used to measure the frequency of oscillation and the peak voltage amplitude. Using the above formula to find the peak acceleration expected from the mechanical movement (ignoring the sign):

$a\ (peak) = (2\pi \times 16)^2 \cdot (0.25 in/s^2) = 2524 in/s^2 = 6.58g$

Where $g = 32\ ft/s^2$

To check the output of the signal conditioning circuit, use the formula:

$$a\ (peak) = \frac{Peak\ voltage\ output}{Sensor\ output \cdot Gain}$$

$$= 128\ mV \frac{g}{1.80\ mV} \frac{1}{11} = 6.46\ g$$

Using the typical x–axis output = 1.80mV/g, there is good agreement between the two calculations.

Nintendo Exhibit 1066
IPR2024-00668 - Page 547

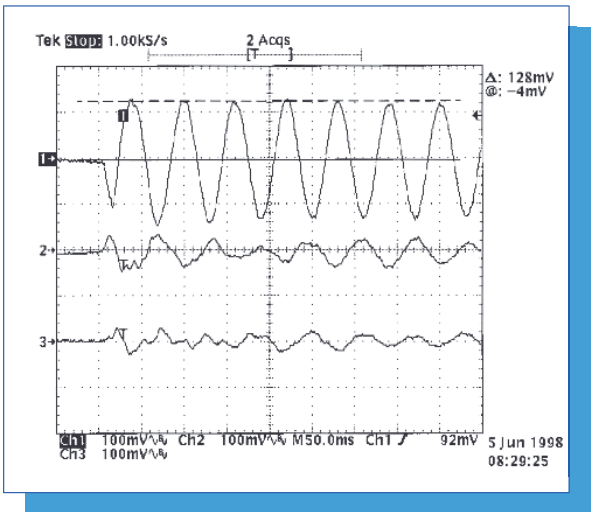


Figure 5–4. Output Displayed on Oscilloscope

Note that output is seen on the y-axis and z-axis. The ACH-04-08-05 data sheet specifies a transverse sensitivity of 15%. Fifteen percent of the x-axis peak signal output is 19.2 mV. The peak y axis signal is 40 mV and the peak z-axis signal is 26 mV. Transverse sensitivity does not account for the observation. While the primary motion was in the x-axis, motion was noticed in the other 2 axes as well.

5.3 TLV1544 EVM

For this application the fast conversion mode of the TLV1544 ADC is used and three of the four analog inputs are converted one after the other. This results in a sampling frequency of 28 ksps. By Nyquist's sampling theorem the frequency content of the input analog signal must be insignificant for frequencies ½ the sampling frequency and above. In this system, the signal is attenuated by over 40 dB at the Nyquist frequency.

5.3.1 Interfacing the Signal Conditioning Circuit to the TLV1544 EVM

The TLV1544 EVM provides a power supply, analog signal conditioning circuitry, ADC (TLV1544), and circuitry to support the interface to a DSP or micro controller.

Refer to the TLV1544 EVM User's Guide, literature #SLAU014, for detailed descriptions of the board and its functions.

To interface the shock sensor and signal conditioning circuit to the TLV1544 EVM, minor modifications are required on the TLV1544 EVM. To ease circuit realization, place the output filter for each axis signal, R5 and C3 in Figure 4–1, on the TLV1544 EVM.

The TLV1544 has 4 analog inputs. In this application, channel 0 samples the reference voltage from the signal conditioning circuit, channel 1 samples the x–axis output, channel 2 samples the y–axis output, and channel 3 samples the z-axis output. Make the following modifications to the TLV1544 EVM, REV–:

Channel 0 Modifications:

- Remove U4, R26, R27, and R28.
- Jumper U4–2 to U4–3.
- Place a 1-kΩ resistor for R28.
- Place a 22-µF capacitor between A0 and ground.

Channel 1 Modifications:

- Remove U5, R29, and C19.
- Jumper U5–3 to U5–6.
- Place a 1-kΩ resistor for R29.
- Place a 0.22-µF capacitor for C19.

Channel 2 Modifications:

- Place a 1-kΩ resistor for JP3.
- Place a 0.22-µF capacitor across D6.

Channel 3 Modifications:

- Place a 1-kΩ resistor for JP4.
- Place a 0.22-µF capacitor across D8.

Switch SW1 to operate the TLV1544 EVM at 3 V. Set the TLV1544 reference voltage input to 2.4 V by installing jumpers JP1–1, 2 and JP2–1, 2. Use the 3 V power supply on the TLV1544 EVM to supply power to the shock sensor and the signal conditioning circuit.

Table 5–4 shows the interface connections between the signal conditioning circuit and the TLV1544 EVM, REV–.

Table 5–4. Interface Between Signal Conditiioning Circuit and TLV1544 EVM

SIGNAL CONDITIONING CIRCUIT	TLV1544 EVM
Board 1 V1+	AV_{DD}
Board 1 GND1	GND
Board 1 VREF1 (signal reference)	JP19 (U2–2)
Board 1 A1OUT (X axis output)	Analog Input 1
Board 1 B1OUT (Y axis output)	Analog Input 2
Board 2 A1OUT (Z axis output)	Analog Input 3

Figure 5–5 is a schematic drawing for the interface between the signal conditioning circuit and the TLV1544.

Nintendo Exhibit 1066
IPR2024-00668 - Page 548

5.4 Interfacing the TLV1544 EVM to the TMS320C5C EVM

Figure 5–6 shows the connections required to interface the TLV1544 EVM to the TMS320C5X EVM. For further details refer to *Interfacing the TLV1544 Analog-to-Digital Converter to the TMS320C50 DSP Applications Report* literature # SLAA025.

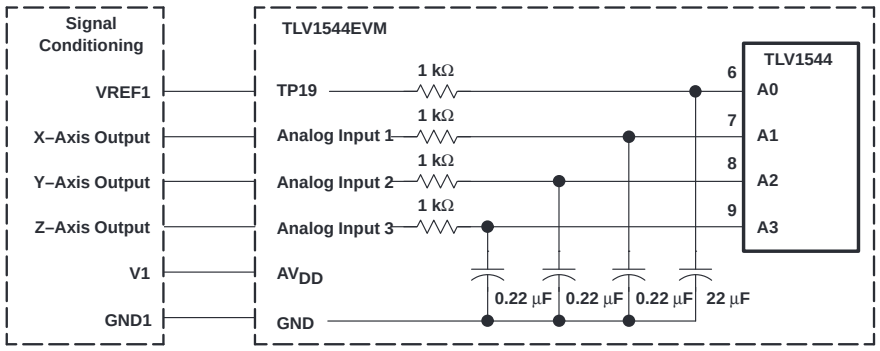


Figure 5–5. Schematic – Signal Conditioning to TLV1544 ADC

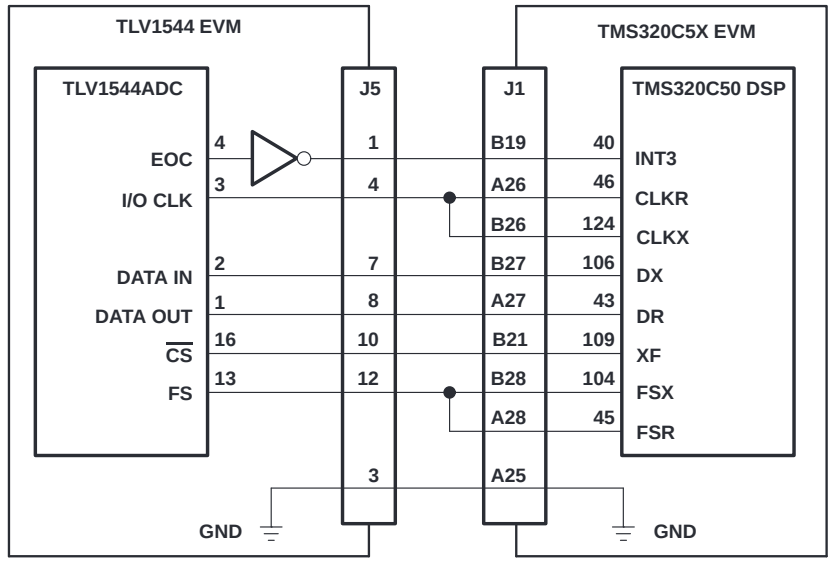


Figure 5–6. Interface Between TLV1544 EVM and TMS320C5X EVM

5.5 The TMS320C5X EVM

The TMS320C5X EVM plugs into an ISA slot in a PC. Refer to *TMS320C5X Evaluation Module Technical Reference* literature # SPRU087 for detailed information on its use. The TMS320C5X C Source Debugger is also required. Refer to *TMS320C5X C Source Debugger User's Guide* literature # SPRU055B for user information.

Nintendo Exhibit 1066
IPR2024-00668 - Page 549

6 Error and Noise Analysis

Error analysis can predict the errors to be expected under normal operating conditions. Two analyses are presented: gain error and noise.

Gain errors contribute to uncertainty in the system output given a known input.

Noise is a random electrical event that occurs in all conductors. Noise imposes a statistical uncertainty on the system's electrical signals.

The system can be calibrated to compensate for the effect of gain errors. The uncertainty associated with noise, on the other hand, prohibits any type of compensation.

Two of the most widely used types of error analysis are worst case analysis and sum of squares analysis. The major task in performing an error analysis is to identify and quantify the error sources.

Worst case analysis assumes that all errors compound, one on top of the other. Therefore, the maximum error in all circuit elements is added to arrive at the total system error.

Sum of squares analysis assumes that some errors will tend to cancel each other. By summing the square of all the errors and taking the square root, the result takes this cancellation effect into account. A sum of squares analysis gives a realistic idea of how well the typical system will perform. This is the type of analysis that will be presented. A sum of squares analysis uses the following formula;

$$Total\ System\ Error = \sqrt{\sum_{n=1}^{k} Error_n^2}$$

Where the subscript n indicates an individual error component and k is the total number of error components.

System gain error analysis is presented first, followed by system noise analysis.

6.1 System Gain Error Analysis

Gain errors are errors that contribute to uncertainty in the system output, given a known input.

The system is essentially an ac system in which dc errors can be compensated. Therefore, dc errors caused by reference voltage errors, offset voltages, and the like are not included in this error analysis.

6.1.1 Sensor Gain Error

The shock sensor's output varies, and this contributes to uncertainty in the system output given a known input. The data sheet for the ACH-04-08-05 states the output sensitivity:

CHARACTERISTIC	MIN	TYP	MAX	UNIT
X-axis sensitivity	1.35	1.80	2.25	mV/g
Y-axis sensitivity	1.35	1.80	2.25	mV/g
Z-axis sensitivity	1	1.35	1.70	mV/g

This is a ±25% tolerance in the output voltage for the same acceleration input. Thus the error assigned to this component is 25%.

6.1.2 Signal Conditioning Gain Error

Errors in the signal conditioning circuit also contribute to uncertainty in the system output, given a known input. The analysis is limited to the pass band of the amplifier circuit. In its pass band the gain of the amplifier is given by:

$$A = \left(\frac{1}{b}\right)\left[\frac{1}{1 + \frac{1}{ab}}\right]$$

Where:

a = open loop amplification of the operational amplifier

And

$$b = \frac{R4}{R4 + R3}$$

The term 1/ab is seen as an error term in this equation because it is desired to set the gain of the circuit with the 1/b term (ratio of R3 to R4). To minimize this error, the open loop amplification of the operational amplifier should be as large as possible so that 1/ab is very close to 0. In this application the TLV2772's open loop amplification is the lowest at the upper cutoff frequency. At 1 kHz the open loop amplification is about 75 dB or 5600. Using this value: 1/ab = 0.000016, and the deviation of the amplifier gain from ideal is 0.002%.

The error caused by the op amp gain setting resistors is the tolerance of the resistors. In this case, 1% resistors add an error of 1%.

6.1.3 ADC Gain Errors

Errors caused by sampling of the signal by the ADC also need to be analyzed. Figure 6–1 shows a simplified schematic to use for analysis.

Nintendo Exhibit 1066
IPR2024-00668 - Page 550

Set initial conditions where Vadc = Vo and Vsample =0. To simplify the analysis, notice that the time constant R5C3 = 0.22 ms is much longer than the time constant RadcCadc = 55 ns, because C3 is 4000 times larger than Cadc. In this system the TLV1544's I/O CLK is being driven at 5 MHz. The sampling period = 6 I/O CLK periods = 1.2 µs. Because C3 >> Cadc, when the switch closes during sampling, C3 acts like a voltage reservoir for charging Cadc via Radc. During the sampling period very little charge is transferred from Vo. The sampling period, 1.2 µs = 29 × 55 ns or 29 RadcCadc time constants. Therefore, at the end of the sampling the period, the voltage across Cadc and C3 is essentially equal, the sample voltage is set by the ratio of C3 to Cadc;

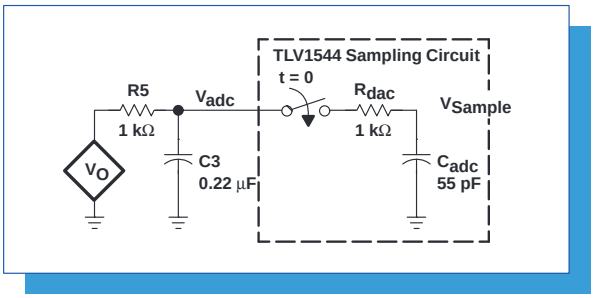


Figure 6–1. Sampling Input Model

$$Vsample = Vadc\left(\frac{C3}{Cadc + C3}\right) = 0.99975\ Vadc$$

The error attributed is 0.025%.

The other sources of error in the ADC can be read from the data sheet. As stated earlier, the system is essentially an ac system, and dc errors are not included in the error analysis. Therefore, only the maximum linearity error from the data sheet, which is ±1 LSB, is included. With 10 bits of resolution or 1024 codes the error = 0.0976%.

6.1.4 Total Gain Error

From this point on in the system, the signal is digital, and it is assumed there are no errors which cannot be corrected for.

Calculating the total error as the square root of the sum of the error squared results in:

$$\sqrt{25\%^2 + 0.002\%^2 + 1\%^2 + 0.025\%^2 + 0.0976\%^2} = 25.02\%$$

The uncertainty associated with the shock sensor output dominates the error analysis. Calibration is required to insure accurate measurement of acceleration.

6.2 System Noise Analysis

The first step to analyzing system noise is to qualify and quantify noise sources within the system. Next, the components must be added to see the overall effect on the system.

In this system the noise sources are the shock sensor, the resistors, and the amplifier. Since all three channels are essentially the same, the noise analysis is performed on one channel. Reference designators from Figure 4–1 are used with the component values as calculated above for channel z.

Because the z-axis of the shock sensor has about 30% less sensitivety than either x-axis or y-axis, 30% more gain is required in channel z. The results of the analysis show the dominant noise source is the sensor. The noise specification for the sensor is given in mg/$\sqrt{Hz}$ and converted to equivalent input noise voltage. Therefore, the noise voltage, as calculated in this analysis, will be higher in channel z, but not significantly so.

It is typical in amplifier circuits to identity equivalent input noise voltage per root Hertz for system components. This is then multiplied by the equivalent noise bandwidth and amplifier noise gain. The result is the total system noise. It is convenient to work in RMS values to compute the total system noise, then to convert to peak-to-peak (pk-pk) and compare to 1 LSB to see the effect on the ADC's output. The following formula is used:

$$\underset{(in\ RMS\ Volts)}{Total\ System\ Noise} = \sqrt{\sum_{m=1}^{k} ENB \cdot en_m^2 \cdot An^2}$$

Where ENB is the equivalent noise bandwidth in hertz, the subscript m indicated an individual equivalent input noise source, en, in RMS volts per root Hertz, An is the noise gain of the amplifier, and k is the total number of noise sources referred to the input.

Normally, noise in RMS voltage is multiplied by numbers ranging from 5 to 7 to convert to peak-to-peak (pk-pk) voltage. This accounts for the large crest factor seen in noise signals. The pk-pk value of noise voltage is of concern when driving the input to an ADC converter. A multiplication factor of 6 is used in this analysis to convert RMS into pk-pk.

The equivalent noise bandwidth (ENB) accounts for the noise transmitted above the upper cutoff frequency as a result of the finite roll-off, or tail of the frequency response curve. For a 2nd order system, ENB is 1.11 times the normal bandwidth. For this system, ENB = 1.11(724 – 0.7) = 802.9 Hz. It is convenient and acceptable to use ENB = 803 Hz.

Nintendo Exhibit 1066
IPR2024-00668 - Page 551

The amplifier noise gain is the noninverting gain of the amplifier, which is equal to 14.3.

6.2.1 Sensor Noise Analysis

From the ACH-04-08-05 data sheet the shock sensor has a specification for equivalent noise at 100 Hz equal to 0.2 mg/$\sqrt{Hz}$. Using the typical z-axis value for sensitivity, 1.35 mV/g, the equivalent noise in volts/$\sqrt{Hz}$ is 0.27 µV/$\sqrt{Hz}$. The data sheet gives no further details as to the spectral shape of the noise from the shock sensor. For this analysis, assume the noise voltage from the ACH-04-08-05 is flat over the bandwidth of the system.

6.2.2 Signal Conditioning Noise Analysis

For Vdd = 2.7 V, the TLV2772 data sheet specifies equivalent input noise voltage of 147 nV/vHz at 10 Hz and 21 nV/$\sqrt{Hz}$ at 1 kHz. Because the TLV2772 is a CMOS input op amp, the input noise current is insignificant with the circuit values being used.

The resistors in the signal conditioning amplifier's input circuit contribute thermal noise voltage:

$$= \sqrt{\frac{4kTR}{Hz}}$$

Where k is Boltzmann's Constant = 1.38×10^{-23}J/K

T is temperature in Kelvin

R is resistance in ohms

Hz if frequency in Hertz

R2 contributes 128 nV/$\sqrt{Hz}$. R3 and R4 appear in parallel at the negative input for noise calculations. Together they contribute 10.7 nV/$\sqrt{Hz}$. Resistor R1 adds 40 nV/$\sqrt{Hz}$.

Resistor R5 adds thermal noise voltage = $\sqrt{(4KTR/Hz)}$ to the system. The value of the resistor is small and the noise is not amplified by the amplifier. Therefore the effect of R5 on the overall system noise is negligible.

Adding the foregoing is straightforward for all components except the amplifier's input noise. Referring to the equivalent input noise voltage vs frequency graph in the data sheet for the TLV2772 (Figure 39) it can be seen that the equivalent input noise voltage is characterized by 1/f noise over the bandwidth of the system's operation. The input noise is a combination of the 1/f noise and the white noise of the op amp: $en^2 = (K^2/f)+e_w^2$ where e_n is the equivalent input noise voltage per root Hertz, K is a proportionality constant and f is frequency in Hertz, and e_w is the white noise specifiction for the op amp. K can be calculated from the values on the equivalent input noise vs frequency graph to be about 450 nV. By integrating the noise density over the frequency range of operation, the input noise can be computed by:

$$e_{oa} = \sqrt{ENB\ e_w^2 + K^2\ ln\ \frac{f_H}{f_L}}$$

Where e_{oa} is the equivalent input noise voltage over the bandwidth in RMS volts

K is a proportionality constant, equal to 450 nV RMS

f_L is the lower cutoff frequency, 0.724 Hz and f_H is the upper cutoff frequency, 724 Hz.

The result is e_{oa} = 1.32 µV RMS.

6.2.3 Total Noise Analysis

Adding the system noise sources results in:

Total System Noise = (in RMS Volts)

$$14.3 \times \sqrt{803\left[(0.27E\text{-}6)^2 + (128E\text{-}9)^2 + (10.7E\text{-}9)^2 + (40E\text{-}9)^2\right] + (1.32E\text{-}6)^2}$$

$$= 0.124\ mV\ RMS$$

To convert to pk-pk voltage, multiply by 6. Then Total System Noise pk-pk = 0.743 mV pk-pk.

The TLV1544 ADC has 10 bits of resolution. With a voltage reference = 2.4 V, 0.743 mV pk-pk of noise is equivalent to about 1/3 LSB.

Nintendo Exhibit 1066
IPR2024-00668 - Page 552

7 System Test and Evaluation

With the shock sensor and signal conditioning circuit interfaced to the TLV1544 EVM and the TMS320C5X EVM, proceed with testing and evaluation of the system performance.

The program listings as published in the *Interfacing the TLV1544 Analog-to-Digital Converter to the TMS320C50 DSP Applications Report* literature #SLAA025 can be used as a starting point. Appendix A contains program listings based on these, except they modify program flow so that the TLV1544 performs consecutive conversions of three of its four channels. When motion in any axis is detected, the program stores 3000h samples in memory from each channel.

Once the data is stored, it can be saved as a COFF file using the “store data” utility provided with the TMS320C5X C-Source Debugger. To read the data into an Excel spread sheet, a utility program is required to convert the hexadecimal numbers into decimal ASCII format. Source code listings are included in Appendix A.

With the data converted and loaded into Excel, it can be converted into equivalent acceleration in g using the formula:

$$g = \left(\frac{ADC\ Sample \times ADC\ Ref\ Volts}{2^{10}} - Sig\ Ref\ Volts\right) \times \left(\frac{1}{Sensor\ output \times Gain}\right)$$

Figure 7–1 shows the x-axis acceleration graphed in Excel from data collected when testing the signal conditioning and shock sensor circuits. It can be seen that the results match the results as presented previously.

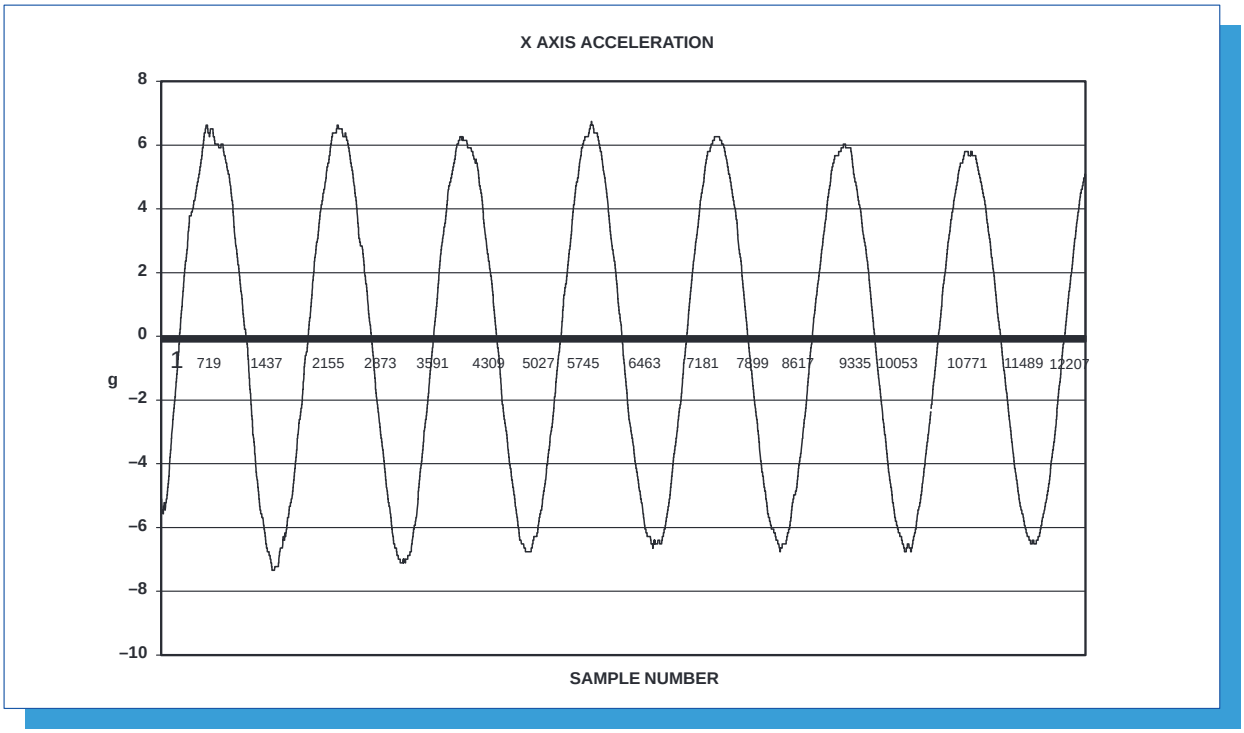


Figure 7–1. X-Axis Acceleration Graphed in Excel

Nintendo Exhibit 1066
IPR2024-00668 - Page 553

8 Calibration Data/Analysis

8.1 Calibration

The acceleration sensor and the signal conditioning circuitry were housed in a Bud CU-234 box, which was machined to mount on a fixture plate for calibrated testing. The calibrated acceleration source used was an Unholtz Dickie T-1000 vibration tester. The specifications for this machine are:

- 1 inch maximum displacement
- 70 in/s maximum velocity
- 75g maximum sine acceleration ±10% operational tolerance
- 5 Hz to 5 kHz frequency range ±1/4 Hz frequency operational tolerance
- Cross axis output 25% maximum

Signals from the signal conditioning circuitry were routed to the TLV1544 ADC via coaxial cables. Sine wave acceleration was used and data was collected at various acceleration levels and frequencies on all 3 axis. Data for each axis was plotted over frequency and acceleration using the mean sensitivity. The data was analyzed and the errors calculated. Tables 8–1 through 8–6 and Figures 8–1 through 8–6 show the result. Figure 8–7 shows the output vs. input for each axis when averaged over frequency.

A maximum cross axis sensitivity of 17.6% from y-axis to x-axis was observed. Resonance was observed in the z-axis at 2 kHz.

Table 8–1. X-Axis Output Vs. Input Using X-Axis Mean Sensitivity = 1.16 mV/g

g/f	10 Hz	20 Hz	50 Hz	100 Hz	500 Hz
1	1.20	1.20	1.20	1.05	0.83
10		11.50	11.00	10.56	8.70
20			21.86	20.94	17.45
50			53.80	51.15	42.60

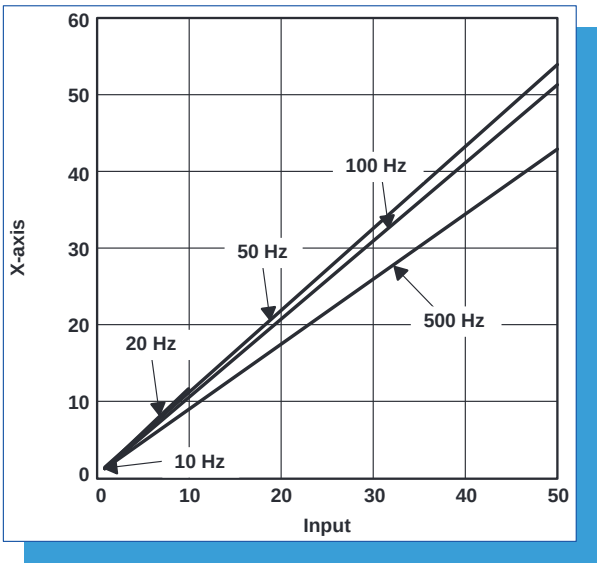


Figure 8–1. X-Axis Output vs. Input

Nintendo Exhibit 1066
IPR2024-00668 - Page 554

Table 8–2. X-Axis % Error

g/f	10 Hz	20 Hz	50 Hz	100 Hz	500 Hz
1	20.00%	20.00%	20.00%	5.00%	–17.50%
10		15.00%	10.00%	5.60%	–13.00%
20			9.30%	4.70%	–12.75%
50			7.60%	2.30%	–14.80%

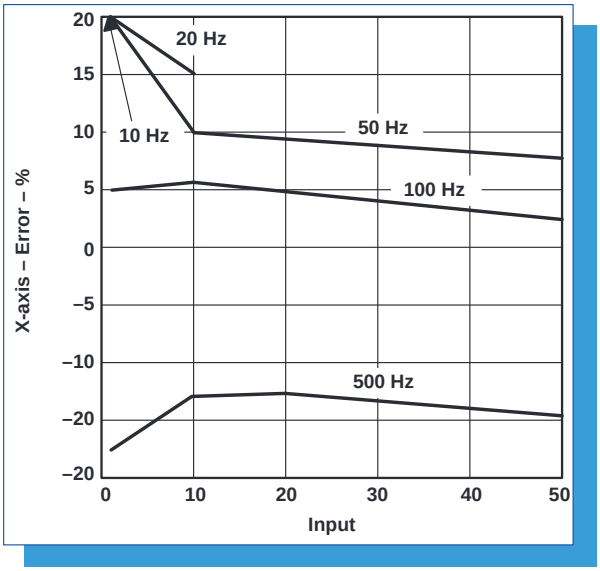


Figure 8–2. X-Axis % Error

Table 8–3. Y-Axis Output Vs. Input Using Y-Axis Mean Sensitivity = 1.35 mV/g

g/f	10 Hz	20 Hz	50 Hz	100 Hz	500 Hz
1	1.03	1.03	1.11	1.03	0.88
10		10.50	9.80	9.70	9.85
20			19.65	19.18	20.10
50			49.65	47.00	52.55

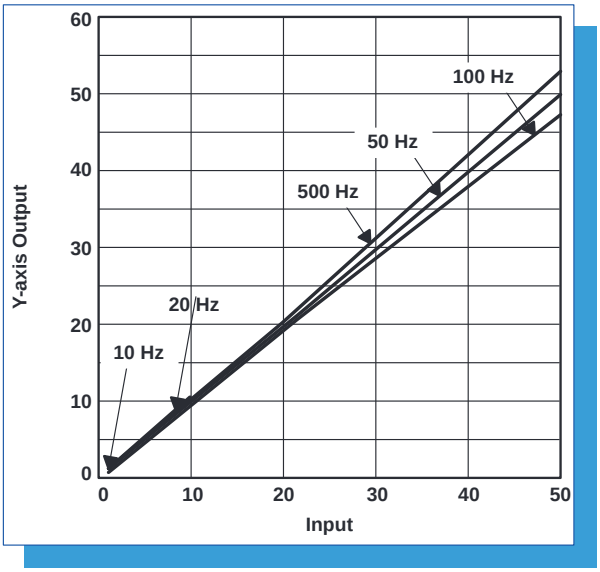


Figure 8–3. Y-Axis Output vs. Input

Nintendo Exhibit 1066
IPR2024-00668 - Page 555

Table 8–4. Y-Axis % Error

g/f	10 Hz	20 Hz	50 Hz	100 Hz	500 Hz
1	2.50%	2.50%	10.50%	–2.50%	–12.50%
10		5.00%	–2.00%	–3.00%	–1.50%
20			–1.75%	–4.13%	0.50%
50			–0.70%	–6.00%	5.10%

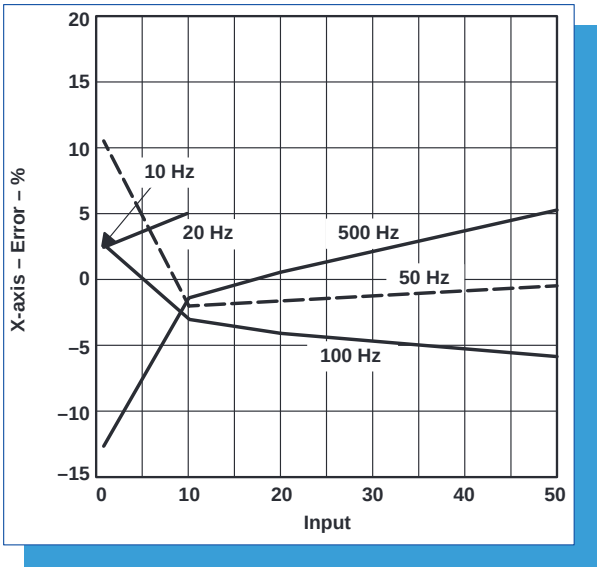


Figure 8–4. Y-Axis % Error

Table 8–5. Z-Axis Output Vs. Input Using Z-Axis Mean Sensitivity = 1.01 mV/g

g/f	10 Hz	20 Hz	50 Hz	100 Hz	500 Hz
1	0.89	0.97	0.97	0.97	1.13
10		8.20	8.35	8.20	11.70
20			16.80	16.55	23.40
50			41.30	41.55	59.10

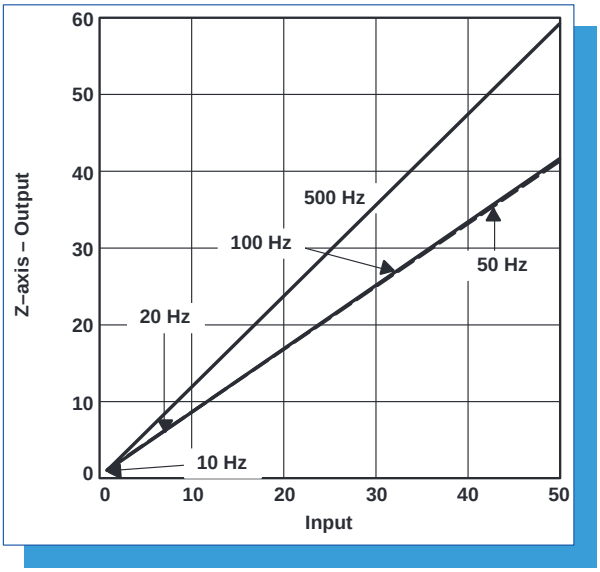


Figure 8–5. Z-Axis Output vs. Input

Nintendo Exhibit 1066
IPR2024-00668 - Page 556

Table 8–6. Z-Axis % Error

g/f	10 Hz	20 Hz	50 Hz	100 Hz	500 Hz
1	–11.00%	–3.00%	–3.00%	–3.00%	13.00%
10		–18.00%	–16.50%	–18.00%	17.00%
20			–16.00%	–17.25%	17.00%
50			–17.40%	–16.90%	18.20%

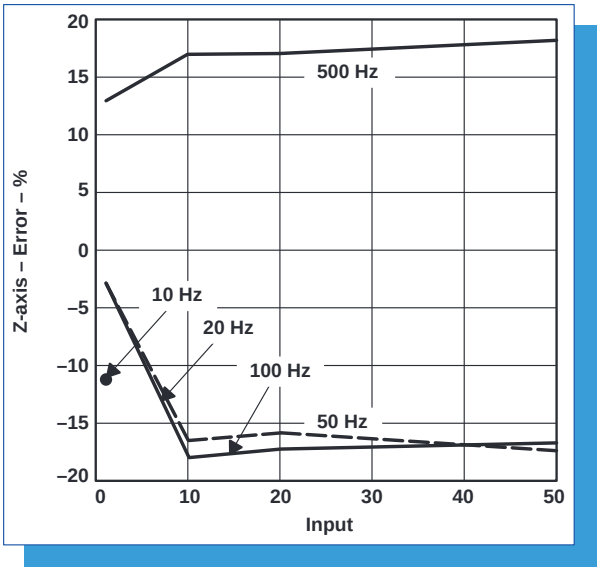


Figure 8–6. Z-Axis % Error

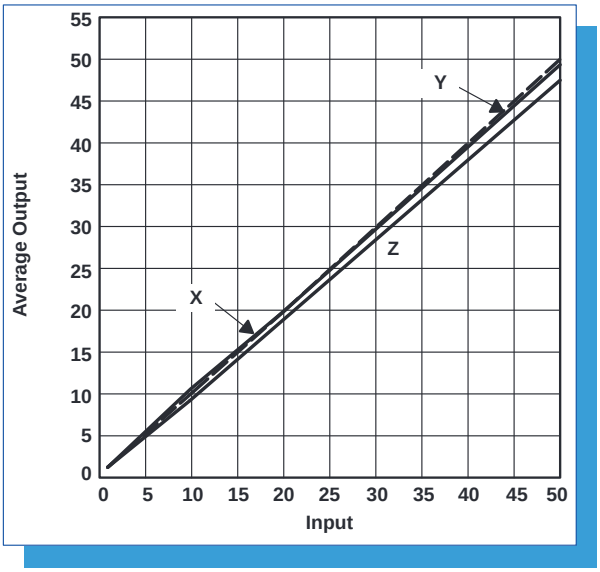


Figure 8–7. Average Output vs. Input Over Frequency for Each Axis

9 References

1. *ACH04-08-05 Data Sheet* http://www.amp.com/sensors
2. *TLV2772 Data Sheet*, literature #SLOS209
3. *Universal Operational Amplifier EVM User's Manual*, literature #SLVU006
4. *TLV1544 Data Sheet*, literature #SLAS139B
5. *TLV1544 EVM User's Manual*, literature #SLAU014
6. *Interfacing the TLV1544 Analog-to-Digital Converter to the TMS320C50 DSP Applications Report*, literature #SLAA025
7. *TMS320C5X Evaluation Module Technical Reference*, literature #SPRU087
8. *TMS320C5X C Source Debugger User's Guide*, literature #SPRU055B
9. *TMS320C5X EVM Technical Reference*, literature #SPRU087

Nintendo Exhibit 1066
IPR2024-00668 - Page 557

Appendix A. Source Code Listings

```
*******************************************************************************************
* TITLE         : ADC Interface routine                                                   *
* FILE          : ACCELER1.ASM                                                            *
* FUNCTION      : MAIN                                                                    *
* PROTOTYPE     : void MAIN ()                                                            *
* CALLS         : Wait ()                                                                 *
*                 Channels ()                                                             *
* PRECONDITION  : N/A                                                                     *
* POSTCONDITION : N/A                                                                     *
* DESCRIPTION   :
* AUTHOR        : AAP Application Group, Dallas                                           *
*                 CREATED 1998(C) BY TEXAS INSTRUMENTS INCORPORATED.                      *
* REFERENCE     : TMS320C5x User's Guide, TI 1997                                         *
*               : Data Aquisation Circuits, TI 1998                                       *
*******************************************************************************************
    .mmregs
    .sect ".vectors"
    .copy "vectors.asm"

    .sect ".data"
    .copy "values.asm"
    .def    _MAIN
    .def    ACT_CHANNEL
    .def    ADWORD
    .def    ADCOUNT
    .def    ADMEM
    .def    isr save
    .def    FINITO
    .def    data_loc_point0
    .def    data_loc_point1
    .def    data_loc_point2
    .def    data_loc_point3
    .def    MEMCOUNT
    .def    TST_CH1;
    .def    TST_CH2;
    .def    TST_CH3;
AD_DP       .usect ".variabl", 0        ;
ACT_CHANNEL .usect ".variabl", 1        ; jump address to init. new channel
ADWORD      .usect ".variabl", 1        ; send-bytes to the ADC
ADCOUNT     .usect ".variabl", 1        ; counter for one channel
ADMEM       .usect ".variabl", 1        ; points to act. memory save location
```


Nintendo Exhibit 1066
IPR2024-00668 - Page 558

```
isr_save    .usect ".variabl", 1              ; memory location to save AR7 during interrupts
FINITO      .usect ".variabl", 1              ; shows, that the sampling is completed
MEMCOUNT    .usect ".variabl", 1              ; counter for samples per channel
TST_CH1     .usect ".variabl", 1              ;
TST_CH2     .usect ".variabl", 1              ;
TST_CH3     .usect ".variabl", 1              ;
data_loc_point0 .usect ".variabl", 1          ;
data_loc_point1 .usect ".variabl", 1          ;
data_loc_point2 .usect ".variabl", 1          ;
data_loc_point3 .usect ".variabl", 1          ;
    .sect ".text"
_MAIN:
*******************************************************************************
* INITIALIZATION BODY
*******************************************************************************
* DSP INITIALIZATION
    SETC    INTM                        ; DISABLE GLOBAL INTERRUPTS
    LDP     #0;
    OPL     #0038h, PMST                ; Configure PMST (allocate IRQ)
    APL     #0000h, PDWSR               ; clear PDWSR (zero wait states)
    APL     #00F0h, CWSR                ; clear CWSR  (zero wait states)

* SERIAL PORT INITIALIZATION
SPI_INI:
    APL     #07F38h,SPC                 ; clear Res, DLB, FO, XRST, RRST  and FREE in SPC
    OPL     #00038h,SPC                 ; Set Burst Mode,
                                        ; CLKX=1/4CLKOUT1,
                                        ; FSX generated by DSP
    OPL     #080C0h,SPC                 ; activate transmitter and receiver
* INITIALIZE USER INFORMATIONS FOR DATA AQUISITION
    CALL    CHANNELS                    ; load informations about ADC channel and
                                        ; memory location for data saving
* Enable Interrupts
    LDP     #0
    OPL     #00014h,IMR                 ; Unmask RINT and INT3
    CLRC    INTM                        ; enable global interrups
* FIRST SEND OPERATION MODE TO TLV1544
    LDP     #ADWORD
    LACL    ADWORD
    CLRC    XF                         ; Enable Chip Select
    SAMM    DXR                        ; move ADWORD into DXR (DXR = fast conversation mode)
*******************************************************************************
* initialize MEMCOUNT and data_loc_pointx
*******************************************************************************
```


Nintendo Exhibit 1066
IPR2024-00668 - Page 559

```
    SPLK    #data_loc_0,data_loc_point0  ;
    SPLK    #data_loc_1,data_loc_point1  ;
    SPLK    #data_loc_2,data_loc_point2  ;
    SPLK    #data_loc_3,data_loc_point3  ;
    SPLK    #TRIG_REF,TST_CH1  ;
    SPLK    #TRIG_REF,TST_CH2  ;
    SPLK    #TRIG_REF,TST_CH3  ;
    SPLK    #numb_data_all,MEMCOUNT  ;
*********************************************************************************************
* MAIN BODY FOR A PROGRAM, UNRELATED TO AD-CONVERTING                                       *
* PROCESSOR SLEEP AT NONACTIVITY TIMES                                                      *
* INSTEAD OF THE IDLE INSTRUCTION, USER CAN RUN THEIR OWN PROGRAM                           *
*********************************************************************************************
USERINTERFACE:
    SPLK    #00000h,FINITO      ; sampling not finished yet                                   *

*********************************************************************************************
* testing the input samples against trigger values to start                                 *
* the final sampling of the accelerator                                                     *
*********************************************************************************************
TRIP_LOOP:
    LDP     #TST_CH1            ;
    LACC    TST_CH1             ;
    SUB     #TRIP_HIGH          ;
    BCND    TRIG,GEQ            ;
    LACC    TST CH1             ;
    SUB     #TRIP_LOW           ;
    BCND    TRIG,LEQ            ;
    LDP     #TST_CH2            ;
    LACC    TST_CH2             ;
    SUB     #TRIP_HIGH          ;
    BCND    TRIG,GEQ            ;
    LACC    TST_CH2             ;
    SUB     #TRIP_LOW           ;
    BCND    TRIG,LEQ            ;
    LDP     #TST_CH3            ;
    LACC    TST_CH3             ;
    SUB     #TRIP_HIGH          ;
    BCND    TRIG,GEQ            ;
    LACC    TST_CH3             ;
    SUB     #TRIP_LOW           ;
    BCND    TRIG,LEQ            ;
    B       TRIP_LOOP           ;
*********************************************************************************************
```


Nintendo Exhibit 1066
IPR2024-00668 - Page 560

```
* start the final sampling of the accelerator
*********************************************************************************************
TRIG:
    SPLK    MAIN_CHANNEL0,ACT_CHANNEL  ; set the next INTERRUPT-BRANCH-ADDRESS to the
                                       ; MAIN sampling
M1:
    LDP     #FINITO;
    LACC    FINITO ;
    SUB     #00001h                   ;
    BCND    M1, LT
*********************************************************************************************
* sampling is done, wait until user interrupt
*********************************************************************************************
M2:
    NOP                             ; no operation
    B       M2;
*********************************************************************************************
* END_CONV_IRQ:
*   Interrupthandler for the external INT3-IRQ, which is the end of conversation signal
*   of the ADC. The Routine will enable the Chip Signal again and send the next sample
*   instruction, contained in ADWORD, to the ADC.
*********************************************************************************************
END CONV_IRQ:
* MAIN IRQ ROUTINE
    LDP     #ADWORD
    LACL    ADWORD
    CLRC    XF                      ; Enable Chip Select
    SAMM    DXR                     ; move ADWORD into DXR
    RETE                            ; Return to Wait loop
*********************************************************************************************
* RECEIVE_IRQ:
*   Interrupthandler for serial receive of the SPI interface. The Routine will disable the
*   Chip Signal and store the received sample into the by ADMEM specified memdory location.
*   It also checks, how many samples were made of the actual channel and if all done, it
*   will call the procedure CHANNELS to load the next channel specifications.
*********************************************************************************************
RECEIVE IRQ:
* save AR7 before handling the IRQ routine
    ldp     #isr_save
    sar     ar7,isr_save          ; save AR7 in isr_save

* MAIN IRQ ROUTINE (Data collection from ADC)
    CLRC    SXM                   ; Clear sign bit
    LDP     #0;
```


Nintendo Exhibit 1066
IPR2024-00668 - Page 561

```
    LACC    DRR,10                ; load content of DRR in ACCh; shift 10
    LDP     #ADMEM;
    MAR     *,AR7;
    LAR     AR7, ADMEM            ; AR7 = ADMEM
    SACH    *+                    ; save sample in the memory
    SAR     AR7, ADMEM            ; ADMEM++
    LAR     AR7, ADCOUNT;         ; AR7 = ADCOUNT
    LACL    ADCOUNT;
    SUB     #1                    ; increment ACC
    SACL    ADCOUNT               ; ADCOUNT=ADCOUNT–1
    BCND    KEEP_ON,NEQ           ; if ADCOUNT not 0 jump to KEEP_ON
    LACC    ACT_CHANNEL           ; load addr. to set new sampling channel
    CALA                          ; jump into the subroutine
KEEP_ON:
    SETC    XF                    ; Disable Chip Select
* restore AR7 before jump back into the user software
    ldp     #isr_save
    lar     ar7,isr_save          ; load old AR0
    RETE                          ; Return from Interrupt

   .copy ”channels.asm”
   .end
*************************************************************************************************
* TITLE         : TLV1544C ADC Interface routine                                                *
* FILE          : Channels.ASM                                                                  *
* FUNCTION      : CHANNELS                                                                      *
* PROTOTYPE     : void CHANNELS ()                                                              *
* CALLS         : N/A                                                                           *
* PRECONDITION  : N/A                                                                           *
* POSTCONDITION : N/A                                                                           *
* DESCRIPTION   :
* AUTHOR        : AAP Application Group, Dallas                                                 *
*                 CREATED 1998(C) BY TEXAS INSTRUMENTS INCORPORATED.                            *
* REFERENCE     : TMS320C5x User’s Guide, TI 1997                                               *
*               : Data Aquisation Circuits, TI 1998                                             *
*************************************************************************************************
    .text
CHANNELS:
WAKE_UP:
    LDP     #AD_DP                  ; point to AD Data Page
    SPLK    #fast_conv,ADWORD       ; The first Word to send is fast_conv to wake up the ADC
                                    ; from power down
    SPLK    #tresh,ADMEM            ; DATA LOCATION = THRES, because first received byte
                                    ; is meaningless
```


Nintendo Exhibit 1066
IPR2024-00668 - Page 562

```
    SPLK    #1,ADCOUNT                  ; NUMBER OF DATA 0
    SPLK    #one_more,ACT_CHANNEL       ; set new jump level
    RET
one_more:
    LDP     #AD_DP                      ; point to AD Data Page
    SPLK    #channel_1,ADWORD           ; The first Word to send is fast_conv to
                                       ; wake up the ADC from power down
    SPLK    #tresh,ADMEM                ; DATA LOCATION = THRES, because first
                                       ; received byte is meaningless
    SPLK    #4,ADCOUNT                  ; NUMBER OF DATA 0
    SPLK    #CHANNEL1,ACT_CHANNEL       ; set new jump level
    RET
CHANNEL1:
    LDP     #AD_DP                      ; point to AD Data Page
    SPLK    #channel_1,ADWORD           ; SELECT CHANNEL 0
    SPLK    #TST_CH3,ADMEM              ; DATA LOCATION 0
    SPLK    #00001h,ADCOUNT             ; NUMBER OF DATA 0
    SPLK    #CHANNEL2,ACT_CHANNEL       ; set new jump level\
    RET

CHANNEL2:
    LDP     #AD_DP                      ; point to AD Data Page
    SPLK    #channel_2,ADWORD           ; SELECT CHANNEL 0
    SPLK    #TST_CH1,ADMEM              ; DATA LOCATION 0
    SPLK    #00001h,ADCOUNT             ; NUMBER OF DATA 0
    SPLK    #CHANNEL3,ACT_CHANNEL       ; set new jump level
    RET
CHANNEL3:
    LDP     #AD_DP                      ; point to AD Data Page
    SPLK    #channel_3,ADWORD           ; SELECT CHANNEL 0
    SPLK    #TST_CH2,ADMEM              ; DATA LOCATION 0
    SPLK    #00001h,ADCOUNT             ; NUMBER OF DATA 0
    SPLK    #CHANNEL1,ACT_CHANNEL       ; set new jump level
   RET
MAIN_CHANNEL0:
    LDP     #AD_DP                      ; point to AD Data Page
    SPLK    #channel_0,ADWORD           ; SELECT CHANNEL
    LACL    data_loc_point3             ;
    SACL    ADMEM                       ; load actual memory pointer
    ADD     #1                          ; increment ACC
   SACL    data_loc_point3             ; save new memory pointer
    SPLK    #00001h,ADCOUNT             ; NUMBER OF DATA
    SPLK    #MAIN_CHANNEL1,ACT_CHANNEL  ; set new jump level
    RET
```


Nintendo Exhibit 1066
IPR2024-00668 - Page 563

```
MAIN_CHANNEL1:
    LDP     #AD_DP                      ; point to AD Data Page
    SPLK    #channel_1,ADWORD           ; SELECT CHANNEL
    LACL    data_loc_point0             ;
    SACL    ADMEM                       ; load actual memory pointer
    ADD     #1                          ; increment ACC
   SACL    data_loc_point0             ; save new memory pointer
    SPLK    #00001h,ADCOUNT             ; NUMBER OF DATA
    SPLK    #MAIN_CHANNEL2,ACT_CHANNEL  ; set new jump level\
    RET

MAIN_CHANNEL2:
    LDP     #AD_DP                      ; point to AD Data Page
    SPLK    #channel_2,ADWORD           ; SELECT CHANNEL
    LACL    data_loc_point1             ;
    SACL    ADMEM                       ; load actual memory pointer
    ADD     #1                          ; increment ACC
   SACL    data_loc_point1             ; save new memory pointer
    SPLK    #00001h,ADCOUNT             ; NUMBER OF DATA
    SPLK    #MAIN_CHANNEL3,ACT_CHANNEL  ; set new jump level
    RET
MAIN_CHANNEL3:
    LDP     #AD_DP                      ; point to AD Data Page
    SPLK    #channel_3,ADWORD           ; SELECT CHANNEL
    LACL    data_loc_point2             ;
    SACL    ADMEM                       ; load actual memory pointer
    ADD     #1                          ; increment ACC
   SACL    data_loc_point2             ; save new memory pointer
    SPLK    #00001h,ADCOUNT             ; NUMBER OF DATA
    LACL    MEMCOUNT                    ;
    SUB     #1                          ; increment ACC
    SACL    MEMCOUNT                    ; ADCOUNT=ADCOUNT-1
    BCND    FINITISIMO,EQ               ; if ADCOUNT not 0 jump to KEEP_ON
    SPLK    #MAIN_CHANNEL0,ACT_CHANNEL  ; set new jump level
   RET
FINITISIMO:
    SPLK    #00001h,FINITO              ; set finish sign
    SPLK    #CHANNEL_END,ACT_CHANNEL    ; set new jump level
   RET
* TLV1544 POWER DOWN AFTER TRANSITIONS
CHANNEL_END:
    LDP     #AD_DP                      ; point to AD Data Page
    SPLK    #power_down,ADWORD          ; SELECT CHANNEL 0
    SPLK    #0,ADCOUNT                  ; NUMBER OF DATA 0
```


Nintendo Exhibit 1066
IPR2024-00668 - Page 564

```
    SPLK    #CHANNEL_END,ACT_CHANNEL ; set new jump level
    RET
*************************************************************************************************
* TITLE         : TLV1544C ADC Interface routine                                                *
* FILE          : values.ASM                                                                    *
* FUNCTION      : N/A                                                                           *
* PROTOTYPE     : N/A                                                                           *
* CALLS         : N/A                                                                           *
* PRECONDITION  : N/A                                                                           *
* POSTCONDITION : N/A                                                                           *
* DESCRIPTION   : contains the control data for the TLV 1544, the starting address to          *
*                 save the samples to the DSP memory and the number of samples                  *
*                 according each channel                                                         *
* AUTHOR        : AAP Application Group, Dallas                                                 *
*                 CREATED 1998(C) BY TEXAS INSTRUMENTS INCORPORATED.                            *
* REFERENCE     : TMS320C5x User's Guide, TI 1997                                               *
*               : Data Aquisation Circuits, TI 1998                                             *
*************************************************************************************************
channel_0       .set    0000h                   ; Select TLV1544 channel 0
channel_1       .set    2000h                   ; Select TLV1544 channel 1
channel_2       .set    4000h                   ; Select TLV1544 channel 2
channel_3       .set    6000h                   ; Select TLV1544 channel 3
power_down      .set    8000h                   ; Software Power Down
fast_conv       .set    9000h                   ; Fast Conversion Rate
slow_conv       .set    0A00h                   ; Slow Conversion Rate
test_200        .set    0B00h                   ; (Vreg+ – Vreg–)/2
test_000        .set    0C00h                   ; Vreg–
tets_3FF        .set    0D000h                  ; Vreg+
num_data_0      .set    1FFh                    ; Number of Data from channel 0
num_data_1      .set    200h                    ; Number of Data from channel 1
num_data_2      .set    200h                    ; Number of Data from channel 2
num_data_3      .set    200h                    ; Number of Data from channel 3
tresh           .set    1000h                   ; address to waste the first input sample
                                                ; after initialization
data_loc_0      .set    01000h                  ; Start data location for channel 0
data_loc_1      .set    04000h                  ; Start data location for channel 1
data_loc_2      .set    07000h                  ; Start data location for channel 2
data_loc_3      .set    0A000h                  ; Start data location for channel 3
numb_data_all   .set    03000h                  ; how many samples per channel to do
TRIP_HIGH       .set    023bh                   ; high trigger value = 1.34 V
TRIP_LOW        .set    01e7h                   ; low trigger value = 1.14 V
TRIG_REF        .set    0211h                   ; mean value of no triggering = 1.24 V
*************************************************************************************************
* TITLE         : TLV1544C ADC Interface routine                        *
```


Nintendo Exhibit 1066
IPR2024-00668 - Page 565

```
* FILE          : vectors.ASM                                                    *
* FUNCTION      : N/A                                                            *
* PROTOTYPE     : N/A                                                            *
* CALLS         : N/A                                                            *
* PRECONDITION  : N/A                                                            *
* POSTCONDITION : N/A                                                            *
* DESCRIPTION   : defines the interrupt vector table.                            *
*                 if RINT occurs: vector points to RECEIVE_IRQ subroutine        *
*                 if INT3 occurs: vector points to END_CONV_IRQ subrout.         *
* AUTHOR        : AAP Application Group, Dallas                                  *
*                 CREATED 1998(C) BY TEXAS INSTRUMENTS INCORPORATED.             *
* REFERENCE     : TMS320C5x User's Guide, TI 1997                                *
*********************************************************************************
   .mmregs

RS      b   _MAIN             ;0x00; RESET
INT1    b   INT1              ;0x02; external user interrupt #1
INT2    b   INT2              ;0x04; external user interrupt #2
INT3    b   END_CONV_IRQ      ;0x06; external user interrupt #3
TINT    b   TINT              ;0x08; internal timer interrupt
RINT    b   RECEIVE_IRQ       ;0x0A; Serial Port receive interrupt
XINT    b   XINT              ;0x0C; Serial Port transmit interrupt
TRNT    b   TRNT              ;0x0E; TDM receive interrupt
TXNT    b   TXNT              ;0x10; TDM transmit interrupt
INT4    b   INT4              ;0x12; external user interrupt #4
   .space  14*16             ;0x14-0x21; reserved area
TRAP    b   TRAP              ;0x22; trap instruction vector
NMI     b   NMI               ;0x24; non-maskable interrupt
/*********************************************************************************/
/* TITLE         : Hexadecimal to ASCII - Decimal Converter                      */
/* FILE          : B_H_C502.PAS                                                  */
/* FUNCTION      : N/A                                                           */
/* PROTOTYPE     : N/A                                                           */
/* CALLS         : N/A                                                           */
/* PRECONDITION  : N/A                                                           */
/* POSTCONDITION : N/A                                                           */
/* DESCRIPTION   : strip header from COFF file and convert                       */
/*                                 hexadecimal numbers into ASCII-decimal        */
/* AUTHOR        : AAP Application Group, Dallas                                 */
/*                 CREATED 1998(C) BY TEXAS INSTRUMENTS INCORPORATED.            */
/* REFERENCE     :                                                               */
/* NOTE       : Written in PASCAL                                                */
/*********************************************************************************/
uses crt,dos,printer;
```


Nintendo Exhibit 1066
IPR2024-00668 - Page 566

```
type
   positionstyp=record
   AAAA :word;
   END;
var
   pos          :positionstyp;
   satz1  :file of positionstyp;
   inpfile,ffile        :string[20];
   na,c         :char;
   s2           :string[2];
   i            :integer;
   A,n          :char;
   AA           :byte;
   tin          :file of byte;
   tout         :text;
   offset       :byte;
   nb           : byte;
   number       :longint;
   number_low   :longint;
   number_high  :longint;
begin
repeat
  clrscr;
  writeln;
  writeln(' TEXAS INSTRUMENTS (C) SOFTWARE');
  writeln(' 1998 ');
  writeln;
  write(' hard drive for input binary hexadecimal file(16bit) : ');  na:=readkey;
writeln(na,':);
  write(' file name: ');
  readln(ffile);ffile:=na+':+ffile;
  assign(tin,ffile);{$i-} reset(tin);{$i+}
  i:=IoResult;
  if (i<>0) then
    begin
     repeat
       writeln(' file not found, new Input Name? [Y/N]');
       n:=upcase(readkey);
     until ((n='Y') or (n='N'));
    end;
  if i=0 then n:='w';
until ((n='N') or (n='w'));
if n<>'N' then
begin
```


Nintendo Exhibit 1066
IPR2024-00668 - Page 567

```
inpfile:=ffile;
repeat
  writeln;
  write(' hard drive for decimal output file : ');  na:=readkey; writeln(na,':');
  write(' file name: ');  readln(ffile);ffile:=na+':+ffile;
  assign(tout,ffile);{$i-} reset(tout);{$i+}
  i:=IoResult;
  if (i=0) then
    begin
     repeat
       writeln(' file already found, should I overwrite it? [Y/N]');
       n:=upcase(readkey);
     until ((n='Y') or (n='N'));
    end
  else n:='Y';
until n='Y';
    rewrite(tout);writeln;
    writeln(tout,'binary Hex_dec-convertion, made by  TI: ');
    writeln(tout,'Input_file: ',inpfile);
    read(tin,nb);
    reset(tin);
   for i:=1 to 70 do read(tin,nb);
   repeat
     read(tin,nb);
     number_low:=nb;
     read(tin,nb);
     number_high:=nb;
     number:=number_high*256+number_low;
     writeln(number);
     writeln(tout,number,';');
   until eof(tin);
   close(tin);
   close(tout);
   readln;
end;
end.
{A=97 0=48}
```


Nintendo Exhibit 1066
IPR2024-00668 - Page 568

EXHIBIT 1063C

MEASUREMENT SPECIALTIES

Piezo Film Sensors

Technical Manual

Measurement Specialties, Inc.
Sensor Products Division
950 Forge Avenue
Norristown, PA 19403
Tel: 610.650.1500
FAX: 610.650.1509
Internet: www.msiusa.com
e-mail: sensors@msiusa.com

P/N 1005663-1 REV B 02 APR 99

-- TABLE OF CONTENTS –

Introduction 1
Background 1
Piezoelectric Film Properties 2
    Table 1. Typical properties of piezo film 3
    Table 2. Comparison of piezoelectric materials 4
Operating Properties for a Typical Piezo Film Element 4
Lead Attachment Techniques for Piezo Film Sensors 8
Frequency Response 13
Piezo Film at Low Frequencies 14
    Table 3. Capacitance values of common piezo film components . . . 15
Temperature Effects 25
Piezoelectric Cable and Properties 26
    Table 4. Piezo Cable Typical Properties 26
Piezoelectric Basics 27
Pyroelectric Basics 34
    Table 5. Comparison of pyroelectric materials 35
Basic Circuit Concepts 36
Manufacturing 43
Applications 43
    Switches 43
    Beam Switch 44
    Snap-Action Switches 44
    Impact Sensors 45
        Impact Printers 45
        Sports Scoring 45
        Musical Instruments 45
        Traffic Sensors 46
    Vibration Sensing 47
        Music Pickups 47
        Machine Monitoring 48
        Bearing Wear Sensors 48
        Fan Flow Sensor 48
        Thread Break Sensor 48
        Vending Sensors 49
    Accelerometers 49
        Table 6. Accelerometer Family 50
        Table 7. Accelerometer Applications 51

Nintendo Exhibit 1066
IPR2024-00668 - Page 571

Ultrasound Applications 52
Medical Imaging Ultrasound 52
NonDestructive Testing (NDT) 53
Acoustic Emission 53
Fluid Level Sensor 53
Air Ranging Ultrasound 54
Audio 55
Speakers 55
Microphones 55
SONAR 56
Future Applications 56
Active Vibration Damping 56
Sensors on Silicon 57
Smart Skin 57
Appendix A – Applications of Piezo Film 58
Appendix B – Index of Piezo Film Articles 61
Appendix C – Application Notes 79

Nintendo Exhibit 1066
IPR2024-00668 - Page 572

INTRODUCTION

Transducer materials convert one form of energy into another, and are widely used in sensing applications. The tremendous growth in the use of microprocessors has propelled the demand for sensors in diverse applications. Today, **PIEZOELECTRIC POLYMER SENSORS** are among the fastest growing of the technologies within the $18 billion worldwide sensor market. Like any new technology, there have been an extraordinary number of applications where **"PIEZO FILM"** has been considered for the sensor solution. In the 20 years since the discovery of piezoelectric polymer, the technology has matured, practical applications have emerged from a long list of possibilities, and the rate of commercialization of the technology is accelerating.

These documents provide an overview of piezoelectric polymer technology and nomenclature, its properties, and sensor design considerations. It also explores a range of sensor applications that have been successfully developed in recent years.

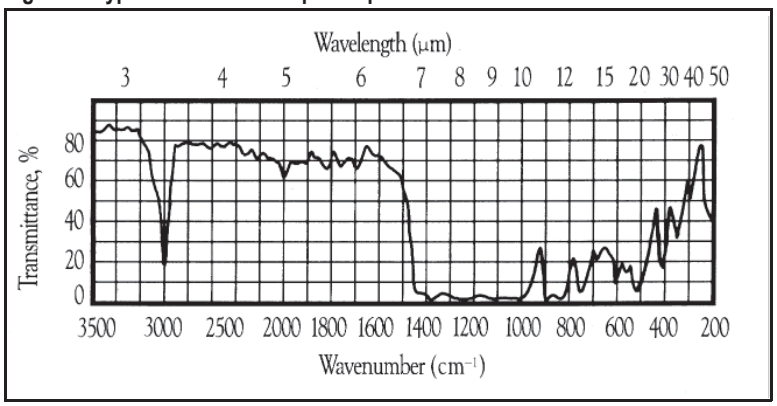
Solving unique sensor problems is a particular strength of our group of applications engineers. We welcome the opportunity to provide assistance to you during your evaluation of piezo film sensors for your design.

BACKGROUND

Piezoelectricity, Greek for "pressure" electricity, was discovered by the Curie brothers more than 100 years ago. They found that quartz changed its dimensions when subjected to an electrical field, and conversely, generated electrical charge when mechanically deformed. One of the first practical applications of the technology was made in the 1920's by another Frenchman, Langevin, who developed a quartz transmitter and receiver for underwater sound - the first SONAR. Before World War II, researchers discovered that certain ceramic materials could be made piezoelectric when subjected to a high polarizing voltage, a process analogous to magnetizing a ferrous material.

By the 1960's, researchers had discovered a weak piezoelectric effect in whale bone and tendon. This began an intense search for other organic materials that might exhibit piezoelectricity. In 1969, Kawai found very high piezo-activity in the polarized fluoropolymer, polyvinylidene fluoride (PVDF). While other materials, like nylon and PVC exhibit the effect, none are as highly piezoelectric as PVDF and its copolymers.

Figure 1. Typical infrared absorption spectrum of PVDF film.



Like some other ferroelectric materials, PVDF is also pyroelectric, producing electrical charge in response to a change in temperature. PVDF strongly absorbs infrared energy in the 7-20μm wavelengths (see Figure 1), covering the same wavelength spectrum as heat from the human body. Accordingly, PVDF makes a useful human motion sensor as well as pyroelectric sensor for more sophisticated applications like vidicon cameras for night vision and laser beam profiling sensors. A dense infrared array has been recently introduced that identifies one's fingerprint pattern using the pyro effect of piezo polymer.

Nintendo Exhibit 1066
IPR2024-00668 - Page 573

New copolymers of PVDF, developed over the last few years, have expanded the applications of piezoelectric polymer sensors. These copolymers permit use at higher temperatures (135°C) and offer desirable new sensor shapes, like cylinders and hemispheres. Thickness extremes are possible with copolymer that cannot be readily attained with PVDF. These include ultrathin (200 Å) spin-cast coatings that enable new sensor-on-silicon applications, and cylinders with wall thicknesses in excess of 1200μm for sonar. Piezo cable is also produced using copolymer.

PIEZOELECTRIC FILM PROPERTIES

Piezo film is a flexible, lightweight, tough engineering plastic available in a wide variety of thicknesses and large areas. Its properties as a transducer include:

- Wide frequency range—0.001 Hz to 10^9 Hz.
- Vast dynamic range (10^{-8} to 10^6 psi or μ torr to Mbar).
- Low acoustic impedance—close match to water, human tissue and adhesive systems.
- High elastic compliance
- High voltage output—10 times higher than piezo ceramics for the same force input.
- High dielectric strength—withstanding strong fields (75V/μm) where most piezo ceramics depolarize.
- High mechanical strength and impact resistance (10^9—10^{10} Pascal modulus).
- High stability—resisting moisture (<0.02% moisture absorption), most chemicals, oxidants, and intense ultraviolet and nuclear radiation.
- Can be fabricated into unusual designs.
- Can be glued with commercial adhesives.

One major advantage of piezo film over piezo ceramic is its low acoustic impedance which is closer to that of water, human tissue and other organic materials. For example, the acoustic impedance ($Z_O = \rho \upsilon$) of piezo film is only 2.6 times that of water, whereas piezo ceramics are typically 11 times greater. A close impedance match permits more efficient transduction of acoustic signals in water and tissue.

Piezo film does have some limitations for certain applications. It makes a relatively weak electromechanical transmitter when compared to ceramics, particularly at resonance and in low frequency applications. The copolymer film has maximum operating/storage temperatures as high as 135ºC, while PVDF is not recommended for use or storage above 100 °C. Also, if the electrodes on the film are exposed, the sensor can be sensitive to electromagnetic radiation. Good shielding techniques are available for high EMI/RFI environments.

Table 1 lists typical properties of piezo film. Table 2 provides a comparison of the piezoelectric properties of PVDF polymer and two popular piezoelectric ceramic materials.

Piezo film has low density and excellent sensitivity, and is mechanically tough. The compliance of piezo film is 10 times greater than the compliance of ceramics. When extruded into thin film, piezoelectric polymers can be directly attached to a structure without disturbing its mechanical motion. Piezo film is well suited to strain sensing applications requiring very wide bandwidth and high sensitivity. As an actuator, the polymer's low acoustic impedance permits the efficient transfer of a broadband of energy into air and other gases.

Nintendo Exhibit 1066
IPR2024-00668 - Page 574

Table 1. Typical properties of piezo film

Symbol	Parameter		PVDF	Copolymer	Units
t	Thickness		9, 28, 52, 110	<1 to 1200	μm (micron, 10^{-6})
d_{31}	Piezo Strain Constant		23	11	10^{-12} $\frac{m/m}{V/m}$ *or* $\frac{C/m^2}{N/m^2}$
d_{33}			-33	-38	
g_{31}	Piezo Stress constant		216	162	10^{-3} $\frac{V/m}{N/m^2}$ or $\frac{m/m}{C/m^2}$
g_{33}			-330	-542	
k_{31}	Electromechanical Coupling Factor		12%	20%	
k_t			14%	25-29%	
C	Capacitance		380 for 28μm	68 for 100μm	pF/cm^2, @ 1KHz
Y	Young's Modulus		2-4	3-5	10^9 N/m^2
V_0	Speed of Sound	stretch:	1.5	2.3	10^3 m/s
		thickness:	2.2	2.4	
p	Pyroelectric Coefficient		30	40	10^{-6} C/m^2 °K
ε	Permittivity		106-113	65-75	10^{-12} F/m
$\varepsilon/\varepsilon_0$	Relative Permittivity		12-13	7-8	
ρ_m	Mass Density		1.78	1.82	10^3kg/m
ρ_e	Volume Resistivity		$>10^{13}$	$>10^{14}$	Ohm meters
$R_\square$	Surface Metallization Resistivity		<3.0	<3.0	Ohms/square for NiAl
$R_\square$			0.1	0.1	Ohms/square for Ag Ink
tan δ_e	Loss Tangent		0.02	0.015	@ 1KHz
	Yield Strength		45-55	20-30	10^6 N/m^2 (stretch axis)
	Temperature Range		-40 to 80...100	-40 to 115...145	°C
	Water Absorption		<0.02	<0.02	% H_2O
	Maximum Operating Voltage		750 (30)	750 (30)	V/mil(V/μm), DC, @ 25°C
	Breakdown Voltage		2000 (80)	2000 (80)	V/mil(V/μm), DC, @ 25°C

Nintendo Exhibit 1066
IPR2024-00668 - Page 575

Table 2. Comparison of piezoelectric materials

Property	Units	PVDF Film	PZT	$BaTi0_3$
Density	10^3kg/m3	1.78	7.5	5.7
Relative Permittivity	$\varepsilon/\varepsilon_0$	12	1,200	1,700
d_{31} Constant	(10^{-12})C/N	23	110	78
g_{31} Constant	(10^{-3})Vm/N	216	10	5
k_{31} Constant	% at 1 KHz	12	30	21
Acoustic Impedance	(10^6)kg/m^2-sec.	2.7	30	30

OPERATING PROPERTIES FOR A TYPICAL PIEZO FILM ELEMENT

The DT1 element is a standard piezo film configuration consisting of a 12x30 mm active area printed with silver ink electrodes on both surfaces of a 15x40 mm die-cut piezo polymer substrate.

1. **Electro-Mechanical Conversion**
   (1 direction) 23 x 10^{-12}m/V, 700 x 10^{-6}N/V
   (3 direction) -33 x 10^{-12}m/V

2. **Mechano-Electrical Conversion**
   (1 direction) 12 x 10^{-3}V per microstrain, 400 x 10^{-3}V/μm, 14.4V/N
   (3 direction) 13 x 10^{-3}V/N

3. **Pyro-Electrical Conversion**
   8V/ ^{o}K (@ 25 ^{o}C)

4. **Capacitance**
   1.36 x 10^{-9}F; Dissipation Factor of 0.018 @ 10 KHz; Impedance of 12 KΩ @ 10 KHz

5. **Maximum Operating Voltage**
   DC: 280 V (yields 7 μm displacement in 1 direction)
   AC: 840 V (yields 21 μm displacement in 1 direction)

6. **Maximum Applied Force (at break, 1 direction)**
   6-9 kgF (yields voltage output of 830 to 1275 V)

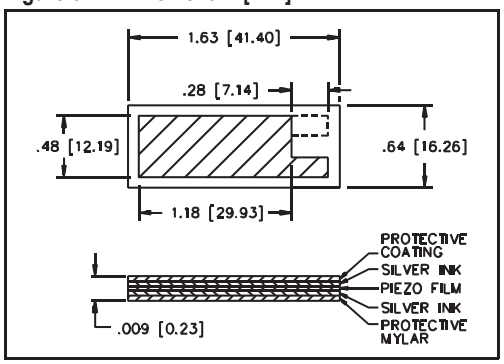
Electrical to Mechanical Conversion

Large displacements of forces are not generally available from piezo film. This becomes apparent when designing loudspeaker elements for instance, as low frequency performance (below 500Hz) tends to be limited. Even a large sheet of film is unable to create high amplitude pressure pulses as low audio frequencies. This does not apply, however, to low to high frequency ultrasonic frequencies, as seen in current designs for ultrasound air ranging transducers (40-50 KHz) and in medical ultrasonic imaging applications. In enclosed air cavities (headset speakers, hearing aids), the low frequency response of piezo film is excellent. For air ranging ultrasound, the piezo film element height controls vertical beam angle and the curvature and width of the transducer controls horizontal beam pattern. Piezo film air ranging transducers can provide up to 360 ^{o} field of view, ranging object from a few centimeters to several meters with high resolution.

Nintendo Exhibit 1066
IPR2024-00668 - Page 576

Bimorph configurations (like a bimetal strip) allow the small differential displacement of two reverse-connected elements to be translated into substantial flexural motion. Small fans or optical deflectors can thus be created. Such devices consume very little real power (being capacitive in nature). Large devices may be difficult to drive due to high capacitance, especially when transformers are used to step up the drive voltage. Good amplifier design is important. Nevertheless, conventional fan and blower technologies generate higher flow rates and back pressures than piezo bimorphs.

Figure 3. DT1 Element in [mm]



Although the forces involved are small, the film can be used to excite other mechanical structures over a very wide frequency range. If a second element of film is used to receive the induced vibration, the system can possess a very high dynamic range, even though the overall "insertion loss" due to the film is about -66 dB typically for a structure at resonance. If sufficient gain is applied between these elements, the structure will self-oscillate at its natural frequency. For these resonant mechanical systems, high voltage drive is not required. The amplifier circuit may function adequately from a normal dual rail op-amp supply, or even from a single 9 volt battery. For analysis purposes, even lower applied voltages, e.g., the noise source of a spectrum analyzer at 70 mVrms, are sufficient to insert the mechanical energy into a structure when piezo film is also used to monitor the result.

Mechanical to Electrical Conversion

The sensitivity of piezo film as a receiver of mechanical work input is awesome. In its simplest mode the film behaves like a dynamic strain gage except that it requires no external power source and generates signals greater than those from conventional foil strain gages *after* amplification. Frequency response is thus free from any limitations imposed by the need for high gains and will extend up to the wavelength limit of the given transducer.

The extreme sensitivity is largely due to the format of the piezo film material. The low thickness of the film makes, in turn, a very small cross-sectional area and thus relatively small longitudinal forces create very large stresses within the material. It is easy to exploit this aspect to enhance the sensitivity parallel to the machine axis. If a laminated element of film (for example an LDT1-028K) is placed between two layers of compliant material then any compressive forces are converted into much larger longitudinal extensive forces. In fact, this effect tends to predominate in most circumstances since most substances are compliant to some extent and the ratio of effective sensitivity in the 1 (length) vs 3 (thickness) directions is typically 1000:1.

Piezo film transducers may often cover a much larger area than normal strain gages so any direct comparisons should be performed in a *uniform* strain field for meaningful results. Obviously "point"-type transducers could be used where required although the capacitance of a very small area will require consideration. The low frequency limit of operation will be defined by the greatest resistive load achievable, or by the largest capacitance load that still allows the signal to be easily detected. Operation down to fractions of Hz can be achieved using either conventional charge amplifiers or, since signal levels are relatively high, simple high impedance FET buffer circuits.

Pyro to Electrical Conversion

Piezo film absorbs strongly in the region of 7 to 20 μm which corresponds to well beyond both operating temperature limits of the film. It thus makes a sensitive pyroelectric detectors for, say, human body radiation. Since the pyro sensitivity is strong, care must be taken when designing low (<0.01 to 1Hz) frequency mechanical sensors to avoid ambient temperature changes swamping

Nintendo Exhibit 1066
IPR2024-00668 - Page 577

the output with pyro-generated signal. If a very long time constant is in use, then the film will generate a voltage corresponding to the change in temperature since switch-on. Since the output will be several volts per degree C, substantial offsets may be noticed.

In general, however, most piezo applications will have a cut-off frequency of several Hertz or more. Connecting a device of 1nF capacitance to an oscilloscope input, even at 10 MΩ impedance, will produce a roll off below 16 Hz. Only a more rapid change in the film temperature will generate a detectable signal.

Common-mode rejection can be used to isolate either very low frequency mechanical strain from simultaneous pyro-effects or vice-versa. These straight-forward techniques are quite familiar to MSI applications engineers who are available for design assistance.

Electrical Design Considerations

A useful model for piezo film which applies for most cases except ultrasonic applications is a strain-dependent voltage source in series with a capacitance. Thus any resistive load will form a divider network with a simple RC high-pass filter characteristic. The cut-off frequency is given by $f_o = \frac{1}{2\pi RC}$ and the time constant $\tau = RC$. Operation below the cut-off frequency will give an output signal proportional to the rate of change of the input parameter (differentiator). Application of a constant stress will generate an initial level followed by an exponential decay of rate $\exp(RC)^{-1}$.

A capacitive load will extend the time constant but reduce the magnitude of the response. Energy is always lost when transferring charge from one capacitor to another. Large capacitive loads are useful for attenuating the very large signals arising from powerful impacts—often hundreds of volts.

When driving the film at high voltage and high frequency, the dissipation factor of the film may result in substantial energy loss in the form of heat. Also, the surface resistivity of the electrodes may become significant, especially with vacuum metallized film. Very high localized currents may be encountered. Operation within the field limits given in the Technical Manual is strongly recommended since any arcing will normally destroy the device.

Silver ink, screenprinted onto both film surfaces, has been developed to withstand high voltage and high localized currents. The silver ink metallization has been successfully used in tweeters and active vibration damping applications. The DT1 sample is electroded with the silver ink. The unmetallized border mitigates potential for arcing across the film's thickness. The offset lead attach tabs also preclude high voltage breakdown, as the conductor at each lead attach site is on one side only.

Mechanical Design Considerations

The output energy is proportional to the volume of film stressed. Film thickness may be chosen to optimize the electrical signal or in view of mechanical strength considerations. Thicker films generate higher voltages but form smaller capacitors, so a laminate of thinner film with a compatible, passive material such as polyester (i.e. the LDT1-028K) may be preferable to a single thicker film. Any area of film that is not undergoing stress will act as a capacitive load on the "active" area and should be minimized if required.

Most metallizations are subject to corrosion, especially when handled. Thin conformal coatings or laminates are frequently applied to maintain surface quality. Acrylics adhesives, synthetic rubber resins, epoxies and cyano-acrylates are all frequently employed in lamination and assembly.

Some designs may use external metallic or conductive substrates as the electrodes, in which case unmetallized film may be used to good advantage. The external metal surface can be in direct

Nintendo Exhibit 1066
IPR2024-00668 - Page 578

contact with the unmetallized film to collect the charge, or, capacitive coupling through thin adhesive tapes or epoxy layers can be employed for ac applications. Patterning of the electrodes is especially useful for defining specific active areas on a continuous sheet and also to allow die-cutting of elements with a clear border around the cut area. Displacement (offset) of upper and lower electrode tabs at the connection point is good practice to prevent unpredictable piezo behavior in this area caused by the influence of the wire terminations. This also allows low cost penetrative lead-attach methods to be used (crimps or eyelets).

Joint Electrical and Mechanical Design Considerations

The capacitive nature of piezo film devices implies that they are susceptible to Electro Magnetic Interference (EMI). This becomes increasingly more important as the output signal level drops. EMI can be ignored where the output is high or when the film is being driven in a non-critical environment. A.C. mains interference may become a problem with unshielded devices. Another potential problem exists when one electrode element is being driven and an another is receiving the vibration signal. Care must be taken to avoid "crosstalk".

Use of ready-made shielded elements (SDT1-028K) supplied with coaxial cable eliminates these problems, but simple measures may be taken with any device to avoid interference.

Unwanted frequencies may be filtered out electronically. If the sensor is to be mounted on a conductive substrate, then this may form one half of a grounded envelope, with the outer electrode forming the other half. Lightweight shielded cable is readily available and is an alternative to twisted pair wires. Attention should be paid to the point of connection itself as this is also an area of EMI vulnerability.

Durable lead attachment techniques have been fully developed by MSI, and most products are supplied with leads preattached. As indicated, some form of coaxial cable is often employed and must be interfaced to a very thin flexible material. Reinforcement at the lead attach site may be required, which can introduce some acoustic effects into the transducer if the interconnection site is free to vibrate.

Thin copper foil backed with a conductive adhesive can provide excellent but non-permanent connections to the film. An area of 1 cm^2 will give a contact resistance of a few mΩ s. Crimp-through connectors as used for flexible circuits are routinely used with offset electrode patterns, but thin films require some physical reinforcement for good results. Polyester reinforcement at the lead attach site is a common method to ruggedize the interconnection. The stiffener may lie between the crimp and the electrode with only minor degradation of contact resistance. Typical values are 150-500 mΩ. Miniature rivets, eyelets and even nuts and bolts, with washers, all combine great strength with good contact resistance at typically less than 100 mΩ. These techniques may be used to connect to cables using solder tags, or direct onto printed circuit boards.

Clamping methods, either direct to the conductive traces on the PCB or using conductive rubber, ZEBRA® connectors, lugs and washers have all been used with success. Direct connection using silver-loaded (conductive) epoxy also works well, but requires curing time, often at elevated temperature, for best results.

As indicated earlier, other materials may form the electrodes themselves, such as PCB traces or conductive rubber. Capacitive coupling through thin adhesive layers is practical under some a.c. circumstances, allowing some unusual transducer designs with apparently no lead attachment at all!

ZEBRA is a registered trademark of Fujipoly.

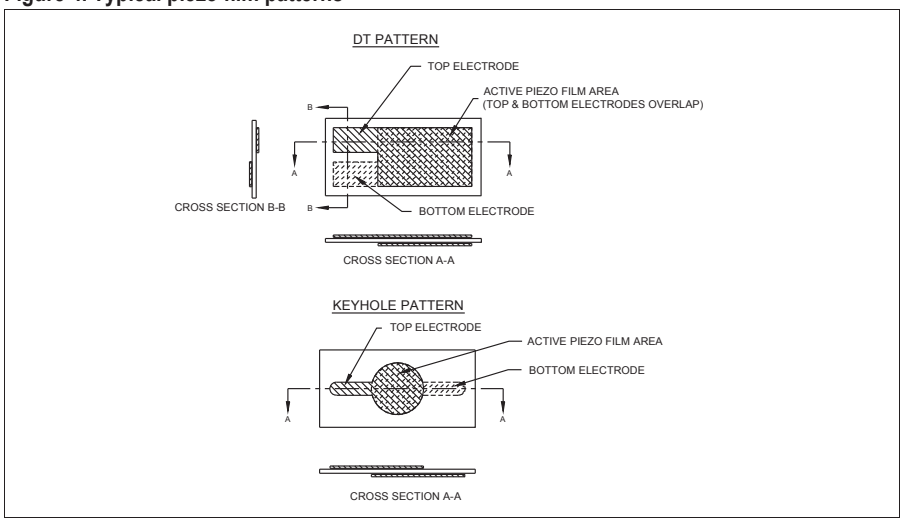
Nintendo Exhibit 1066
IPR2024-00668 - Page 579

LEAD ATTACHMENT TECHNIQUES FOR PIEZO FILM SENSORS

Introduction

How to make reliable interconnection to piezo film is one of the most frequently asked customer questions. With this in mind, MSI has paid great attention to the development of techniques to simplify interconnection to piezo film elements. Today, most of the sensor elements supplied to customers from our Division have leads already attached. The aim of this article is to examine and discuss available interconnection options.

Figure 4. Typical piezo film patterns



Some of the most convenient interconnection techniques require that MSI apply patterned electrodes on one or both surfaces of the piezo film—this can always be done to customers' requirements during manufacture— alternatively, a simple method achieving the same goal is presented at the end of the text. In general, patterned electrodes are achieved during piezo film manufacturing by screen printing conductive inks, metal masking during sputtered electrode deposition, or chemically etching patterns by photolithographic techniques.

The Targets

Considered here are the design objectives desired for the lead-attach method. Not all objectives can be achieved with any one technique. Designers should identify the most important objectives and select among the interconnection options accordingly.

- High conductivity/low resistance — surprisingly, high conductivity interconnection is not a particularly important parameter for most piezoelectric applications. Piezo transducers are frequently used in high-impedance circuits where inclusion of a few ohms does not usually affect performance. More important, however, is consistence—the resistance should not fluctuate during use since this will introduce a source of electrical noise.
- Low mass — this is especially important when the piezo film is not to be clamped to a mechanical support structure. The acoustic effect created by the mechanical vibration of the mass of the interconnection on an otherwise flexible structure can be dramatic.
- Low profile — many piezo film applications arise by virtue of the low thicknesses of piezo film. Interrupting this with bulk terminations is often prohibited. Contact vibration sensors can show distinct resonances if film is not bonded flush to the contact surface to include the interconnection.
- Flexibility — here again is a property that must often match that of the film itself. Some degree of flexibility is a distinct advantage in many applications.
- Low area — useful piezo devices can be quite literally be employed as "point" receivers. Small piezo-active areas (where the top and bottom conductors fully overlap) can be configured with

Nintendo Exhibit 1066
IPR2024-00668 - Page 580

displaced or off-set lead-attach tabs. The top and bottom tabs are off-set with respect to each other (when viewed through the film thickness). This allows a precisely defined active area (overlapped electrodes) with non-piezo conductors (off-set tabs) leading to remote bonding sites, a technique most frequently employed for "small" devices.

- Mechanical Strength — very often the greatest strain experienced by a polymer transducer is around the connection, whether by accident (tripping over the cable) or by design. In general, those methods which involve the interconnection penetrating through the film at the off-set tab locations with crimps, eyelets or rivets yield the best ultimate strain resistance. Often the lead attach area is reinforced with polyester to improve the strength of the penetrative interconnection.
- Long-term Stability — including all the usual environmental parameters. Most interconnections have unlimited life (crimps, eyelets, conductive rubber connectors). Others have a more limited shelf life (conductive tapes)
- Speed and Ease of application — of particular importance when high volume production is planned. Many interconnection techniques are supported by semi-automatic equipment for volume production (crimps, eyelets) while others are labor intensive (conductive adhesives).
- Electrical strength — an issue associated mainly with electrically driven (high voltage) elements such as loudspeakers and actuators.

The Design Considerations

Two major issues control the selection of lead-attach methods:

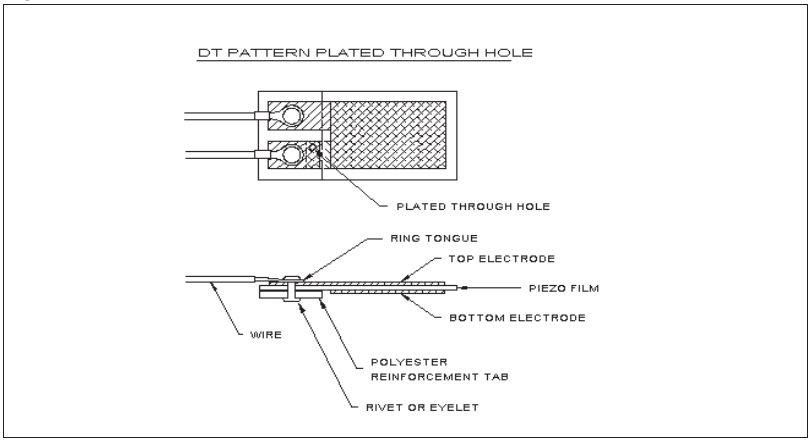
- Is anchorage of the film allowed at the site of lead-attach? This can be a major advantage, for example, direct connection or capacitive coupling to the conductive traces of a printed-circuit board.
- Is special patterning of the film available, which would allow penetrative techniques? (with MSI Sensors custom patterning service, the answer is almost always "yes.") Simple experimental methods allow the same result.

This concludes the "questions" section—now, hopefully, are the "answers."

The Methods

Penetrative - Here the techniques involve piercing the film (and possibly additional reinforcing laminates to give sufficient thickness and strength), and thus the film should be patterned with a displaced or off-set lead-out arrangement to prevent shorting of upper and lower electrodes by the inserted connector.

Figure 4.

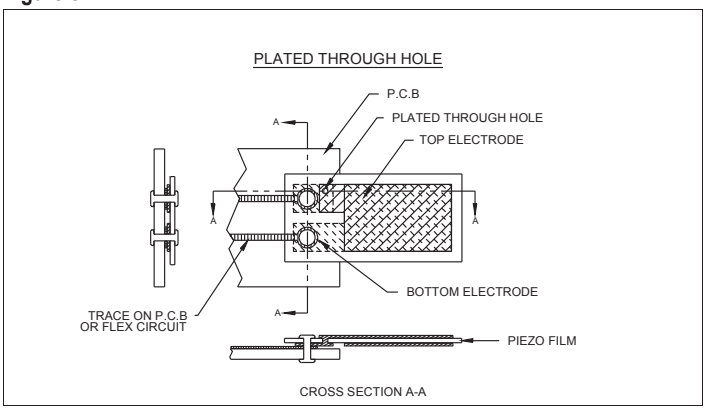


- Rivets or eyelets can be affixed to the off-set conductive traces on the piezo film. Included between the eyelet or rivet can be a ring tongue lug terminal with wire attached. The eyelet or rivet mechanically presses the conductive ring against the off-set patterned electrode to make reliable interconnection.

Nintendo Exhibit 1066
IPR2024-00668 - Page 581

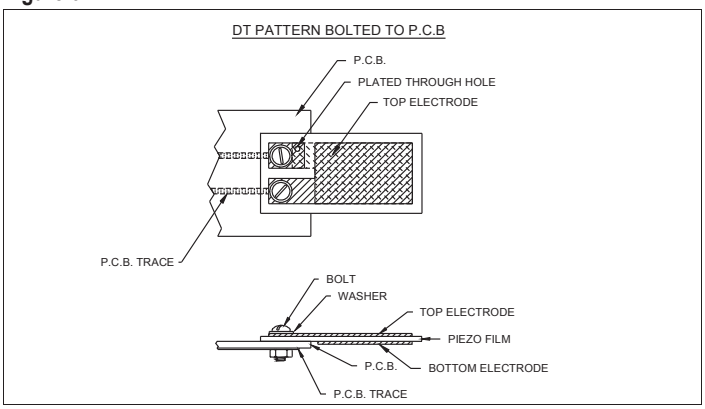
! To affix the piezo film directly to a PCB, small "POP" or "blind" rivets or eyelets can be used in conjunction with patterned film electrodes and the conductive tracks on the PCB to allow a single operation to form the interconnection. During screen printing of conductive ink electrodes, a small “plated through hole” can be formed in one of the off-set tabs, thereby bringing both conductors to the same side of the piezo film. This greatly facilitates riveting the film electrode tabs to the corresponding PCB traces. If the “plated through hole” technique is not used, then the top film electrode can be electrically connected by the rivet to a conductive trace on the underside of the PCB. The bottom film electrode is electrically connected to a corresponding trace on the top of the PCB and held in intimate contact by the pressure exerted by the rivet.

Figure 5.



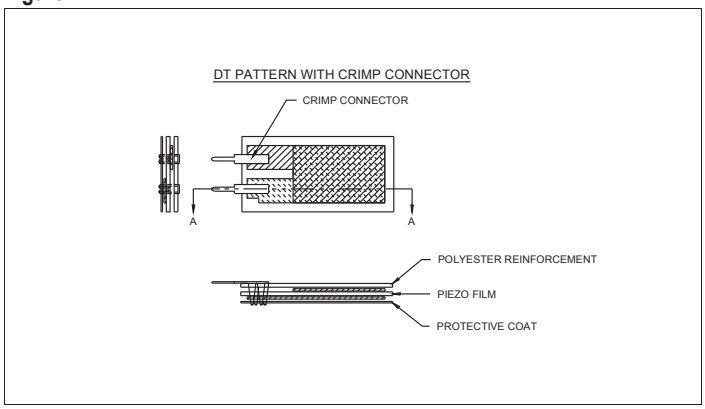
! Nuts and bolts - Wires terminated with washers, ring-tongue lugs, solder-tags, etc. can easily be incorporated with small nuts and bolts.

Figure 6.



! Crimp Connectors — generally, crimps designed for flexible circuit technology work well with piezo film elements. Crimps can have solder tabs for affixing wires, or the crimp ends can be inserted into corresponding holes in a PCB and soldered to the underside of the PCB (maximum of a few second soldering time so as not to overheat the film). Like the eyelets mentioned above, crimps are normally designed to work with a specified thickness of "substrate," so film may require "padding" on one side (i.e., polyester reinforcement) to accommodate the crimp connectors. Additionally, a complete multi-way connector may be crimped to a more complex device, giving straight plug-in compatibility with other connectors.

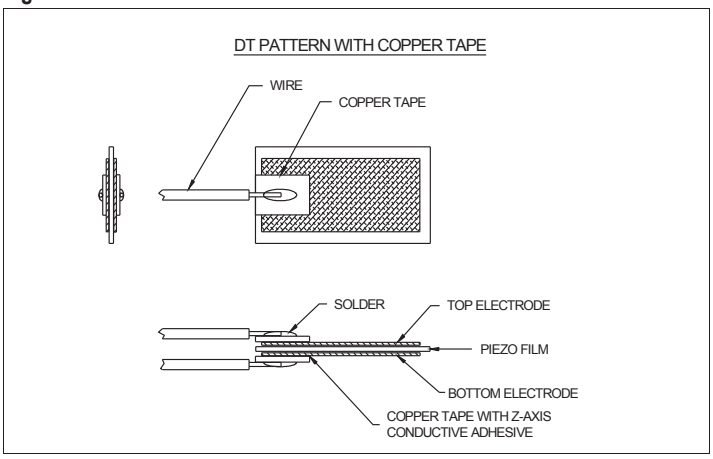
Figure 7.



Nintendo Exhibit 1066
IPR2024-00668 - Page 582

Non-penetrative (and temporary) - Conductive-adhesive coated Copper Foil Tape (e.g., 3M #1181)—available in widths from 3mm up to 25mm. Best results are obtained by...

Figure 9.

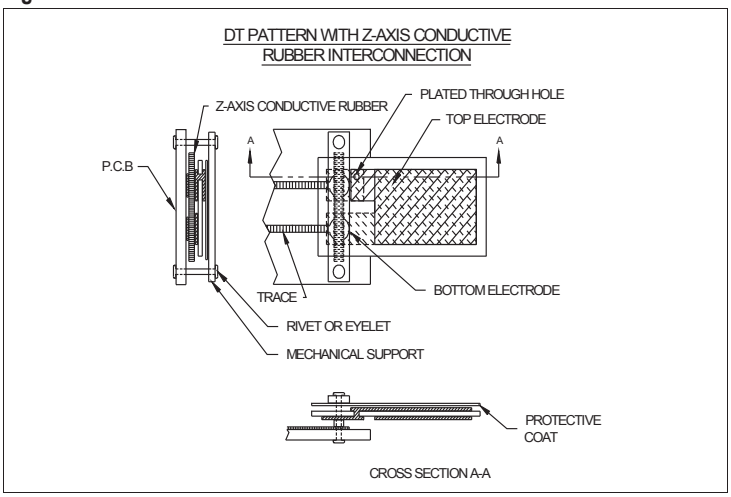


- Using a "reasonable" area of tape (perhaps about 1cm or more). Small pieces do tend to lift off easily.
- Soldering wires to the tape FIRST, then removing the liner and adhering with gentle pressure to film. If small areas are to be used, solder before cutting the contact pad down to size, thus leaving the excess area to act as a heat sink. Soldering does appear to degrade the adhesive properties in the vicinity of the joint. NOTE: 3M does not recommend relying on the conductive adhesive in this way and suggest an embossed version of the same tape. The tape is really designed for large area contacts to metal, but results have shown this method to be an effective, if not guaranteed, technique. An aluminum version of this product is available (Part No. 1170). Beware of similar tapes that do not have conductive adhesives (although these can be used for shielding, etc.)
- Conductive Transfer Tape—e.g., 3M #9702 (Preliminary product). An acrylic adhesive layer loaded with conductive particles giving excellent "Z-axis" conductivity (i.e., through the thickness of the tape) with very high resistivity in the X and Y axes. Thus single or multiple-way connections may be made with a single strip. This material is relatively new. Initial results seem very promising. Obviously this can be used to make direct connection with PC board or strip, or to sections of foil with soldered leads.
- Negative aspects are a) high cost, and b) like all transfer adhesives, there is a tendency for the material to adhere to its own liners around the edge so that "stringing" occurs on liner removal. NOTE: Since time of writing, this product has been superseded by an improved version (#9703) with an easy-release liner. This may not yet be generally available.
- Conductive Epoxy. This is usually available in two-part form (adhesive and hardener). Precise metering and mixing of the small quantities usually required is rather difficult and messy. One-part, pre-mixed material is available as a product which is stored at very low temperature and should be used and cured at room temperature. Curing of any epoxy mix can usually be accelerated by use of higher temperature, but since the piezo film has a modest high-temp capability, curing is often a long term process (many hours, a day). Some mechanical clamping is usually required on the parts to be bonded. Final reinforcement with "ordinary" epoxy can be reassuring. Negative aspects: difficulty of use, cure time, higher cost, short "shelf life."
- Low melting-point Alloys—some alloys (e.g., Indium/Tin/Bismuth) which are known as "fusible alloys" rather than "solders," melt at temperatures which allow them to be used on piezo film with suitable metallization (e.g., gold, cooper, silver or silver ink). Rather aggressive fluxes are often required, and the joint may be brittle. Mechanical strength is limited by the adhesion of the metallization onto the film surface, so once again, reinforcement with epoxy may help. For joints that must be very small and do not need undue mechanical strength this may prove a valuable technique. Negative aspects: only certain metallizations are appropriate, sample quantities hard to come by. Mechanical strength limited [Indium Corp.]
- Zebra® Connectors — Conductive rubber spliced with insulating rubber as used to form contacts to LCD displays. High density multiple-way contacts may be made. External clamping of contacts is required.

Nintendo Exhibit 1066
IPR2024-00668 - Page 583

- Mechanical clamping—simply sandwiching the film between two conductive surfaces (possibly using a thin layer of conductive-loaded rubber) can provide excellent results. Two rings can provide useful support for diaphragms, speakers, etc.
- Capacitive Coupling - In certain applications, no metal electrode is required on the piezo film itself. Thin, non-conductive adhesives can affix the unmetallized film to a conductive surface. The conductive surface in effect provides the film's electrodes in ac applications. A PCB, having conductive pads on one surface corresponding to the desired active sensor area, is an embodiment of this concept. The opposite piezo film surface can be metallized with a ground electrode. The film can be sandwiched between two conductive surfaces with or without adhesive to form electrodes.

Figure 10.



User Etching of Piezo Film Electrodes

Patterned electrodes are available from MSI in either silver screen printed ink or as sputtered electrodes. In some instances, customers purchase fully metallized sheets for experimentation, and want to produce their own patterns. This is very difficult with screen printed inks as they cannot be easily etched or mechanically braided. For sputtered electrodes, standard photolithographic techniques work quite well.

In order to pattern piezo film in such a way as to allow penetration of film without shorting top and bottom electrodes, a very simple technique may be employed which works on any vacuum deposited electrodes (NOTE: not recommended for Ag Ink.)

One terminal of a power source (bench p.s.u. or 9 volt battery) is connected via a conductor pad or block by mechanical pressure to the piece of film in question. The other terminal is brought to a conductive point (needle, wire-end, blunt scalpel, etc.) and the area required to be isolated simply drawn around. Sufficient current normally passes to cause arcing at the point contact and the metallization is vaporized. Concentric "guard rings" may be drawn for extra confidence.

For more complex patterning of thin sputtered metallization, it is possible to coat the piezo film with photoresist aerosol (both sides if necessary). The cured spray can then be exposed through a mask using UV light, as with conventional PCB techniques, and then dipped in an etchant. Complete etching of the very thin metal layer occurs in seconds.

Copper/Nickel metallizations etch very well with standard PCB etchant (ferric chloride). Other metals require special etchants for good results (Aquaregia for gold). Remember that the metallization layer may only be a few hundred atoms thick (300-700 Å), and therefore fine traces are very vulnerable to scratching or cracking.

Nintendo Exhibit 1066
IPR2024-00668 - Page 584

High Voltage Techniques

The use of piezo film as a vibration exciter requires separate consideration. Since the impedance of a capacitive transducer decreases with frequency and approaches infinity for low frequencies, very high voltages (a few hundred volts typically) may be required to drive, for example, full audio-range loudspeakers. Frequently, transformers are used to step up moderate voltages to supply the required drive signal. Under these circumstances, extreme stresses may be placed upon the connections. Consider first applying a voltage step of 30V to a capacitor of 100nF with an overall circuit resistance of 2 ohms. The initial current pulse peaks at 15 amps (assuming the supply is capable of supplying this). Such a current "spike" may well show up defects in connectors.

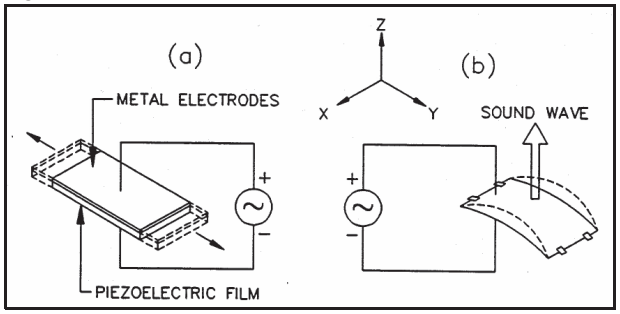
Consider next a transformer which steps 12V signals up to 240V. A DC current in the primary of 200 μA (corresponding to an applied voltage of 0.5 volts), when broken, may cause a voltage surge of 830 volts across the secondary circuit, well in the excess of the expected X 20 magnification factor. Even with heavy capacitive loading, high voltages may be seen. Worse still, if the secondary circuit is broken, current pulses exceeding 60A with durations of only tens of nanoseconds may arise. Such phenomena should not trouble well-formed connections. But if a lead-attach method has been used which has any trapped air, the effect of the reduced dielectric constant may be to promote breakdown. Such events may be catastrophic, as the familiar crackling sound and lively blue sparks will testify.

Solutions are:
1. Silver ink electrodes are a must - the thin sputtered electrodes cannot withstand the high voltages
2. Large area contacts to reduce stress. We paint silver ink around eyelets/rivets to provide extra conduction paths to the film electrode.
3. (Possibly) a semi-resistive contact pad to reduce current surges—equivalent to including a series resistance in the circuit. Practical values up to about 1 k will produce only a fractional loss in output and will reduce the magnitude of current spikes.

FREQUENCY RESPONSE

Unlike piezo ceramic transducers, piezo film transducers offer wide dynamic range and are also broadband. These wide band characteristics (near dc to 2GHz) and low Q are partly attributable to the polymers' softness. As audio transmitters, a curved piezo film element, clamped at each end, vibrates in the length (d_{31}) mode, as shown in Figure 10. Piezo film is a very high fidelity tweeter, also used in novelty speakers for toys, inflatables and apparel. The d_{31} configuration (Figure 10) is also used for air ultrasound ranging applications up to frequencies of about 50 KHz.

Figure 10. Clamped film in d_{31} mode produces sound



When used as a high ultrasonic transmitter (generally >500KHz), piezo film is normally operated in the thickness (d_{33}) mode. Maximum transmission occurs at thickness resonance. The basic half-wavelength resonance of 28μm piezo film is about 40 MHz:

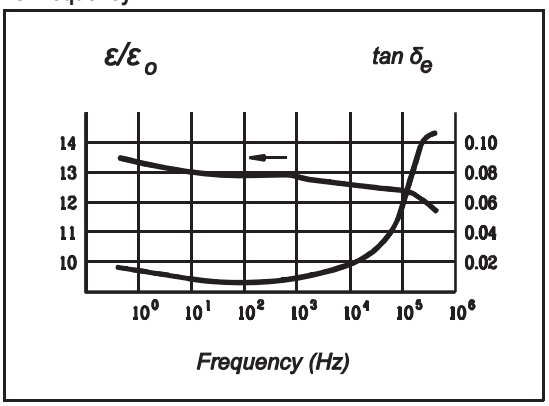
$$f_r = \frac{v}{2t} = \frac{2.2x10^3 m/\sec}{2x28x10^{-6}m}$$

Nintendo Exhibit 1066
IPR2024-00668 - Page 585

Resonance values thus depend on film thickness. They range from low MHz for thick films (1,000μm) to >100MHz for very thin films.

Figure 11 shows the effect that frequency has on permittivity and dissipation factor at room temperature. As a result of its very low permittivity ε (1 percent that of piezo ceramics), the film exhibits *g*-constants (voltage output coefficients) that are significantly greater than piezo ceramics ($g = d/\varepsilon$).

Figure 11. Dielectric permittivity and dissipation factor vs. frequency



PIEZO FILM AT LOW FREQUENCIES

Introduction

The behavior of a piezo film component at low frequencies is fairly straightforward to describe in electrical terms, yet is quite frequently misunderstood. Since any practical application of the technology will most likely involve some consideration of this topic, it is the intent of this article to examine the subject at some length. The treatment is made as non-mathematical as possible, with verbal descriptions and real-world examples being used to illustrate the concepts. Some familiarity with the use of FFT techniques to transform between time-domain and frequency-domain descriptions is assumed, but not essential.

Connecting Up

In most instances, the first evaluation of piezo film begins with connecting a piezo component to an oscilloscope via a probe ("scope probe"). Under normal electronics circumstances, a scope probe can be considered to be an "infinite impedance" - so high, that its effect on the circuit under test can be neglected. **Not so with piezo film** - in many cases, a scope probe can act almost like a short-circuit. Typical probes, when plugged in to an oscilloscope, have an effective *resistance* of 1MΩ (one million ohms). Others may be fixed at 10MΩ, while many are conveniently switchable between "x1" (1MΩ) and "x10" (10MΩ). Note that the physical element comprising the 1MΩ resistance is usually built into the oscilloscope input stage, rather than being a discrete component within the probe itself. A "x1" probe is thus basically a length of shielded cable with suitable contacts attached to each end.

Source Capacitance

To analyze what will happen when the probe is connected, we now need to consider the properties of the piezo film element. Perhaps the most important characteristic (after the piezoelectric property, of course) is the material's *capacitance*. Capacitance is a measure of any component's ability to store electrical charge, and is always present when two conductive plates are brought close together. In our case, the conductive plates are the conductive electrodes printed or metallized onto each surface of the film. The capacitance of the device is strongly affected by the properties of the insulator serving to space the plates apart, and the measure of the insulator's capacity to store charge is given by its *dielectric constant* or *permittivity*.

Nintendo Exhibit 1066
IPR2024-00668 - Page 586

PVDF has a high dielectric constant compared with most polymers, with its value being about 12 (relative to the permittivity of free space).

Obviously, the capacitance of an element will increase as its plate area increases, so a large sheet of film will have a larger capacitance than a small element. Capacitance also increases as the film thickness *decreases*, so for the same surface geometry, a thin film will have a higher capacitance than a thick film.

These factors are formally related in the equation: $$C = \varepsilon \frac{A}{t}$$

where C is the capacitance of the film,
ε is the permittivity (which can also be expressed in the form

$\varepsilon = \varepsilon_r \varepsilon_0$ where ε_r is the relative permittivity (about 12 for PVDF), and ε_0 is the permittivity of free space (a constant, 8.854×10^{-12} F/m)

A is the active (overlap) area of the film's electrodes
and t is the film thickness

The units of capacitance are Farads (F), but usually much smaller sub-multiples are encountered: microfarads (μF or 10^{-6} F), nanofarads (nF or 10^{-9} F) and picofarads (pF or 10^{-12} F).

The capacitance of any piezo film element can be calculated using the formula, or measured directly using a hand-held capacitance meter, or bench-top instrument such as an "LCR bridge".

Capacitance values should be quoted at a given measurement frequency - where this is not given, a frequency of 1 KHz is often assumed. Capacitance values of piezo film components usually decrease as the measurement frequency increases.

Table 3. Capacitance values of common piezo film components

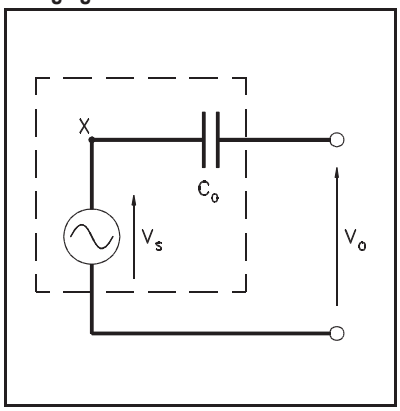
Description	Part No.	Capacitance
LDT0-028K/L	0-1002794-1	500 pF
DT1-028K/L	1-1002908-0	1.3 nF
DT1-052K/L	2-1002908-0	650 pF
DT2-028K/L	1-1003744-0	2.6 nF
DT4-028K/L	1-1002150-0	9 nF
8" x 11" 28 μm	1-1003702-4	30 nF
HYD-CYL-100	0-1001911-1	43 pF

Equivalent Circuit of Piezo Film

We are now ready to draw out an electrical equivalent of the piezo film element. There are two equally valid "models" - one is a *voltage* source in series with a capacitance, the other a *charge* generator in parallel with a capacitance - but the latter is uncommon in electrical circuit analysis and we will concentrate on the voltage source (see Figure 12).

The dashed line represents the "contents" of the piezo film component. The voltage source V_S is the piezoelectric generator itself, and this source is directly proportional to the applied stimulus (pressure, strain, etc). It is not the purpose of

Figure 12. Piezo film element as a simple voltage generator



Nintendo Exhibit 1066
IPR2024-00668 - Page 587

this article to elaborate further on the calculations involved, but it is important to realize that this voltage will absolutely follow the applied stimulus - it is a "perfect" source.

Note, however, that the node marked "X" can never be accessed! The film's capacitance C_0 will always be present and connected when we monitor the "output" of the film at the electrodes.

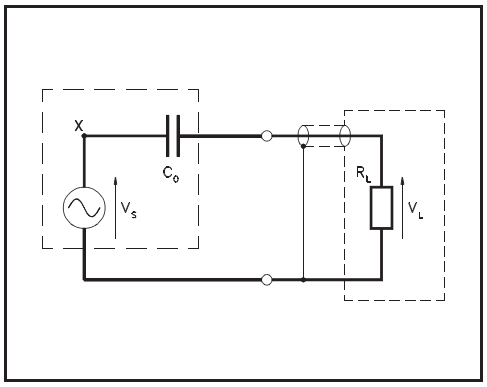
Adding in a resistive load

Now we can add in the effect of connecting up to the oscilloscope. The oscilloscope and its probe are modeled simply as a pure resistance, although in reality there will be a very small capacitance associated with the probe and the cable (usually in the region of 30 to 50 pF). This can be neglected if the film capacitance is significantly higher in value.

The voltage measured across the load resistor R_L will **not** necessarily be the same voltage developed by the "perfect" source (V_S).

To see why, it is helpful to redraw this circuit in another way.

Figure 13. Adding the oscilloscope as resistive load



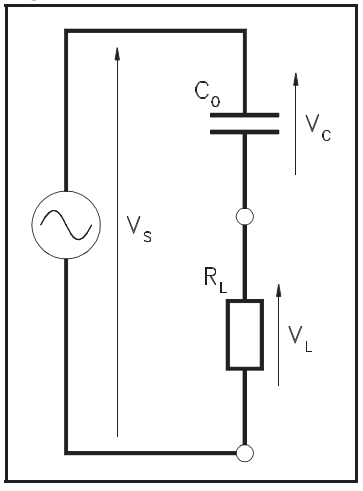
Potential Divider

With the circuit shown in Figure 13 redrawn as in Figure 14, it is easier to see why the full source voltage does not always appear across the resistive load.

A *potential divider* is formed by the *series* connection of the capacitance and the resistance. Since the capacitance has an impedance which varies with frequency, the share of the full source voltage which appears across R_L also varies with frequency.

The proportion (V_L) of V_S which appears across R_L is given by:

Figure 14. Potential divider



$$\frac{V_L}{V_S} = \frac{R_L}{R_L + Z_C}$$

where

$$Z_C = -jX_C = -\frac{j}{2\pi fC}$$

(j denoting √-1, and X_C being the reactance of the capacitive element. For simplicity, we ignore any resistive component of the film's impedance).

The above equations may be used in simple ways to calculate the voltage level expected to be observed in simple cases where the frequency of excitation is constant, and so a value of f can simply be substituted. In many real-world cases, however, there may be a distribution of signal energy over a band of frequencies. Then it becomes useful to consider the "frequency response" of the network.

Nintendo Exhibit 1066
IPR2024-00668 - Page 588

Frequency Response

This is illustrated in the following example graphs. First, a lin/lin plot is shown (Figure 15, linear y-scale or amplitude, plotted against linear x-scale or frequency) with the corresponding phase plot (Figure 16) also shown in lin/lin form. Following these is a log/log plot (Figure 17), which will be dealt with in a little greater detail.

Note that the phase curve indicates that at very low frequencies, the observed voltage will show significant phase deviation from the source (limiting at -90° or -π/2 radians at "dc" or zero Hz). The significance of this effect is great if the piezo film element is to be used as part of a control loop.

Figure 15. Magnitude response of R-C filter

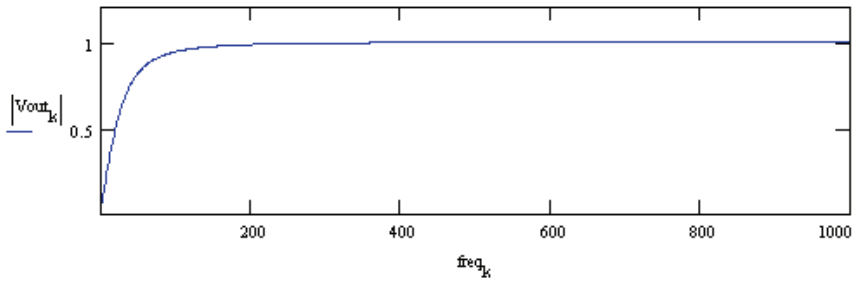


Figure 16. Phase response of R-C filter

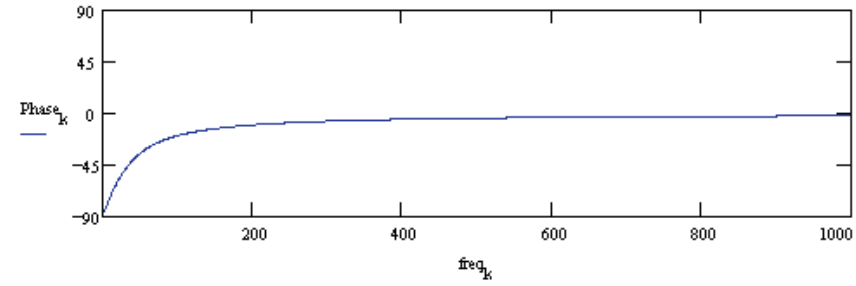
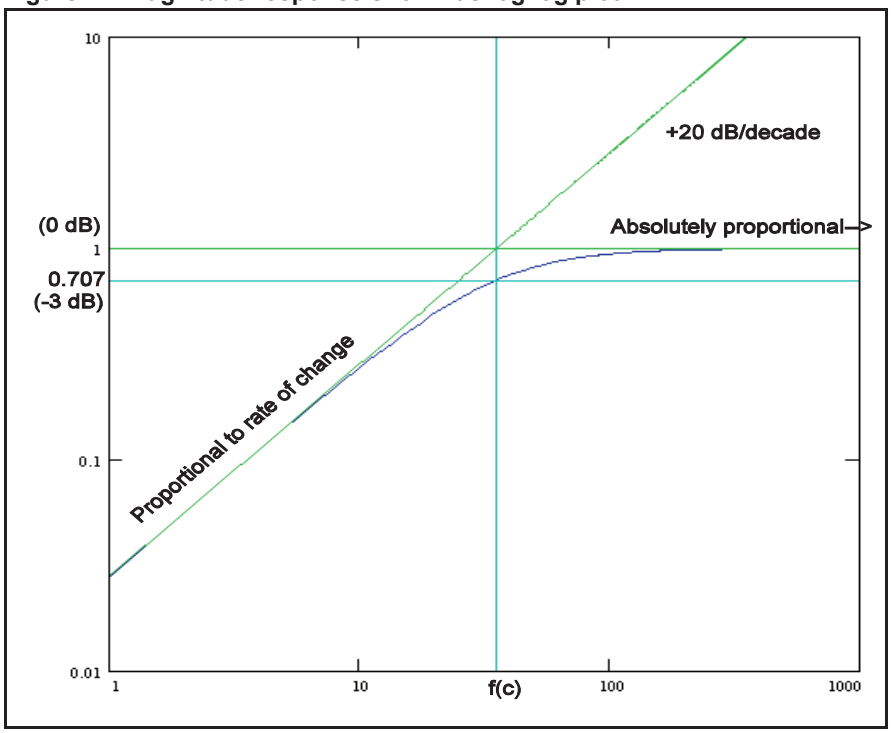


Figure 17. Magnitude response shown as log/log plot



Nintendo Exhibit 1066
IPR2024-00668 - Page 589

Analysis of the log/log R-C frequency response curve

Some key features:

- the overall characteristic of this network is known as a high-pass filter
- the frequency at which the magnitude falls to 0.707 or -3 dB is known as the "cut-off" or "corner" frequency of the high-pass filter
- this frequency can be calculated as $f(c) = 1/(2\pi RC)$, when both the resistance R and capacitance C are known
- at frequencies well *below* the cut-off frequency, the plot has the form of a straight line with gradient +20 dB/decade (in other words, doubling the frequency will double the signal amplitude) - this characteristic is identical with that of a *differentiator* network, and gives an output which is proportional to the *rate of change* of the input quantity
- at frequencies well *above* the cut-off frequency, the plot is level at "unity gain" and the output is directly proportional to the input quantity
- the filter characteristic can be approximated by these two intersecting straight lines, but the magnitude actually follows an asymptotic curve, with magnitude -3 dB at the cut-off frequency where the straight lines cross
- the filter characteristic can then be applied to the frequency-domain description of any practical signal by multiplying the filter transfer characteristic with the spectrum of the input signal, and deriving a response curve (output) which can in turn be transformed back into a time-domain signal.

Some practical examples of the effect of this filter characteristic will be shown next. For each signal, the time-domain description of the "perfect source" (e.g. the waveform which would be seen on an oscilloscope if the filter characteristic was absent) is given first, followed by its spectrum (obtained by use of the FFT [Fast Fourier Transform] algorithm supplied in the analysis software), then the filter characteristic (identical for all examples, but shown to emphasize the effect), then the resulting output signal spectrum obtained by multiplying the complex input spectrum by the complex filter characteristic, and finally the corresponding time-domain description obtained by inverse FFT, which shows the waveform an engineer would expect to observe in reality.

Note: in Figures 15, 16 and 17 the R-C values used to generate the curve were R = 1MΩ and C = 4.5 nF. In the following plots, the value of C was reduced to 1.5 nF. These values were chosen somewhat arbitrarily to demonstrate the principle, and so the scaling on the curves has not been annotated. But the time waveforms can be read in x units of seconds, and the frequency curves with x units of Hz. The cut-off frequency for R = 1MΩ and C = 1.5 nF is approximately 106 Hz.

Nintendo Exhibit 1066
IPR2024-00668 - Page 590

Key to following figures

Figure 18 shows a relatively high-frequency sine wave passing through the network. In the input spectrum, the signal is represented by a single spectral line at the appropriate frequency. This frequency is just below the filter "cut-off", and so is only slightly attenuated by the network. The resulting output wave is diminished in amplitude, and slightly shifted in phase.

Figure 19 shows the same process applied to a slower sine wave. In this case, the attenuation is much greater, and the phase shift more significant. This situation occurs when trying to monitor steady vibration at "too low" a frequency using a piezo sensor. The phase behavior may be significant if a control loop is to be implemented.

Figure 20 shows a harmonic series, with a number of discrete spectral lines all lying below the cut-off frequency. Each is attenuated to a different extent, and so the "balance" of harmonics in the output signal is altered.

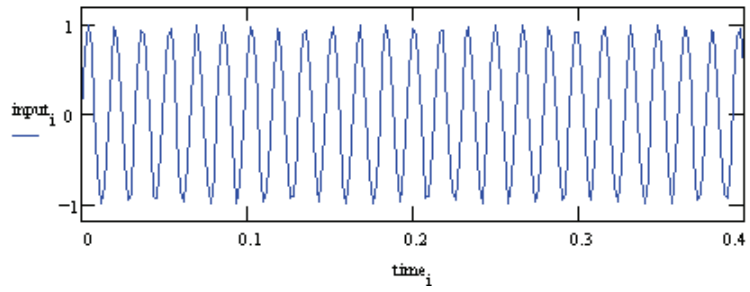
Figure 21 shows a slow half-sine input pulse (typical of many mechanical impact signals). Although the high-frequency content is largely unaltered, the output waveform appears heavily "distorted" and clearly shows both positive and negative excursions, whereas the input waveform is unipolar.

Figure 22 shows a sawtooth waveform with slowly rising "leading edge" followed by a "snap" descent back to zero. Many piezo switches detect this form of mechanical event. In the output waveform, the "leading edge" has almost disappeared, but the "snap" gives almost full amplitude. Note the polarity of the output pulse relative to the input waveform.

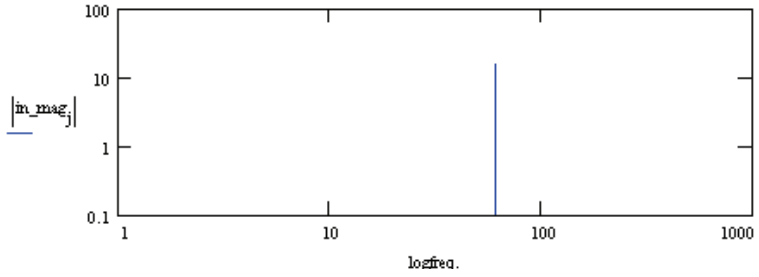
Nintendo Exhibit 1066
IPR2024-00668 - Page 591

Figure 18. Effect of R-C filter on High Frequency Sine Wave input waveform

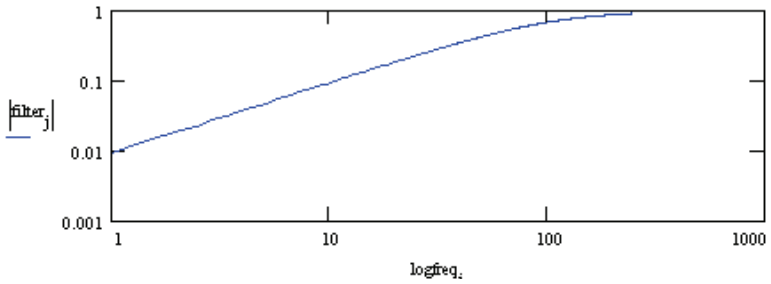
a) Input waveform



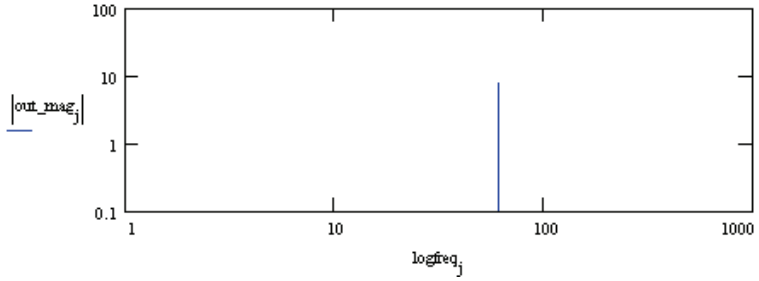
b) Input spectrum



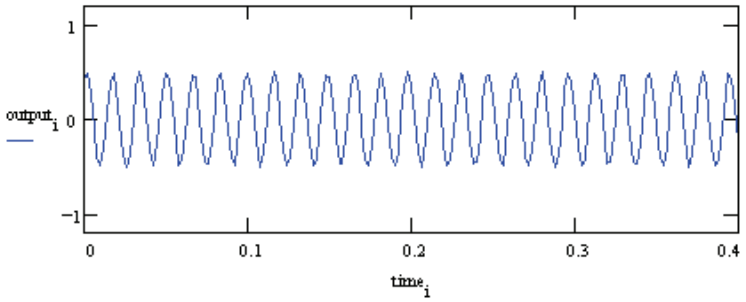
c) Filter characteristic



d) Output spectrum



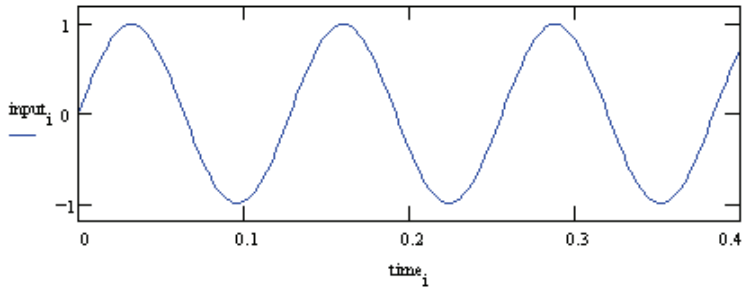
e) Output waveform



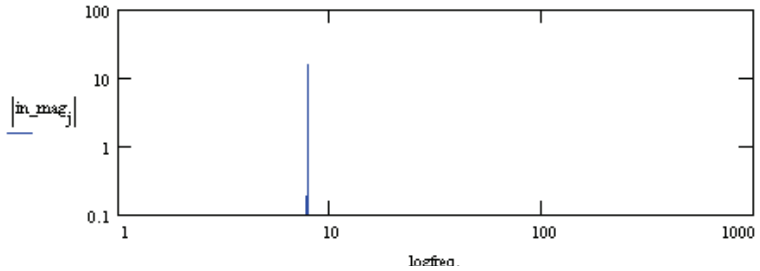
Nintendo Exhibit 1066
IPR2024-00668 - Page 592

Figure 19. Effect of R-C filter on Low Frequency Sine Wave input waveform

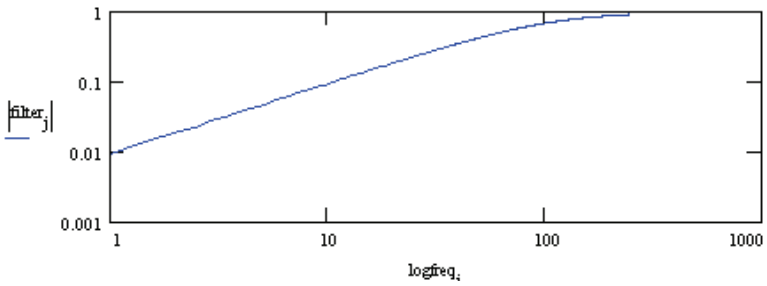
a) Input waveform



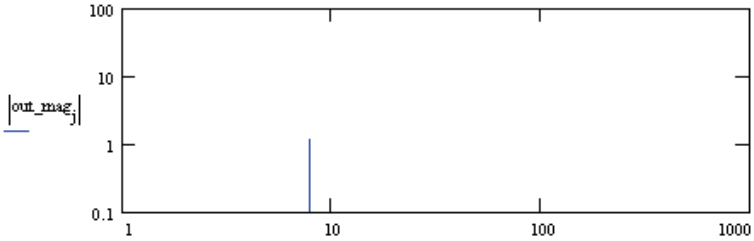
b) Input spectrum



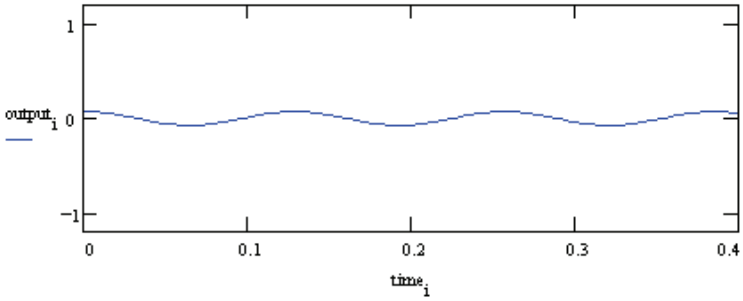
c) Filter characteristic



d) Output spectrum



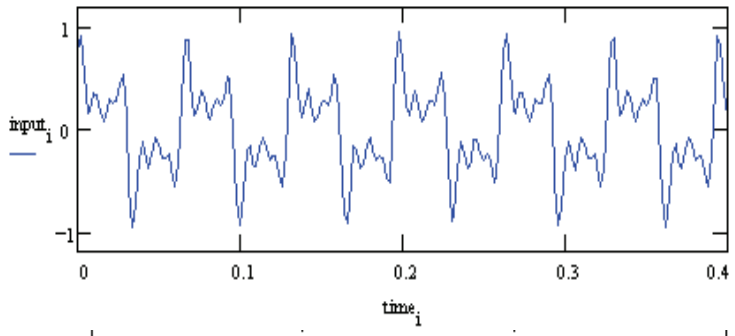
e) Output waveform



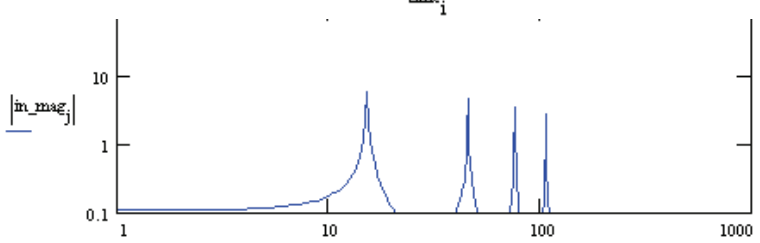
Nintendo Exhibit 1066
IPR2024-00668 - Page 593

Figure 20. Effect of R-C filter on Harmonic Series input waveform

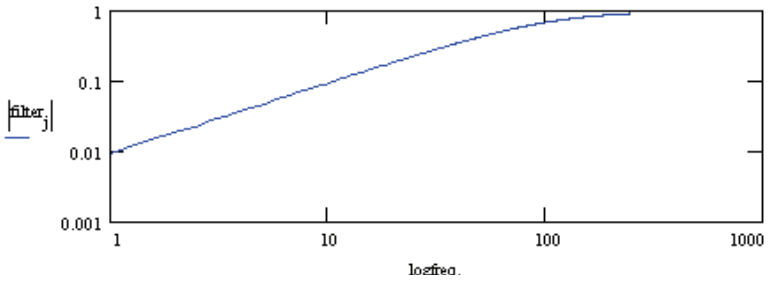
a) Input waveform



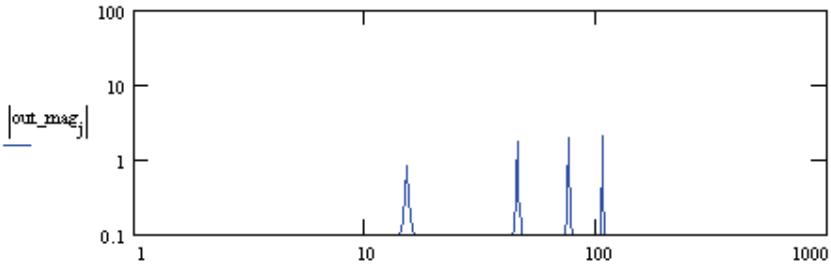
b) Input spectrum



c) Filter characteristic



d) Output spectrum



e) Output waveform

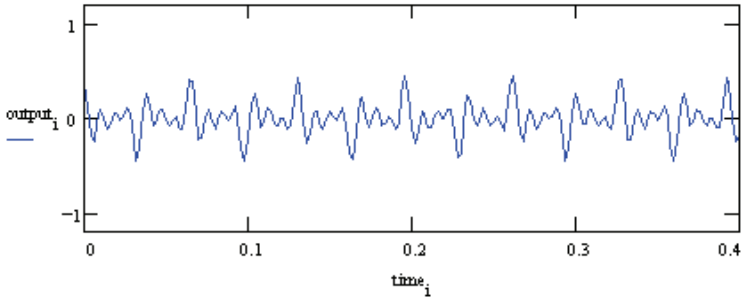
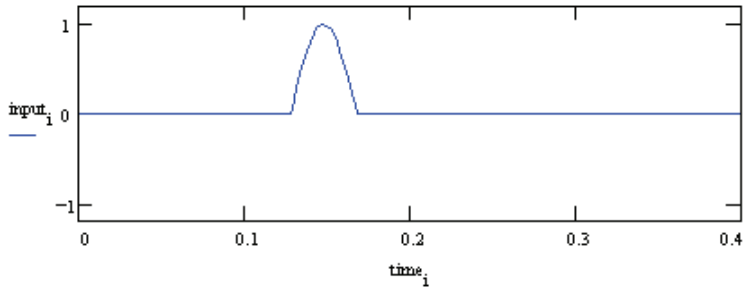
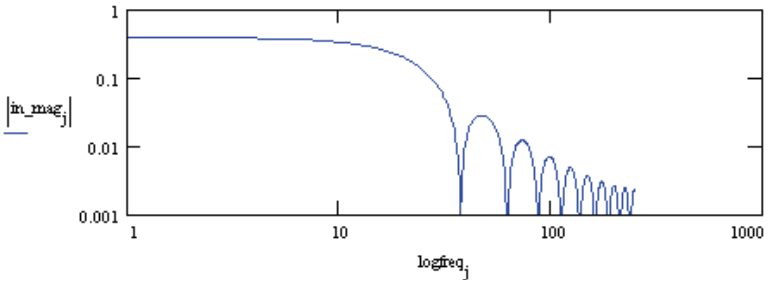


Figure 21. Effect of R-C filter on Slow Half-Sine Transient input waveform

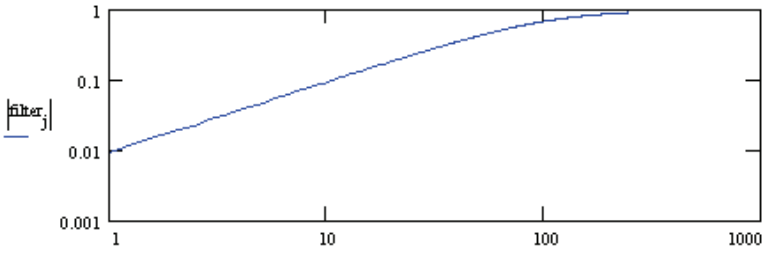
a) Input waveform



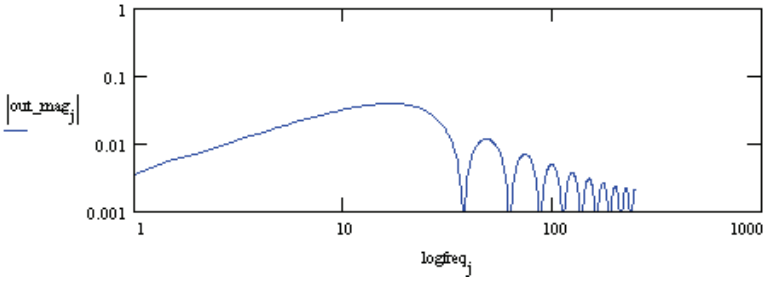
b) Input spectrum



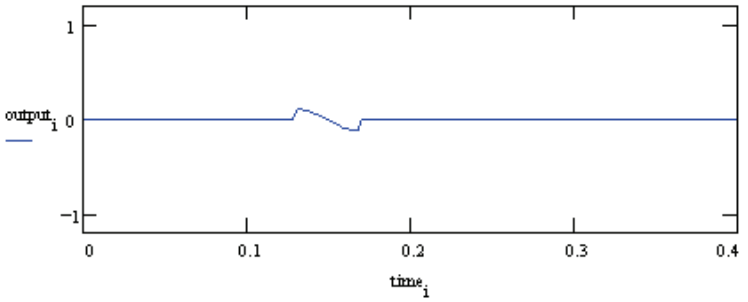
c) Filter characteristic



d) Output spectrum



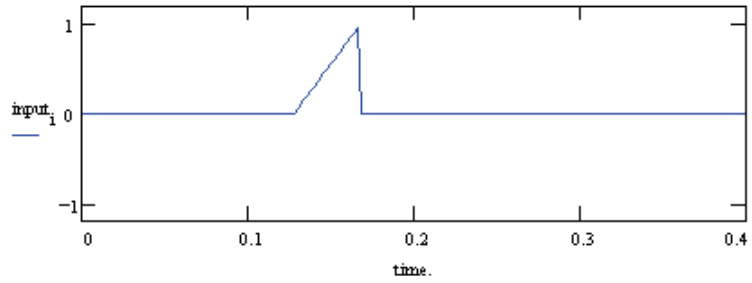
e) Output waveform



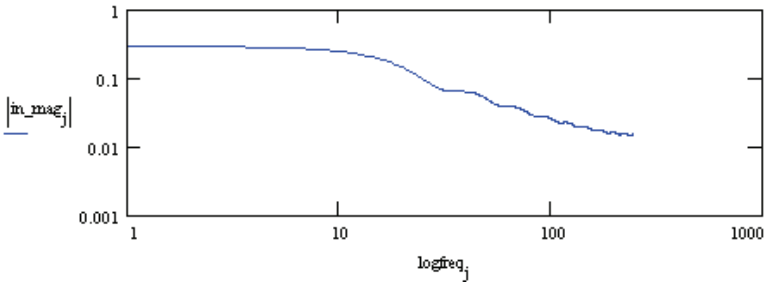
Nintendo Exhibit 1066
IPR2024-00668 - Page 595

Figure 22. Effect of R-C filter on Slow Sawtooth Transient input waveform

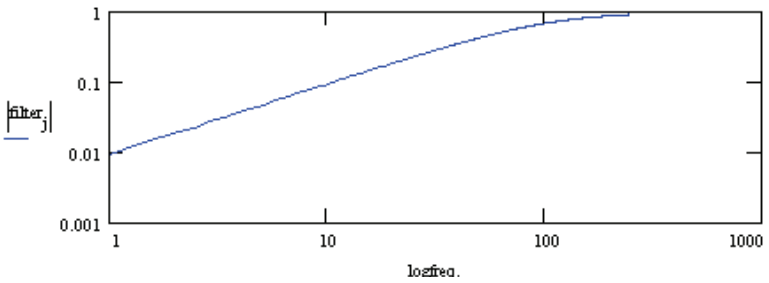
a) Input waveform



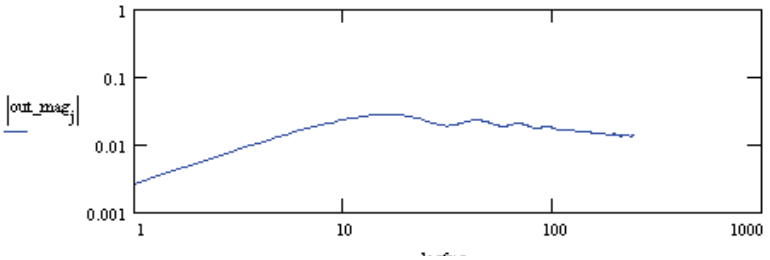
b) Input spectrum



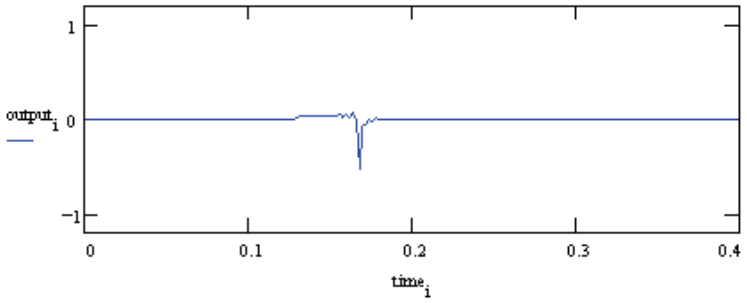
c) Filter characteristic



d) Output spectrum



e) Output waveform



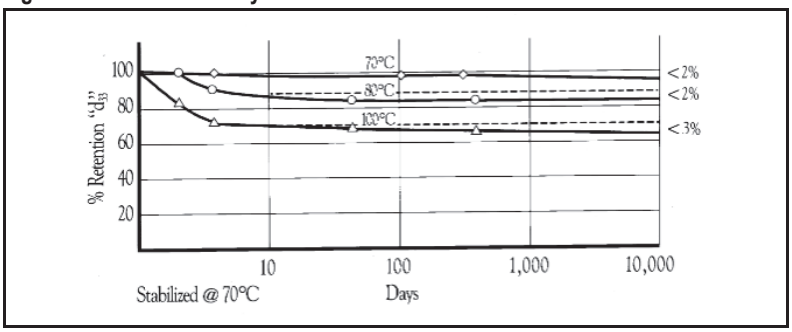
Nintendo Exhibit 1066
IPR2024-00668 - Page 596

TEMPERATURE EFFECTS

Many of the properties of piezo film change with excitation frequency and temperature. These properties are reversible and repeatable with either frequency or temperature cycling.

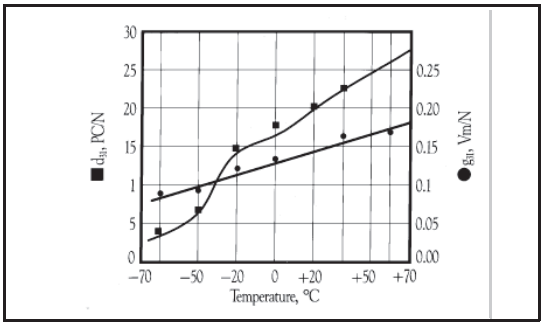
In addition, Figure 23 shows the permanent decay of the piezoelectric strain constant d_{33} for PVDF, annealed at 70°C, after long term exposure to elevated temperatures.

Figure 23. Thermal stability of d_{33} constant - 70 C annealed PVDF



Having reached a stabilizing temperature, the material properties then remain constant with time. Piezo film can be annealed to specific operating (or maximum storage) temperatures to achieve long-term stability for high temperature applications. Figure 24 shows the reversible temperature effects on d_{33} and g_{31} coefficients for PVDF.

Figure 24. Temperature coefficient for d_{33} and g_{31} constants - PVDF



In Figures 25a and 25b, the effect of temperature on the dielectric constant $(\varepsilon/\varepsilon_O)$ and dissipation factor $(\tan \delta_e)$ are shown for copolymer films.

Piezo films have been shown to offer excellent transducer properties at very low (cryogenic) temperatures.

Figure 25a. Dielectric loss tangent vs. temperature COPOLYMER

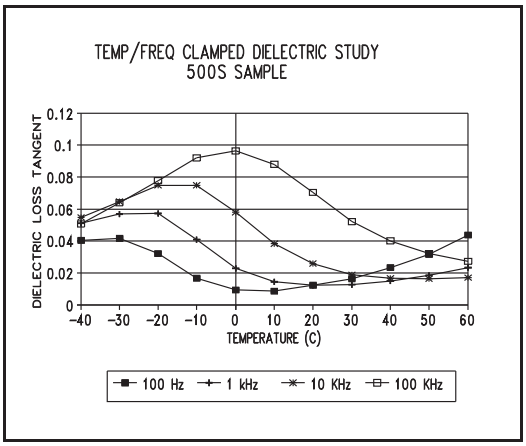
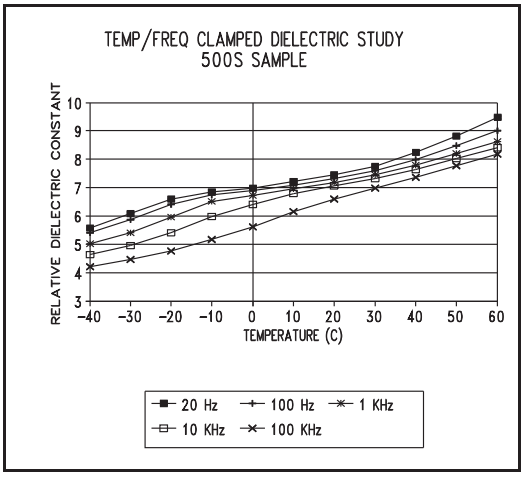


Figure 25b. Dielectric constant vs. temperature COPOLYMER



Nintendo Exhibit 1066
IPR2024-00668 - Page 597

PIEZOELECTRIC CABLE AND PROPERTIES

One of the most recent developments in piezo polymer technology is piezo cable. The cable has the appearance of standard coaxial cable, but is constructed with a piezoelectric polymer insulator between the copper braid outer shield and the inner conductor (Figure 26).

Protected by a rugged polyethylene jacket, the cable is used in buried or fence security systems, traffic sensors including vehicle classification and weight-in-motion systems, and taxiway sensors for aircraft identification, safety and security applications. Other applications include sensors for anti-tampering, door edge safety monitoring, floor mats, touch pads and panels, and patient mattress monitors. The new cables feature the same piezoelectric properties that are characteristic of piezo film sensors. The electrical output is proportional to the stress imparted to the cable. The long, thin piezoelectric insulating layer provides a relatively low output impedance (600 pF/m), unusual for a piezoelectric device. The dynamic range of the cable is substantial (>200 dB), sensing distant, small amplitude vibrations caused by rain or hail, yet responding linearly to the impacts of heavy trucks. The cables have withstood pressures of 100 MPa. The typical operating temperature range is -40 to +125°C. Table 4 lists typical properties for piezo cable.

Figure 26. Piezo cable construction

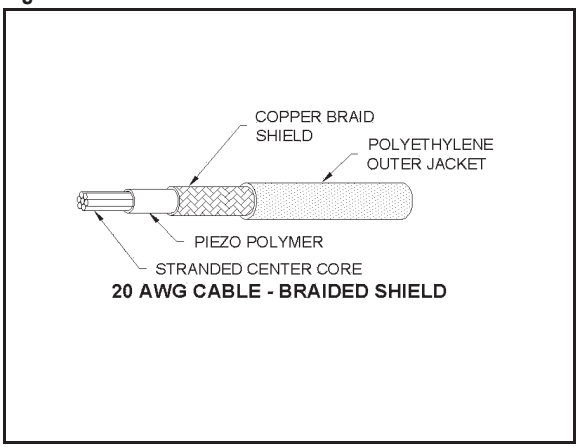


Table 4. Piezo Cable Typical Properties

Parameter	Units	Value
Capacitance @ 1KHz	pF/m	600
Tensile Strength	MPa	60
Young's Modulus	GPa	2.3
Density	kg/m^3	1890
Acoustic Impedance	MRayl	4.0
Relative Permittivity	@1KHz	9
tan δ_e	@1KHz	0.017
Hydrostatic Piezo Coefficient	pC/N	15
Longitudinal Piezo Coefficient	Vm/N	250×10^{-3}
Hydrostatic Piezo Coefficient	Vm/N	150×10^{-3}
Electromechanical Coupling	%	20
Energy Output	mJ/Strain (%)	10
Voltage Output	kV/Strain (%)	5

Nintendo Exhibit 1066
IPR2024-00668 - Page 598

Cable Typical Properties

The output sensitivity of piezo cable in response to increasing impact load is shown in Figure 27a. The linearity in output for increasing force as shown in Figure 27b is typical of all piezo cable gages.

PIEZOELECTRIC BASICS

Figure 27a. Sensitivity vs. load

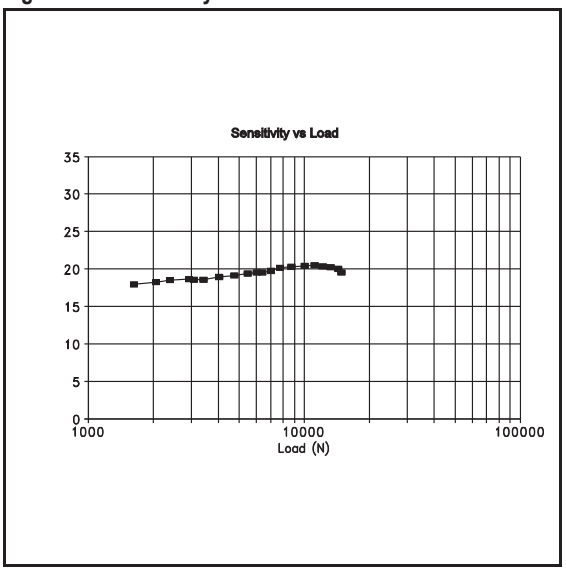
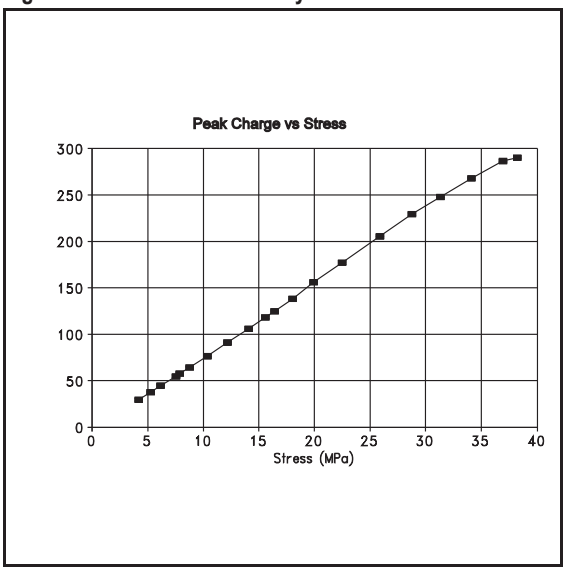


Figure 27b. Piezo cable linearity



Mechanical to Electrical

Like water from a sponge, piezoelectric materials generate charge when squeezed. The amplitude and frequency of the signal is directly proportional to the mechanical deformation of the piezoelectric material. The resulting deformation causes a change in the surface charge density of the material so that a voltage appears between the electroded surfaces. When the force is reversed, the output voltage is of opposite polarity. A reciprocating force thus results in an alternating output voltage.

Piezo film, like all piezoelectric materials, is a dynamic material that develops an electrical charge proportional to a change in mechanical stress. Piezoelectric materials are not suitable static measurements (true dc) due to their internal resistance. The electrical charges developed by piezo film decay with a time constant that is determined by the dielectric constant and the internal resistance of the film, as well as the input impedance of the interface electronics to which the film is connected. Practically speaking, the lowest frequency measurable with piezo film is in the order of 0.001Hz. There are methods to achieve true dc response, but these require using the piezo film as both an actuator and sensor, monitoring change in the actuation resulting from the dc event.

The fundamental piezoelectric coefficients for charge or voltage predict, for small stress (or strain) levels, the charge density (charge per unit area) or voltage field (voltage per unit thickness) developed by the piezo polymer.

Nintendo Exhibit 1066
IPR2024-00668 - Page 599

Charge Mode:

Under conditions approaching a short circuit, the generated charge density is given by:

$D = Q/A = d_{3n}X_n$ (n = 1, 2, or 3)

The mechanical axis *(n)* of the applied stress (or strain), by convention, is:

1 = length (or stretch) direction
2 = width (or transverse) direction
3 = thickness direction

where

D = charge density developed
Q = charge developed
A = conductive electrode area
d_{3n} = appropriate piezoelectric coefficient for the axis of applied stress or strain
n = axis of applied stress or strain
X_n = stress applied in the relevant direction

It is important to note that the d_{3n} coefficient is commonly expressed in pico-Coulombs per Newton (pC/N), but the more correct form would be $(pC/m^2)/(N/m^2)$ since the areas (m^2) upon which the stresses or strains apply are very often different and cannot be "canceled".

Voltage Mode:

The open-circuit output voltage is given by:

$V_o = g_{3n}X_nt$ (*n* = 1, 2, or 3, as above)

where

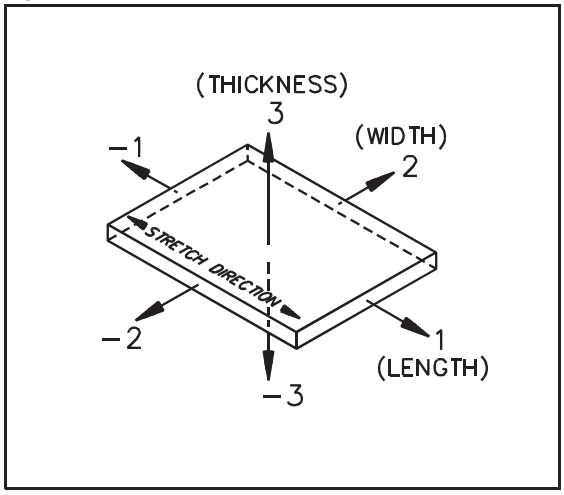
g = appropriate piezoelectric coefficient for the axis of applied stress or strain
X_n = applied stress in the relevant direction
t = the film thickness

Piezo Coefficients:

The most widely used piezo coefficients, d_{3n} and g_{3n}, charge and voltage respectively, possess two subscripts. The first refers to the electrical axis, while the second subscript refers to the mechanical axis. Because piezo film is thin, the electrodes are only applied to the top and bottom film surfaces. Accordingly, the electrical axis is always "3", as the charge or voltage is always transferred through the thickness (n = 3) of the film. The mechanical axis can be either 1, 2, or 3, since the stress can be applied to any of these axes, as shown in Figure 28.

Typically, piezo film is used in the mechanical 1 direction for low frequency sensing and actuation (< 100KHz) and in the mechanical 3 direction for high ultrasound sensing and actuation (> 100KHz).

Figure 28. Numerical classification of axes



Nintendo Exhibit 1066
IPR2024-00668 - Page 600

Directionality:

Piezoelectric materials are anisotropic. This means that their electrical and mechanical responses differ depending upon the axis of applied electrical field or axis of mechanical stress or strain. Calculations involving piezo activity must account for this directionality.

EXAMPLE 1:

A 1.45 psi load (10,000 N/m^2) is applied to a piezo film switch of 2.54 cm length, 2.54 cm width and 110μm in film thickness. The switch element is rigidly backed, so the force acts to compress the film's thickness (therefore g_{33} mode). In this example the load acts on the length by width area of the piezo film. The open circuit voltage developed across the thickness of the piezo film is:

$$V_o = -g_{33} X t$$

$$g_{33} = -339 \times 10^{-3} \frac{V/m}{N/m^2}$$

where:

V/m is Volts out per meter of piezo film thickness

N/m^2 is stress applied to the relevant film area. The conversion from psi to N/m^2 is approximately 7,000.

$$V_o = -\left(-339 \times 10^{-3} \frac{V/m}{N/m^2} \right) (-10{,}000\, N/m^2)(110 \times 10^{-6} m)$$

$$V = -0.373 \text{ volts}$$

EXAMPLE 2:

The same piezo film element as in EXAMPLE 1 is subjected to a force (10,000 N/m^2 x $0.0254 m^2$ = 6.45 Newtons), but in this example, the film switch is configured as a membrane having a compliant backing. Now, the force acts on the thickness cross-sectional area (wt). The piezo film is being stretched by the load, so it is acting in the g_{31} mode.

$$V_o = -(3g_{31})\left(\frac{F}{wt}\right)(t) = -(g_{31})\left(\frac{F}{w}\right)$$

$$g_{31} = 216 \times 10^{-3} \frac{V/m}{N/m^2}$$

$$V_o = -\left(216 \times 10^{-3} \frac{V/m}{N/m^2} \right)\left(\frac{6.45 N}{2.54 \times 10^{-2} m} \right)$$

$$V_o = -54.9 \text{ volts}$$

The sharp increase in output voltage results because the force is applied to the much smaller cross-sectional area of the film. The small area results in a correspondingly higher stress.

Nintendo Exhibit 1066
IPR2024-00668 - Page 601

Dynamic Range

Piezo film has a vast dynamic range. The sensor has been used to detect the impact of high speed particles in space having a mass of 10^{-12} grams, and at the other extreme, measures shock waves at 300,000 atmospheres produced during weapons testing. A recent study was conducted to determine the maximum output energy of a 52μm thick film, having an area of 155.5 mm x 18.5 mm. The film was subjected to approximately 350 MPa (in the stretch or "n = 1" direction) without failure. The charge generated was found to be very linear, with the following measurements made at maximum applied stress:

Maximum Charge Observed: 20μC, giving 6.95 mC/m^2
Maximum Voltage Observed: 1600 V, giving 30.8 x 10^6 V/m
Maximum Energy Converted: 30.9 mJ, giving 207 kJ/m^3

Later experiments showed that about 10% of the above energy levels can be sustained for long periods of time without measurable damage to the piezo film element.

Electrical to Mechanical

When a voltage is applied to a sheet of piezo film, it causes the film to change dimensions due to the attraction or repulsion of internal dipoles to the applied field.. With one voltage polarity is applied, the piezo film becomes thinner, longer and wider. The opposite polarity causes the film to contract in length and width and become thicker. An ac voltage causes the film to "vibrate".

The amount of deformation is given by the piezoelectric "d_{3n}" constant:

for **length** change $\Delta l = l d_{31} V/t$

where

Δl = change in film length in meters
l = original film length in meters
d_{31} = piezoelectric coefficient for length ("n=1" direction) change in meters per volt
V = applied voltage across the thickness (t)

for **width** change $\Delta w = w d_{32} V/t$

where

d_{32} = piezoelectric coefficient for width ("n=2" direction) change

for **thickness** change $\Delta t = t d_{33} V/t = d_{33} V$

where

d_{33} = piezoelectric coefficient for thickness ("n=3" direction) change

Nintendo Exhibit 1066
IPR2024-00668 - Page 602

EXAMPLE 3:

A piezo film of 3 cm length (l), 2 cm width (w) and 9μm thickness (t) is subjected to an applied voltage of V=200 volts in the 3 (thickness) direction. The amount of strain S resulting from this electrical input is d times the applied field.

In the 1 direction:

$$S_1 = \frac{\Delta l}{l} = d_{31}(V/t) \quad \text{where } d_{31} = 23 \times 10^{-12} \frac{m/m}{V/m}$$

$$\Delta l = d_{31}(V/t)\, l = \left(23 \times 10^{-12} \frac{m/m}{V/m}\right) \frac{(200\,V)(3 \times 10^{-2} m)}{(9 \times 10^{-6} m)}$$

$$\Delta l = 1.53 \times 10^{-5} m \quad \text{or} \quad 15.3\ \mu m$$

In the t direction:

$$\Delta t = t d_{33}(V/t)\, l = d_{33} V = \left(-33 \times 10^{-12} \frac{m/m}{V/m}\right)(200\,V) = 6.6 \times 10^{-9} m \text{ or } 66 Å$$

Actuators

Generally, piezo film actuator designs depend on the application requirements such as operating speed, displacement, generated force, and available electrical power. Piezo film technology offers various design options to meet such application requirements. Those design options include:

- Customized electrode patterns on one or both sides of the piezo film sheet.
- Multilaminate structures or bimorphs.
- Fold-over or scrolled multilayer structures.
- Extruded piezo tubes and piezo cables.
- Cast piezo polymer on various substrates
- Molded 3-D structures.

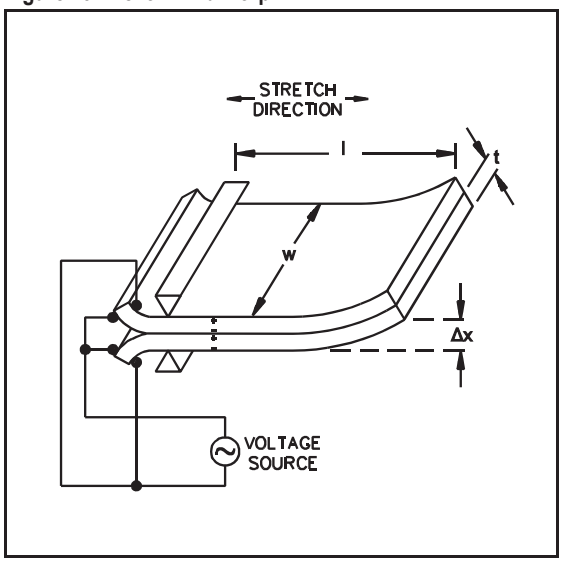
Each design option mentioned above has advantages and disadvantages. For example, scrolled multilayer actuators can generate a higher force but may sacrifice some displacement.

Bimorph

Like a bimetal strip, two sheets of piezo film of opposite polarities, adhered together form a bending element, or "bimorph" (Figure 29). An applied voltage causes one film to lengthen, while the other contracts, causing the unit to bend. An applied voltage of opposite polarity bends the bimorph in the opposite direction.

The bimorph configuration converts small length changes into sizable tip deflections, but producing low force.

Figure 29. Piezo film bimorph



Nintendo Exhibit 1066
IPR2024-00668 - Page 603

Thicker films and multilayers improve the force developed by the bimorph, but sacrifice displacement unless the unit can be operated at higher fields.

The amount of tip deflection and the force developed are given by:

$$\Delta x = 3/4 d_{31}(l^2/t^2)V \quad \text{meters}$$

and

$$F = 3/2 Y w d_{31}(t/l)V \quad \text{Newtons}$$

where

Δx = displacement at dc
F = generated force
d_{31} = piezoelectric coefficient in the "1" direction
l,t,w = length, thickness, and width of piezo film
V = applied voltage (Volts)
Y = Young's modulus of piezo film ($2 \times 10^9 N/m^2$)

By applying an ac voltage, the bimorph can act as a fan, similar to an insect wing. Although the piezo film bimorph does exhibit a dc response, maximum tip deflections are obtained when the unit is operated at resonance, determined by the length and thickness of the bimorph beam.

EXAMPLE 4:

100 volts are applied across a 2 cm long cantilever bimorph comprised of two strips of 9 μm PVDF. The resultant tip displacement Δx is:

$$\Delta x = \frac{3/4 V d_{31} l^2}{t^2}$$

$$\Delta x = \frac{3/4(100\,V)\left(23 \times 10^{-12}\,\frac{m/m}{V/m}\right)(2 \times 10^{-2}\,m)^2}{(9 \times 10^{-6}\,m)^2}$$

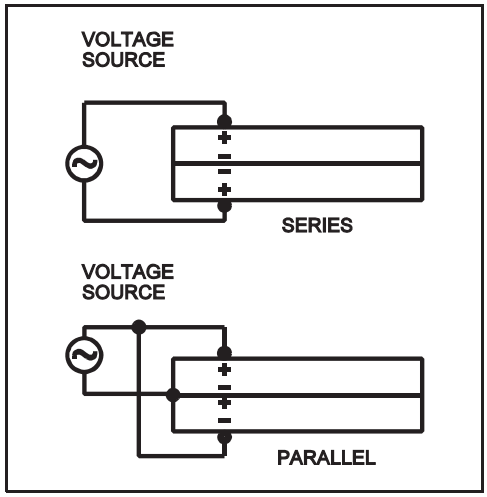
$$\Delta x = 8.52mm$$

As shown in the equations, more displacement can be obtained from a longer bimorph. Larger forces can be obtained from a wider bimorph. The ratio of displacement at a resonance frequency and dc is defined by Q which indicates a mechanical gain. A typical Q value for a piezo film bimorph is 20 to 25.

For example, a 5 mm long 70μm thick bimorph with 120 volts dc creates a displacement of 57μm. With the same bimorph, however, displacement can be 1.4 mm at the resonant frequency of 580 Hz. For applications that require a higher force, such as cooling fans, multilayer construction can be considered. The resulting output force is proportionally increased by the number of layers.

In terms of electrical connections to the bimorph, there are two basic methods as shown in Figure 30 — parallel and series connections. In order to generate the same amount of displacement, the parallel connection requires a lower voltage than the series connection. Series connections, on the other hand,

Figure 30. Lead attachment methods for a bimorph



Nintendo Exhibit 1066
IPR2024-00668 - Page 604

draw less current than parallel connections. For both parallel and series connections, the total electrical power to the actuator is identical. However, it is obvious that the lead attachment of the series connection is much simpler than that of the parallel connection for manufacturing purposes. Typical applications of the bimorph bender are cooling fans, toys, and decoratives.

Scrolled Actuator

The generated force and displacement of a scrolled piezoelectric cylinder in Figure 31 are expressed as follows:

$x = d_{31}El$ Meters

$E = V/t$ Volts/meters

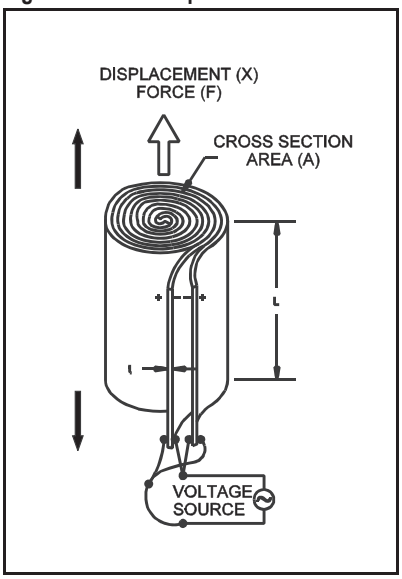
$F = Yd_{31}EA$ Newtons

$$f = (1/2\pi)\sqrt{YA/l(M_e + 0.405M_p)}$$

where

x = displacement at dc (meter)
F = generated force (Newton)
f = resonance frequency
l,t = Length, thickness of piezo film (meters)
M_e = externally loaded mass (kilograms)
M_p = piezo actuator mass (kilograms)
A = cross sectional area (m^2)
Y = Young's modulus (N/m^2)
E = electrical field (volt/meter)

Figure 31. Scrolled piezo film actuator



As shown in the equations, a scrolled actuator can generate more force and can respond with a higher resonant frequency by increasing the cross sectional area. A longer actuator generates more displacement but reduces the response speed. Note that the actuator output, with $M_e = 0$, will be maximized when the length *l* is adjusted to satisfy the resonant condition. As an example, the performance of a 12 mm diameter, 25 mm long scrolled actuator can be maximized at 32 KHz operation.

Folded Actuator

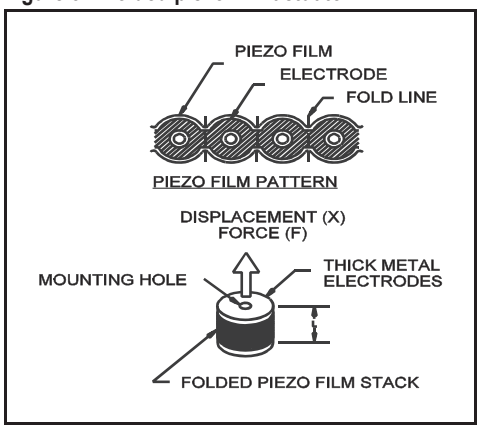
Another design option for a high speed, high force actuator is to fold over a long sheet of piezo film as shown in Figure 32. This design effectively creates a parallel wired stack of piezo film discs. The center hole is used to secure the actuator to a base. Design equations of the scrolled actuator also can be applied to this type of actuator. In the previous equations, d_{31} should be replaced with d_{33} ($-33x10^{-12}$ C/m^2) for a folded actuator. An example of specifications for the folded actuator is shown below:

Displacement: 1 μm/1 mm length
Generated force: 15 kg/10 mm dia.
Frequency: dc - 100 kHz
Drive voltage: 800 volts

Nintendo Exhibit 1066
IPR2024-00668 - Page 605

Compared to mechanical or piezo ceramic actuators, multilayer piezo film actuators have fewer ringing problems due to their lower Q. Applications of multilayer actuators are micropositioners for industrial equipment, acoustic wave generators and ink jet printers.

Figure 32. Folded piezo film actuator

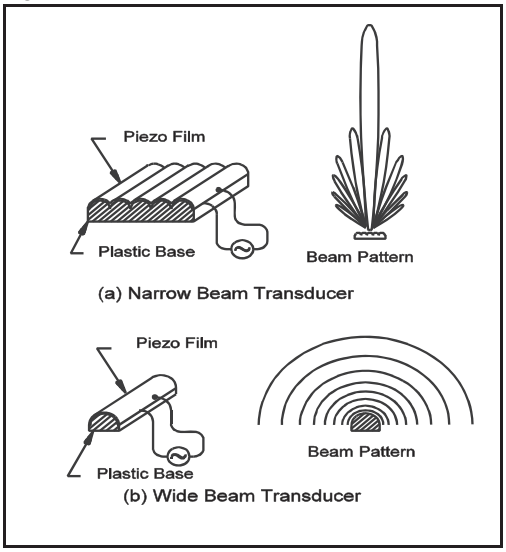


Ultrasonic Actuators

Ultrasonic actuators, as discussed in this section, exclude very high frequency (> 1 MHz) transmitter applications. The use of piezo film in these very high frequency applications, like medical ultrasound imaging and nondestructive testing, use thickness mode operation, d_{33}.This section deals with low frequency ultrasound (20-100 KHz) where the piezo film can be used in the length change (d_{31}) mode.

The advantage of piezo film in low frequency ultrasound can be found from the flexibility of the material. Piezo film can be easily curved or formed to make circular transducers as shown in Figure 33. The beam pattern is determined by the number of half circular elements and their diameter. The operating frequency is determined by the diameter of the half circular elements. Note that the difference between Figures 33(a) and 33(b) is their number of active elements and diameters. To widen the beam coverage, the number of active elements should be reduced. With a cylindrical transducer, a 360° beam pattern is obtained.

Figure 33. Piezo film ultrasound transducers



In ultrasound applications, a narrow beam with minimum side lobes is required for remote distance measurements. On the other hand, a wide beam, as wide as 180° or more, is required for applications like automobile rear bumper proximity sensing. Figure 33 shows design configurations for both narrow beam and wide beam ultrasound transducers. The applications for piezo film in through-air ultrasonic actuators include distance ranging for air pen, air mouse, white board digitizer, collision avoidance, physical security systems, air flow velocity (doppler) sensors, and inter-object communications. Similar constructions can be produced for underwater or fluid sensing, including flow sensors, level sensors, and communications.

PYROELECTRIC BASICS

Piezoelectric polymers, such as PVDF and its copolymers of VF_2/VF_3, are also pyroelectric. Pyroelectric sensor materials are normally dielectric materials with a temperature-dependent dipole moment. As these materials absorb thermal energy, they expand or contract, thereby inducing secondary piezoelectric signals. As piezo film is heated, the dipoles within the film exhibit random motion by thermal agitation. This causes a reduction in the average polarization of the film, generating a charge build up on the film surfaces. The output current is proportional to the rate of temperature change (ΔT). The amount of electrical charge produced per degree of temperature increase (or decrease) is described by the pyroelectric charge coefficient, ρ.

Nintendo Exhibit 1066
IPR2024-00668 - Page 606

The charge and voltage produced in a given film of area A permittivity ε, and thickness t is given by :

$Q = p\Delta TA$

$V = pt\Delta T/\varepsilon$

EXAMPLE 5:

A piezo film pyroelectric detector having a film thickness (t) of 9μm, a permittivity (ε) of 106×10^{-12} C/Vm and a pyroelectric coefficient (p) of 30×10^{-6} C/(m^{2o}K), undergoes a temperature increase (ΔT) of 1°K due to incident IR radiation. The output voltage is given by:

$$V = \frac{(30 \times 10^{-6} C/m^{2\circ}K)(9 \times 10^{-6} m)(1^\circ K)}{(106 \times 10^{-12} C/Vm)}$$

$V = 2.55$ volts

The pyroelectric voltage coefficient of piezo film is about an order of magnitude larger than those of Lead Zirconate Titanate (PZT) and Barium Titanate ($BaTiO_3$). Table 5 compares the pyroelectric properties of these materials, but a far lower figure of merit due to the low capacitance of PVDF.

Table 5. Comparison of pyroelectric materials

Material	TGS	$LiTaO_3$	$BaTiO_3$	PZT	$PbTiO_3$	PVDF	VF_2VF_3
ρ_Q	350	200	400	420	230	30	50
$\varepsilon/\varepsilon_O$	30	45	1000	1600	200	10.7	8.0
α	.16	1.31	1.00	.44	.67	.06	.06
L	225	646	564	374	461	138	138
P_v	1.32	.50	.05	.03	.10	.47	.71
M_l	.53	.16	.02	.01	.03	.20	.31
Pyroelectric Charge Coefficient				$(\rho_Q)\mu Coul/[m^2 \bullet {}^\circ K]$			
Dielectric Constant				$(\varepsilon/\varepsilon_o)$,where $\varepsilon_o = 8.85pF/m$			
Thermal Diffusivity				$(\alpha)m^2/sec \bullet 10^{-6}$			
Thermal Diffusion Depth @ 1Hz				$(L)\mu m$			
Pyroelectric Voltage Coefficient				$(P_V)\rho_Q/\varepsilon$, $V/[\mu m \bullet {}^\circ K]$			
Figure of Merit				$(M_l)\rho_Q/[C_V \bullet \varepsilon]$, $V \bullet mm^2/J$			

Nintendo Exhibit 1066
IPR2024-00668 - Page 607

Piezo film advantages including:

— moisture insensitivity (<.02% H_2O absorption)
— low thermal conductivity
— low dielectric constant
— chemical inertness
— large detector sizes

The pyroelectric response of piezo film can also become a noise source for piezo sensor applications at low frequencies. In piezoelectric applications where low frequency strain sensing is desired, there are several convenient methods to "common-mode reject" the pyroelectric response. Examples include:

- Two equal sized electrode patterns on one piezo film element; one electrode oriented parallel to the d_{31} and the other electrode pattern is perpendicular to the d_{31} direction. Both develop equal signals in response to pyro, but the electrode area parallel to the d_{31} develops about 10X the perpendicular electrode pattern. Subtracting the signals yields a pure piezo response.
- Two equal sized piezo film elements, laminated in a stacking configuration; one film has d_{31} parallel to strain surface, the other has d_{31} perpendicular to strain surface. As above, signals are subtracted to isolate the piezo response from pyro.
- Several other common mode rejection techniques can be described by MSI's applications engineers.

For higher frequencies, where the rate of temperature change seen by the piezo film element is slower than the strain event to be measured, frequency filters readily sort out the unwanted pyro signal.

BASIC CIRCUIT CONCEPTS

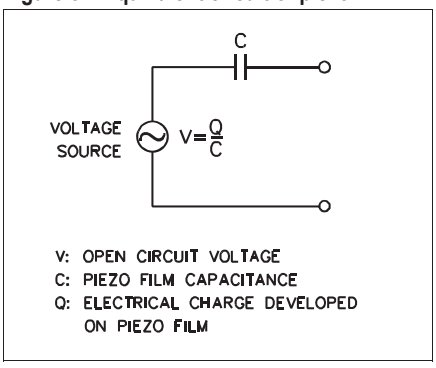
A properly designed interface circuit plays a key role in the optimization of piezo film sensors. The applications of piezo film span from toys to military sensors and interfacing to electronics is highly application dependent. In many cases, piezo film can be directly connected to electronic circuits without special interface considerations. However, for those cases where an interface circuit is required, the following 3 steps are recommended:

1. Consider the frequency range and signal amplitude requirements over the desired dynamic range.
2. Choose a proper load resistance to assure the low end operating frequency and to minimize signal loss due to the loading effect.
3. Select a buffer circuit if the signal level is small. If a high value load resistance is needed (such as 22MΩ or higher value), a low leakage high impedance buffer amplifier is recommended. JFET's or CMOS operational amplifiers are commercially available for a buffer.

Simplified Equivalent Circuits

The first step in an interface circuit design is to understand the piezo film characteristics as part of an electrical equivalent circuit. Figure 34 shows a simplified equivalent circuit of piezo film. It consists of a series capacitance with a voltage source. The series capacitance C_f represents piezo film capacitance which is proportional to the film

Figure 34. Equivalent circuit of piezo film

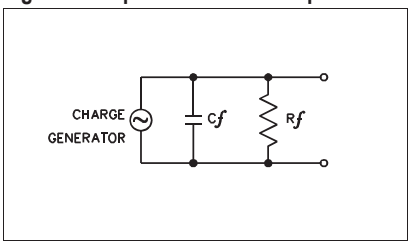


Nintendo Exhibit 1066
IPR2024-00668 - Page 608

permittivity and area and inversely proportional to film thickness. The voltage source amplitude is equal to the open circuit voltage of piezo film and varies from microvolts to 100's of volts, depending on the excitation magnitude. This simplified equivalent circuit is suitable for most applications but is of limited value at very high frequencies such as that used in ultrasound transducers.

Figure 35 shows an equivalent circuit as a charge generator. This equivalent circuit has film capacitance C_f, and internal film resistance R_f. The induced charge Q is linearly proportional to the applied force as described earlier. The capacitance C_f is proportional to the surface area of film and is inversely proportional to the film thickness. In low frequency applications, the internal film resistance R_f is very high and can be ignored. The open circuit output voltage can be found from the film capacitance; i.e., $V=Q/C_f$.

Figure 35. Equivalent circuit for piezo film

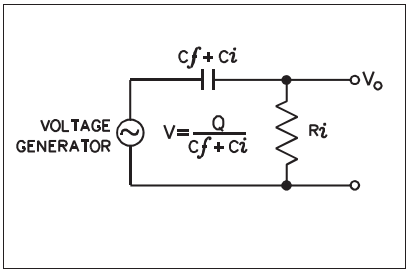


Input Resistance

The most critical part of an interface circuit is the input resistance. The input resistance affects low frequency measurement capability as well as signal amplitude. This is called the "loading effect".

Piezo film capacitance can be regarded as an equivalent source impedance. It is important to note that this source impedance increases with decreasing film capacitance and decreasing frequency of operation. This source impedance combined with the input resistance produces a voltage divider. As the ratio of input resistance to source impedance is decreased, the overall output voltage is reduced. Therefore, choosing a proper input resistance for the electronic interface is critical in minimizing the loading effect.

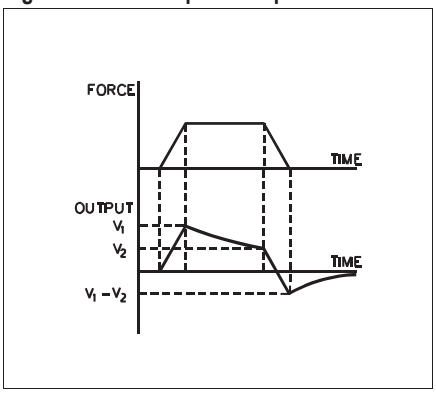
Figure 36. Equivalent circuit of piezo film with input resistance of electronic interface



Time Constant

In addition to input resistance, the input capacitance of an interface circuit can also affect the output. Figure 36 shows the equivalent circuit of film with input resistance R_i and input capacitance C_i. A typical time domain response of piezo film is shown in Figure 37 . The charge developed on the film due to an applied force decays with a time constant which is defined by $R_i(C_f + C_i)$.

Figure 37. Time response of piezo film



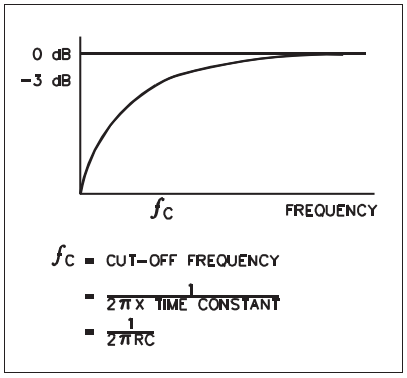
This time constant represents the time required for a signal to decay to 70.7% (-3dB) of its original amplitude. The smaller the time constant, the quicker the signal decays. Because of this finite time constant, piezo film is suitable for dynamic measurements rather than static measurement (0.001 Hz minimum).

If a long time constant is desired, a high input resistance and film capacitance can be used. It should be understood, however, that a high input resistance can also produce higher noise, requiring compensation through shielding, etc.

Nintendo Exhibit 1066
IPR2024-00668 - Page 609

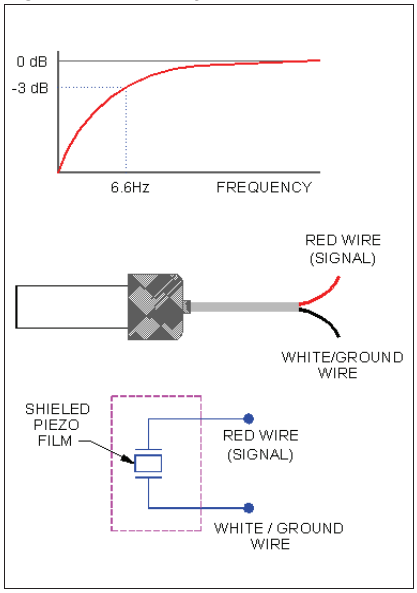
Frequency Response

Figure 38. High pass filter characteristic of piezo film



Another important aspect of the time constant can be seen in the frequency response of the equivalent circuit. The circuit exhibits an RC high-pass filter characteristic as shown in Figure 38. In this figure, the vertical axis implies the ratio of observable output signal to the developed signal (open circuit voltage of the piezo film). Zero dB implies no loss of signal. The cutoff frequency (3 dB down) is inversely proportional to the time constant. When a piezo film sensor is operated below this cut-off frequency, the output signal is significantly reduced. For a low frequency measurement, an input resistance needs to be high enough so that the cut-off frequency is well below the desired operating frequency. This consequence can be verified from consideration of the time constant as well as the loading effect.

Figure 39. Frequency response of SDT1



As an example, the frequency response of a shielded piezo film sensor (model SDT1) is shown in Figure 39. In this example, the SDT is interfaced with a circuit which contains a 10MΩ load resistor and an FET. The capacitance of the piezo film is 2.4 nF. With 10MΩ load resistance, the time constant becomes 24 msec and thus, the cut-off frequency is 6.6 Hz. For comparison, the cut-off frequency can be reduced to 0.66 Hz if a 100MΩ resistor is used instead of the 10MΩ resistor. This sensor component can be used for any application operating above the cut-off frequency determined by the resistance value.

In applications where the electronic circuit cannot be placed near the sensor, a buffer circuit is recommended close to the sensor. The buffer circuit converts the high output impedance of the piezo film element into a low output impedance and thus minimizes the signal loss and noise through the cable. For large size (i.e., high capacitance) piezo film sensors a buffer may not be required, even with small signals and long cables.

When a high piezo film output impedance is required, a low-leakage, high impedance buffer is necessary. For example, infrared motion sensor and accelerometer applications require up to 50GΩ of input resistance to obtain a very low frequency response. For such cases, the input impedance of the buffer must be much higher than the output resistance of the piezo film in order to maintain the low frequency response. In addition, minimum leakage current of the buffer is critical in order to maximize the measurement accuracy. Some examples of low leakage buffer electronics include: JFET - 4117 (Siliconix, Sprague); Operational amplifiers — LMC660, LF353 (National Semiconductor), OP80 (PMI), and 2201 (Texas Instruments).

Figure 40. Unity gain buffer for piezo film sensors

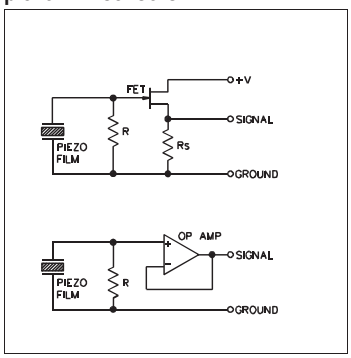


Figure 40 shows unity gain buffer circuit examples for general applications. Operational amplifiers offer a great deal of versatility as both buffers and amplifiers. They can be used as either charge-mode or voltage-mode amplifiers. Figure 41 shows basic charge and voltage amplifier configurations. The voltage output of the charge

Nintendo Exhibit 1066
IPR2024-00668 - Page 610

amplifier is determined by Q/C_f. Q is the charge developed on the piezo film and C_f is the feedback capacitance of the charge amplifier.

The output voltage of the charge amplifier depends on the feedback capacitance, not the input capacitance. This indicates that the output voltage of a charge amplifier is independent of the cable capacitance. The major advantage of a charge amplifier can be realized when a long cable is used between a piezo film sensor and electronics. In addition, it also minimizes charge leakage through the stray capacitance around the sensor. Otherwise, simple voltage amplifiers are sufficient for most applications. Included in Figure 41 is a typical non-inverting voltage amplifier.

The advantage of a voltage amplifier can be seen when ambient temperature is considered. The voltage sensitivity (g-constant) variation over temperature is smaller than the charge sensitivity (d-constant) variation. Consequently, voltage amplifiers with piezo film exhibit less temperature dependence. In Figure 41, the time constants for the charge amplifier and voltage amplifier are determined by RC_f and RC respectively.

As a design example, a traffic sensor interface is described. Because of its flexibility, piezo cable is an ideal sensor material for traffic measurement applications. MSI's BL traffic sensor is constructed with a piezo cable sheathed in a compressed brass tube, with a variety of signal cable lengths tailored to the installation requirements. The BL is available in sensing lengths of more than 3 meters. In this specific example, the BL sensor is 2 meters long. This electrically shielded sensor has 100 feet of coax cable. The electrical specifications of this sensor include:

Capacitance = 9.5 nF (including piezo cable and signal cable capacitances)
Output = 500mV (for a wheel load of 800 pounds at 55mph and 70°F)
Signal : Noise = 10:1

The basic requirements of an interface circuit are:
Low end frequency = 1.6 Hz
Circuit output = Digital pulse count

An interface circuit to meet these requirements is shown in Figure 42. This circuit works as a comparator. A 10MΩ input resistance is chosen in order to reduce the cut-off frequency to about 1 Hz. The actual cut-off frequency with this resistor can be calculated as 1.6 Hz. A 10MΩ potentiometer is used to adjust the threshold voltage, V and the diode is included to protect the electronics from high voltage damage. Typical piezo film and interface circuit output signals from a passenger car at 55 mph are shown in Figure 42.

Figure 41. Typical amplifiers for piezo film sensors

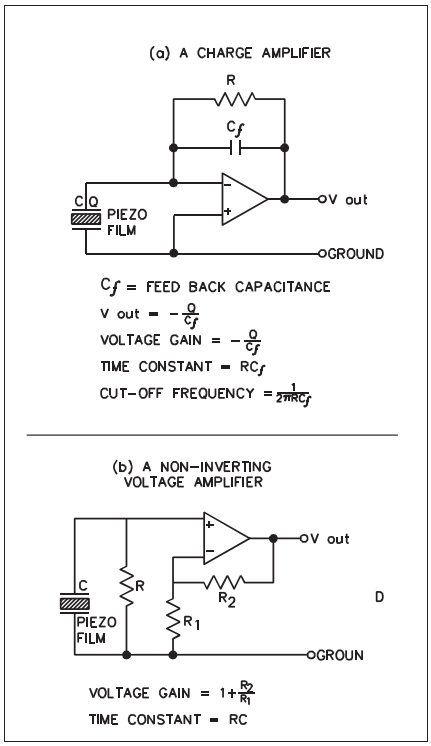
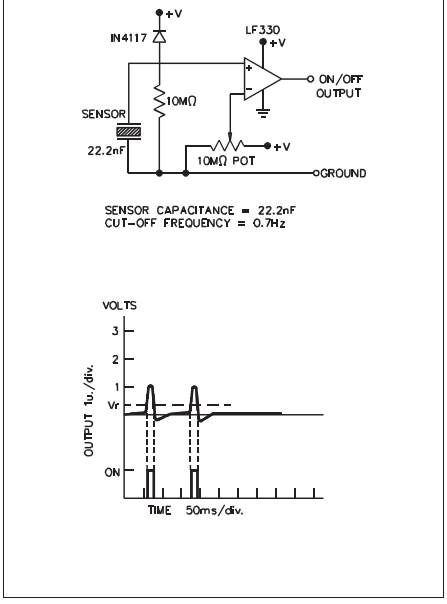


Figure 42. An interface circuit of a traffic sensor



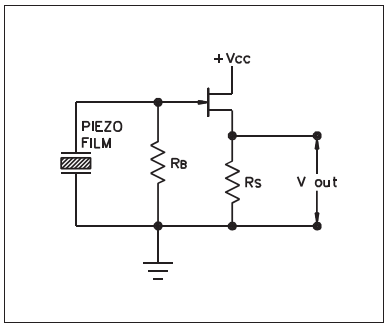
Nintendo Exhibit 1066
IPR2024-00668 - Page 611

Signal Conditioning

Because piezo film is both piezoelectric and pyroelectric, some provision must be made to eliminate—or at least reduce—the effect of unwanted signals. The primary principles of signal conditioning include:

- Filtering—Electrical filters designed to give the desired band-pass and band-rejection characteristics.
- Averaging—If the desired signal exhibits periodicity, while the undesired signal is random, signal averaging can increase the signal-to-noise ratio.
- Common Mode Rejection—By wiring two equal areas of a piezo film electrode out-of-phase, unwanted common-mode signals can be made to cancel.

Figure 43. High frequency, low gain FET circuit interface

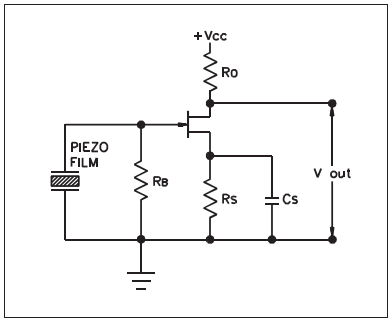


Basic Switch Circuitry

A variety of circuits are available to electronically interface with piezo film including field effect transistors (FETs), operational amplifiers (Op Amps), and low-current digital logic (CMOS).

FETs lend themselves to applications of small size since they are readily available in surface mount technology. Important characteristics to consider when using FETs are switching frequency, piezo film capacitance, leakage current of the FET in the off-state, input bias resistance, and shielding from electromagnetic interference (EMI).

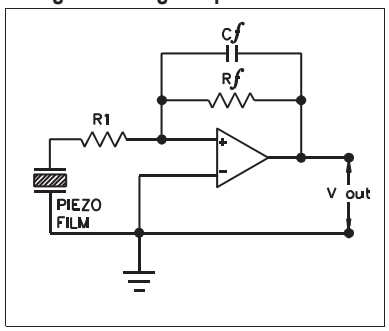
Figure 44. Low frequency, high gain FET circuit interface



Figures 43 and 44 show typical FET circuit configurations for a piezo film switch. Figure 43, the common drain or source follower, applies well in applications where simple buffering is important. Here, the circuit voltage gain is approximately one.

The common source circuit in Figure 44 is suitable for low frequency applications where voltage gain is required. The gain is determined by resistances R_D and R_S. As the gain increases, frequency bandwidth decreases by a factor of one decade per 20 dB of gain.

Figure 45. Op Amp Interface circuit acting as a charge amplifier



Operational amplifiers offer a great deal of versatility for piezo film switch applications. Adaptation to a particular application is often as simple as making a few wiring changes. Important op amp circuit characteristics include input bias resistance, film switch capacitance, and EMI shielding.

The op amp circuit of Figure 45, a charge amplifier, suits applications where a detected vibration actuates the switch. It also works well in small signal applications. A charge amplifier eliminates the effects of the time constants of both the piezo film and connecting cable. The charge amplifier is a current operated circuit with zero input impedance, which results in no voltage being generated across the film. The charge amplifier quickly absorbs charges developed by the film. With no charge left on its electrodes, the film exhibits no time constant.

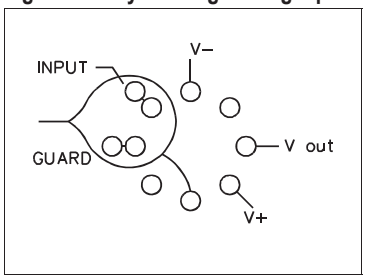
The capacitance of the film and connecting cable have no adverse effect on the circuit's transfer function. Thus tolerances on film size and cable length need not be exceptionally tight. The charge is

Nintendo Exhibit 1066
IPR2024-00668 - Page 612

transferred from the film to the capacitor in the amplifier's feedback loop, which determines the output voltage: $V = Q/C_f$.

The charge amplifier requires an op amp having a high input resistance and low bias current. A high input resistance avoids bleed-off of the charge on the feedback capacitor, and low bias current prevents the feedback capacitor from charging and discharging at excessive rates. The layout of the charge amplifier circuit is critical. The op-amp casing must be well grounded and the inputs should be guarded and connected to the same ground as the casing.

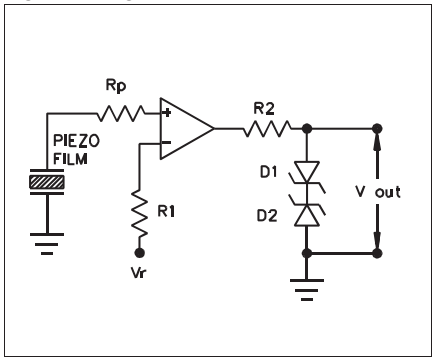
Figure 46. Layout for guarding inputs



A layout with guarded inputs is shown in Figure 46. Also, to prevent leakage noise from being amplified by the op-amp, the input cable should be terminated using a well-insulated stand-off connector.

Even with the above precautions, it is likely that the output voltage will drift. To compensate for drift, a reset switch is generally designed into the circuit to manually reset the output to zero at intervals. One technique is to place a reed switch in series with a resistor, which is in parallel with the feedback capacitor C_f. Activating the reed switch closes the switch, discharging the voltage stored in the feedback capacitor.

Figure 47. Signal level detector

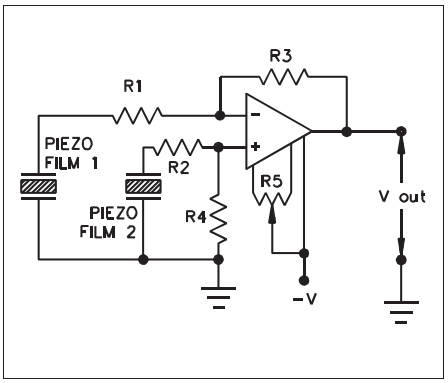


Another method is to use a MOSFET device in which the maximum output voltage and off-gate voltage determine the minimum gate voltage of the FET. In practice, a supply voltage greater than the amplifier voltage is applied to the gate of the MOSFET, thereby lowering its drain/source resistance and creating a current path for discharge of the feedback capacitor.

The third alternative is to place a bleed resistor across the feedback. This resistor creates a time constant (C_fR_f), which is independent of the film capacitance and can be accurately controlled.

The signal level detector of Figure 47 fits applications where large signal-to-noise ratios are desirable. This circuit is perfect for detecting an impact among low-level vibrations. For situations where signal to noise ratios are low and where impacts or pressures must be discerned from background vibration, the differential amplifier circuit of Figure 48 is appropriate. This circuit consists of two sensors driving a differential amplifier.

Figure 48. Differential Op Amp interface circuit



This configuration uses a common-mode rejection concept. The two switches are mechanically coupled to cancel unwanted vibrations that stimulate both. An input or pressure on one switch but not the other, will produce an output.

CMOS logic offers a low-cost way to interface with piezo film. As mentioned earlier, low-power circuits implemented with CMOS technology are ideally suited to piezo film switches. CMOS applications for piezo film are generally for low frequency operation. Other characteristics to consider include device input leakage current and input impedance,

Nintendo Exhibit 1066
IPR2024-00668 - Page 613

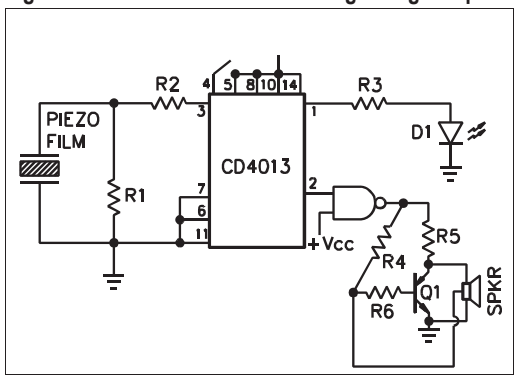
input bias resistance, and the effect of EMI. A CMOS circuit can be used, for example, in applications to sense a single impact or a single pressure.

The D-Flip Flop in Figure 49 indicates the presence of either the impact or pressure to set off an audible alarm.

The circuit in Figure 50, senses multiple impacts or pressures for counting applications.

Many different CMOS circuit configurations are possible to interface with piezo film. Common to all of them is an input bias resistor in parallel with the piezo film, and an input resistor in series with the film. The bias resistor handles leakage current and the series resistor limits current to protect against electrostatic discharge.

Figure 49. CMOS circuit for detecting a single impact

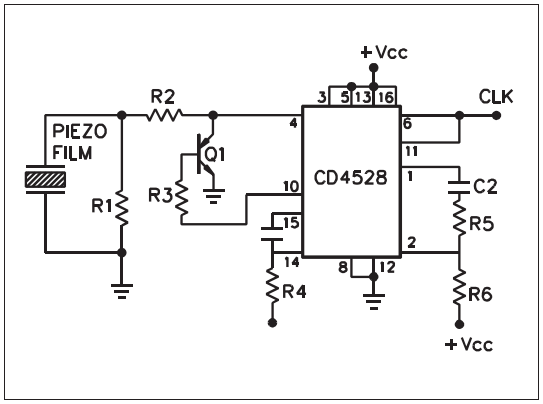


Cables

In applications where it is not possible to place the amplification circuit in close proximity to the piezo film transducer, considerable care must be exercised in selecting the connecting cable that carries the high-impedance signal.

Shielded coaxial cable, while used for noise reduction, can add problems associated with cable leakage and added capacitance. In most cases the cable's primary insulation should consist of highly resistant, non-polar plastics such as high-purity polyethylene or Teflon® (PTFE). It is equally important to make the cable as vibration-free as possible since cable movements generate noise that interferes with signal transmission.

Figure 50. CMOS interface circuit for counting applications



Nintendo Exhibit 1066
IPR2024-00668 - Page 614

MANUFACTURING

Rolls of piezo film are produced in a clean room environment The process begins with the melt extrusion of PVDF resin pellets into sheet form, followed by a stretching step that reduces the sheet to about one-fifth its extruded thickness. Stretching at temperatures well below the melting point of the polymer causes chain packing of the molecules into parallel crystal planes, called “beta phase”. To obtain high levels of piezoelectric activity, the beta phase polymer is then exposed to very high electric fields to align the crystallites relative to the poling field. Copolymers of PVDF are polarizable without stretching.

Evaporatively deposited metals are typically 500 to 1000 Å in thickness, and almost any metal can be deposited. Popular metals are nickel, aluminum, copper, gold and alloys . Electrode patterns are made by sputtering through masks or by chemical etching continuous metallizations using photoresists. Resolution to 25μm line widths has been achieved. Screen printed electrodes of conductive silver ink are much thicker, about 5-10 μm, and can be applied in complex patterns to form multiple sensors on a single sheet. Foils are adhered with thin adhesive layers and capacitively coupled to the piezo film. Each electrode alternative has advantages and disadvantages.

Generally, sputtered metals are for very high resolution arrays, pyroelectric applications requiring a low thermal mass, or for inertness, as with invasive medical applications. Fully metallized sheets can by carefully cut with a razor blade without shorting across the film thickness. Screened inks are very robust and compliant, withstand very high strains (>10%), can operate at high voltages without breakdown, and are easy to pattern on a continuous basis. However, unmetallized borders are required for cutting elements out of a sheet of screen printed electrodes, since there is a high likelihood of shorting across the films thickness with the thick inks. Foils may mechanically restrict the piezo film from responding to externally applied stresses and strains in the plane of the film, but foils are useful in pure "thickness mode" operation.

After metallization, a wide variety of possible processing steps are followed to produce a packaged sensor. Generally, the piezo film is laminated in a protective carrier film, die cut to size, and packaged with lead wires or crimp connectors and, often, signal conditioning electronics. The wide range of packaged sensors, from a few square millimeters (including an ASIC chip) as a shipping damage sensor, to multiple square meter sensors for sports scoring targets suggests the versatility of this technology.

APPLICATIONS

The sensor applications described below represent a good cross-section of the products now using piezo film sensors.

Switches

The reliability of contact switches is reduced due to contaminates like moisture and dust which foul the contact points. Piezo film offers exceptional reliability as it is a monolithic structure, not susceptible to this and other conventional switch failure modes. One of the most challenging of all switch applications is found in pinball machines.

A pinball machine manufacturer uses a piezo film switch manufactured by MSI as a replacement for the momentary rollover type switch. The switch is constructed from a laminated piezo film on a spring steel beam, mounted as a cantilever to the end of a circuit board.

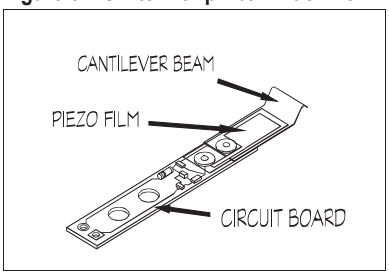
Nintendo Exhibit 1066
IPR2024-00668 - Page 615

The "digital" piezo film switch features a simple MOSFET circuit that consumes no power during the normally-open state. In response to a direct contact force, the piezo film beam momentarily triggers the MOSFET. This provides a momentary "closure" for up to a 50 V maximum voltage. The output of this low profile contactless switch is well suited to logic-level switching. The unit does not exhibit the corrosion, pitting or bounce that are normally associated with contact switches.

The company has tested these switches in excess of 10 million cycles without failure. The switch solves the nagging problem of fouled contacts in pinball machines, a significant source for machine downtime and lost revenue. The simplicity of the design makes it effective in applications which include:

- Counter switches for assembly lines and shaft rotation
- Switches for automated processes
- Impact detection for machine dispensed products
- Panel switches
- Foot pedal switches
- Door closure switches

Figure 51. Switch for pinball machine

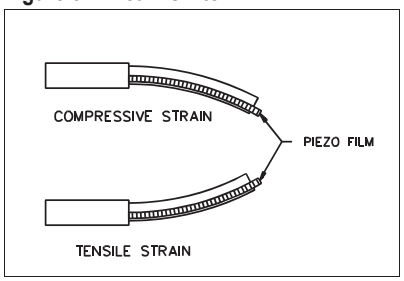


The cantilever beam that carries the piezo film can be modified to adjust switch sensitivity for high to low impact forces. Figure 51 shows the construction of the digital switch.

Beam Switch

Piezo film switches can be used to measure the amplitude, frequency and direction of an event and are useful in object detection and recognition, counting, wakeup switches and bidirectional encoding applications. The construction of the beam-type switch is shown in Figure 52.

Figure 52. Beam switch



Note that the piezo film element is laminated to a thicker substrate on one side, and has a much thinner laminate on the other. This moves the neutral axis of the structure out of the piezo film element, resulting in a fully tensile strain in the piezo film when deflected downward, and a fully compressive strain when deflected in the opposite direction. Were the neutral axis in the center of the piezo film element, as would be the case if the two laminae were of equal thickness, the top half of the piezo film would be oppositely strained from the bottom half under any deflection condition, and the resulting signals would therefore be canceled.

Beam switches are used in shaft rotation counters in natural gas meters and as gear tooth counters in electric utility metering. The beam switch does not require an external power source, so the gas meter is safe from spark hazard. Other examples of applications for the beam switch include a baseball target that detects ball impact, a basketball game where a hoop mounted piezo film sensor counts good baskets, switches inside of an interactive soft doll to detect a kiss to the cheek or a tickle (and the sensor is sewn into the fabric of the doll), coin sensors for vending and slot machines and as digital potentiometer for high reliability.

Snap-Action Switches

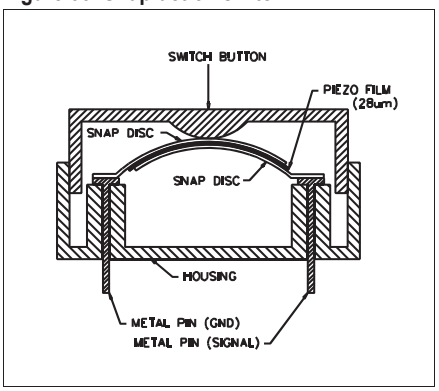
Piezoelectric materials do not have a true dc response. Very slow events, 0.0001 Hz, for example, are not normally possible to detect with piezoelectric film.

Nintendo Exhibit 1066
IPR2024-00668 - Page 616

In switch applications where dc response is required, piezo film in combination with a snap dome provides a high voltage pulse.

When the snap device actuates, the film is rapidly strained, typically generating a 10 volt pulse into a one megohm circuit as shown in Figure 53. This concept is especially well suited for wakeup switches, where an electronic device can be dormant for long periods without power consumption until the snap action device is actuated. The piezoelectric pulse turns on the electronics. Battery operated parking meters, where battery life is very critical, are an example of a piezo snap action switch application. A thermal snap action device also employs this principle.

Figure 53. Snap-action switch



Impact Sensors

Impact Printers

High speed impact printers require very accurate print head timing. Impact must occur the instant that a high speed revolving steel band, embossed with print characters, is properly positioned in front of the print hammer. Any advance or delay in energizing the print hammer will result in an offset print of the desired character.

Piezo film sensor strips, built into the printer platen, monitor the impact timing and force of the bank of print heads, and transmit the information to the controller. Automatic adjustment is made in the actuator timing to accommodate any minor change in print head timing. The very high speed of the embossed steel ribbon, about 300 inches per second, requires a very fast switch response. Alternative impact switches are quickly destroyed by the large impact forces of the print head. Piezo film switches have been in use in this application for more than five years without failure.

Sports Scoring

Piezo film sensors can be used to measure impact time, location (accuracy) and force. These parameters are desirable in several sports scoring applications. The energy of a 90 mph pitch has instantaneous power of about 50,000 watts! The great challenge in this application is target ruggedness without the introduction of severe bounceback into the design.

A second sports scoring application is electronic dartboards, where piezo film monitors the many impact zones in the game. Scoring is electronically recorded.

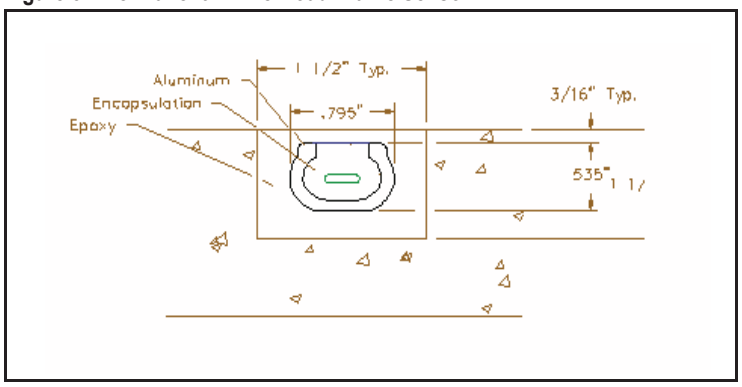
Musical Instruments

The popularity of electronics for musical instruments presents a special problem in drums and pianos. The very high dynamic range and frequency response requirements for drum triggers and piano keyboards are met by piezo film impact elements. Laminates of piezo film are incorporated in foot pedal switches for bass drums, and triggers for snares and tom-toms. Piezo film impact switches are force sensitive, faithfully duplicating the effort of the drummer or pianist. In electronic pianos, the piezo film switches respond with a dynamic range and time constant that is remarkably similar to a piano key stroke.

Nintendo Exhibit 1066
IPR2024-00668 - Page 617

Traffic Sensors

Figure 54. Permanent In-The-Road Traffic Sensor

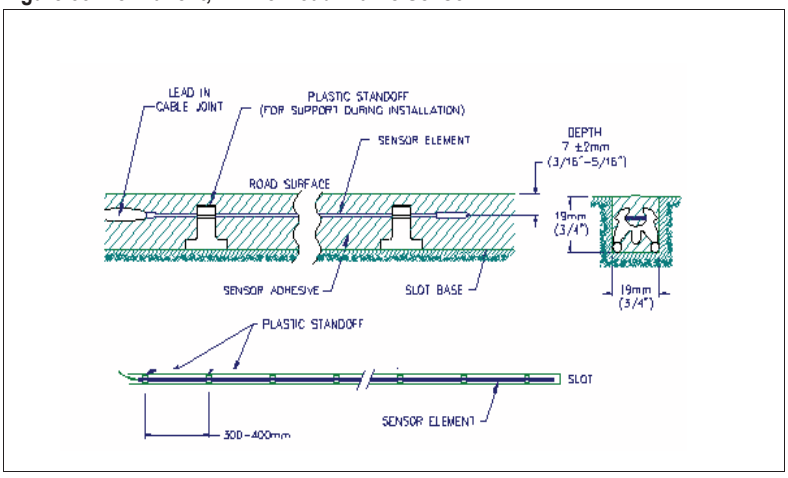


The U.S. Government is actively studying "smart highways" as an alternative to major new highway construction. The idea is that existing highways can accommodate greater vehicle densities if electronically managed. In addition to conventional traffic monitoring for highway studies and enforcement, the Intelligent Vehicle/Highway System (IVHS) programs create the need for new classes of "smart highway" high speed sensors to count and classify vehicles, provide lane control, and to monitor weight and speed. IVHS also requires "smart car" sensors, and advanced vehicle surveillance, communications, and software.

Futuristic programs like the IVHS, and more contemporary projects like the Strategic Highway Research Program (SHRP), require traffic data collection to provide the necessary information required by the Federal Highway Administration on highway structures. Recent advancements in signal processing open the door to greatly improved real-time vehicle data analysis, provided that inexpensive reliable sensor technologies are developed.

Pneumatic road tubing has long been the workhorse of traffic data collection. Road tubes provide a pneumatic pulse to a piezoelectric membrane, which triggers nearby electronics when an axle is detected.

Figure 55. Permanent, In-The-Road Traffic Sensor



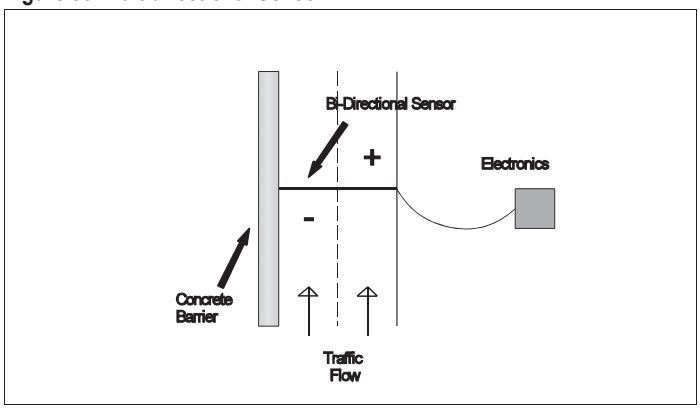
The evaluation of alternative sensor technologies has shown piezo cable provides the necessary sensitivity, linearity, noise immunity and environmental stability for high traffic interstate vehicle classification and weight-in-motion systems. Piezo cable BL sensors are used for traffic data collection from Saskatchewan to Florida.

Piezo cable traffic sensor constructions are shown in Figures 54 and 55. There are two basic categories of traffic sensor ... permanent and temporary. Generally, permanent sensors are mounted in the road with the top of the sensor flush to the highway surface, while temporary units are adhesively applied to the road surface for shorter monitoring periods. Permanent sensors, used for toll booths and interstate highway data collection, are flush mounted to a road surface and must withstand the rigors of years of high density traffic, snow plows, salt, sand, water and dragging mufflers.

Nintendo Exhibit 1066
IPR2024-00668 - Page 618

"New Jersey barriers", the modern concrete barriers that separate opposing lanes on highways, introduce problems for multilane sensing of four lane highways. Piezo cable can solve this problem with a single sensor that has opposite polarities corresponding to each lane. Vehicles crossing the near lane produce a signal of opposite sign from vehicles in the far lane (Figure 56). This ability to provide lane activity in a single sensor is a significant development.

Figure 56. Multidirectional Sensor



Traffic sensors can monitor vehicle speed, count axles, weigh vehicles, provide direction, and vehicle classification. Recently, these sensors have also proven valuable on airport taxiways. From the output, one can discern the ground speed of an aircraft (time lag between two sensors), its direction, weight (fueled), number of axles, and the span of the aircraft (determined from the speed and the known fixed distance between sensors). This information can be used to classify the aircraft and provides taxiway traffic control and safety information at airports.

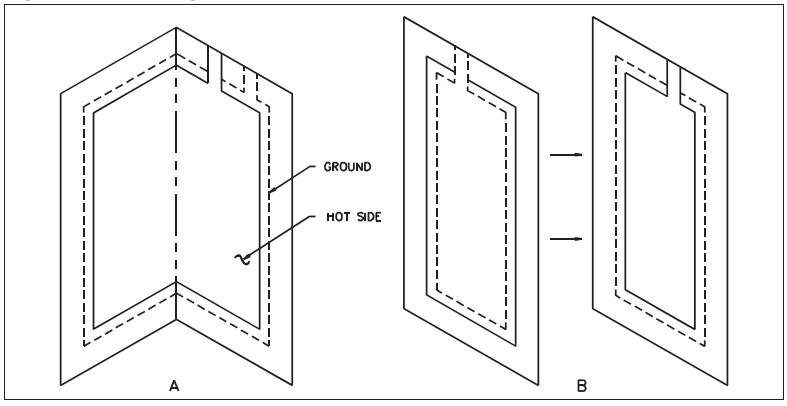
VIBRATION SENSING

One of the first applications for piezo film was as an acoustic pickup for a violin. Later, piezo film was introduced for a line of acoustic guitars as a saddle-mounted bridge pickup, mounted in the bridge. The very high fidelity of the pickup led the way to a family of vibration sensing and accelerometer applications.

Music Pickups

Piezo film is used today in several guitar pickup designs; one is a thick film, compressive (under the saddle) design; another is a low cost accelerometer, while another is an after market pickup design that is taped to the instrument. Because of the low Q of the material, these transducers do not have the self-resonance of hard ceramic pickups. Shielding can be achieved by a foldover design as shown in Figure 57. The hot side is the slightly narrower electrode on the inside of the fold. The foldover technique provides a more sensitive pickup than alternative shielding methods because the shield is formed by piezoelectric material. Conventional shielding laminates can be easily fabricated by a multilayer laminate of piezo film, adhesive and shielding foil.

Figure 57. Shielding piezo film



Nintendo Exhibit 1066
IPR2024-00668 - Page 619

Machine Monitoring

The fidelity of a shielded piezo film sensor in musical instruments led to the development of vibration sensors for machines. In its simplest mode, piezo film vibration sensors behave essentially like dynamic strain gages. The film does not require an external power source, yet typically generates signals greater than strain gages **after** amplification. A typical piezo film sensor produces four orders of magnitude higher voltage signal than a foil-type strain gage, and two orders higher than semiconductor types. The frequency response of the piezo film strain gage is also superior.

The extreme sensitivity is due to the form of the piezo film material. The low thickness of the film results in a very small cross sectional area. Thus very small longitudinal forces create very large stresses within the material.

Piezo film sensors can be affixed to a vibrating surface and monitor the amplitude and frequency of the vibrating structure. The sensors can cover larger areas than normal strain gages so any direct comparisons should be performed in **uniform** strain fields for meaningful results. Obviously, point-type transducers may be used where required, although the low capacitance of the small sensor area will require additional consideration. Operation down to fractions of Hz can be achieved by either conventional charge amplifiers or, since signal levels are relatively high, simple high impedance FET buffer circuits.

Bearing Wear Sensors

A shielded piezo film sensor has been used to monitor bearings for wear and evidence of spall. The sensors are permanently affixed to the outer surface of the bearing race with epoxy. The low mass and thin profile allow its use as a built-in nondestructive testing sensor, rather than the time consuming use of accelerometers for periodic fault-condition checks.

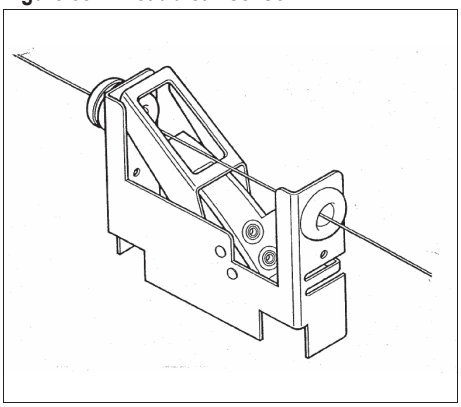
Fan Flow Sensor

A laminated beam type sensor is used in ducted airflow as a centrifugal fan failure sensor. The presence of air flow is detected by the vibrations in the sensor caused by the turbulence of air flow at about 100 Hz. The absence of this signal is used for trigger electronics. The sensor and switching electronics are based around a TL084 quad bi- FET op amp, with typical input signals of 80 mV. Sensor reliability is the key feature. Since the sensor is subjected to virtually no operating stresses, it has an indefinite working life.

Thread Break Sensor

Textile plants require the continuous monitoring of often thousands of lines of thread for breakage. An undetected break event can require that a large volume of material be discarded, as the labor costs to recover the material exceed the manufacturing cost. Drop switches, where switch contact closure occurs when the thread breaks, are very unreliable. Lint fouls the contact points, resulting in no output signal. A piezoelectric film vibration sensor, mounted to a thin steel beam, monitors the acoustic signal caused by the abrasion of the thread running across the beam, analogous to a violin string (Figure 58). The absence of the vibration instantly triggers the machinery to stop. Thread tension and defects in man-made fibers are also monitored with piezo film textile sensors.

Figure 58. Threadbreak sensor



Nintendo Exhibit 1066
IPR2024-00668 - Page 620

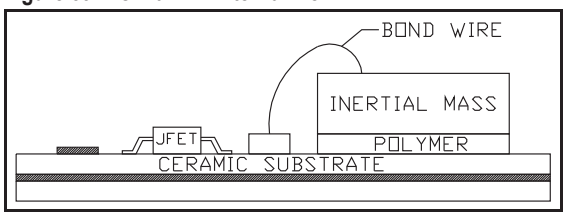
Vending Sensors

Shielded dynamic strain gages of piezo film are affixed to the underside of a vending product delivery tray to verify that product was properly vended. The absence of the impact induced vibration triggers an "Out of Order" warning. In a second application, slot machine coin counting is provided by a piezo film element. The sensors confirm delivery of coins won, discouraging gamblers from falsely claiming equipment defects. A ticket dispensing machine counts tickets delivered with a piezo beam design. Coin sensors also trigger or wake-up vending machines and coin changer electronics to verify coin authenticity.

ACCELEROMETERS

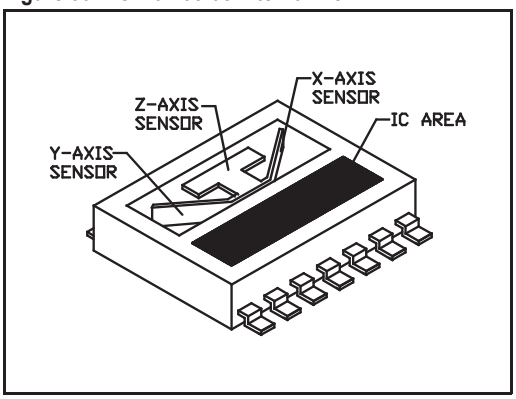
A logical outgrowth of the many vibration sensor applications of MSI's piezoelectric technology are accelerometers. These accelerometer designs are based on more traditional piezoelectric ceramic, as well as piezoelectric polymer materials. The choice of base materials allows the product to be tailored for specific applications. Table 6 lists the key specifications for the MSI Accelerometer product family.

Figure 59. ACH-01-XX internal view



Like more conventional sensors, these accelerometers are configured as either compression-design type or beam-design type. Compression-design accelerometers typically have higher resonant frequencies providing wide useful frequency ranges. An internal view of MSI's ACH-01-XX compression-design accelerometer is shown in Figure 59.

Figure 60. ACH-04-08-05 internal view



Beam-design accelerometers tend to have lower resonant frequencies and useful frequency ranges. Beam-design accelerometers also have another very interesting feature: They can be oriented to sense acceleration in multiple-axes with one monolithic sensing element using MSI's patented "Origami" beam technology ("Origami" is the Japanese word for the art of paper folding). An internal view of the ACH-04-08-05 three axis beam-design accelerometer, with its origami sensing element, is shown in Figure 60.

To reduce system costs as well as simplify use, all of MSI's accelerometers include buffers. JFET biasing and signal processing is implemented external to the device.

The ACH-01 family of products is typically used in applications which require broad frequency capability, high sensitivity, low noise, and low cost. Such applications include: speaker feedback and control systems, automotive anti-theft systems, acoustic pick-ups, machine-health and pump and centrifuge monitoring systems, and medical body motion monitoring.

The ACH-04-08 product family is used in a very broad range of applications such as speaker feedback and control systems, appliance fault monitoring, virtual reality systems, automotive systems, medical body motion monitoring, shipment damage and material-handling monitoring systems, vibration switches and earthquake shut-off switches. OEM applications that require acceleration or vibration measurements in more than one axis are perfect for the ACH-04-08-05.

MSI is constantly developing and upgrading its accelerometer product line. Please contact MSI for further details on these products or on customizing one of our other products.

Nintendo Exhibit 1066
IPR2024-00668 - Page 621

Table 6. Accelerometer Family

Production Qualified Accelerometers				
		ACH-01-XX	**ACH-04-08-05**	**ACH-04-08-09**
Key Features		-Wide Frequency Range -Wide Dynamic Range -High Sensitivity -Low Noise -JFET Buffer	-Low Frequency Operation -3 Simultaneous Analog Outputs -Low current generation - JFET Buffer	-Low Frequency Operation -Low Current Operation - JFET Buffer
Sensitive Axes	X-Axis	---	X	--
	Y-Axis	---	X	X
	Z-Axis	X	X	--
Sensitivity (Nominal)		10 mV/g	1.8 mV/g	6mV/g
Frequency Range (±3 dB)		1.0 Hz-20 kHz	0.5 Hz to 4 kHz	0.2 to 1500 Hz
Dynamic Range		±250 g	±250 g	±40 g
Resolution (@ 100 Hz)		$40\mu g/\sqrt{Hz}$	$200\mu g/\sqrt{Hz}$	$40\mu g/\sqrt{Hz}$
Resonant Frequency		>35 kHz	9.2 kHz	3.4 kHz
Resonant Q (Hz/Hz)		30	10	10
Transverse Sensitivity		5%	15%	<20%
Linearity		0.1%	0.1%	0.1%
Operating Temperature		-40 ºC to +85 ºC	-40 ºC to +85 ºC	-40 ºC to +85 ºC
Storage Temperature		-40 ºC to +85 ºC	-40 ºC to +85 ºC	-40 ºC to +85 ºC
Maximum Shock		1000 g	1000 g	1000 g
Supply Voltage		3 V to 40 V	3 V to 40 V	3 V to 28 V
Supply Current		2µ A Typical	6µ A Typical	2µ A Typical
Weight		3 grams	0.35 grams	0.35 grams
Size (mm)		13 x 19 x 6	11 x 10 x 1.8	11 x 10 x 1.8
Mounting Method		Adhesive	Hand Solder to PCB	Hand Solder to PCB

Nintendo Exhibit 1066
IPR2024-00668 - Page 622

Table 7. Accelerometer Applications

	ACCELEROMETER PRODUCTS			
Industry	**Application**	**ACH-01-XX**	**ACH-04-08-05**	**ACH-04-08-09**
Aerospace & Defense Electronics	Anti-Tamper Sensors	X	X	X
	Surveillance	X		
	Modal Analysis	X	X	
Automotive	Antitheft	X	X	X
	Skid/Rain Sensing	X		
Computers & Peripherals	Computer Mouse Sensor		X	
	Virtual Reality Sensor		X	
Household Appliances	Out-of-Balance Sensor	X	X	X
	Spray Arm Jam Sensor		X	X
	μ wave Acoustic Sensor	X		
Consumer Electronics	Speaker Feedback	X		
	Acoustic Pick-ups	X		
	Security		X	X
Industrial	Machine Health Monitor	X	X	
	Bearing Monitor	X	X	
Instruments & Measuring Equipment	Active Vibration Damping	X	X	X
	Predictive Maintenance	X	X	X
Medical	Motion Sensor	X	X	
	Pacemaker	Consult Factory for further Information		
Power & Utilities	Earthquake Shut-Off		X	X
	Machine Monitoring	X	X	
Transport & Material Handling	Shipment Monitoring	X	X	
	Railroad Systems	X	X	X

Nintendo Exhibit 1066
IPR2024-00668 - Page 623

ULTRASOUND APPLICATIONS

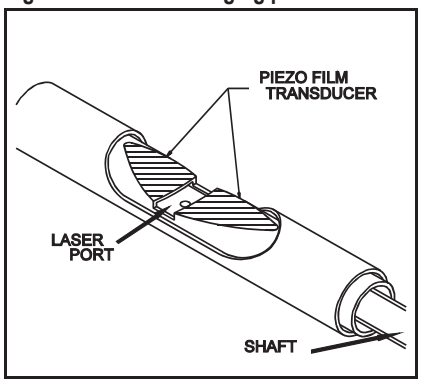
The wide frequency response and physical attributes of its polymeric construction makes piezo film a material of choice in certain medical probes and in nondestructive testing applications. Additionally, the film sensors are found in applications in ultrasonic based sensing devices, like air-ranging ultrasound for distance measurement, in fluid level sensors, and in-flow measurement instruments using doppler shift of sound velocity perturbations which are proportional to fluid flow.

Medical Imaging Ultrasound

Piezoelectric ceramic materials are used in medical imaging transducers because of their high sensitivity and broad bandwidth. The d_{33} constant, strain developed for an applied voltage, is about an order of magnitude higher for piezo ceramics than for piezo polymer. A disadvantage of piezo ceramic is its high acoustic impedance, about 30 MRayls (1 MRayl = 10^6 kg/m^{2}s) in contrast to about 1.5 MRayls for body tissue. This impedance mismatch can be compensated by quarter wavelength matching layers, but these can degrade the ultrasonic pulse due to adhesive layers and construction methods. The acoustic impedance of piezo film is about 4 MRayls, a much better match. Additionally, in higher frequency applications requiring very thin piezo elements, ceramics are too fragile, and cannot be shaped to desired geometries.

Invasive imaging requires lower powered devices than external probes. Resolution of the image is considerably improved at the higher frequencies of invasive catheters. A medical imaging company has developed an invasive imaging probe with piezo film for a therapeutic laser prostate catheter (Figure 61). The piezo film sensor is about 30 microns thick, and is located near the catheter tip. The unit operates at frequencies of 7 MHz and higher.

Figure 61. Invasive imaging probe



Steered *in-vivo* phased-array images using piezo polymer film have been produced for the first time by researchers at Duke University. A 32 element array of 11 mm x .56 mm elements was fabricated and tested with a well matched circuit designed to optimize the transducer. The result was 28 dB lower sensitivity than PZT transducers at 2.5 MHz operating frequency. However, the piezo film array had improved axial resolution, better angular response (6 dB pulse-echo response at 30 degrees), and a low interelement cross-coupling of -35 dB. It is exceptionally difficult to diamond blade saw PZT ceramic into these small elements; while, for piezo film, complex patterns are readily etched into the surface gold electrode. PZT must be diced due to the severe interelement coupling problem. Duke University researchers plan to improve the polymer probe by expanding the number of array elements to 128.

Very high resolution arrays have been traditionally formed by etching an electrode pattern on the surface of a piezo film. Newer techniques include deposition of the copolymer directly onto silicon wafers. The wafers are etched to minimize interelement coupling, then the copolymer is applied by spin-coating, followed by poling. Then a top ground electrode is applied and inter-connections made. This advance results in a very high resolution imaging. Capacitively coupling copolymer film to a dense array of conductive traces on a PCB has achieved remarkable performance as a Tx/Rx array.

Nintendo Exhibit 1066
IPR2024-00668 - Page 624

NonDestructive Testing (NDT)

Advanced composite materials are very desirable as structural members. Light weight, high strength, corrosion resistance, and non-magnetic are among the advantages for these materials. The need for very routine nondestructive testing of such structures to prevent catastrophic failure due to delamination, is one of technology's greatest concerns. Flexible sheets of piezoelectric polymer transducer arrays, acoustically well matched to the composites, are desirable for use for non-destructive testing. One example is as an NDT array for testing rocket motor housings prior to launch. These arrays can be applied to the surfaces of composite fuel housings, and each element sequentially activated to provide a pulse-echo response. An array element size of about 0.5 to 1 square inch is sufficient for this application, as well as most large area NDT. Center frequencies of 3-10 MHz and -6 dB fractional bandwidths exceeding 100% are typical with such transducer arrays.

Systems and Instrumentation, Ltd. personnel use piezo film for NDT of aerospace engine parts. NDT transducers capable of detecting flaws down to 1/64th inch are now required. Further, the frequency response range of these new materials are broader than the bandwidth of conventional transducers. S&I, Ltd. find that a single broadband transducer covers the bandwidth of interest. Their transducers are also used in near-surface NDT applications, where high resolution and short pulse duration are required. Defects of 0.8 mm in size, lying within 1 mm of the surface, have been detected with the S&I probes.

Critical points or inaccessible test areas within a composite structure, like support strut mounts, where delamination or other damage is especially likely, can have custom fabricated NDT arrays permanently affixed for in-service testing and monitoring. It is possible to achieve uniformity of ±1 dB between the elements of a multi-element transducer array. Special shaped transducers, providing special focal characteristics, have also been built with these polymer transducers.

Acoustic Emission

Acoustic emission of materials including fiber-reinforced composites, aluminum, steel and glass can be performed with contact microphones of piezo film, or, as with NDT, by large area arrays. These arrays can continuously monitor structures for 0.1 - 1.0 MHz acoustic emission, the precursor to structural failure. Piezo film, being broad band, responds well at these frequencies. This capability is especially necessary for critical application like tank rail cars carrying toxic products, underground fuel storage tanks, nuclear plants, etc.

Fluid Level Sensor

There are a variety of fluid level sensing transducer technologies available to the designer. A float arm, attached to a sliding potentiometric device is still widely used in automobiles. Ultrasonic pulse-echo devices that measure the distance from a fixed transducer to the fluid surface from above through air, or from below through the fluid, are popular. Newer capacitance types, where the fluid becomes the dielectric, are also used. Each of these technologies represent tradeoffs in system cost, performance and reliability. A new ultrasound level sensor, in development by MSI, holds promise as a digital, solid state ultrasonic level sensor.

The novel construction is a level sensor with ultrasonic through-transmission with multiple transmitters and a single, common receiver. The sensor is fabricated by attaching an unmetallized strip of piezo film to a printed circuit board containing electrode patterns, conductors, and interconnections to circuitry on the opposite side of the board. The electrode patterns are capacitively coupled to the piezo film layer, becoming the multiple transmitter elements. A second conductor bar, parallel to the patterned elements becomes the common receiver.

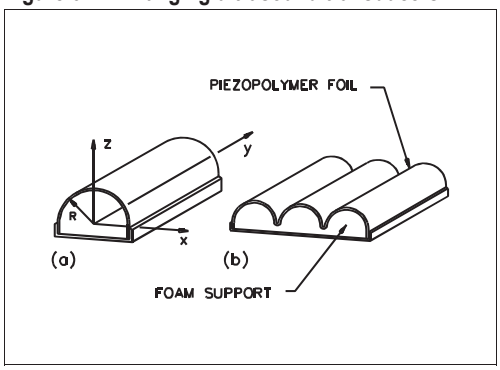
Nintendo Exhibit 1066
IPR2024-00668 - Page 625

The presence of fluid couples the transmit signal to the receiver to a much greater extent (60dB) than when the ultrasound energy is coupled by the air above the fluid. The excitation signal for the transmitter is a 1.1 MHz sine wave tone burst with an amplitude of 20 volts peak to peak. The required circuitry consists of a high frequency oscillator and clock, an array of analog switches, a single receiver amplifier with input gate, and a threshold detector. These electronics can be reduced to the chip level, and are incorporated on the backside of the circuit board.

Resolution of the level sensor is determined by the resolution of the patterned transmit electrodes on the circuit board. Parallel elements of 2 mm width and 0.5 mm spacing between elements is a representative capability. The ground electrode for the transmitters is a fully gold metallized surface on the fluid side of the piezo film transmitter array. The receiver is formed by the same piece of piezo film, capacitively coupled to the signal electrode which is a separate conductor trace on the printed circuit board (PCB). Again, the ground is the backside electrode on the film.

The new level sensor has several unique advantages. The spacing between transmitter elements need not be uniform For tanks that do not have a uniform volume throughout the tank height, a simple PCB layout can linearize the nonlinear tank volume by setting the transmitter element spacing accordingly. The output of the device is digital—no expensive A/D conversion is required. The level sensor is small in width, less than 1 inch, so it can be inserted into a small diameter tube. The tube confines the motion of the fluid, reducing large swings in fluid height readings caused by motion, as with an automobile fuel tank during cornering. Reliability is greatly improved. The level sensor is self diagnostic to the extent that the transmitter/receiver pair must be operational to deliver a meaningful signal. The absence of the signal indicates a fault condition. For a detailed discussion on Ultrasonic Ink Level Sensing, see Appendix C.

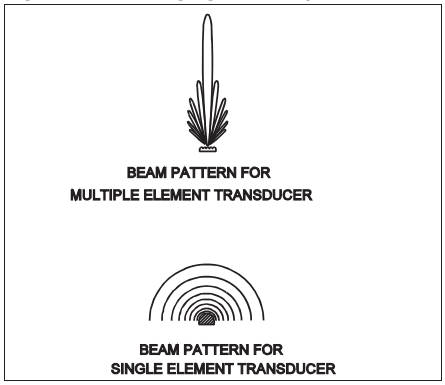
Figure 62. Air ranging ultrasound transducers



Air Ranging Ultrasound

Ultrasonic devices used in pulse-echo modes are used in robotics, vehicle safety and control system, object recognition systems and other remote distance measurement devices. The sensors provide high resolution in the targeted direction, and can be used to measure the elapsed time from transmit to receive to determine the distance to an object. Unlike piezo ceramic and electrostatic devices, piezo film can deliver a very short pulse (due to its low Q), allowing the same device to be used as both transmitter and receiver, even in the near field of the transducer.

Figure 63. Air-ranging directivity patterns



Multiple piezo film elements can be easily fabricated, as shown in Figure 62. The geometries of these cylindrically shaped elements (length, radius of curvature, number of elements) can be designed to control the directivity pattern and acoustic properties. Transducers with operating frequencies from 40-200 KHz have been made. Average values of transducer sensitivity are 0.1-1 mV/Pa in the receive mode (noise was < 1μV) and 15-75 mPa/Vcm^2 in the transmit mode for 1 m of distance. The minimum distances measured in pulse-echo mode was 30 mm. Distances to 15 meters have been measured with a main beam width of less than 10 degrees, and maximum side lobe amplitudes that are 12 dB down at 60 KHz. Examples of directivity patterns for single and multiple element transducers are shown in Figure 63. Multiple

Nintendo Exhibit 1066
IPR2024-00668 - Page 626

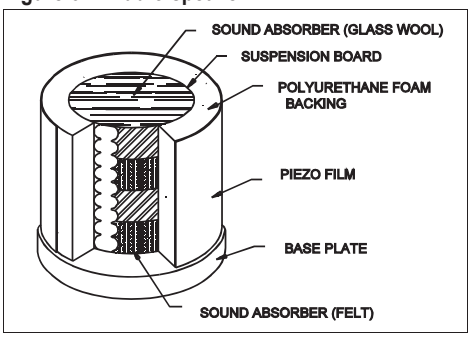
elements can also be used for scanning of objects without physically moving the transducer. Each element within the transducer can be activated sequentially, as with ultrasonic arrays.

AUDIO

Speakers

One of the earliest applications for piezo film was in stereo tweeters (Figure 64) and headset speakers developed by Pioneer Electronics. There is strong renewed interest in these applications as a result of the improvements in the reliability of the electrodes and lead attachment and packaging techniques. Gallo Acoustics has developed a high fidelity omnidirectional tweeter using a cylinder of 52 um thick piezo film. The tweeter rolls off at frequencies below 2 KHz, and features:

Figure 64. Audio speaker



- 330 degrees of horizontal dispersion at high frequencies, which is as much as ten times the dispersion of conventional tweeters,
- very wide dynamic range,
- linear frequency response,
- very fast impulse response, faithfully reproducing the highest frequencies.

Novelty audio speakers have also been developed. These devices make use of the thin, light weight, conformal nature of the piezo film. Examples include speakers for inflatables (like balloons and air inflatable toys), speakers in apparel (including headgear) and paper thin speakers for magazine advertising, greeting cards and posters.

Microphones

A diaphragm of piezo film, affixed in a retaining ring or mounted over a hole in a plate, makes an excellent microphone. Vacuum formed domes on a support can be introduced into the design to take the membrane slightly out of its neutral axis with a foam backing, a small post, bar or structure to give the film membrane a slight radius of curvature. A self-supporting, cylindrically curved film also achieves the mechanical bias. A typical radius of curvature for piezo film microphones which optimizes sensitivity and electroacoustic efficiency is R_o = 25 mm, similar to that of an electrostatic microphone construction.

Sennheiser reports a frequency response for a typical foam backed piezo film microphone of 25 mm diameter, having R_o = 25 mm. The free field sensitivity of the device measured at 1 KHz, for sound pressure incident on the membrane perpendicularly, was -58 dB re 1 V/Pa. Harmonic distortion approaches 1% only at sound pressure levels exceeding 122 dB, and are not significantly higher for the range of higher frequencies.

Microphones built with piezo film are low cost, but more importantly, are inherently immune to moisture, unlike electrostatic types.

Electrostatics dominate the market due to the low cost that has been achieved through very high volume manufacturing. Nonetheless, piezo film microphones are finding application in designs where

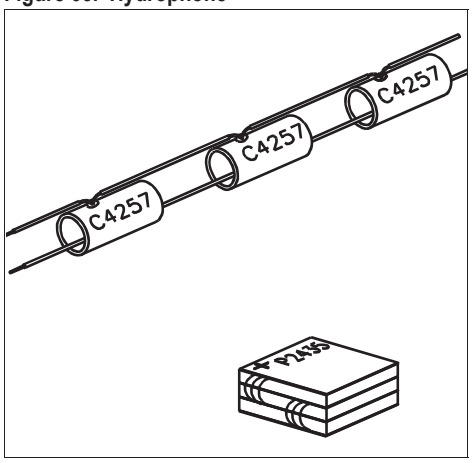
Nintendo Exhibit 1066
IPR2024-00668 - Page 627

environmental stability is critical. Waterproof microphones are being supplied for divers, withstanding total immersion in salt water without damage.

SONAR

Piezo ceramic materials have been used in hydrophones for SONAR since the 1940's. Ceramics have many desirable features as hydrophones including high hydrostatic sensitivity, high capacitance, ability to fabricate into shapes, and availability in thick cross-section (sensitivity is proportional to piezo element thickness). However, the weight of ceramic is much greater than water, so buoyancy must often be added to structures as compensation.

Figure 65. Hydrophone



The current trend in SONAR is toward higher numbers of hydrophone sensors per vehicle. Longer towed arrays and larger and more numerous hull mounted hydrophone panels are being employed by the fleet. This trend requires the advancement of much lower weight hydrophones making piezo film an excellent choice for these applications.

New piezo polymer hydrophones of thick film (1200μm) have been made into sheet and cylinder form (Figure 65). The cylinders, about 2-3 cm in length and <1 cm in diameter, are strung together into a continuous hydrophone line array. The hydrophones are very light weight (0.60 g/cm^3), yet have excellent hydrostatic sensitivity.

Piezo polymer hull mounted hydrophones in panels, of about one square meter in area and greater than 1000μm in piezo polymer thickness, are used by the British and French Navies for submarines. Called "Flank Arrays", these units work in combination with towed arrays in advanced SONAR systems. Piezo film sheets are not fragile, conform to the radius of curvature of the hull, and are low cost. Typical sensitivities for the piezo film thick sheet hydrophones are similar to ceramic type (-192 to -195 dB re 1 V/μ Pa). The lower capacitance of the piezo film hydrophones is compensated by the large area and number of parallel hydrophones used.

New hydrophone technologies, including underwater ultrasound imaging for divers and related applications are also in development.

FUTURE APPLICATIONS

Piezo film research is underway into an exciting new array of applications. A sampling of this R&D activity is highlighted below:

Active Vibration Damping

Piezo film sensor and actuator pairs are in development for active vibration damping. In this application, a piece of piezo film is employed as a strain gauge to detect vibration and another piece of piezo film is employed as an actuator to dampen the vibrational noise by applying a 180 degree phase-

Nintendo Exhibit 1066
IPR2024-00668 - Page 628

shifted signal. Wide coverage of piezo film, with distributed electrode patterns, can be used to create individual sensor/actuator pairs. Critical damping has been achieved with this piezo film laminate by researchers at Massachusetts Institute of Technology and elsewhere.

The applications for this technology include the reduction in harmful vibrations in space-based structures, fuselage for aircraft to cancel engine noise, quiet cars, quiet appliances, and a wide range of other possibilities.

Sensors on Silicon

Piezoelectric polymers can be solution cast (spin coated) onto silicon, polarized in place, metallized in pattern arrays, and interconnected with the integrated circuits on the chip. Minor modifications to wafer processing make the silicon suitable for the piezo Polymer Sensor-On-Silicon (PSOS). Early work in PSOS technology at Stanford University was frustrated by the need to adhesively bond thin sheet piezo film onto silicon. The adhesive layer was difficult to apply to the silicon, introducing air bubbles, wrinkles, nonuniform thickness layers, etc. The advent of new piezo polymer processing that eliminates the adhesive makes the PSOS technology practical. R&D work at MSI and elsewhere includes the development of pyroelectric arrays for infrared cameras, fingerprint readers, and thermal imaging devices, ultrasound arrays for high resolution NDT and invasive medical imaging, and integrated accelerometers for microminiature components.

Smart Skin

Piezoelectric film can both sense surface energy and can microdeflect the surface. These capabilities may be of interest in active surfaces for sound cancellation, extension of laminar to turbulent flow boundaries, etc. Considerable work is under way at university and government laboratories in these and related applications.

Nintendo Exhibit 1066
IPR2024-00668 - Page 629

Appendix A – Applications of Piezo Film

APPLICATIONS OF PIEZO FILM

COMPUTER INPUT/OUTPUT

Keypad arrays
- Digitizer
- Air Mouse
- Joystick
- Pen (Signature verification; Handwriting Recognition)

Printers
- Impact Flight Time
- Ink Drop Generation and Detection
- Toner and Ink Jet Level
- Toner Activation

Business Equipment
- Antitamper for ATM Machine
- Coin Counters
- Copiers
  - Switches
  - Paper Path Switches
  - Toner Level and Activation

Disc Drives
- Shock Sensing Accelerometers

INDUSTRIAL

Switches
- Solid State Momentary
- Snap Action
- Cantilever Beam
- Keypad
- Vandal-Proof
- Intrinsically Safe
- CMOS Wake-up
- Low-Deflection
- Singing Switch (a.c. switch)
- Coin Counter
- Acoustic Switch
- Shaft Rotation Counter

Robotics
- Tactile Sensor
- Micropositioner
- Safety Mats & Switches
- Bumper Impact

Physical Security & Energy Management
- Glass Break Detectors
- Floor/Mat Sensor
- Penetration Detection
- Contact Microphone
- Piezo Cable Perimeter Protection
- Pyrometer/Flame Sensor

Flow/Level
- Vortex
- Fluidic Oscillator
- Air Flow
- Doppler Ultrasound
- Solid State Fluid Level
- Laminar/Turbulent Boundary Layer
- Fan Failure

INSTRUMENTATION

Machine Health Monitor
- Accelerometers
- Contact Microphones
- Hi-Strain Dynamic Strain Gages

Weather Sensors
- Rain Intensity
- Hail Detection
- Wind Velocity

Active Vibration Damping
- Strain Gages Sensor Arrays
- Actuator Arrays

Non Destructive Engineering
- Flexible Contact NDT Probes
- NDT Arrays
- Acoustic Emission Sensors

Air Ranging Ultrasound
- Safety
- Distance

Adaptive Optics
- Fiber Optic Shutters/Modulators
- Deformable Mirrors
- Laser Scanners

Oil Exploration
- Hydrophones
- Seismic Geophones

Nintendo Exhibit 1066
IPR2024-00668 - Page 630

MEDICAL

Diagnostics
- Apnea Monitor
- Ambulatory/Gait Monitors
- Blood Pressure Cuff
- Pulse Counter
- Stethoscope
- Sleep Disorder Monitors
- Respiratory Air Flow
- Isokinetics
- Patient Bed Monitor

Ultrasound
- Near Field Imaging
- Prostate
- Transdermal
- Transluminal
- Coronary Arterial
- Breast
- Lithotripter
- Hydrophone Calibration Probes

Handicapped Aides
- Switches
- Braille Reader
- Hearing Aid
- Speech Intensification

Implantables
- Pacemaker Activity Monitor
- Implantable Switch
- Vascular Graft Monitor
- Micropower Source

Instrumentation
- Intravenous Drop Counter
- IV Air Bubble Detection
- Laser Switch/Modulator

AUTOMOTIVE

- Accelerometers
- Occupancy Seat Sensor

Switches
- Passenger Compartment Switches
- Horn Switch
- Control Panel

Fuel Level, Tire Rotation, Security
- Keyless Entry
- Motion (Theft) Sensor

CONSUMER

Musical Instruments
- Piano Keys
- Pick-up
- Drum Trigger

Sports Equipment
- Target Location
- Reaction Time
- Foul Line
- Force (Karate, Impact)
- Sweet Spot

Toys/Games
- Switches
- Proximity (Air Ranging Ultrasound, Pyro)
- Novelty Speakers (Microphones)
- Target Scoring

Audio
- Tweeter
- Balloon Speakers
- Novelty Speakers (Visor, Poster)
- Microphone
- Speaker distortion Feedback Accelerometer

Appliance
- Washer Imbalance
- Vacuum Soil Sensing
- Dishwasher Spray Arm
- Level Sensing Switches

MILITARY/GOVERNMENT

Hydrophones
- Towed Cable Array
- Hull Mounted Arrays
- Sonobuoys
- Active Noise Suppression

Ballistics
- Safety and Arming Fuses
- Shock Wave Gages
- Seismic Accelerometers

Physical Security
- Perimeter Security Cable (Buried or Fence)
- Seismic/Geophones
- Covert Microphones

Traffic Sensors
- Vehicle Classification
- Weight-In-Motion
- Speed, Red Light Enforcement
- Lane Designation
- Toll Booth

Nintendo Exhibit 1066
IPR2024-00668 - Page 631

Appendix B - INDEX OF PIEZO FILM ARTICLES

[NOTE: THIS LIST IS ONLY A REFERENCE. COPIES OF THESE ARTICLES ARE NOT SUPPLIED BY MSI, INC.]

CODE	AUTHOR AND REFERENCE	TITLE
DEFOULING		
DF1	U.S Patent, 4,170,185 P.V. Murphy, M.J. Latour, Lectret S.A. (Switzerland) Oct. 9 1979.	Preventing Marine Fouling.
DF2	US DOD, Small Bus. Innovation Research Program; Ocean Power Technologies, Inc. Topic #DARPA 90-111	Piezoelectric Copolymer Antifouling System
ACTUATORS (Electromotional Devices)		
EM1	M. Toda & S. Osaka (RCA, Japan.) Proceedings of the IEEE.67(8). August, 1979.	Vibrational Fan Using the Piezoelectric Polymer PVF2.
EM2	M. Toda & S. Osaka (RCA Japan). Transactions of the IECE of Japan. 61(7). July 1978.	Electromotional Devices Using PVF2 Multilayer Bimorph.
EM3	M. Toda (RCA, Japan) Transactions of the IECE of Japan 61(7). July, 1978.	Design of Piezoelectric Polymer Motional Devices with Various Structures.
EM4	Gale E. Nevil, Jr. & Alan F. Davis. Paper from "Robotics Research: The next Five Years and Beyond". Aug. 14-16, 1984.	The Potential of Corrugated PVDF Bimorphs for Actuation and Sensing.
EM5	U.S. Patent, 4,666,198 Heiserman, David L., Microflex Technology.	Piezoelectric Polymer Microgripper.
EM6	Linvill, J.G. Stanford University. ©1986 IEEE	Piezoelectric Polymer Transducer Arrays.
EM7	Clive Robertson, Pennwalt (Europe) Application note.	Bimorph Drivers - An Electronic Solution.
EM8	M. Toda, K. Park, Atochem Sensors	Update on Novel Piezo Film Actuators and Ultrasound Transducers.
EM20	Amr M. Baz, Jeng-Jong Ro. Sound & Vibration, March 1994.	The Concept and Performance of Active Constrained Layer Damping Treatments
EM21	M. Sasaki, P.K.C. Wang, F. Fujisawa.	Stability Analysis of Piezo Polymer Flexible Twisting Micro-Actuator with a Linear Feedback Control.
EM22	US Patent 5,295,014, Minoru Toda	Two-Dimensional Laser Beam Scaner Using PVDF Bimorph.

Nintendo Exhibit 1066
IPR2024-00668 - Page 632

EM23	Minoru Toda, Ferroelectrics, 1979, Vol.22, pp 911-918	Theory of Air Flow Generation By A Resonant Type PVF2 Bimorph Cantilever Vibrator.

FORCE TRANSDUCERS

F1	G.R. Crane (Bell Labs, Holmdel) Transactions on Sonics and Ultrasonics. SU-25(6). November, 1978.	Poly(vinylidene)Fluoride Used for Piezoelectric Coin Sensors.
F4	D.S. Leitner (Columbia U.) & M.C. Rosenberger (N.Y. Psych. Inst) Behaviour Research Methods and Instrumentation. 15(5). 1983.	A Simple and Inexpensive Startle Transducer with High Output.
F5	U.S. Patent 4,282,532 R.G. Markham (Xerox Corp.) August 4, 1981.	Ink Jet Method and Apparatus Using a Thin Film piezoelectric Excitor for Drop Generation.
F15	National Bureau of Standards NBSIR 76;1078. June 1976.	Piezo Polymer Transducers for Dynamic Pressure Measurements.
F17	K.T. Park et al, IEEE 1986 International Symposium on the Applications of Ferroelectrics.	A charge Readout Algorithm for Piezo Force Transducers.
F18	Seh-leh Chou et al. From Proceedings of the 1986 SEM Spring Conference on Experimental Mechanics. New Orleans, LA. June 3-18, 1986.	Interlaminar Normal Stresses in a Multilayered Plate -Theory and Experiment.
F22	Scottish Schools Science Equip. Research Centre. January, 1987.	Electronic Balances using Kynar Piezo Film.
F27	A.A.H.P. Megans, J. et al Janssen Pharmaceutica Psychopharmacology(1987)93:	Behavioral activity of rats measured by a new method based on the piezo-electric principle.
F30	USA Patent 4,807,482. Kyung T. Park, Upper Darby; Richard D. Klafter, Wyncote, both of Pa.	Method and Apparatus for Measuring Stimuli applied to a Piezoelectric Transducer.
F32	USA Patent 4,512,431. April 23 1985.	Weight Sensing Apparatus Employing Polymeric Piezoelectric Film
F35	A. G. Bagnall, Harrow School, Harrow, Middlesex. UK	Investigations Using Piezo Film
F41	A. J. Tuzzolino; Nuclear Instruments & Methods in Physics Research 00 (1991) NIM06317, North-Holland; Elsevier Science Purlibhsers B.N.	Two-dimensional position-sensing PVDF dust detectors for measurement of dust particle trajectory, velocity, and mass

Nintendo Exhibit 1066
IPR2024-00668 - Page 633

F42	D. A. Dillard, G. L. Anderson, D. D. Davis; 35th Sagamore Army Matls Res. Conf., Manchester, NJ June 26-30, 1988.	A Preliminary Study of the use of Kynar Piezoelectric Film to Measure Peel Stresses in Adhesive Joints
F43	Randy Fromm, RePlay Magazine, November 1991.	Gottlieb's System 3 Pinball
F44	W. Nitsche, M. Swoboda, P. Mirow, Berlin; Z. Flugwiss. Weltraumforsch. 15(1991) 223-226. Springer-Verlag 1991	Shock Detection by means of Piezofoils.
F45	W. N. Nitsche, P. Mirow, J. Szodruch, Berlin; Experiments in Fluids, Springer-Verlag 1991	Piezo-electric foils as a means of Sensing Unsteady Surface Forces
F46	Pieter de Bruyne, Laboratory for Communication Technology, Zurich, Switzerland; presented at International Graphics Symposium, Tempe AZ, Oct 27-30, 1993.	A Piezo-Electric Recording Device of Writing Velocity
F47	UK Patent, 2,235,802A; John Ronald Parks, National Research Development Corporation, London, 03-13-91.	Capturing Information in Drawing or Writing
F48	A.J. Tuzzolino, J.Z. Simpson, R.B. McKibben, H.D. Voss, H. Gursky. Adv Space Res., Vol 13, no 8, pp 133-136.	An Instrument For Discrimination Between Orbital Debris and Natural Particles In Near-Earth Space.
F49	A.J. Tuzzolino. Nuclear Instruments and Methods in Physics Research 1992.	PVDF Copolymer Dust Detectors: Particle Response and Penetration Characteristics.

FLOW

FL1	Pennwalt News Release. May 1982	Piezo Film is key to Unique Flowmeter in New Perkin-Elmer Monitoring System.
FL4	Clive Robertson, Pennwalt Piezo Film Ltd. Edinburgh	The Use of Piezo Film for Sensing Fan Failure.
FL5	K. Sakai, Tokyo Gas Co, M. Okabayashi, Osaka Gas Co, Yasuda, Toho Gas Co.	Fluid Flowmeter - Gas Flowmeter Based on Fluidic Dynamic Oscillation.
FL8	Richard Brown, Pennwalt Piezo Film Ltd. Edinburgh, 7/23/90	Fuel Level Sensor using Multiple Transducers
FL9	E. J. Stefanides, *Design News*, p. 107; 7/23/91	Piezo Sensor Upgrades Wastewater Sampler's Accuracy
FL10	U.S. Patent 4,920,794 Ingman, 1988	Fluid Flow Meter
FL11	Richard Brown, Elf Atochem Sensors, Ltd., July 1992	Fuel Tank Level Sensor with Digital Output
FL12	Richard Brown, AMP Sensors EMEA	Discussion of Ultrasonic Ink Level Sensing

Nintendo Exhibit 1066
IPR2024-00668 - Page 634

GENERAL

G6	M. Toda (RCA Japan). J.Appl. Phys. 51(9), September 1980.	Elastic Properties of Piezoelectric PVF2.
G15	Pennwalt Corporation. Material Safety Data Sheet. Nov. 15, 1986.KYNAR Piezo Film	
G19	U.S. Patent, 4,633,122 P.F. Radice (Pennwalt) Dec. 30, 1986.	Means for Electrically Connecting Electrodes on Different Surfaces of Piezoelectric Polymer Films.
G23	N.A. Suttle, Marconi Research Centre. GEC Journal of Research, Vol.5, No. 31987	New Piezoelectric Polymers
G24	Invention Record, Pennwalt Piezo Film Ltd., Edinburgh.	Forming mechanical and electrical connections to printed circuit boards.
G27	Francois Bauer, Lucien Eyraud Saint-Louis, France.	Ferroelectric Homopolymer PVDF and P(VDF-TrFE) Copolymers.
G30	Encyclopedia of Polymer Science and Engineering, Vol. 17, p. 532	Vinlydene Fluoride Polymers
G31	U.S. Patent 4,931,019, Kyung T. Park, 1 Sep 1988.	Electrostatic Image Display Apparatus
G32	Richard A. Ferren, Atochem Sensors, Inc. 1990	Polymeric Piezoelectric Transducers
G34	Steve Garrison, The Science Teacher, Feb. 92	Piezoelectric Film. . Investigate its Flexibility
G35	U.S. Patent 5,089,741, K. Park, F. Gastgeb, G. Daniels, Atochem Sensors, Inc. 1990	Piezo Film Impact Detector with Pyro Effect Elimination
G36	W. Campbell, Jr., J. J. Scialdone, Goddard Space Flight Center, Greenbelt, MD; NASA Reference Publication 1124 Revision 2	Outgassing Data for Selecting Spacecraft Material
G37	B.A. Auld (Stanford U.) & J.J. Gagnepain. J. Appl Physics. 50(8). August 1979.	Shear Properties of Polarized PVF2 Film Studied by the Piezoelectric Resonance Method.
G38	Nicola A. Suttle	New Piezoelectric Polymers
G41	D. Clarkson, Maplin Magazine, Jan 1993, pp 36-39	Piezoelectric Technology
G42	D. M. Brown, B&D Insts & Avionics, Inc. Valley Center, KS. Sensors Expo Proc, 1991; pp 105A-1 - 105A-11	Applications of PVDF for Aircraft Sensors

Nintendo Exhibit 1066
IPR2024-00668 - Page 635

G43	F. Bauer, St. Louis, FR; J. Simonne, Toulouse, FR; L. Audaire, Grenoble, FR. 8th IEEE Int'l Symp. on Applic. of Ferroelectrics, Greenville, SC, Aug 31- Sep 2, 1992	Ferroelectric Copolymer and IR Sensor Technology applied to Obstacle Detection
G44	US Patent 5,424,716. Kyung Park	Penetration Detection System
G45	Joseph Dougherty. Penn State Mat'l Research Lab Report	PVDF Copolymer - Piezoelectric Powder Composites.
G46	Ken Turner. Schaumburg High School	Smart Sensors Module Report
G47	Glen MacGibbon. Appliance Engineer	Piezo Film Sensors For Appliance Applications.
G48	M.G. Broadhurst, G.T. Davis, J.E. McKinney, R.E. Collins	Piezoelectricity & Pyroelectricity in PVDF-A-Model

HYDROPHONES

H1	T.D. Sullivan & J.M. Powers (U.S. Navy). J. Acoust. Soc. Am. 63(5). May 1978.	Piezoelectric Polymer Flexural Disk Hydrophone.
H3	B. Woodward & R.C. Chandra (EE Dept., Lonborough U of Tech.) Electrocomponent Sci & Tech. 5. 1978.	Underwater Acoustic Measurements on Polyvinylidene Fluoride Transducers.
H4	Powers (U.S. Navy). Naval Underwater Systems Center, New London, CT 06320	Piezoelectric Polymer - An Emerging Hydrophone Technology.
H6	R.H. Tancrell, D.T. Wilson, D.T. and D. Ricketts, Raytheon Research Division.	Properties of PVDF Polymer for Sonar.
H8	J.M. Powers (U.S. Navy).	Long range Hydrophones.
H10	M. A. Josserand and C. Maerfeld, Thomson-CFS, France.	PVF_2 Velocity Hydrophones.
H11	David R. Fox, IEEE Journal of Oceanic Engineering, Vol. 13, No. 4, Oct. 1988	A Low-Density Extended Acoustic Sensor for Low-Frequency Arrays
H13	Atochem Sensors, Inc. 12/31/90	Piezoelectric Polymer Hydrophones
H14	Innovative Transducers Inc., 1990	PISCIS MS-4 Marsh/Swamp Hydrophone PISCIS MS-5 Marsh/Swamp Hydrophone PISCIS BC-4 Bottom Cable Hydrophone
H15	Gregory Kaduchak, Christopher Kwaitkowski, Philip Marstan. J. Acoustic Soc. Am. 97 (5) Pt 1, May 1995	Measurement and Interpretation of the Impulse Response For Backscattering By A Thin Spherical Shell Using A Broad-Bandwidth Source That Is Nearly Acoustically Transparent.

Nintendo Exhibit 1066
IPR2024-00668 - Page 636

H16	Clayton Spikes, Christopher Clark. Sea Technology, April 1996	Whales 95 - Revolutionizing Marine Mammal Monitoring Technology

IMPACT SENSORS

I1	U.S. Patent 4,904,894 Henry et al. February 1990	Hail Sensor
I2	Joseph Paradiso, Craig Abler, Kai-yuh Hsiao, Matthew Reynolds	The Magic Carpet: Physical Sensing for Immersive Environments

KEYBOARDS

K2	Patent 4,234,813 Heishaburo et al. (Toray Ind) November 18, 1980.	Piezoelectric or Pyroelectric Polymer Input Element for Use as a Transducer in Keyboards.
K6	U.S.Patent 4,328,441. F.R.Kroeger & R.A. Norquist (3M) May 4, 1982.	Output Circuit for Piezo-electric Polymer Pressure.
K9	J.V.Chatigny, Atochem Sensors	Novel Switch Ideas Using Piezo pyroelectric Polymer films.
K10	U.S. Patent, 4,633,123. P.F. Radice (Pennwalt) Dec. 30, 1986	Piezoelectric Polymer Keyboard Apparatus.
K11	U.S. Patent, 4,975,616. K.T. Park	Piezoelectric Transducer Array.
K12	U.S. Patent, 5,315,204. Kyung Park	Piezoelectric Snap Action Switch.

MICROPHONES

M1	H.Naono, T.Gotch, M. Matsumoto (Acoustic Research Lab, Japan).	Design of an Electro-Acoustic Transducer using Piezoelectric Polymer Film.
M2	G.M. Garner (Allen Clark Research Centre). Systems Technology. 27 November 1977.	A new Microphone for Telephone Handsets.
M3	Pioneer Electric Corp.	Electroacoustic Transducer with Piezoelectric High Polymer Films.
M5	J.F. Sear & R. Carpenter (Allen Clerk - UK). Electronic Letters. 11. 1975.	Noise-Cancelling Microphone using a Piezoelectric Plastic Transducing Element.
M6	Reihard Lerch (Darmstadt, FRG). J. Acoust. Soc. Am. 66(4) October, 1979	Electroacoustic Transducers using Piezoelectric Polyvinylidene fluoride Films.

Nintendo Exhibit 1066
IPR2024-00668 - Page 637

M11	R. Lerch & G.M. Sessler. J. Acoust. Soc. Am. 76(4) April 1980	Microphone with Rigidly Supported Piezo Polymer membranes.
M15	I. Veit, Sennheiser Electronic Wedemark, Germany. Presented at 84th Convention of Audio Engrg Society, March 14, 1988	The Piezoelectric PVDF Film. Its properties and application in electroacoustic transducers.
M17	Edward F. Downs, Jr. NCSC IR415-89	Independent Exploratory Development Piezoelectric Diver's Microphone Development.

MEDICAL APNEA

MA2	UK Patent, 2,138,144, A J. Fraden ,Timex Medical, USA 14 February 1984.	Cardio-Respiration Transducer.
MA5	D.DeRossi and P Dario University Pisa and NCR Institute, Pisa.	Biomedical Applications of Piezoelectric and Pyro-Electric Polymers.
MA6	F. Steenkeste and &. Moschetto et al. Lille, France.	An Application of PVF2 Fetal Phonocardiographic Transducers.
MA7	K. Kobayashi & T. Yasuda Tokyo Ins. of Technology.	An Application of PVDF Film to Medical Transducers.
MA8	D. Dario, D De Rossie, R. Bedini, R. Francesconi & M.G. Trivella, Pisa, Italy.	PVF2 Catheter-Tip Transducers for Pressure, Sound & Flow Measurements.
MA10	Sally L. Hope et.al. Park Lane Surgery, Woodstock, Oxford UK. Journal of Ambulatory Monitoring 1988, Vol. 1 no. 1, 39-51.	Validation of the Accuracy of the Medilog ABP non-invasive blood-pressure monitor.
MA11	J. Fraden, Journal of Clinical Engineering. Vol.13, No3, Mar-April 1988.	Applications of Piezo/Pyroelectric Films in Medical Transducers.
MA14	U.S. Patent, 4,690,143, E. A. Schroeppel, Miramar, FL, Jan. 24, 1986	Pacing Lead with Piezoelectric Power Generating Means
MA16	D. Cavaye, M. Tabbara, G. Kopchok, R. White. Harbor-UCLA Med Ctr. Presented at So Cal Vascular Surgical Society Annual Scientific Mtg, Marina Del Ray, CA 9/91	Continuous Piezoelectric Pulse-Sensor Monitoring of Peripheral Vascular Reconstructions.
MA17	J. French, A. Siebens, Div of Rehab Medicine, Johns Hopkins Univ. Presented at RESNA 13 Annual Conf, Washington DC 1990	Interfacing Piezoelectric/ Pyroelectric Sensors for use with Communication Devices
MA18	C. K. McKibben, N. V. Reo, Dept of Chemistry, Kettering-Scott Magnetic Resonance Lab, Wright State Univ & Kettering Medical Center, Dayton OH	A Piezoelectric Respiratory Monitor for In Vivo NMR

Nintendo Exhibit 1066
IPR2024-00668 - Page 638

MA19	Medical Electronics Buying Guide. Sept 1994	Buyers Guide and Market Analysis
MA20	SBIR Research Proposal, Phase I Abstract	A Bilaminate Electronic Bioinductive Wound Seal.
MA21	Allen Zuckerwar, Robert Pretlow, John Stoughton, Donald Baker. IEEE Vol 40, No 9, September 1993	Development of a Piezopolymer Pressure Sensor for a Portable Fetal Heart Rate Monitor.
MA22	Chris Henry. July 1988	Vascucare Respiration Air Monitor (R.A.M.) Phase II, Engineering Report.
MA23	S. Chonan, Z.W.Jiang, Y. Tanahashi, M. Tanaka, Y. Suga	A Soft Palpation Sensor & its Application to Measurement of the Stiffness of Prostate Glands
MA24		North American Science Research Associates Inc. RESEARCH REPORT ON TOXICITY

MEDICAL OSTEOGEN

MO1	J.J. Ficat, R. Durroux et al (France). Univ Paul Sabatien	Osteogen material/Piezoelectric Polymer.

MUSIC

MS4	Pennwalt Press Release. June 1985.	Virtuoso Qualities in Electric Violin Made Possible by New Transducer Material.
MS5	Pennwalt Press Release. July 1985.	Piezo Film Pickup puts "The Sound of Magic" in New Gibson Guitar Line.

MEDICAL ULTRASOUND

MU5	Toray Industries, Tokyo, Japan. Ind. publication.	Piezoelectric Polymer Transducers for High Resolution Ultrasound Imaging.
MU6	J. Callerame et al. (Raytheon) in 1978 Ultrasonics Symposium, J. DeKerk & B.R. McAvoy, Editors IEEE Cat. No. 78 1344-ISU.V	Comparison of Ceramic and Polymer Transducers for Medical Imaging.
MU7	N. Chubachi (Japan). Paper presented at Joint Meeting of the Acoustical Society of America and Acoustical Society of Japan (Honolulu, 1978).	Piezoelectric Polymer Transducer and its application to Acoustics.
MU10	Mark Schafer & Peter A. Lewin. IEEE Transactions on Sonics and Ultrasonics, Vol. SU-31 No 4. July 1984	The Influence of Front-End hardware on Digital Ultrasonic Imaging.

Nintendo Exhibit 1066
IPR2024-00668 - Page 639

MU13	F.S. Foster et.al. Ultrasound in Med. & Biol. 9(2) 151-164 1983.	Breast Imaging with a Conical Transducer/Annular Array Hybrid Scanner.
MU16	Peter A. Lewin & Mark Schafer. Drexel University, Philadelphia, PA.	Piezoelectric Polymer Transducers for Ultrasound Dosimetry Application.
MU17	M. Platte.	A Polyvinylidene Fluoride Needle Hydrophone for Ultrasonic Applications.
MU18	C.T. Lancee, J. Souquet, H. Ohigashi and N. Bom, Fifth Symposium on Echo-cardiology, Rotterdam, 1983.	Ferroelectric ceramics versus polymer piezoelectric materials.
MU23	D.W. Fitting et al. IEEE Transactions on Ultrasonics, Ferroelectrics, vol. UFFC-34 No. 3, May 1987.	A Two-Dimensional Array Receiver for Reducing Refraction Artifacts in Ultrasonic Computed Tomography of Attenuation.
MU24	M. D. Shearer, F. S. Foster, University of Toronto.	A 100 MHz PVDF Ultrasound Microscope with Biological Applications.
MU25	Valerie P. Jackson, M.D. et al. RADIOLOGY, Vol. 159, No. 3, Pages 679-684, June 1986.	Automated Breast Sonography Using a 7.5MHz PVDF Transducer: Preliminary Clinical Evaluation.
MU26	L. F. Brown & D. L. Carlson.IEEE Trans. on Ultrasonics, Ferroelectrics & Freq Control. Vol.36, No3, May 1989.	Ultrasound Transducer Models for Piezoelectric Polymer Films.
MU28	Stephen W. Smith, Principle Investigator, ERC	Ultrasound Transducers
MU30	B. Granz, R. Holzapfel, G. Kohler, IEEE 1989 Ultrasonics Symposium	Measurement of Shock Waves in the Focus of a Lithotripter
MU31	P. A Contla, D. K. Das-Gupta, IEEE 1991	Ultrasonic Piezoelectric Transducer for Biomedical Applications
MU32	R. Goldberg, S. Smith, Dept. Biomedical Engrg, Duke Univ., Durham, NC; L. Brown, Atochem Sensors, Inc., Valley Forge, PA	In Vivo Imaging using a Copolymer Phased Array
MU33	L. F. Brown, PhD., Elect Engrg Dept, So Dakota St Univ; Presented at 1992 SPIE International Symposium on Optical Applied Science and Engineering, 7/21/92, San Diego, CA	New Developments in Piezoelectric Polymer Ultrasound Transducers and Transducer Systems

NON-DESTRUCTIVE TESTING

NDT1	R.Stiffler & E.G. Henneke, 11 (VPI). Materials Evaluation, 41. July, 1983.	Application of Polyvinylidene Fluoride as an Acoustic Emission Transducer for Fibrous Composite Materials.

Nintendo Exhibit 1066
IPR2024-00668 - Page 640

NDT4	Systems & Instrumentation Ltd. Pershore, Worcs, England.	Polymer Film Transducers.
NDT8	Lewis F. Brown, Ph.D. Pennwalt Corp., Valley Forge, PA. Presented at ASNT 1989 Fall Conference Oct 9-13 1989.	Piezoelectric Polymer Ultrasound Transducers for Nondestructive Testing.
NDT9	Lewis F. Brown, Ph.D. Pennwalt Corp., Valley Forge, PA. Presented at 7th Intl Symposium on Applic. of Ferroelectrics, June 6-8, 1990	New Ferroelectric Polymer Ultrasound Contact Transducers for Non-destructive Testing Applications
NDT10	Lewis F. Brown, Ph.D. Pennwalt Corp., Valley Forge, PA. Presented at 1990 Review of Progress in Quantitative NDE, July 15-20, 1990	Permanently Mounted Piezo Film Sensors for Structural Quantitative NDE
NDT11	Lewis F. Brown, PhD. Atochem Sensors, Inc. Valley Forge, PA. Presented at 1991 Review of Progress in Quantitative NDE, July 28-Aug. 2, 1991	PFS-Gap: A Large Area Ultrasonic Gap Profile Measurement System
NDT12	J. Bulteel, Sensor Review, Vol. 11 No. 3. 1991. pp. 23-24	Polymer Materials for Ultrasonic Transducers
NDT13	L.F. Brown, PhD. So Dakota St Univ, Brookings, SD; W.M. Sisson, United Technologies Res. Ctr, East Hartford, CT; C.P. Guerin, Elf Atochem Sensors, Valley Forge, PA. Presented at 1992 Conf on Review of Progress in Quantitative Nondestructive Evaluation, July 23, 1992, Univ of Cal-San Diego	Custom PVDF Transducers for Pulse-Echo Testing of Solid Rocket Motors for Detection of Propellant-to-Boot-Liner Unbonds
NDT14	L.F. Brown, PhD. So Dakota St Univ, Brookings, SD. Presented at 1992 IEEE Fall Ultrasonics Symposium, Oct 20-23, 1992, Tucson, AZ	Ferroelectric Polymers: Current and Future Ultrasound Applications
NDT16	Lewis Brown. 1992 IEEE 8th International Symposium	New Extremely Broadband Ferroelectric Polymer Ultrasound Transducers

OPTICAL

OP1	T. Sato, H. Ishida & Co. Ikeda (Japan). Applied Optics. 19(9).	Adaptive PVDF Piezoelectric Deformable Mirror System.
OP2	H. Ohigashi, R. Shigenari, & M. Tokota (Toray, Japan) Japan J. Appl. Phys. 14(7) 1975.	Light Modulation by Ultrasonic Waves from Piezoelectric Polyvinylidene Fluoride Films.
OP3	D. Broussoux & F. Micheron (France). J. Appl. Phys. 51(4). April, 1980.	Electro-optic and Elastoptic Effects in Polyvinylidene Fluoride.
OP4	T. Sato, Y. Ueda & O. Ikeda (Japan). Applied Optics 20(2). January, 1981.	Transmission-type PVDF 2-D Optical Phrase Modulator.

Nintendo Exhibit 1066
IPR2024-00668 - Page 641

OP5	S.A. Kokorowski (Hughes Research). J Opt. Soc. Am. 69(1) January, 1979.	Analysis of Adaptive Optical Elements Made from Piezoelectric Bimorphs.
OP6	R. Kashyap & P. Pantelis. Second Symposium on Optic Fibre Measurements, Oct. 13-14 1982	Measurement of Optical Fibre Absorption Loss: A Novel Technique.
OP7	P. D. DeSouza, M. D. Mermelstein, Applied Optics, Dec. 1, 1982.	Electric Field Detection with a Piezoelectric Polymer-jacketed Single-Mode Optical Fiber
OP8	H. Coufal (IBM) Applied Physics Letters. 44(1) January 1, 1984.	Photothermal Spectroscopy Using a Pyroelectric Thin-Film Detector.
OP9	U.S. Patent 4,748,366 George Taylor, Sept. 2, 1986	Novel uses of Piezoelectric Materials for Creating Optical Effects
OP10	H. Sasabe, T. Nakayama et al. (Japan). Polymer Journal 13(10). 1981.	Photovoltaic Effect in Poly(vinylidene fluoride)
OP11	A. Mandelis (Toronto) Chemical Physics Letters 108(4). July 13, 1984.	Frequency-Domain Photopyroelectric Spectroscopy of Condensed Phrases (PPES): A New Simple and Powerful Spectroscopic Technique.
OP12	V. S. Sudarshanam, R. O. Claus, Fiber & Electro Optics Res Ctr, VA Polytechnic Inst & State Univ, Blacksburg, VA. Accepted for publication in Proc Optical Fiber Sensors '93) Firenze, Italy, May 1993.	Fiber Optic Polarization and Phase Modulator Utilizing a Transparent Piezofilm with Indium Tin Oxide Electrodes

PYROELECTRIC

P5	K. Shigiyama & K. Miura (Matsushita Comm. Inds. Co.,Japan). Presentation.	PVDF Infrared Detector and Microphone for Monitoring.
P7	U. Korn, Z. Rav-Noy & S. Shtrikman (Israel). Applied Optics 20(11). June 1981.	Pyroelectric PVF2 Infrared Detector Arrays.
P12	U.S. Patent 3,824,098 J.G. BERGMAN et al. (Bell Labs) July 16, 1974.	Pyroelectric Copying Device.
P17	L.E. Ravich. Electronic Imaging. June 1984.	Pyroelectric Infrared Detectors.
P19	Pennwalt Corporation	KYNAR Properties.
P24	H. Meixner, G. Mader, P. Kleinschmidt. Siemens Entwickl. - Ber.Bd.15(1986)Nr.3.	Infrared sensors based on the Pyroelectric Polymer Poly-Vinylidene Fluoride (PVDF).

Nintendo Exhibit 1066
IPR2024-00668 - Page 642

P25	Microwatt Applications. Sea Cliff, New York. U.S.A.	Comparisons of Pyroelectric and Piezoelectric Properties and Manufacturing of Several Detector Materials for Military and Scientific Applications.
P26	Microwatt Applications. Sea Cliff, New York. U.S.A.	Motion Detection Systems with Pyroelectric IR Detectors.
P27	Alan P Doctor, Microwatt Applications Inc., Martin Rost, Servo Corporation.	Pyroelectrics for Smart Munitions.
P29	M. Hammerich and A. Olafsson, Physics Lab., HC Orsted Inst.	A Versatile, low-cost pyroelectric Laser Power Monitor for the 1mW to 50W range.
P30	Reinhard Freitag, Hans Meixner Siemens AG, Corporate Research and Development, Munich, West Germany.	PVDF Sensor Array for Human Body Detection.
P33	U.S. Patent 4,797,840 Jacob Fraden, Hamden, Conn. Jan 10, 1989	Infrared Electronic Thermometer and Method for Measuring Temperature
P34	Richard Brown, ASL; 14 Dec 1990	Thermal Detector
P36	M. Thompson, Atochem Sensors, Valley Forge, PA. Presented at the 1991 Sensors Conference, Chicago, IL	Advances in Passive Infrared Sensors Based on Pyroelectric Polymer Films
P37	Edward Tom, Atochem Sensors, Valley Forge, PA	Polymer Passive Infrared Design for Long Range Detection
P38	Edward Tom. SENSORS Sept 1994	Polymer Film Arrays in Pyroelectric Applications

POWER GENERATION

PW2	Hausler, E. & Stein L. Paper presented at Ocenas '85.	Hydromechanic-Electric Power Converter.
PW3	Richard Brown, Pennwalt (Europe). Appl. note.	The LED Report.
PW9	Richard Brown, ASL; 1 Jan 1991	Piezo Film Power Supply; Tyre Sensor
PW10	Richard Brown, ASL; 3 Mar 1991	Energy Generation Using Piezo Film
PW11	G.E. Taylor, J. R. Burns, OPT	Hydropiezoelectricity
PW12	Otter Controls Ltd, Derbyshire, England; OTT2P2, June, 1991	Otter Signals an End to High-Speed Tyre Blow-outs
PW13	USA Patent 3,665,226. R. Sinker, G. Williams; (Hughes Aircraft) May 23, 1972	Electric Power Source

Nintendo Exhibit 1066
IPR2024-00668 - Page 643

PW14	V. Hugo Schmidt. 1992 Ultrasonics Symposium	Piezoelectric Energy Conversion in Wildmills.
PW15	V. Hugo Schmidt. IEEE, 1986	Theoretical Electrical Power Output Per Unit Volume of PVF2 and Mechanical-To-Electrical Conversion Efficiency as Functions of Frequency.

ROBOTICS

R4	P. Dario, C. Domenici, R. Bardelli et al. Unpublished paper.	Piezoelectric Polymers: New Sensor Materials for Robotic Applications.
R5	P. Dario, R. Bardelli, D. de Rossie et al. Sensor Review. October, 1982.	Touch-sensitive Polymer Skin Uses Piezoelectric properties to Recognize Orientation of Objects.
R8	Allen R. Grahn and Lynn Astle. Salt Lake City.	Robotic Ultrasonic Force Sensor Arrays.
R9	D. DeRossi & P. Ario. Paper from "Robotics Research: The Next Five Years and Beyond." Aug. 14-16, 1984.	Multiple Sensing Polymeric Transducers for Object Recognition Through Active Touch Exploration.
R11	Greg Toto	Polyvinylidene Fluoride Tactile Transducers.
R12	P. Dario et al. University of Pisa, Italy.	Ferroelectric Polymer Tactile Sensors with Anthropomorphic Features.
R13	K.T. Park, R.D. Klafter, P.E. Bloomfield	A PVDF Tactile Sensor for Industrial Robots.
R14	U.S. Patent 4,634,917 J.E. Dvorsky, B.A. Kelly, R.B. McCown, D.F. Renner, (Battelle) Dec. 26, 1984	Active Multi-Layer Piezoelectric Tactile Sensor Apparatus and Method.
R15	R. Klafter, K.T. Park. Sensors Expo Sept. 16, 1987	Applications of a Piezoelectric Polymer Film to Robotic Sensing.
R16	D. DeRossi, A. Nannini, C. Domenici. Univers Pisa.	A Biominetic Tactile Sensor with Stress-Component Discrimination Capability.
R19	Sensors, June 1992	Ultrasonic Force Sensor Technology

SPEAKERS

S1	M. Tamura, T. Yamaguchi et al. (Pioneer Electronic Corp., Japan) Journal of the Audio Engineering Society. 23(1) January February, 1975.	Electroacoustic Transducers with Piezoelectric High Polymer Films.

Nintendo Exhibit 1066
IPR2024-00668 - Page 644

S2	Pioneer	Pioneers New High Polymer Molecular Transducer Technology Will Alter the Course of High Fidelity.
S3	B.Locanthi, K. Maekawa, K. Sugano et al. (Pioneer, Japan) Unpublished paper.	Development of a Loudspeaker System with Omni-Directional Horn Loaded High Polymer Tweeter.
S4	S. Edelman & A.S. DeReggi (NBS) Journal of the Audio Engineering Society. 24(7) September 1976.	Comments on "Electroacoustic Transducers with piezoelectric High Polymer Films.
S6	Jesse Klapholz, Klapholz Technologies. Presented at 79th Convention of the Audio Engrg Society. Oct. 12-16, 1985.	High Polymer piezo film in Electroacoustial Transducer Applications.
S8	Jesse Klapholz. db Magazine Nov-Dec. 1985.	Polymer Film for Transducers.
S11	U.K. Patent 8,626,712. Nov 8 1986. Clive Robertson, Pennwalt Piezo Film Ltd, Dunfermline, Scotland.	Integrating Amplifiers.
S12	K. Hatakeyama, S. Kinoshita, A. Haeno, T. Asanuma, Pioneer Electronic Corp. (Tokorozawa, Japan)	Development of a Loudspeaker System with Omni-Directional High Polymer Tweeters
S13	U.S. Patent 5,115,472. May 19, 1992. K. T. Park, P. F. Radice	Electroacoustic Novelties
S14	Joseph Paradiso, MIT Media Lab. IBM Systems Journal, November 1995	The Interactive Balloon: Sensing, Actuation and Behavior in a Common Object.
S15	U.S. Patent. 5,309,519. May 3, 1994 Kyung Park, Peter Radice	Electroacoustic Novelties
S16	Research Proposal	Thin Film Transducers as Implantable Hearing Aids
S17	Hong Wang	Piezoelectric Polymer Speaker
S18	J.A. Paradiso	The Interactive Balloon: Sensing, actuation, and behavior in a common object

SPORT

SP1	PCT. Patent No. WO 84/04692. P.P. Vanderreydt. 6 December 1984	Device for Localizing the Impact of a Ball or an Object on a Sports Court.

Nintendo Exhibit 1066
IPR2024-00668 - Page 645

SP2	PCT. Patent No. WO 89/05174 ENCICCA, Traian, Anghel. 15 June 1989.	Signalling System for Localizing in-out Ball Impacts by Ball Games
SP3	U. S. Patent No. 4,824,107 Larry J. French, Bay Village, Ohio. April 25 1989.	Sports Scoring Device including a Piezoelectric Transducer

TRAFFIC

TR1	R.M. Tyburski. ITE Journal, August 1989.	A Review of Road Sensor Technology for Monitoring Vehicle Traffic
TR3	W. Cunagin, A. Grubbs	Automated Acquisition of Truck Tire Pressure Data
TR5	S. Majdi; W. Cunagin, Texas Trans. Inst.; Nat'l Traffic Data Acquisition Tech. Conf., Austin, TX; 8/31/90	Piezoelectric Film Technology
TR6	R.C. Moore, Transport and Road Res. Lab, UK.	Piezo-electric Axle Load Sensors.

ULTRASOUND

U1	C. Alquie, J. Lewiner & C. Friedman (Paris). Applied Physics Letters. 29(2). July 15, 1976.	Piezoelectric Electret Transducers for Ultrasonic Generation and Detection Up to Microwave Frequencies.
U2	A.S. DeReggi, S.C. Roth et al. (NBS). J. Acoust, Soc. Am. 69(3), March 1981.	Piezoelectric Polymer Probe for Ultrasonic Applications.
U4	J. Schoenwald & J.F. Martin 1983. Ultrasonics Symposium.	PV2 Transducer for Acoustic Ranging and Imaging in Air.
U13	G.M. Garner. Plessey Research & Technology. Research Review 88.	A Short Range Ultrasonic Detector.
U15	A. Fiorillo, P. Dario, J. Vander Spiegel, C. Domenick, J. Foo, 1987 Ultrasonics Symposium V2. pp 667-670	Spinned P(VDF-TrFE) Copolymer Layer for a Silicon-Piezoelectric Integrated US Transducer
U16	P. H. Brown, Thorn EMI Central Research Laboratories	Ultrasonic Imaging with an Electric Beam Scanned PFDF Sensor
U21	F. Harnisch, Elotech GmgH; N. Kroemer, W. Manthey, Technical University. Sensors and Actuators A. 25-27 (1991) pp. 549-552	Ultrasonic Transducers with Piezoelectric Polymer Foil

Nintendo Exhibit 1066
IPR2024-00668 - Page 646

U22	E. Carome, K. Fesler, J. Shaw, D. Weinstein, L. Zitelli; Edward L. Ginzton Lab, Stanford Univ; 1979 Ultrasonics Symposium	PVF2 Surface Wave Transducers
U23	R. Wagers, Central Research Labs, TI, Dallas; 1979 Ultrasonics Symposium	Saw Transduction on Silicon Substrates with PVF2 Films
U24	R.G. Swartz & J.D. Plummer (Stanford). IEEE Transactions and Ultrasonics. SU-27(6) November 1980.	On the Generation of High-Frequency Acoustic Energy with Polyvinylidene Fluoride.
U25	F. Mattiocco, E. Dieulesaint, D. Royer. Electronics Letters 16(7). March 27, 1980.	PVF_2 Transducers for Rayleigh Waves.
U27	K. Park, M. Toda, AMP Flexible Film Sensors, Valley Forge, PA. April 1992	Piezo Film Ultrasound Distance Transducer for Automobile Obstacle Detection Applications
U28	Lewis Brown, Joel Mason	Disposable PVDF Ultrasonic Transducers For Nondestructive Testing Applications
U30	U.S. Patent 5,442,592 August 15, 1995. Minoru Toda, Kyung Park.	Ultrasonic Distance Meter
U32	Antonio Fiorillo. IEEE Transactions on Ultrasonics, Ferroelectrics and Frequency Control, Vol 39, No 6, November 1992	Design and Characterization of a PVDF Ultrasonic Range Sensor
U33	Lewis Brown, David Carlson	Ultrasound Transducer Models for Piezoelectric Polymer Films

VIBRATION AND ACCELERATION

VA1	T. Bailey & J.E. Hubbard, Jr. (MIT). Unpublished paper.	Distributed Piezoelectric-Polymer Active Vibration Control of a Cantilever Beam.
VA8	E. Tom, R.Bowman, D. McGovern. 1986 Carnahan Conf. on Security Technology May 14, 1986	Ferroelectric Sensor Technology Development, Intrusion Detection Using Ferroelectric Sensor Technology.
VA10	Richard H. Brown, Pennwalt Piezo Film Group, Edinburgh.	New Techniques for Model Analysis.
VA11	J.E. Hubbard, Jr., The Charles Draper Laboratory.	Distributed Transducers for Smart Structural Components.
VA15	Research Report C.K. Lee, IBM and F.C. Moon, Cornell University.	Laminated Piezopolymer Plates for Torsion and Bending Sensors and Actuators.
VA19	Richard H Brown, Pennwalt Piezo Film Ltd.	Piezo Film, Form and Function.

Nintendo Exhibit 1066
IPR2024-00668 - Page 647

VA22	C.K. Lee, IBM Research Div. Intern'l Conf. on Adv. Mechatronics, Tokyo May 21-24 1989.	Theory of Laminated Piezopolymer Plates for Torsional and Bending Control.
VA24	C.K. Lee, W.W.. Chiang, and T.C. O'Sullivan. Almaden Research Centre. IBM ACCESS Vol III. No.3 1989.	Piezoelectric Modal Sensors and Actuators Achieving Critical Active Damping on a Cantilever Plate.
VA35	J. Plump, Dr. J. Hubbard, Jr. (M.I.T.), T. Bailey, (Draper Laboratories); ASME Winter Annual Meeting 1985	Nonlinear Control of a Distributed System: Simulation and Experimental Results
VA36	D. W. Miller, S. A. Collins, S. P. Peltzman (M.I.T.); 31st AIAA/ASME/ASCE/AHS Structures, Structural Dynamics & Matls Conf, Long Beach, CA 4/2-4/90; pp 2283-2297	Development of Spatially Convolving Sensors for Structural Control Applications
VA37	S. W. Sirlin, Caltech; AAS/AIAA Astrodynamics Specialist Conf. Aug 10-13, 1987	Piezoelectric Polymer-Based Isolation Mount for Articulated Pointing Systems on Large Flexible Aircraft
VA39	S. Collins, C. Padilla, et al. AIAA/ASME/ASCE/AHS Structures, Structural Dyn. & Matls Conf Apr 2-4, 1990	Design, Manufacture and Application to Space Robotics of Distributed Piezoelectric Film Sensors
VA40	Prof. A. H. von Flotow, Charles Stark Draper, November, 1989	A Solid State Heliogyro (A PVDF Application)
VA43	C. K. Lee, T. C. O'SUllivan, IBM Res. Div. San Jose, CA, Research Rpt RJ 7636 (71083) 8/14/90	Piezoelectric Strain Rate Gages
VA47	S. J. Kim, H. D. Jones; Ray W. Herrick Laboratories, Sch. of Mech. Engrg., Purdue University, W. Lafayette, IN	Optimization of Piezo-Actuator/Substructure Coupling for Active Noise and Vibration Control
VA48	NASA Lewis Research Center, June 1992	Active Umbilical System for Microgravity Experiments (Piezo-PVDF Actuator Design Concept)
VA49	W. Nitsche, P. Mirow, T. Dorfler, ICIASF '89 Record, Res. Ctr Gottingen, W. Germany, 9/18-21, 1989 (IEEE Pub 89CH2762-3)	Application of Piezoelectric Foils in Experimental Aerodynamics
VA50	W. Nitsche, J. Szodruch, ICAS paper 90-6.1.4, 17th ICAS Congress, Stockholm, Sept, 1990	Concepts and Results for Laminar Flow Research in Wind Tunnel & Flight Experiments
VA51	W. Nitsche, P. Mirow, T. Dorfler, Berlin; Proceedings of ICIASF '89, Research Center Gottingen, W. Germany, 9/18-21/1989	Application of Piezoelectric Foils in Experimental Aerodynamics
VA52	D. Tasker, P. Gustavson, W. Wilson, Naval Surface Warfare Center, Res & Tech Dept. NAVSWCTR91-640, November 1991	A PVDF Trigger and Tilt Detector for Projectile Impact Experiments

Nintendo Exhibit 1066
IPR2024-00668 - Page 648

VA55	C.K. Lee. Intelligent Structural Systems	Piezoelectric Laminates: Theory and Experiments for Distributed Sensors and Actuators
VA56		Preliminary Piezo Film/Rail Assessment
VA57	U.S. Patent. 4,869,101 Sept 26, 1989. James Dvorsky Batelle Memorial Institute	Texture Softness Sensing
VA59	C.K. Lee, F.C. Moon. Journal of Applied Mechanics June 1990, Vol 112	Modal Sensors/Actuators
VA60	James E. Hubbard Jr, Calvin Lowe. December 1995 Charles Stark Draper Laboratory, Inc.	The Active Vibration Control of A Cantilever Beam Using PVF2 In A Simulated Space Environment.
VA61	Ki Won Yoon, Seung Jo Kim, Seoul Nat'l University; Wie Dae Kim, Pusan Nat'l University	Active Control of Sound Fields in Plate-Cavity System By Anisotropic Piezoelectric Polymers

Nintendo Exhibit 1066
IPR2024-00668 - Page 649

APPENDIX C -- APPLICATION NOTES

Nintendo Exhibit 1066
IPR2024-00668 - Page 650

INTRODUCTION

A loudspeaker is a transducer which transforms electrical signals into acoustic sound. Conventional speakers usually consist of a vibrating surface (called a diaphragm) and a driving units which is, in most cases, a voice coil driven by a magnetomotive force or a piezoelectric ceramic actuator. In piezoelectric polymer speakers, the active driving element and the air-pushing diaphragm are combined into a single unit. Utilizing the piezoelectric effect of polyvinylidene fluoride (PVDF) material and the flexibility of the polymer film, a unique speaker can be formed from PVDF which vibrates under the stimulus of an AC electric field applied to the surface electrodes on the film.

There are two principal types of loudspeakers. The first uses a vibrating surface to radiate sound directly into the air. The second uses an acoustic element (a horn, e.g.) which is inserted between the diaphragm and the air. The direct radiator type is used most often in small radios, residential, and automotive stereo systems. The horn type is used in high fidelity systems, large sound systems for auditoriums and theaters, and outdoor music and PA systems. Here we will only discuss piezo polymer speakers for direct radiating systems. The uses and effects will be discussed in a separate application note.

SPEAKER STRUCTURE

An extremely crude speaker element can be created by simply hanging a sheet of piezo polymer film in air and applying an AC electrical signal. Sound will emanate from the film and its audio characteristics will vary as you flex and bend the film in different directions. Although this demonstrates basic operation, the performance is marginal and unpredictable at best. By controlling the shape of the film and the support structure of the mounting, a very acceptable speaker can be created.

Please refer to Figure 1. A simple speaker design consists of two parts. The first is the vibrating PVDF diaphragm and the second is the speaker enclosure and support structure. Because PVDF film is anisotropic in its surface piezoelectric parameters, it is important to orient the film properly in this design. The maximum displacement per volt applied is along the machine direction (or “1” direction) of the film. As such, the highest acoustic output is achieved when the machine direction is oriented in the length L direction. The width W is perpendicular to the machine direction and the total height of the speaker consists of the enclosure depth H_2 and the film height H_1.

The function of the enclosure is to isolate the front side of the film from the rear side. The film is curved in one direction (the direction of highest piezoelectric activity) and clamped rigidly onto each end of the enclosure. The curvature of the film is maintained by the sides of the enclosure. When a voltage is applied to the film electrodes, it creates a mechanical strain in the film in both the normal direction and in-plane active direction. Because the film is very thin, the strain in the normal direction is negligible. However, the larger displacement caused by in-plane strains is converted to radial motion along the radius of curvature and perpendicular to the film surface.

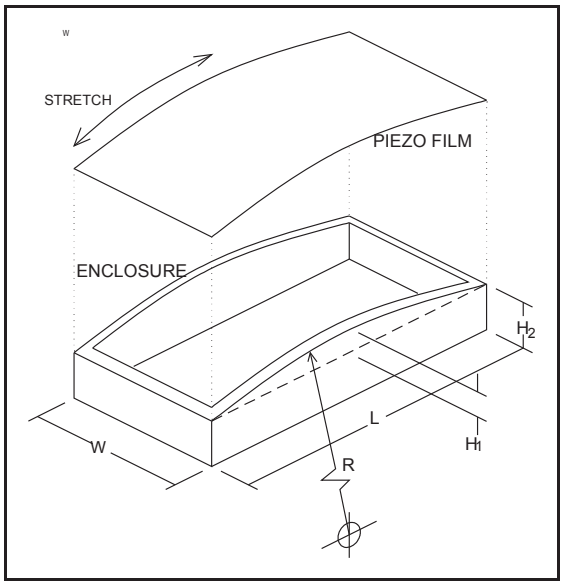


Figure 1

Nintendo Exhibit 1066
IPR2024-00668 - Page 651

Because of the curvature, the film surface basically moves in and out of the enclosure. The large film area effectively couples acoustic energy into the surrounding air. This speaker design has very good high frequency characteristics. The acoustic output is constant for frequencies up to 20 kHz.

Sound pressure levels at a specified distance, and the frequency response curves of a piezoelectric polymer speaker can be analytically calculated by solving the wave equation for a curved plate in conjunction with the electro-mechanical equations of piezoelectricity.
The calculations involve the size and shape of the film element, amplitude of the driving signal, piezoelectric properties and dielectric and mechanical loss properties of PVDF film materials, radiation impedance effects, and the mass loading effects of the electrode materials, among other parameters. MSI has developed a computer program to obtain numerical results from a wide variety of parameters. Because of the complexities, the details of these calculations will not be presented here. Discussed below, however, are the effects of key structure parameters on the acoustic performance of a typical speaker design.

DESIGN PARAMETERS

PVDF FILM THICKNESS - Piezoelectric film is available in various thickness'. Standard thickness' from MSI are 28 µM, 52 µM, and 110 µM. Other thickness' are available on a special order basis. The sound pressure level produced by a piezo polymer speaker at a certain distance is directly proportional to the applied electric field strength. Therefore, for a given voltage, in principle, the thinner the film, the higher the sound pressure produced. Sound Pressure Level (SPL) is usually used to measure the output performance of a speaker and is defined by the following equation:

$$SPL = 20 \log_{10} \frac{P}{P_{ref}} (dB)$$

P is sound pressure at a certain distance from the speaker and $P_{ref} = 2 \times 10^{-5}$ Pascal. Reducing the film thickness by half will generate a 6 dB increase in SPL. However, reducing film thickness will increase the capacitance of the speaker element, resulting in a higher current draw from the power amplifier (this will be discussed later). The use of thinner films can also cause deformation of the film curvature especially for speakers requiring large area of PVDF film. This deformation of curvature can cause irregularities in the frequency response curve.

CURVATURE OF PIEZOELECTRIC POLYMER FILM - The curvature radius of a film speaker is an important parameter for determining the frequency range of the speaker. For a rough estimation, the low frequency cutoff of a speaker is proportional to the square root of the ratio of Young's modulus of PVDF film to its density, and inversely proportional to the radius of curvature. Substituting the material property parameters, this low frequency can be estimated by the following equation:

$$f \sim \frac{21}{R(cm)} kHz = \frac{53}{R(inch)} kHz$$

R is the radius of curvature and *f* is the low frequency corner. See Figure 2. Note that the above equation does not take the mass loading effect of the electrodes into consideration. When the PVDF film is thin and heavy electrode materials such as silver ink are used, the above equation should be modified.

Nintendo Exhibit 1066
IPR2024-00668 - Page 652

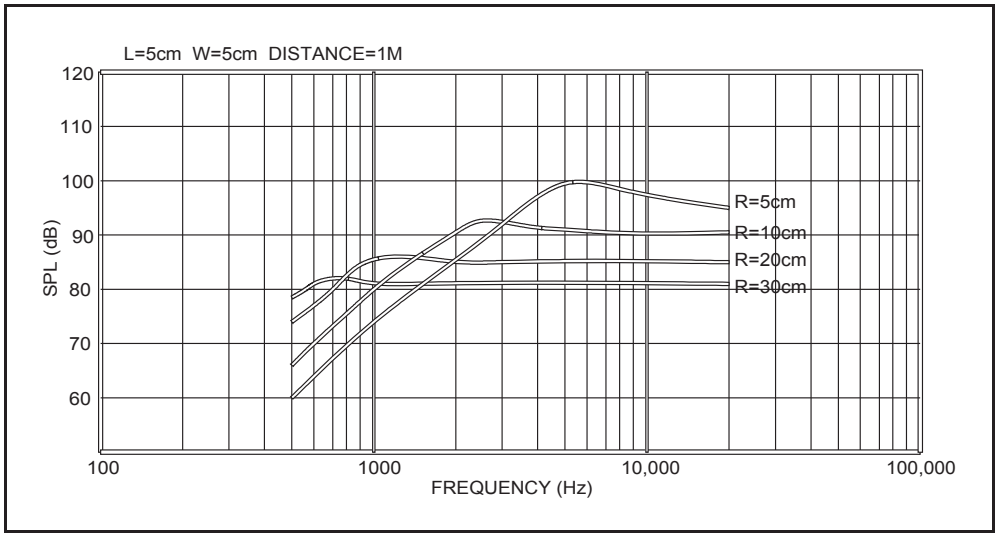


Figure 2

In the design of a piezo polymer speaker, the curvature of the film needs to be considered along with other structural parameters. For example, for a small area speaker, especially with a short length L, a large radius makes the film close to a flat plane, resulting in a lower acoustic output. On the other hand, for a large area speaker, a small radius makes the speaker deeper which requires a larger space.

Changing the radius not only controls the cutoff frequency, but also affects the sound pressure level at certain distances from the speaker. Figure 3a shows the relationship between low frequency corner and radius of curvature. Figure 3b shows the relationship between SPL at 10 kHz and radius of curvature for the same speaker. As seen from the graphs, the cutoff frequency and SPL are both inversely proportional to the radius.

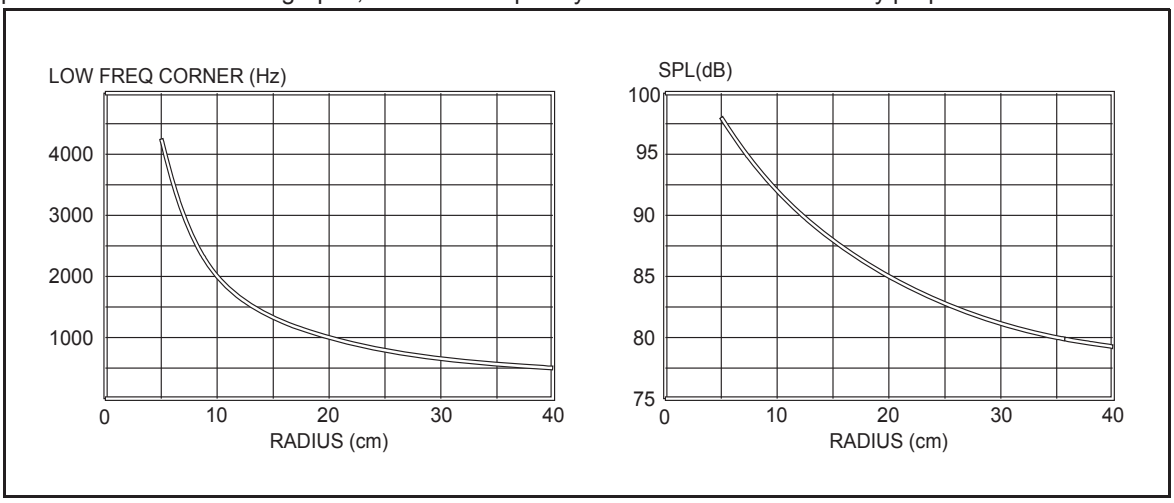


Figure 3a **Figure 3b**

Nintendo Exhibit 1066
IPR2024-00668 - Page 653

LENGTH AND WIDTH OF SPEAKER FILMS - The acoustic output of a PVDF speaker is directly related to the length and width dimensions which are, in turn, determined by each different application. The sound pressure generated by a speaker at a certain distance is linearly proportional to the active area of PVDF film. Therefore, SPL is a logarithmic function of the PVDF film dimensions if the speaker area is rectangular. Figures 4a & 4b show the relation between SPL and film length and width respectively at 10 kHz.

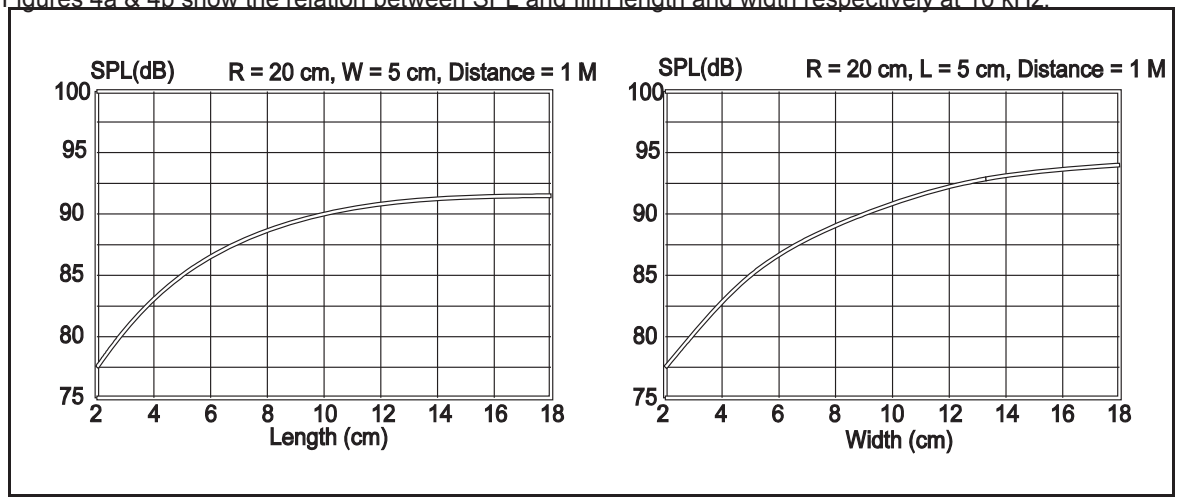


Figure 4a Figure 4b

POWER CONSIDERATIONS

In order to obtain a significant displacement from PVDF film to radiate sound, a high voltage is usually required. A step-up audio transformer can be used to increase the output voltage of an audio amplifier. The designer should give consideration to the electrical properties of the PVDF film speaker and the capabilities of the audio amplifier when selecting or designing the transformer. The input/output voltage ratio is directly proportional to the primary/secondary turns ratio of a transformer:

$$\frac{V_{sec}}{V_{pri}} = -\frac{N_{sec}}{N_{pri}}$$

The primary/secondary impedance ratio is proportional to the square of the turns ratio. The transformer must have an output impedance that is equal to or less than the PVDF film impedance at the highest specified frequency. If these impedances are not matched, significant distortion may result.

Conventional speakers present a resistive load to the power amplifier output while a PVDF film speaker presents a capacitive load to the output. Because of this the piezo film speaker impedance changes with frequency. For a 28 µm thick film with an area of 10 cm X 10 cm, the typical capacitance is about 35 nF. In the high frequency audio range, the impedance of such a speaker is quite low resulting in a high current draw from the amplifier. This current is about 90 degrees out of phase with the voltage applied to the PVDF film. With the high applied voltage and large current at higher frequencies, the apparent power, defined as the transformer output current times the voltage applied to the PVDF film, is somewhat higher when compared to conventional speakers. This power issue needs to be considered when choosing amplifiers and transformers. Because of the capacitive nature of a PVDF film speaker, an electrical resonance is introduced when using a transformer. This resonance should be avoided within the frequency range of interest or carefully damped.

PRACTICAL DESIGN TIPS FOR SPEAKERS

A reasonably good tweeter can be made using the basic design shown in Figure 1**.** Keeping the film smooth and wrinkle free will reduce distortion and provide a flat frequency response. The support should also be as rigid as possible to maximize the film surface displacement.

Nintendo Exhibit 1066
IPR2024-00668 - Page 654

The lead attachment area should not be on the PVDF film radiating surface because any non-uniformity in the radiating element can be a source for distortion of air cavity. Filling the enclosure with a sound absorbing materials such as fiberglass or absorbing foams will reduce resonances and improve the sound quality**.** The enclosure should be made as rigid as possible to reduce structural resonances.

APPLICATIONS AND ADVANTAGES

Piezoelectric polymer speakers can be made in just about any imaginable shape or size. Square or rectangular elements can be sized to fit any available space. Wide horizontal or vertical dispersion angles can be obtained by wrapping the film in a 180 degree or 360 degree shape. The film can form a stand alone speaker element or can be laminated or attached to other structures to become an integrated speaker. A single film held in a shape with different curvatures in different areas of the film can provide unusual and unique frequency response characteristics. Piezo film speakers have the advantages of flat frequency response, high sound quality, low weight, flexible form factor, low cost, and ease of manufacturability. PVDF film speakers have a wide range of applications including home stereo, home theater, automotive, personal stereo, multi-media, and stereo headphones.

SAMPLE SPECIFICATION

PARAMETER	VALUE
Frequency Range	3.5 kHz - 20 kHz
SPL @ 40 cm	105 dB +/- 5 dB
Drive Voltage	125 V_{rms}
Enclosure Dimensions	13 cm X 11 cm X 6 cm
Radius of Curvature	7 cm
PVDF Thickness	52 µM
PVDF Capacitance	24 nF

* * * * * * * *

Nintendo Exhibit 1066
IPR2024-00668 - Page 655

DISCUSSION OF ULTRASONIC INK LEVEL SENSING

Q: What is MSI's concept for detecting low ink level?

A: Right now, ink level in an ink-jet print cartridge can be measured using resistance (if the ink is partially conductive), or can be estimated by simply counting the number of droplets ejected. There are situations where neither approach will work – when the ink does not contain carbon, or where the cartridge is replaceable separately from the print head. MSI has based their approach on other work involving high-frequency ultrasound, and propose a kind of ultrasonic switch for each chamber of the cartridge. This "switch" would be a small patch of piezoelectric polymer, stuck onto the outside of the cartridge, which can send and receive an ultrasonic pulse into the wall. If the ink level is above the point where the patch is located, then most of the ultrasonic signal will travel on into the ink, and only a weak echo returns to the sensor. If the ink level is below the patch, then most of the signal returns, and the echo is strong. A simple voltage threshold is used to detect which condition exists.

Q: Sounds easy. What's the catch?

A: The basic principle is pretty straightforward, and has been demonstrated in the lab using electronics based on readily available discrete components. We know it has to be a low-cost solution, both for the sensor and the associated electronics. The integration of the electronics into an ASIC should be quite practical. The operating frequency of the device is high (about 20 MHZ) and we need some gain (+40 dB seems likely) – but the development of mobile phones and high capacity hard disk drives has made this requirement seem quite realistic. Our biggest challenge is, quite simply, fixing the sensor onto the wall. If we don't achieve good consistency in this area, the sensor would not be reliable. It is unlikely that MSI will be doing this part of the assembly, so we need to work together to make sure that the process works.

Q: What about multiple chambers in a single cartridge? I'm interested in monitoring color cartridges.

A: Obviously, we could arrange separate sensors for each chamber. With our piezo film technology, this is easy since we can form independent patterns on a single piece of film. So an arrangement with three active signal electrodes, and a common ground, would work well – but this would require four contacts, and some mutiplexing on the receiver amplifier input.

At this point, we began to think of ways to combine three sensors (for example) into a single, extended one, to simplify the interconnection and the associated electronics.

The obvious possibility is to treat the three separate walls as if they were one, allowing the three echoes to "add up" on arrival. If any one out of the three echoes were to increase in amplitude (as the ink level fell below the sensing point), we could detect this and flag the condition. This sounds fine until we consider the influence of tolerances on the echo amplitude. The basic piezoelectric coefficients of our material don't vary much along the length of a roll of film, but we would need to consider roll to roll variation, temperature influence on sensitivity, adhesive bonding variations, adhesive property temperature variations, wall tolerances on thickness and parallelism, and the variation of these with temperature.

Q: It's beginning to sound "risky". What is the basic signal/noise ratio?

A: Typically around +10 dB amplitude change, from ink to air on the inside of the wall. The precise value depends on the wall material, and slightly on the ink composition. But if we allow ± 3 dB on the starting level to cover all tolerance ranges, then add up three return echoes, we don't think we would have a very good "switch"!

That's why we exploited another concept we originally developed for a different kind of liquid level sensor – creating different path lengths for the ultrasonic signal for each chamber. This would simply be done by arranging fractional differences in the wall thickness of each chamber. This separates the three returning echoes so they arrive one after another, with approximately equal amplitude. We still have a tolerance associated with the amplitudes, but they don't add, and a single threshold should suffice to detect any one out of the three going "dry". The same principle applies for any number of chambers (within reason!).

Q: How much thickness change is required for each chamber?

Nintendo Exhibit 1066
IPR2024-00668 - Page 656

A: Difficult to say, before we optimize many of the variables, but 0.2 to 0.5 Mr. & Mrs. steps look practical right now. So 1.0, 1.5 and 2.0 Mr. & Mrs. walls would certainly work – if necessary, the imbalance in internal volume could be made up by adding or subtracting material elsewhere in the chamber. The step size could be smaller, if we push for "perfect" ultrasonic waveform and possibly higher frequency.

Q: My cartridges have sponges inside. Will this affect the performance?

A: We believe not. It seems so far that a dry sponge looks just like air, and a wet sponge just like ink. It really is quite difficult to get good ultrasonic coupling at 20 MHZ frequency, and the dry sponge simply lying in contact with the wall does not, as far as we can tell, absorb any of the ultrasonic energy at the interface. Even pushing a solid, flat block of polymer against the inside wall doesn't affect the signal unless a significant amount of force is applied, or liquid is allowed to penetrate into the gap.

Q: It sounds like the fixing of the sensor onto the wall is going to be quite a challenge!

A: The ideal case would be a very thin layer of liquid adhesive, which then cured to reach a hard state – epoxy works great! But we appreciate that a liquid process may not prove acceptable in production. We may be able to procure an off-the-shelf "transfer adhesive" (in tape form) which we can laminate to our film during our production cycle. Alternatively, we may need to enter into a dialog with a tape converter who could develop and apply a coating (with release liner) onto our film.

We envisage supplying reels of self-adhesive "labels", kiss-cut to allow easy application onto cartridges.

Q: I understand the principle of the sensor. Now, how do we connect to this "label"?

A: We're working on this! One possibility is lightly-sprung contacts, which would be brought into contact only when the cartridge is at rest. Our electrode surface will be either sputtered metallization (around 500 Å thick) or printed silver ink (about 7 µm), so we don't think a wiping contact would be appropriate. Another possibility is capacitive coupling, if we can arrange some reasonable area of electrode surface (for both signal and ground tracks) to come into proximity with a similar arrangement fixed to the printer. There would be further signal losses, and probably additional tolerance variations, if this method were adopted. This is partly a cost issue – if we add too much area to the sensor just for capacitive coupling, the cost of this inactive area may jeopardize the economics of the whole solution.

The connection scheme also has to take into account the physical layout and practicalities of the printer itself. We can't design the solution in a vacuum – we need input from both the mechanical and electronic design teams responsible for the printer.

Q: Where should the interface electronics be located? Can I integrate these into an ASIC on the main pcb?

A: We think so. The sensor will be designed to have as low an impedance as practical at the operating frequency – ideally 50 ohms. Although we have, in theory, a small "antenna" connected to the gain stage, in practice we don't see noise pick-up as being a major problem. Shielded cable, or "gnd-sig-gnd" coplanar wiring would be preferred for carrying the signals over any significant distance within the printer. Our measurement process should only take a few microseconds, so it is possible that a "quiet time" (as far as intentional digital or control activity is concerned) could be selected to make the measurement. Noise radiation and immunity would need to be considered and reviewed throughout the design process.

Q: What control do I have over the "switching point"?

A: The placement of the sensor, of course, dictates the basic depth of ink where the "switch" will change state. Ideally, the active electrode area would be a narrow horizontal line. In practice, we prefer to use a rectangular element to increase the capacitance of the sensor (which allows better matching to practical electronics). The "switching point" will nominally occur at the vertical midpoint of the sensor. A "height" in the region of 5 to 10 Mr. & Mrs. appears likely for the overall "label", so the lowest sensing depth may be 2.5 to 5.0 Mr. & Mrs. Temperature effects may vary the apparent location of this switching point, but worst-case uncertainty would be determined by the active electrode height.

Q: What factors would MSI wish to influence in my cartridge design?

A: The base material has an influence on the effectiveness of the solution. Some polymers (such as Nylon and acetyl) have high attenuation in the ultrasonic region. A close match of acoustic impedance

Nintendo Exhibit 1066
IPR2024-00668 - Page 657

(speed of sound x density) to the ink would be preferred. Given several choices, we would evaluate and select the most favorable.

The wall thickness(es) have already been discussed, but it is also important to have the best possible parallelism at the sensing area. We appreciate that a finite draw angle is required for the moulding process, but if this can be minimized in the region of interest, then it makes our job much easier.

Smooth surfaces (outside and inside) work best – a spark-eroded on the outside surface would make ultrasonic coupling extremely difficult.

Q: I'm interested. How do we proceed?

A: We would split up the development effort into phases. Before commencing, we would seek to establish performance and economic targets for the solution, including timescales for the various stages of effort.

As a guideline, MSI would propose the following:

In Phase 1, MSI would build and supply concept demonstration units based on available cartridge samples, using discrete electronics. These units would not be qualified for temperature dependence or noise immunity, nor would the transducers or electronics be optimized, but they would serve as a discussion point when considering future effort. Basic performance would be documented in the form of a brief engineering report, together with candidate interconnection schemes and their characteristics.

Phase 2 would involve investigations into candidate adhesive systems and processing, study of temperature and other environmental effects on transducer performance, preparation of budgetary estimates for production equipment design and procurement, budgetary estimates of unit cost in production volumes. A series of prototype transducers would be supplied for customer evaluation and qualification.

A separate (perhaps parallel) effort may be required to qualify the selected interconnection scheme. This is highly dependent upon specific details of the printer design, and it is possible that this effort may best be performed by the printer manufacturer.

Phase 3 would lead towards product launch, including the design and procurement of production tooling.

Nintendo Exhibit 1066
IPR2024-00668 - Page 658

EXHIBIT 1063D

web.archive.org/web/19990221083428/http://www.msiusa.com/piezo_film_manual.htm

http://www.msiusa.com/piezo_film_manual.htm Go JAN FEB APR

18 captures 21 Feb 1999 - 10 Apr 2021

1998 21 1999 2000 About this capture



Home
MSI Profile
Investors
Consumer
Sensors
Piezo Film
Accelerometers
Piezo Cable
Shockwriter
Sonar Hydrophones
Traffic Sensors
Vibration and Dynamic Strain Sensors
Transducers
Search
Contact Us





Technical Manual

Contents

PART1-INT.pdf
PART2-INT.pdf
PART3-INT.pdf
PART4-INT.pdf
PART5-INT.pdf
PART6-INT.pdf
PART7-INT.pdf
PART8-INT.pdf
PART9-INT.pdf
PART10-INT.pdf
PART11-INT.pdf
PART12-INT.pdf
PART13-INT.pdf
PART14-INT.pdf
PART15-INT.pdf
PART16-INT.pdf
PART17-INT.pdf
PART18-INT.pdf

Product Information

Accelerometer ACH Specifications
805SPEC3.pdf

Accelerometer ACH Analog Test PCB
805SPCB1.pdf

Piezo Coax Cable
Piezo_Cable.pdf

BL Sensor Package
BL Traffic Info.pdf

Piezo-Polymer Speakers
AN1242138.pdf

Solid State Switches
1141084.pdf

Download Our Piezo Film Products Guide!

Sensors_Product_Guide.pdf

The Wayback Machine - https://web.archive.org/web/19990221083428/http://www.msiusa.com:80/piezo_film…



back_button.gif

info_downloads.gif (2044 bytes)

Home
MSI Profile
Investors
Consumer
Sensors
Piezo Film
Accelerometers
Piezo Cable
Shockwriter
Sonar Hydrophones
Traffic Sensors
Vibration and Dynamic Strain Sensors
Transducers
Search
Contact Us

Technical Manual

Contents

PART1-INT.pdf
PART2-INT.pdf
PART3-INT.pdf
PART4-INT.pdf
PART5-INT.pdf
PART6-INT.pdf
PART7-INT.pdf
PART8-INT.pdf
PART9-INT.pdf
PART10-INT.pdf
PART11-INT.pdf
PART12-INT.pdf
PART13-INT.pdf
PART14-INT.pdf
PART15-INT.pdf
PART16-INT.pdf
PART17-INT.pdf
PART18-INT.pdf

Product Information

Accelerometer ACH Specifications
805SPEC3.pdf

Accelerometer ACH Analog Test PCB
805SPCB1.pdf

Piezo Coax Cable
Piezo_Cable.pdf

BL Sensor Package
BL Traffic Info.pdf

Piezo-Polymer Speakers
AN1242138.pdf

Solid State Switches
1141084.pdf

Download Our Piezo Film Products Guide!

Sensors_Product_Guide.pdf

Can't read PDF files?

Get Acrobat Reader

Transducers | Piezo Film
Home | Profile | Investors | Consumer | Sensors | Contact | Search

MEASUREMENT SPECIALTIES

Nintendo Exhibit 1066
IPR2024-00668 - Page 661

web.archive.org/web/20000925200634/http://www.msiusa.com/PART11-INT.pdf

http://www.msiusa.com/PART11-INT.pdf Go AUG SEP 25 OCT

1 capture
25 Sep 2000

1999 2000 2001 About this capture

MEASUREMENT SPECIALTIES

Piezo Film Sensors

Technical Manual

Nintendo Exhibit 1066
IPR2024-00668 - Page 662

MEASUREMENT SPECIALTIES

Piezo Film Sensors

Technical Manual

Internet Version

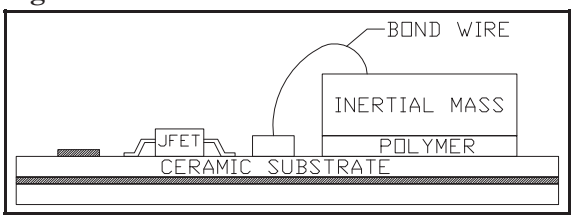
Part 11 of 18

Accelerometers
Table 6. Accelerometer Family
Table 7. Accelerometer Applications

ACCELEROMETERS

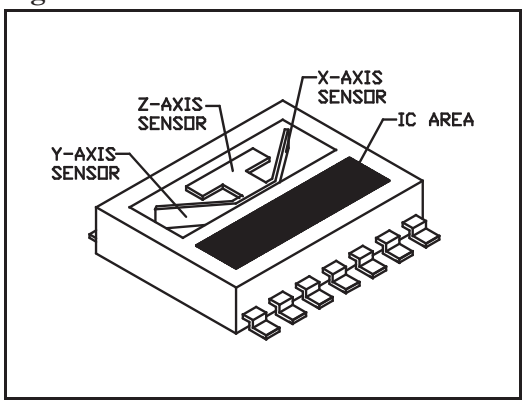
A logical outgrowth of the many vibration sensor applications of MSI's piezoelectric technology are accelerometers. These accelerometer designs are based on more traditional piezoelectric ceramic, as well as piezoelectric polymer materials. The choice of base materials allows the product to be tailored for specific applications. Table 6 lists the key specifications for the MSI Accelerometer product family.

Figure 59. ACH-01-XX internal view



Like more conventional sensors, these accelerometers are configured as either compression-design type or beam-design type. Compression-design accelerometers typically have higher resonant frequencies providing wide useful frequency ranges. Consequently, they also tend to have lower sensitivities. An internal view of MSI's ACH-01-XX compression-design accelerometer is shown in Figure 59.

Figure 60. ACH-04-08-05 internal view



Beam-design accelerometers, on the other hand, tend to have lower resonant frequencies and useful frequency ranges but higher sensitivities. Beam-design accelerometers also have another very interesting feature: They can be oriented to sense acceleration in multiple-axes with one monolithic sensing element using MSI's patented "Origami" beam technology ("Origami" is the Japanese word for the art of paper folding). An internal view of the ACH-04-08-05 beam-design accelerometer, with its origami sensing element, is shown in Figure 60.

To reduce system costs as well as simplify use, all of MSI's accelerometers include some type of integral electronic sensor interface. The ACH-01 family of accelerometers and the ACH-04-08-05 multiple-axis accelerometer both use simple JFET impedance buffers. With these sensors, JFET biasing and signal processing is implemented external to the device. The rest of the ACH-04-08 multiple-axis accelerometer family uses custom ASIC's (**A**pplication **S**pecific **I**ntegrated **C**ircuit) to provide impedance matching, gain, and signal processing. The system gain, output type (analog or digital), and output axis can be programmed (via on-chip EEPROM) to allow the sensors to be easily configured for a specific application. A SLEEP mode, to minimize power requirements, is also included.

The ACH-01 family of products is typically used in applications which require broad frequency capability, high sensitivity, low noise, and low cost. Such applications include: speaker feedback and control systems, automotive anti-theft systems, acoustic pick-ups, machine-health and pump monitoring systems, and medical body motion monitoring.

The ACH-04-08 product family, because of the products wide capabilities, is used in a very broad range of applications such as computer hard-disk-drive shock sensing, speaker feedback and control systems, appliance fault monitoring, virtual reality systems, automotive systems, medical body motion monitoring, shipment damage and material-handling monitoring systems, GPS systems, vibration switches and earthquake shut-off switches. OEM applications that require acceleration or vibration measurements in more than one axis are perfect for the ACH-04-08.

MSI is constantly developing and upgrading its accelerometer product line. Please contact MSI for further details on these products or on customizing one of our other products.

Nintendo Exhibit 1066
IPR2024-00668 - Page 664

Table 6. Accelerometer Family

Production Qualified Accelerometers					
		ACH-01-XX	**ACH-04-08-01**	**ACH-04-08-07/08**	**ACH-04-08-05**
Key Features		-Wide Frequency Range -Wide Dynamic Range -High Sensitivity -Low Noise -Very High Resonance -JFET Buffer IC	-Integrated ASIC -Programmable -Digital & Analog Output -SLEEP Mode -NOT for New Designs	-Integrated ASIC -Programmable -Digital & Analog Output -SLEEP Mode -IR Reflow Solder	-Low Frequency Operation -3 Simultaneous Analog Outputs
Sensitive Axes	X-Axis	---	----	---	X
	Y-Axis	---	X	X	X
	Z-Axis	X	X	---	X
	Angular @ Z	---	X	X (08 only)	---
Sensitivity		10 mV/g	15 to 150 mV/g 0.3 mV/rad/s^2	22 to 250 mV/g 0.4 mV/rad/s^2 (08 only)	1.8 mV/g
Frequency Range (±3 dB)		1.0 Hz-20 kHz	30 Hz to 3 kHz	11 Hz to 3 kHz	0.5 Hz to 5 kHz
Dynamic Range		±250 g	±67 g (Max)	±45 g (Max)	±250 g
Resolution (@ 100 Hz)		20μg/$\sqrt{Hz}$	1800μg/$\sqrt{Hz}$	390μg/$\sqrt{Hz}$	200μg/$\sqrt{Hz}$
Resonant Frequency		>35 kHz	6.5 kHz	6.5 kHz	9.2 kHz
Resonant Q (Hz/Hz)		30	10	10	10
Transverse Sensitivity		5%	25%	10%	15%
Linearity		0.1%	0.1%	1%	0.1%
Operating Temperature		-40 °C to +85 °C	0 °C to +70 °C	0 °C to +70 °C	-40 °C to +85 °C
Storage Temperature		-40 °C to +85 °C	-40 °C to +85 °C	-40 °C to +105 °C	-40 °C to +85 °C
Maximum Shock		1000 g	1000 g	1000 g	1000 g
Supply Voltage		3 V to 40 V	4.5 V to 5.5 V	4.5 V to 5.5 V	3 V to 40 V
Supply Current (mA)		2μ A Typical	2m A Typical	2m A Typical	2μ A Typical
Weight		3 grams	0.35 grams	0.35 grams	0.35 grams
Size (mm)		13 x 19 x 6	11 x 10 x 1.8	11 x 10 x 1.8	11 x 10 x 1.8
Mounting Method		Adhesive	Hand Solder to PCB	Reflow Solder to PCB	Hand Solder to PCB

Nintendo Exhibit 1066
IPR2024-00668 - Page 665

Table 7. Accelerometer Applications

	ACCELEROMETER PRODUCTS				
Industry	**Application**	**ACH-01-XX**	**ACH-04-08-01**	**ACH-04-08-07/08**	**ACH-04-08-05**
Aerospace & Defense Electronics	Anti-Tamper Sensors	X	X	X	X
	Surveillance	X			
	Modal Analysis	X	X	X	X
Automotive	Frontal Airbag		Consult factory for multiple-axis airbag accelerometer information		
	Side Airbag				
	Antitheft	X	X	X	X
	Skid/Rain Sensing	X	X		
Computers & Peripherals	Disc Drive Shock Sensor		X	X	
	Computer Mouse Sensor				X
	Virtual Reality Sensor				X
Household Appliances	Out-of-Balance Sensor		X	X	X
	Spray Arm Jam Sensor		X	X	X
	μ wave Acoustic Sensor	X		X	
	Vibration Switch		X	X	
Consumer Electronics	Speaker Feedback	X		Consult factory for Other Options	
	Acoustic Pick-ups	X			
	Security		X	X	X
Industrial	Machine Health Monitor	X		X	X
	Bearing Monitor	X		X	X
Instruments & Measuring Equipment	Active Vibration Damping	X			X
	Vibration Switches		X	X	
	Predictive Maintenance	X		X	X
Medical	Motion Sensor		X	X	X
	Pacemaker	Consult Factory for further Information			
Power & Utilities	Earthquake Shut-Off				X
	Machine Monitoring	X		X	X
Telecom-munications	GPS Systems		X	X	
	Vibration Switches		X	X	
Transport & Material Handling	Shipment Monitoring	X			X
	Railroad Systems	X			X

Nintendo Exhibit 1066
IPR2024-00668 - Page 666

EXHIBIT 1064A

https://web.archive.org/web/20151106170116/https://www.analog.com/media/en/technical-documenta 133%
https://www.analog.com/media/en/technical-documentation/obsolete-data-sheets/66309706ADXL05.pdf Go
4 captures
6 Nov 2015 - 6 Jun 2024
OCT NOV MAY
2014 06 2015 2024
About this capture

ANALOG DEVICES

±1 *g* to ±5 *g* Single Chip Accelerometer with Signal Conditioning

ADXL05*

FEATURES
5 milli-*g* Resolution
Noise Level 12× Less than the ADXL50
User Selectable Full Scale from ±1 *g* to ±5 *g*
Output Scale Selectable from 200 mV/*g* to 1 V/*g*
Complete Acceleration Measurement System on a Single Chip IC
Self Test on Digital Command
+5 V Single Supply Operation
1000 *g* Shock Survival

floor is 500 μ*g*/√Hz, (12× less than the ADXL50), allowing signals below 5 milli-*g* to be resolved. The ADXL05 is a force balanced capacitive accelerometer with the capability to measure both ac accelerations (typical of vibration) or dc accelerations (such as inertial force or gravity). Three external capacitors and a +5 volt regulated power supply are all that is required to measure accelerations up to ±5 *g*. Three resistors are used to configure the output buffer amplifier to set scale factors from 200 mV/*g* to 1 V/*g*. External capacitors may be added to the resistor network to provide 1 or 2 poles of filtering. No addi-

Nintendo Exhibit 1066
IPR2024-00668 - Page 668

±1 *g* to ±5 *g* Single Chip Accelerometer with Signal Conditioning

ADXL05*

FEATURES
5 milli-*g* Resolution
Noise Level 12× Less than the ADXL50
User Selectable Full Scale from ±1 *g* to ±5 *g*
Output Scale Selectable from 200 mV/*g* to 1 V/*g*
Complete Acceleration Measurement System on a Single Chip IC
Self Test on Digital Command
+5 V Single Supply Operation
1000 *g* Shock Survival

APPLICATIONS
Low Cost Sensor for Vibration Measurement
Tilt Sensing with Faster Response than Electrolytic or Mercury Sensors
More Sensitive Alarms and Motion Detectors
Affordable Inertial Sensing of Velocity and Position

OBSOLETE

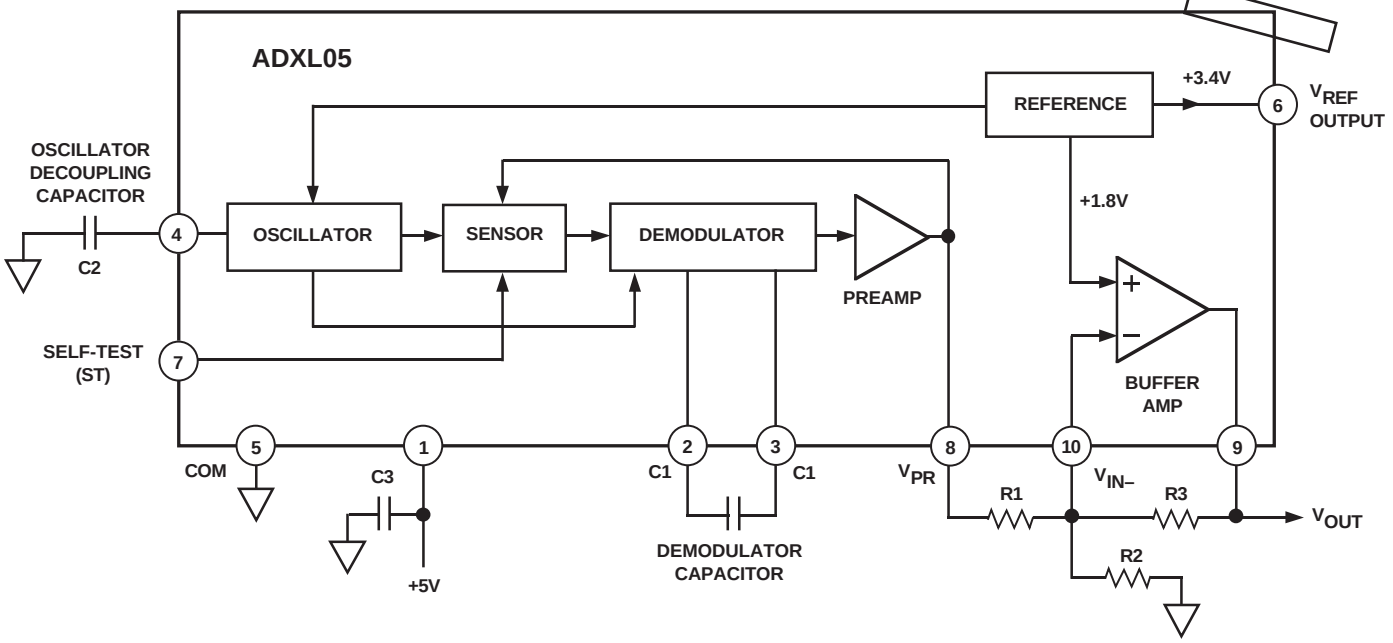
GENERAL DESCRIPTION

The ADXL05 is a complete acceleration measurement system on a single monolithic IC. The ADXL05 will measure accelerations with full-scale ranges of ±5 *g* to ±1 *g* or less. Typical noise floor is 500 μ*g*/√Hz, (12× less than the ADXL50), allowing signals below 5 milli-*g* to be resolved. The ADXL05 is a force balanced capacitive accelerometer with the capability to measure both ac accelerations (typical of vibration) or dc accelerations (such as inertial force or gravity). Three external capacitors and a +5 volt regulated power supply are all that is required to measure accelerations up to ±5 *g*. Three resistors are used to configure the output buffer amplifier to set scale factors from 200 mV/*g* to 1 V/*g*. External capacitors may be added to the resistor network to provide 1 or 2 poles of filtering. No additional active components are required to interface directly to most analog to digital converters (ADCs).

The device features a TTL compatible self-test function that can electrostatically deflect the sensor beam at any time to verify that the sensor and its electronics are functioning correctly.

The ADXL05 is available in a hermetic 10-pin TO-100 metal can, specified over the 0°C to +70°C commercial, and –40°C to +85°C industrial temperature ranges. Contact factory for availability of automotive grade devices.

FUNCTIONAL BLOCK DIAGRAM



*Patents pending.

REV. B

Information furnished by Analog Devices is believed to be accurate and reliable. However, no responsibility is assumed by Analog Devices for its use, nor for any infringements of patents or other rights of third parties which may result from its use. No license is granted by implication or otherwise under any patent or patent rights of Analog Devices.

© Analog Devices, Inc., 1996

One Technology Way, P.O. Box 9106, Norwood. MA 02062-9106, U.S.A.
Tel: 617/329-4700 Fax: 617/326-8703

ADXL05–SPECIFICATIONS ($T_A = T_{MIN}$ to T_{MAX}, T_A = +25°C for J Grade Only, V_S = +5 V, @ Acceleration = 0 *g*, unless otherwise noted)

Parameter	Conditions	ADXL05J/A Min	Typ	Max	Units
SENSOR INPUT					
Measurement Range	Guaranteed Full Scale	–5		+5	*g*
Nonlinearity	Best Fit Straight Line, 5 *g* FS		0.2		% of FS
Alignment Error[1]			±1		Degrees
Transverse Sensitivity[2]			±2		%
SENSITIVITY					
Initial Sensitivity at V_{PR}	+25°C	175	200	225	mV/*g*
Initial Sensitivity at V_{OUT}	+25°C, R3/R1 = 5	0.875	1.000	1.125	V/*g*
Temperature Drift[3]			±0.5		% of Reading
ZERO *g* BIAS LEVEL	at V_{PR}				
Initial Offset		1.50	1.80	2.10	V
vs. Temperature[3]			±25/40		mV
vs. Supply	V_S = 4.75 V to 5.25 V		10	32	mV/V
NOISE PERFORMANCE	at V_{PR}				
Voltage Noise Density	BW = 4 Hz to 1 kHz		500	1000	$\mu g/\sqrt{Hz}$
Noise in 100 Hz Bandwidth			5		m*g* rms
Noise in 10 Hz Bandwidth			1.6		m*g* rms
FREQUENCY RESPONSE					
3 dB Bandwidth[4]	C1 = 0.022 µF (See Figure 9)	1000	1600		Hz
3 dB Bandwidth[4]	C1 = 0.010 µF		4		kHz
Sensor Resonant Frequency			12		kHz
SELF TEST INPUT					
Output Change at V_{PR}[5]	ST Pin from Logic "0" to "1"	–0.85	–1.00	–1.15	V
Logic "1" Voltage		2.0			V
Logic "0" Voltage				0.8	V
Input Resistance	To Common		50		kΩ
+3.4 V REFERENCE					
Output Voltage		3.350	3.400	3.450	V
Output Temperature Drift[3]			±5		mV
Power Supply Rejection	DC, V_S = +4.75 V to +5.25 V		1	10	mV/V
Output Current	Sourcing	500			µA
PREAMPLIFIER OUTPUT					
Voltage Swing		0.25		V_S – 1.4	V
Current Output	Source or Sink	30	80		µA
Capacitive Load Drive			100		pF
BUFFER AMPLIFIER					
Input Offset Voltage[6]	Delta from Nominal 1.800 V		±10	±25	mV
Input Bias Current			5	20	nA
Open-Loop Gain	DC		80		dB
Unity Gain Bandwidth			200		kHz
Output Voltage Swing	I_{OUT} = ±100 µA	0.25		V_S – 0.25	V
Capacitive Load Drive		1000			pF
Power Supply Rejection	DC, V_S = +4.75 V to +5.25 V		1	10	mV/V
POWER SUPPLY					
Operating Voltage Range		4.75		5.25	V
Quiescent Supply Current			8.0	10.0	mA
TEMPERATURE RANGE					
Operating Range J		0		+70	°C
Specified Performance A		–40		+85	°C
Automotive Grade*		–40		+125	°C

OBSOLETE

NOTES

[1]Alignment error is specified as the angle between the true and indicated axis of sensitivity, (see Figure 2).

[2]Transverse sensitivity is measured with an applied acceleration that is 90° from the indicated axis of sensitivity. Transverse sensitivity is specified as the percent of transverse acceleration that appears at the V_{PR} output. This is the algebraic sum of the alignment and the inherent sensor sensitivity errors, (see Figure 2).

[3]Specification refers to the maximum change in parameter from its initial at +25°C to its worst case value at T_{MIN} to T_{MAX}.

[4]Frequency at which response is 3 dB down from dc response assuming an exact C1 value is used. Maximum recommended BW is 6 kHz using a 0.010 µF capacitor, refer to Figure 9.

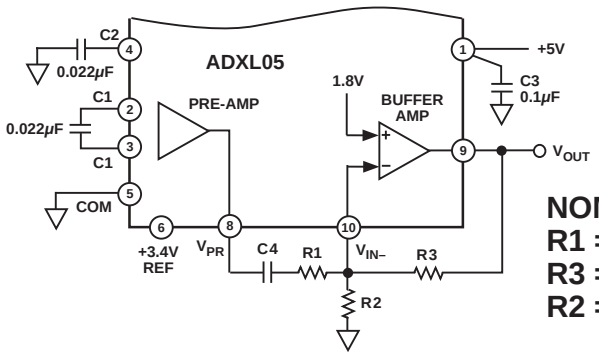
[5]Applying logic high to the self-test input has the effect of applying an acceleration of –5 *g* to the ADXL05.

[6]Input offset voltage is defined as the output voltage differential from 1.800 V when the amplifier is connected as a follower. The voltage at this pin has a temperature drift proportional to that of the 3.4 V reference.

*Contact factory for availability of automotive grade devices.

All min and max specifications are guaranteed. Typical specifications are not tested or guaranteed.
Specifications subject to change without notice.

Nintendo Exhibit 1066
IPR2024-00668 - Page 670



NOMINAL VALUES:
R1 = 49.9kΩ
R3 = 249kΩ
R2 = 640kΩ

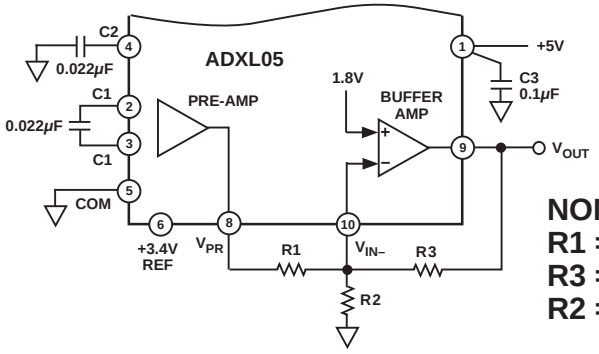
AC COUPLED CONNECTION (±1.5 *g* Full Scale)

(@ V_{OUT} Terminal (Pin 9), unless otherwise noted. 0 *g* Bias Level = +2.5 V, C1 = 0.022 μF, R2 = 2.57 R3

OBSOLETE

Parameter	Conditions	ADXL05J/A Min	Typ	Max	Units
Buffer Gain	G = R3/R1*		5		
FULL-SCALE RANGE		–1.5		+1.5	*g*
SENSITIVITY	@ +25°C	875	1000	1,125	mV/*g*
Temperature Drift	T_{MIN} to T_{MAX}		±0.5		% of Reading
ZERO *g* BIAS LEVEL	@ +25°C		2.5		V
Temperature Drift	+25°C to T_{MIN} or T_{MAX}		2/5		mV
FREQUENCY RESPONSE	C4 = 3.3 μF, R1 = 49.9 kΩ	1		1000	Hz

*Note: Resistor tolerance will affect system accuracy. Use of ±1% (or better) metal film resistors is recommended.



NOMINAL VALUES:
R1 = 49.9kΩ
R3 = 100kΩ (G=2)
R2 = 255kΩ (G=2)

DC COUPLED CONNECTION (±2 *g* Full Scale)

(@ V_{OUT} Terminal (Pin 9), unless otherwise noted. 0 *g* Bias Level = +2.5 V, C1 = 0.022 μF, R2 = 2.57 R3)

Parameter	Conditions	ADXL05J/A Min	Typ	Max	Units
Buffer Gain	G = R3/R1*		2		
FULL-SCALE RANGE		–2		+2	*g*
SENSITIVITY	@ +25°C	350	400	450	mV/*g*
Temperature Drift	T_{MIN} to T_{MAX}		±0.5		% of Reading
ZERO *g* BIAS LEVEL	@ +25°C	1.75	2.5	3.2	V
Temperature Drift	+25°C to T_{MIN} or T_{MAX}		±50/80		mV
FREQUENCY RESPONSE		dc		1000	Hz

*Note: Resistor tolerance will affect system accuracy. Use of ±1% (or better) metal film resistors is recommended.

ABSOLUTE MAXIMUM RATINGS*

Acceleration (Any Axis, Unpowered for 0.5 ms) . . . . . 1000 *g*
Acceleration (Any Axis, Powered for 0.5 ms) . . . . . 500 *g*
$+V_S$ . . . . . –0.3 V to +7.0 V
Output Short Circuit Duration
(V_{PR}, V_{OUT}, V_{REF} Terminals to Common) . . . . . Indefinite
Operating Temperature . . . . . –55°C to +125°C
Storage Temperature . . . . . –65°C to +150°C

*Stresses above those listed under "Absolute Maximum Ratings" may cause permanent damage to the device. This is a stress rating only; the functional operation of the device at these or any other conditions above those indicated in the operational sections of this specification is not implied. Exposure to absolute maximum rating conditions for extended periods may affect device reliability.

Package Characteristics

Package	θ_{JA}	θ_{JC}	Device Weight
10-Pin TO-100	130°C/W	30°C/W	5 Grams

ORDERING GUIDE

Model	Temperature Range
ADXL05JH	0°C to +70°C
ADXL05AH	–40°C to +85°C

OBSOLETE

CAUTION

ESD (electrostatic discharge) sensitive device. Electrostatic charges as high as 4000 V readily accumulate on the human body and test equipment and can discharge without detection. Although the ADXL05 features proprietary ESD protection circuitry, permanent damage may occur on devices subjected to high energy electrostatic discharges. Therefore, proper ESD precautions are recommended to avoid performance degradation or loss of functionality.

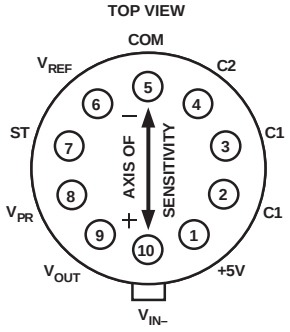


Drops onto hard surfaces can cause shocks of greater than 1000 *g* and exceed the absolute maximum rating of the device. Care should be exercised in handling to avoid damage.

PIN DESCRIPTION

+5 V	The power supply input pin.
C2	Connection for an external bypass capacitor (nominally 0.022 μF) used to prevent oscillator switching noise from interfering with other ADXL05 circuitry. Please see the section on component selection.
C1	Connections for the demodulator capacitor, nominally 0.022 μF. See the section on component selection for application information.
COM	The power supply common (or "ground") connection.
V_{REF}	Output of the internal 3.4 V voltage reference.
ST	The digital self-test input. It is both CMOS and TTL compatible.
V_{PR}	The ADXL05 preamplifier output providing an output voltage of 200 mV per *g* of acceleration.
V_{OUT}	Output of the buffer amplifier.
V_{IN-}	The inverting input of the uncommitted buffer amplifier.

CONNECTION DIAGRAM
10-Header (TO-100)



NOTES:
AXIS OF SENSITIVITY IS ALONG A LINE BETWEEN PIN 5 AND THE TAB.
THE CASE OF THE METAL CAN PACKAGE IS CONNECTED TO PIN 5 (COMMON).
ARROW INDICATES DIRECTION OF POSITIVE ACCELERATION ALONG AXIS OF SENSITIVITY.

Nintendo Exhibit 1066
IPR2024-00668 - Page 672

GLOSSARY OF TERMS

Acceleration: Change in velocity per unit time.

Acceleration Vector: Vector describing the net acceleration acting upon the ADXL05 (A_{XYZ}).

g: A unit of acceleration equal to the average force of gravity occurring at the earth's surface. A *g* is approximately equal to 32.17 feet/s^2, or 9.807 meters/s^2.

Nonlinearity: The maximum deviation of the ADXL05 output voltage from a best fit straight line fitted to a plot of acceleration vs. output voltage, calculated as a % of the full-scale output voltage (@ 5 *g*).

Resonant Frequency: The natural frequency of vibration of the ADXL05 sensor's central plate (or "beam"). At its resonant frequency of 12 kHz, the ADXL05's moving center plate has a peak in its frequency response with a Q of 3 or 4.

Sensitivity: The output voltage change per *g* unit of acceleration applied, specified at the V_{PR} pin in mV/*g*.

Sensitive Axis (X): The most sensitive axis of the accelerometer sensor. Defined by a line drawn between the package tab and Pin 5 in the plane of the pin circle. See Figures 2a and 2b.

Sensor Alignment Error: Misalignment between the ADXL05's on-chip sensor and the package axis, defined by Pin 5 and the package tab.

Total Alignment Error: Net misalignment of the ADXL05's on-chip sensor and the measurement axis of the application. This error includes errors due to sensor die alignment to the package, and any misalignment due to installation of the sensor package in a circuit board or module.

Transverse Acceleration: Any acceleration applied 90° to the axis of sensitivity.

Transverse Sensitivity Error: The percent of a transverse acceleration that appears at the V_{PR} output. For example, if the transverse sensitivity is 1%, then a +10 *g* transverse acceleration will cause a 0.1 *g* signal to appear at V_{PR} (1% of 10 *g*). Transverse sensitivity can result from a sensitivity of the sensor to transverse forces or from misalignment of the internal sensor to its package.

Transverse Y Axis: The axis perpendicular (90°) to the package axis of sensitivity in the plane of the package pin circle. See Figure 2.

Transverse Z Axis: The axis perpendicular (90°) to both the package axis of sensitivity and the plane of the package pin circle. See Figure 2.

Polarity of the Acceleration Output

The polarity of the ADXL05 output is shown in the Figure 1. When oriented to the earth's gravity (and held in place), the ADXL05 will experience an acceleration of +1 *g*. This corresponds to a change of approximately +200 mV at the V_{PR} output pin. Note that the polarity will be reversed to a negative going signal at the buffer amplifier output V_{OUT}, due to its inverting configuration.

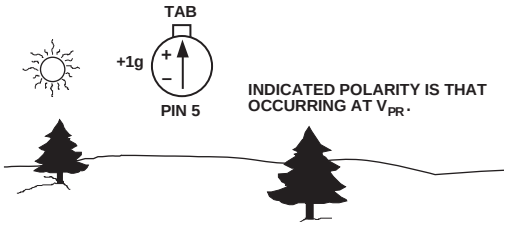


Figure 1. Output Polarity at V_{PR}

Acceleration Vectors in Three Dimensions

The ADXL05 is a sensor designed to measure accelerations that result from an applied force. The ADXL05 responds to the component of acceleration on its sensitive X axis. Figures 2a and 2b show the relationship between the sensitive "X" axis and the transverse "Z" and "Y" axes as they relate to the TO-100

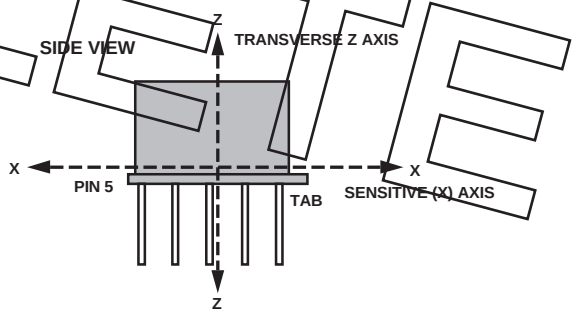


Figure 2a. Sensitive X and Transverse Z Axis

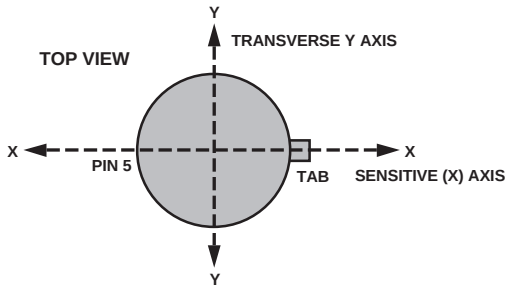


Figure 2b. Sensitive X and Transverse Y Axis

OBSOLETE

package. Figure 2c describes a three dimensional acceleration vector (A_{XYZ}) which might act on the sensor, where A_X is the component of interest. To determine A_X, first, the component of acceleration in the XY plane (A_{XY}) is found using the cosine law:

$$A_{XY} = A_{XYZ}\,(cos\theta_{XY}) \text{ then}$$

$$A_X = A_{XY}\,(cos\theta_X)$$

Therefore: Nominal $V_{PR} = 200\ mV/g\ (A_{XYZ})\ (cos\theta_{XY})\ cos\theta_X$

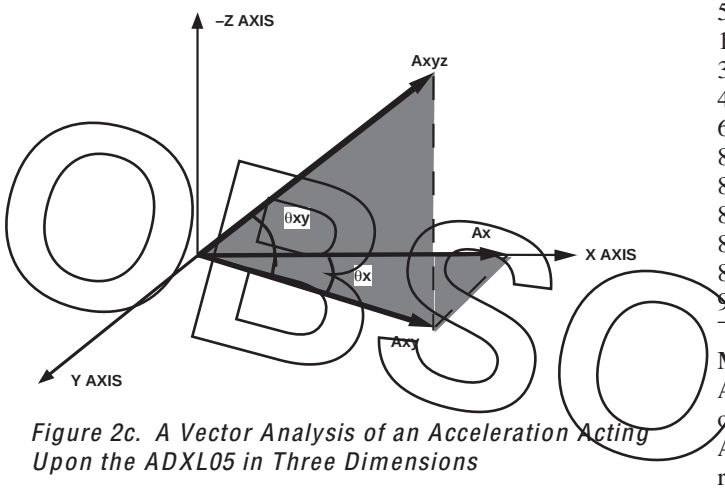


Figure 2c. A Vector Analysis of an Acceleration Acting Upon the ADXL05 in Three Dimensions

Note that an ideal sensor will react to forces along or at angles to its sensitive axis but will reject signals from its various transverse axes, i.e., those exactly 90° from the sensitive "X" axis. But even an ideal sensor will produce output signals if the transverse signals are not exactly 90° to the sensitive axis. An acceleration that is acting on the sensor from a direction different from the sensitive axis will show up at the ADXL05 output at a reduced amplitude.

Table I shows the percentage signals resulting from various θ_X angles. Note that small errors in alignment have a negligible effect on the output signal. A 1° error will only cause a 0.02% error in the signal. Note, however, that a signal coming 1° off of the transverse axis (i.e., 89° off the sensitive axis) will still contribute 1.7% of its signal to the output. Thus large transverse signals could cause output signals as large as the signals of interest. Table I may also be used to approximate the effect of the ADXL05's internal errors due to misalignment of the die to the package. For example: a 1 degree sensor alignment error will allow 1.7% of a transverse signal to appear at the output.

Table I. Ideal Output Signals for Off Axis Applied Accelerations Disregarding Device Alignment and Transverse Sensitivity Errors

θ_X	% of Signal Appearing at Output	Output in *g*s for a 5 *g* Applied Acceleration
0	100%	5.000 (On Axis)
1°	99.98%	4.999
2°	99.94%	4.997
3°	99.86%	4.993
5°	99.62%	4.981
10°	98.48%	4.924
30°	86.60%	4.330
45°	70.71%	3.536
60°	50.00%	2.500
80°	17.36%	0.868
85°	8.72%	0.436
87°	5.25%	0.263
88°	3.49%	0.175
89°	1.7%	0.085
90°	0%	0.000 (Transverse Axis)

Mounting Fixture Resonances

A common source of error in acceleration sensing is resonance of the mounting fixture. For example, the circuit board that the ADXL05 mounts to may have resonant frequencies in the same range as the signals of interest. This could cause the signals measured to be larger than they really are. A common solution to this problem is to dampen those resonances by mounting the ADXL05 near a mounting post or by adding extra screws to hold the board more securely in place.

When testing the accelerometer in your end application, it is recommended that you test the application at a variety of frequencies in order to ensure that no major resonance problems exist (refer to Analog Devices Application Note AN-379).

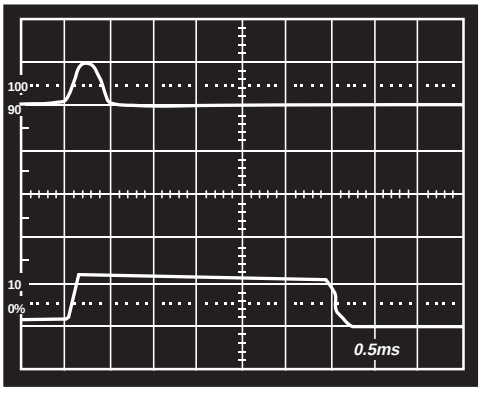


Figure 3. 500 g Shock Overload Recovery. Top Trace, PCB Reference Accelerometer Output: 500 g/Vertical Division. Bottom Trace, ADXL05 Output at V_{PR}

OBSOLETE

Typical Characteristics (@ +25°C, C1 = C2 = 0.022 µF, V_S = +5 V unless otherwise noted)

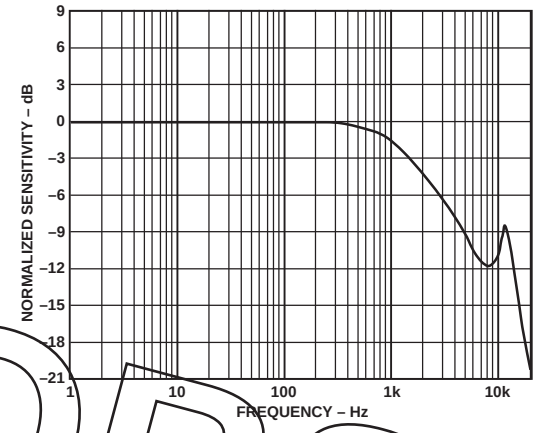


Figure 4. Normalized Sensitivity vs. Frequency

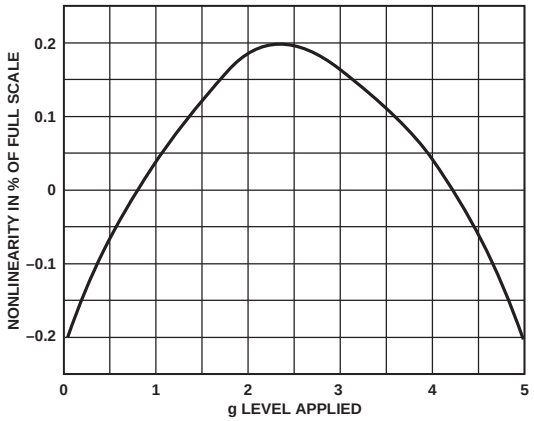


Figure 7. % Nonlinearity vs. g Level Applied

OBSOLETE

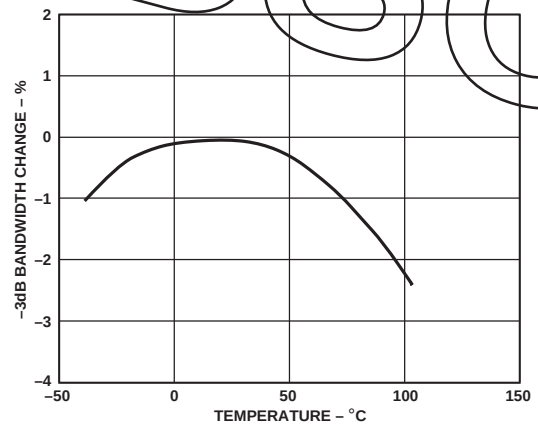


Figure 5. –3 dB Bandwidth vs. Temperature

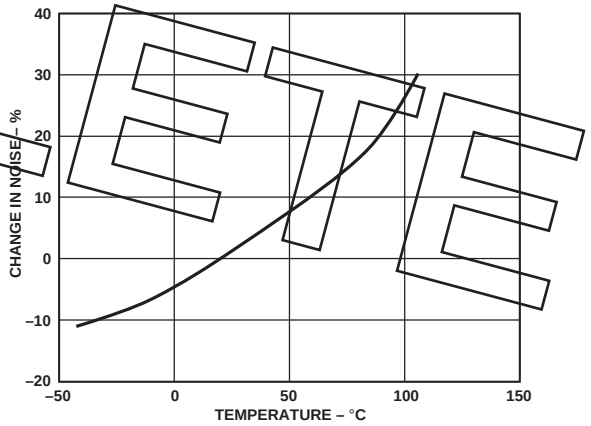


Figure 8. % Change in Noise from +25°C vs. Temperature

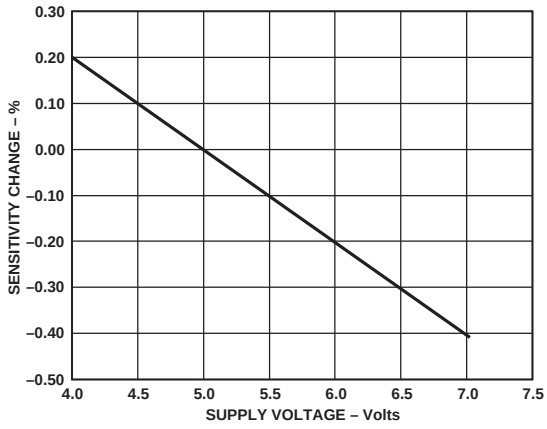


Figure 6. Sensitivity Change at V_{PR} vs. Supply Voltage

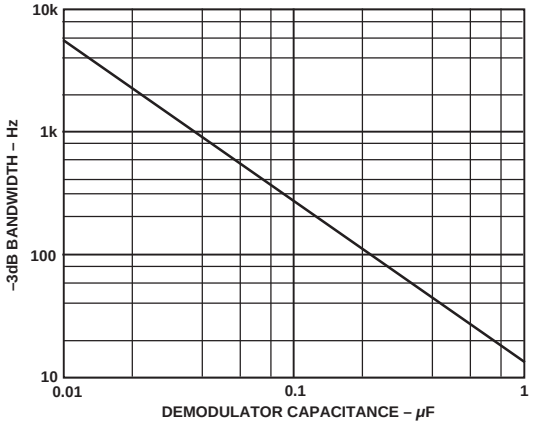


Figure 9. –3 dB Bandwidth vs. Demodulator Capacitance

Typical Characteristics (@ +25°C, C1 = C2 = 0.022 μF, V_S = +5 V unless otherwise noted)

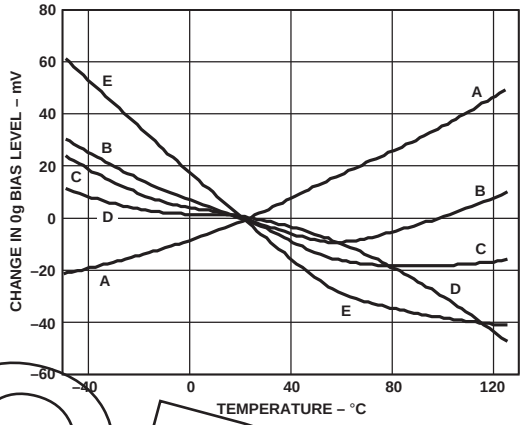


Figure 10. Change in 0 g Bias Level vs. Temperature (Characteristic Curves from Five Typical Units)

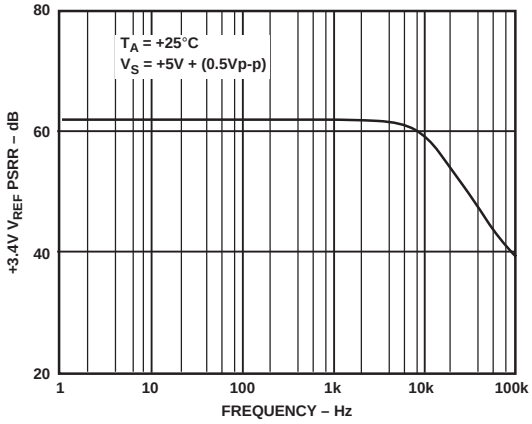


Figure 13. +3.4 V V_{REF} PSRR vs. Frequency

OBSOLETE

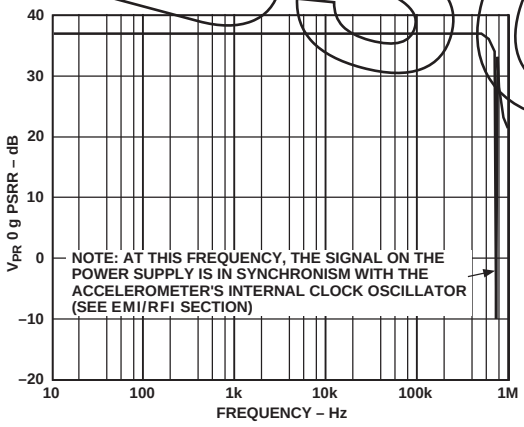


Figure 11. 0 g PSRR vs. Frequency

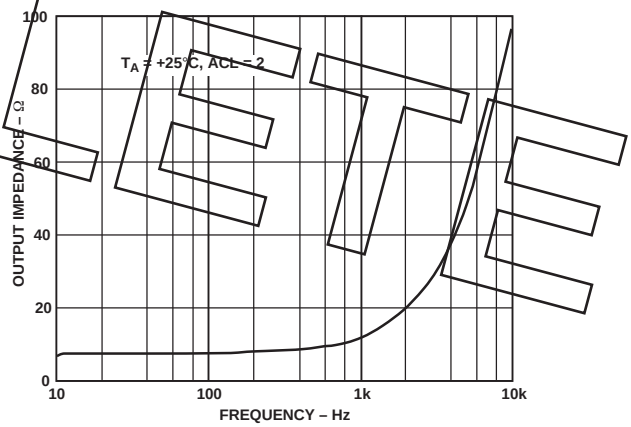


Figure 14. Buffer Amplifier Output Impedance vs. Frequency

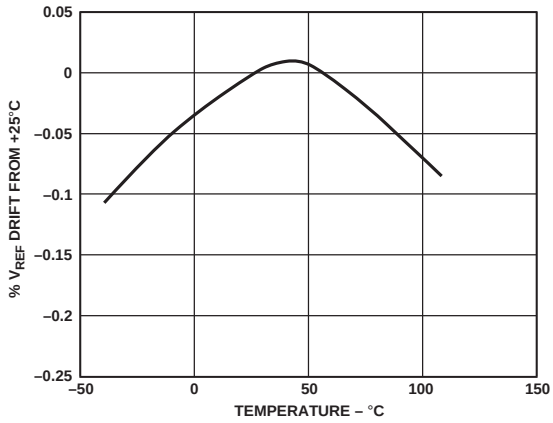


Figure 12. % V_{REF} Drift vs. Temperature

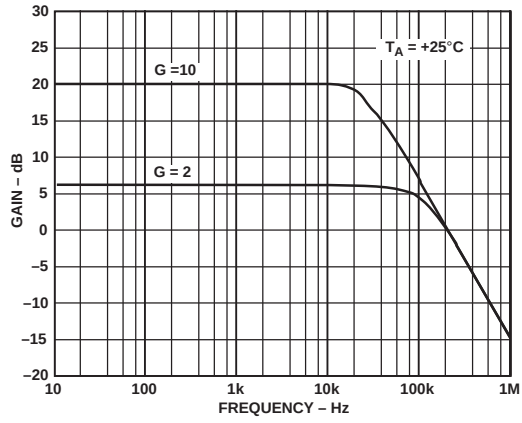


Figure 15. Buffer Amplifier Closed-Loop Gain vs. Frequency

THEORY OF OPERATION

The ADXL05 is a complete acceleration measurement system on a single monolithic IC. It contains a polysilicon surface-micro machined sensor and signal conditioning circuitry which implements a force-balance control loop. The ADXL05 is capable of measuring both positive and negative acceleration to a maximum level of ±5 *g*.

Figure 16 is a simplified view of the ADXL05's acceleration sensor at rest. The actual structure of the sensor consists of 46 unit cells and a common beam. The differential capacitor sensor consists of independent fixed plates and central plates attached to the main beam that moves in response to an applied acceleration. The two capacitors are series connected, forming a capacitive divider with a common movable central plate. The sensor's fixed capacitor plates are driven differentially by a 1 MHz square wave; the two square wave amplitudes are equal but are 180° out of phase from one another. When at rest, the values of the two capacitors are the same, and therefore, the voltage output at their electrical center (i.e., at the center plate) is zero.

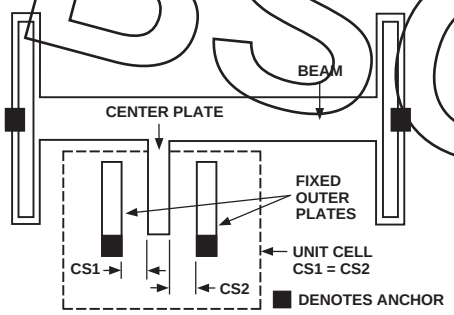


Figure 16. A Simplified Diagram of the ADXL05 Sensor at Rest

Figure 17 shows the sensor responding to an applied acceleration. When this occurs, the common central plate or "beam" moves closer to one of the fixed plates while moving further from the other. This creates a mismatch in the two capacitances, resulting in an output signal at the central plate. The output amplitude of the signal varies directly with the amount of acceleration experienced by the sensor.

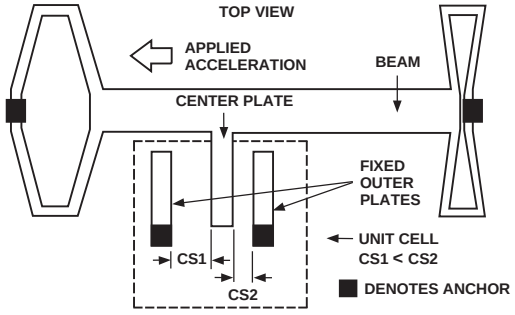


Figure 17. The ADXL05 Sensor Momentarily Responding to an Externally Applied Acceleration

Figure 18 shows a block diagram of the ADXL05. The voltage output from the central plate of the sensor is buffered and then applied to a synchronous demodulator which is clocked, in phase, with the same oscillator that drives the fixed plates of the sensor. If the applied voltage is in sync and in phase with the clock, a positive output will result. If the applied voltage is in sync but 180° out of phase with the clock, then the demodulator's output will be negative. All other signals will be rejected. An external capacitor, C1, sets the bandwidth of the demodulator.

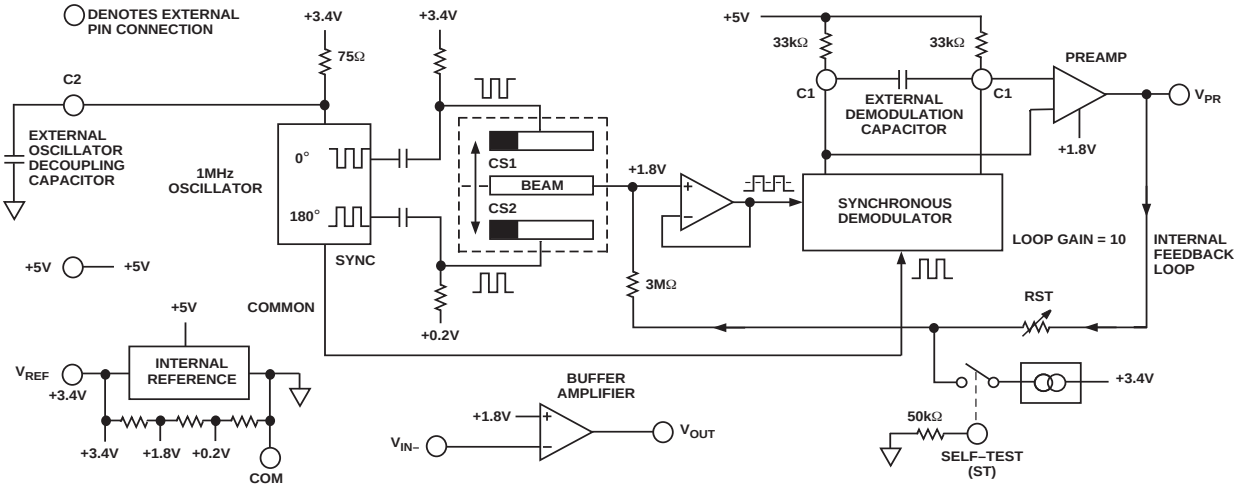


Figure 18. Functional Block Diagram

OBSOLETE

The output of the synchronous demodulator drives the preamp—an instrumentation amplifier buffer which is referenced to +1.8 volts. The output of the preamp, V_{PR}, is fed back to the outer plate of the sensor through a 3 MΩ isolation resistor. The V_{PR} voltage electrostatically resets the sensor back to its 0 *g* position and is a direct measure of the applied acceleration.

The output of the ADXL05's preamplifier is 1.8 V ± 200 mV/*g*, with an output range of ±1 V for a ±5 *g* input. An uncommitted buffer amplifier provides the capability to adjust the scale factor and 0 *g* offset level over a wide range. An internal reference supplies the necessary regulated voltages for powering the chip and +3.4 volts for external use.

A self-test is initiated by applying a TTL "high" level voltage (> +2.0 V dc) to the ADXL05's self-test pin, which causes the chip to apply a deflection voltage to the beam which moves it an amount equal to –5 *g* (the negative full-scale output of the device). Note that the ±15% tolerance of the self-test circuit is not proportional to the sensitivity error, see Self-Test section.

BASIC CONNECTIONS FOR THE ADXL05

Figure 19 shows the basic connections needed for the ADXL05 to measure accelerations in the ±5 *g* range with an output scale factor 400 mV/*g*, a 2.5 V 0 *g* level, a ±2.0 V full-scale swing around 0 *g*, and a 3 dB bandwidth of approximately 1.6 kHz.

Using the circuit of Figure 19, the overall transfer function is:

$$V_{OUT} = \left(\frac{R3}{R1}\left(1.8\ V - V_{PR}\right)\right) + \left(\frac{R3}{R2}\left(1.8\right)\right) + 1.8\ V$$

OBSOLETE

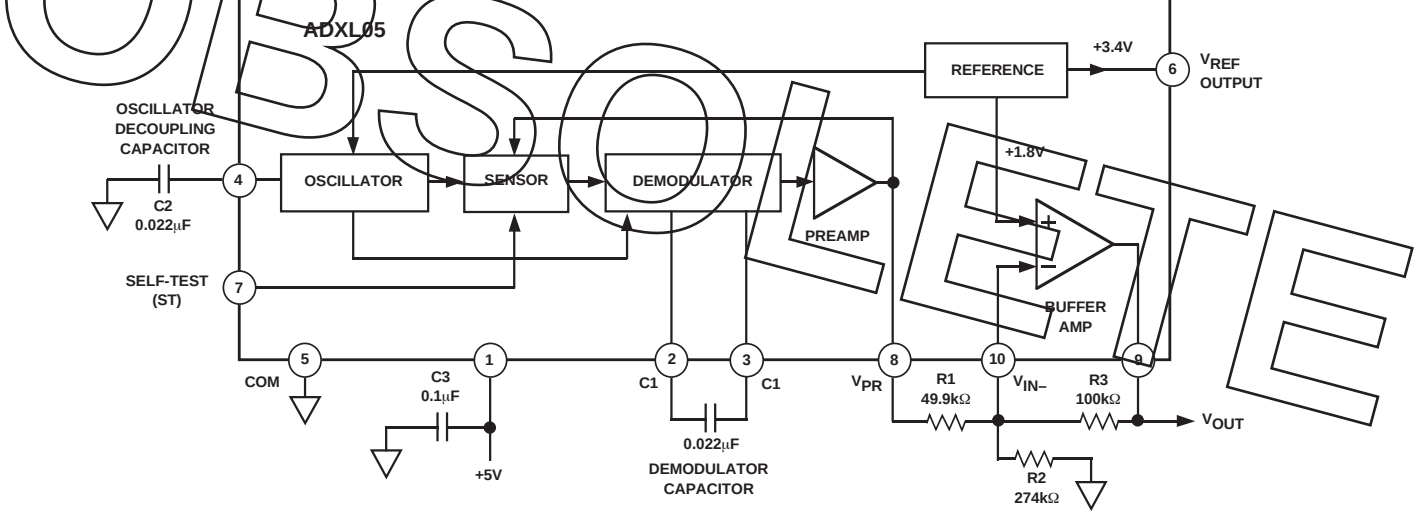


Figure 19. ADXL05 Application Providing an Output Sensitivity of 400 mV/g, a +2.5 V 0 g Level and a Bandwidth of 1 kHz

USING THE INTERNAL BUFFER AMPLIFIER TO VARY THE ACCELEROMETER'S OUTPUT SCALE FACTOR AND 0 *g* BIAS LEVEL

The ADXL05 accelerometer has an onboard buffer amplifier that allows the user to change the output scale factor and 0 *g* bias level.

The output scale factor of an accelerometer is simply how many volts output are provided per *g* of applied acceleration. This should not be confused with its resolution. The resolution of the device is the lowest *g* level the accelerometer is capable of measuring. Resolution is principally determined by the device noise and the measurement bandwidth.

The 0 *g* bias level is simply the dc output level of the accelerometer when it is not in motion or being acted upon by the Earth's gravity.

Setting the Accelerometer's Scale Factor

Figure 20 shows the basic connections for using the onboard buffer amplifier to increase the output scale factor. The nominal output level in volts from V_{PR} (the preamplifier output) is equal to the *g* forces applied to the sensor (along its sensitive axis) times 200 mV/*g*. The use of the buffer is always recommended even if the preset scale factor is adequate, as the buffer helps prevent any following circuitry from loading down the V_{PR} output.

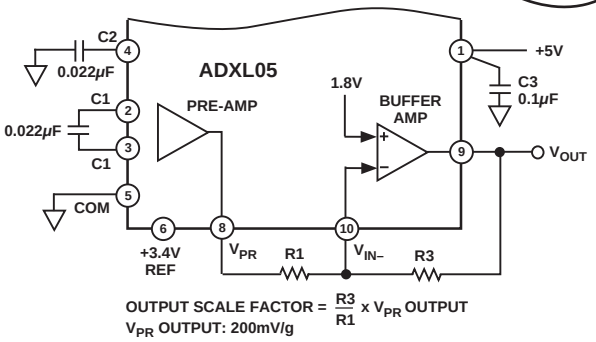


Figure 20. Basic Buffer Connections

In Figure 20, the output scale factor at Pin 9 (V_{OUT}) is the output at V_{PR} times the gain of the buffer, which is simply the value of resistor R3 divided by R1. Choose a convenient scale factor, keeping in mind that the buffer gain not only amplifies the signal but any noise or drift as well. Too much gain can also cause the buffer to saturate and clip the output wave form.

The circuit of Figure 20 is entirely adequate for many applications, but its accuracy is dependent on the pretrimmed accuracy of the accelerometer and this will vary by product type and grade. For the highest possible accuracy, an external trim is recommended. As shown by Figure 21, this consists of a potentiometer, R1a, in series with a fixed resistor, R1b.

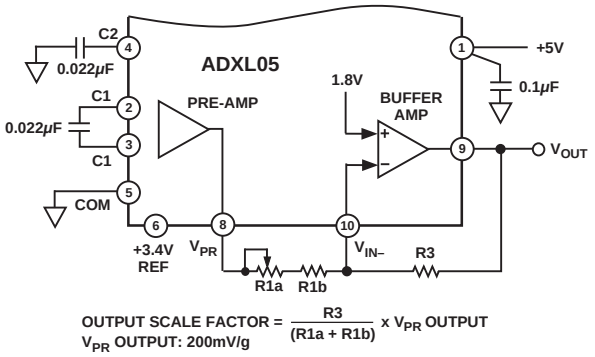


Figure 21. External Scale Factor Trimming

Setting the Accelerometer's 0 *g* Bias Level, AC Coupled Response

If a dc (gravity) response is not required—for example in motion sensing or vibration measurement applications—ac coupling can be used between the preamplifier output and the buffer input as shown in Figure 22. The use of ac coupling between V_{PR} and the buffer input virtually eliminates any 0 *g* drift and allows the maximum buffer gain without clipping.

Resistor R1 and capacitor C4 together form a high pass filter whose corner frequency is $1/(2\pi R1\,C4)$. This means that this simple filter will reduce the signal from V_{PR} by 3 dB at the corner frequency, and it will continue to reduce it at a rate of 6 dB/octave (20 dB per decade) for signals below the corner frequency.

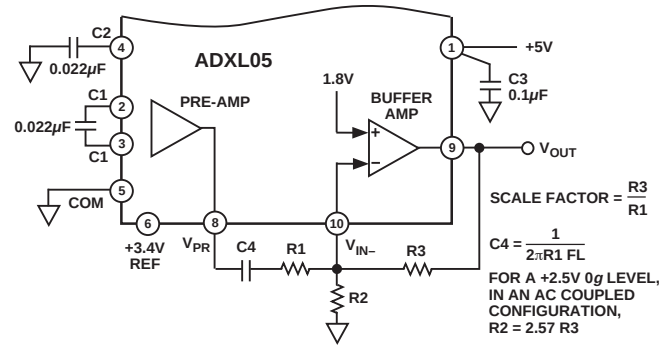
Note that capacitor C4 should be a nonpolarized, low leakage type. If a polarized capacitor is used, tantalum types are preferred, rather than electrolytic. With polarized capacitors, V_{PR} should be measured on each device and the positive terminal of the capacitor connected toward either V_{PR} or V_{IN}—whichever is more positive

The 0 *g* offset level of the ADXL05 accelerometer is preset at +1.8 V. This can easily be changed to a more convenient level, such as +2.5 V which, being at the middle of the supply voltage, provides the greatest output voltage swing.

When using the ac coupled circuit of Figure 22, only a single resistor, R2, is required to swing the buffer output to +2.5 V. Since the "+" input of the buffer is referenced at +1.8 V, its summing junction, Pin 10, is also held constant at +1.8 V. Therefore, to swing the buffer's output to the desired +2.5 V 0 *g* bias level, its output must move up +0.7 V (2.5 V – 1.8 V = 0.7 V). Therefore, the current needed to flow through R3 to cause this change, IR3, is equal to:

$$IR3 = \frac{0.7\ Volts}{R3\ in\ Ohms}$$

Nintendo Exhibit 1066
IPR2024-00668 - Page 679



RECOMMENDED COMPONENT VALUES

FULL SCALE RANGE	SCALE FACTOR IN mV/*g*	DESIRED LOW FREQUENCY LIMIT, F_L	R1 IN kΩ	CLOSEST C4 VALUE	R3 IN kΩ	R2 VALUE IN kΩ FOR +2.5V 0*g* LEVEL
±2*g*	1000	30Hz	49.9	0.10μF	249	640
±5*g*	400	30Hz	127	0.039μF	249	640
±2*g*	1000	3Hz	49.9	1.0μF	249	640
±5*g*	400	1Hz	127	1.5μF	249	640
±5*g*	400	0.1Hz	127	15μF	249	640

Figure 22. Typical Component Values for AC Coupled Circuit

In order to force this current through R3, the same current needs to flow from Pin 10 to ground through resistor R2. Since Pin 10 is always held at +1.8 V, R2 is equal to:

$$R2 = \frac{1.8\ Volts}{IR3}$$

Therefore, for an ac coupled connection and a +2.5 V 0 *g* output:

$$R2 = \frac{1.8\ Volts \times R3}{0.7\ Volts} = 2.57 \times R3$$

If ac coupling is used, the self-test feature must be monitored at V_{PR}, rather than at the buffer output (since the self test output is a dc voltage).

Setting the Accelerometer's 0 *g* Bias Level, DC Coupled Response

When a true dc (gravity) response is needed, the output from the preamplifier, V_{PR}, must be *dc coupled* to the buffer input. For high gain applications, a 0 *g* offset trim will also be needed. The external offset trim permits the user to set the 0 *g* offset voltage to exactly +2.5 volts, since this is at the center of the +5 volt power supply it will allow the maximum output swing from the buffer without clipping.

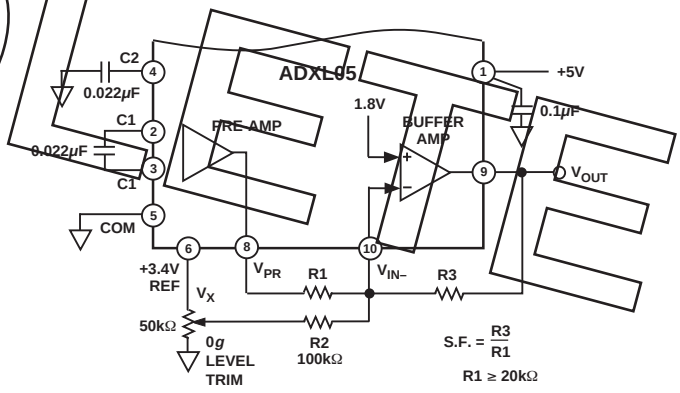
With a dc coupled connection, any difference between a non-ideal +1.8 V 0 *g* level at V_{PR} and the fixed +1.8 V level at the buffer's summing junction will be amplified by the gain of the buffer. If the 0 *g* level only needs to be approximate and the buffer is operated a low gain, a single fixed resistor, R2, can still be used. But to obtain the exact 0 *g* output desired or to allow the maximum output voltage swing from the buffer, the 0 *g* offset will need to be externally trimmed using the circuit of Figure 23. Normally, a value of 100 kΩ is typical for R2.

The buffer's maximum output swing should be limited to ±2 volts, which provides a safety margin of ±0.25 volts before clipping. With a +2.5 volt 0 *g* level, the maximum gain the buffer should be set to (R3/R1) equals:

$$\frac{2\ Volts}{200\ mV/g\ Times\ the\ Max\ Applied\ Acceleration\ in\ gs}$$

Note that the value of R1 should be kept as large as possible, 20 kΩ or greater, to avoid loading down the V_{PR} output.

The device scale factor and 0 *g* offset levels can be calibrated using the Earth's gravity as explained in the section "calibrating the ADXL05."



RECOMMENDED COMPONENT VALUES FOR VARIOUS OUTPUT SCALE FACTORS

FULL SCALE	mV per *g*	R1 kΩ	R3 kΩ
±1*g*	2000	30.1	301
±2*g*	1000	40.2	200
±4*g*	500	40.2	100
±5*g*	400	49.2	100

Figure 23. Typical Component Values for Circuit with External 0 g Trimming

Nintendo Exhibit 1066
IPR2024-00668 - Page 680

DEVICE BANDWIDTH VS. MEASUREMENT RESOLUTION

Although an accelerometer is usually specified according to its full scale (clipping) *g* level, the limiting resolution of the device, i.e., its minimum discernible input level, is extremely important when measuring low *g* accelerations.

The limiting resolution is predominantly set by the measurement noise "floor" which includes the ambient background noise and the noise of the ADXL05 itself. The level of the noise floor varies directly with the bandwidth of the measurement. As the measurement bandwidth is reduced, the noise floor drops, improving the signal-to-noise ratio of the measurement and increasing its resolution.

The bandwidth of the accelerometer can be easily reduced by adding low-pass or bandpass filtering. Figure 24 shows the typical noise vs. bandwidth characteristic of the ADXL05.

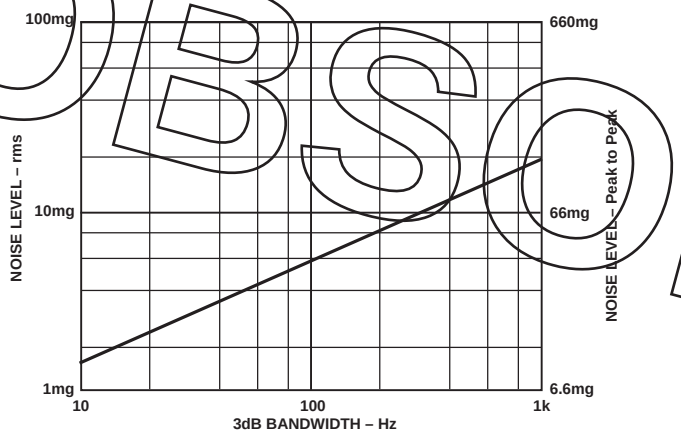


Figure 24. Noise Level vs. 3 dB Bandwidth

The output noise of the ADXL05 scales with the square root of the measurement bandwidth. With a single pole roll-off, the equivalent rms noise bandwidth is π divided by 2 or approximately 1.5 times the 3 dB bandwidth. For example, the typical rms noise of the ADXL05J using a 100 Hz one pole post filter is:

$$Noise\,(rms) = 500\ \mu g/\sqrt{Hz} \times \sqrt{100(1.5)} = 6{,}124\ \mu g\ or\ 6.1\ mg\ rms$$

For the bandpass filter of Figure 27 where both ac coupling and low pass filtering are used, the low frequency roll-off, F_L, is determined by C4 and R1 and the high frequency roll-off, F_H, is determined by the 1-pole post filter R3, C5.

The equivalent rms noise of the bandpass filter is equal to

$$500\ \mu g/\sqrt{Hz} \times \sqrt{(1.5\ F_H) - (F_L/1.5)}\,.$$

For example, the typical rms noise of the ADXL05 using 1 pole ac coupling with a bandwidth of 10 Hz and 1 pole low-pass filter of 100 Hz is:

$$Noise\,(rms) = 500\ \mu g/\sqrt{Hz} \times \sqrt{1.5(100) - (10/1.5)}$$

$$= 5{,}987\ \mu g\ rms\ or \approx 5.9\ mg\ rms$$

Because the ADXL05's noise is for all practical purposes Gaussian in amplitude distribution, the highest noise amplitudes have the smallest (yet nonzero) probability. Peak-to-peak noise is therefore difficult to measure and can only be estimated due to its statistical nature. Table II is useful for estimating the probabilities of exceeding various peak values, given the rms value.

Table II.

Nominal Peak-to-Peak Value	% of Time that Noise Will Exceed Nominal Peak-to-Peak Value
2.0 × rms	32%
4.0 × rms	4.6%
6.0 × rms	0.27%
6.6 × rms	0.1%
8.0 × rms	0.006%

RMS and peak-to-peak noise (for 0.1% uncertainty) for various bandwidths is estimated in Figure 24. As shown by the figure, device noise drops dramatically as the operating bandwidth is reduced. For example, when operated in a 1 kHz bandwidth, the ADXL05 typically has an rms noise level of 19 mg. With ±5 *g* applied accelerations, this 19 mg resolution limit is normally quite satisfactory; but for smaller acceleration levels the noise is now a much greater percentage of the signal. As shown by the figure, when the device bandwidth is rolled off to 100 Hz, the noise level is reduced to approximately 6 mg, and at 10 Hz it is down to less than 2 mg.

Alternatively, the signal-to-noise ratio may be improved considerably by using a microprocessor to perform multiple measurements and then compute the average signal level. When using this technique, with 100 measurements, the signal-to-noise ratio will be increased by a factor of 10 (20 dB).

OBSOLETE

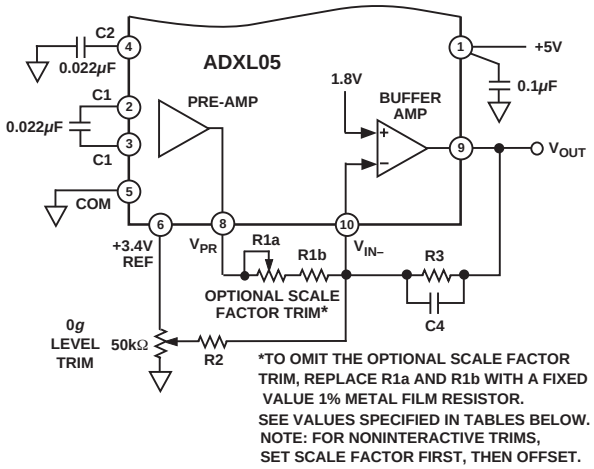
Low-Pass Filtering

The bandwidth of the accelerometer can easily be reduced by using post filtering. Figure 25 shows how the buffer amplifier can be connected to provide 1-pole post filtering, 0 *g* offset trimming, and output scaling. The table provides practical component values for various full-scale *g* levels and approximate circuit bandwidths. For bandwidths other than those listed, use the formula:

$$C4 = \frac{1}{(2\pi R3)\,Desired\ 3\ dB\ Bandwidth\ in\ Hz}$$

or simply scale the value of capacitor C4 accordingly, i.e., for an application with a 50 Hz bandwidth, the value of C4 will need to be twice as large as its 100 Hz value. If further noise reduction is needed while maintaining the maximum possible bandwidth, then a 2- or 3-pole post filter is recommended. These provide a much steeper roll-off of noise above the pole frequency. Figure 26 shows a circuit that uses the buffer amplifier to provide 2-pole post filtering. Component values for the 2-pole filter were selected to operate the buffer at unity gain. Capacitors C3 and C4 were chosen to provide 3 dB bandwidths of 10 Hz, 30 Hz, 100 Hz, and 300 Hz.

In this configuration, the nominal buffer amplifier output will be +1.8 V ± the 200 mV/*g* scale factor of the accelerometer. An AD820 external op amp allows noninteractive adjustment of 0 *g* offset and scale factor. The external op amp offsets and scales the output to provide a +2.5 V ± 2 V output over a wide range of full-scale *g* levels.

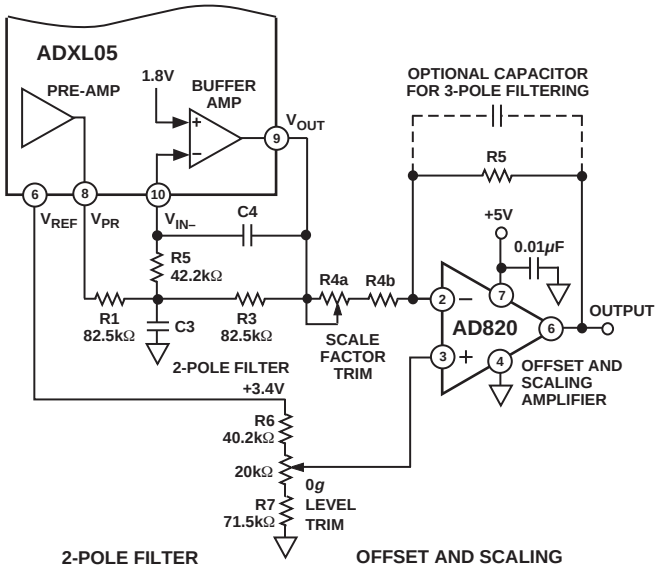


COMPONENT VALUES FOR VARIOUS FULL-SCALE RANGES AND BANDWIDTHS

FULL SCALE	mV per *g*	3dB BW (Hz)	R1a kΩ	R1b kΩ	R3 kΩ	R2 kΩ	C4 μF
±1*g*	2000	10	10	24.9	301	100	0.056
±2*g*	1000	100	10	35.7	200	100	0.0082
±4*g*	500	200	10	35.7	100	100	0.0082
±5*g*	400	300	10	45.3	100	100	0.0056

$$3dB\ BW = \frac{1}{2\pi\ R3\ C4}$$

Figure 25. Using the Buffer Amplifier to Provide 1-Pole Post Filtering Plus Scale Factor and 0 g Level Trimming



2-POLE FILTER COMPONENT VALUES

3dB BW (Hz)	C3μF	C4μF
300	0.027	0.0033
100	0.082	0.01
30	0.27	0.033
10	0.82	0.1

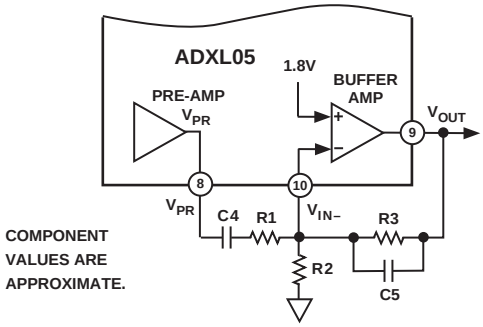
OFFSET AND SCALING AMPLIFIER COMPONENT VALUES

FULL SCALE	mV per *g*	GAIN	R4a kΩ	R4b kΩ	R5 kΩ
±1*g*	2000	10.00	10	24.9	301
±2*g*	1000	4.98	10	35.7	200
±4*g*	500	2.50	10	35.7	100
±5*g*	400	2.00	10	45.3	100

Figure 26. Two-Pole Filtering Circuit with Gain and 0 g Offset Adjustment

Bandpass Filtering

Figure 27 shows how the combination of ac coupling and low-pass filtering together form a bandpass filter that provides an even greater improvement in noise reduction.



SCALE FACTOR IN mV/*g*	DESIRED LOW FREQUENCY LIMIT, F_L	R1 VALUE IN kΩ	CLOSEST C4 VALUE	DESIRED HIGH FREQUENCY LIMIT, F_H	R3 IN kΩ	CLOSEST C5 VALUE	VALUE OF R2 FOR +2.5V 0*g* LEVEL
1000	30	49.9	0.10μF	300	249	0.002μF	640kΩ
200	30	249	0.022μF	300	249	0.002μF	640kΩ
1000	3	49.9	1.0μF	100	249	0.0068μF	640kΩ
200	1	249	0.68μF	100	249	0.0068μF	640kΩ
200	0.1	249	6.8μF	10	249	0.068μF	640kΩ

Figure 27 AC Coupling and Low-Pass Filtering Used Together to Provide a Bandpass Function

OBSOLETE

Additional Noise Reduction Techniques

Shielded wire should be used for connecting the accelerometer to any circuitry that is more than a few inches away—to avoid 60 Hz pickup from ac line voltage. Ground the cable's shield at only one end and connect a separate common lead between the circuits; this will help to prevent ground loops. Also, if the accelerometer is inside a metal enclosure, this should be grounded as well.

Methods for Reducing 0 *g* Offset Drift

When using any accelerometer with a dc (gravity sensing) response, the 0 *g* offset level will exhibit some temperature drift. For very high accuracy applications, one very straightforward approach is to use a low cost crystal oven to maintain the accelerometer at a constant temperature. These ovens are available in a variety of different temperatures. After the circuit has been built and is operating correctly, the crystal oven can be mounted over the accelerometer and powered off the same +5 V power supply.

The ovens may be purchased from Isotemp Research, Inc., P.O. Box 3389, Charlottesville, VA 22903, phone 804-295-3101. For more details on crystal oven compensation, refer to application note AN-385.

Other methods for 0 *g* drift compensation include using a low cost temperature sensor such as the AD22100 to supply a microprocessor with the device temperature. If the drift curve of the accelerometer is stored in the µP, then a software program can be used to subtract out the drift. Alternatively, a simple 1st order (straight line) correction circuit can be used to subtract out the linear portion of the accelerometer's drift by using a temperature sensor and op amp to supply a small compensation current. For more details on software and hardware drift compensation, refer to application note AN-380.

ACCELEROMETER APPLICATIONS

Popular applications for low *g* accelerometers tend to fall into three categories: measurement of tilt and orientation, inertial measurement of acceleration, velocity and distance, and vibration or shock measurement.

The ADXL05 is a "dc" accelerometer, meaning that it is capable of measuring static accelerations such as the Earth's gravity. The ADXL05 differs from other acceleration measurement technologies such as piezoelectric and piezofilm sensors which can only respond to ac signals greater than approximately 1 Hz. This dc capability is required for tilt and inertial measurement. For ac shock or vibration the ADXL05 can measure frequencies of up to 4 kHz and has the added benefit of measuring all the way down to dc.

Using the ADXL05 in Tilt Applications

The ADXL05's precision dc characteristics make it suitable for tilt measurement. It can directly measure the Earth's gravity and use this constant force as a position reference to determine inclination. As shown in Figure 28, the accelerometer should be mounted so that its sensitive axis is perpendicular to the force of gravity, i.e., parallel to the Earth's surface. In this manner, it will be most sensitive to changes in orientation (when it is orientated 90° to the force of gravity). Its output can be then described by the sine function; a tilt occurring at an angle θ will cause a voltage output equal to:

$$V_{OUT} = \left[Accelerometer\ \ Scale\ Factor\left(\frac{V}{g}\right) \times \sin(\theta) \times 1g \right] + zero\ g\ output(V)$$

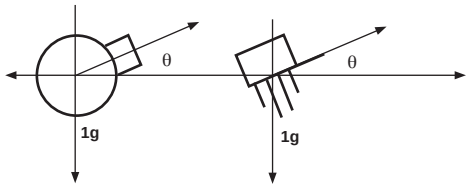


Figure 28. Two Possible Orientations for Tilt Measurement

Conversely, for a given acceleration signal and assuming no other changes in the axis or interfering signals, the tilt angle is proportional to the voltage output as shown in Figure 29. The angle, θ can be calculated using:

$$\theta = \arcsin\left(1g \times \left[\frac{V_{OUT} - zero\ g\ output(V)}{Scale\ Factor\ (V/g)}\right]\right)$$

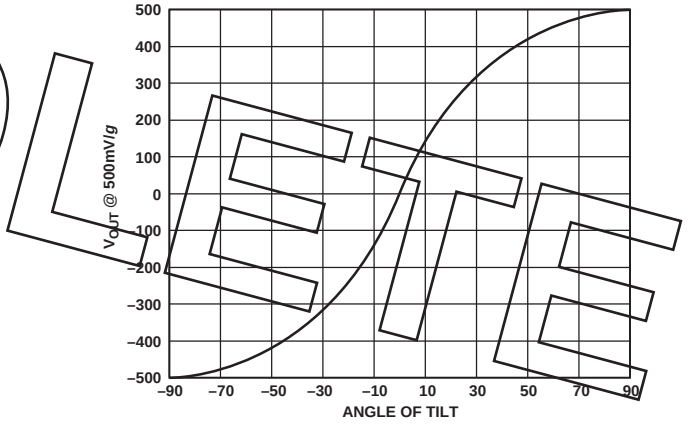


Figure 29. V_{OUT} vs. Tilt Angle

The use of an accelerometer in tilt applications has several advantages over the use of a traditional tilt sensor. A traditional tilt sensor consists of glass vial filled with a conductive liquid, typically a mercury or electrolytic solution. Besides being larger than an XL05, it requires additional signal conditioning circuitry. The settling time and frequency response is limited by the amount of time required for the liquid to stop sloshing around in the vial. In high vibration environments, or where high lateral accelerations may be present, it may not be possible to resolve the tilt signal above the "slosh" noise. The accelerometer has faster frequency (up to 50 ×) response and settling time. Interfering vibrations may be filtered out if necessary, an impossibility with a liquid tilt sensor, since one cannot filter the liquid. Finally, in the presence of lateral accelerations, an accelerometer provides more useful information, i.e., an acceleration signal, which if cleverly signal processed, can provide both a tilt and an acceleration output. A single accelerometer can be used to measure tilt over a 180° range; two accelerometers gives a complete 360° of measurement.

An important characteristic for an accelerometer used in a tilt application is its 0 *g* offset stability over temperature. The ADXL05 typically exhibits offsets that deviate no more than 0.1 *g* over the 0°C to +70°C temperature range, corresponding

OBSOLETE

to a 5° tilt error over the entire temperature range. Straightforward calibration schemes discussed in this data sheet may be used to reduce or compensate for temperature drift to improve the absolute accuracy of the measurement.

Using the ADXL05 in Inertial Measurement Applications
Inertial measurement refers to the practice of measuring acceleration for the purpose of determining the velocity of an object and its change in position, or distance traveled. This technique has previously required expensive inertial guidance systems of the type used in commercial aircraft and military systems. The availability of a low cost precision dc accelerometer such as the ADXL05 enables the use of inertial measurement for more cost sensitive industrial and commercial applications.

Inertial measurement makes use of the fact that the integral of acceleration is velocity and the integral of velocity is distance. By making careful measurements of acceleration and mathematically integrating the signals, one can determine both velocity and the distance traveled. The technique is useful for applications where a traditional speed and distance measurement is impractical, or where a non-contact, relative position measurement must be made.

A practical inertial measurement system uses multiple accelerometers to measure acceleration in three axes, and gyroscopes to measure rotation in three axes, the requirement for a 6 degree of freedom system. For simpler systems where one or more of the axes can be constrained, it is possible to build a system with fewer accelerometers and gyros.

The measurement system must take the acceleration sensor and calibrate out all static errors including any initial inaccuracy or temperature drift. A mathematical model is used to describe the performance of the sensor in order to calibrate it. If these errors are not removed, then the process of double integration will quickly cause any small error to dominate the result. Most practical systems use microprocessors for error correction and a temperature sensor for temperature drift compensation. Another approach is to maintain all of the sensors at a controlled temperature. The microprocessors have the additional advantage of providing a low cost method of performing the single and double integration of the acceleration signal.

The stability and repeatability of the accelerometer is the most important specification in an inertial system. The ADXL05 is "well behaved" that is, its response and temperature characteristics are easy to model and correct, and once modeled they are very repeatable. For example, temperature performance can be adequately modeled using first order, (straight line) approximations for most applications, and other errors such as on-axis and pendulous rectification are minimal. This greatly simplifies the math required to correct the sensor.

Vibration and Shock Measurement Applications
The ADXL05 can measure shocks and vibrations from dc to 4 kHz. Typical signal processing for vibration signals includes fast Fourier transforms, and single and double integration for velocity and displacement. It is possible to build a single integrator stage using the ADXL05's output buffer amplifier in order to provide a velocity output.

The sensitivity of the accelerometer will typically vary only ±0.5% over the full industrial temperature range, making it one of the most stable vibration measurement devices available. In vibration measurement applications, mechanical mounting and control of system and mounting resonances are critical to proper measurement. Refer to the application note AN-379, available from Analog Devices.

CALIBRATING THE ADXL05

If a calibrated shaker is not available, both the 0 *g* level and scale factor of the ADXL05 may be easily set to fair accuracy by using a self-calibration technique based on the 1 *g* (average) acceleration of the earth's gravity. Figure 30 shows how gravity and package orientation affect the ADXL05's output. Note that the output polarity is that which appears at V_{PR}; the output at V_{OUT} will have the opposite sign. With its axis of sensitivity in the vertical plane, the ADXL05 should register a 1 *g* acceleration, either positive or negative, depending on orientation. With the axis of sensitivity in the horizontal plane, no acceleration (the 0 *g* bias level) should be indicated.

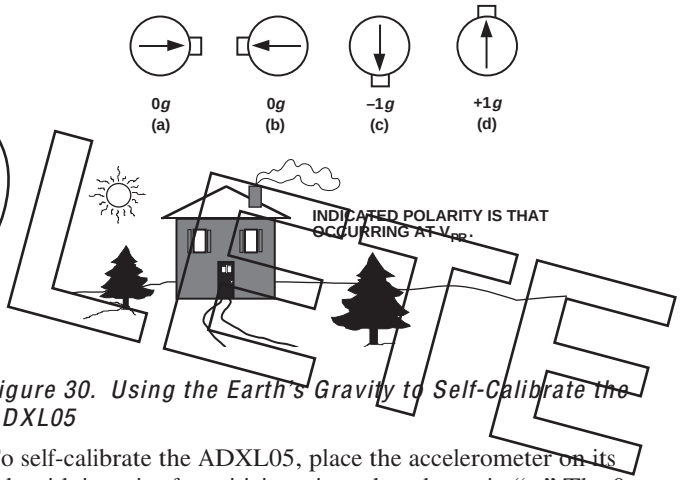


Figure 30. Using the Earth's Gravity to Self-Calibrate the ADXL05

To self-calibrate the ADXL05, place the accelerometer on its side with its axis of sensitivity oriented as shown in "a." The 0 *g* offset potentiometer, Rt, is then roughly adjusted for midscale: +2.5 V at the buffer output (see Figure 25).

Next, the package axis should be oriented as in "c" (pointing down) and the output reading noted. The package axis should then be rotated 180° to position "d" and the scale factor potentiometer, R1a, adjusted so that the output voltage indicates a change of 2 *g*s in acceleration. For example, if the circuit scale factor at the buffer output is 400 mV per *g*, then the scale factor trim should be adjusted so that an output change of 800 mV is indicated.

Adjusting the circuit's scale factor will have some effect on its 0 *g* level so this should be readjusted, as before, but this time checked in both positions "a" and "b." If there is a difference in the 0 *g* reading, a compromise setting should be selected so that the reading in each direction is equidistant from +2.5 V. Scale factor and 0 *g* offset adjustments should be repeated until both are correct.

REDUCING POWER CONSUMPTION

The use of a simple power cycling circuit provides a dramatic reduction in the ADXL05's average current consumption. In low bandwidth applications such as shipping recorders, this simple, low cost circuit can provide substantial power reduction.

If a microprocessor is available, only the circuit of Figure 31 is needed. The microprocessor supplies a TTL clock pulse to gate buffer transistor Q1 which inverts the output pulse from the µP

OBSOLETE

so that the duty cycle is correct when the pulse is re-inverted again by transistor, Q2, which cycles the accelerometer's supply voltage on and off.

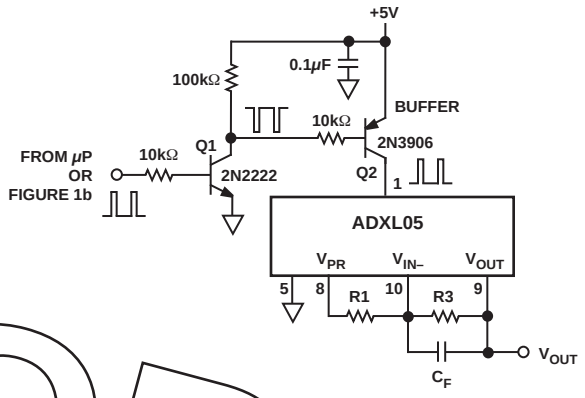


Figure 31. Basic Power Cycling Circuit

Figures 32 and 33 show typical waveforms of the accelerometer being operated with a 10% duty cycle: 1 ms on, 9 ms off. This reduces the average current consumption of the accelerometer from 8 mA to 800 μA, providing a power reduction of 90%. The μP should sample acceleration during the interval between the time the 0 *g* level has stabilized (≈ 400 μs using a 0.022 μF demod cap) and the end of the pulse duration. The measurement bandwidth of a power-cycled circuit will be set by the clock pulse rate and duty cycle. In this example, 1 sample can be taken every 10 ms which is 100 samples per second or 100 Hz. As defined by the "Nyquist criteria," the best case measurement bandwidth is $F_S/2$ or half the clock frequency. Therefore 50 Hz signals can be processed if adequate filtering is provided.

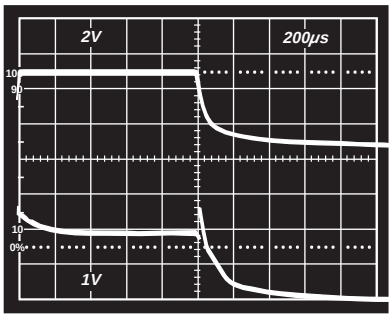


Figure 32. Top Trace: Voltage at Pin 1; Bottom Trace: Output at V_{PR}

Higher measurement bandwidths can be achieved by reducing the size of the demodulation capacitor below 0.022 μF and increasing the pulse frequency. A 0.01 μF capacitor was connected across the feedback resistor of the ADXL05 buffer to improve its transient characteristics. The optimum value for this capacitor will change with buffer gain and the cycling pulse rate. For more details, refer to application note AN-378.

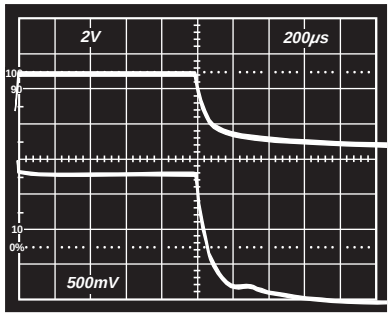


Figure 33. Top Trace: Voltage at Pin 1; Bottom Trace: Buffer Output With R1 = R3 = 100 kΩ, C_F = 0.01 μF

COMPONENT SELECTION

LOAD DRIVE CAPABILITIES OF THE V_{PR} AND BUFFER OUTPUTS

The V_{PR} and the buffer amplifier outputs are both capable of driving a load to voltage levels approaching that of the supply rail. However, both outputs are limited in how much current they can supply, affecting component selection.

V_{PR} Output

The V_{PR} pin has the ability to source current up to 500 μA but only has a sinking capability of 30 μA which limits its ability to drive loads. It is recommended that the buffer amplifier be used in most applications, to avoid loading down V_{PR}. In standard ±5 *g* applications, the resistor R1 from V_{PR} to V_{IN-} is recommended to have a value greater than 20 kΩ to reduce loading effects.

Capacitive loading of the V_{PR} pin should be minimized. A load capacitance between the V_{PR} pin and common will introduce an offset of approximately 1 mV for every 10 pF of load. The V_{PR} pin may be used to directly drive an A/D input or other source as long as these sensitivities are taken into account. It is always preferable to drive A/D converters or other sources using the buffer amplifier (or an external op amp) instead of the V_{PR} pin.

Buffer Amplifier Output

The buffer output can drive a load to within 0.25 V of either power supply rail and is capable of driving 1000 pF capacitive loads. Note that a capacitance connected across the buffer feedback resistor for low-pass filtering does not appear as a capacitive load to the buffer. The buffer amplifier is limited to sourcing or sinking a maximum of 100 μA. Component values for the resistor network should be selected to ensure that the buffer amplifier can drive the filter under worst case transient conditions.

Self-Test Function

The digital self-test input is compatible with both CMOS and TTL signals. A Logic "l" applied to the self-test (ST) input will cause an electrostatic force to be applied to the sensor which will cause it to deflect to the approximate negative full-scale output of the device. Accordingly, a correctly functioning accelerometer will respond by initiating an approximate –1 volt

OBSOLETE

output change at V_{PR}. If the ADXL05 is experiencing an acceleration when the self-test is initiated, the V_{PR} output will equal the algebraic sum of the two inputs. The output will stay at the self-test level as long as the ST input remains high and will return to the 0 *g* level when the ST voltage is removed.

A self-test output that varies more than ±15% from the nominal –1.0 V change indicates a defective beam or a circuit problem such as an open or shorted pin or component.

Operating the ADXL05's buffer amplifier at Gains > 2, to provide full-scale outputs of less than ±5 *g*, may cause the self-test output to overdrive the buffer into saturation. The self-test may still be used in the case, but the change in the output must then be monitored at the V_{PR} pin instead of the buffer output.

Note that the value of the self-test delta is not an exact indication of the sensitivity (mV/*g*) of the ADXL05 and, therefore, may not be used to calibrate the device for sensitivity error.

In critical applications, it may be desirable to monitor shifts in the zero-*g* bias voltage from its initial value. A shift in the 0 *g* bias level may indicate that the 0 *g* level has shifted which may warrant an alarm.

Power Supply Decoupling
The ADXL05 power supply should be decoupled with a 0.1 µF ceramic capacitor from +5 V pin of the ADXL05 to common using very short component leads. For other decoupling considerations, see EMI/RFI section.

Oscillator Decoupling Capacitor, C2
An oscillator decoupling capacitor, C2, is used to remove 1 MHz switching transients in the sensor excitation signal, and is required for proper operation of the ADXL05. A ceramic capacitor with a minimum value of 0.022 µF is recommended from the oscillator decoupling capacitor pin to common. Small amounts of capacitor leakage due to a dc resistance greater than 1 MΩ will not affect operation (i.e., a high quality capacitor is not needed here). As with the power supply bypass capacitor, very short component leads are recommended. Although 0.022 µF is a good typical value, it may be increased for reasons of convenience, but doing this will not improve the noise performance of the ADXL05.

Demodulator Capacitor, C1
The demodulator capacitor is connected across Pins 2 and 3 to set the bandwidth of the force balance control loop. This capacitor may be used to approximately set the bandwidth of the accelerometer. A capacitor is always required for proper operation.

The frequency response of the ADXL05 exhibits a single pole roll-off response, see Figure 4.

A nominal value of 0.022 µF is recommended for C1. In general, the design bandwidth should be set 40% higher than the minimum desired system bandwidth due to the ±40% tolerance, to preserve stability C1 should be kept > 0.01 µF.

The demodulation capacitor should be a low leakage, low drift ceramic type with an NPO (best) or X7R (good) dielectric.

In general, it's best to use the recommended 0.022 µF capacitor across the demodulator pins and perform any additional low-pass filtering using the buffer amplifier. The use of the buffer for low-pass filtering generally results in smaller capacitance values and better overall performance. It is also a convenient and more precise way to set the system bandwidth. Post filtering allows bandwidth to be controlled accurately by component selection and avoids the ±40% demodulation tolerance. Note that signal noise is proportional to the square root of the bandwidth of the ADXL05 and may be a consideration in component selection—see section on noise.

Care should be taken to reduce or eliminate any leakage paths from the demodulator capacitor pins to common or to the +5 V pin. Even a small imbalance in the leakage paths from these pins will result in offset shifts in the zero-*g* bias level. As an example, an unbalanced parasitic resistance of 30 MΩ from either demodulator pin to ground will result in an offset shift at V_{PR} of approximately 50 mV. Conformal coating of PC boards with a high impedance material is recommended to avoid leakage problems due to aging or moisture.

MINIMIZING EMI/RFI
The architecture of the ADXL05 and its use of synchronous demodulation make the device immune to most electromagnetic (EMI) and radio frequency (RFI) interference. The use of synchronous demodulation allows the circuit to reject all signals except those at the frequency of the oscillator driving the sensor element. However, the ADXL05 does have a sensitivity to RFI that is within ±5 kHz of the internal oscillator's nominal frequency of 1 MHz and also to any odd harmonics of this frequency. The internal oscillator frequency will exhibit part to part variation in the range of 0.5 MHz to 1.4 MHz.

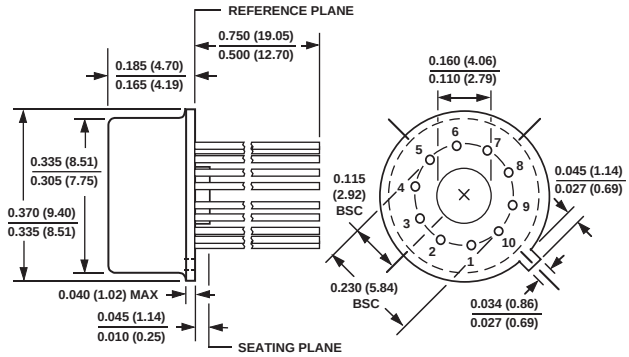
In general the effect is difficult to notice as the interference must match the internal oscillator within ±5 kHz and must be large in amplitude. For example: a 1 MHz interference signal of 20 mV p-p applied to the +5 V power supply pin will produce a 200 mV p-p signal at the V_{PR} pin if the internal oscillator and interference signals are matched exactly or at odd harmonics. If the same 20 mV interference is applied but 5 kHz above or below the internal oscillator's frequency, the signal level at V_{PR} will only be 20 mV p-p in amplitude.

Power supply decoupling, short component leads (especially for capacitors C1 and C2), physically small (surface mount, etc.) components and attention to good grounding practices all help to prevent RFI and EMI problems. Good grounding practices include having separate analog and digital grounds (as well as separate power supplies or very good decoupling) on the printed circuit boards. A single ground line shared by both the digital and analog circuitry can lead to digital pulses (and clock signals) interfering with the sensor's onboard oscillator. In extreme cases, a low cost radio frequency choke (≈10 µH) may be needed in series with the accelerometer's power supply pin. This, together with the recommended 0.1 µF power supply bypass capacitor, will form an effective RF filter. The use of an RF choke is preferred over a resistor since any series resistance in the power supply will "unregulate" the device from the supply, degrade its power supply rejection and reduce its supply voltage.

OBSOLETE

OUTLINE DIMENSIONS

Dimensions shown in inches and (mm).



OBSOLETE

OBSOLETE

C2028b–5–3/96

PRINTED IN U.S.A.

EXHIBIT 1064B

web.archive.org/web/19970606212637/http://www.analog.com/publications/press/products/ADXL05_050195.html
http://www.analog.com/publications/press/products/ADXL05_050195.html Go
FEB JUN FEB
8 captures 06
10 Feb 1997 - 12 Jul 2001 1996 1997 1999 About this capture

ANALOG DEVICES



Multi-Purpose Accelerometer Measures Low g Forces with 0.005g Resolution [ADXL05]

NORWOOD, Mass. (May 1, 1995) -- Analog Devices' ADXL05 is the industry's first single-chip integrated low-g accelerometer which resolves minute changes in acceleration (from 0 g to ±5 g full scale) with 0.005 g resolution-ten times more precise than the ADXL50 ±50 g airbag version. More than a sensor, the ADXL05 contains all the signal processing blocks of a complete acceleration system on a single chip. It combines a tiny micromachined sensor, modulator, demodulator, voltage reference, signal conditioning, amplification, and on-command self-test circuitry on one polysilicon die.

The ADXL05 is designed to simplify system complexity, improve performance, and reduce engineering costs in automotive, industrial, and commercial applications where tilt, inertial, shock, vibration, velocity and acceleration characteristics must be measured. Unlike piezoelectric devices, the ADXL05 provides a true dc (gravity) response for precision tilt and inertial measurement systems. Piezoresistive devices are less precise and more expensive.

The Wayback Machine - https://web.archive.org/web/19970606212637/http://www.analog.com:80/publication…

Multi-Purpose Accelerometer Measures Low g Forces with 0.005g Resolution [ADXL05]

NORWOOD, Mass. (May 1, 1995) -- Analog Devices' ADXL05 is the industry's first single-chip integrated low-g accelerometer which resolves minute changes in acceleration (from 0 g to ±5 g full scale) with 0.005 g resolution-ten times more precise than the ADXL50 ±50 g airbag version. More than a sensor, the ADXL05 contains all the signal processing blocks of a complete acceleration system on a single chip. It combines a tiny micromachined sensor, modulator, demodulator, voltage reference, signal conditioning, amplification, and on-command self-test circuitry on one polysilicon die.

The ADXL05 is designed to simplify system complexity, improve performance, and reduce engineering costs in automotive, industrial, and commercial applications where tilt, inertial, shock, vibration, velocity and acceleration characteristics must be measured. Unlike piezoelectric devices, the ADXL05 provides a true dc (gravity) response for precision tilt and inertial measurement systems. Piezoresistive devices are less precise and more expensive. The ADXL05 operates from a single +5-V power supply and produces a user-selectable output signal of up to 1 V/g with a typical nonlinearity of 0.3% full scale (FS). Its flexibility and guaranteed specifications enable new design opportunities in virtual reality headsets, machine health monitors, seismic instruments, medical diagnostic equipment, automotive autoskid breaking systems (ABS) and suspension control, embedded shipping recorders, and any number of applications involving movement. Adjustable control via an internal buffer lets users set the device's sensitivity and zero-output to accommodate various system techniques. External capacitors can be added to provide one or two poles of filtering. No additional components are needed for interface to most analog-to-digital converters and microcontrollers.

Analog Devices' ±50 g accelerometer, the ADXL50, is now used in a variety of 1995 General Motors cars as the crash sensor in airbag deployment systems. The same high-volume, proven reliability benefits of this 50 g device are now available in the new 5 g ADXL05 version.

The ADXL05 is packaged in a hermetic 10-pin TO-100 metal can with guaranteed specifications over the 0 to +70°C commercial, and -40° to +85°C industrial temperature ranges; delivery is from stock. Contact the factory for the availability of devices for operation over the -40° to +105°C automotive and -55° to +125°C military temperature ranges.

With fiscal 1994 revenues of $773 million, Analog Devices is a Fortune 500 company that designs, manufactures, and markets precision high-performance integrated circuits used in analog and digital signal processing applications. The company employs approximately 5,500 people worldwide and has manufacturing facilities in Massachusetts, California, North Carolina, Ireland, Japan, the Philippines and Taiwan.

Revised March 4, 1997

Nintendo Exhibit 1066
IPR2024-00668 - Page 691

For more information contact us.

© Copyright 1995-1997 Analog Devices, Inc. All rights reserved.

Nintendo Exhibit 1066
IPR2024-00668 - Page 692

EXHIBIT 1064C

web.archive.org/web/19970606201119/http://www.analog.com/products/sheets/ADXL05.html

http://www.analog.com/products/sheets/ADXL05.html Go MAY JUN NOV

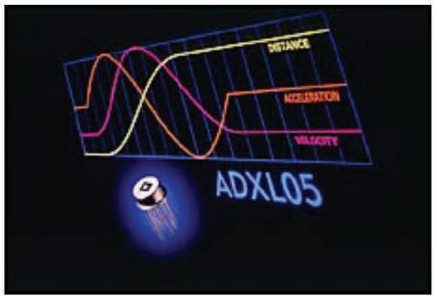
23 captures

6 Jun 1997 - 11 Feb 2021

1996 06 1997 2001 About this capture

ADXL05

General Description



The ADXL05 is a complete acceleration measurement system on a single monolithic IC. The ADXL05 will measure accelerations with full-scale ranges of ±5 g to ±1 g or less. Typical noise floor is 500 μg/(root)Hz, (12x less than the ADXL50), allowing signals below 5 milli-g to be resolved. The ADXL05 is a force balanced capacitive accelerometer with the capability to measure both ac accelerations (typical of vibration) or dc accelerations (such as inertial force or gravity). Three external capacitors and a +5 volt regulated power supply are all that is required to measure accelerations up to ±5 g. Three resistors are used to configure the output buffer amplifier to set scale factors from 200 mV/g to 1 V/g. External capacitors may be added to the resistor network to provide 1 or 2 poles of filtering. No additional active components are required to interface directly to most analog to digital converters (ADCs).

The device features a TTL compatible self-test function that can electrostatically deflect the sensor beam at any time to verify that the sensor and its electronics are functioning correctly.

The ADXL05 is available in a hermetic 10-pin TO-100 metal can, specified over the 0°C to +70°C commercial, and -40°C to +85°C industrial temperature ranges.

© Copyright 1995-1997 Analog Devices, Inc. All rights reserved.

web.archive.org/web/19970606201119/http://www.analog.com/products/sheets/ADXL05.html

http://www.analog.com/products/sheets/ADXL05.html Go MAY JUN NOV

23 captures 06

6 Jun 1997 - 11 Feb 2021 1996 1997 2001 About this capture

ADXL05

Description

Datasheets

Press Releases

the sensor and its electronics are functioning correctly.

The ADXL05 is available in a hermetic 10-pin TO-100 metal can, specified over the 0°C to +70°C commercial, and -40°C to +85°C industrial temperature ranges.

Datasheets

Listed below is the datasheet for this product. This datasheet is available in Adobe Acrobat PDF format. To view Acrobat files you must install Adobe Acrobat Reader. Acrobat Reader is available free of charge. To download Adobe Acrobat visit their website.

Get Acrobat® Reader

- ±1g to ±5g Single Chip Accelerometer with Signal Conditioning

Press Releases

Listed below are any Analog press releases that pertain to this product. Press Releases contain the latest news and information about specific products.

- Analog Devices Dedicates New FAB to Micromachined Products
- Multi-Purpose Accelerometer Measures Low g Forces with 0.005g Resolution
- ADXL Accelerometer Evaluation Kits Simplify System Development, Reduce Design Time

ANALOG DEVICES

HOME SEARCH SITE MAP HELP GLOSSARY FEEDBACK ORDER PRODUCTS

© Copyright 1995-1997 Analog Devices, Inc. All rights reserved.

EXHIBIT 1064D

DONATE

Explore more than 928 billion web pages saved over time

http://www.analog.com/products/sheets/

Calendar · Collections · Changes · Summary · Site Map · URLs

3,081 URLs have been captured for this URL prefix.

Filter results by URL or MIME Type (i.e. '.txt')

URL ↑	MIME Type	From	To	Captures	Duplicates	Uniques
http://www.analog.com:80/products/sheets/ADSP2162.html	text/html	Jun 6, 1997	Nov 15, 1997	3	1	2
http://www.analog.com:80/products/sheets/ADSP2164.html	text/html	Jun 6, 1997	Nov 15, 1997	3	1	2
http://www.analog.com:80/products/sheets/ADSP2166.html	text/html	Jun 6, 1997	Nov 15, 1997	3	1	2
http://www.analog.com:80/products/sheets/ADSP216X.html	text/html	Jun 6, 1997	Jul 6, 1997	2	0	2
http://www.analog.com:80/products/sheets/ADSP2171.html	text/html	Jun 6, 1997	Nov 15, 1997	3	1	2
http://www.analog.com:80/products/sheets/ADSP2172.html	text/html	Jun 6, 1997	Nov 15, 1997	3	1	2
http://www.analog.com:80/products/sheets/ADSP2173.html	text/html	Jun 6, 1997	Nov 15, 1997	3	1	2
http://www.analog.com:80/products/sheets/ADSP218.html	text/html	Jun 6, 1997	Jul 6, 1997	2	1	1
http://www.analog.com:80/products/sheets/ADSP2181.html	text/html	Jun 6, 1997	Nov 15, 1997	3	1	2
http://www.analog.com:80/products/sheets/ADSP2183.html	text/html	Jun 6, 1997	Nov 15, 1997	3	0	3
http://www.analog.com:80/products/sheets/ADSP2185.html	text/html	Jun 6, 1997	Dec 18, 2005	18	13	5
http://www.analog.com:80/products/sheets/ADSP2186.html	text/html	Jun 6, 1997	Nov 15, 1997	3	1	2
http://www.analog.com:80/products/sheets/ADSP21CSP01.html	text/html	Jun 6, 1997	Jul 6, 1997	2	1	1

Nintendo Exhibit 1066
IPR2024-00668 - Page 697

URL ↑	MIME Type	From	To	Captures	Duplicates	Uniques
http://www.analog.com:80/products/sheets/ADSP21MOD870.html	text/html	Nov 15, 1997	Nov 15, 1997	1	0	1
http://www.analog.com:80/products/sheets/ADSP21MSP58.html	text/html	Jun 6, 1997	Nov 15, 1997	3	1	2
http://www.analog.com:80/products/sheets/ADSP21MSP59.html	text/html	Jun 6, 1997	Nov 15, 1997	3	1	2
http://www.analog.com:80/products/sheets/ADSP21XX.html	text/html	Jun 6, 1997	Nov 15, 1997	3	0	3
http://www.analog.com:80/products/sheets/ADSP21XXEZICE.html	text/html	Jun 6, 1997	Nov 15, 1997	3	1	2
http://www.analog.com:80/products/sheets/ADSP21XXEZKITLITE.html	text/html	Jun 6, 1997	Nov 15, 1997	3	1	2
http://www.analog.com:80/products/sheets/ADSP21XXEZLAB.html	text/html	Jun 6, 1997	Nov 15, 1997	3	1	2
http://www.analog.com:80/products/sheets/ADSP21XXSOFTWAREDEVTOOLS.html	text/html	Jun 6, 1997	Nov 15, 1997	3	1	2
http://www.analog.com:80/products/sheets/ADSP28MSP02.html	text/html	Jun 6, 1997	Nov 15, 1997	3	1	2
http://www.analog.com:80/products/sheets/ADT14.html	text/html	Jun 6, 1997	Nov 15, 1997	3	1	2
http://www.analog.com:80/products/sheets/ADT41.html	text/html	Jun 6, 1997	Nov 15, 1997	3	1	2
http://www.analog.com:80/products/sheets/ADT42.html	text/html	Jun 6, 1997	Nov 15, 1997	3	1	2
http://www.analog.com:80/products/sheets/ADT43.html	text/html	Jun 6, 1997	Nov 15, 1997	3	1	2
http://www.analog.com:80/products/sheets/ADV101.html	text/html	Jun 6, 1997	Nov 15, 1997	3	1	2
http://www.analog.com:80/products/sheets/ADV453.html	text/html	Jun 6, 1997	Nov 15, 1997	3	1	2
http://www.analog.com:80/products/sheets/ADV471.html	text/html	Jun 6, 1997	Nov 15, 1997	3	1	2
http://www.analog.com:80/products/sheets/ADV473.html	text/html	Jun 6, 1997	Nov 15, 1997	3	1	2
http://www.analog.com:80/products/sheets/ADV476.html	text/html	Jun 6, 1997	Nov 15, 1997	3	1	2
http://www.analog.com:80/products/sheets/ADV478.html	text/html	Jun 6, 1997	Nov 15, 1997	3	1	2
http://www.analog.com:80/products/sheets/ADV601.html	text/html	Jun 6, 1997	Apr 3, 2005	12	5	7

Nintendo Exhibit 1066
IPR2024-00668 - Page 698

URL ↑	MIME Type	From	To	Captures	Duplicates	Uniques
http://www.analog.com:80/products/sheets/ADV601LC.html	text/html	Nov 15, 1997	Mar 22, 2005	11	7	4
http://www.analog.com:80/products/sheets/ADV7120.html	text/html	Jun 6, 1997	Nov 15, 1997	3	1	2
http://www.analog.com:80/products/sheets/ADV7121.html	text/html	Jun 6, 1997	Nov 15, 1997	3	1	2
http://www.analog.com:80/products/sheets/ADV7122.html	text/html	Jun 6, 1997	Nov 15, 1997	3	1	2
http://www.analog.com:80/products/sheets/ADV7128.html	text/html	Jun 6, 1997	Nov 15, 1997	3	1	2
http://www.analog.com:80/products/sheets/ADV7129.html	text/html	Jun 6, 1997	Nov 15, 1997	3	1	2
http://www.analog.com:80/products/sheets/ADV7150.html	text/html	Jun 6, 1997	Nov 15, 1997	3	0	3
http://www.analog.com:80/products/sheets/ADV7151.html	text/html	Jun 6, 1997	Nov 15, 1997	3	1	2
http://www.analog.com:80/products/sheets/ADV7152.html	text/html	Jun 6, 1997	Nov 15, 1997	3	1	2
http://www.analog.com:80/products/sheets/ADV7160.html	text/html	Jun 6, 1997	Nov 15, 1997	3	1	2
http://www.analog.com:80/products/sheets/ADV7162.html	text/html	Jun 6, 1997	Nov 15, 1997	3	1	2
http://www.analog.com:80/products/sheets/ADV7175.html	text/html	Jun 6, 1997	Nov 15, 1997	3	1	2
http://www.analog.com:80/products/sheets/ADV7176.html	text/html	Jun 6, 1997	Nov 15, 1997	3	1	2
http://www.analog.com:80/products/sheets/ADVFC32.html	text/html	Jun 6, 1997	Nov 15, 1997	3	1	2
http://www.analog.com:80/products/sheets/ADXL05.html	text/html	Jun 6, 1997	Feb 11, 2021	15	9	6
http://www.analog.com:80/products/sheets/ADXL150.html	text/html	Nov 15, 1997	Nov 15, 1997	1	0	1
http://www.analog.com:80/products/sheets/ADXL150EM1.html	text/html	Jun 6, 1997	Jul 6, 1997	2	1	1

Showing 801 to 850 of 3,081 entries

First Previous 1 … 16 17 18 … 62 Next Last

Nintendo Exhibit 1066
IPR2024-00668 - Page 699

The Wayback Machine is an initiative of the Internet Archive, a 501(c)(3) non-profit, building a digital library of Internet sites and other cultural artifacts in digital form. Other projects include Open Library & archive-it.org.

Your use of the Wayback Machine is subject to the Internet Archive's Terms of Use.

Nintendo Exhibit 1066
IPR2024-00668 - Page 700

EXHIBIT 1065A

https://web.archive.org/web/19970707142701/http://www.analog.com/pdf/adxl50.pdf 133%
http://www.analog.com/pdf/adxl50.pdf Go JUN JUL APR
6 captures 07
7 Jul 1997 - 15 Jan 2006 1996 1997 2003 About this capture

ANALOG DEVICES

Monolithic Accelerometer With Signal Conditioning

ADXL50*

FEATURES

Complete Acceleration Measurement System on a Single Monolithic IC
Full-Scale Measurement Range: ±50 g
Self-Test on Digital Command
+5 V Single Supply Operation
Sensitivity Precalibrated to 19 mV/g
Internal Buffer Amplifier for User Adjustable Sensitivity and Zero-g Level
Frequency Response: DC to 10 kHz
Post Filtering with External Passive Components

For convenience, the ADXL50 has an internal buffer amplifier with a full 0.25 V to 4.75 V output range. This may be used to set the zero-g level and change the output sensitivity by using external resistors. External capacitors may be added to the resistor network to provide 1 or 2 poles of filtering. No external active components are required to interface directly to most analog-to-digital converters (ADCs) or microcontrollers.

The ADXL50 uses a capacitive measurement method. The analog output voltage is directly proportional to acceleration, and is fully scaled, referenced and temperature compensated, resulting

Nintendo Exhibit 1066
IPR2024-00668 - Page 702

Monolithic Accelerometer With Signal Conditioning

ADXL50*

FEATURES

Complete Acceleration Measurement System on a Single Monolithic IC
Full-Scale Measurement Range: ±50 g
Self-Test on Digital Command
+5 V Single Supply Operation
Sensitivity Precalibrated to 19 mV/g
Internal Buffer Amplifier for User Adjustable Sensitivity and Zero-g Level
Frequency Response: DC to 10 kHz
Post Filtering with External Passive Components
High Shock Survival: >2000 g Unpowered
Other Versions Available: ADXL05 (±5 g)

GENERAL DESCRIPTION

The ADXL50 is a complete acceleration measurement system on a single monolithic IC. Three external capacitors and a +5 volt power supply are all that is required to measure accelerations up to ±50 g. Device sensitivity is factory trimmed to 19 mV/g, resulting in a full-scale output swing of ±0.95 volts for a ±50 g applied acceleration. Its zero g output level is +1.8 volts.

A TTL compatible self-test function can electrostatically deflect the sensor beam at any time to verify device functionality.

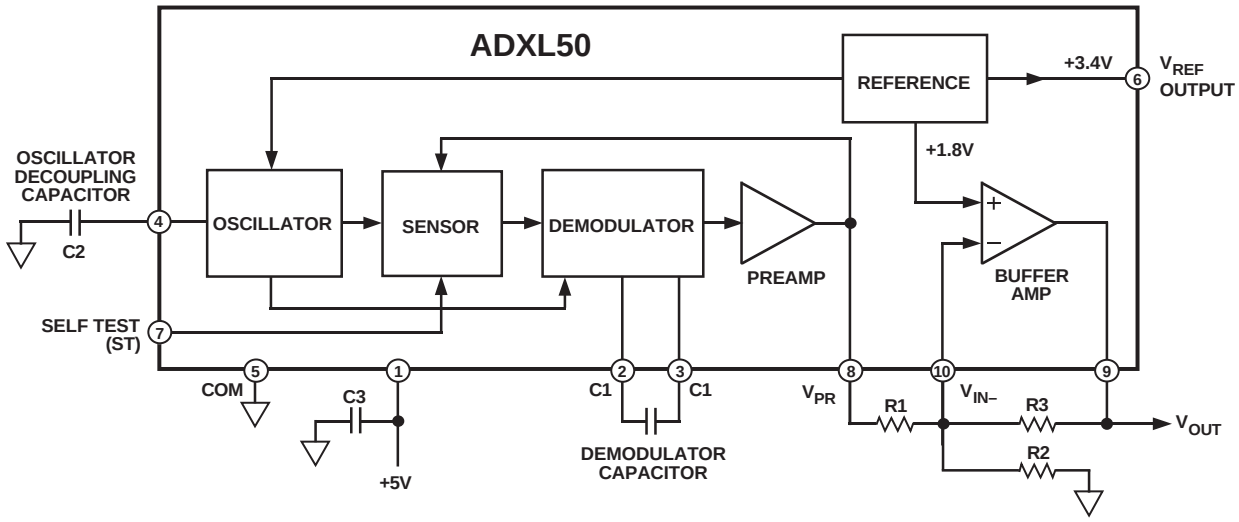
For convenience, the ADXL50 has an internal buffer amplifier with a full 0.25 V to 4.75 V output range. This may be used to set the zero-g level and change the output sensitivity by using external resistors. External capacitors may be added to the resistor network to provide 1 or 2 poles of filtering. No external active components are required to interface directly to most analog-to-digital converters (ADCs) or microcontrollers.

The ADXL50 uses a capacitive measurement method. The analog output voltage is directly proportional to acceleration, and is fully scaled, referenced and temperature compensated, resulting in high accuracy and linearity over a wide temperature range. Internal circuitry implements a forced-balance control loop that improves accuracy by compensating for any mechanical sensor variations.

The ADXL50 is powered from a standard +5 V supply and is robust for use in harsh industrial and automotive environments and will survive shocks of more than 2000 g unpowered.

The ADXL50 is available in a hermetic 10-pin TO-100 metal can, specified over the 0°C to +70°C commercial, and –40°C to +85°C industrial temperature ranges. Contact factory for availability of devices specified for operation over the –40°C to +105°C automotive temperature range.

FUNCTIONAL BLOCK DIAGRAM



*Patents pending.

REV. B

Information furnished by Analog Devices is believed to be accurate and reliable. However, no responsibility is assumed by Analog Devices for its use, nor for any infringements of patents or other rights of third parties which may result from its use. No license is granted by implication or otherwise under any patent or patent rights of Analog Devices.

© Analog Devices, Inc., 1996

One Technology Way, P.O. Box 9106, Norwood, MA 02062-9106, U.S.A.
Tel: 617/329-4700 Fax: 617/326-8703

ADXL50–SPECIFICATIONS ($T_A = T_{MIN}$ to T_{MAX}, T_A = +25°C for J Grade Only, V_S = +5 V, @ Acceleration = 0 *g*, unless otherwise noted)

Parameter	Conditions	ADXL50J/A Min	Typ	Max	Units
SENSOR INPUT					
Measurement Range	Guaranteed Full Scale	–50		+50	*g*
Nonlinearity	Best Fit Straight Line, 50 *g* FS		0.2		% of FS
Alignment Error[1]			±1		Degrees
Transverse Sensitivity[2]			±2		%
SENSITIVITY					
Initial Sensitivity at V_{PR}	+25°C	16.1	19.0	21.9	mV/*g*
Temperature Drift[3]			0.75/1.0		% of Reading
ZERO *g* BIAS LEVEL	at V_{PR}				
Initial Offset		1.55/1.60	1.80	2.05/2.00	V
vs. Temperature[3]			±15/35		mV
vs. Supply	V_S = 4.75 V to 5.25 V		10	32	mV/V
NOISE PERFORMANCE	at V_{PR}				
Voltage Noise Density	BW = 10 Hz to 1 kHz		6.6	12	m*g*/√Hz
Noise in 100 Hz Bandwidth			66		m*g* rms
Noise in 10 Hz Bandwidth			20		m*g* rms
FREQUENCY RESPONSE					
3 dB Bandwidth[4]	C1 = 0.022 µF (See Figure 22)	800	1300		Hz
3 dB Bandwidth[4]	C1 = 0.0068 µF		10		kHz
Sensor Resonant Frequency			24		kHz
SELF TEST INPUT					
Output Change at V_{PR}[5]	ST Pin from Logic "0" to "1"	–0.85	–1.00	–1.15	V
Logic "1" Voltage		2.0			V
Logic "0" Voltage				0.8	V
Input Resistance	To Common		50		kΩ
+3.4 V REFERENCE					
Output Voltage		3.350	3.400	3.450	V
Output Temperature Drift[3]			±10		mV
Power Supply Rejection	DC, V_S = +4.75 V to +5.25 V		1	10	mV/V
Output Current	Sourcing	500			µA
PREAMPLIFIER OUTPUT					
Voltage Swing		0.25		V_S – 1.4	V
Current Output	Source or Sink	30	80		µA
Capacitive Load Drive			100		pF
BUFFER AMPLIFIER					
Input Offset Voltage[6]	Delta from Nominal 1.800 V		±10	±25	mV
Input Bias Current			5	20	nA
Open-Loop Gain	DC		80		dB
Unity Gain Bandwidth			200		kHz
Output Voltage Swing	I_{OUT} = ±100 µA	0.25		V_S – 0.25	V
Capacitive Load Drive		1000			pF
Power Supply Rejection	DC, V_S = +4.75 V to +5.25 V		1	10	mV/V
POWER SUPPLY					
Operating Voltage Range		4.75		5.25	V
Quiescent Supply Current			10	13	mA
TEMPERATURE RANGE					
Operating Range J		0		+70	°C
Specified Performance A		–40		+85	°C
Automotive Grade*		–40		+125	°C

NOTES

[1]Alignment error is specified as the angle between the true and indicated axis of sensitivity, (see Figure 2).

[2]Transverse sensitivity is measured with an applied acceleration that is 90° from the indicated axis of sensitivity. Transverse sensitivity is specified as the percent of transverse acceleration that appears at the V_{PR} output. This is the algebraic sum of the alignment and the inherent sensor sensitivity errors, (see Figure 2).

[3]Specification refers to the maximum change in parameter from its initial at +25°C to its worst case value at T_{MIN} to T_{MAX}.

[4]Frequency at which response is 3 dB down from dc response assuming an exact C1 value is used. Maximum recommended BW is 10 kHz using a 0.007 µF capacitor, refer to Figure 22.

[5]Applying logic high to the self-test input has the effect of applying an acceleration of –52.6 *g* to the ADXL50.

[6]Input offset voltage is defined as the output voltage differential from 1.800 V when the amplifier is connected as a follower (i.e., Pins 9 and 10 tied together). The voltage at Pin 9 has a temperature drift proportional to that of the 3.4 V reference.

*Contact factory for availability of automotive grade devices.

All min and max specifications are guaranteed. Typical specifications are not tested or guaranteed.
Specifications subject to change without notice.

Nintendo Exhibit 1066
IPR2024-00668 - Page 704

ABSOLUTE MAXIMUM RATINGS*

Acceleration (Any Axis, Unpowered for 0.5 ms) . . . . . 2000 g
Acceleration (Any Axis, Powered for 0.5 ms) . . . . . 500 g
$+V_S$ . . . . . –0.3 V to +7.0 V
Output Short Circuit Duration
(V_{PR}, V_{OUT}, V_{REF} Terminals to Common) . . . . . Indefinite
Operating Temperature . . . . . –55°C to +125°C
Storage Temperature . . . . . –65°C to +150°C

*Stresses above those listed under "Absolute Maximum Ratings" may cause permanent damage to the device. This is a stress rating only; the functional operation of the device at these or any other conditions above those indicated in the operational sections of this specification is not implied. Exposure to absolute maximum rating conditions for extended periods may affect device reliability.

Package Characteristics

Package	θ_{JA}	θ_{JC}	Device Weight
10-Pin TO-100	130°C/W	30°C/W	5 Grams

ORDERING GUIDE

Model	Temperature Range
ADXL50JH	0°C to +70°C
ADXL50AH	–40°C to +85°C

CAUTION

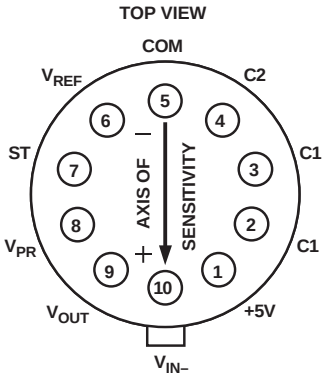
ESD (electrostatic discharge) sensitive device. Electrostatic charges as high as 4000 V readily accumulate on the human body and test equipment and can discharge without detection. Although the ADXL50 features proprietary ESD protection circuitry, permanent damage may occur on devices subjected to high energy electrostatic discharges. Therefore, proper ESD precautions are recommended to avoid performance degradation or loss of functionality.



PIN DESCRIPTION

+5 V	The power supply input pin.
C2	Connection for an external bypass capacitor (nominally 0.022 μF) used to prevent oscillator switching noise from interfering with other ADXL50 circuitry. Please see the section on component selection.
C1	Connections for the demodulator capacitor, nominally 0.022 μF. See the section on component selection for application information.
COM	The power supply common (or "ground") connection.
V_{REF}	Output of the internal 3.4 V voltage reference.
ST	The digital self-test input. It is both CMOS and TTL compatible.
V_{PR}	The ADXL50 preamplifier output providing an output voltage of 19 mV per g of acceleration.
V_{OUT}	Output of the uncommitted buffer amplifier.
V_{IN-}	The inverting input of the uncommitted buffer amplifier.

CONNECTION DIAGRAM
10-Header (TO-100)



NOTES:

AXIS OF SENSITIVITY IS ALONG A LINE BETWEEN PIN 5 AND THE TAB.

THE CASE OF THE METAL CAN PACKAGE IS CONNECTED TO PIN 5 (COMMON).

ARROW INDICATES DIRECTION OF POSITIVE ACCELERATION ALONG AXIS OF SENSITIVITY.

Nintendo Exhibit 1066
IPR2024-00668 - Page 705

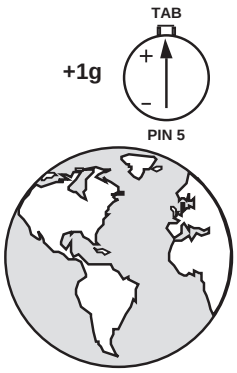


Figure 1. Output Polarity at V_{PR}

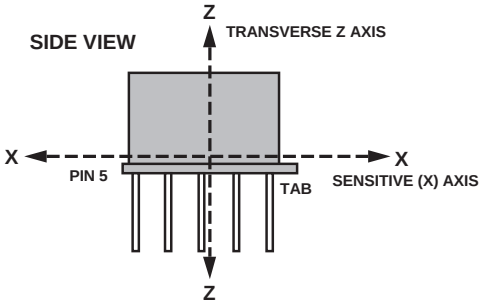


Figure 2a. Sensitive X and Transverse Z Axis

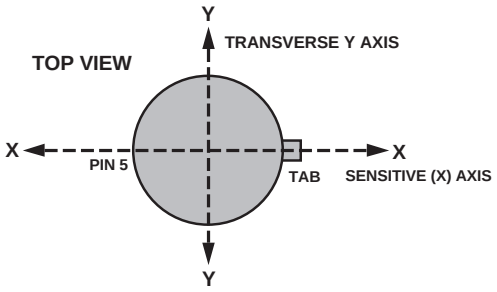


Figure 2b. Sensitive X and Transverse Y Axis

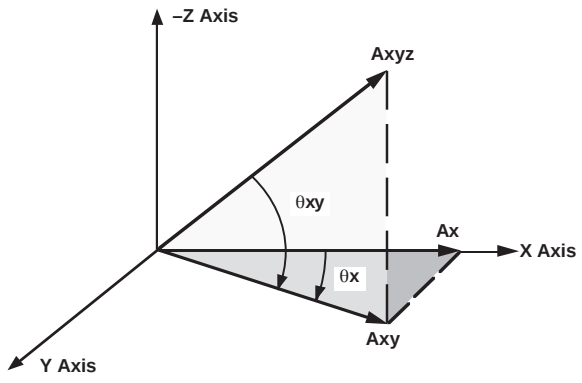


Figure 2c. A Vector Analysis of an Acceleration Acting Upon the ADXL50 in Three Dimensions

Polarity of the Acceleration Output

The polarity of the ADXL50 output is shown in the Figure 1. When oriented to the earth's gravity (and held in place), the ADXL50 will experience an acceleration of +1 g. This corresponds to a change of approximately +19 mV at the V_{PR} output pin. Note that the polarity will be reversed to a negative going signal at the buffer amplifier output V_{OUT}, due to its inverting configuration.

Mounting Considerations

There are three main causes of measurement error when using accelerometers. The first two are alignment and transverse sensitivity errors. The third source of error is due to resonances or vibrations of the sensor in its mounting fixture.

Errors Due to Misalignment

The ADXL50 is a sensor designed to measure accelerations that result from an applied force. Because these forces act on the sensor in a vector manner, the alignment of the sensor to the force to be measured may be critical.

The ADXL50 responds to the component of acceleration on its sensitive X axis. Figures 2a and 2b show the relationship between the sensitive "X" axis and the transverse "Z" and "Y" axes as they relate to the TO-100 package.

Figure 2c describes a three dimensional acceleration vector (A_{XYZ}) which might act on the sensor, where A_X is the component of interest. To determine A_X, first, the component of acceleration in the XY plane (A_{XY}) is found using the cosine law:

$$A_{XY} = A_{XYZ}\,(cos\theta_{XY})\ then$$

$$A_X = A_{XY}\,(\cos\theta_X)$$

$$Therefore:\ Typical\ V_{PR} = 19\ mV/g\ (A_{XYZ})\ (cos\theta_{XY})\ cos\theta_X$$

Note that an ideal sensor will react to forces along or at angles to its sensitive axis but will reject signals from its various transverse axes, i.e., those exactly 90° from the sensitive "X" axis. But even an ideal sensor will produce output signals if the transverse signals are not exactly 90° to the sensitive axis. An acceleration that is acting on the sensor from a direction different from the sensitive axis will show up at the ADXL50 output at a reduced amplitude.

Table I. Ideal Output Signals for Off Axis Applied Accelerations Disregarding Device Alignment and Transverse Sensitivity Errors

θ_X	% of Signal Appearing at Output	Output in gs for a 50 g Applied Acceleration
0	100%	50 (On Axis)
1°	99 98%	49.99
2°	99.94%	49.97
3°	99.86%	49.93
5°	99.62%	49.81
10°	98.48%	49.24
30°	86.60%	43.30
45°	70.71%	35.36
60°	50.00%	25.00
80°	17.36%	8.68
85°	8.72%	4.36
87°	5.25%	2.63
88°	3.49%	1.75
89°	1.7%	0.85
90°	0%	0.00 (Transverse Axis)

Nintendo Exhibit 1066
IPR2024-00668 - Page 706

Table I shows the percentage signals resulting from various θ_X angles. Note that small errors in alignment have a negligible effect on the output signal. A 1° error will only cause a 0.02% error in the signal. Note, however, that a signal coming 1° off of the transverse axis (i.e., 89° off the sensitive axis) will still contribute 1.7% of its signal to the output. Thus large transverse signals could cause output signals as large as the signals of interest.

Table I may also be used to approximate the effect of the ADXL50's internal errors due to misalignment of the die to the package. For example: a 1 degree sensor alignment error will allow 1.7% of a transverse signal to appear at the output. In a nonideal sensor, transverse sensitivity may also occur due to inherent sensor properties. That is, if the sensor physically moves due to a force applied exactly 90° to its sensitive axis, then this might be detected as an output signal, whereas an ideal sensor would reject such signals. In every day use, alignment errors may cause a small output peak with accelerations applied close to the sensitive axis but the largest errors are normally due to large accelerations applied close to the transverse axis.

Errors Due to Mounting Fixture Resonances
A common source of error in acceleration sensing is resonance of the mounting fixture. For example, the circuit board that the ADXL50 mounts to may have resonant frequencies in the same range as the signals of interest. This could cause the signals measured to be larger than they really are. A common solution to this problem is to dampen these resonances by mounting the ADXL50 near a mounting post or by adding extra screws to hold the board more securely in place.

When testing the accelerometer in your end application, it is recommended that you test the application at a variety of frequencies in order to ensure that no major resonance problems exist.

GLOSSARY OF TERMS
Acceleration: Change in velocity per unit time.

Acceleration Vector: Vector describing the net acceleration acting upon the ADXL50 (A_{XYZ}).

g: A unit of acceleration equal to the average force of gravity occurring at the earth's surface. A g is approximately equal to 32.17 feet/s^2, or 9.807 meters/s^2.

Nonlinearity: The maximum deviation of the ADXL50 output voltage from a best fit straight line fitted to a plot of acceleration vs. output voltage, calculated as a % of the full-scale output voltage (@ 50 g).

Resonant Frequency: The natural frequency of vibration of the ADXL50 sensor's central plate (or "beam"). At its resonant frequency of 24 kHz, the ADXL50's moving center plate has a peak in its frequency response with a Q of 3 or 4.

Sensitivity: The output voltage change per g unit of acceleration applied, specified at the V_{PR} pin in mV/g.

Sensitive Axis (X): The most sensitive axis of the accelerometer sensor. Defined by a line drawn between the package tab and Pin 5 in the plane of the pin circle. See Figures 2a and 2b.

Sensor Alignment Error: Misalignment between the ADXL50's on-chip sensor and the package axis, defined by Pin 5 and the package tab.

Total Alignment Error: Net misalignment of the ADXL50's on-chip sensor and the measurement axis of the application. This error includes errors due to sensor die alignment to the package, and any misalignment due to installation of the sensor package in a circuit board or module.

Transverse Acceleration: Any acceleration applied 90° to the axis of sensitivity.

Transverse Sensitivity Error: The percent of a transverse acceleration that appears at the V_{PR} output. For example, if the transverse sensitivity is 1%, then a +10 g transverse acceleration will cause a 0.1 g signal to appear at V_{PR} (1% of 10 g). Transverse sensitivity can result from a sensitivity of the sensor to transverse forces or from misalignment of the internal sensor to its package.

Transverse Y Axis: The axis perpendicular (90°) to the package axis of sensitivity in the plane of the package pin circle. See Figure 2.

Transverse Z Axis: The axis perpendicular (90°) to both the package axis of sensitivity and the plane of the package pin circle. See Figure 2.

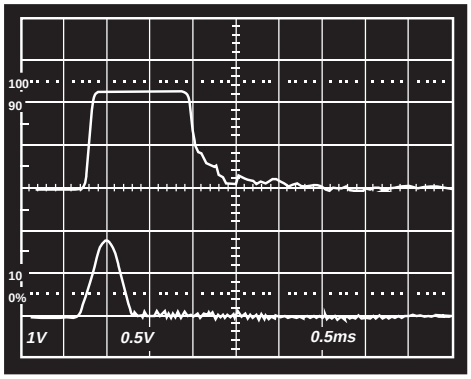


Figure 3. 500 g Shock Overload Recovery. Top Trace: ADXL50 Output. Bottom Trace: Reference Accelerometer Output

Nintendo Exhibit 1066
IPR2024-00668 - Page 707

ADXL50–Typical Characteristics

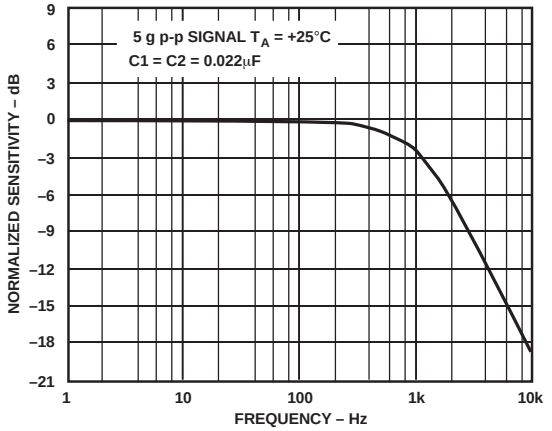


Figure 4. Normalized Sensitivity vs. Frequency

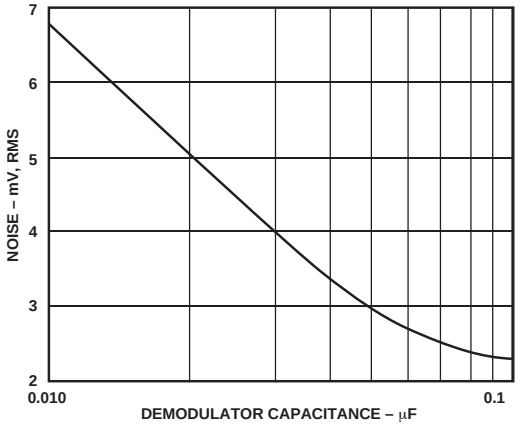


Figure 7. RMS Noise vs. Value of Demodulator Capacitor, C1

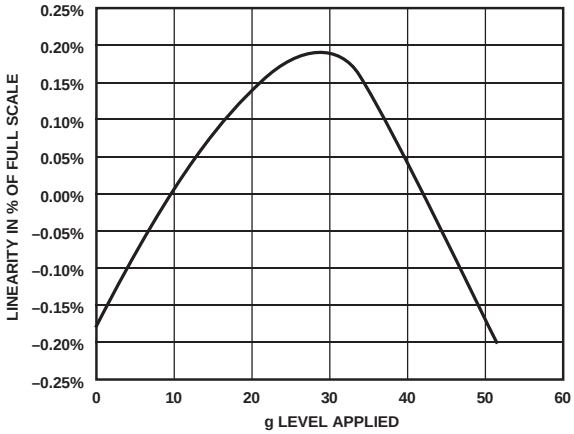


Figure 5. Linearity in Percent of Full Scale

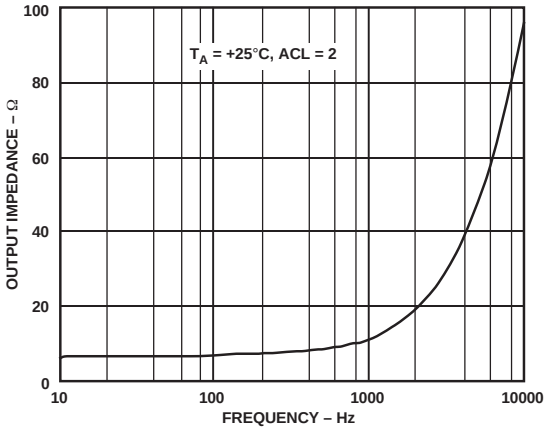


Figure 8. Buffer Amplifier Output Impedance vs. Frequency

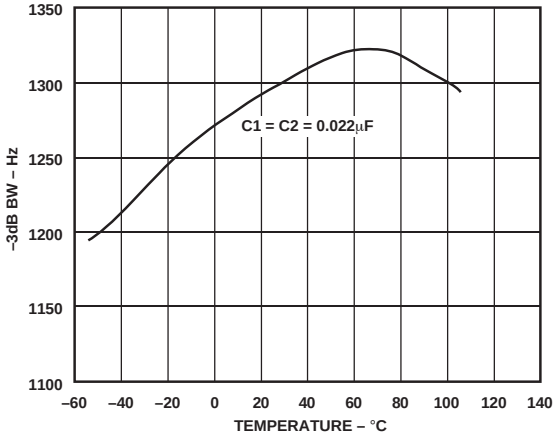


Figure 6. –3 dB Bandwidth vs. Temperature at V_{PR}

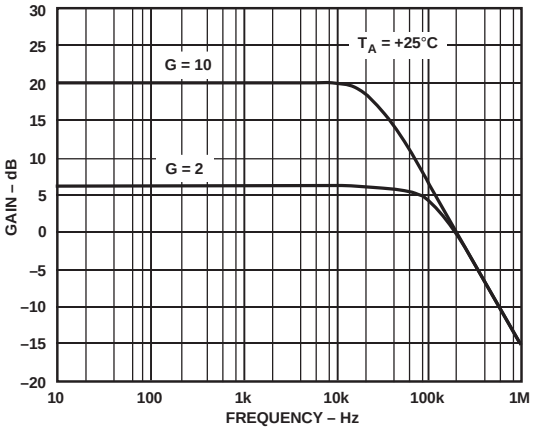


Figure 9. Buffer Amplifier Closed-Loop Gain vs. Frequency

Nintendo Exhibit 1066
IPR2024-00668 - Page 708

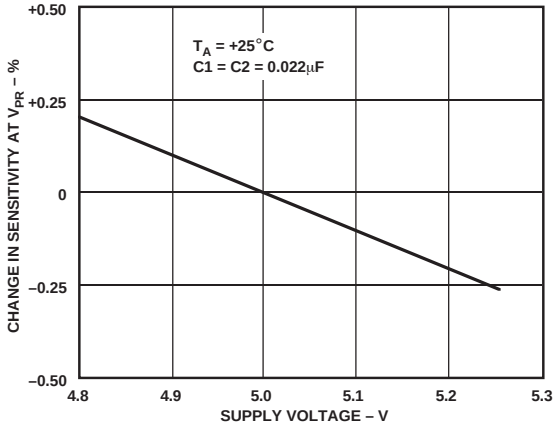


Figure 10. Change in Sensitivity vs. Supply Voltage

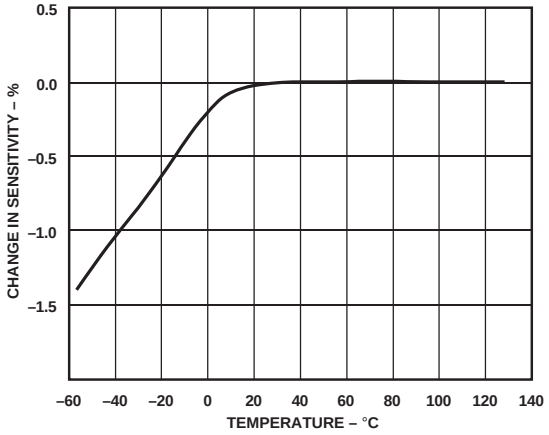


Figure 13. Percent Change in Sensitivity at V_{PR} vs. Temperature

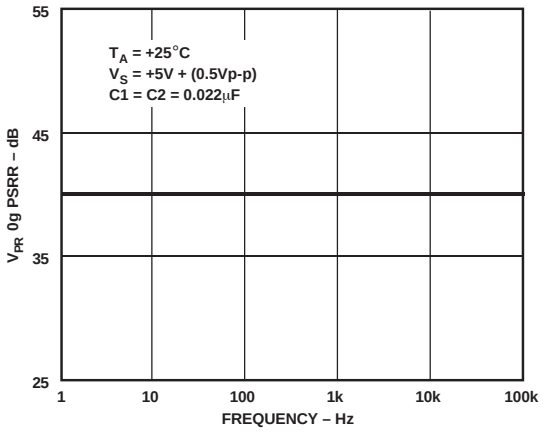


Figure 11. V_{PR} 0 g PSRR vs. Frequency

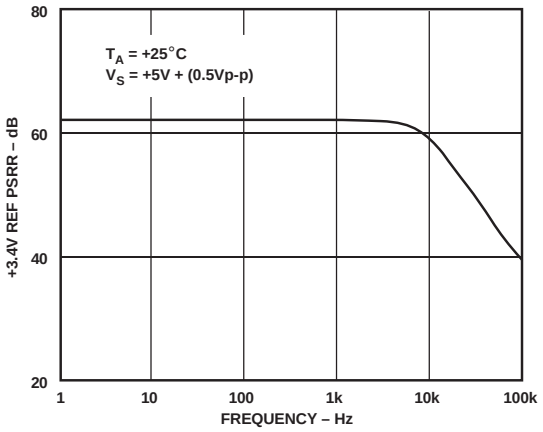


Figure 14. +3.4 V REF PSRR vs. Frequency

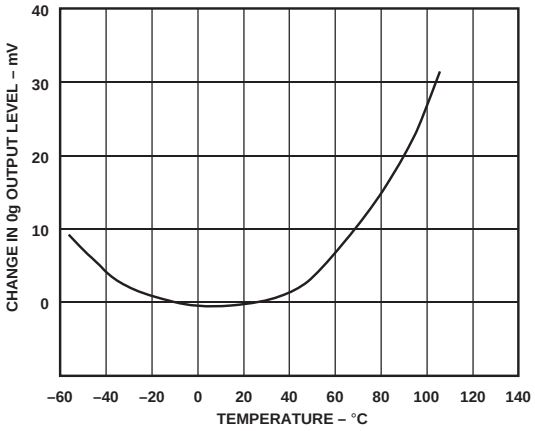


Figure 12. 0 g Bias Level vs. Temperature

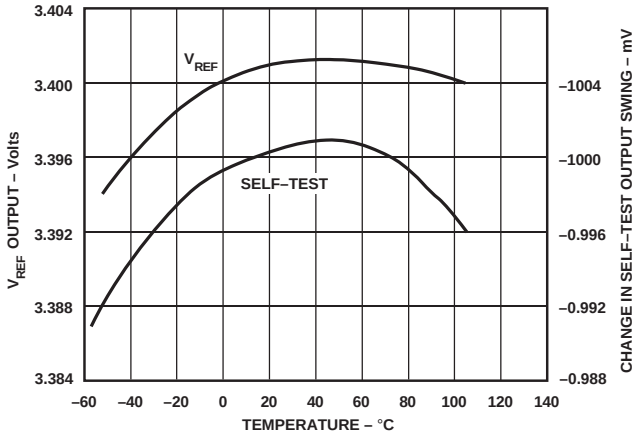


Figure 15. V_{REF} Output and Change in Self-Test Output Swing vs. Temperature

Nintendo Exhibit 1066
IPR2024-00668 - Page 709

THEORY OF OPERATION

The ADXL50 is a complete acceleration measurement system on a single monolithic IC. It contains a polysilicon surface-micro machined sensor and signal conditioning circuitry. The ADXL50 is capable of measuring both positive and negative acceleration to a maximum level of ±50 g.

Figure 16 is a simplified view of the ADXL50's acceleration sensor at rest. The actual structure of the sensor consists of 42 unit cells and a common beam. The differential capacitor sensor consists of independent fixed plates and a movable "floating" central plate which deflects in response to changes in relative motion. The two capacitors are series connected, forming a capacitive divider with a common movable central plate. A force balance technique counters any impeding deflection due to acceleration and servos the sensor back to its 0 g position.

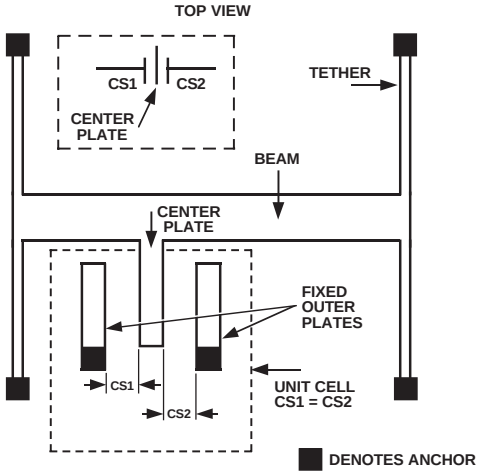


Figure 16. A Simplified Diagram of the ADXL50 Sensor at Rest

Figure 17 shows the sensor responding to an applied acceleration. When this occurs, the common central plate or "beam" moves closer to one of the fixed plates while moving further from the other. The sensor's fixed capacitor plates are driven deferentially by a 1 MHz square wave: the two square wave amplitudes are equal but are 180° out of phase from one another. When at rest, the values of the two capacitors are the same and therefore, the voltage output at their electrical center (i.e., at the center plate) is zero.

When the sensor begins to move, a mismatch in the value of their capacitance is created producing an output signal at the central plate. The output amplitude will increase with the amount of acceleration experienced by the sensor. Information concerning the direction of beam motion is contained in the phase of the signal with synchronous demodulation being used to extract this information. Note that the sensor needs to be positioned so that the measured acceleration is along its sensitive axis.

Figure 18 shows a block diagram of the ADXL50. The voltage output from the central plate of the sensor is buffered and then applied to a synchronous demodulator. The demodulator is also supplied with a (nominal) 1 MHz clock signal from the same oscillator which drives the fixed plates of the sensor. The demodulator will rectify any voltage which is in sync with its clock signal. If the applied voltage is in sync and in phase with the clock, a positive output will result. If the applied voltage is in sync but 180° out of phase with the clock, then the demodulator's output will be negative. All other signals will be rejected. An external capacitor, C1, sets the bandwidth of the demodulator.

The output of the synchronous demodulator drives the preamp —an instrumentation amplifier buffer which is referenced to +1.8 volts. The output of the preamp is fed back to the sensor through a 3 MΩ isolation resistor. The correction voltage required to hold the sensor's center plate in the 0 g position is a direct measure of the applied acceleration and appears at the V_{PR} pin.

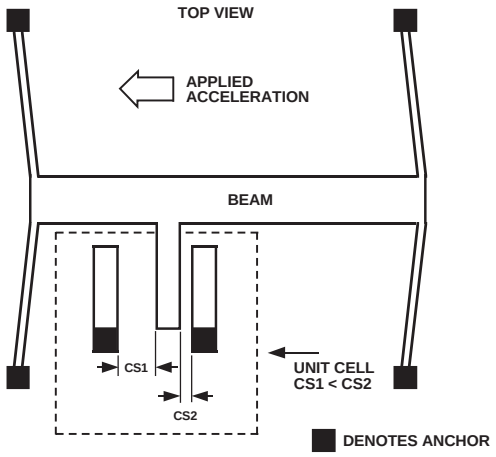


Figure 17. The ADXL50 Sensor Momentarily Responding to an Externally Applied Acceleration

When the ADXL50 is subjected to an acceleration, its capacitive sensor begins to move creating a momentary output signal. This is signal conditioned and amplified by the demodulator and preamp circuits. The dc voltage appearing at the preamp output is then fed back to the sensor and electrostatically forces the center plate back to its original center position.

At 0 g the ADXL50 is calibrated to provide +1.8 volts at the V_{PR} pin. With an applied acceleration, the V_{PR} voltage changes to the voltage required to hold the sensor stationary for the duration of the acceleration and provides an output which varies directly with applied acceleration.

The loop bandwidth corresponds to the time required to apply feedback to the sensor and is set by external capacitor C1. The loop response is fast enough to follow changes in g level up to and exceeding 1 kHz. The ADXL50's ability to maintain a flat response over this bandwidth keeps the sensor virtually motionless. This essentially eliminates any nonlinearity or aging effects due to the sensor beam's mechanical spring constant, as compared to an open-loop sensor.

An uncommitted buffer amplifier provides the capability to adjust the scale factor and 0 g offset level over a wide range. An internal reference supplies the necessary regulated voltages for powering the chip and +3.4 volts for external use.

Nintendo Exhibit 1066
IPR2024-00668 - Page 710

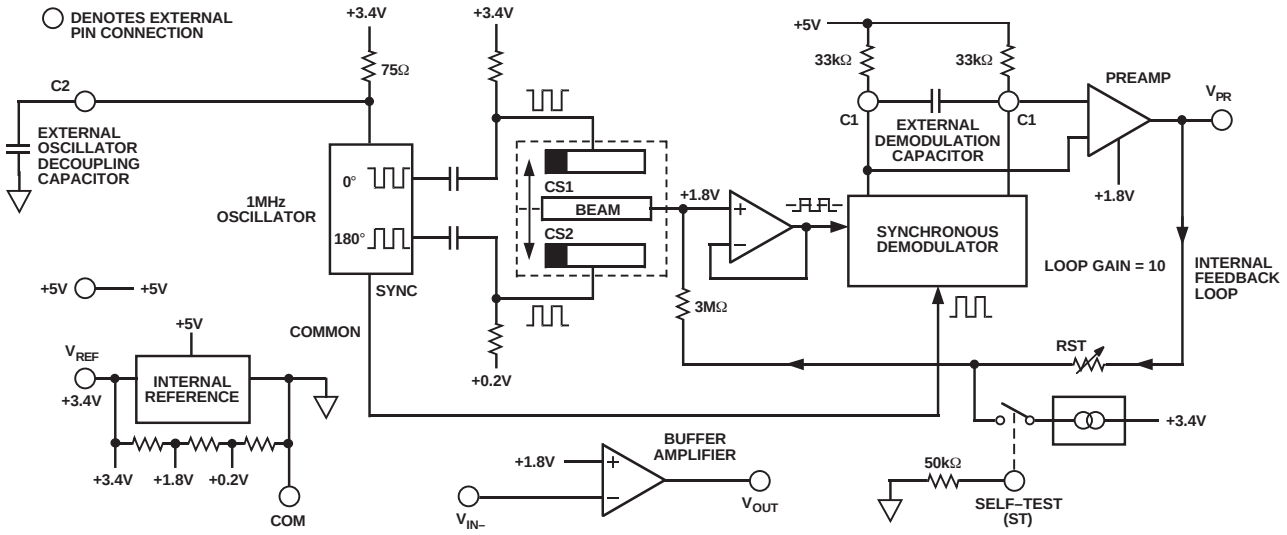


Figure 18. Functional Block Diagram

The sensor's tight mechanical spacing allows it to be electrostatically deflected to full scale while operating on a 5 volt supply. A self-test is initiated by applying a TTL "high" level voltage (>+2.0 V) to the ADXL50's self-test pin which causes the chip to apply a deflection voltage to the beam which moves it an amount equal to –50 g (the negative full-scale output of the device). Note that the ±10% tolerance of the self-test circuit is not proportional to the sensitivity error, see Self-Test section.

The output of the ADXL50's preamplifier is 1.8 V at 0 g acceleration with an output range of ±0.95 V for a ±50 g input, i.e., 19 mV/g. An uncommitted buffer amplifier has been included on-chip to enhance the user's ability to offset the 0 g signal level and to amplify and filter the signal. Access is provided to both the inverting input and the output of this amplifier via pins V_{OUT} and V_{IN-}, while the noninverting input is connected internally to a +1.8 V reference. The +1.8 V is derived from a resistor divider connected to the 3.4 V reference.

BASIC CONNECTIONS FOR THE ADXL50

Figure 19 shows the basic connections needed for the ADXL50 to measure accelerations in the ±50 g range with an output scale factor 40 mV/g corresponding to a 2.5 V 0 g level, a ±2.0 V full-scale swing around 0 g and a 3 dB bandwidth of approximately 1 kHz.

In general, the designer will need to take into account the initial zero g bias when designing circuits. For the ADXL50J this offset is 1.8 V ± 250 mV. When microprocessors and software

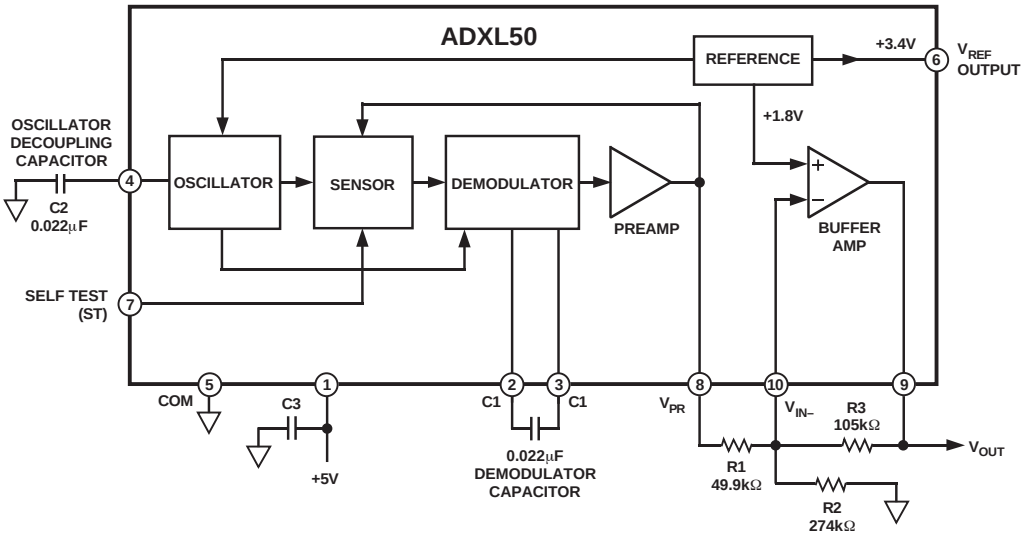


Figure 19. ADXL50 Application Providing an Output Sensitivity of 40 mV/g, a +2.5 V 0 g Level and a Bandwidth of 1 kHz

Nintendo Exhibit 1066
IPR2024-00668 - Page 711